

Isabel Franco Castillo

Preventing biodeterioration of cultural heritage using nanostructured materials

Director/es

George Mitchell, Scott
Martínez De La Fuente, Jesús

<http://zaguan.unizar.es/collection/Tesis>



Universidad
Zaragoza

Tesis Doctoral

**PREVENTING BIODETERIORATION OF CULTURAL
HERITAGE USING NANOSTRUCTURED
MATERIALS**

Autor

Isabel Franco Castillo

Director/es

George Mitchell, Scott
Martínez De La Fuente, Jesús

UNIVERSIDAD DE ZARAGOZA
Escuela de Doctorado

Programa de Doctorado en Bioquímica y Biología Molecular

2022

Preventing biodeterioration of cultural heritage using nanostructured materials

Memoria presentada para optar al título de Doctor
por la Universidad de Zaragoza

Isabel Franco Castillo

Directores

Scott G. Mitchell

Jesús Martínez de la Fuente

CSIC – Universidad de Zaragoza

Instituto de Nanociencia y Materiales de Aragón

Programa de Doctorado de Bioquímica y Biología Molecular

Zaragoza, 2022

Thesis in the modality of compendium of publications

The PhD thesis *“Preventing biodeterioration of cultural heritage using nanostructured materials”* is presented by compendium of the following publications:

- Article 1:** I. Franco-Castillo, L. Hierro, J. M. de la Fuente, A. Seral-Ascaso, S. G. Mitchell. “Perspectives for antimicrobial nanomaterials in cultural heritage conservation”. *Chem*, **2021**, 7(3), 629-669.
- Article 2:** I. Franco-Castillo, L. De Matteis, C. Marquina, E. G. Guillén, J. M. de la Fuente, S. G. Mitchell. “Protection of 18th century paper using antimicrobial nano-magnesium oxide”. *International Biodeterioration & Biodegradation*, **2019**, 141, 79-86.
- Article 3:** I. Franco-Castillo, E. G. Guillén, J. M. de la Fuente, F. Silva, Mitchell, S. G. “Preventing fungal growth on heritage paper with antifungal and cellulase inhibiting magnesium oxide nanoparticles”. *Journal of Materials Chemistry B*, **2019**, 7(41), 6412-6419.
- Article 4:** I. Franco-Castillo, A. G. Enderle, E. Atrián-Blasco, R. Martín-Rapún, L. Lizarraga, M. J. Culzoni, M. Bollini, J. M. de la Fuente, F. Silva, C. Streb, S. G. Mitchell. “Hybrid Antimicrobial Films Containing a Polyoxometalate-Ionic Liquid” *ACS Applied Polymer Materials*, **2022**, 4, 4144–4153.
- Article 5:** I. Franco-Castillo, A. Misra, S. Laratte, M. Gommeaux, R. Perarnau, N. Vaillant-Gaveau, C. Pierlot, C. Streb, S. G. Mitchell, S. Eyssautier-Chuine. “New protective coatings against lampenflora growing in the Pommery Champagne cellar”. *International Biodeterioration & Biodegradation*, **2022**.
- Article 6:** K. Rajkowska, A. Koziróg, A. Otlewska, M. Piotrowska, E. Atrián-Blasco, I. Franco-Castillo, S. G. Mitchell. “Antifungal activity of polyoxometalate-ionic liquids on historical brick”. *Molecules*, **2020**, 25(23), 5663.

The following publications have been part of the doctoral student's training, and have been added in the Appendix section:

- Appendix 3:** I. Franco-Castillo, A. Misra, D. P. Müller, C. González, S. Eyssautier-Chuine, A. Ziegler, J. M. de la Fuente, S. G. Mitchell, C. Streb. "Polyoxometalate-ionic liquids (POM-ILs) as anticorrosion and antibacterial coatings for natural stones". *Angewandte Chemie International Edition*, **2018**, 57(45), 14926-14931.
- Appendix 4:** A. Misra, C. Zambrzycki, G. Kloker, A. Kotyrba, M. H. Anjass, I. Franco-Castillo, S. G. Mitchell, R. Güttel, C. Streb. "Water purification and microplastics removal using magnetic polyoxometalate-supported ionic liquid phases (magPOM-SILPs)". *Angewandte Chemie International Edition*, **2020**, 59(4), 1601-1605.
- Appendix 5:** H. Soria-Carrera, I. Franco-Castillo, P. Romero, S. Martín, J. M. de la Fuente, S. G. Mitchell, R. Martín-Rapún. "On-POM Ring-Opening Polymerisation of N-Carboxyanhydrides". *Angewandte Chemie*, **2021**, 133(7), 3491-3495.
- Appendix 6:** D. J. Wales, S. Miralles-Comins, I. Franco-Castillo, J. M. Cameron, Q. Cao, E. Karjalainen, J. A. Fernandes, G. N. Newton, S. G. Mitchell, V. Sans. "Decoupling manufacturing from application in additive manufactured antimicrobial materials". *Biomaterials Science*, **2021**, 9(16), 5397-5406.

Table of Contents

Thesis in the modality of compendium of publications.....	1
List of Abbreviations.....	7
1. Abstract.....	9
2. Introduction	13
2.1. Biodeterioration of cultural heritage artifacts and architectures: causes and threats	13
2.1.1. Microorganisms responsible of the biodeterioration	14
2.1.2. Interaction of microorganisms with heritage objects.....	16
2.1.2.1 Organic materials.....	17
2.1.2.2. Inorganic materials	20
2.1.3. Consequences and solutions to biodeterioration.....	24
2.2. Traditional methods to prevent and combat biodeterioration	25
2.3. New biocidal compounds based on nanoparticles	28
2.3.1. Desired characteristics of the NPs	29
2.3.2. Most used NPs in heritage	30
2.3.3. Magnesium oxide nanoparticles (MgO NPs)	32
2.3.4. Polyoxometalate-ionic liquids (POM-ILs).....	32
2.4. Coatings: application methods and characterization.....	35
Article 1: Perspectives for antimicrobial nanomaterials in cultural heritage conservation.....	37
3. Objectives and Structure	78
4. Methodology	81
4.1. Nanoparticle synthesis.....	81
4.1.1. Magnesium oxide nanoparticles (MgO NPs)	81
4.1.2. Polyoxometalate (POM) and polyoxometalate-ionic liquid (POM-IL) syntheses	81
4.1.2.1. $K_8[\alpha\text{-SiW}_{11}\text{O}_{39}] \times 13\text{H}_2\text{O}$	81
4.1.2.2. Polyoxometalate-ionic liquids (POM-IL 1, POM-IL 2 and DOTMG-1)	82
4.2. Microorganisms and growth conditions.....	82
4.3. Antimicrobial susceptibility testing.....	84
4.3.1. Microbial proliferation in presence of the antimicrobial compound	84

Table of Contents

4.3.1.1. Antimicrobial activity of water-compatible compounds (MgO NPs)	84
4.3.1.2. Organic-soluble compounds (POM-ILs).....	85
4.3.2. Cell viability assays	86
4.3.2.1. Viability assay for prokaryotic cells (bacteria)	86
4.3.2.2. Viability assay for eukaryotic cells (moulds)	86
4.3.3. Cell morphology damage study by microscopy	87
4.3.3.1. Environmental Scanning Electron Microscopy (ESEM)	87
4.3.3.2. Transmission Electron Microscopy (TEM)	88
4.3.3.3. Optical microscopy	89
4.4. Coatings on real heritage samples.....	89
4.4.1. XVIII Century paper coating with MgO NPs	89
4.4.1.1. Colorimetric measurement after the MgO NPs coating	90
4.4.1.2. Paper coating visualization by ESEM	90
4.4.1.3. Inductively coupled plasma mass spectrometry (ICP–MS)	90
4.4.2. Stone surfaces coated with POM-ILs	91
4.4.3. DOTMG-1 films	91
4.5. Determination of the antimicrobial activity <i>in situ</i>	92
4.5.1. MgO NPs paper coating antimicrobial activity evaluation	92
4.5.1.1. MgO NPs <i>in situ</i> activity against <i>E. coli</i>	92
4.5.1.2. Antifungal activity under optimal growth conditions	92
4.5.1.3. <i>In situ</i> antifungal activity under more realistic growth conditions	93
4.5.1.4. Evaluating the cellulose degradation capacity of moulds	93
4.5.2. POM-ILs coating on stone surfaces	94
4.5.2.1. Pommery chalk slabs.....	94
4.5.2.2. 19 th century historical bricks	95
4.5.2.3. Surface antimicrobial activity of the POM-IL DOTMG-1	95
5. Results and Discussion	97

Table of Contents

5.1. MgO NPs to prevent heritage paper colonization	97
5.1.1. Synthesis and characterization of MgO NPs	97
5.1.2. Antimicrobial activity of the MgO NPs	98
5.1.2.1. Microbial proliferation and viability in presence of the MgO NPs	98
5.1.2.2. Study of the bacterial cell viability and morphology after treatment with the MgO NPs	100
5.1.3. Characterization of the MgO NPs coating on real heritage samples	102
5.1.4. Antimicrobial performance of the MgO NP on paper samples	104
5.1.4.1. Diffusion ability of the MgO NPs	104
5.1.4.2. MgO NPs <i>in situ</i> activity against <i>E. coli</i>	105
5.1.4.3. Antifungal activity under optimal growth conditions	105
5.1.4.4. <i>In situ</i> antifungal activity under more realistic growth conditions	106
5.1.4.5 Ability of MgO NP to prevent cellulose degradation by moulds	108
5.1.5. Conclusions	110
Article 2: Protection of 18th century paper using antimicrobial nano-magnesium oxide	111
Article 3: Preventing fungal growth on heritage paper with antifungal and cellulase inhibiting magnesium oxide nanoparticles	123
5.2. Polyoxometalate-ionic liquids (POM-ILs) as broad-spectrum antimicrobial coatings to protect stone materials from microbial contamination	135
5.2.1. Antimicrobial activity of the POM-ILs against bacteria and fungi	135
5.2.1.1. Microbial proliferation and viability in presence of the POM-ILs	135
5.2.1.2. Study of the microbial morphology after treatment with the POM-IL DOTMG-1	139
5.2.1.3. Surface antimicrobial activity of the POM-ILs	141
5.2.2. POM-ILs antimicrobial performance as stone coatings to prevent lampenflora growth	142

Table of Contents

5.2.2.1. Evaluation of the colour change after application of the coatings	143
5.2.2.2. Biocidal performance of the coatings against lampenflora.....	144
5.2.3. POM-ILs as disinfectant agents of 19 th bricks	147
5.2.4. Conclusions.....	149
Article 4: Hybrid Antimicrobial Films Containing a Polyoxometalate-Ionic Liquid	150
Article 5: New protective coatings against lampenflora growing in the Pommery Champagne cellar	175
Article 6: Antifungal Activity of Polyoxometalate-Ionic Liquids on Historical Brick	217
6. Conclusions.....	231
7. Perspectives	237
8. References	240
Appendix.....	261
Appendix 1: Impact factor and Thematic Area of the journals.....	261
Appendix 2: Doctoral student's contribution.....	263
Appendix 3: Polyoxometalate-Ionic Liquids (POM-ILs) as Anticorrosion and Antibacterial Coatings for Natural Stones	266
Appendix 4: Water Purification and Microplastics Removal Using Magnetic Polyoxometalate-Supported Ionic Liquid Phases (magPOM-SILPs)	272
Appendix 5: On-POM Ring-Opening Polymerisation of N-Carboxyanhydrides.....	277
Appendix 6: Decoupling manufacturing from application in additive manufactured antimicrobial materials	282
Appendix 7: Bacterfield - ¡Las bacterias entran en juego!	292

List of Abbreviations

BB	Belgian Blue Stone
BHIA	Brain Heart Infusion Agar
CECT.....	Colección Española de Cultivos Tipo
CFU	Colony Forming Units
CON.....	Conidia
DMSO	Dimethyl Sulfoxide
DNA.....	Deoxyribonucleic acid
DNS.....	3,5-dinitrosalicylic acid
DO	Dom Stone
DOTMG.....	<i>N,N,N',N'</i> -tetramethyl- <i>N'',N''</i> -dioctylguanidinium
ESEM	Environmental Scanning Electron Microscopy
IL	Ionic Liquid
LB	Luria-Bertani medium
MBC	Minimum Bactericidal Concentration
MEP.....	Malt Dextrin Peptone
MHA.....	Mueller Hinton Agar
MIC	Minimum Inhibitory Concentration
NB	Nutrient Broth
NPs.....	Nanoparticles
OD	Optical Density
PBS	Phosphate-Buffered Saline
PDA.....	Potato Dextrose Agar
PMMA	Poly(methyl methacrylate)
POM.....	Polyoxometalate
POM-IL.....	Polyoxometalate-Ionic Liquid
RO	Rommery Stone
ROS	Reactive Oxygen Species
RPMI.....	Roswell Park Memorial Institute 1640 Medium

Table of Contents

SA.....	Savonnieres Stone
SDA.....	Sabouraud Dextrose Agar
TBX.....	Tryptone Bile X-Glucuronide
TEM	Transmission electron microscopy
THA	Tetraheptyl Ammonium
THTDA.....	Trihexyl Tetradecyl Ammonium
TSA	Tryptone Soy Agar
VTEC.....	Verotoxigenic <i>E. coli</i>
XTT.....	2,3,5-triphenyltetrazoliumchlorid
YMA.....	Yeast Malt Agar
YMB	Yeast Malt Broth

1. Abstract

The biodeterioration of artistic and architectural heritage represents a serious and recurring problem for museums, local authorities, and private collectors alike, where irreparable damage to unique artifacts can result in immeasurable losses to our shared cultural heritage. This biodeterioration is mainly caused by microorganisms, which not only threat heritage materials such as paper, leather, or stones, but also poses a health risk to restorers and general public. The overall aim of this thesis is to engineer a range of molecular and hybrid nanomaterials with modular and tuneable antimicrobial properties, which act to help prevent the biodeterioration of cultural heritage objects. To achieve this goal, there have been used magnesium oxide nanoparticles (MgO NPs) and polyoxometalate-ionic liquids (POM-ILs) against different bacterial and fungal strains. The MgO NPs (average diameter 10-12 nm), synthesized by sol-gel method, have been used as protective coating for 18th century paper samples. *In vitro* assays demonstrated the antimicrobial activity of the MgO NPs against two bacteria (*E. coli* and *B. subtilis*) and three moulds commonly found colonizing paper heritage (*A. niger*, *C. cladosporioides* and *T. reesei*). Moreover, the MgO NPs not only inhibit the bacterial and fungal growth over the paper samples, but also the cellulase activity of *T. reesei* and *A. niger*, preventing the degradation of the paper. On the other hand, three POM-ILs, based on the monolacunary Keggin-type polyoxometalate ($[\alpha\text{-SiW}_{11}\text{O}_{39}]^{8-}$) and combined with three different cations, have been used to protect different types of mineral-based building materials from microbial colonization. The broad-spectrum antimicrobial activity of POM-IL DOTMG-1 has been studied against non-pathogenic (*E. coli* DH5- α , *B. subtilis*) and pathogenic (VTEC, *L. monocytogenes*) bacteria and against environmental moulds (*A. niger*, *C. cladosporioides*) as well as alimentary mycotoxin-producing moulds (*A. ochraceus*, *P. expansum*), obtaining low biocidal concentrations. POM-IL 1 and POM-IL 2 were used to limit the growth of lampenflora on chalk stones, and the results showed both POM-ILs were more effective than commercial Preventol RI80 against two algal strains isolated from the Pommery Champagne cellar bas reliefs, *Pseudostichococcus monallantoides* and *Chromochloris zoefingiensis*. The antifungal activity of different POM-ILs as disinfectant agents to eradicate mould contamination inhabiting historical bricks was also studied, being POM-IL 2 one of the compounds with better performance. Based on these results, we can conclude that both MgO NPs and POM-ILs are promising compounds for the

Abstract

conservation of cultural heritage objects and architecture. They can be applied as colourless coatings, which won't modify the aesthetics of the materials, and display broad-spectrum antimicrobial activity, preventing the colonisation of the surface.

1. Resumen

El biodeterioro del patrimonio artístico y arquitectónico representa un grave y recurrente problema tanto para museos y autoridades locales como para los coleccionistas privados, donde un daño irreparable en ciertos objetos únicos puede ocasionar grandes pérdidas para nuestro patrimonio cultural. El biodeterioro está causado principalmente por microorganismos, que no solo suponen una amenaza para los materiales patrimoniales como el papel, el cuero o las piedras, sino que también ponen en riesgo la salud de los restauradores y del público en general. El objetivo general de esta tesis es diseñar una gama de nanomateriales moleculares e híbridos con propiedades antimicrobianas modulables, que puedan ayudar a prevenir el biodeterioro del patrimonio cultural. Para lograr este objetivo se han sintetizado nanopartículas de óxido de magnesio (MgO NPs) y líquidos iónicos de polioxometalatos (POM-ILs), y se ha probado su eficacia frente a diferentes cepas de bacterias y mohos. Las NPs de MgO (con un diámetro medio de 10-12 nm), sintetizadas mediante un método sol-gel, se han utilizado como un recubrimiento protector en muestras de papel del siglo XVIII. Diferentes ensayos *in vitro* demostraron la actividad antimicrobiana de las NP de MgO frente a dos bacterias (*E. coli* y *B. subtilis*) y tres mohos que suelen encontrarse contaminando papel (*A. niger*, *C. cladosporioides* y *T. reesei*). Además, con estudios complementarios se ha comprobado que las NPs de MgO no solo inhiben el crecimiento bacteriano y fúngico sobre las muestras de papel, sino que también inhiben la actividad celulasa de *T. reesei* y *A. niger*, evitando así la degradación del papel. Por otro lado, tres POM-ILs (basados en el polioxometalato monolacunar tipo Keggin $[\alpha\text{-SiW}_{11}\text{O}_{39}]^{8-}$ combinado con tres cationes diferentes) se han utilizado para proteger diferentes tipos de materiales de construcción (de base mineral) de la colonización microbiana. Se ha estudiado la actividad antimicrobiana de amplio espectro de uno de estos compuestos (POM-IL DOTMG-1) frente a un amplio abanico de microorganismos: bacterias no patógenas (*E. coli* DH5- α , *B. subtilis*), bacterias patógenas (VTEC, *L. monocytogenes*), mohos ambientales (*A. niger*, *C. cladosporioides*) y mohos alimentarios productores de micotoxinas (*A. ochraceus*, *P. expansum*), obteniendo una buena actividad biocida a baja concentración frente a todos los microorganismos. Por otra parte, el POM-IL 1 y POM-IL 2 se utilizaron como recubrimientos antimicrobianos en piedra caliza para limitar el crecimiento de lampenflora. Los resultados obtenidos demostraron que ambos POM-ILs eran más efectivos que un compuesto comercial (Preventol RI80) frente a dos cepas de

Resumen

algas aisladas de los bajorrelieves de la bodega de Champagne de Pommery, *Pseudostichococcus monallantoides* y *Chromochloris zofingiensis*. También se estudió la actividad antifúngica de diferentes POM-ILs como agentes desinfectantes en muestras de ladrillos históricos previamente contaminados por mohos, siendo el POM-IL 2 uno de los compuestos que presentó mayor actividad. A la vista de estos resultados, se puede concluir que tanto las NPs de MgO como los POM-ILs son compuestos prometedores para la conservación del patrimonio cultural, ya que se pueden aplicar como recubrimientos incoloros, que no van a modificar la apariencia estética de los materiales, y que presentan actividad antimicrobiana de amplio espectro, evitando así la colonización microbiana de la superficie.

2. Introduction

2.1. Biodeterioration of cultural heritage artifacts and architectures: causes and threats

The tangible cultural heritage of a country or region is largely based on their artistic and architectural heritage. This heritage is constituted by a wide range of objects and materials, from books and paintings to textiles and buildings, all of which are constituted by different types of raw natural and handmade materials. However, they share one common feature in that almost all heritage material types are highly susceptible to deterioration over time. The global societal issue concerning the decay of our shared cultural heritage not only poses a threat to the historical value of the object; it also includes important economic considerations caused by lack of proper preservation of the artifacts.¹ Singular tragic events such as wars, fires and floods pose serious and often unforeseen threats, but other silent but relentless threats arising from environmental aspects (such as alterations in humidity, temperature, light, CO₂ concentration, atmospheric pressure, and pH) and geological conditions have an extremely deleterious effect on all types of heritage materials. The chemical composition of the material will affect the ageing process of the material and its bioreceptivity, which can be defined as the *“ability or aptitude of a material to be colonised by one or several groups of living organisms”*.^{2,3} Although this colonisation does not necessarily preclude any noticeable damage, changes in environmental conditions could easily lead to biodeterioration—*“any undesirable change in the properties of a material caused by the vital activities of organisms”*⁴— of the object, which poses a persistent problem in the conservation of cultural heritage. Biodeterioration involves a combination of physical and chemical damages, together with aesthetic alteration (Table 1), and occurs in both outdoors and indoors environments, from the façade of the buildings to artifacts displayed in exhibition rooms or stored in depots and is caused, mainly, by microorganisms.⁵ These microorganisms (such as bacteria, fungi, cyanobacteria, and algae) are highly proficient at inhabiting and decaying artistic and architectural heritage objects, constituted by inorganic and organic materials such as paper, leather, stone, textile, ceramic, metal, and glass.²

Table 1. Types of biodeterioration

Type of biodeterioration	Description	Example
Physical and mechanical	The material is damaged by the organism's growth.	Penetration of fungal hyphae or moss rhizoids into the stone, causing holes.
Aesthetic	Microorganism growth alters the aesthetics of the object.	Microbial biofilms growing over stone supports.
Chemical assimilation	The microorganisms use the material as their carbon and energy source.	Dissolution of stone substrates by epilithic cyanobacteria. Cellulose degradation into glucose by cellulolytic fungi.

2.1.1. Microorganisms responsible of the biodeterioration

All types of historic artifact are at risk of biodeterioration by microorganisms, from outdoor environments like palaeolithic wall art or external façades of buildings and stone sculptures, to indoor environments, which include both museums or private art collections; not to mention underground heritage, which includes caves, catacombs, and cellars. It therefore follows that biodeterioration of such a wide variety of substrate materials over such different local environments can be caused by a wide and heterogeneous community of colonising microbes constituted by prokaryote (bacteria and cyanobacteria) and eukaryote microorganisms (fungi and algae).⁶ The different characteristics of each environment will influence the type of microorganisms colonising the heritage object, making some of them prevail over others (Figure 1).

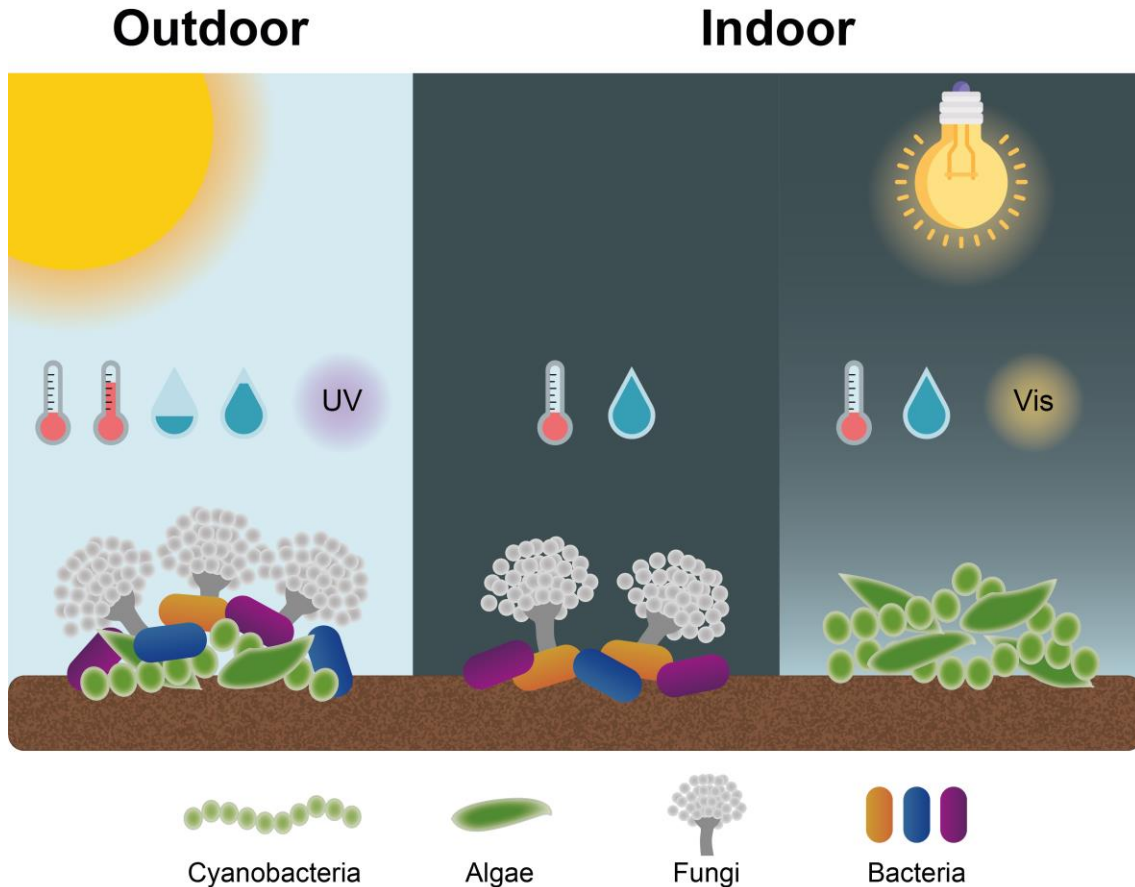


Figure 1. Schematic representation of the different characteristics of outdoor and indoor environments and its influence in microbial colonisation. Outdoor environments constitute high energy systems where weather conditions can vary from extreme hot environments with high doses of sun radiation to colder and humid conditions. In general, the pioneer colonisers are phototrophic microorganisms such as cyanobacteria, algae and lichens, followed by the heterotrophic microorganisms (secondary colonisers) such as bacteria and fungi. Indoor environments represent low energy systems characterized for their dark and humid conditions, which favour the growth of heterotrophic microorganisms like moulds and bacteria among the autotrophic ones. However, human activity has disrupted the natural ecosystem, causing new and undesired contaminations such as the lampenflora (photosynthetic cave microorganisms) growth due to artificial lighting.

Outdoor environments constitute high energy systems, with large amount of nutrients and light. In this scenario, the main colonizers will be those microorganisms that are best able to use these energy sources. In general, the pioneer colonisers of outdoor heritage are those capable of using light as a carbon source, namely, autotrophic microorganisms such as algae, cyanobacteria and lichens, which are able to perform photosynthesis. Note that lichen result from the symbiosis between an autotrophic microorganism (algae or cyanobacteria) and a fungus.⁷⁻⁹ These autotrophic microorganisms can obtain their nutrients from the inorganic compounds present in the surface and the sunlight and, once

they have obtained a foothold on the surface, the heterotrophic microorganisms (such as bacteria and fungi) can establish themselves as secondary colonisers, obtaining organic nutrients from the autotrophs that have established themselves previously, thereby creating a multispecies biofilm over the surface.⁸

On the other hand, indoor environments represent low energy systems, with little availability of energy and nutrients. Natural and artificial indoor environments, like caves, cellars, or depots are characterized for their dark and humid conditions, which favour the growth of heterotrophic microorganisms like moulds and bacteria among the autotrophic ones.^{8,10} Nonetheless, human activity has led to new sources of contamination, for example introducing new bacterial strains during restoration processes. Piñar and co-workers described a dominance of bacteria over fungi on Leonardo Da Vinci's drawings, partly due to the manipulation of the drawing during restoration works, which led to a high proportion of bacteria, typical of the human microbiome, contaminating the artworks.¹¹ Moreover, artificial lighting on caves and cellars has caused an increase of "lampenflora" (photosynthetic cave communities constituted by algae and cyanobacteria) growth. This problem has been described in show caves like the Carlsbad Cavern¹² or the Postojna and the Škocjan cave, in Slovenia,¹³ and also in the Pommery Champagne cellar,¹⁴ among other caves worldwide, where the lampenflora growth mar the aesthetics and can degrade the stone surfaces. This increased influence of the human activity on different heritage scenarios disrupts the natural ecosystem, causing new and undesired contaminations and accelerating the biodeterioration process, which sometimes ends with the closure of the monuments to the public, like in the paleolithic cave of Altamira (Spain), that was closed to the public in 2002 due to the deterioration of prehistoric paintings caused by photosynthetic bacteria and fungi.^{11-13,15}

2.1.2. Interaction of microorganisms with heritage objects

Historic artifacts are constituted by a wide range of materials, from the organic paper, leather and textiles used for clothes, books and book binding, to inorganic materials like natural stone used for architectural surfaces and sculptures or the glass and ceramics used for stained glass windows or glazed tiles. All these materials are readily colonised by fungi and bacteria, whether they are exposed in outdoor environments or are exhibited in public museums and in private art collections.^{2,6,16}

Introduction

The principal materials susceptible of biodeterioration and the microorganisms involved are described in the following sections, and summarized in Figure 2.

Damage caused by microorganisms (Aesthetic and affecting structural integrity)		
Fungi	Bacteria	Cyanobacteria and algae
Main affected materials		
Paper, parchment, wood, textiles, stained glass, metal	Paper, parchment, textiles, stained glass, metal, stones	Textiles, glazed tiles, stones
Characteristics and specific microorganisms causing biodeterioration		
Mycotoxin production Biopitting of stones	Microbiologically influenced corrosion (MIC) on metals	First colonisers of outdoor environments (specially stones) Green and red pigments production Biopitting on stones
Cellulolytic activity (degrades paper) Proteolytic activity (degrades parchment) Production of acids (discoloration, metal corrosion) Pigment production (black, brown, red, orange and yellow)		
Moulds: <i>Aspergillus</i> , <i>Trichoderma</i> , <i>Cladosporium</i> , <i>Chrysosporium</i> , <i>Fusarium</i> , <i>Penicillium</i> , <i>Alternaria</i> Black meristematic fungi: <i>Hortaea</i> , <i>Sarcinomyces</i> , <i>Coniosporium</i> , <i>Capnobotryella</i> , <i>Exophiala</i> , <i>Trimmatostroma</i> Wood decay fungi: <i>Ganoderma</i> , <i>Heterobasidion</i> , <i>Inonotus</i> , <i>Phellinus</i>	<i>Bacillus</i> <i>Actinobacteria</i> <i>Corynebacterium</i> <i>Achromobacter</i> <i>Streptomyces</i> <i>Paenibacillus</i> <i>Kocuria</i>	Cyanobacteria: <i>Gloeocapsa</i> <i>Phormidium</i> <i>Chroococcus</i> <i>Chroococcidiopsis</i> Green algae (Chlorophyta): <i>Chlorella</i> <i>Stichococcus</i> <i>Chlorococcum</i>

Figure 2. Summary of the principal microorganisms causing biodeterioration, their specific harmful activity and the materials affected.

2.1.2.1 Organic materials

Paper: Paper is one of the most susceptible materials to biodeterioration. Its organic cellulose composition represents a favoured nutritional source for many microorganisms, especially fungi and bacteria. The degree of polymerization of cellulose (a linear chain of glucose) determines, along with the presence of pulp like lignin and the percentage ratio between the two types of cellulose (crystalline or amorphous), the biodegradability of the paper. The enzymatic hydrolysis of the glycosidic bonds the cellulose into glucose monomers is carried out by microorganisms with cellulolytic activity, where fungi play a major role, due to their growth mode and ecology, in comparison to cellulolytic bacteria.^{17,18} The fungal mycelium allows the fungi to rapidly colonise and penetrate the substrate

Introduction

material, while the fungal hyphae move the products of the cellulose degradation through the mycelial network (Figure 3E).¹⁹ The deteriorating fungi that damage paper are usually filamentous fungi, also known as moulds, adapted to colonise indoor environments, and can be divided into two main functional groups: i) opportunistic fungi (which are not capable of degrading the material enzymatically) and the real 'material pathogens' (fungi that produce different enzymes to degrade the substrate material), like the aforementioned cellulases, causing serious the decay of the material.¹⁸ These moulds can be easily dispersed in the air through conidia and spores, increasing their colonization ability. *Aspergillus*, *Trichoderma*, *Cladosporium*, *Chrysosporium*, *Fusarium*, *Penicillium* and *Alternaria* are some such moulds commonly found contaminating heritage paper,^{18,20,21} and can damage the paper in different ways, affecting the aesthetics (causing foxing or discoloration or by the production of coloured pigments (melanin) which causes stains) or structural integrity of the object by penetration of the hyphae into the cellulose fibrils, or degrading the cellulose by the production of organic acids and degrading enzymes, such as cellulases or proteases.^{6,17–19,22}

Wood: Wood is a traditional building material exposed to biodeterioration and degradation due to its organic nature, composed by cellulose fibers embedded in a matrix of lignin. This biodeterioration lead to disruption of the wood structure, which depends on abiotic factors, such as moisture and temperature, but also resides on fungal colonisation, whose development can alter the chemical and physical properties of wood.²³ The different fungal communities have been studied and it was observed that environmental fungi represent the first colonizers (Figure 3C). They increase and retain moisture of the substrate, increasing the bioreceptivity for the subsequent colonisation of wood decay fungi, able to digest moist wood. The species coexist with cooperative effect between them at the beginning but, subsequently, wood decay fungus replace the environmental fungi due to better exploitation of the resources through their specific enzymatic battery. The environmental fungi are easily detectable by human eyes and only affect the aesthetic appearance of the material, therefore traditional clean protocols can be used to remove them. Otherwise, wood decay fungi, the principal consequence of the loss of wooden heritage, often emerge visually when structural damage is irreversible. Hence, the appearance of environmental fungi could serve as an indicator of the need to treat the material

Introduction

to prevent further colonisation by the wood decay fungi. The environmental fungi belong to the genera *Alternaria* sp., *Aureobasidium* sp., *Cladosporium* sp., *Mucor* sp., *Rhizopus* sp. and *Epicoecum* sp.,²⁴ while many of the most serious decay-causing fungi are *Ganoderma lucidum*, *Heterobasidion annosum*, *Inonotus tomentosus*, *Inonotus dryadeus*, *Phellinus nigroimitatus* and *Phellinus weirii*.²⁵ Aside from the fungal communities, the wood species is another factor to consider. The differences in the microstructure, cell morphology and amount of extractives (such as fungistatic biocides) present in the wood species can alter the fungi development, making some species more resistant than others.

Parchment: Before its substitution by paper, parchment was the most used writing material utilized, for example, in the making of official and private documents. Parchment is made from the skin of animals such as sheep, goats, labs or pigs, and is rich in collagen, a natural biopolymer. This organic composition, rich of nitrogen present on the collagen, make it easily degradable by microorganisms, like filamentous bacteria and proteolytic fungi, being the collagenases producing microorganisms especially harmful, since they are able to digest the proteins of the parchment through hydrolysis.^{18,22} In the case of proteolytic bacteria, *Actinomycetes* has been discovered to play a major role in the deterioration of parchment based documents, due to the production of many types of enzymes, among them, collagenase.²⁶ Parchment is a very robust and durable material, ant its degradation is a complex process that involves oxidative chemical deterioration of the amino acid chains and the hydrolytic cleavage of the peptide backbone. However, this material is very hygroscopic, making it highly susceptible to bacteria and moulds colonisation (Figure 3B). It is interesting noticing that the degradation of parchment not only varies depending on the origin or the part of the animal used, but also depends on the side of the parchment. The degradation usually starts in the “flesh” side and, as the colonization increases, the “hair” side becomes colonized too.^{22,27–30} Several fungi genera have been isolated and identified from contaminated parchment, among them: *Aspergillus*, *Alternaria*, *Penicillium*, *Cladosporium*, *Fusarium* and *Trichoderma*.²²

Textile: Among with paper, wood and parchment, textile materials represent an important heritage to human history, from the ancient Pre-Columbian and Native clothes, tapestries, and carpets, to more modern Olympic winner swimsuits and spacesuits. Like other artworks, textiles can also suffer from

deterioration and degradation due to their organic composition (i.e., cotton, cellulose, wool, silk, linen and synthetic fibres, among others) (Figure 3G). The environmental conditions (e.g., the UV of solar radiation, humidity, heat and oxygen) can cause alterations such as discoloration, decrease on tensile and tear strength and damage to the textile fibres.^{31,32} Along with the physical and chemical damage, this material can also be biodeteriorated by microorganisms whose proliferation is favoured under hot and humid conditions. Bacteria and fungi can colonize textiles and damage them by the production of enzymes, pigments, and acids, but also using the textile components (carbon, nitrogen, sulphur and phosphorous) as a nutrient and energy source.³³ The composition of the textiles affects their susceptibility to biodeterioration, plant-derived fabrics host a microbial flora very different from animal-derived fabrics, and synthetic fabrics are usually too hydrophobic to allow biodegradation (except for polyurethane, which can bind water).³⁴ The presence of light and humidity can support the growth of phototrophic bacteria (cyanobacteria), that generate green pigments,³⁵ and non-phototrophic bacteria (*Bacillus*, *Corynebacterium*, *Achromobacter*, *Streptomyces*), that generate black, brown, red, orange, and yellow pigments along with fungi of different genera such as *Penicillium*, *Aspergillus*, and *Cryptococcus*. On the other hand, the microorganism can also cause the opposite phenomenon, discoloration, due to the production of enzymes, surfactants and organic solvents, which can even lead to the depolymerization of the fabric and loss of the strength and elasticity.³⁶

2.1.2.2. Inorganic materials

Glass: Recent studies on glass-based historical materials has shown how biocolonisation can affect both the aesthetics and the morphology of the glass surface, which can suffer from iridescence, etching, cracks, and corrosion pits.¹⁶ Glass is a non-crystalline, amorphous inorganic solid, containing about 70-74 % silica by weight, and can be coloured by adding powdered metals to the mixture while the glass is still molten. The inorganic composition and the physical features of the glass do not promote biofilm growth, but glass can be covered by organic residues (such as dust deposits, dead microbial material, and bird droppings) that can be a source of nutrients to the colonising microorganisms.³⁷ Stained glass windows are mainly colonised by fungi and bacteria, while glazed tiles are mostly colonised by macroalgae and cyanobacteria. Fungi of the genera *Aspergillus*, *Cladosporium* and *Penicillium* were found to be the most common

Introduction

ones, along with the bacteria genera *Bacillus*, *Paenibacillus*, and *Kocuria* bacteria. Regarding the phototrophic microorganisms, *Chroococcidiopsis* and *Chlorella* were the most diverse genera of cyanobacteria and green algae, respectively, identified on glazed tiles. These differences in the colonizer microorganisms cause differences in the type of biodeterioration, causing serious damage on the glass, from the chemical and physical properties to the aesthetic one, since glass can lose its transparency (Figure 3H).¹⁶

Metal: Microorganisms can also cause biocorrosion or microbiologically influenced corrosion (MIC) on metals through the utilization and release of electrons, which can lead to electrochemical corrosion.^{37–39} The microbial activity of biofilms on metallic surfaces can transport electrons via organic molecules and may affect the kinetics of cathodic and anodic reactions, modifying the chemistry of protective layers.^{37,38,40} Iron, copper, aluminium and their alloys are some of the metals that can be affected by the microorganisms growth and this interaction can cause different affections on the metals, such as pitting, crevice formation, under-deposit corrosion to stress corrosion cracking.⁴¹ The microorganisms involved in the biocorrosion are usually aerobic and anaerobic bacteria,⁴² and there has been described that the extracellular polymeric substances (EPS) of the biofilm are able to bind metal ions by the interaction between the metal ions and anionic functional groups commonly present on the protein and carbohydrate components of the EPS, such as carboxyl, phosphate, sulfate, glycerate, pyruvate, and succinate groups.^{38,43} On the other hand, the influence of fungi has been also studied, where *Aspergillus niger* was found to be responsible of metal corrosion via the production of oxalic acid, which can cause irregularities and discoloration of the objects.^{41,44} This biodeterioration associated to biocorrosion has been described on surfaces of archaeological objects recovered from terrestrial and aquatic environments (Figure 3F).⁴⁵

Mineral-based building materials: From a biological point of view, mineral-based building materials, such as stones or bricks, represent an extreme environment. They constitute an extreme microniche for microbial growth due to the lack of nutrients, the changes of humidity, the mechanical erosion due to wind and rain and the high doses of UV radiation.^{46–48} These factors, along with the physico-chemical properties of the mineral-based building materials, such as surface roughness, porosity and mineralogical nature, affect the bioreceptivity of the material.⁴⁹ Stone-inhabiting microorganisms, such as bacteria and fungi, may

Introduction

grow as epilithic microorganisms – living on the surface of the stone – and endolithic microorganisms – living inside of pores and fissures. Endolithic colonisation is an adaptive strategy developed by cyanobacteria, algae, fungi, and lichens, where fungi represent the most pertinent endolithic microorganisms on building stone, mortar and other building materials due to their aggressive physical and chemical interaction with the material.^{37,50–54}

There are two main groups of fungi isolated from stone monuments, hyphomycetes and black meristematic fungi, according to the environmental conditions. Hyphomycetes, commonly known as moulds, dominate moderate or humid climates. Some of the representative species of hyphomycetes are: *Alternaria*, *Aspergillus*, *Cladosporium*, *Epicoccum*, *Fusarium*, *Penicillium*, *Aureobasidium* and *Phoma*.^{47,55} Many hyphomycetes, notably *Aspergillus*, *Fusarium*, and *Penicillium* genera, as a result of their metabolic activity, produce toxic metabolites (mycotoxins) and excrete corrosive organic acids (oxalic, citric, acetic, formic, gluconic, glyoxylic, fumaric, malic, succinic, and pyruvic) that can act as chelators and degrade minerals, particularly the oxalic acid. The increased solubility of the material in water and the fungal hyphae penetration into the pores cause important structural damage on the mineral-based building material.^{37,51,54} On the other hand, in arid and semi-arid environments the fungal community shifts towards black yeasts and microcolonial fungi. Black fungi belong to the genera *Hortaea*, *Sarcinomyces*, *Coniosporium*, *Capnobotryella*, *Exophiala* and *Trimmatostroma*, have thick pigmented walls and form small black colonies on and inside the stone. The pigments produced by these microcolonial fungi (such as melanin and carotenoids) not only protect them from UV irradiation, but also provides them with extra-mechanical strength, making hyphae able to grow better in fissures, making them stress-tolerant colonizers involved in biodeterioration.^{47,50} The black endolithic fungi can cause biopitting, the formation of little holes close together in a size range of up to 2 cm in diameter and depth on stone (Figure 3D). The stone frequently associated with this kind of deterioration is marble (53%), followed by carbonate rocks (44%), granite, and concrete (3%). These fungi can be found invading caves and catacombs, being the Lascaux cave a representation of the damage these microorganism can do.⁵⁶ Some examples of mineral-based buildings deteriorated by fungi are the Acropolis of Athens, marble monuments of the Crimea and the antique temples of Delos^{51,57}, but it is important to note that fungi-induced biodeterioration is observed not

Introduction

only on cultural heritage architectures and artefacts, but also on modern buildings, museums, storerooms and a variety of other materials.^{40,58,59}

In extreme environments with high doses of sun irradiation, like the hyper-arid Atacama Desert (Chile), the stones are colonized by endolithic algae and cyanobacteria, which synthesize pigments (carotenoids and scytonemin, respectively) to protect themselves from the UV light.⁶⁰ Stone cultural heritage from the European countries of the Mediterranean Basin also suffer from this autotrophic microorganisms' colonisation and deterioration, mostly by three cyanobacteria genus (*Gloeocapsa*, *Phormidium* and *Chroococcus*) and three chlorophyta (a taxon of green algae) genus (*Chlorella*, *Stichococcus* and *Chlorococcum*). Cyanobacteria and microalgae are usually the first colonisers of stone surfaces, where they develop coloured phototrophic biofilms that not only affects the aesthetics of the stone, but also cause water retention and damage due to the freeze-thaw cycles.^{37,52} Besides, cyanobacteria is also responsible of the biopitting phenomenon, along with fungi, and followed by lichens and algae.⁶¹

Subterranean cultural heritage, as ancient tombs and caves, is also at risk of biodeterioration, especially by *Actinobacteria*, whose predominance in that kind of environments has been described worldwide.^{62–65} These bacteria represent a supercompetitive microorganism due to different mechanisms. On the one hand, *Actinobacteria* produce organic acids, cellulolytic enzymes, and form biofilms, which lead to the biodeterioration of the material,^{55,66,67} but the dominance of these bacteria among others could be explained by interspecies mutualism that help the dispersal of the microorganism,⁶⁸ and the production of antibiotics.⁶⁹ This behaviour has been described in Dahuting Han Dynasty Subterranean Tomb in China, which was closed to visitors in the 1990s to avoid unintended human impacts such as those reported for Lascaux Cave (Dordogne, France)⁵⁶ and Altamira Cave (Cantabria, Spain).⁷⁰ In this tomb, the family *Pseudonocardiaceae* (within the phylum *Actinobacteria*) was found to be the dominant organism due to mutualism interaction with arthropods, the production of a powerful mixture of cellulases and antimicrobial substances that exclude bacterial competitors.

Mural paintings: Mural paintings (a painting on a wall or ceiling) may have a “double nature”, inorganic and organic. Over the course of history, numerous different artistic techniques have been employed, from the water-soluble pigments used in the well-known frescos, to the actual oils, tempera, or acrylic

Introduction

colours. Both the inorganic and the organic component are susceptible of biodeterioration, particularly by fungi of the genera *Penicillium*, *Cladosporium*, *Alternaria*, *Curvularia*, *Drechslera*, *Chaetomium*, *Fusarium*, *Trichoderma*, *Gliomastix*, and *Aureobasidium*. This colonisation can lead into discoloration of pigments, formation of stains and biofilms, salt efflorescence, cracking and disintegration of paint layers, and even degradation of binders, which can cause the detachment of the paint layers (Figure 3A).^{2,18,54,71}

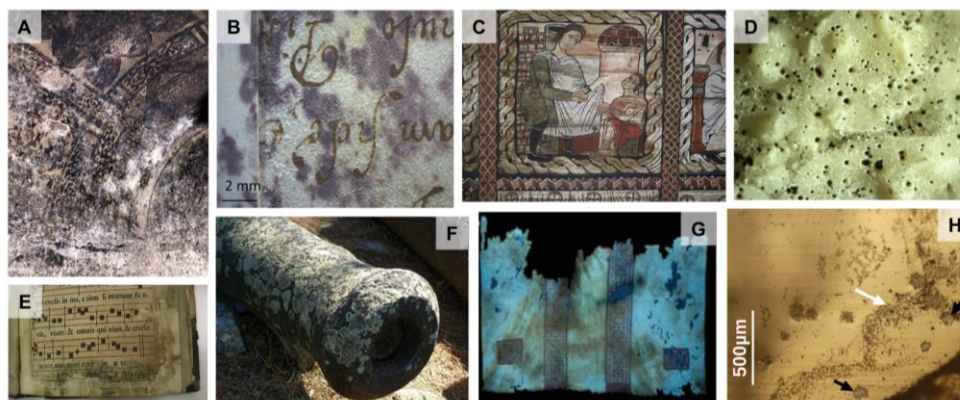


Figure 3. Examples of biodeteriorated materials. A) Picture of the Dahuting Han Dynasty Tomb, colonised by white colonies;⁷² B) Purple stains on parchment caused by halophilic microorganisms;²² C) 12th painted century wood ceiling deteriorated by *Aspergillus* sp.;⁵⁰ D) Marble facade of the Celsus library in Ephesos (Turkey) with biopitting caused by microcolonial fungi;⁵⁰ E) Historical book colonised by *Trichoderma* sp.;⁵⁰ F) Ancient cannon of Ioannina (Greece) covered by lichen;³⁷ G) Visible damages in the back side of the Coptic tunic of the Egyptian Museum of Turin (Italy);³² H) Optical microscopy results of a glass surface, the black arrows indicate crystal formation on the surface and the white arrows. show the mycelia growth⁷³

2.1.3. Consequences and solutions to biodeterioration

All these colonising microorganisms are a threat to heritage materials, and this deterioration of artistic and architectural heritage results in a loss in several ways. From the immense financial damage for museums, local authorities, and private collectors, to the immeasurable cultural and societal losses. Along with the economic issue, the extreme proliferation of microorganisms, especially in closed spaces such as museums, poses health risks for employees and visitors.⁷⁴ Certain fungi that are often found colonizing museum spaces, archives and libraries may be dangerous to professionals and visitors alike.^{75–79} Although moulds rarely cause serious diseases in healthy individuals, the repeatedly exposure to the moulds and the inhalation of their spores can cause immune system issues and allergic diseases, develop of asthma, rhinitis, superficial and systemic infections (mycoses) and mycotoxicosis.^{6,20,80} *Aspergillus*, *Penicillium* and *Stachybotrys* genera

Introduction

produce mycotoxins, compounds with mutagenic, teratogenic, carcinogenic, dermatotoxic, hepatotoxic, neurotoxic properties, that can be inhaled in form of aerosols along with fungal spores.^{76,77}

Effective climate control, frequent cleaning, and phenomenological monitoring can help to reduce the biogenic damage to historical objects, but other factors such as inadequate storage conditions, dampness and antimicrobial-resistance require the development of new and more active biocides.⁵ A limited range of methods to control biodeterioration is available and, frequently, these methods are inadequate and don't display long-term activity.⁸¹ The main traditional methods used to date and new biocides based on nanoparticles are described in the following sections.

2.2. Traditional methods to prevent and combat biodeterioration

Biodeterioration has been a recurring problem for the conservation of cultural heritage materials for a long time. To minimize the consequences of biodeterioration, different methods have been used, from preventive (or indirect) methods such as environmental monitoring and control, to a wide variety of corrective (or direct) methods (chemical, physical or biological). The principal characteristics of the corrective methods are summarised in Table 2.

Table 2. Traditional corrective methods applied to prevent biodeterioration

Method	Advantages	Disadvantages
Chemical (Biocides)		Cyto and eco-toxicity.
		Limited long-term effect.
	Wide variety of compounds available.	Poor antimicrobial selectivity.
	Cheap and easy to apply.	Development of antimicrobial resistance.
	Effective against a broad range of microorganisms.	Possible modification of biofilm structures favouring the growth of more harmful biodeteriogens.
	Application in remote areas.	Repeated use may damage the heritage material.
Physical (Mechanical removal, UV-C irradiation, Gamma radiation, Laser cleaning)	Do not require the use of toxic compounds.	Repeated use may damage the heritage material.

		Require specialized staff.
		Costly.
		Not selective against specific biodeteriogens.
Biological (Natural biocides: essential oils)	Safer for human beings and the environment.	The extract composition has a lot of variability.
	Easy to apply.	Few products available on the market.
	Effective against a broad range of microorganisms.	Poor antimicrobial selectivity.
	Application in remote areas.	The interference with the heritage material has not been reported yet.

From here we will focus on the characteristics and limitations of the traditional biocides used in heritage conservation (Figure 4). These kinds of chemicals usually come from the agricultural and health sector and have not been specifically designed for the cultural heritage field, making them present some limitations when applied on heritage materials. In general, the biocides used have limited long-term effect and are quite toxic for both the professionals working with them and the environment. They can also affect the treated materials, causing discoloration or change in the chemical and physical characteristics.⁸² More information about specific traditional biocides can be found in “Article 1”.

Biocides have been used for any kind of cultural heritage material both indoors and outdoors, and can be organic and inorganic, being the inorganic the ones that provide a longer-lasting action, especially in outdoor environments, where the organic compounds deteriorate more rapidly. Exposure to outdoor environments, coupled with low efficacy in elimination of microorganisms, make reapplications of the products necessary to prevent recolonisation. It is also important to remark that the use of ineffective products can induce to adaptation of the microorganisms, leading to development of antimicrobial resistance.⁸³

To be applied on heritage materials, the biocidal compounds should meet some requirements. Taking into consideration the heritage material itself, the biocide applied must be chemically inert, stable, and colourless, to avoid interference

Introduction

with the material, possible interactions with other compounds used in the intervention such as consolidants, which may subsequently change the appearance of the object. In addition, there are other important aspects to consider, such as the reversibility of the application, the resistance of the coating to external agents and the compatibility with the substrate, for example, maintaining adequate permeability of a stone not obstructing the porosity. Moreover, the product should ideally be ecologically acceptable (eco-safe) and by extension possess low cytotoxicity to end users.⁸⁴

The effectiveness of the treatment applied to prevent biodeterioration will depend on the one hand on the characteristics of the product itself and, on the other hand, on the material treated. Regarding the product, the stability, the method of application, the concentration and the solvent used, the pH of the solution are some issues to consider. The type of substrate and its condition, the possible interaction with the product applied, along with the climate (temperature, light, humidity) are also important factors to study to maximize the efficacy of the treatment.⁸⁵

Some commercially available products commonly used to prevent microbial colonization in heritage material are based on isothiazolones (Biotin R, Biotin T) and quaternary ammonium compounds (Preventol RI80), that have been used against lichens, fungi, bacteria, algae and cyanobacteria.^{86–89} Quaternary ammonium salts and formaldehyde are other chemical agents that have been used over the last century to disinfect objects, however these compounds also pose a risk to human health due to their high cytotoxicity.⁹⁰ Ethylene oxide was used for fumigation, against insects and fungi, but it has been banned in several countries due to carcinogenic and mutagenic features.⁹¹ Hydrogen peroxide has displayed comparable activity when vaporized in cardboard at the Auschwitz–Birkenau State Museum in Oświęcim, Poland.⁹² Ethanol, a universally acknowledged disinfectant, antiseptic, and preservative, has been used as an antifungal treatment for paper, being able to inhibit complete the germination of the spores at a concentration of 70%. Although under appropriate conditions can form complexes with the cellulose and remain stable for long periods, these complexes are not stable in humid conditions, where the moist in the air can displace the ethanol.^{93,94}

Introduction

It is also worth mentioning essential oils, natural biocides that present relevant antibacterial activity, and are being used in other areas, e.g., active food packaging, air-purification, etc. Essential oils are composed of a variety of volatile compounds that come from plant extracts, and, in principle, are safe to humans and the environment. However, few products based on essential oils are available on the market, and more studies applied to the heritage field are needed; particularly since material-essential oil interactions have not been studied in detail.^{95,96}

Despite the wide range of available products, the lack of long-term effects, the need of reapplication (which can lead into antimicrobial resistance), along with the toxic effects associated with these biocides, make it necessary to continue the search for new compounds and materials with improved antimicrobial properties with more selectivity towards specific microorganisms and less adverse effects, for both the heritage substrate material, the professionals and the environment.^{97,98}

In the last decade, nanomaterials have gained importance in the field of cultural heritage conservation, being used to protect stone monuments, textiles, murals, glass, and paper. Although silver and titanium nanoparticles are the most studied, a variety of multifunctional nanomaterials, such as magnesium oxide nanoparticles and polyoxometalate ionic-liquids, that have been shown to serve as alternative solutions to heritage biodeterioration issues.^{99–101}

2.3. New biocidal compounds based on nanoparticles

Nanoparticles (NPs), defined by the IUPAC as "a particle of any shape with dimensions in the 1 and 100 nm (1×10^{-9} and 1×10^{-7} m) range", although generally considered an invention of modern science, have a very long history. They were used by glassmaker and potter artisans since long time ago, albeit without knowledge of their nature, for generating a glittering effect. The best-known examples are the Roman Lycurgus cup, of dichroic glass, from the fourth century, and the lusterware pottery made in Mesopotamia in the ninth century, characterized by silver and copper nanoparticles dispersed in the glassy glaze.^{102,103}

Silver and copper, along with zinc oxide, are also known for their antimicrobial properties since time immemorial. Egyptians used copper or silver containers to make drinkable water, and, in the Wild West, silver coins were used to preserve

the freshness of milk and to prevent algae and bacteria from contaminating the water. It is also known that the ZnO was used as far back as 2000 BC as a treatment for boils and injuries.⁹⁷

Reducing the size of these materials to the nanoscale brings with it a change in the physicochemical properties of the material. The surface-to-volume ratio increases, affecting the surface and interphase properties, and these reduction in size also facilitated the interaction with cellular components such as proteins or DNA, which can therefore lead to improved antimicrobial properties.^{104,105}

Nanomaterials (materials in which at least one dimension is in the 1 and 100 nm range) have been thoroughly investigated as antimicrobials in different areas, such as water disinfection, food packaging and healthcare and, during the last decade, they have gained attention as antimicrobial coatings and treatments (deacidification, consolidations and cleaning) for heritage conservation.¹⁰⁶

2.3.1. Desired characteristics of the NPs

However, for being considered as a potential candidate for application in the heritage field, a nanomaterial should possess some characteristics (Figure 4). In first instance, it should present high and long-lasting antimicrobial activity, to avoid microbial contamination over time, but, on the other hand, should be safe, displaying low cytotoxicity and ecotoxicity.¹⁰⁷ Besides, the treatment with NPs should not affect the aesthetic appearance of the heritage object (colour, brightness or texture) and any intervention should be removable, according to the guidelines of conservation.¹⁰⁸ Also, to be commercially viable, the synthesis processes must be as simple and reproducible as possible, and the price of raw materials should be low. In fact, the most studied NPs in the heritage conservation field are those ones easily commercially available (TiO₂, Ag and ZnO NPs),^{109,110} and wet-chemistry methods (sol-gel, soft-chemistry and autoclave processes) have been the most utilized synthesis methods to produce the NPs, because of the simplicity and low cost of these synthesis.^{111,112} The most common synthesis methods used in the heritage field are described with more detail in “Article 1”.

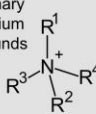

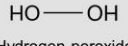
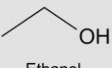

Limitations of traditional biocides	Desired characteristics of the NPs
<p>Quaternary ammonium compounds</p>  <p>Ethylene oxide</p>  <p>Hydrogen peroxide</p>  <p>Ethanol</p> 	<p>Nanoparticle</p>  <p>1 – 100 nm</p>
<p>Not specifically designed for the cultural heritage field</p> <p>Limited long-term effect</p> <p>Eco- and cytotoxic</p> <p>Can affect the treated material</p> <p>Reapplications needed</p> <p>Can induce antimicrobial resistance</p>	<p>High and long-lasting antimicrobial activity</p> <p>Low eco- and cytotoxicity</p> <p>Removable</p> <p>Do not affect the aesthetic appearance</p> <p>The synthesis should be:</p> <p>Simple</p> <p>Reproducible</p> <p>Low cost</p>

Figure 4. Summary of the limitations of the traditional biocides and the characteristics the nanoparticles should possess to become a competitive candidate in the heritage field.

Only by fulfilling these characteristics we will be able to develop a competitive market-ready nanomaterial to prevent the biodeterioration and protect our shared cultural heritage. This presents a challenge for the development of novel biocides based on nanomaterials, furthermore since the long-term effects are still under study due to the short time they have been used. In order to enlarge the characteristics and limitations the nanomaterials present, the most common NPs used to prevent biodeterioration are described in the next section.

2.3.2. Most used NPs in heritage

As mentioned above, titanium dioxide (TiO₂), silver (Ag), and zinc oxide (ZnO) nanoparticles are, in this order, the most recurrently applied nanomaterials to prevent or treat microbial colonization of heritage substrate materials. Other frequently reported nanomaterials are based on silicon dioxide (SiO₂), copper (Cu), magnesium oxide (MgO) and zinc-derivates. Other nanomaterials that have gained interest recently in heritage conservation are the polyoxometalate-ionic liquids (POM-ILs). These compounds (inorganic metal-oxo anionic clusters combined with a bulky organic cation) can be highly tailorable, obtaining different antimicrobial properties.

These nanomaterials have been applied over a range of cultural heritage items and architectures, which include organic substrates (parchment, wool, silk, paper, wood, and cotton) and those obtained from inorganic resources (stone,

Introduction

glass, and plaster). The principal characteristics and limitations of these NPs are described in Table 3. For a broader description the characteristics of each nanoparticle consult the “Article 1”. The nanomaterials studied during the thesis (MgO and POM-ILs) are described in more detail below.

Table 3. Principal characteristics and limitations of the NPs

Type of NP	Characteristics	Limitations
TiO ₂ NPs	The most utilized NPs	Bacteriostatic effect (not strong enough to perform biocidal action)
	Inexpensive	
	Chemically stable	Little or no antimicrobial activity in the absence of light
	Photoactivity (release of ROS upon exposure to UV light)	
Ag NPs	Broad-spectrum antimicrobial	Strong colour variation
	ROS production	
	Interfere with nutrient transport	The aggregation increases the colour change
	Disrupts metabolic processes	
	Release Ag ⁺ ions (which impede DNA replications and inhibit enzymes)	More active against vegetative cells than for spores
ZnO NPs	Photoactivity (release of ROS upon exposure to UV light)	Hormetic behaviour (low doses accelerate sporulation, induce earlier production of secondary metabolites and change the appearance of the biofilm)
	Active under dark conditions due to the release of Zn ²⁺ and internalization of ZnO NPs	
	Activity increased under UV light	
	Self-cleaning properties	
	UV-light protection	
SiO ₂ NPs	Hybridized with other NPs (TiO ₂ , ZnO or Ag NPs) display consolidating and hydrophobic properties.	Need to be used in combination with other NPs to have relevant antimicrobial activity.
Cu and CuO NPs	Formation of ROS	Rapid oxidation
	Highly effective when applied together with consolidants	Possible nanotoxicity
	Underexploited in heritage conservation	Strong colour variation

2.3.3. Magnesium oxide nanoparticles (MgO NPs)

Magnesium oxide nanoparticles (MgO NPs) have received significant attention as antibacterial agents in recent years due to their high stability and low cost based on their preparation from economical precursors.^{113,114} Although the exact mechanism of action is still unknown, the antimicrobial activity has been attributed to the formation of reactive oxygen species (ROS), which induce oxidative stress and lipid peroxidation in bacteria,¹¹⁵ as well as non-ROS mediated bacterial toxicity mechanisms, like interaction with the cell wall or the cell membrane of the microorganisms, or an alkaline effect due to the increase of the pH.^{113,115–117} This antimicrobial activity is species- and genus-dependent, and the size of the nanoparticles plays a major role, since the smaller the particle, the larger the surface area and the easier interaction with the microorganisms cell wall and membrane.

Although MgO NPs are generally regarded as safe and present low cytotoxicity,¹¹⁸ they have been shown to display toxicity on early and larval stages of zebrafish.¹¹⁹ Despite their possible toxic effects, that are highly dependent on the physicochemical properties of each individual nanoparticle as well as on the types of cells tested,¹²⁰ they have been used in diverse areas. The MgO NPs have been used, for example, as an additive in heavy fuel-oil,¹²¹ for the cleaning of fuel-oil pipelines, and also as a mineral supplement source for magnesium¹²² or for the relief of cardiovascular disease and stomach problems and as anti-cancer therapy.¹²³ Regarding the heritage field, they have been used in restoration processes, such as in the deacidification of paper or canvases.^{124,125} They can be mixed with other nanomaterials that will act as supports (such as hydroxyethyl cellulose (HEC) or hydroxypropyl cellulose (Klucel E)), or they can be doped to improve the catalytic and antifungal properties (e.g. Zn doped MgO NPs), to prepare protective and antimicrobial coatings for heritage paper and stones.^{106,126}

2.3.4. Polyoxometalate-ionic liquids (POM-ILs)

Polyoxometalate-ionic liquids (POM-ILs) have recently gained attention as antimicrobials in heritage conservation due to the tailorable antimicrobial properties offered by the structural and compositional versatility of these materials. They are constituted by a polyoxometalate (POM), a nanoscale molecular metal-oxide anion, and bulky organic cations, typically alkylammonium or phosphonium cations, which provide the ionic liquid

Introduction

characteristics. Importantly, both the POM anion and the organic cation can be independently tuned, offering access to a multifunctional materials library.⁹⁷

Polyoxometalates (POMs) are defined as inorganic metal-oxo anionic clusters of the generic formula $[M_xO_y]^{n-}$ with multiple (≥ 2) high-valent transition metals in their highest oxidation state. The first polyoxometalate was reported in 1826, a phosphomolybdate $[PMo_{12}O_{40}]^{3-}$ with Keggin structure ($[XM_{12}O_{40}]^{n-}$), obtained by treating ammonium molybdate $(NH_4)_2MoO_4$ with an excess of phosphoric acid.¹²⁷ This POM self-assembles in acidic aqueous solution (e.g. between pH 5-6 for silicotungstates) and forms a very stable structure.¹²⁸ POMs exhibit an enormous assortment of physicochemical properties, like ionic conductivity,¹²⁹ electrochromism and photochromism,¹³⁰ magnetism,¹³¹ superacidity,¹³² and luminescence.¹³³ Besides, their redox properties and high oxidation activity make them useful to a wide variety of applications, from industrial applications such as catalysis,^{134,135} removal of multiple pollutants from drinking water,¹³⁶ energy-storage systems,¹³⁷ acid-corrosion protection of metal discs¹³⁸ or natural limestones,⁹⁹ to molecular medicine,¹³⁹ and drug-delivery.¹⁴⁰ In this thesis it has been used the *lacunary* POM $[\alpha-SiW_{11}O_{39}]^{8-}$, a Keggin POM cluster with a vacant site, combined with tetraalkylammonium or alkylguanidinium cations to obtain different polyoxometalate-ionic liquids (Figure 5A).¹²⁷

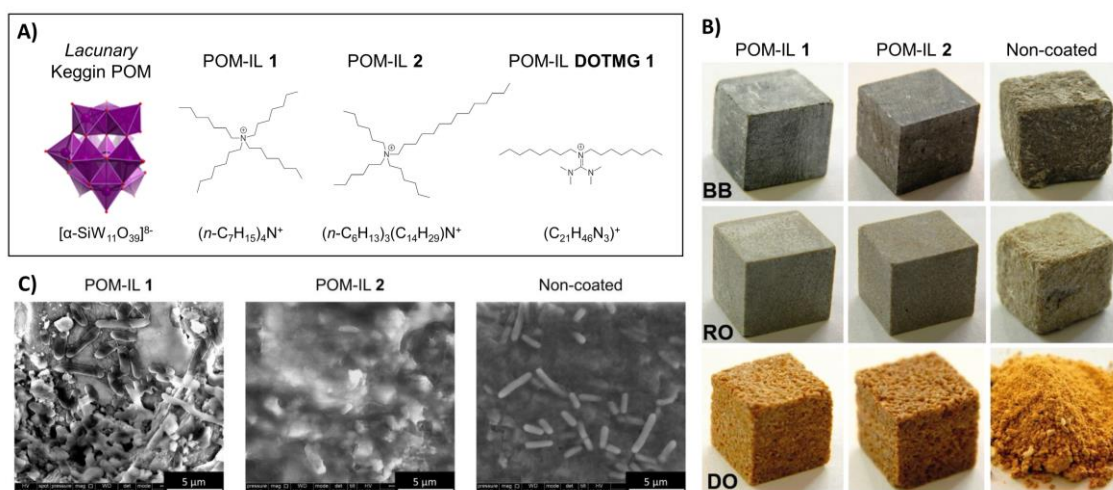


Figure 5. A) Illustration of the *lacunary* Keggin POM $[\alpha-SiW_{11}O_{39}]^{8-}$ and the cations used as components for POM-ILs 1, POM-IL 2 and POM-IL DOTMG-1. B) Acid-vapour corrosion protection of POM-IL-coated stone samples, studied by exposing the samples to acetic acid vapour for 72 h. RO: Romery stone; BB: Belgian Bluestone; DO: Dom stone. Both POM-ILs display high protection against acid corrosion, especially for the most porous stone DO.⁹⁹ C) Environmental Scanning Electron Microscopy (ESEM) images of *E. coli* incubated over a BB stone coated with POM-IL 1 and 2, (and over a non-coated sample as a reference sample). While bacteria incubated over the non-treated BB stone present a normal and healthy morphology, the coatings

Introduction

have affected *E. coli* growth. Bacteria over POM-IL 1 coated stone has released its intracellular content, and bacteria incubated over the sample coated with POM-IL 2 seem to be generating exopolysaccharides and creating an extracellular matrix.⁹⁹

Ionic liquids (ILs) are salts with a melting point below 100 °C and are in liquid or wax state at room temperature.¹⁴¹ The interest in ILs has increased in the recent years due to their application in catalysis¹⁴² and biocatalysis,¹⁴³ electrochemical devices,¹⁴⁴ or engineering fluids.^{127,145} Recently, ionic-liquids have attracted widespread interest also as antimicrobial agents (e.g. overcoming challenges related to acquired antibiotic resistance)¹⁴⁶ and POM-ILs, specifically, have gained relevance in cultural heritage conservation as bioactive surface coatings. The anticorrosive properties and hydrophobicity, along with the high antimicrobial activity displayed by the POM-ILs make them highly suitable candidates for cultural heritage conservation (Figure 5B and 5C). Furthermore, modulating the chemical composition of the anion and the cation there can be obtained broad-spectrum antimicrobials, with enough antimicrobial activity to be applied as an invisible coating which will not alter the aesthetics of the material. The antimicrobial activity of the POMs is generally suggested to arise from interactions with amino acids of proteins and production of reactive oxygen species (ROS), affecting the viability of the microbial cell.¹⁴⁷ Once combined with the cation to form the POM-IL, the antimicrobial activity of the compound increases due to the interaction of the aliphatic chain with the lipid membranes of the cells. The Keggin-type POM $[\alpha\text{-SiW}_{11}\text{O}_{39}]^{8-}$, combined with tetraalkylammonium cations, has displayed antimicrobial activity against important human pathogens such as *E. coli*, *P. aeruginosa*, and especially against the Gram positive *S. aureus*.¹⁴⁸ Moreover, these POM-ILs have been tested as coatings on mineral stone surfaces, providing not only antimicrobial and antibiofilm effect on natural limestone samples (Figure 5C),^{14,99} but also acting as a disinfectant agent to eliminate mould colonisation over brick surfaces.¹⁴⁹

While such materials may be quite promising, their application and associated nanotoxicological profile is a major concern. One of the great challenges of nanotechnology is the environmental safety implications of the nanomaterials, which widespread use lead into inevitably release to the terrestrial, aquatic and atmospheric environments, where their toxicity, behaviour and ultimate fate are largely unknown.¹⁵⁰

2.4. Coatings: application methods and characterization

Choosing the most appropriate mode of application is a crucial step to guarantee the success of the protective coating. For nanomaterials, the first thing to consider is the solvent where the NPs will be diluted, which is usually a polar protic solvent like water or ethanol that quickly evaporates.^{106,151,152} To improve the longevity of the antimicrobial coating, the NPs can be combine with commercial varnished and consolidants. Once the NPs solution is prepared, it can be applied by different methods (brushing,¹²⁶ spraying,¹⁵³ immersion,¹⁵⁴ drop-casting,^{155,156} spreading with a spatula,¹⁵⁷ misting,¹⁵⁸ capillary absorption¹⁵⁹ or spin-coating¹⁶⁰) that should ensure a homogeneous coating.⁹⁷

Prior to the coating characterization, the nanomaterial should be characterized itself: the nanoparticles size and shape, the crystallinity and purity, and elemental composition and distribution. To study that there are several analytical techniques. The size and morphology of the NPs are most often studied by electron microscopy (scanning electron microscopy (SEM) and transmission electron microscopy (TEM)),^{126,161} while the NP size distribution in solution can be analysed by dynamic light scattering.^{157,162} The reliability of this technique, however, is limited to particles with spherical shape. The crystallinity of the NPs, defects, and doping can be studied by TEM and X-ray diffraction (XRD).^{126,163}

The NPs coating over the heritage sample can be characterized also by SEM, and by energy-dispersive X-ray spectroscopy (EDX) and electron energy loss spectroscopy (EELS) (techniques present in most electron microscopes) which will provide insights about the elemental composition of the coating and the substrate.^{161,164} To quantify with more detail the amount of NPs there are several techniques that can be used: X-ray photoelectron spectroscopy (XPS), elemental analysis, or inductively coupled plasma (ICP) spectroscopy or spectrometry.

The homogeneity of the coating and the presence of microorganisms can also be studied by SEM. Moreover, environmental scanning electron microscopy (ESEM), a technique that operates under a controlled gaseous atmosphere instead of vacuum and allows the imaging of wet samples, allow the visualization of samples with high sensitivity to vacuum or that cannot be coated with a conductive layer. Thus, we are able to visualize the microorganisms under conditions similar to their natural state.^{101,106}

Introduction

Optical microscopy can be combined with cell staining to study the efficiency of the coatings. For example, Live/Dead viability assays are designed to dye alive and dead cells in green and red, respectively, which allow the study of the antimicrobial properties on the surface using a epifluorescence microscope.⁹⁷

The colour variation is a very useful method in the heritage field since it allows to determine if a coating is changing the aesthetic appearance of the material, and do not require expensive equipment or high specialized staff. The colour of the surface that is going to be treated is characterized before and after the nanomaterial application by spectrophotometric techniques, and the chromatic change (ΔE^*) is calculated in the CIE 1976 L^* a^* b^* color space. In general, chromatic change below three ($\Delta E^* \leq 3$) is the desirable value, but usually values below five ($\Delta E^* \leq 5$) are accepted, since it is limit value when the colour change becomes visible to the naked eye.^{165,166} This technique can be also used to study the microbial colonization over a surface, due to the colour change made by the microorganisms growth.¹⁴ The percentage of the surface on a heritage item colonized by microorganisms can be also determined by digital image analysis, a simple and low-cost tool with which the colour variation originated as a consequence of microbial growth can be studied.^{162,167}

It is also important to take into consideration the use of large scientific facilities, like Neutron¹⁶⁸ and Synchrotron X-Ray Tomography^{169,170}, which can provide high resolution images of the coating and substrates, yielding valuable information about the porosity and morphology of samples.¹⁷¹ More focused on the heritage field, the European Union recently created E-RISH, the European Research Infrastructure for Heritage Science. The E-RISH supports research on heritage characterization and preservation by delivering integrated access to expertise, large-scale and medium-scale instrumentation, portable technologies, and data science. This organisation offers a competitive advantage since it exploits the synergy of the cooperation among the academy, research centres, museums, and cultural institutions, making it highly attractive especially to small research groups.¹⁷²

Article 1: Perspectives for antimicrobial nanomaterials in cultural heritage conservation

Chem

CellPress

Review

Perspectives for antimicrobial nanomaterials in cultural heritage conservation

Isabel Franco-Castillo,^{1,2} Lara Hierro,^{1,2} Jesús M. de la Fuente,^{1,2} Andrés Seral-Ascaso,^{1,2,*} and Scott G. Mitchell^{1,2,*}

SUMMARY

The biodeterioration of artistic and architectural heritage represents a serious and recurring problem for museums, local authorities, and private collectors alike, where irreparable damage to unique artifacts can result in immeasurable losses to our shared cultural heritage. Here, we present an overview of the current trends in antimicrobial products used to protect heritage items from microbial colonization and prevent their deterioration. From a conservation-restoration standpoint, we contrast and compare traditional antimicrobial products with the state of the art in antimicrobial nanomaterials applied in the heritage conservation field, highlighting the promising potential of various different nanomaterials, as well as points of concern and clear red flags from some of the emerging research. Through an examination of the growing body of research in the academic literature we offer recommendations and practical advice on selecting appropriate microbiological assays and characterization techniques to better evaluate the *in vitro* and *in situ* antimicrobial properties of nanomaterials.

INTRODUCTION

Artistic and architectural heritage in the form of books, paintings, clothing, historic monuments, and buildings, among many other artifacts, represents significant tangible aspects of a community, region, or country's cultural heritage, from which current and future generations will embrace, study, and share. The preservation of our shared cultural heritage constitutes a global societal and economic priority;¹ yet, the problems caused by lack of proper preservation of tangible heritage often only come to attention when tragedies occur, such as a fire, collapse, or water damage. However, there are many silent threats lurking permanently in our heritage items and buildings, far from the eyes of the great majority of people. Environmental aspects (humidity, temperature, light, CO₂ concentration, atmospheric pressure, and pH) and geological conditions are two important factors affecting heritage objects; however, chemical composition (organic versus inorganic), the quality of the materials and aging process, internal mechanical stress, and biological colonization (originating specifically bacteria, fungi, algae, moss, lichen, and insects) constitute the other principle actors leading to the decay and deterioration of artifacts.²

In particular, biodeterioration—"any undesirable change in the properties of a material caused by the vital activities of organisms"³—poses a persistent problem in the conservation of cultural heritage. Contamination and spoilage of artifacts displayed in exhibition rooms or stored in depots is not exceptional; but rather frequent, in both old and newly built museums. Microorganisms such as bacteria, fungi,

The bigger picture

Microorganisms are highly proficient at inhabiting and decaying cultural heritage objects and architectures. Unfortunately, only a limited range of physical and chemical methods are available for preventing or removing microbiological damage to heritage items where, all too often, the available methods are frequently inadequate to clean effectively and prevent recolonization. Our shared cultural heritage is an invaluable social and environmental resource as well as a key global economic driver. So how can we protect our shared tangible cultural heritage from biodeterioration and preserve it for future generations? The use of antimicrobial nanomaterials in the heritage science field represents challenging new research opportunities for chemists and materials scientists, where an integrated multidisciplinary approach is required to tackle the heterogeneous composition, uniqueness, and value of each individual heritage piece.





CellPress

Chem
Review

cyanobacteria, and algae are highly proficient at inhabiting and decaying artistic and architectural heritage objects. Paper, leather, stone, textile, ceramic, and glass are all blighted by this problem, which incurs substantial difficulties for the conservation of cultural heritage.²

All types of historic artifacts in public museums and in private art collections are at risk of attack from fungi and bacteria: from textiles and leathers used for clothes and weaponry to paper and books; not to mention architectural surfaces and stone monuments in outdoor environments along with mural paintings in churches, caves, and catacombs.⁴ In mural paintings, for example, microbial colonization can be the root cause of a host of serious problems: discoloration of pigments and mortars, formation of stains and biofilms, salt efflorescence, exfoliation, cracking and disintegration of paint layers, formation of paint blisters, and degradation of binders that results in detachment of the paint layer(s). Fungi of the genera *Penicillium*, *Cladosporium*, *Alternaria*, *Curvularia*, *Drechslera*, *Chaetomium*, *Fusarium*, *Trichoderma*, *Gliomastix*, and *Aureobasidium* are abundant in degraded mural paintings.^{2,5} In fact, fungi are particularly threatening to heritage materials because their hyphae undergo rapid proliferation and penetrate deep into all types of organic and inorganic materials. Meanwhile their spores, in a dormant state, are ever present and available for germination when the local growth conditions become more favorable.⁵ Furthermore, carboxylic acids produced through fungal metabolism (e.g., oxalic, citric, succinic, formic, malic, acetic, fumaric, glyoxylic, gluconic, and tartaric acids) can produce a highly aggressive second wave of corrosive chemical attack.

Consequently, the deterioration of artistic and architectural heritage results in immense financial damage for museums, local authorities, and private collectors alike. More important still are the immeasurable cultural and societal losses caused by irreparable damage to unique artifacts, which represent our shared cultural heritage and identity, as well as an important social and economic resource for communities, regions, and countries. Although effective climate control, frequent cleaning, and phenomenological monitoring all help to reduce biogenic damage to historical objects; there are other factors, such as acquired resistance to antibacterial agents and environmental damage (inadequate storage conditions, dampness, floods, transportation/relocation, etc.) that require a wider range of more suitable biocides.⁶ Moreover, extreme proliferation of bacterial and fungal biofilms in closed spaces also present inherent (often severe) health risks for employees and visitors to museums and indoor public environments.⁷ Unfortunately, the chemical community has not risen to this grand challenge and only a limited range of methods is available to disinfect recent and progressive microbiological deterioration to heritage objects. In addition, the available methodologies are frequently inadequate for cleaning and preventing long-term biofilm growth; plus, certain coatings, paints, and varnishes are themselves subject to microbial attack.⁸

Recently, there has been a drive for greater use of nanomaterials in the conservation of cultural heritage. Recent examples include their use for protecting stone monuments, textiles, murals, glass, and paper. Of course, products based on nano-silver and nano-titanium are studied frequently, but a variety of other readily available multifunctional nanomaterials have been shown to serve as alternative solutions to heritage biodeterioration issues.^{9–11}

In this review, we provide a critical summary of the state of the art in traditional and nanomaterials-based antimicrobial treatments for heritage items from a multidisciplinary perspective in order to include key considerations from the heritage

¹Instituto de Nanociencia y Materiales de Aragón (INMA), Consejo Superior de Investigaciones Científicas (CSIC)-Universidad de Zaragoza, Zaragoza 50009, Spain

²CIBER-BBN, Instituto de Salud Carlos III, Madrid 28029, Spain

*Correspondence: aseral@unizar.es (A.S.-A.), scott.mitchell@csic.es (S.G.M.)

<https://doi.org/10.1016/j.chempr.2021.01.006>

conservation-restoration, materials science, and microbiological standpoints. We aim to provide an overview and comprehensive analysis of the principal and most effective nanomaterial types and the most appropriate analytical biochemical techniques that can be used to accurately evaluate their antimicrobial properties, both *in vitro* in laboratory cell cultures under model conditions and *in situ* applied to samples in realistic settings. From a functional materials perspective, the first and most important step is to properly characterize the physicochemical properties of the nanomaterials (i.e., size, morphology, stability, and so on); however, the second stage requires a precise evaluation of the antimicrobial properties of the nanomaterials against relevant microorganisms to screen potential candidates, develop structure-property relationships, and thus select the most active agent to be used as a protective method in cultural heritage objects. Crucially, it is in the interests of the field to attempt to standardize analytical methods and demand fundamental materials characterization and more comprehensive antimicrobial assessment in order to have confidence in the data and to obtain comparable results. Choosing the wrong biochemical method or performing non-standard antimicrobial assays could lead to irreproducible and non-comparable results, or even to false-negative or -positive results. Consequently, at the heart of this review we outline standardized characterization techniques and biochemical assays/protocols used to evaluate antimicrobial compounds or materials more rigorously to help interested readers to select the most appropriate antimicrobial and antibiofilm methods, depending on the physicochemical properties and desired end use of each nanomaterial on different heritage substrates.

In most of the literature examples, articles cited in this review, model substrate materials—most of which possess no true cultural or economic value—are used to evaluate the efficacy of antimicrobial treatments. In many cases these might include, for example, stone from the same quarries as those used in the construction of heritage buildings,^{9,10,12} ceramic tiles or glass prepared using historically accurate production methods, filter paper, glass slides or freshly made bricks,¹³ or plaster, among others. These initial proof-of-concept model laboratory studies represent one of the first and most vital stages in evaluation, since any unforeseen and undesired effects that the antimicrobial treatments might cause to the heterogeneous character of an original heritage item preclude their direct use in mitigating biodeterioration. However, numerous antimicrobial nanomaterial treatments have also been evaluated on unique antique artifacts and architectures in their local environmental conditions at various cultural heritage sites around the world, which highlights the scope of the heritage biodeterioration problem as well as the global research effort being used to understand and address it (Figure 1). These reports include colorimetric measurements,¹⁴ *in situ* long-term monitoring of microbial recolonization,^{15,16} and studies of the biocidal efficiency of the treatments.^{17,18} A complete description of the type of test performed on the cultural heritage items, their location, dating, and the image references is provided in Table S1.

CURRENT TRENDS IN CHEMICAL PRODUCTS USED TO PREVENT BIODETERIORATION

Biodeterioration represents a serious ongoing problem for the conservation of cultural heritage materials, and consequently, a number of different preventive or indirect methods (such as environmental monitoring and control) and corrective or direct methods (mechanical, biological, physical, or chemical) are currently used to reduce this threat. In this section, we focus on commonly used or commercial chemical biocides whose function is to inhibit or eliminate the growth of different



CellPress

Chem
Review

Figure 1. World distribution and heritage items used in antimicrobial studies of nanomaterials

(A and B) (A) Walls on Palacio da Pena¹⁴ and (B) glaze tiles at Marquis of Pombal Palace,¹⁷ both in Portugal.

(C) Paper sheet from the archive of the Royal Botanic Garden (Spain).¹⁰

(D–F) (D) Plaster wall from the Fiesole archaeological area,¹⁵ (E) Church of San Leonardo di Siponto,¹⁹ and (F) Villa dei papyri, all three from Italy.²⁰

(G) Cathedral of Seville (Spain).²¹

(H) Old manuscript from Iran.²²

(I) Monument at Teotihuacan, Mexico.¹⁶

(J) Pre-Columbian wool from La Plata Museum in Argentina.²³

(K) Temple of Concordia, Italy.²⁴

(L–N) (L) Wall paintings at Valley of the Kings,²⁵ (M) funerary mask,²⁶ and (N) columns from the Mosque of Amir Altinbugha al-Maridani,²⁷ all three from Egypt. All images were adapted with permission of the corresponding editorials. The references along with additional details are listed in Table S1.

Note: *1, *2, and *3 denote additional heritage items whose picture has not been included. Please refer to Table S1 in the Supplemental information for further details. (a, d, f, g, h, i, j, and l) adapted from (see ref.) and reprinted with permission of Elsevier Masson SAS. Copyright © all rights reserved; (b) adapted from (see ref.) and reproduced with permission of John Wiley and Sons Copyright © all rights reserved; (e and n) adapted from (see ref.), Springer Nature, under creative commons license CC BY; (k) adapted from (see ref.) and reproduced under creative commons license CC BY; (m) adapted from (see ref.), and reproduced with permission of the editor, Mediterranean Archaeology and Archaeometry, all rights reserved.

microorganisms. Many of these products offer limited long-term effect, are highly toxic, and frequently are also corrosive. This is due to the fact that many of these biocides have not been designed specifically with the heritage material in mind and instead have been transferred from the agricultural or health sector. Moreover, some also present unwanted negative effects in the treated works, such as the discoloration of the heritage material or changes to its chemical and physical characteristics.²⁸

Biocides can be both organic and inorganic, where the latter provide a longer-lasting action than organic products (which deteriorate rapidly, especially in outdoor environments). It is important to clarify that most of the biocidal products typically used in heritage conservation are overall quite ineffective in the elimination of microorganisms, and especially if they have been applied to materials exposed to outdoor environments. It is therefore necessary to reapply products at regular intervals to prevent recurring recolonization of the material and also consider how acquired antimicrobial resistance can develop as microorganisms adapt to poorly chosen or ineffective biocides.²⁹

When applying a biocidal product, it is important that it be chemically inert, stable, and colorless in order to avoid interference with the material or its possible interaction with other compounds used in the intervention (such as consolidants). The cytotoxicity and ecotoxicity must be also considered. Also, these materials must meet other requirements, such as resistance to external alteration agents, offer the potential for reversible application without causing damage to the substrate or in the case of stone materials, for example, maintaining adequate permeability without obstructing their porosity.³⁰

The effectiveness of the products used to prevent biodeterioration, as well as the results obtained with their application, will depend on a variety of factors such as the concentration and stability of the product, the duration and method of the application, the type of solvent, the pH of the solution, the presence of cracks in the substrate or organic materials, the type of substrate and its content in water, the existence of wind and rain during and after the treatment, the ambient temperature, the light intensity, or the colonization entity.³¹

It is also important to keep in mind that the chemical composition of some materials can modify the activity of these products and may affect the longevity of action over time, depending on the material on which the biocide has been applied. These factors are often responsible for the success or failure of these products, in different interventions carried out worldwide. However, and even though commercial biocides are routinely used in the field of heritage conservation, it must be said that not enough studies have been carried out to assess their long-term efficacy, as well as the possible negative effects caused to the treated materials.²⁸

The commercially available chemical products currently applied in the prevention of biodeterioration caused by heterotrophic and autotrophic microorganisms (such as lichen, algae, cyanobacteria, yeast, molds, and bacteria), and plants (like moss and bryophyte), are summarized in Table 1.

Essential oils, although not directly marketed as antimicrobials for heritage conservation, are worthy of special mention since they represent relevant antibacterial agents used routinely in other areas, e.g., active ingredients in food packaging, and are likely to receive added attention in the coming years. The volatile compounds present in essential oils extracted from plants present good antimicrobial activity against target microorganisms and are eco-friendly, naturally occurring biocides. However, their high antioxidant capacity and migration issues should be considered. For a more comprehensive analysis on the topic, readers are referred to the following reviews.^{40,41} Pioneering reports on nanoencapsulated essential oils in heritage conservation are discussed at the end of the following section.

ANTIMICROBIAL AGENTS IN CULTURAL HERITAGE CONSERVATION

Antimicrobial nanoparticles

The antimicrobial properties of materials such as silver, zinc oxide or copper have been known since time immemorial. For example, it is known that the water was already stored by the Egyptians in copper or silver containers to make it drinkable, or that during the exploration of the Wild West, silver coins were used to preserve the freshness of milk and to conserve drinking water against algae and bacteria. In the case of ZnO, it is also known that it was used as far back as 2000 BC as a treatment for boils and injuries. The antimicrobial properties of such materials increase upon reductions in particle size down to the nanoscale, because of fundamental changes



Table 1. Commercial chemical products most commonly applied in the prevention of biodeterioration

Chemical classification	Active commercial ingredient name	Substrate and targeted microorganism	Efficacy	Examples/notes	Refs.
Alcohols	ethanol	stone materials, paper, bacteria, lichen, fungi, algae	contradictory results: not effective against <i>Trebouxia</i> sp., <i>Gloeocapsa</i> sp. and <i>Chroococcus</i> sp. applied by brushing at 96% ethanol solutions (30%, 70%, and 100%) revealed antifungal activity over short and long term on paper	granite (laboratory test) filter paper (laboratory test) can act as a conidia activator	Sequeira et al. ²²
Isothiazolones	2-methyl-4-isothiazolone-3-one	ProClin 950-Sigma Aldrich	low efficacy: killed 20%–40% algae cells	laboratory test	Bartolini et al. ³³ Kumar and Kumar ³⁴
	2-octyl-2H-isothiazolone-3-one + didecyl dimethyl ammonium chloride in propanol + formic acid	Rocima 103- Dow Chemical	efficient applied by brushing, at 2% in water	archaeological site at Ostia Antica, Rome, Italy must be properly diluted for use	Fonseca et al. ¹⁴ Coutinho et al. ¹⁷
	5-chloro-2-methyl isothiazolinone, 2-methyl isothiazolone, methylbenzisoxazol-2-ylcarbanate + 2-n-octylisothiazolinone	Mergal 597-Troy corporation	effective	laboratory test crystallization on stone pores which could make penetration of the solution difficult	
	n-octyl-isothiazolone		effective, applied at 5% in ethanol	agar diffusion tests, (laboratory test)	
	di-n-decyl-dimethyl ammonium chloride, 2-N-octyl-2H-isothiazol-3-one + isopropanol + formic acid	bioin T-CTS	contradictory results: not effective at 2% v/v efficient, but recolonization occurred after 6 months	Palacio Nacional da Pena, Sintra, Portugal fishing House of the Marquis of Fontal Palace, Oeiras, Portugal the use of anionic surfactants and hard waters should be avoided	

(Continued on next page)

Table 1. Continued				
Chemical classification	Active commercial ingredient name	Substrate and targeted microorganism	Efficacy	Examples/notes
Mixes	imidazole + isothiazolinone	stone materials plastic materials textile metals fungi, algae	high efficiency. Effective after 4 years	Angkor Wat, (Cambodia) ethanol (70%) was applied first to destabilize. Avoid use with alkaline solutions
	iodopropynyl butyl carbamate + <i>n</i> -octyl-isothiazolone dissolved in 2(2'-oxydiethanol)	stone materials ceramic materials wall paintings fungi, lichen, bryophyte, cyanobacteria, bacteria	contradictory results: effective applied by brushing at 5% until saturation not effective after 4% v/v ethanol by brushing application	Segovia cathedral cloister, (Spain) Limestone, Classic Karst plateau (Italy) barely miscible in water
	sodium dimethyldithiocarbamate + sodium 2-mercaptobenzothiazole	stone materials cotton wood paper metals plaster works fungi, algae, lichen	good efficiency against bacteria and fungi, applied three times by brushing, at 1% in isopropanol good efficiency for 1–2 years	marbles, (laboratory test)
	tributyltin oxide + quaternary ammonium salt	stone materials woods lacking artistic interest wall paintings algae, moss, lichen	effective applied by spraying, but after 3 years almost completely washed-out by the rain reapplication every 4 to 8 years	Copan monuments, (Honduras)

(Continued on next page)



Table 1. Continued

Chemical classification	Active commercial ingredient name	Substrate and targeted microorganism	Efficacy	Examples/notes	Refs.
Oxidizing agents	calcium hypochlorite	stone materials	good efficiency applied at 5% in hot water	Palace of Saints George and Michael, Corfu, (Greece) Washington Legislative Building (USA)	Pantazidou and Theoulakis ³⁷ Pantazidou and Theoulakis ³⁷ Kumar and Kumar ³⁴
		algae, cyanobacteria, lichen		its activity is not maintained long (recolonization after 1 year)	
	hydrogen peroxide	stone materials	contradictory results: not effective applied by brushing, at 10% in water	historic cemetery of Drapano, Kefalonia, (Greece)	
		algae, bacteria, lichen	effective applied by sprayed at 15% (v/v) in water and carbonate/bicarbonate buffer solution	Slovenian caves can bleach materials	
	sodium hypochlorite	stone materials water saturated wood algae, cyanobacteria, lichen	good efficiency applied at 3.5% in hot water	Palace of Saints George and Michael, Corfu, (Greece) interferes with some stone materials, (excessive bleaching or secondary yellowing action) may react with wood lignin its activity is not maintained long	
phenolic compounds	duron 3-[3,4-dichlorophenyl]-1,1-dimethylurea	plasters algae	effective	laboratory test it can produce a darkening of limestone surfaces and a less detectable change on granite surfaces	Blazquez et al. ³⁵ Sawides et al. ³⁶
	n-butyl-1,2-benzisothiazolin-3-one	stone materials bacteria, algae, lichen, fungi	good efficiency at 3% v/v in water	Acropolis, Athens, Greece a first application is recommended to devitalize microflora, (3%-5% benzalkonium chloride in aqueous solution), followed by the mechanical removal of necrotized residues	
	parabens (p-hydroxybenzoates) + calcium propionate	paper fungi	very effective for inhibition using methyl paraben at 0.5% or propyl paraben at 1% with 5% calcium propionate	laboratory test it can be used to avoid fungal growth and as a treatment when is already infected	
	resin alkyleneoxide+ alkylaminotriazine+ N-(3,4-dichlorophenyl)-N,N-dimethyl urea + denaturated alkyl trihydroxyben-zene polyoxide	stone materials lichen	highly effective	Trieste Karst, (Italy) it produces color changes in the surfaces and the absorption of water by the capillary action of certain types of stones	

(Continued on next page)

Table 1. Continued

Chemical classification	Active commercial ingredient name	Substrate and targeted microorganism	Efficacy	Examples/notes	Refs.
Quaternary ammonium compounds	alkyl dimethyl benzyl ammonium chloride	Preventol R50, Preventol R80, Preventol R90-Lannexess, Hyamine 3,500-Lorza Company, Céquatyl-Rhone Poulenc	stone materials wood ceramic materials bacteria, lichen, fungi, algae	contradictory results: not effective at 4% w/v in ethanol efficient, but recolonization occurred after 6 months	Acropolis, Athens, Greece Fishing House of the Marquis of Pombal Palace, Oeiras, Portugal it is recommended to apply another coat (after 24 h) corrosive to metals
	benzalkonium chloride	Wet & Forget-Wet & Forget	stone materials Wood	contradictory results: not effective at 1% effective at 10% in water	statues of La Recoleta Cemetery, Buenos Aires, (Argentina) Felai Feng limestone, (China), (laboratory test) corrosive and toxic
	benzalkonium chloride + 2-phenyl-phenol	acticide 50X-Thor	bacteria, lichen, fungi, algae stone materials wood bacteria, lichen, fungi, algae	not effective at 5%	Felai Feng limestone, (China), (laboratory test)
	didecyl dimethyl ammonium chloride + excipients		wood bricks plaster bacteria, molds	contradictory results: very effective against bacteria and low efficacy against molds, after 28 days effective after 12 months	wood and brick fragments from Auschwitz II – Birkenau State Museum, (Oświęcim, Poland), (laboratory test) laboratory test
Essential oils	N, N-dodecyl-N, N-dimethylammonium	New Des 50-CTS	stone materials ceramic bacteria, biofilm, algae	contradictory results: effective. Higher efficacy against Gram-positive bacteria low efficacy applied at 2% and not effective for killing phototrophic organisms	laboratory test processional cloister of the Monastery of San Martín Pinario (Spain) could be used, in a lower concentration range than that indicated by producer decrease tension superficial and interfacial of the water in which it has been dissolved caused visible color changes on a granite wall
	N, n-didecyl-n-methyl-poly(oxyethyl) ammonium propionate + alkyl-propylene-diamine guanidium acetate	Anios DDSH-Anios laboratories	compatible with all kinds of materials yeast, lichen, algae, moss, bacteria	not efficient	walls on buildings in Sintra, (Portugal) ready-to-use spray foam
	thyme oil	doterra thyme oil	bacteria, fungi	reduction 12%–100% depending on the microorganism	Pietrzak et al. ¹⁸



CellPress

Chem
Review

in the physics of electron properties in the crystalline solid, combined with the better interaction with cells and intercellular components such as proteins, DNA, ion channels, etc.

Nanomaterials have been thoroughly investigated as antimicrobials in applications as diverse as water disinfection, food packaging, and healthcare. It is perhaps then not surprising that during the last decade nanomaterials have also emerged as antimicrobial coatings and treatments in the field of heritage conservation. However, this area is still in its infancy and only a limited number of reports have been published over the last 10 years. As part of this review a total of 84 papers have been identified, primarily using the keywords <nanoparticles>, <antibacterial>, <antifungal>, <antimicrobial>, <biodeterioration>, <biocidal>, <bactericidal>, <fungicidal>, <cultural heritage>, <relics>, and <monuments>, which equates to 15, 27, and 42 papers in the periods 2010–2013, 2014–2016, and 2017–2020, respectively. Nanomaterials have also been broadly used in heritage science for deacidification, consolidation, and cleaning processes,⁴² where a number of commercial products already exist, however, such studies are outside the scope of this review.

In the first instance, in order to be considered as a potential candidate for application in the heritage conservation field, a nanomaterial should present a potent and long-lasting antimicrobial activity and also display low cytotoxicity and ecotoxicity.⁴³ This presents a challenge for the development of novel biocides based on nanomaterials, since the long-term toxicity or the effect on the environment of many of them are still under study. Moreover, the guidelines of conservation state that, following a coating application, the aesthetic appearance of the heritage object (color, texture) should not be perceived to have been changed and any intervention must be susceptible to be reverted in the future,⁴⁴ which also implies a challenge in the design of nanomaterials-based coatings. Finally, regarding the commercialization of conservation products based on nanomaterials, the synthesis processes must be as simple and reproducible as possible, and the price of raw materials should be low, in order to develop competitive market-ready nanomaterial-based formulations.

Nanoparticles (NPs) of titanium dioxide (TiO₂), silver (Ag), and zinc oxide (ZnO) are, in this order, the most recurrently applied nanomaterials to prevent or treat microbial colonization of heritage substrate materials. Other frequently reported NPs include silicon dioxide (SiO₂), copper (Cu), magnesium oxide (MgO), zinc-derivates such as calcium zinc hydroxide dihydrate, Ca[Zn(OH)₃]₂·2H₂O, carbon nanomaterials (graphene, graphene oxide, and fullerene), and layered double hydroxides (LDH). To date, nanomaterials have been applied over a range of cultural heritage items and architectures, either model replicas or original artifacts, which include substrates originating from animals (parchment, wool, and silk tissues) and plants (paper, wood, and cotton fabrics) plus those obtained from inorganic resources (stone, glass, and plaster). Figure 2 provides an overview of the occurrence of publications that have used antimicrobial nanomaterials to prevent biodeterioration on different types of heritage materials. Our analysis shows that the most studied type of nanomaterial has been nano-TiO₂, which has been applied to most of the heritage substrates but is followed closely by Ag NPs. On the other hand, stone—in its many different varieties—has undoubtedly been the most studied heritage substrate material, being the focus of a total of 47 relevant publications to date.

Synthesis and properties of the nanomaterials tested as biocides in heritage

Wet-chemistry methods (sol-gel, soft-chemistry and autoclave processes) have been utilized to synthesize up to 51% of nanomaterials reported herewithin (see

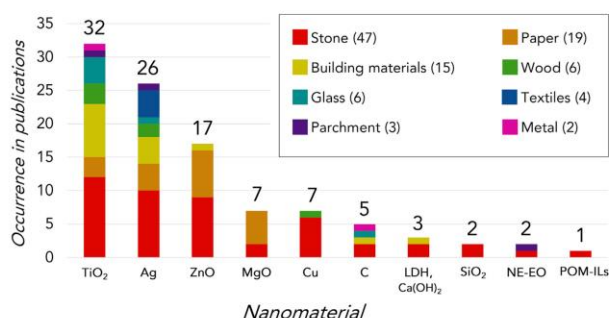


Figure 2. Frequency of studies of a nanomaterial for each type of heritage item substrate
C denotes carbon nanomaterials (graphene, graphene oxide, and fullerenes); NE-EO, nanoencapsulated essential oils; and POM-ILs, polyoxometalate-ionic liquids. For further clarity, similar heritage materials have been grouped: stone includes limestone, marble, calcareous stone, and a fossil. Textiles include canvas and fabrics such as silk, wool, and cotton. Building materials include a miscellanea of materials obtained from the transformation of inorganic sources used in construction and usually located in the outer side of buildings: bricks, ceramic tiles, plaster, adobe, and mortar. Oil painting over paper has been included in paper, since the article refers mainly to the support and not the pigments. It must be highlighted here that some of the publications compare more than one nanomaterial or apply them over more than one type of substrates, which has been considered to the elaboration of this graph. Journal articles were acquired by searching for the keywords "antimicrobial," "bactericidal," "fungicidal," "antibacterial," "antifungal," "biocidal," "biodegradation," "nanoparticles," "cultural heritage," "relics" and "monuments."

Figure 3).^{21,45} Some of these syntheses have been complemented with a calcination treatment (9%) to produce oxides such as TiO₂, MgO, or ZnO.^{10,46} Commercial materials have also been broadly utilized (in up to 27% of the published literature) but generally have been limited to TiO₂, ZnO, and Ag NPs.^{47,48} The availability of these three materials for purchase directly from commercial suppliers has undoubtedly rendered them as some of the most studied antimicrobial materials in the heritage conservation field, as previously shown in [Figure 2](#). Although a variety of other synthetic approaches have also been used, including the use of microorganisms, so-called biosynthesis (8%), used for ZnO,⁴⁹ Cu NPs,⁵⁰ and Ag NPs.^{16,51} Electrochemical methods (4%) have also been used to prepare ZnO¹⁹ and Cu NPs,⁵² and sonochemical methods (4%) are currently trending as a convenient, rapid, and cost-effective route to obtain NPs such as ZnO.^{53,54} Physical vapor deposition has also been used for the synthesis of In-doped ZnO.⁵⁵ Finally, it is worth mentioning that 6% of the reviewed publications failed to even specify the origin or synthetic procedure for the NPs used in the study.

In these studies, the heterogeneous nature of the synthesis methods (including the commercial materials, whose processes remain undisclosed) causes a broad distribution of the average particle size, ranging from diameters of a few nm to more than 100 nm. Moreover, the difference of concentration applied over the specimen, ranging several orders of magnitude, and other factors (size distribution within each sample, particle aggregation, type of substrate, environmental conditions, and type of microorganisms) involve so many variables that it is not possible to have a direct comparison or a statistical analysis of the results in terms of the effectiveness or durability of the conservation treatment. In order to be able to compare the effectiveness of the treatments, the heritage conservation research field would benefit greatly

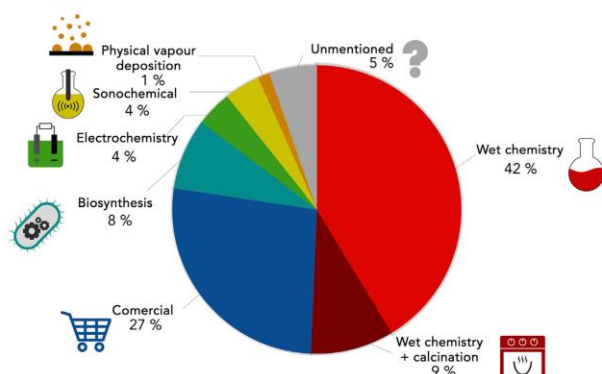


Figure 3. Origin of the antimicrobial nanomaterials used in heritage conservation

The graph includes chemical, physical, and biological synthetic methods, commercial sources, and those of unspecified origin.

from establishing a series of standardized protocols or assays to evaluate the antimicrobial activity of NP coatings or treatments. Such considerations are discussed in more detail in the final section of this review.

Nanomaterial application methods

If choosing the right antimicrobial nanomaterial is essential, the selection of the most appropriate mode of application (considering the properties of both the nanomaterial and the heritage material surface) is the next key step in the process. The techniques most commonly used so far have been brushing^{56,57} and spraying,¹³ which are adequate for most substrates and ensure a homogeneous NP coating, as well as others like immersion,⁵⁸ drop-casting,^{59,60} spreading with a spatula,⁶¹ misting,²³ capillary absorption,⁶² and even spin-coating for a glass test specimen.⁶³ In most of the studies, the nanomaterials were dispersed in polar protic solvents that quickly evaporate, like water or ethanol;^{12,64,65} however, some studies took further the idea of stabilizing the coatings versus environmental conditions, and organic or inorganic matrices were incorporated for this purpose. These includes commercial varnishes⁴⁶ and consolidants^{15,19,22,50,52,56,60,63,66–68} and natural and synthetic polymers such as polyvinyl butyral,⁴⁷ starch,⁵⁴ siloxanes,^{59,62,69,70} acrylic resins,^{27,71} wax,⁷² estearates,⁷³ nanocellulose,⁵³ hydroxyethylcellulose,⁷⁴ and hydrogels.^{48,75} These hybrids generally enhanced the attachment properties of the NPs, thus improving the longevity of the antimicrobial coatings.

Types of microorganisms used to evaluate the potential of antimicrobial nanomaterials

Following the nanomaterials deposition on the substrate, the antimicrobial efficiency must be assessed. Biodeterioration processes are usually caused by a wide and heterogeneous community of colonizing microbes constituted by prokaryote (bacteria and cyanobacteria) and eukaryote microorganisms (fungi and algae), where the presence and prevalence of one type of microorganism over another will typically depend on the available nutrients and on the environmental conditions to which they are exposed. For example, the availability of natural light naturally favors the proliferation of photosynthetic microorganisms such as algae and

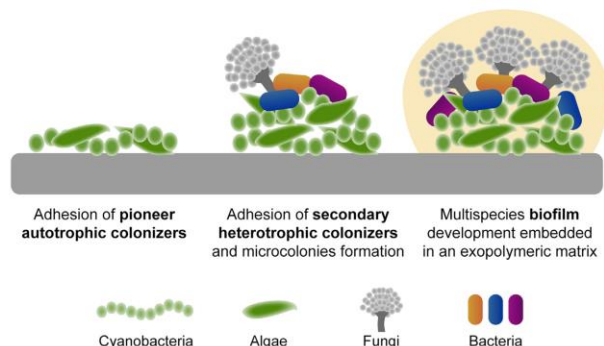


Figure 4. Outdoor stone surface colonization process

First, pioneering autotrophic colonizers (cyanobacteria and algae) attach to the surface, facilitating colonization by secondary heterotrophic colonizers (typically fungi and bacteria). Thereafter, multispecies biofilm development begins with the formation of microcolonies composed of different microorganisms which then evolves into a mature biofilm as the microorganisms become embedded in the matrix formed from the excretion of extracellular polymeric substances.

cyanobacteria; while in dark and humid conditions heterotrophic microorganisms like molds and bacteria will be the more prevailing and abundant species.^{16,18,21,76} The microbial colonization of different types of heritage object, from stone monuments and other architectures to paper heritage, textiles, metals, and other works of art, is discussed in detail in several excellent books and reviews.^{2,77,78} Briefly, to better understand this process, here, we will take an outdoor stone surface as an example (Figure 4), where the pioneering colonizers are typically autotrophic cyanobacteria and algae that can obtain their nutrients from the inorganic compounds on the stone surface and the sunlight. Once the autotrophic microorganisms have obtained a foothold on the stone surface, the heterotrophic microorganisms can establish themselves as secondary colonizers, obtaining organic nutrients from the autotrophic cyanobacteria and algae.⁷⁸ We recommend that interested readers consult the aforementioned texts for detailed discussion of the different types of microorganisms and the environmental conditions favoring their proliferation.

To date, a variety of different microorganisms relevant to the decay of heritage objects and architectures have been used to evaluate the efficacy and potential of antimicrobial nanomaterials.⁷⁹ Figure 5 shows the occurrence of bacteria, fungi, and algae in the studies in this review, specifying the type of heritage substrate and the type of nanomaterial. Fungi (in particular molds) and bacteria are the most studied microorganisms. Regarding fungal studies, *Aspergillus niger* is by far the most common of the more than 30 fungal species studied, which also includes *Penicillium oxalicum*, *Candida albicans*, and *Alternaria alternata*, among others. The biocidal activity of nanomaterials has been tested against more than 20 types of bacteria, with *Escherichia coli* being the most common strain, together with *Staphylococcus aureus*, *Bacillus subtilis*, and *Bacillus cereus*. It is important to remark that, even though bacteria are not always the main colonizing microorganisms, they present some characteristics (e.g., rapid growth, can be cultured and evaluated in the laboratory through reproducible protocols) that make them highly suitable as model microorganisms for the first *in vitro* assays. Besides, some very recent studies have

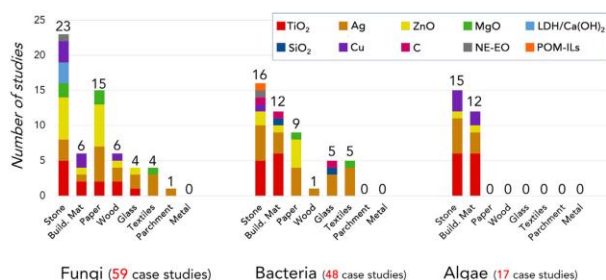


Figure 5. Frequency of studies for bacteria, fungi, and algae
C, carbon nanomaterials (graphene, graphene oxide, fullerene); NE-EO, nanoencapsulated essential oils; POM-ILs, polyoxometalate-ionic liquids. The studies are groups for type of substrate of cultural heritage. Each column details the number of studies per nanomaterial, in different colors (see legend).

demonstrated the presence of different bacterial species in heritage objects, deposited through vectors, such as insects, or even due to human contamination during restoration or other processes. This research opens the door to the study of a new source of contamination, making non-environmental bacteria relevant to biodeterioration processes.⁸⁰ It is worth mentioning cyanobacteria as a special case of study. While this bacteria domain represents a relevant pioneering colonizer of outdoor heritage objects, very few studies were carried out with this microorganism. Just six papers of the consulted bibliography studied the effect of Ag NPs^{13,61,81} and TiO₂ NPs^{14,21,82} on cyanobacteria. *Chlorella vulgaris* is the most utilized algae from a list of more than ten different algal species. Only a few studies concerning treatments specifically for lichens have been performed—not included in the figure—over stone with TiO₂¹⁴ and Cu NPs.¹⁵ Algae, lichens, cyanobacteria, and moss require a supply of water and light to grow, and so the research projects involving these microorganisms were focused in stone and building materials in outdoor environments. Yet, studies preventing algal growth on wood, glass, and metal in cultural heritage objects are non-existent, even though algae are known to be pioneering microorganisms in extreme environments.

Although most studies employ easily culturable laboratory strains, some have gone as far as to analyze the type of microorganisms present in the heritage object, which were identified by traditional culture methods (microscopy, gram staining, and enzymes activity) and molecular techniques (PCR amplification, sequencing).^{15–18,20,21,26,27,61,76,82,83} In these cases, the effectiveness of the biocidal treatments was tested either *in vitro* (on culturable strains) or *in situ* (on the heritage item itself), which provide the added value of dealing with the microorganisms that cause the biodeterioration of the heritage material. Some studies were carried out under the exact environmental conditions that caused the deterioration,^{17,20} while others have used similar conditions simulated in the laboratory.^{21,82}

The type of studies that have been performed are based primarily on the identification of the microorganisms present in real samples by sequencing the 16S rRNA gene and the determination of the minimum inhibitory concentration (MIC) of the compounds against the different microorganisms. Our analysis has shown that broth dilution methods and agar diffusion test were the preferred means of determining

the MIC, and, as we will explain later in the review, these may not be the most suitable methods depending on the characteristics of the compound. Although some studies performed more accurate microbiological assays to determine the activity of the compounds⁷⁶ there is a clear need to establish more standardized protocols to determine the antimicrobial and antibiofilm properties of a compound or nanomaterial *in vitro* but also over the heritage material being protected. To this end, this weakness is addressed in the final section of this review ([Overview of biochemical techniques for determining antimicrobial and antibiofilm properties](#)), where a comprehensive description of appropriate techniques is detailed.

Nanomaterial and nanomaterial-heritage substrate characterization techniques

This section overviews the principal analytical techniques that have been used to characterize the nanomaterials, as well as their interaction with the substrate heritage material.

Size and morphology of the NPs are most often reported using images from scanning electron microscopy (SEM) and transmission electron microscopy (TEM).^{26,56} NP size distribution in solution has been frequently analyzed by dynamic light scattering.^{61,81} The reliability of this technique, however, is limited to particles with spherical shape. This technique is affected by aggregation and, therefore, can be used to study the stability of the NP dispersion prior application.^{21,65} It must be highlighted that, although NP antimicrobial activity is often size dependent,⁸⁴ ca. 30% of the publications cited herein contain no such analysis of the NP dimensions.

Crystallinity of the NPs, defects, and doping. TEM and X-ray diffraction (XRD) analyses provide key information about the crystallinity of the samples, the presence of defects, and doping.^{56,85}

Compositional analysis. Additional techniques present in most electron microscopes, such as energy-dispersive X-ray spectroscopy (EDX) and electron energy loss spectroscopy (EELS), provide insights into the elemental composition of the NPs and substrate.^{26,50} For quantitative compositional analysis, the preferred techniques are X-ray photoelectron spectroscopy (XPS), elemental analysis, or inductively coupled plasma (ICP).

Homogeneity and degree of penetration of the NP coatings in the substrates have been extensively studied by SEM, EDX,^{60,71} and also by XPS.⁶³

Presence and growth of microorganisms on different surfaces have been characterized by SEM and optical microscopies. For samples with high sensitivity to vacuum or those which cannot be coated with a conductive layer, environmental scanning electron microscopy (ESEM) is the preferred tool.^{11,12} This technique operates under a controlled gaseous atmosphere instead of vacuum and allows the imaging of wet samples where the microorganisms are under conditions similar to their natural state. Optical microscopies are non-invasive techniques, useful to study the structure of the substrate, the microorganisms, and the antimicrobial performance of the coatings.^{26,48} Combined with cell staining (for example, death/alive bacteria) they are useful to evaluate the effectiveness of a given treatment. Digital image analysis is a useful tool to evaluate the percentage of the surface of a heritage item that has been colonized by the microorganisms that cause a color variation on the same, such as algae or fungi.^{81,82} Spectroscopies using infrared, ultraviolet-visible radiation, and photoluminescence have also been reported as convenient and universal methods for the characterization of the NPs and coatings.^{22,56,86} Fourier



transformed infrared (FTIR) spectroscopy has been revealed as a useful tool to study the evolution of organic substrates during accelerated aging studies.^{22,47,53}

Color variation. As mentioned previously, any mitigating biodeterioration prevention coating must not alter the aesthetic appearance of the heritage object to a noticeable degree. Most of the articles in this review address this issue by performing colorimetric studies. The surface color is characterized before and after the nanomaterial application by spectrophotometric techniques and the chromatic change calculated as ΔE in the CIE 1976 L*a*b* color space.^{10,12,45,52,60,68,74} Most authors refer to a $\Delta E \leq 1$ as being a perceivable change but assume $\Delta E \leq 5$ to be acceptable.

Aging studies. Ideally, an antimicrobial coating should possess a long-lasting effect. However, most research projects are time limited, and only in some cases it has been possible to study the performance of the treatment *in situ* during a period of several years. Some examples found in literature include TiO₂ on glazed tiles (2 years),¹⁷ TiO₂/wax on marble in underwater marine environment (2 years),⁷² and Cu NPs mixed with commercial consolidants on several inorganic substrates (3 to 8 years).^{15,68} Nevertheless, in most of the projects it is necessary to perform accelerated aging tests to assess the durability and resistance of the antimicrobial coatings within the project time frame, as follows:

(1) Biofouling accelerated growth: tests have been performed by introducing the coated samples within climatic chambers with controlled conditions of humidity, temperature, and simulated sunlight. Water supply was ensured by using sprinkling systems,^{82,87} or direct immersion.^{21,61} More recently, Becerra et al. have proposed capillarity system for wetting the substrate. This is considered a more realistic simulation since multiple applications of culture are avoided compared with sprinkling systems.⁸¹

(2) Accelerated environmental factors (light, temperature, and humidity): the use of climate chamber studies, or similar, is also common.⁵³ The exposition of the substrates to UV light to simulate solar aging has showed that TiO₂/Mg(OH)₂ hybrids improve the tensile strength resistance of paper under UV radiation,⁵⁶ or that the presence of Ag NPs do not alter the stability or the color of cotton fabrics during accelerated light aging.⁸⁸ The avoidance of color fading in pigments/colorants and the improvement of tensile strength in paper by ZnO and TiO₂ NPs,^{46,66} has also been studied. Other authors reported a positive effect on the stability of the organic matrix that contains the NPs.^{27,62,67} The photoactivity of ZnO^{12,62} and TiO₂^{67,86,87} was also evaluated by the discoloration of rhodamine or methylene blue solutions upon UV-vis light irradiation.

(3) Freeze-thaw cycles: cycles of freezing and thawing⁸⁹ and heating treatments (60°C–90°C) inside chambers,^{22,62} in occasions with high, controlled humidity⁴⁷ showed improved performance of the NP-coated substrates versus the uncoated ones. Other aging studies include the evaluation of the treated surface after several months exposed to environmental conditions to check the decrease of the accumulation of dirtiness on TiO₂-treated substrates.⁴⁶

(4) NP-release studies: It must be highlighted here that the evolution of the coatings regarding the release of NPs, lixiviates of the organic matrices, and the possible toxicity related to this has only been studied in the release of Zn from ZnO via a rainwater-mimicking study.⁶³ In fact, the evolution of the treatments is a critically

important issue to sustainable conservation practices because of the implication on the health of curators, museum visitors, and the environment.⁹⁰ It is our view that thorough toxicological and ecotoxicological research should be developed in parallel to nanomaterial research in heritage conservation to ensure their safe and sustainable use.

Heritage substrate material studies. Broadly speaking, the properties of the heritage materials (substrates) are unevenly characterized in the literature cited in this review. Stone is usually analyzed by a comprehensive set of techniques, which include several of the following: porosimetry, surface area, roughness, water vapor permeability, capillary water absorption, and static contact angle,^{12,15,45,50,58,62,67,68} while paper usually includes basic tensile strength measurements to evaluate changes in resistance.^{46,66,74,83} However, it must be stated here that it should be necessary to perform a more systematic study of the heritage object in terms of composition and structural arrangement. In general, for all types of materials, certain properties must be present in any study, such as their typology, size, composition, pH, and density, as well as their color. However, in addition to this, there are other characteristics specific to certain materials, simple to determine, and that provide great information, as for example the grammage of the paper.⁹¹

Looking to the future, it is becoming increasingly clear that studies should also involve the use of large scientific facilities, like Neutrons⁹² and Synchrotron radiation,^{93,94} whose use in heritage science has increased considerably in recent years. Valuable information about the porosity and morphology of samples can be provided by computer-tomography-based techniques.⁹⁵ The use of such facilities enables non-destructive analysis with high spatial resolution and accurate compositional information, as well as high resolution imaging of the coatings and substrates, therefore providing a better characterization and deeper understanding of surface properties and enhanced information on aging studies. It is also important to note that the heritage science community is supported by the European Research Infrastructure for Heritage Science (ERIHS), which supports research on heritage interpretation, preservation, documentation, and management through transnational access (TNA) to a wide range of high-level scientific instruments, methodologies, data, and tools for advancing knowledge and innovation in the field of heritage science.

TiO₂ NPs

TiO₂ is the most utilized nanomaterial in heritage conservation, as it is inexpensive, chemically stable, and environmentally benign. The well-documented antimicrobial properties of TiO₂ rely on its photoactivity: this semiconducting material releases reactive oxygen species (ROS) upon exposure to UV light or solar radiation. ROS are formed from molecules present in the atmosphere (O₂ and H₂O) and include superoxide anion radicals (·O₂), hydroxide radicals (·OH), and hydrogen peroxide (H₂O₂), which are capable of killing microorganisms by oxidative attack of their cell membrane.⁹⁶

Fonseca et al. were the first to report the use of nanoparticulated TiO₂ to prevent biodeterioration on heritage items in 2010, demonstrating the efficiency of pure and Fe³⁺-doped 20 nm anatase to decrease the growth of cyanobacteria and algae on mortars.¹⁴

The majority of reports in the literature show that TiO₂ is bacteriostatic and generally only slows down the growth of microorganisms on the surface of heritage items when

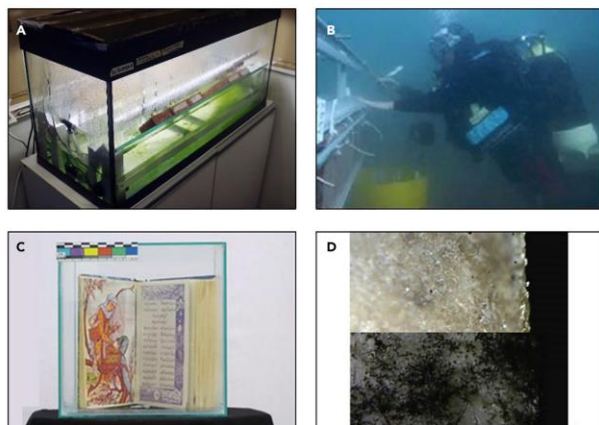


Figure 6. Images taken from studies of TiO_2 NPs as antimicrobial in heritage conservation (A–D) (A) Climatic chamber used in the accelerated algal growth test,⁸⁷ (B) positioning of TiO_2 -coated marble specimens under marine underwater environment,⁷² (C) picture of a book inside the TiO_2 -coated glass box,⁶⁶ and (D) parchment colonized by *Penicillium chrysogenum* after (upper side) and before (lower side) the cleaning with TiO_2 in gellan gum.⁴⁸ (A) adapted from (see ref.) and reprinted with permission of MDPI under creative commons license CC BY (MDPI Editorial); (B), (C), and (D) adapted from (see ref.) and reproduced with permission of Elsevier Masson SAS, Copyright © all rights reserved.

activated by UV or visible light, and it is typically not strong enough for a complete biocidal action.^{20,62,66,67,97} Further, TiO_2 presents null^{58,61} or poor^{26,47} antimicrobial activity in the absence of light.

TiO_2 has been shown to diminish the growth of algae on bricks and stone in under water environments and when subject to humid conditions (Figures 6A and 6B).^{82,87} Similarly, Coutinho et al. reported the partial detachment of the biofilm in the glazed wall tiles of Palacio da Pena (Portugal) under natural sunlight conditions even 2 years after application.¹⁷ Afsharpour et al. designed a TiO_2 -coated glass box for paper-art-works preservation⁶⁶ that protects the objects inside from the damaging effects of microorganisms, UV light, and pollutants (Figure 6C).

An interesting approach was developed by De Filipo et al. (Figure 6A) whereby a removable coating of TiO_2 -loaded gellan gum was applied over parchment producing a dual antimicrobial functionality: first, organic contaminants (spores and hyphae) were removed after being trapped in the 3D polymeric network, and second, UV-light-activated TiO_2 NPs had a biocidal effect, and no fungal regrowth was observed, although the testing time for the fungal growth was limited to 15 days. One particular advantage for this treatment is its reversibility, since the gellan gum can be removed after finishing, leaving no residual gel on the parchment surface. However, some of the TiO_2 NPs were observed to remain in the parchment that continued to function as antimicrobial reservoirs afterward.⁴⁸

One of the limitations on the use of TiO_2 as antimicrobial is that, due to its band gap, this material absorbs photons mainly in the UV region. La Russa and Ruffolo

pioneered the use of Ag-doped TiO₂ to prevent heritage deterioration, where the presence of Ag shifts the absorbance of photons into the visible region and enhances its photoactivity under sunlight.^{85,86} NPs of TiO₂ and Ag-doped TiO₂ were synthesized by wet-chemistry methods and their capacity to prevent the growth of microorganisms on marble slabs under a simulated marine habitat was studied. No microbial colonization was observed after 72 h in samples containing Ag-TiO₂, in contrast to untreated samples, which were extensively colonized by algae. Regarding samples treated with only TiO₂, these authors reported a remarkable higher activity for TiO₂ against bacteria at a concentration of 0.01% versus 0.1% (w/w in distilled water), reporting a 0% bacterial survival at 0.01% versus a >19% survival for the higher TiO₂ concentration.⁸⁵ Other authors have studied doping TiO₂ with Fe, Sr,⁸⁶ and Ce,⁷⁰ which resulted in complete inhibition of bacterial growth on stone for Sr-Ag-TiO₂ and Ce-TiO₂. In this instance it must be highlighted that, although doping TiO₂ improves the performance of the coatings, the absorbance of photons in the visible region causes color variations that might alter the color of the heritage item.

Another strategy to improve the antimicrobial properties of TiO₂ has been to explore the synergic effects arising from using a combination of nanomaterials. Hybrids of Ca(OH)₂/TiO₂,⁵⁸ ZnO/TiO₂,⁴⁷ and Zn:Al LDH/TiO₂⁹⁸ were employed as effective antifungal agents on limestone, wood, and bricks, respectively. ZnO/TiO₂ showed an effective protection of wood even during aging tests performed at high relative humidity and using further UV irradiation.⁴⁷ For their part, Vidakovic et al. reported that the aging of the TiO₂/LDH coating is substrate dependent, and the treatment should be renewed every 4–7 months.⁹⁸

Hybrids of TiO₂ and Ag NPs showed superior antimicrobial activity, achieving a complete or significant reduction (>98%) of microbial growth,^{21,61,67,69,72,82,85} although authors state that the inherent antimicrobial activity of Ag NPs might be key in these cases. The antimicrobial properties of Ag NPs by themselves will be discussed in the following section.

Interesting enough, several authors have observed that the testing conditions and the properties of the substrate strongly determine the efficacy of the antimicrobial treatments. As stated by Graziani et al. "the efficiency of any coating cannot be assessed without testing them directly on each substratum they could be applied."¹³ Ruffolo et al. showed that, for a given TiO₂ coating on plaster in a heritage site, the presence of soil humidity decreased the antimicrobial effectiveness of the TiO₂ when applied close to the ground in comparison to upper zones.²⁰ Porosity and roughness of the heritage substrate are also a key factor in treatment effectiveness. Graziani et al. studied the effect of surface roughness on a TiO₂ treatment against algae on fired bricks with 36% porosity. The initial surface roughness of 8 μm was smoothed to 1 μm with sandpaper. Even in absence of a treatment, a 20% lower algal coverage was observed in the clay bricks with lower roughness. The treatment of the bricks with 4-nm-diameter TiO₂ showed no decrease in the algal coverage in the rougher sample; however, a reduction of algal coverage of 40% was observed in the lower roughness bricks compared with the blank.⁸⁷ The same authors observed a similar effect regarding porosity, where the initial algal coverage were 95% and 20% for untreated stone specimens with a porosity of 37% and 19%, respectively. Antimicrobial treatments in the stone with 19% porosity showed an algal coverage of 3.6% for TiO₂, while it reached 6.7% with Ag NPs/TiO₂ and 8.2% with Cu NPs/TiO₂. However, no antibiofouling effect was observed for these treatments on the 37% porous stone.¹³ Other authors reported a similar effect of the porosity/roughness on

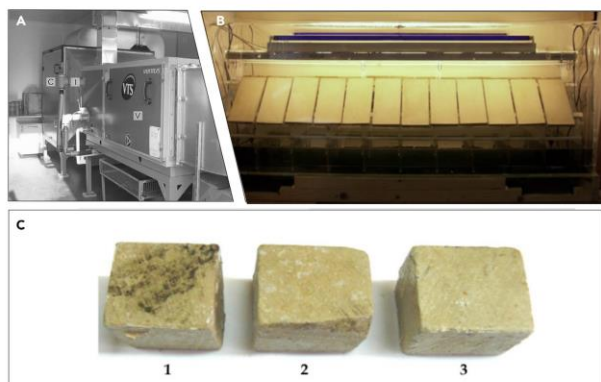


Figure 7. Images illustrating the studies of Ag NPs as antimicrobial in heritage conservation (A–C) (A) Misting chamber used for Ag NPs disinfection,¹⁰⁰ (B) culture streaming tank,⁷³ and (C) limestone blocks treated with a silicon polymer loaded with Ag NPs against *Aspergillus flavus*.⁷¹ (A–C) adapted from (see ref.) and reproduced with permission of Elsevier Masson SAS. Copyright all rights reserved.

ceramics and limestone.⁵⁸ The porosity of the substrate contributes to retain nutrients and moisture while decreases the coating efficiency due to diffusion of the nanomaterials within the pores. Roughness is also important since some microorganisms, like algae, require asperities to adhere. Moreover, Becerra et al. noted that the chromatic changes for a given treatment are related to the porosity, as the diffusion of the NPs into the pores led to a smaller ΔE in more porous materials.⁶¹

All these examples illustrate the difficulty in developing an antimicrobial coating on a proof-of-concept sample in the laboratory, before even taking into consideration its successful implementation on a real heritage surface in more realistic natural setting, outside of the laboratory.

Ag NPs

Ag NPs present broad-spectrum antimicrobial activity resulting from the attack on multiple microbial cellular processes: Ag NPs increase the oxidative stress via ROS formation, interfere with nutrient transport processes in the cytoplasmic membranes, and disrupts metabolic processes. This activity is boosted by the release of Ag^+ ions, which impede DNA replication and inhibit enzymes and peptides that eventually leads to the microorganism death.⁹⁹

Gutarowska et al. pioneered the use of biocidal Ag NPs in heritage preservation, demonstrating their potential as a powerful disinfectant for the surface of archival documents and historical objects.⁷⁶ These authors isolated microbial strains from the air and surfaces from different museums and archives from Warsaw and Lodz, Poland, (see Table S1) and removed up to 94% of those microorganisms using a 45 ppm loading of Ag NPs. Thereafter, the Lodz team optimized a method to disinfect heritage objects within a misting chamber (see Figure 7A) in which Ag NPs from a dispersion were nebulized over textiles, paper, or canvas.¹⁰⁰ These authors found that this misting disinfection process was sensitive to the degree of relative humidity,

since moisture eases the penetration of the NPs in the microbial walls. Moreover, these authors also observed that vegetative cells (bacteria and mycelium) are more sensitive to the antimicrobial effect of Ag NPs than the corresponding bacterial or fungal spores. Further experiments with pre-Columbian fabrics from Peru (wool, cotton, and sisal) showed that the reduction of microbial number depended on the type and initial amount of microbial species: while it ranges 30.8%–99.9% for some species of bacteria and fungi, some other species (mostly endospore-forming *Bacillus*) were insensitive to Ag-NPs-misting treatments.²³

Reports by other authors have shown that Ag NPs effectively reduce the cell viability of bacteria on sandstone by 80%,⁵⁹ biofouling on mortar by 40% under humid conditions (see Figure 7B),⁷³ and the growth of aerial algae on facades by 98%.¹⁰¹

The amount of Ag NPs that can be used for an antimicrobial treatment is notably limited by the color change produced (such NPs absorb strongly in the range of 390–470 nm). Becerra et al. reported a limit on the efficiency of the antimicrobial properties of Ag NPs that can be achieved in low porosity stone due to esthetical considerations.⁶¹ Essa et al. reported a complete growth inhibition of microorganisms *in vitro* using a 60 µg/mL suspension of Ag NPs, although to avoid color change on stone surfaces the maximum concentration that could be used as part of *in situ* assays was 40 µg/mL (Figure 7C). To mitigate this undesired color change, Ag NPs were further combined with a silicon polymer, which sharply reduced the growth of both bacteria and fungi on the coated stones (*Streptomyces parvulus* growth displayed a reduction of 98.6% and the growth of *A. niger*, determined visually, was almost inexistent).⁷¹ The color limitation associated with Ag NPs can be moderated by embedding them in a removable hydrogel,¹⁰² similarly as described for TiO₂ in the previous section.⁴⁸ In this case, Ag and AgCl NPs were embedded within a poly(vinyl)alcohol-borax hydrogel and authors demonstrated an effective elimination of the microorganisms present in the stone. However, the microorganisms were not isolated for identification, and so the absence of quantitative antimicrobial data means that the results should be treated with caution.¹⁰²

Carrillo et al. carried out an *in vitro* study on the effect of the size and concentration of biosynthesized Ag NPs against fungal and bacterial strains isolated from the citadel of Teotihuacan (Mexico). In this particular case, NPs of 12 different sizes in the range of 39–367 nm were tested, but no clear trend was observed for the inhibitory effect versus the NP size. However, these authors found that the effectiveness was dose sensitive, reaching a maximum of effectiveness above 90% against some bacteria, although a clear dose-effect trend against molds was not observed. In a further *in vivo* study, the reduction of microbial colonization ranged from 90% to 98% for *Pectobacterium carotovorum* and *A. alternata* on three different types of heritage building materials (stucco, basalt, and calcite).¹⁶ Gámez-Espinosa et al. reported a 100% inhibition on the growth of *Aspergillus versicolor* and *Cladosporium cladosporioides* on bricks coated with a 2% Ag NPs loading on silane.⁵¹

Pietrzak et al. used ancient books from a public library in Lodz (Poland) and the National Archive in Prague (Czech Republic) to compare the efficiency of three different antimicrobial treatments: Ag NPs, essential thyme oil, and a low-temperature plasma treatment (generation of ROS from air by electric discharges). The Ag NPs were found to be the most effective against bacteria, which underwent a 60%–100% growth reduction versus 12%–100% for the other treatments, although all three approaches showed a similar performance against fungal contaminants (0%–98.8%). For all three treatments, the effectiveness was lower for fungi than for



bacteria and depended on the type book, the area of sampling and the tested microorganisms. Efficiencies as low as 0% and as high as 100% in viability reduction tests were reported for the three types of treatments in different samples containing bacteria and fungi. The authors stated that the low efficiency of Ag NPs in this study may be due to the presence of strains of mold that were unaffected by the Ag NPs.¹⁸ Similar resistance was observed for the bacteria obtained from pre-Columbian archaeological cotton textiles compared with those from laboratory strains.

Becerra et al. observed that the performance of Ag NPs and the Ag NPs/TiO₂ hybrid against the formation of a bio-patina on stone could be further improved by stabilizing the nanomaterials with the citrate ligand. These authors reported that, for a given initial quantity of Ag NPs, the ΔE is directly related to the aggregation of the NPs: the more they tend to aggregate (zeta potential closer to 0 and higher hydrodynamic diameter) the higher the ΔE. The presence of citrate increases the zeta potential while decreasing the hydrodynamic diameter, which avoids aggregation, while the presence of TiO₂ has the opposite effect.²¹

Another important factor on the effectiveness of treatments is the pH of the NP dispersion, as reported by Noeiaghahi et al., who demonstrated that the pH defined the stability of ZnO and Ag NPs against aggregation. For example, the same treatment of ZnO NPs on a partially deteriorated mortar caused a 55%–59% growth inhibition of *E. coli* over the pH range 6–10 versus a 100% inhibition at pH 12; while for *B. cereus* the efficiency ranged 25%–31% at pH in the range of 6–10 versus 12% inhibition at pH 12.⁶⁵

This clearly indicates the importance of the testing conditions on the antimicrobial performance of the treatments and emphasizes the need to study the native microorganisms present in the heritage objects as opposed to the more commonly studied strains.

ZnO NPs

The photocatalytic properties of ZnO are similar to those of TiO₂, with the advantage that ZnO is also an active antimicrobial agent under dark conditions. This is due to the toxic effect of zinc ions released into the local environment and/or from ZnO NPs internalization by the microorganisms.¹⁰³ Gómez-Ortiz et al. successfully tested the antimicrobial features of pure ZnO and ZnO/Ca(OH)₂ hybrids on limestone in both dark and light conditions,⁵⁸ and they also tried coatings containing Ca [Zn(OH)₃]₂·2H₂O that inhibited the growth of *A. niger* and *P. oxalicum*.¹⁰⁴ Another test case with calcium zinc hydroxide or ZnO is the work of Soria-Castro et al. (2019), who stated that the tested ZnO and [Ca(Zn(OH)₃]₂·2H₂O NPs showed good activity against *S. aureus*, *E. coli*, *A. niger*, *P. oxalicum*, and *C. albicans*.

ZnO can completely inhibit the fungal growth, as reported for *A. niger* on stone (Figure 8A),^{19,27,53} *Trichoderma viride* on paper,⁵⁴ and *A. niger*, *A. versicolor* and *Rhizopus solani* on paper.⁵³ The efficiency of the treatment was increased under UV light (Figure 8B).⁵⁴ Ditaranto et al. reported a complete inhibition of *A. niger* growth in *in vitro* assays, although the corresponding *in situ* assay on stone did not provide significant results because, after 6 months, no growth was observed even in the control sample.⁶³ Other authors reported the inhibition of fungal growth in the range of 13%–68% for four types of fungus (*A. alternata*, *A. niger*, *P. chrysogenum*, and *Penicillium pinophilum*) isolated from an Egyptian tomb at the Valley of the Kings,²⁵ 89.7% for *P. chrysogenum* isolated from an archaeological

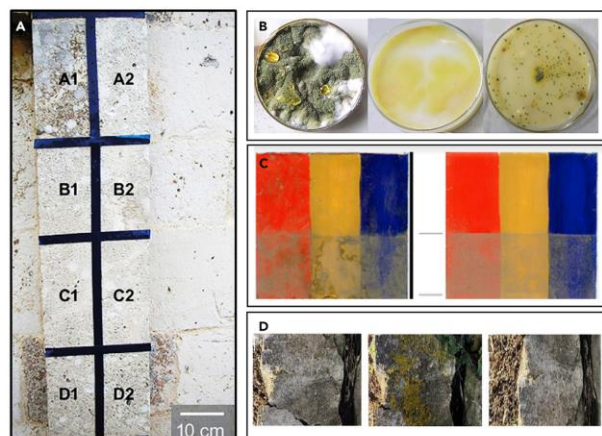


Figure 8. Images of the studies of ZnO NPs as antimicrobials in heritage conservation
 (A) Test areas at the wall of the church of San Leonardo di Siponto (Italy). Zones C1 and C2 were cleaned with ZnO NPs combined with commercial consolidants.¹⁹ (B) Growth of mold on starch paste (left), starch treated with ZnO under light (center), and in absence of light (right).⁵⁴ (C) Comparison of ZnO-treated oil paintings (upper part) and untreated (lower part) after 6 months of aging (left side) and once cleaned with a brush (right side).⁴⁶ (D) Artwork surface original (left), stained by algae (center) and protected by ZnO NPs (right).⁵⁵ (A) adapted from (see ref.), Springer Nature, under creative commons license CC BY; (B) adapted from (see ref.) and reproduced with permission of John Wiley and Sons. Copyright all rights reserved; (C) and (D) adapted from (see ref.) and reproduced with permission of Elsevier Masson SAS. Copyright all rights reserved.

manuscript deposited at Al-Azhar Library of Cairo, Egypt,⁴⁹ 98.2% for *A. niger* isolated from the book "Descriptio de L'Egypte," deposited at Misr library, Mansoura city, Egypt,⁸³ and 97% for *C. Albicans* and 7% for *A. niger* on paper works.²² A comprehensive publication by El-Feky et al. reported a reduction in the growth of *Trichoderma reesei* and *A. niger* on fresh oil paintings on paper and the reduction of the accumulation of dirt when left in the open air for 6 months (See Figure 8C).

ZnO has also been reported to completely inhibit the growth of *B. subtilis* and *P. chrysogenum* on paper (these strains were isolated from a manuscript from XVII century deposited at Al-Azhar Library, Cairo, Egypt)⁴⁹ and inhibit the growth of *S. aureus* and *E. coli* by 98.7% and 94.2% also on paper.⁵³ ZnO also delivers a 50% reduction on the growth of the algae *C. vulgaris* and *Scenedesmus quadricauda* on adobe mud and earthen artworks within 1 week (Figure 8D)⁵⁵ and presents an anti-fouling capacity close to 70% reduction on limestone.⁶¹ In-doped ZnO can also reduce the growth of algae on stone.⁵⁵ Moreover, ZnO can provide additional features such as self-cleaning properties, UV-light protection,⁴⁶ or structural reinforcement⁸³; aging tests with UV light for 150 h showed a reduction of color fading in samples treated with ZnO, and no appreciable change in the tensile strength of the NP-treated paper.⁴⁶

Gambino et al. reported a dose-response effect of ZnO against *A. niger* similar to a hormetic behavior: a ZnO low-dose (0.25%) led to the accelerated sporulation, an



earlier production of secondary metabolites and a change in the appearance of the biofilm, while a higher dose (0.5%) inhibited the fungal growth.²⁵ This phenomenon must be considered when designing an antimicrobial treatment due to the important consequences on the conservation of the heritage items. Recently, Schifani et al. have used ZnO nanorods supported on graphene to reduce the growth (60%–90%) of the bacteria *Arthrobacter aureus* and *Achromobacter spanius* on Noto stone, Carrara marble, and bricks. Those strains were previously isolated from the Temple of the Concordia (Italy).²⁴

SiO₂ NPs

The previous antimicrobial studies on these NPs have focused on hybrids of SiO₂ NPs with photocatalytic materials based on TiO₂ and ZnO, organic biocides or biocidal metals or NPs, such as Ag NPs. These mixtures are of particular interest in the field of heritage conservation because, besides their antimicrobial features, they also possess consolidating and hydrophobic properties.^{45,57} Zarzuela et al.⁴⁵ developed silica-based nanocomposites with copper(II) oxide, via sol-gel route, as a multifunctional treatment in the protection of building stone. The compound, applied by impregnation to natural limestone, improves the mechanical resistance of the stone and reduces the growth of *E. coli* and *Saccharomyces cerevisiae*. Compared with the control samples, they obtained the highest inhibition with 87% for *E. coli* and 80% for *S. cerevisiae*, according to the colony-forming unit (CFU) data of the cell recovery assay, with the compound containing a proportion of 0.15% w/v of CuO.

In other cases, the biocidal activity of Ag/SiO₂ NPs hybrids grafted into a modified silicate matrix on xerogel samples has been evaluated.⁵⁷ These hybrids were applied on four stone samples of different origin: Lecce Stone from the Salento region (Italy), granite from Meis quarry (Pontevedra, Spain), and limestone from the Estepa quarries (Seville, Spain) and Cabra (Córdoba, Spain); noting that Ag/SiO₂ NPs products increased biocidal effect by up to >90%, typically achieving ca. 80%–98% bacterial inhibition against *E. coli* and *S. cerevisiae*.

Cu and CuO NPs

The bioactivity of Cu NPs against microorganisms relies on the formation of ROS, which causes multiple toxic effects, including membrane lipid peroxidation and degradation, protein oxidation, or the degradation of DNA.⁷⁹ Despite the known antimicrobial surface properties and widespread commercial use of Cu and CuO NPs in the biomedical field, they have been relatively underexploited in heritage conservation, particularly when compared with other common antibacterial agents such as TiO₂ or Ag NPs. In this respect, one of the inherent limitations of copper is its rapid oxidation and its possible nanotoxicity. However, the available literature affirms that Cu NPs applied together with consolidants are highly effective in the treatment of stone surfaces colonized by bacteria, fungi, algae, or lichens.^{15,50}

Following an 8-year-long study, Pinna et al. (2018) evaluated the effectiveness of Cu NPs, together with several commercial consolidants and water-repellents (Silo 111, Acrilico 30, and Estel 1000), after their application to pre-cleaned substrates (sandstone, marble, and plaster), from the archaeological site area of Fiesole (Florence, Italy).¹⁵ The authors concluded that the recolonization of the substrates after the treatment applied in 2008 was related to their bioreceptivity and the weather conditions. In this case, although the applied materials reduced colonization, after 2-to-3 years they failed to prevent the reappearance of lichens and biofilms.

The biogenic synthesis of CuO NPs from *E. coli* Z1 has been reported, including a study of the antimicrobial activity of Cu NPs and CuSO₄ solution against bacterial and fungal strains.⁵⁰ These NPs were also suspended in two commercial consolidation polymers (Primal AC33 and a silicon polymer), to be applied on stone, where *E. coli*, *S. parvulus* and *B. subtilis* was reduced by between 61% and 68%. Helmi et al. also reported a promising antimicrobial activity of CuO NPs, comparable with that of Ag NPs, against strains of bacterial and fungi isolated from funeral masks from Saqqara necropolis (Egypt).²⁶ However, these authors recommend using Ag NPs for heritage-related applications instead of CuO, due to the stronger color variation of the latter.

MgO NPs

Nano-MgO is known to possess important antimicrobial activity due to the small particle size and a larger surface area, which lead to the increased generation of superoxide radicals and the increase in pH associated with the hydration of MgO. Both the radicals and high pH damage the cell membrane and induce lysis, which, after the loss of the intracellular content, lead to the death of the microorganisms.¹⁰⁵ In addition to combating microbial biodeterioration, MgO NPs can be used in other restoration processes, such as in the deacidification of paper or canvases.^{106,107}

Typically, MgO or Mg(OH)₂ NPs are mixed with other nanomaterials acting as supports, such as hydroxyethyl cellulose (HEC) or hydroxypropyl cellulose (Klucel E), and the hybrids are subsequently applied to heritage materials such as paper or stone. For example, the antifungal activity of MgO NPs and Mg(OH)₂ NPs with hydroxypropyl cellulose, on cotton paper sheets (Rotilabo, Carl Roth) was evaluated by introducing samples into a growth medium containing *S. cerevisiae* and *E. coli*.⁵⁶ The treated samples showed wider zones of inhibition than others treated with non-nanosized MgO. MgO NPs only presented biocidal activity against fungi, while Mg(OH)₂ NPs showed antifungal and antibacterial activity. The authors concluded that nanometer-sized MgO particles were more effective than non-nanometer-sized particles due to better penetrability between paper fibers and that the use of hydroxypropyl cellulose provides an improved surface coating of paper.

Recently, Franco-Castillo et al. evaluated the use of 12-nm diameter nano-MgO, prepared using a simple sol-gel synthesis, on three samples of 18th century paper from the archives of the Royal Botanical Gardens (Madrid, Spain). MgO NPs were shown to be bactericidal to both the Gram-negative and Gram-positive species at low concentrations (1.5 mg/mL for *E. coli* and 0.75 mg/mL for *B. subtilis*). This antibacterial effect was verified using both cell proliferation assays and colorimetric resazurin cell viability tests. An *in situ* assay based on a chromogenic agar was used to determine the activity of the nano-MgO coating over the papers, which illustrated how the nano-MgO-treated paper samples remained free of microbial colonization (Figure 9). The low cytotoxicity of the particles to eukaryotic cells was also confirmed.¹⁰ A subsequent article by the same team showed that the same MgO NPs possessed fungicidal properties against the fungi *A. niger*, *T. reesei*, and *C. cladosporioides* *in vitro*. When applied to original heritage paper samples, the particles retained their fungicidal properties against two of the three molds tested. Microscopy inspection of the paper samples showed how the untreated paper samples were fully colonized by fungal mycelium, while the coated paper samples remained free from colonization (Figure 9). Further assays were carried out to determine the ability of the MgO NPs to inhibit the cellulase enzyme activity of *A. niger* and *T. reesei*. These assays demonstrated how the MgO NPs inactivate the cellulases in both fungi at concentrations below the fungicidal concentration, making

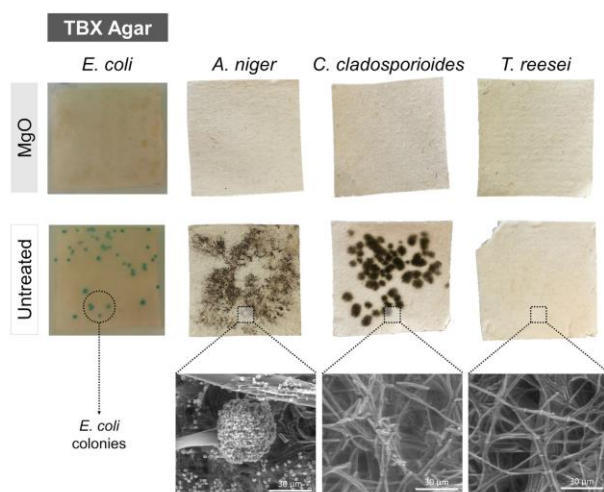


Figure 9. Use of antimicrobial MgO NPs in heritage paper conservation
Digital image analysis of 18th century paper samples (2 × 2 cm), coated with a 10 mg/mL MgO NPs solution and untreated control samples. The chromogenic TBX agar assay, performed with *E. coli*, reveals the growth inhibition properties of the MgO NPs (top left: absence of blue colonies of *E. coli*). MgO NPs also prevent fungal colonization of the paper samples, but visible fungal growth was evident in the untreated paper samples. ESEM imaging (below) confirmed the results.^{10,11} Adapted and reproduced with permission of Elsevier Masson SAS and Royal Society of Chemistry (see ref.). Copyright all rights reserved.

the molds unable to degrade the cellulose of the paper to obtain their nutrients. It is important to remark that none of the concentrations used to protect the paper samples result in a color change of the paper ($\Delta E < 3$).¹¹

Recently, Sierra-Fernandez et al. have also reported the use of MgO NPs and Zn-doped MgO NPs ($\text{Mg}_{1-x}\text{Zn}_x\text{O}$, $x = 0.096$) as protective antifungal coatings for dolomitic and calcitic stones. The authors found that Zn-doping significantly improved the photocatalytic and antifungal capabilities of MgO and that $\text{Mg}_{1-x}\text{Zn}_x\text{O}$ NP-based treatment prevented microbial colonization on calcareous stone materials.¹² The MIC of the MgO NPs was determined to be 1.25 mg/mL for *A. niger* and *P. oxalicum*, and similarly, for the Zn-doped MgO NPs, 1.25 mg/mL for *A. niger* and 0.625 mg/mL for *P. oxalicum*. Regarding the stone samples treated with Zn-doped MgO, *A. niger* colonization decreased from 50.13% to 8.35% (on dolostone) and from 19.93% to 9.84% (on limestone); while the overall *P. oxalicum* colonization reduction was found to be 78.8% (on dolostone) and 88.2% (on limestone), compared with the untreated control substrates.

Other nanomaterials

Other nanomaterials recently tested as antimicrobial in heritage conservation include polyoxometalate-ionic liquids (POM-ILs), graphene oxide, and polymer-nanoencapsulated essential oils. POM-ILs have recently gained attention due to the tailorable antimicrobial properties offered by the structural and compositional

versatility of these materials. These ionic liquid materials (salts with a melting point below 100°C)¹⁰⁸ are a combination of nanoscale molecular metal-oxide anions (polyoxometalates) and bulky organic cations, typically alkylammonium or phosphonium cations. Importantly, both the POM anion and the organic cation can be independently tuned, offering access to a multifunctional materials library. The anticorrosive and antimicrobial properties of the POM-ILs along with their hydrophobicity make them highly suitable candidates for cultural heritage conservation. Importantly, broad-spectrum antimicrobial POM-IL materials can be obtained by modulating the chemical composition of the POM-IL, providing microbicidal activity in the µg/mL range against different bacterial and fungal strains. Furthermore, the application of a transparent coating that will not modify the aesthetic properties of the object make them applicable on heritage materials. Recently, Misra and co-workers have obtained successful results applying POM-ILs as a coating over different natural limestone samples of different porosity from the north-east France and Belgium. Two types of POM-ILs, POM-IL 1 ((*n*-C₇H₁₅)₄N)₈[α-SiW₁₁O₃₉] and POM-IL 2 ((*n*-C₆H₁₃)₃(C₁₄H₂₉)N)₈[α-SiW₁₁O₃₉], which share identical POM structure with different counter-cations were used in this study. A 200 mg/mL solution (in acetone) of both POM-ILs was applied by brush as a protective coating over three types of stones—Belgian Blue (0.3% porosity), Romery (5% porosity), and Dom (30% porosity)—to protect them against simulated acid corrosion. The weight loss after the experiment shows how both POM-ILs are capable of protecting the integrity of the stones, especially for the porous Dom stone, where the weight loss after exposed to simulated acid-vapor corrosion was only 0.4% for the POM-IL 1-coated stone, while the uncoated Dom stone underwent complete loss of structure. These compounds were also tested against two bacterial strains, Gram-positive *B. subtilis* and Gram-negative *E. coli*. Both POM-ILs possessed bactericidal activity in solution at concentrations between 0.5 and 500 µg/mL, and a modified Japanese Industrial Standard (JIS Z 2801) analysis verified the surface bactericidal activity of the POM-ILs, reaching up to 100% bacterial reduction for the Belgian blue stone. A new protocol using the chromogenic Tryptone Bile X-glucuronide (TBX) agar was established to determine the biofilm prevention activity of the POM-ILs when applied as a coating (Figure 10). Those quantitative results were also commensurate with qualitative analysis by ESEM, fluorescence, and confocal microscopy.⁹ A recent study has demonstrated the antifungal activity of these POM-ILs against a mixed culture of molds (*Engyodontium album*, *Cladosporium cladosporioides*, *Alternaria alternata*, and *Aspergillus fumigatus*) isolated from the surface of historical bricks from the Auschwitz II-Birkenau State Museum (Poland). These POM-ILs were applied as a coating on 19th-century brick samples and then inoculated with the mixture of molds and incubated in a climate chamber for three weeks. The POM-IL coating showed very high antifungal activity, being able to completely inhibit the mold growth over the surface. ESEM analysis performed with the inoculated bricks demonstrated the toxic effect of the POM-ILs on the conidia.¹⁰⁹

Regarding carbon nanomaterials, González-Domínguez et al. have recently patented the use of graphene oxide for preventing the colonization of ornamental rocks by lichens and moss.¹¹⁰ Finally, Romano et al. have introduced the use of polymer-encapsulated essential oils (170-nm-diameter capsules) to eliminate the bacteria *E. coli* and *Kocuria rhizophila* from the red marble surface of an 18th century church altar.¹¹¹ Meanwhile, Saada et al. studied the effectiveness of a lemongrass oil nanoemulsion using Tween 20 as surfactant. Microorganisms isolated from a 9th-century parchment were reduced by 100% (*Aspergillus fumigatus*), 98.7% (*Byssoschlamys spectabilis*), 83.5% (*Cladosporium xanthochromaticum*), and 100%

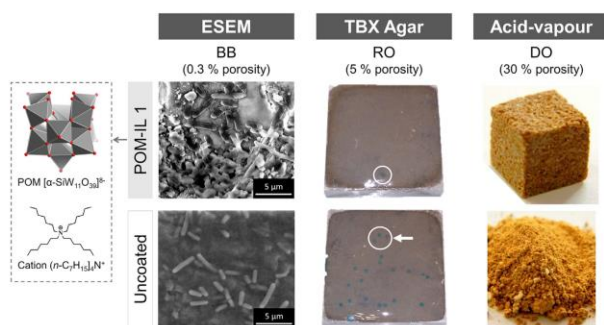


Figure 10. Antimicrobial and anticorrosive POM-ILs in heritage conservation

ESEM, TBX agar assay, and acid-vapor test performed with the three different stones: Belgian blue (BB), Romery (RO), and Dom (DO), respectively, coated with POM-IL 1 (images above) and without coating (images below). Both BB and DO stones, POM-IL 1 coated and uncoated, were inoculated with a solution of *E. coli*. As it can be observed in the ESEM results, bacteria incubated over the BB POM-IL 1 coated sample have lost their integrity and present serious morphology damage, whereas in the uncoated stone they show a normal and healthy morphology. These results were commensurate with the TBX agar assay performed with the RO stone. As in the ESEM assay, *E. coli* was inoculated over a POM-IL 1 coated and uncoated RO stone and, after the incubation time, almost no growth was observed on the POM-IL 1 coated sample, while multiple colonies (blue spots) were found covering the uncoated stone. Furthermore, acid-vapor tests exposing the stone samples to acetic acid vapor for 72 h demonstrated the corrosion protection properties of the POM-ILs. This anticorrosive effect was particularly evident for the POM-IL 1 coating over the DO stone sample when compared with the uncoated control sample, which lost its structural integrity following the acid-vapor assay.⁹ Adapted from (see ref.) and reproduced with permission of John Wiley and Sons. Copyright all rights reserved.

(*Streptomyces albidoflavus*).¹¹² Consequently, it is our opinion that micro- and nano-encapsulated antimicrobial agents will be ever more present in future publications.

OVERVIEW OF BIOCHEMICAL TECHNIQUES FOR DETERMINING ANTIMICROBIAL AND ANTIBIOFILM PROPERTIES

Designing optimal antimicrobial agents to prevent biodeterioration of cultural heritages

Several key points must be deemed when designing antimicrobial agents to prevent biodeterioration of heritage materials. Even before antimicrobial activity is considered, one of the main issues is the chemical stability of the compound or nanomaterial being studied along with any possible adverse interaction with the heritage substrate material. For this reason, chemically stable agents are preferred. Importantly, the type of heritage material, its elemental composition, and key properties, such as porosity, stability, and so on, should be carefully considered to prevent undesired interactions with the antimicrobial agent. As a brief example, metal-oxide NPs (e.g., TiO₂, ZnO, Ca(OH)₂) are, a priori, good candidates for the protection of porous stone, since they can become integrated into the physical structure of the substrate material (Figure 2); whereas others, such as Ag NPs, are less stable, more prone to oxidation and release of metal ions that could induce unwanted damage to the stone in the long term. Furthermore, sustainable and reversible conservation practices must also be considered meaning that removal and reapplication are also desirable characteristics. We must also add to this consideration of generating safe and sustainable materials that the use of antimicrobial agents that simultaneously possess

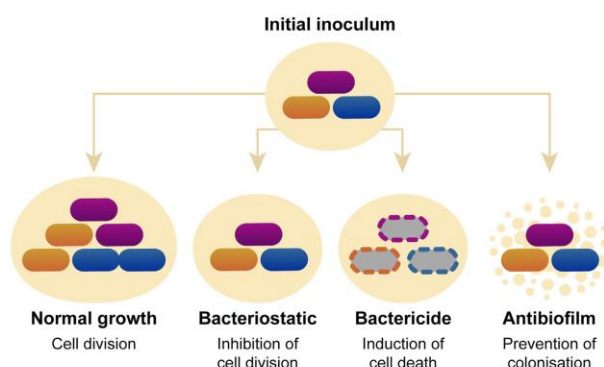


Figure 11. The effect of an antimicrobial agent to a bacterial inoculum

When the inoculum is not exposed to any drug, cell division occurs, and the culture grows. Bacteriostatic agents are capable of disable cell division, stopping bacterial growth, while bactericide agents kill the bacterial cells. Antibiofilm agents act by destroying the biofilm or preventing its formation.

low cyto- and ecocytotoxicity must be a priority, especially in outdoor environments and objects frequently manipulated by the restorers or the public.^{30,44} As a result of our review, we can confirm that this is one of the key sustainable aspects that frequently goes unaddressed in the published literature and one that will come under increasing scrutiny.

Focusing solely on antimicrobial properties, there are two main ways in which a microbial community can be removed using chemical methods: by preventing proliferation of the microorganism (antimicrobial properties) or by inhibiting biofilm generation (antibiofilm properties) (Figure 11). When using an agent with antimicrobial properties, it is critically important to distinguish between bacteriostatic and bactericidal effect. While a “bacteriostatic” compound inhibits bacterial growth, a “bactericidal” agent will act to kill the bacteria. However, these two pure categories (bacteriostatic and bactericidal) only apply *in vitro* and can be influenced by growth conditions, the initial bacterial inoculum, test duration, temperature of incubation, and multiple other conditions. Besides, bactericidal compounds are usually concentration dependent, and there is a required minimum dose to exhibit the bactericidal effect.¹¹³ The same categories can be attributed to antifungal compounds, those that inhibit the fungal growth will exhibit a “fungistatic” effect, and those that kill the fungi will exhibit a “fungicidal effect.” These categories are also influenced by the length of incubation, the medium, temperature, etc. and only apply *in vitro* studies.¹¹⁴ In general, a bactericidal (or fungicidal) compound or material is preferred over one that exhibits a bacteriostatic (or fungistatic) effect, since the latter offers greater opportunity for the microorganism to mutate and create resistance to the compound, enabling a recolonization of the substrate material.¹¹⁵ Besides these principal antimicrobial characteristics, the way each microbe interact with the substrate has to be studied, especially in the case of biodeterioration through chemical assimilation, where the microorganisms obtains their carbon source and energy from the substrate. In this special case, the addition of another property that inhibits or avoids the use of the substrate as the nourishment source could be preferable and complement a bacteriostatic (or fungistatic) effect. For example, MgO NPs, which



require relatively high concentrations to prevent fungal growth (>1 mg/mL) also inhibit cellulase activity—the enzyme secreted by the molds to obtain glucose from the cellulose of the paper substrate—at sub-MIC concentrations, meaning that they effectively prevent the microbial colonization of heritage paper through bifunctional mode of action.¹¹

In addition to the importance of considering the wide variety of characteristics of different classes of microorganisms, the protection offered by biofilms must also be considered when designing an antimicrobial treatment. Biofilms are defined as a community of microbial cells - interacting with one another and with the surface - embedded in a matrix of extracellular polymeric substances.¹¹⁶ The biofilm community can act to shield the microorganisms inside the matrix from the external aggressions, such as antimicrobials or harsh environmental conditions.¹¹⁷ Therefore, the use of specifically designed antibiofilm agents is essential for combating biodegradation of any surface. There are two ways to tackle biofilm growth: (1) preventing initial formation (or regrowth) or (2) removing a pre-existing biofilm. Nowadays, most antibiofilm compounds being developed are based on non-toxic molecules that do not directly affect the bacterial survival, to prevent future resistance to the compound.^{117,118} These molecules can inhibit the microbial colonization on surfaces and the biofilm formation by regulating the expression of certain genes, inhibit the synthesis of the exopolymeric matrix or interrupting the molecular communication between bacteria—known as quorum sensing signals—that regulate the expression of a wide range of genes involved in virulence, antibiotic production, motility, or biofilm formation, among others. Some examples of these molecules that are currently being used to prevent biofilm formation are indoles and their derivatives, peptides, D-aminoacids, free fatty acids, nitric oxide, ionic liquids⁹ or quorum sensing inhibitors, among others. Other approaches to prevent biofilm formation consist of physical modification of the surface via 3D patterning or conferring new physicochemical properties such as hydrophobicity.¹¹⁸ It is worth mentioning that, for some conservators, the microbial growth over a heritage surface (bio-patina) is considered as an integral part of the object. Consequently, there are cases where conservation and restoration methods should take this into consideration and attempt to preserve this patina.¹¹⁹

Some studies have reported on the synergistic effects promoted by antimicrobials in combination with antibiofilm agents. Darouiche and co-workers evaluated the combination of the antimicrobial triclosan with an antibiofilm enzyme against Gram-positive cocci and yeasts and demonstrated a synergistic activity between them, due to the increase of antimicrobial susceptibility induced by the antibiofilm enzyme.¹²⁰ This study is in agreement with previous reports, where the synergic effect of different antibiofilm agents in combination with antibiotics and non-antibiotic compounds was already reported.^{121,122}

Applicable techniques for antimicrobial activity determination

In this section we summarize different techniques from the microbiology field that can be used to establish the antimicrobial properties of a compound or material. Determining the antimicrobial activity *in vitro* using rapid and accurate biochemical techniques is the first crucial step in evaluating and selecting the most appropriate antimicrobial agent to be used in real samples. Choosing the wrong assay or method could easily lead to false-negative results (e.g., promising compounds may be mistakenly discarded) or false positive results (e.g., bacteriostatic compounds selected for aggressive microbial colonization). Furthermore, determining the antimicrobial activity with non-standardized assays makes it almost impossible to

compare results between other reports in the literature. For all this, knowing how to select the right combination of assays to perform for different compounds or materials is required in order to obtain a true understanding of their activity and proceed with meaningful subsequent research.

Table 2 contains an overview of these techniques, the antimicrobial property information that can be extracted from the assays, the effect of the compound on the microorganisms, the mechanism of action of the technique as well as any inherent limitations. To facilitate the reading of the table some important definitions and criteria are discussed in this paragraph. First, the MIC is defined as the minimum concentration of an antimicrobial agent at which the growth of a microorganism stops. While the minimum bactericidal concentration (MBC) and minimum fungicidal concentration (MFC) are both defined as the lowest concentration of an antimicrobial agent at which 99.9% of the final inoculum is killed.¹²³ In general, dilution methods—performed in liquid media—are preferred over diffusion methods—performed in agar-based solid media—to determine quantitative antimicrobial activities, like the MIC value. However, diffusion methods (Kirby-Bauer test or agar well diffusion test) are useful for screening of a large number of compounds and determine the susceptibility of the microorganism, since the bioactivity of each compound can be determined easily, cheaply, and quickly. Most crucially of all, the solubility properties of a compound or material must also be taken into account when planning assays, since many water-insoluble compounds could lead to false-negative activities if the aqueous culture media precipitates such materials from solution. In such cases new methods have been described, like the agar microdilution method, which allows the determination of the MIC of non-water-soluble compounds, like essential oils.^{123,124} There are also specific methods for antifungal effects, like the poisoned food method, which provides information about the fungistatic effect of the compound against molds. Microbial viability and, consequently, the MBC, is usually determined by colorimetric assays, using chromogenic compounds as Resazurin¹²⁵ or XTT tetrazolium salt, which stain the bacterial cells and depends on their metabolic activity, allowing the differentiation between viable and non-viable bacteria. Fluorescence assays work in a similar way and can provide a more complete picture of the metabolic processes and the cell cycle using specialized equipment such as a flow cytometer or confocal and fluorescence microscope; however, this requires access to expensive equipment and costly reagents as well as extensive user training. As additional information, the best and easiest method to confirm bacterial viability is the culture of the bacteria in solid media after performing the mentioned techniques. For further information about these techniques and other and more specific methods we highly recommend the recent review by Balouiri and co-workers on “Methods for *in vitro* evaluating antimicrobial activity: a review” (and relevant references therewithin).¹²³

Specific methods used to determine the antibiofilm properties of an antimicrobial agent are described in Table 3, which defines the nature of the data obtained (quantitative or qualitative), the mechanism of action of the technique, and the primary advantages and disadvantages. As for the antimicrobial activity, the biofilm can also be studied by colorimetric and fluorescence methods. Fluorescence staining provides quantitative and qualitative results, obtaining information also about the bacterial viability and can also provide information on mechanism of action; however, it also requires access to expensive equipment, fully trained users, and data analysis is often time consuming. On the other hand, the crystal violet assay is an easy and inexpensive method to quantify biofilms and does not require high-tech equipment, although it does not distinguish between viable and dead bacterial cells. Electron microscopy can provide qualitative information about the cell morphology and cell-wall integrity, which can be useful to



Table 2. Methods used to determine the antimicrobial activity of a compound or nanomaterial

Technique	Antimicrobial property	Information obtained	Mechanism of action	Remarks of the technique
Agar (disk) diffusion test (Kirby-Bauer test) ²³	inhibition of bacterial growth – bacteriostatic effect	antimicrobial susceptibility. Not distinguish between bacteriostatic and bactericide effect.	diffusion of the antimicrobial into de agar	qualitative, not suitable for determining the MIC. The drug may not diffuse into de agar
Agar well diffusion test ²³	inhibition of bacterial growth – bacteriostatic effect	antimicrobial activity of plant or microbial extracts.	Diffusion of the antimicrobial into de agar	qualitative, not suitable for determining the MIC. The drug may not diffuse into de agar
Poisoned food method ²³	inhibition of fungal growth – fungistatic effect	antifungal effect against molds	inhibition of fungal growth over agar with the compound incorporated	need to use a positive control (a known antimicrobial)
Broth dilution method ²³	inhibition of microbial growth – microbiostatic and microbicide effect	MIC MBC can be obtained subculturing	turbidity of the solution is proportional to the microbial growth	the compound can mask the microbial growth
Agar microdilution method ^{123,124}	inhibition of microbial growth – Microbostatic effect	MIC	inhibition of microbial growth over agar with the compound incorporated	preferred to the "Broth method" when having multiple isolates or if the compound mask the detection of growth
Time kill Curve ¹²³	bactericidal and fungicidal effect	MBC, MFC	this method reveals a time-dependent or concentration-dependent effect	this method can be used to determine the synergism of antagonism between two drugs
Resazurin/Alamar blue ^{123,125}	cell viability assay for prokaryotic and eukaryotic cells	MIC, MBC	oxidation-reduction indicator	change color from blue to pink in the presence of living organisms
XTT ¹²³	cell viability assay for eukaryotic cells (fungal cells)	MBC	quantification of metabolic activity of the cells	allows the study of intact biofilms. Not suitable for comparison between different strains or species
Fluorescence ^{123,126}	cell viability assay for prokaryotic and eukaryotic cells	MBC	stains DNA discriminate between viable and dead cells based on membrane integrity (live/dead staining)	avoids viable but nonculturable bacteria. ¹²⁷ expensive equipment required (flow cytometer, confocal or fluorescence microscopy). time-consuming image processing

Table 3. Methods to assess biofilm growth

Technique	Type	Mechanism of action	Advantages	Limitations
Fluorescence staining ²⁸	quantitative and qualitative	stains the cells or the matrix of the biofilm with a fluorescent dye	high resolution images, 3D images information about cellular viability, shape, and function information about spatial structures	cost of the equipment (confocal scanning laser microscopy, fluorescence microscopy or flow cytometry) user training use of specific and time-consuming software (e.g., Image J, COMSTAT)
Dry mass ²⁸	quantitative - indirect	biofilm quantification by the difference in weight between biomass on the substrate and the substrate with no biomass (achieved by temperature)	inexpensive, easy and quick low-tech equipment	destructive The substrate must be heat resistant or easily separated from the biofilm
Crystal violet ²⁸	quantitative - indirect	triphenyl dye, cell membrane permeable in both Gram-positive and Gram-negative bacteria	inexpensive, easy, reproducible, and quick	non-specific (does not distinguish between live and dead cells) need for a standardized protocol
ATP bioluminescence ²⁸	quantitative - indirect	uses light (commonly produced by luciferase) to correlate the amount of ATP with the biofilm viability and biomass	simple and quick can be performed in both suspended or attached cells availability of commercial kits optional non-destructive assay with recombinant bacteria expressing GFP	requires a luminometer, which must be calibrated regularly
Quartz crystal microbalance ²⁸	quantitative - indirect	uses the shift in resonance frequency due to program changes in mass to measure the biofilm accumulation as it is forming	non-destructive measurement of the biofilm accumulation in real time additional information about the viscoelastic properties can be obtained	cost of the equipment, software, and consumables measurements are highly sensitive to changes in temperature and pressure
Chlorophyll a ²⁹	quantitative - indirect	quantification of the concentration of chlorophyll to estimate the amount of photosynthetic biomass	allows measurement over the sample (without removing the biofilm)	only suitable for photosynthetic microorganisms (e.g., algal biomass)
Fluorescein diacetate (FDA) ²⁹	quantitative - indirect	estimator of microbial biomass by measuring metabolic activity	allows measurement over the sample (without removing the biofilm) great sensitivity and rapid detection suitable for non-scientific personnel with a minimum of scientific equipment	enzymes released by damaged or inactive cells can overestimate the activity
Scanning Electron Microscopy ²⁸	qualitative	concentrated beam of electrons provides information about surfaces	high resolution images possibility to perform elemental analysis (EDX)	not suitable for living samples due to the high vacuum sample preparation of living samples includes fixation, dehydration and sometimes coating with a conductive metal
Environmental scanning electron microscopy ²⁸	qualitative	concentrated beam of electrons provides information about surfaces	no need for fixation process	lower resolution than conventional SEM the electron beam can harm the living sample if not fixed



determine the interaction between the cell and the compound. Besides, there are also specific assays for photosynthetic microorganisms that enables the quantification of chlorophyll (the green pigments found in cyanobacteria, algae, and plants, essential for photosynthesis) in a sample. Some of these methods are non-destructive and allow the study of the biofilms *in situ*. The metabolism of the cell can also be an indicator of biofilm mass and can be studied by ATP (adenosine triphosphate) bioluminescence and fluorescein diacetate assays but do not provide information about the cell morphology. For in-depth information concerning the most appropriate techniques for studying biofilms we recommend the comprehensive review by Wilson and co-workers "Quantitative and qualitative assessment methods for biofilm growth: a mini-review" (and references therein).¹²⁸

Monitoring biofilm growth *in situ* is an important goal relevant to the cultural heritage field. Biofilm formation and evolution can be studied *in situ* using the techniques in Table 3; however, some other more specific methods have been developed for specific substrate materials. For example, attenuated total reflectance-Fourier transform infrared (ATR-FTIR) spectroscopy allows the study of the biofilm at the molecular level, *in situ*, and at real time, making it possible to study the evolution of the biofilm in response to environmental condition changes. Nonetheless, the biofilm must be grown over a specific ATR crystal with high refractive index to allow the detection of the infrared fingerprint of the sample, which may enable the study of the antibiofilm properties of a compound, but only applied on the ATR crystal and not applied on a real heritage sample or substrate material.¹³⁰

Raman spectroscopy can also be used to study biofilms but suffers from the same limitations as the ATR-FTIR method, in that it requires a specific substrate and does not allow the quantification of biofilm mass on real heritage samples. Furthermore, this technique frequently requires the use of colloidal metal NPs (usually Ag or Au) to enhance the signal.^{131,132}

With ESEM microscopy microbial growth over real samples can be studied, providing information about cell structure and morphology. However, this technique can only be applied on small laboratory samples (<approx. 5 cm in diameter).¹²⁸

To the best of our knowledge, one of the best, most convenient and low-cost techniques to monitor biofilm growth *in situ* over a real heritage sample involves the determination of total color difference (ΔE^*). The total color difference is a non-destructive method that can be applied *in situ* and can be used to quantify the biofilm growth over real samples, as reported by Prieto et al.¹²⁹ This method is easy to perform and does not require expensive equipment, only a colorimeter to measure the three values to obtain the total color difference (ΔE^*), the lightness (L^*), and the two chromaticity coordinates (a^* , red-green; b^* , yellow-blue). This color difference can be used as an indicator of microbial growth over the surface, enabling the quantification of the biofilm.¹²⁹ On the other hand, digital image analysis also allows the quantification of microbial colonization over different surfaces, and this simple straightforward technique can rapidly assess the growth of colored biofilms and microorganisms on heritage materials.^{81,82}

CONCLUSIONS AND PERSPECTIVE

This multidisciplinary perspective review has been written to provide chemists, heritage scientists, and restoration and conservation professionals with a comprehensive overview on the use of antimicrobial nanomaterials for the conservation of

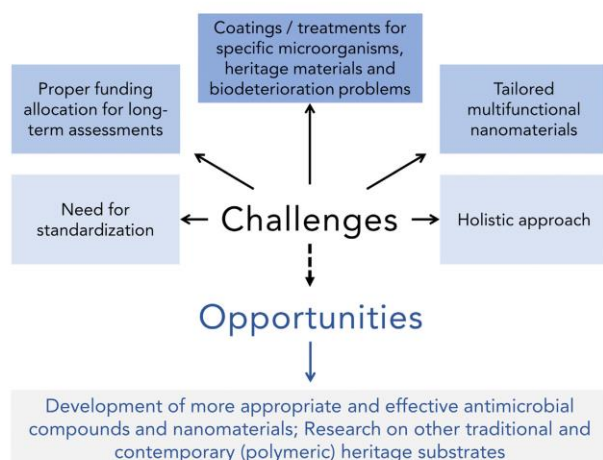


Figure 12. Challenges and opportunities in heritage conservation science

cultural heritage objects and architectures. In summarizing the literature to date, we have strived to show how nanomaterials can provide alternatives to the traditional or commercial antimicrobial products used to prevent the biodeterioration of heritage objects by offering tailored and durable solutions for safeguarding different substrate materials. By addressing the question from a multidisciplinary standpoint, we hope that this review will be useful to readers initiating in the field as well as for expert readers who require a snapshot of the current state of the art in order to provide cutting-edge technological solutions for heritage conservation-restoration. Our conclusions and perspectives herein give rise to several key challenges and opportunities for the area (summarized in Figure 12).

Breakthroughs leading to substantial leaps for the field will arise from combining multifunctional antimicrobial agents with advanced materials characterization to understand and engineer next-generation precision biocides that meet the particular needs of heritage conservation. Currently, however, there are still a limited number of examples where the fundamental physico-chemical properties of the nanomaterial can be adapted or improved to function without significantly altering the integrity of the object of interest. Herein lies the grand challenge for chemists and materials scientists: to chemically tailor nanomaterials to target specific microorganisms for particular end uses in the conservation-restoration field, e.g., conservation of heritage items, removal of biofilms (or indeed prevent their formation), paralyze the formation of the bio-patina, avoid microbially influenced corrosion of metals and glass, or purify the air in museum display cases.

Over the last five years or so, there has been a clear move toward developing multifunctional coatings, where consolidation, antimicrobial, and water repellence properties, among others, are combined into one material. In our opinion, the key to success lies in developing libraries of such materials, but with the perspective of the conservator-restorer in mind. Moreover, the design of such antimicrobial agents



should aim to meet the needs of the local environment (e.g., effect of ambient temperature, rainfall, humidity, UV exposure, and so on) and properly consider desired mode of action (i.e., either durable and long lasting or highly active over a short period). This will permit researchers to develop materials that: (1) target specific microorganisms responsible for deterioration and degradation of the heritage material, for example, cellulase-producing bacteria and fungi (wood and paper biodeteriogens), or cyanobacteria and algae (the pioneering autotrophic colonizers of outdoor heritage), and so on; (2) function by direct application (e.g., as hydrophobic, antimicrobial, or anticorrosive protective coatings), and (3) function indirectly (e.g., incorporated into display case filters or used as biosensors) to provide non-contact approaches to prevent microbial colonization.

Our analysis of the available literature on antimicrobial nanomaterials confirmed our premise that a variety of different classes of nanomaterials are being used to prevent biodeterioration of cultural heritage objects. Yet, few can be applied to a broad range of heritage surfaces or provide long-term antimicrobial action, essentially eliminating the potential for commercial application. It is patently clear that the time continuity of the projects is an issue, and it is necessary to evaluate the performance of the antimicrobial treatments over longer periods of time, for instance from five to ten years, or longer. In this respect, a more frequent use of climate chamber tests for coatings and treatments would be a significant step forward; however, it is also clear that studies should ideally be performed in real-world *in situ* settings (outdoors, in archives, in display cases, etc.), where anthropogenic conditions can be evaluated properly. The duration of research projects should consider the time frames that are necessary for the implementation of medium-to-long-term *in situ* evaluation through stable, collaborative programs involving museums, conservation-restoration professionals, and research centers.

Such studies should be limited not only to the effectiveness of the treatment as antimicrobial but also the whole process of designing, applying, testing the temporal evolution of the treatment—detachment, leaching, or ions release—and the final disposing (when applicable): i.e., a holistic approach for the design of antimicrobials for the protection of cultural heritage items. Furthermore, one of the inherent disadvantages of many antimicrobial agents is that their bioactivity is generally non-specific, and so the cytotoxicity of such agents should be more completely evaluated. For example, Ag NPs and materials based on quaternary ammonium or phosphonium compounds are frequently cytotoxic and therefore have corresponding health, safety, and environmental implications for restorers-conservators, curators, and general public. In addition, ecotoxicological aspects should also be considered to comprehensively assess the release of NPs (or products of degradation) during deposition or preparation of the coatings, during the coating lifetime. Finally, protocols for their removal or disposal should also be considered, since any such application should, of course, be reversible to facilitate its removal from the heritage surface, in line with conservation guidelines. Globally, these key considerations would more strictly adhere to the sustainable conservation principles that underpin the principal goals of the heritage science community at the moment.

The literature illustrates how a combination of antimicrobial procedures together with advanced materials characterization techniques can be used to comprehensively evaluate the properties of different nanomaterials against biodeterioration. Consequently, a thorough understanding of the biodeterioration process and choice of appropriate microbiological assays is imperative. Our review of the literature leads us to emphasize the need for more precise evaluation of the antimicrobial



properties of the materials being reported; with a specific need to identify more bactericidal and fungicidal agents, as opposed to bacteriostatic or fungistatic materials (which covers the vast majority of materials published to date). This characteristic affects the potential use of any antimicrobial agent, and it is our view that there is a need to clearly distinguish between bacteriostatic, bactericide, and antibiofilm so that it can be considered appropriately for the proposed end use. It is therefore important that the heritage science and biodeterioration community should work to establish systematic, standardized microbiological approaches to properly address the design and evaluation of antimicrobials to protect and preserve heritage items.

Finally, the heritage science field offers challenging research opportunities for chemists and materials scientists aiming to safeguard our shared cultural heritage for generations to come. In this respect, there is an ongoing requirement to develop antimicrobial solutions for lesser studied heritage materials, such as ivory,¹³³ soft and hard tissues in mummies,¹³⁴ papyrus and palm tree leaves, textiles,¹³⁵ or pigments¹³⁶ in prehistoric paintings. What is more, contemporary artworks produced from plastic polymers, acrylic resins, other organic substrates and varnishes, and other protective substances that act as a protective barriers also require significant attention in coming years.¹³⁷ In summary, a series of multidisciplinary challenges to more effectively preserve our past and present cultural heritage for generations to come.

IMAGES COPYRIGHT

The images in this article have been taken/adapted from third sources. If you wish to reproduce/adapt any of the images of this paper, the corresponding editorials holding the rights of the original source must be contacted to obtain the corresponding permissions.

SUPPLEMENTAL INFORMATION

Supplemental information can be found online at <https://doi.org/10.1016/j.chempr.2021.01.006>.

ACKNOWLEDGMENTS

A.S.-A. "This project has received funding from the European Union's Horizon 2020 research and innovation program under the Marie Skłodowska-Curie grant agreement no 840375." S.G.M. acknowledges financial support from Ministerio de Ciencia Innovación y Universidades (Spain) for Proyecto I+D+i PID2019-109333RB-I00, and professional support from the CSIC Interdisciplinary Thematic Platform Open Heritage: research and Society (PTI-PAIS). I.F.-C. acknowledges the Gobierno de Aragón for a doctoral scholarship (2018–2022). L.H. acknowledges the Consejo Superior de Investigaciones Científicas (CSIC) for a JAE Intro fellowship (JAEINT19_EX_0430).

AUTHOR CONTRIBUTIONS

All authors contributed equally to the writing of this manuscript.

DECLARATION OF INTERESTS

The authors declare no competing interests.



REFERENCES

- Steinbauer, M.J., Gohlke, A., Mahler, C., Schmiedinger, A., and Beierkuhnlein, C. (2013). Quantification of wall surface heterogeneity and its influence on species diversity at medieval castles—implications for the environmentally friendly preservation of cultural heritage. *J. Cult. Herit.* 14, 219–228.
- R. Mitchell, and J. Clifford, eds. (2018). *Biodeterioration and Preservation in Art, Archaeology and Architecture* (Archetype Publications).
- Hueck, H.J. (1965). The biodeterioration of materials as a part of phylobiology. *Mater. Organ.* 7, 5–34.
- Strzelczyk, A.B. (2004). Observations on aesthetic and structural changes induced in Polish historic objects by microorganisms. *Int. Biodeterior. Biodegrad.* 53, 151–156.
- Sterflinger, K., and Pinzari, F. (2012). The revenge of time: fungal deterioration of cultural heritage with particular reference to books, paper and parchment. *Environ. Microbiol.* 14, 559–566.
- Allsopp, D., Seal, K.J., and Gaylarde, C.C. (2004). *Introduction to Biodeterioration* (Cambridge University Press).
- Gaylarde, C.C., and Morton, L.H.G. (1999). Deteriogenic biofilms on buildings and their control: a review. *Biofouling* 14, 59–74.
- Paulus, W. (2005). *Directory of Microbicides for the Protection of Materials: A Handbook* (Springer Science & Business Media).
- Misra, A., Franco Castillo, I., Müller, D.P., González, C., Eyssautier-Chuine, S., Ziegler, A., de la Fuente, J.M., Mitchell, S.G., and Streib, C. (2018). Polyoxometalate-ionic Liquids (POM-ILs) as anticorrosion and antibacterial coatings for natural stones. *Angew. Chem. Int. Ed. Engl.* 57, 14926–14931.
- Castillo, I.F., De Matteis, L., Marquina, C., Guillén, E.G., Martínez de la Fuente, J., and Mitchell, S.G. (2019). Protection of 18th century paper using antimicrobial nanomagnesium oxide. *Int. Biodeterior. Biodegrad.* 141, 79–86.
- Franco Castillo, I., García Guillén, E., M de la Fuente, J., Silva, F., and Mitchell, S.G. (2019). Preventing fungal growth on heritage paper with antifungal and cellulase inhibiting magnesium oxide nanoparticles. *J. Mater. Chem. B* 7, 6412–6419.
- Sierra-Fernandez, A., De la Rosa-García, S.C., Gomez-Villalba, L.S., Gómez-Cornelio, S., Rabanal, M.E., Fort, R., and Quintana, P. (2017). Synthesis, photocatalytic, and antifungal properties of MgO, ZnO and Zn/Mg oxide nanoparticles for the protection of calcareous stone heritage. *ACS Appl. Mater. Interfaces* 9, 24873–24886.
- Graziani, L., Quagliarini, E., and D'Orazio, M. (2016). The role of roughness and porosity on the self-cleaning and anti-biofouling efficiency of TiO₂-Cu and TiO₂-Ag nanocoatings applied on fired bricks. *Constr. Build. Mater.* 129, 116–124.
- Fonseca, A.J., Pina, F., Macedo, M.F., Leal, N., Romanowska-Deskins, A., Laiz, L., Gómez-Bolea, A., and Saiz-Jimenez, C. (2010). Anatase as an alternative application for preventing biodeterioration of mortars: evaluation and comparison with other biocides. *Int. Biodeterior. Biodegrad.* 64, 388–396.
- Pinna, D., Galeotti, M., Perito, B., Daly, G., and Salvadori, B. (2018). In situ long-term monitoring of recolonization by fungi and lichens after innovative and traditional conservative treatments of archaeological stones in Fiesole (Italy). *Int. Biodeterior. Biodegrad.* 132, 49–58.
- Carrillo-González, R., Martínez-Gómez, M.A., González-Chávez, M.D.C.A., and Mendoza Hernández, J.C. (2016). Inhibition of microorganisms involved in deterioration of an archaeological site by silver nanoparticles produced by a green synthesis method. *Sci. Total Environ.* 565, 872–881.
- Coutinho, M.L., Miller, A.Z., Martín-Sánchez, P.M., Mirão, J., Gomez-Bolea, A., Machado-Moreira, B., Cerqueira-Alves, L., Jurado, V., Saiz-Jimenez, C., Lima, A., et al. (2016). A multiplex approach to evaluate biocidal treatments on biodeteriorated majolica glazed tiles. *Environ. Microbiol.* 18, 4794–4816.
- Pietrzak, K., Otlewska, A., Danielewicz, D., Dybka, K., Pangallo, D., Kraková, L., Puškárová, A., Bucková, M., Scholtz, V., Durović, M., et al. (2017). Disinfection of archival documents using thyme essential oil, silver nanoparticles misting and low temperature plasma. *J. Cult. Herit.* 24, 69–77.
- Van der Werf, I.D., Ditaranto, N., Picca, R.A., Sportelli, M.C., and Sabbatini, L. (2015). Development of a novel conservation treatment of stone monuments with bioactive nanocomposites. *Herit. Sci.* 3, 29.
- Ruffolo, S.A., De Leo, F., Ricca, M., Arcudi, A., Silvestri, C., Bruno, L., Urzi, C., and La Russa, M.F. (2017). Medium-term in situ experiment by using organic biocides and titanium dioxide for the mitigation of microbial colonization on stone surfaces. *Int. Biodeterior. Biodegrad.* 123, 17–26.
- Becerra, J., Zaderenko, A.P., Sayagués, M.J., Ortiz, R., and Ortiz, P. (2018). Synergy achieved in silver-TiO₂ nanocomposites for the inhibition of biofouling on limestone. *Build. Environ.* 141, 80–90.
- Afsharpour, M., and Imani, S. (2017). Preventive protection of paper works by using nanocomposite coating of zinc oxide. *J. Cult. Herit.* 25, 142–148.
- Pietrzak, K., Puchalski, M., Otlewska, A., Wrzosek, H., Guiamet, P., Piotrowska, M., and Gutarska, B. (2017). Microbial diversity of pre-Columbian archaeological textiles and the effect of silver nanoparticles misting disinfection. *J. Cult. Herit.* 23, 138–147.
- Schifano, E., Cavallini, D., De Bellis, G., Bracciale, M.P., Felici, A.C., Santarelli, M.L., Sarto, M.S., and Uccelletti, D. (2020). Antibacterial effect of zinc oxide-based nanomaterials on environmental biodeteriogens affecting historical buildings. *Nanomaterials* 10, 1–14.
- Gambino, M., Ahmed, M.A.A., Villa, F., and Cappitelli, F. (2017). Zinc oxide nanoparticles hinder fungal biofilm development in an ancient Egyptian tomb. *Int. Biodeterior. Biodegrad.* 122, 92–99.
- Helmi, F.M., Ali, N.M., and Ismael, S.M. (2015). Nanomaterials for the inhibition of microbial growth on ancient Egyptian funeral masks. *Mediterr. Archaeol. Archaeom.* 15, 87–95.
- Aldosari, M.A., Darwish, S.S., Adam, M.A., Elmarzugi, N.A., and Ahmed, S.M. (2019). Using ZnO nanoparticles in fungal inhibition and self-protection of exposed marble columns in historic sites. *Archaeol. Anthropol. Sci.* 11, 3407–3422.
- Palla, F., and Barresi, G. (2017). *Biotechnology and Conservation of Cultural Heritage* (Springer).
- Kakakel, M.A., Wu, F., Gu, J.D., Feng, H., Shah, K., and Wang, W. (2019). Controlling biodeterioration of cultural heritage objects with biocides: a review. *Int. Biodeterior. Biodegrad.* 143, 104721.
- Sameño Puerto, M. (2018). *El biodeterioro en edificios del patrimonio cultural: metodología de evaluación de tratamientos biocidas* (Sevilla: Tesis Doctoral Inédita. Universidad de Sevilla).
- Caneva, G., Nugari, M.P., and Salvadori, O. (1996). *Il Controllo del Degrado Biologico-I Biocidi nel Restauro dei Materiali Lapidei* (Nardini Editore).
- Sequeira, S.O., Phillips, A.J.L., Cabrita, E.J., and Macedo, M.F. (2017). Ethanol as an antifungal treatment for paper: short-term and long-term effects. *Stud. Conserv.* 62, 33–42.
- Bartolini, M., Pietrini, A.M., and Ricci, S. (2007). Valutazione dell'efficacia di alcuni nuovi biocidi per il trattamento di microflora fotosintetica e di briofite su materiali lapidei. *Bollettino ICR* 14, 101–111.
- Kumar, R., and Kumar, A.V. (1999). *Biodeterioration of Stone in Tropical Environments: An Overview* (Getty Publications).
- Blazquez, A.B., Lorenzo, J., Flores, M., and Gomez-Alarcon, G. (2000). Evaluation of the effect of some biocides against organisms isolated from historic monuments. *Aerobiologia* 16, 423–428.
- Riederer, J. (1986). Protection from weathering of building stone in tropical countries. *Stud. Conserv.* 31, 151–154.
- Pantazidou, A., and Theoulakis, P. (1997). Cyanophytes and associated flora at the neoclassical palace of St George and Michael in Corfu (Greece). Aspects of cleaning procedures, *Proceedings of the 4th International Symposium on the Conservation of Monuments in the Mediterranean Basin* pp. 355–368.
- Savvides, A.L., Nikolakopoulou, T.L., Kyrtasous, N., Katsifas, E.A., Kanini, G., and Karagouni, A.D. (2014). Bacterial deterioration of marble monuments: a case

- study of the conservation project of acropolis monuments. *Geomicrobiol. J.* 31, 726–736.
39. Sammartin, P., Rodríguez, A., and Aguiar, U. (2020). Medium-term field evaluation of several widely used cleaning-restoration techniques applied to algal biofilm formed on a granite-built historical monument. *Int. Biodeterior. Biodegrad.* 147, 104870.
 40. Palla, F., Bruno, M., Mercurio, F., Tantillo, A., and Rotolo, V. (2020). Essential oils as natural biocides in conservation of cultural heritage. *Molecules* 25, 730.
 41. Fidanza, M.R., and Caneva, G. (2019). Natural biocides for the conservation of stone cultural heritage: a review. *J. Cult. Herit.* 38, 271–286.
 42. Sierra-Fernandez, A., Gomez-Villalba, L.S., Rabanal, M.E., and Fort, R. (2017). New nanomaterials for applications in conservation and restoration of stony materials: a review. *Mater. construcc.* 67, 107.
 43. Reyes-Estebanez, M., Ortega-Morales, B.O., Chan-Bacab, M., Granados-Echegoyen, C., Camacho-Chab, J.C., Pereañez-Sacarias, J.E., and Gaylarde, C. (2018). Antimicrobial engineered nanoparticles in the built cultural heritage context and their ecotoxicological impact on animals and plants: a brief review. *Herit. Sci.* 6, 52.
 44. Brandi, C., and De Angelis, G. (1972). Carta di Restauro, 1972 (Circolare n° 117 del 6 aprile 1972). Circolare Ministero della Pubblica Istruzione, Roma, Italy.
 45. Zarzuela, R., Carbú, M., Gil, M.L.A., Cantoral, J.M., and Mosquera, M.J. (2017). CuO/SiO₂ nanocomposites: A multifunctional coating for application on building stone. *Mater. Des.* 114, 364–372.
 46. El-Feky, O.M., Hassan, E.A., Fadel, S.M., and Hassan, M.L. (2014). Use of ZnO nanoparticles for protecting oil paintings on paper support against dirt, fungal attack, and UV aging. *J. Cult. Herit.* 15, 165–172.
 47. Harandi, D., Ahmadi, H., and Mohammadi Achachluei, M. (2016). Comparison of TiO₂ and ZnO nanoparticles for the improvement of consolidated wood with polyvinyl butyral against white rot. *Int. Biodeterior. Biodegrad.* 108, 142–148.
 48. De Filpo, G., Palermo, A.M., Munno, R., Molinaro, L., Formoso, P., and Nicoletta, F.P. (2015). Gellan gum/titanium dioxide nanoparticle hybrid hydrogels for the cleaning and disinfection of parchment. *Int. Biodeterior. Biodegrad.* 103, 51–58.
 49. Fouda, A., Abdel-Maksoud, G., Abdel-Rahman, M.A., Salem, S.S., Hassan, S.E.-D., and El-Sadany, M.A.-H. (2019). Eco-friendly approach utilizing green synthesized nanoparticles for paper conservation against microbes involved in biodeterioration of archaeological manuscript. *Int. Biodeterior. Biodegrad.* 142, 160–169.
 50. Essa, A.M.M., and Khallaf, M.K. (2016). Antimicrobial potential of consolidation polymers loaded with biological copper nanoparticles. *BMC Microbiol.* 16, 144.
 51. Gámez-Espinoza, E., Barbería-Roque, L., Obidi, O.F., Deyá, C., and Bellotti, N. (2020). Antifungal applications for nano-additives synthesized with a bio-based approach. *Adv. Nat. Sci. Nanosci. Nanotechnol.* 11, 015019.
 52. Ditaranto, N., Loperfido, S., van der Werf, I., Mangone, A., Cioffi, N., and Sabbatini, L. (2011). Synthesis and analytical characterisation of copper-based nanocoatings for bioactive stone artworks treatment. *Anal. Bioanal. Chem.* 399, 473–481.
 53. Jia, M., Zhang, X., Weng, J., Zhang, J., and Zhang, M. (2019). Protective coating of paper works: ZnO/cellulose nanocrystal composites and analytical characterization. *J. Cult. Herit.* 38, 64–74.
 54. Luo, Z., Dong, K., Guo, M., Lian, Z., Zhang, B., and Wei, W. (2018). Preparation of zinc oxide nanoparticles-based starch paste and its antifungal performance as a paper adhesive. *Starch* 70, 1700211.
 55. Shariati, M., Mallakin, A., Malekmohammady, F., and Khosravi-Nejad, F. (2018). Inhibitory effects of functionalized indium doped ZnO nanoparticles on algal growth for preservation of adobe mud and earthen-made artworks under humid conditions. *Int. Biodeterior. Biodegrad.* 127, 209–216.
 56. Darcanova, O., Tamute, M., Beganskiene, A., and Kareiva, A. (2016). Synthesis of magnesium oxide nanoparticles via sol-gel method and hydrolysis and application for paper deacidification treatment. *Chemija* 27, 170–178.
 57. Zarzuela, R., Carbú, M., Gil, M.L.A., Cantoral, J.M., and Mosquera, M.J. (2019). Ormosils loaded with SiO₂ nanoparticles functionalized with Ag as multifunctional superhydrophobic/biocidal/consolidant treatments for buildings conservation. *Nanotechnology* 30, 345701.
 58. Gómez-Ortiz, N., De la Rosa-García, S., González-Gómez, W., Soria-Castro, M., Quintana, P., Oskam, G., and Ortega-Morales, B. (2013). Antifungal coatings based on Ca(OH)₂ mixed with ZnO/TiO₂ nanomaterials for protection of limestone monuments. *ACS Appl. Mater. Interfaces* 5, 1556–1565.
 59. Bellissima, F., Bonini, M., Giorgi, R., Baglioni, P., Barresi, G., Mastromei, G., and Perito, B. (2014). Antibacterial activity of silver nanoparticles grafted on stone surface. *Environ. Sci. Pollut. Res. Int.* 21, 13278–13286.
 60. Aslanidou, D., and Karapanagiotis, I. (2018). Superhydrophobic, superoleophobic and antimicrobial coatings for the protection of silk textiles. *Coatings* 8, 101.
 61. Becerra, J., Mateo, M., Ortiz, P., Nicolás, G., and Zaderenko, A.P. (2019). Evaluation of the applicability of nano-biocide treatments on limestones used in cultural heritage. *J. Cult. Herit.* 38, 126–135.
 62. Roveri, M., Gherardi, F., Goidanich, S., Gulotta, D., Castelvetro, V., Fischer, R., Winandy, L., Weber, J., and Toniolo, L. (2018). Self-cleaning and antifouling nanocomposites for stone protection: properties and performances of stone-nanomaterial systems. *IOP Conf. Ser.: Mater. Sci. Eng.* 364, 012070.
 63. Ditaranto, N., van der Werf, I.D., Picca, R.A., Sportelli, M.C., Giannossa, L.C., Bonerba, E., Tantillo, G., and Sabbatini, L. (2015). Characterization and behaviour of ZnO-based nanocomposites designed for the control of biodeterioration of patrimonial stoneworks. *New J. Chem.* 39, 6836–6843.
 64. Soria-Castro, M., De la Rosa-García, S.C., Quintana, P., Gómez-Cornelio, S., Sierra-Fernandez, A., and Gómez-Ortiz, N. (2019). Broad spectrum antimicrobial activity of Ca(Zn(OH)₃)₂·2H₂O and ZnO nanoparticles synthesized by the sol-gel method. *J. Sol Gel Sci. Technol.* 89, 284–294.
 65. Noeiaghaj, T., Dhami, N., and Mukherjee, A. (2017). Nanoparticles surface treatment on cemented materials for inhibition of bacterial growth. *Constr. Build. Mater.* 150, 880–891.
 66. Afsharpour, M., and Hadadi, M. (2014). Titanium dioxide thin film: environmental control for preservation of paper-art-works. *J. Cult. Herit.* 15, 569–574.
 67. La Russa, M.F., Ruffolo, S.A., Rovella, N., Belfiore, C.M., Palermo, A.M., Guzzi, M.T., and Crisci, G.M. (2012). Multifunctional TiO₂ coatings for cultural heritage. *Prog. Org. Coat.* 74, 186–191.
 68. Pinna, D., Salvadori, B., and Galeotti, M. (2012). Monitoring the performance of innovative and traditional biocides mixed with consolidants and water-repellents for the prevention of biological growth on stone. *Sci. Total Environ.* 423, 132–141.
 69. Aflori, M., Simionescu, B., Bordinu, I.-E., Sacarescu, L., Varganici, C.-D., Doroftei, F., Nicolescu, A., and Olaru, M. (2013). Silsesquioxane-based hybrid nanocomposites with methacrylate units containing titania and/or silver nanoparticles as antibacterial/antifungal coatings for monumental stones. *Mater. Sci. Eng. B* 178, 1339–1346.
 70. Gómez-Laserna, O., Lando, G., Kortazar, L., Martínez-Arkarazo, I., Monterrubio, I., Sevillano, E., Cardiano, P., and Olazabal, M.Á. (2019). Eco-friendly nanocomposite products based on BPA-free epoxy-silica hybrid materials for stone conservation. *Archaeol. Anthropol. Sci.* 11, 5799–5812.
 71. Essa, A.M.M., and Khallaf, M.K. (2014). Biological nanosilver particles for the protection of archaeological stones against microbial colonization. *Int. Biodeterior. Biodegrad.* 94, 31–37.
 72. Ruffolo, S.A., Ricca, M., Macchia, A., and La Russa, M.F. (2017). Antifouling coatings for underwater archaeological stone materials. *Prog. Org. Coat.* 104, 64–71.
 73. MacMullen, J., Zhang, Z., Dhakal, H.N., Radulovic, J., Karabela, A., Tozzi, G., Hannant, S., Alshehri, M.A., Buhé, V., Herodotou, C., et al. (2014). Silver nanoparticulate enhanced aqueous silane/siloxane exterior facade emulsions and their efficacy against algae and cyanobacteria biofouling. *Int. Biodeterior. Biodegrad.* 93, 54–62.
 74. Wang, H., Lu, G., Zhang, J., and Zheng, D. (2013). Multifunctional nanocomposites for paper conservation. *Stud. Conserv.* 58, 23–29.



75. De Filipo, G., Palermo, A.M., Tolmino, R., Formoso, P., and Nicoletta, F.P. (2016). Gellan gum hybrid hydrogels for the cleaning of paper artworks contaminated with *Aspergillus versicolor*. *Cellulose* 23, 3265–3279.
76. Gutarowska, B., Skora, J., Zduniak, K., and Rembisz, D. (2012). Analysis of the sensitivity of microorganisms contaminating museums and archives to silver nanoparticles. *Int. Biodeterior. Biodegrad.* 68, 7–17.
77. Pinzari, F., Pasquariello, G., and De Mico, A. (2006). Biodeterioration of paper: a SEM study of fungal spoilage reproduced under controlled conditions. *Macromol. Symp.* 238, 57–66.
78. Martino, P.D. (2016). What about biofilms on the surface of stone monuments? The Open Conference Proceedings Journal 6, 14–28, Proc. J. 7, 14–28.
79. Ortega-Morales, B.O., Reyes-Estebanez, M.M., Gaylarde, C.C., Camacho-Chab, J.C., Sanmartín, P., Chan-Bacab, M.J., Granados-Echegoyen, C.A., and Pereañez-Sacarias, J.E. (2018). Antimicrobial properties of nanomaterials used to control microbial colonization of stone substrata. In *Advanced Materials for the Conservation of Stone*, pp. 277–298.
80. Piñar, G., Sclocchi, M.C., Pinzari, F., Colaizzi, P., Graf, A., Sebastiani, M.L., and Sterflinger, K. (2020). The microbiome of Leonardo da Vinci's drawings: a bio-archive of their history. *Front. Microbiol.* 11, 593401.
81. Becerra, J., Ortiz, P., Zaderenko, A.P., and Karapanagiotis, I. (2020). Assessment of nanoparticles/nanocomposites to inhibit micro-algal fouling on limestone façades. *Build. Res. Inf.* 48, 180–190.
82. Goffredo, G.B., Accoroni, S., Totti, C., Romagnoli, T., Valentini, L., and Munafò, P. (2017). Titanium dioxide based nanotreatments to inhibit microalgal fouling on building stone surfaces. *Build. Environ.* 112, 209–222.
83. Fouda, A., Abdel-Maksoud, G., Abdel-Rahman, M.A., Eid, A.M., Barghoth, M.G., and El-Sadany, M.A.-H. (2019). Monitoring the effect of biosynthesized nanoparticles against biodeterioration of cellulose-based materials by *Aspergillus niger*. *Cellulose* 26, 6583–6597.
84. Lu, Z., Rong, K., Li, J., Yang, H., and Chen, R. (2013). Size-dependent antibacterial activities of silver nanoparticles against oral anaerobic pathogenic bacteria. *J. Mater. Sci. Mater. Med.* 24, 1465–1471.
85. Ruffolo, S.A., Macchia, A., La Russa, M.F., Mazza, L., Urzi, C., De Leo, F., Barberio, M., and Crisci, G.M. (2013). Marine antifouling for underwater archaeological sites: TiO₂ and Ag-doped TiO₂. *Int. J. Photoenergy* 2013, 1–6.
86. La Russa, M.F., Macchia, A., Ruffolo, S.A., De Leo, F., Barberio, M., Barone, P., Crisci, G.M., and Urzi, C. (2014). Testing the antibacterial activity of doped TiO₂ for preventing biodeterioration of cultural heritage building materials. *Int. Biodeterior. Biodegrad.* 96, 87–96.
87. Graziani, L., and D'Orazio, M. (2015). Biofouling prevention of ancient brick surfaces by TiO₂-based nano-coatings. *Coatings* 5, 357–365.
88. Pietrzak, K., Otlewska, A., Puchalski, M., Gutarowska, B., and Guimmet, P. (2016). Antimicrobial properties of silver nanoparticles against biofilm formation by *Pseudomonas aeruginosa* on archaeological textiles. *Appl. Environ. Biotechnol.* 1, 1–9.
89. Veltri, S., Sokullu, E., Barberio, M., Gauthier, M.A., and Antici, P. (2017). Synthesis and characterization of thin-transparent nanostructured films for surface protection. *Superlattices Microstruct.* 101, 209–218.
90. de Silva, M., and Henderson, J. (2011). Sustainability in conservation practice. *J. Inst. Conserv.* 34, 5–15.
91. Stuart, B. (2007). *Analytical Techniques in Materials Conservation* (John Wiley & Sons).
92. Festa, G., Andreani, C., Arcidiacono, L., Grazi, F., and Senesi, R. (2019). Neutron diffraction and (n, γ)-based techniques for cultural heritage. In *Nanotechnologies and Nanomaterials for Diagnostic, Conservation and Restoration of Cultural Heritage*, G. Lazzara and R. Fakhnullin, eds. (Elsevier), pp. 61–77.
93. Possenti, E., Conti, C., Gatta, G.D., Merlini, M., Realini, M., and Colombo, C. (2020). Synchrotron radiation μ X-ray diffraction in transmission geometry for investigating the penetration depth of conservation treatments on cultural heritage stone materials. *Anal. Methods* 12, 1587–1594.
94. Creagh, D. (2007). Synchrotron radiation and its use in art, archaeometry, and cultural heritage studies. In *Physical Techniques in the Study of Art, Archaeology and Cultural Heritage*, D. Creagh and D. Bradley, eds. (Elsevier), pp. 1–95.
95. Cotte, M., Genty-Vincent, A., Janssens, K., and Susini, J. (2018). Applications of synchrotron X-ray nano-probes in the field of cultural heritage. *C. R. Phys.* 19, 575–588.
96. Wolfrum, E.J., Huang, J., Blake, D.M., Maness, P.C., Huang, Z., Fiest, J., and Jacoby, W.A. (2002). Photocatalytic oxidation of bacteria, bacterial and fungal spores, and model biofilm components to carbon dioxide on titanium dioxide-coated surfaces. *Environ. Sci. Technol.* 36, 3412–3419.
97. Afsharpour, M., Rad, F.T., and Malekian, H. (2011). New cellulosic titanium dioxide nanocomposite as a protective coating for preserving paper-art-works. *J. Cult. Herit.* 12, 380–383.
98. Vidaković, A.M., Ranogajec, J.G., Markov, S.L., Lončar, E.S., Hirsberger, H.M., and Sever Škapin, A. (2017). Synergistic effect of the consolidant and the photocatalytic coating on antifungal activity of porous mineral substrates. *J. Cult. Herit.* 24, 1–8.
99. Rai, M., Yadav, A., and Gade, A. (2009). Silver nanoparticles as a new generation of antimicrobials. *Biotechnol. Adv.* 27, 76–83.
100. Gutarowska, B., Rembisz, D., Zduniak, K., Skóra, J., Szykowska, M., Gliścińska, E., and Koziróg, A. (2012). Optimization and application of the misting method with silver nanoparticles for disinfection of the historical objects. *Int. Biodeterior. Biodegrad.* 75, 167–175.
101. Nowicka-Krawczyk, P., Żelazna-Wieczorek, J., and Koźlecki, T. (2017). Silver nanoparticles as a control agent against façades coated by aerial algae—a model study of *Apatococcus lobatus* (green algae). *PLoS One* 12, e0183276.
102. Boccalon, E., Nocchetti, M., Pica, M., Romani, A., and Sterflinger, K. (2020). Hydrogels: a 'stepping stone' towards new cleaning strategies for biodeteriorated surfaces. *J. Cult. Herit.*
103. Espitia, P.J.P., Soares, N.d.F.F., Coimbra, J.S.d.R., de Andrade, N.J., Cruz, R.S., and Medeiros, E.A.A. (2012). Zinc oxide nanoparticles: synthesis, antimicrobial activity and food packaging applications. *Food Bioprocess Technol.* 5, 1447–1464.
104. Gómez-Ortiz, N.M., González-Gómez, W.S., De la Rosa-García, S.C., Oskam, G., Quintana, P., Soria-Castro, M., Gómez-Cornelio, S., and Ortega-Morales, B.O. (2014). Antifungal activity of Ca[Zn(OH)3]2·2H₂O coatings for the preservation of limestone monuments: an invitro study. *Int. Biodeterior. Biodegrad.* 91, 1–8.
105. Tang, Z.-X., and Lv, B.-F. (2014). MgO nanoparticles as antibacterial agent: preparation and activity. *Braz. J. Chem. Eng.* 31, 591–601.
106. Baglioni, P., Chelazzi, D., and Giorgi, R. (2015). Deacidification of paper, canvas and wood. In *Nanotechnologies in the Conservation of Cultural Heritage* (Springer), pp. 117–144.
107. Böhme, N., Anders, M., Reichelt, T., Schuhmann, K., Bridaroli, A., and Chevalier, A. (2020). New treatments for canvas consolidation and conservation. *Heritage Science* 8, 1–10.
108. Rogers, R.D., and Seddon, K.R. (2003). Chemistry, ionic liquids—solvents of the future? *Science* 302, 792–793.
109. Rajkowska, K., Koziróg, A., Otlewska, A., Piotrowska, M., Atrián-Blasco, E., Franco-Castillo, I., and Mitchell, S.G. (2020). Antifungal activity of polyoxometalate-ionic liquids on historical brick. *Molecules* 25, 5663.
110. Fernández Raga, M., and González Domínguez, J.M. (2020). Method for Protecting an Ornamental Object or Surface of Rocky Origin, Exposed to the Elements. 43.
111. Romano, I., Granata, G., Poli, A., Finore, I., Napoli, E., and Geraci, C. (2020). Inhibition of bacterial growth on marble stone of 18th century by treatment of nanoencapsulated essential oils. *Int. Biodeterior. Biodegrad.* 148, 104909.
112. Saada, N.S., Abdel-Maksoud, G., Abd El-Aziz, M.S., and Youssef, A.M. (2020). Evaluation and utilization of lemongrass oil nanoemulsion for disinfection of documentary heritage based on parchment. *Biotreat. Agric. Biotechnol.* 29, 101839.
113. Pankey, G.A., and Sabath, L.D. (2004). Clinical relevance of bacteriostatic versus bactericidal mechanisms of action in the treatment of

- Gram-positive bacterial infections. *Clin. Infect. Dis.* 38, 864–870.
114. Graybill, J.R., Burgess, D.S., and Hardin, T.C. (1997). Key issues concerning fungistatic versus fungicidal drugs. *Eur. J. Clin. Microbiol. Infect. Dis.* 16, 42–50.
 115. Stratton, C.W. (2003). Dead bugs don't mutate: susceptibility issues in the emergence of bacterial resistance. *Emerg. Infect. Dis.* 9, 10–16.
 116. Donlan, R.M. (2002). Biofilms: microbial life on surfaces. *Emerg. Infect. Dis.* 8, 881–890.
 117. Rabin, N., Zheng, Y., Opoku-Temeng, C., Du, Y., Bonsu, E., and Sintim, H.O. (2015). Agents that inhibit bacterial biofilm formation. *Future Med. Chem.* 7, 647–671.
 118. Li, X.H., and Lee, J.H. (2017). Antibiofilm agents: a new perspective for antimicrobial strategy. *J. Microbiol.* 55, 753–766.
 119. Krumbein, W.E. (2002). Patina and cultural heritage - a geomicrobiologist's perspective (Cracow: Cultural Heritage Research: a Pan European Challenge), pp. 16–18.
 120. Darouiche, R.O., Mansouri, M.D., Gawande, P.V., and Madhyastha, S. (2009). Antimicrobial and antibiofilm efficacy of triclosan and DispersinB combination. *J. Antimicrob. Chemother.* 64, 88–93.
 121. Donelli, G., Francolini, I., Romoli, D., Guaglianone, E., Piozzi, A., Ragunath, C., and Kaplan, J.B. (2007). Synergistic activity of dispersin B and cefamandole nafate in inhibition of staphylococcal biofilm growth on polyurethanes. *Antimicrob. Agents Chemother.* 51, 2733–2740.
 122. Izano, E.A., Wang, H., Ragunath, C., Ramasubbu, N., and Kaplan, J.B. (2007). Detachment and killing of *Aggregatibacter actinomycetemcomitans* biofilms by dispersin B and SDS. *J. Dent. Res.* 86, 618–622.
 123. Balouiri, M., Sadiki, M., and Ibrsouda, S.K. (2016). Methods for in vitro evaluating antimicrobial activity: a review. *J. Pharm. Anal.* 6, 71–79.
 124. Golus, J., Sawicki, R., Widelski, J., and Ginalska, G. (2016). The agar microdilution method – a new method for antimicrobial susceptibility testing for essential oils and plant extracts. *J. Appl. Microbiol.* 121, 1291–1299.
 125. Yamaguchi, H., Uchida, K., Nagino, K., and Matsunaga, T. (2002). Usefulness of a colorimetric method for testing antifungal drug susceptibilities of *Aspergillus* species to voriconazole. *J. Infect. Chemother.* 8, 374–377.
 126. Ericsson, M., Hanstorp, D., Hagberg, P., Enger, J., and Nyström, T. (2000). Sorting out bacterial viability with optical tweezers. *J. Bacteriol.* 182, 5551–5555.
 127. McDougald, D., Rice, S.A., Weichert, D., and Kjelleberg, S. (1998). Nonculturable: adaptation or debilitation? *FEMS Microbiol. Ecol.* 25, 1–9.
 128. Wilson, C., Lukowicz, R., Merchant, S., Valquier-Flynn, H., Caballero, J., Sandoval, J., Okuom, M., Huber, C., Brooks, T.D., Wilson, E., et al. (2017). Quantitative and qualitative assessment methods for biofilm growth: a mini-review. *Res. Rev. J. Eng. Technol.* 6.
 129. Prieto, B., Silva, B., and Lantes, O. (2004). Biofilm quantification on stone surfaces: comparison of various methods. *Sci. Total Environ.* 333, 1–7.
 130. Humbert, F., and Quilès, F. (2011). In-situ study of early stages of biofilm formation under different environmental stresses by ATR-FTIR spectroscopy. *Science against microbial pathogens: communicating current research and technological advances* 2, 889–895.
 131. Ivleva, N.P., Wagner, M., Horn, H., Niessner, R., and Haisch, C. (2008). In situ surface-enhanced Raman scattering analysis of biofilm. *Anal. Chem.* 80, 8538–8544.
 132. Efeoglu, E., and Culha, M. (2013). In situ monitoring of biofilm formation by using surface-enhanced Raman scattering. *Appl. Spectrosc.* 67, 498–505.
 133. Pinzari, F., Tate, J., Bicchieri, M., Rhee, Y.J., and Gadd, G.M. (2013). Biodegradation of ivory (natural apatite): possible involvement of fungal activity in biodeterioration of the Lewis Chessmen. *Environ. Microbiol.* 15, 1050–1062.
 134. Piñar, G., Piombino-Mascoli, D., Mainzer, F., Zink, A., and Sterflinger, K. (2013). Microbial survey of the mummies from the Capuchin Catacombs of Palermo, Italy: biodeterioration risk and contamination of the indoor air. *FEMS Microbiol. Ecol.* 86, 341–356.
 135. Szostak-Kotowa, J. (2004). Biodeterioration of textiles. *Int. Biodeterior. Biodegrad.* 53, 165–170.
 136. Breitbach, A.M., Rocha, J.C., and Gaylarde, C.C. (2011). Influence of pigment on biodeterioration of acrylic paint films in Southern Brazil. *J. Coat Technol. Res.* 8, 619–628.
 137. Cappitelli, F., and Sorlini, C. (2008). Microorganisms attack synthetic polymers in items representing our cultural heritage. *Appl. Environ. Microbiol.* 74, 564–569.

3. Objectives and Structure

The principal objective of this doctoral thesis was to study the synthesis and application of magnesium oxide nanoparticles (MgO NPs) and polyoxometalate-ionic liquids (POM-ILs) as antimicrobial coatings to prevent biodeterioration of heritage paper, natural stone and brick. The specific objectives have been the following:

1. Synthesise MgO NPs of average diameter 12 nm and study their antimicrobial activity against two model bacterial strains (*E. coli* and *B. subtilis*) and three fungi (*A. niger*, *C. cladosporioides* and *T. reesei*).
2. Study the application of MgO NPs on a variety of 18th century papers from the Archives of the Real Jardín Botánico in Madrid (Spain) and evaluated their ability to prevent microbial colonisation of the paper material.
3. Study the effect of the MgO NPs to prevent the degradation of the paper by inhibiting the cellulase activity of *A. niger* and *T. reesei*.
4. Synthesise three POM-ILs based on the monolacunary Keggin-type polyoxometalate ($[\alpha\text{-SiW}_{11}\text{O}_{39}]^{8-}$) combined with three different cations (tetraheptylammonium to obtain POM-IL 1, trihexyl tetradecyl ammonium to obtain POM-IL 2 and N, N, N', N'-tetramethyl-N'', N''-dioctylguanidinium to obtain POM-IL DOTMG-1) and study their antimicrobial activity against different microorganisms.
5. Use POM-IL 1 and 2 as antimicrobial coatings to limit the growth of lampenflora on chalk stone and compare the results with the commercial biocide Preventol RI80.
6. Assess the antifungal activity of POM-ILs as disinfectant agents to eradicate mould contamination inhabiting historical bricks.

These goals have been achieved in the articles used as compendium in this thesis. The thesis has been structured in three blocks, based on the six articles, as shown below in the **Thesis Structure Diagram** (Figure 6). The first block includes an overview of the principal and most effective nanomaterial types commonly used

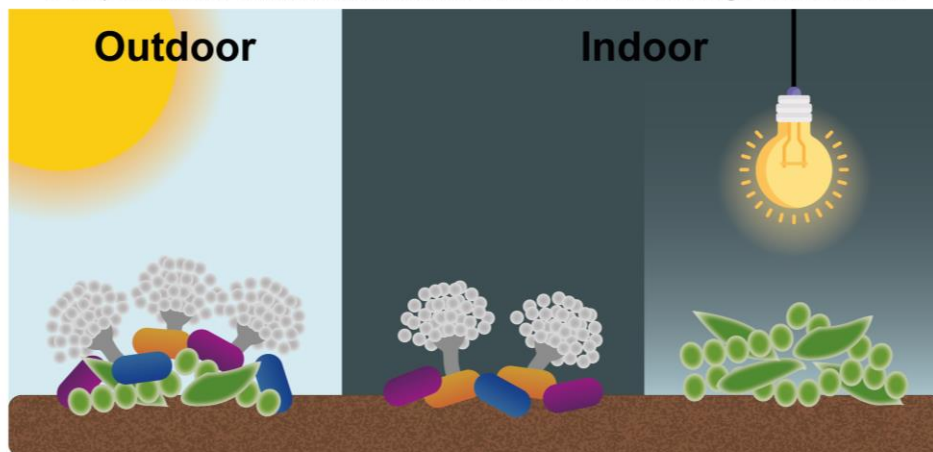
Objectives and Structure

in heritage to prevent biodeterioration, and an analysis of the most appropriate biochemical techniques that can be used to accurately evaluate their antimicrobial properties (published in **Article 1**). This first article, which constitutes a review article, is included in the Introduction of the thesis. The second block refers to the use of MgO NPs to prevent paper colonisation and degradation by microorganisms (**Articles 2 and 3**). **Article 2** probes the antibacterial activity of the MgO NPs against *E. coli* and *B. subtilis*, and **Article 3** reports how the antifungal and anticellulase activity of MgO NPs can be used to prevent paper degradation. The third block explores the use of POM-ILs as protective coatings to prevent colonisation of mineral-based building materials. The antimicrobial activity of POM-IL DOTMG-1 is reported in **Article 4**, where a comprehensive characterisation of the biocidal properties is carried out. The effectiveness of POM-IL 1 and 2 as antimicrobial coatings to limit the growth of lampenflora on chalks stones is reported in **Article 5**. Finally, in **Article 6** we studied the use of POM-ILs as disinfectants to eradicate mould contamination on historical bricks.

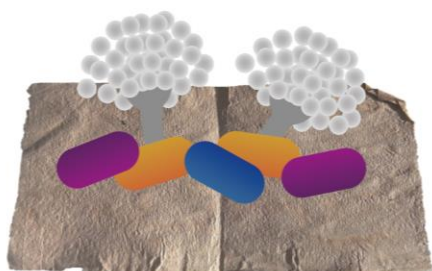
Biodeterioration

Article 1

Perspectives for antimicrobial nanomaterials in cultural heritage conservation



MgO NPs



Article 2

Protection of 18th century paper using antimicrobial nano-magnesium oxide

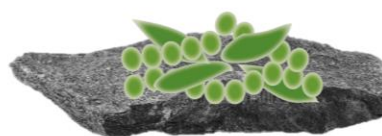
Article 3

Preventing fungal growth on heritage paper with antifungal and cellulase inhibiting magnesium oxide nanoparticles

POM-ILs

Article 4

Hybrid Antimicrobial Films Containing a Polyoxometalate-Ionic Liquid



Article 5

New protective coatings against lampenflora growing in the Pommery Champagne cellar



Article 6

Antifungal Activity of Polyoxometalate-Ionic Liquids on Historical Brick

Figure 6. Thesis Structure Diagram. Schematic summary of the organisation of the thesis in three blocks: the biodeterioration problem, the use of MgO NPs to prevent paper colonisation and degradation, and the use of POM-ILs to protect mineral-based building materials.

4. Methodology

4.1. Nanoparticle synthesis

4.1.1. Magnesium oxide nanoparticles (MgO NPs)

MgO nanoparticles were synthesized by sol-gel method through a modification of protocols already reported in literature.¹⁷³ Briefly, 3.6 mL of magnesium methoxide, $\text{Mg}(\text{OCH}_3)_2$, (2.4 mmol) were added to 20 mL of absolute ethanol under ultrasonication and subsequently 0.9 mL of water (50 mmol) were added to the mixture. The sol was left in the ultrasonic bath for 30 min. The mixture was then kept under gentle stirring for 36 h to facilitate gelation. The water/ethanol gel suspension was heated and stirred in an oil bath and underwent a progressive increase of the temperature from 70 to 90 °C over a period of 5 h. Then a fine magnesium dihydroxide powder was obtained by evaporating the solvent and finally this $\text{Mg}(\text{OH})_2$ powder was completely oxidised to MgO by heating at 600 °C for 30 minutes. Yield = 87 mg (dry particles).

4.1.2. Polyoxometalate (POM) and polyoxometalate-ionic liquid (POM-IL) syntheses

4.1.2.1. $\text{K}_8[\alpha\text{-SiW}_{11}\text{O}_{39}] \times 13\text{H}_2\text{O}$

The synthesis is a modification of the literature procedure.¹⁷⁴ Sodium metasilicate (0.50 g, 4.09 mmol) was dissolved at room temperature in 10 mL of distilled water and filtered (solution A). In a 100 mL beaker, sodium tungstate (8.26 g, 25.18 mmol) was dissolved in 3 mL of boiling distilled water (solution B). To the boiling solution B, an aqueous solution of HCl 4 mol L⁻¹ (8.25 mL) was added dropwise over 5 min with vigorous stirring in order to dissolve the local precipitate of tungstic acid. Solution A was added, quickly followed by addition of 2.50 mL of 4 mol L⁻¹ aqueous hydrochloric acid). The solution was kept boiling for 1 h. After cooling to room temperature, the solution was filtered. KCl (6.80 g, 91.2 mmol) was added to the stirred solution. The resulting white precipitate was collected on a sintered glass funnel (medium porosity), washed with two 20 mL portions of an aqueous KCl solution (1.0 M), then washed with 50 mL of cold water, and finally dried in air (yield: 5.10 g, 1.58 mmol, 69.7 % based on Si). FT-IR (cm⁻¹): 3420 (b), 2364 (w), 2037 (m), 1624 (m), 995 (s), 917 (s), 888 (vs), 793 (vs), 512 (s), 480 (s). ICP-AES (calculated values within brackets): Si 0.86 (0.87), W 64.31 (62.78).

4.1.2.2. Polyoxometalate-ionic liquids (POM-IL 1, POM-IL 2 and DOTMG-1)

The $K_8[\alpha\text{-SiW}_{11}\text{O}_{39}]$ POM was used to synthesize three different POM-ILs, by combining it with three different cations to obtain POM-IL 1, POM-IL 2 and POM-IL DOTMG-1.

For the synthesis of the three POM-ILs an established cation metathesis route^{136,138,148} was used to combine the acid-stable polytungstate anion $[\alpha\text{-SiW}_{11}\text{O}_{39}]^{8-}$ ¹⁷⁵ with two antimicrobial quaternary alkylammonium cations,¹⁷⁶ tetraheptyl ammonium (THA) ($(n\text{-C}_7\text{H}_{15})_4\text{N}^+$) and trihexyl tetradecyl ammonium (THTDA) ($(n\text{-C}_6\text{H}_{13})_3(\text{C}_{14}\text{H}_{29})\text{N}^+$), to give the respective POM-ILs **1** and **2**, and one quaternary alkylguanidinium cation (N, N, N', N'-tetramethyl-N'', N''-dioctylguanidinium, $(\text{C}_{21}\text{H}_{46}\text{N}_3)\text{Br}$) to give POM-IL DOTMG-1.^{138,177}

In a beaker, 1.00 equivalent of the POM $K_8[\alpha\text{-SiW}_{11}\text{O}_{39}] \times 13\text{H}_2\text{O}$ (2.5 g, 0.776 mmol) was dissolved in water (50 mL) and heated at 50 °C until complete dissolution. In another beaker, dissolve 8.00 equivalents of the cation (6.21 mmol: THA-Br (3.047 g), THTDA-Br (3.84 g) or DOTMG-Br (2.66 g)) in 80 mL of toluene for cations THA and THDTA and 80 mL of dichloromethane for cation DOTMG. To ensure high yield of the reaction, the cation was added in excess. Then the cation solution was slowly added to the POM solution and the mixture was stirred for 30 minutes at 50 °C. The mixture was then cooled at room temperature and transferred to a separation funnel and once the two phases were clearly separated, the organic phase—including the POM-IL—was extracted into a round bottom flask. The organic solvent was removed in a rotatory evaporator, and the product was isolated in the form of viscous liquid at room temperature.

The composition and purity of the compounds was verified by elemental analyses and FT-IR spectroscopy. Note that the three compounds are room temperature ILs, they are insoluble in water but show high solubility in a wide range of polar and unipolar organic solvents.

4.2. Microorganisms and growth conditions

A variety of microorganisms were used throughout this doctoral thesis, including:

Four bacterial strains, *Escherichia coli* DH5 α and VTEC (verotoxigenic *E. coli*) as Gram-negative models, *Bacillus subtilis* 1904-E and *Listeria monocytogenes* as Gram-positive models. Bacteria suspensions were stored in the appropriate

Methodology

culture media + 15 % glycerol at -80 °C and were thawed and subculture once prior to use. Before each assay, the bacterial suspension was subcultured in the appropriate liquid culture media and incubated for 24 hours.

Four moulds from the Colección Española de Cultivos Tipo (CECT) *Aspergillus niger* CECT 2088, *Cladosporium cladosporioides* CECT 2111, *Aspergillus ochraceus* CECT 2093 and *Penicillium expansum* CECT 2275 and the mould *Trichoderma reesei* RUT C-30, that was kindly provided by the CICS-UBI – Health Sciences Research Centre, University of Beira Interior, Portugal. Fungal spore suspensions were stored in 0.1% Tween 80, 20% glycerol at -80 °C prior to use. Before each assay, fungal cells were inoculated in the appropriate solid culture media and incubated for 4 days.

All bacterial and fungal growth conditions are summarised in Table 4.

Table 4. Microorganisms and growth conditions

Microorganism	Solid media	Liquid media	Incubation Temperature	Inoculum incubation
Bacteria				
<i>E. coli</i> DH5 α	TSA	LB	37 °C	24 hours
VTEC	MHA	LB	37 °C	24 hours
<i>B. subtilis</i>	TSA	NB	37 °C	24 hours
<i>L. monocytogenes</i>	BHIA	NB	37 °C	24 hours
Fungi				
<i>A. niger</i>	SDA	RPMI	35 °C	4 days
<i>T. reesei</i>	SDA	RPMI	35 °C	4 days
<i>C. cladosporioides</i>	SDA	RPMI	25 °C	4 days
<i>P. expansum</i>	PDA	YMB	25 °C	4 days
<i>A. ochraceus</i>	YMA	MEP	25 °C	4 days

4.3. Antimicrobial susceptibility testing

4.3.1. Microbial proliferation in presence of the antimicrobial compound

Bacterial and fungal growth was recorded measuring the optical density (OD) of the samples at 620 nm after 24 hours of incubation for the bacteria and after 48 hours for the fungi using a microplate reader (Thermo Scientific MULTISKAN GO). Results were compared with the OD variation of a positive control culture containing only bacteria or fungi and a negative control containing the compound in culture media. A negative control containing only culture medium was also added to verify the sterility of the medium. The modal value was chosen as the Minimal Inhibitory Concentration (MIC).

4.3.1.1. Antimicrobial activity of water-compatible compounds (MgO NPs)

Against bacteria. The antimicrobial activity of the MgO NPs was tested against two bacterial strains, *Escherichia coli* DH5-alpha (Gram-negative) and *Bacillus subtilis* 1904-E (Gram-positive). To determine the minimum inhibitory concentration (MIC) an inoculum of 1×10^7 CFU/mL obtained from an overnight culture was prepared (in the corresponding culture media two times concentrated) and added to a 96 well plate (100 μ L on each well). The MgO NPs were dispersed at different concentrations [0.2, 0.5, 1, 1.5, 2 and 3 mg/mL] in the corresponding medium for 30 min under ultrasonication. Then 100 μ L of the MgO NPs dispersion was added to each well and the bacterial growth was recorded by measuring the optical density (OD) of the samples at 620 nm over a period of 24 h. Results were compared with the OD variation of a control culture containing *E. coli* or *B. subtilis* without any NPs.

Against moulds. The antimicrobial activity of the MgO NPs was tested against three moulds, *A. niger*, *C. cladosporioides* and *T. reesei* and the minimum inhibitory concentration (MIC) was determined using a broth microdilution method according to the EUCAST guidelines.¹⁷⁸ The aerial part of the fungi was picked and re-suspended in distilled sterile water with 0.1% Tween to obtain a suspension of 10^6 conidia/mL, which was then diluted to 10^5 conidia/mL in distilled sterile water and added to a 96 well plate to a final concentration of 5×10^4 conidia/mL. Geometric two-fold dilutions of MgO NPs [0.09375, 0.1875, 0.375, 0.75, 1.5, 3, 6, 12 mg/mL] were made by dispersing them in RPMI and sonicated for 30 minutes before adding them to the 96 well-plate. Positive control contained only fungal inocula and culture media while the negative control contained only

Methodology

MgO NPs dispersed in culture medium. After an incubation period of 48 h, at 35 °C for *A. niger* and *T. reesei* and at 25 °C for *C. cladosporioides*, according to CECT recommendations, the MIC values were determined as the lowest MgO concentration able to inhibit fungal growth detectable to the naked eye.

4.3.1.2. Organic-soluble compounds (POM-ILs)

Against bacteria. The minimum inhibitory concentration (MIC) of the POM-ILs was determined against four bacterial strains (*E. coli* DH5 α , VTEC, *B. subtilis* and *L. monocytogenes*). An inoculum of 10⁷ CFU/mL was prepared in the appropriate liquid media and 100 μ L were added to a 96-well plate containing 98 μ L of the appropriate liquid media and 2 μ L of the POM-IL dissolved in DMSO (prepared 100 concentrated to obtain a final concentration of: 500, 250, 125, 62.5, 31.25, 15.62, 7.81, 3.91, 1.95 and 0.98 μ g/mL). Positive controls contained bacteria and liquid media while the negative controls contained only 2 μ L of the POM-IL dissolved in DMSO in culture media. The bacterial growth curves were recorded over a 24 h period by measuring the optical density (OD) of the samples at 620 nm. Results were compared with the OD variation of a control culture containing bacteria without POM-IL.

Against moulds. The determination of the minimum inhibitory concentration (MIC) of the POM-ILs against the four fungal strains (*A. niger*, *A. ochraceus*, *C. cladosporioides* and *P. expansum*) was performed using a broth microdilution method according to the European Committee on Antimicrobial Susceptibility Testing guidelines.¹⁷⁸ The aerial part of the fungi was recovered with a swab and re-suspended in distilled sterile water with 0.1% Tween to obtain a suspension of 10⁶ conidia/mL. This suspension was then diluted to 10⁵ conidia/mL in distilled sterile water. To determine the MIC, the POM-IL was dissolved in DMSO 100 times concentrated and then 2 μ L of each solution was added to each well of a 96-well plate, containing 98 μ L of culture media and 100 μ L of the 10⁵ conidia/mL suspension, to obtain the desired concentrations of the compound (2000, 1000, 500, 250, 125, 62.5, 31.25, 15.625 μ g/mL). Positive control contained only fungal spores and culture media while the negative control contained only DOTMG-1 dissolved in culture media. After an incubation period of 48 h, at 35 °C for *A. niger* and at 25 °C for *A. ochraceus*, *C. cladosporioides*, and *P. expansum*, according to CECT recommendations, the minimum inhibitory concentration (MIC) values were determined as the lowest POM-IL concentration able to inhibit fungal growth visible to the naked eye. The results were confirmed by measuring the

Methodology

optical density (OD) of the samples at 620 nm and comparing with the OD of the positive control.

4.3.2. Cell viability assays

4.3.2.1. Viability assay for prokaryotic cells (bacteria)

Cell viability was analysed using a Resazurin (7-Hydroxy-3H-phenoxazin-3-one 10-oxide) assay in a 96-well plate. A bacterial inoculum (1×10^7 CFU/mL) was incubated with different concentrations of the compound as in the “4.3.1. Microbial proliferation in presence of the antimicrobial compound” section and after 24 h of incubation 30 μ L of 0.1 mg/mL Resazurin prepared in the appropriate culture media were added to each well. The plate was then incubated at 37 °C for 1 h under stirring and the viability of the bacteria was determined by the Resazurin colour change. The blue Resazurin compound reduces to pink resofurin in presence of metabolically active cells, being an indicator of cell viability. Therefore, pink wells indicate presence of viably bacteria, while blue wells indicate a loss of metabolic activity, which is one of the first cascade events in the mechanism of cell death. The bacteria viability was also confirmed by subculturing 10 μ L of each well on solid media. After incubating the plates for 24 h at 37 °C, the MBC values obtained with Resazurin were compared with the lack of colonies on the solid media.

4.3.2.2. Viability assay for eukaryotic cells (moulds)

The MIC values obtained in **Section 4.3.1.** were further confirmed by measuring the OD₆₂₀ and fungal metabolic activity using XTT and menadione. The colorimetric assay based on XTT was carried out by adding 50 μ L of saline containing 1 mg of XTT/mL and 20.2 μ g of menadione/mL (previously dissolved in acetone at a concentration of 430 μ g/mL and then diluted 1/10 in saline) was added to each well to obtain a final concentration of 200 μ g of XTT/mL and 4.3 μ g of menadione/mL (25 μ M). Following an incubation period of 2 h in the dark to allow conversion of the XTT to its formazan derivative, the absorbance at 450 nm was measured.

4.3.3. Cell morphology damage study by microscopy

4.3.3.1. Environmental Scanning Electron Microscopy (ESEM)

The samples were visualised on a Quanta FEG-250 (FEI Company) field emission SEM for high-resolution imaging operating in ESEM mode using a GSED detector.

Bacteria and moulds incubated with MgO NPs. Bacterial cell morphology after incubation with the MgO NPs at MIC concentrations (1.5 mg/mL for *E. coli* and 0.75 mg/mL for *B. subtilis*) was studied by ESEM. All samples were analysed in a Quanta FE6-250 (FEI Company) field emission ESEM for high-resolution imaging working at low vacuum mode. A bacterial inoculum (1×10^7 CFU/mL) of *E. coli* and *B. subtilis* was supplemented with MgO NPs at a final concentration of 1.5 and 0.75 mg/ml, respectively. A sample without MgO NPs was also included in the assay as negative control. After 24 h of incubation the samples were washed twice in PBS, by centrifuging 10 min at 1.400 rpm (300 G) and resuspending the pellet in 1.5 mL of PBS. Then the bacteria were fixed by incubation in 1.5 mL of phosphate buffer 10 mM pH 7.2 + 2.5% glutaraldehyde for two hours in a wheel at room temperature. After two washed in 1.5 mL of PBS the samples were finally resuspended in distilled water.

The effect of the MgO NPs on moulds was also studied by ESEM. Briefly, the moulds were incubated on 2x2 cm 18th century paper samples previously coated with a 10 mg/mL MgO NP solution (dissolved in RPMI). After 2 weeks incubation the samples were fixed with cacodylate buffer 0.1 M and dehydrated with methanol. Then the samples were visualized on a Quanta FEG-250 (FEI Company) field emission SEM for high-resolution imaging working in ESEM mode using a GSED detector under high relative humidity conditions. A more detailed protocol is described in section 4.5.1.3.

Moulds incubated with POM-IL DOTMG-1. The effect of the POM-IL on fungal cells was also studied by Environmental Scanning Electron Microscopy (ESEM). First, a suspension of 10^5 conidia/mL was prepared and incubated 48 h with the compound at concentrations corresponding to the MIC and $\frac{1}{2}$ MIC values for each mould. After the incubation time, the samples were centrifuged at 10000 rpm for 10 min and the supernatant was discarded. The pellet, containing the mould, was resuspended into 1 mL of saline and filtered through a sterile polycarbonate membrane (13 mm diameter, pore size 0.22 μ m). Afterwards, the

Methodology

membranes containing the moulds were placed on a 12-well plate and fixed. The fixation protocol was performed as follows: the membranes were washed once with 2 mL of saline and then fixed with 2 mL of cacodylate buffer 0.1 M at 37 °C for 90 min. To dehydrate the moulds, increasing concentrations of methanol were used (5 min with methanol 30%, 5 min with methanol 50%, 5 min with methanol 70%, 10 min with methanol 100% and 5 min with methanol 100%).

4.3.3.2. Transmission Electron Microscopy (TEM)

TEM images were obtained in a TECNAI T20 electron microscope (FEI) operating at 60 kV.

Bacteria incubated with MgO NPs. Bacterial cell morphology after incubation with MgO NPs was also studied by TEM. The bacteria were incubated at sub-MIC concentrations (0.5 mg/mL and 1 mg/mL) with the MgO NPs for a 24 h period. A control of untreated bacteria was also added. After the incubation the bacteria cells were fixed, dehydrated, embedded in epoxy resin, and sliced into 10 µm slivers using a microtome.

Bacteria incubated with POM-IL. Bacterial morphology after the treatment with the POM-IL DOTMG-1 was studied by TEM. A 10⁷ CFU/mL bacterial suspension of each bacterium (*E. coli* DH5α, VTEC, *B. subtilis* and *L. monocytogenes*) was incubated with the compound at DOTMG-1 concentrations corresponding to the MIC and ½ MIC values for each of them. The assay was performed on a 12-well plate, where each well contained 1 mL of the bacteria suspension, 980 µL of liquid media and 20 µL of the compound at the corresponding concentration. Then, the plate was incubated at 37 °C for 24 h with agitation in an incubator. Fixation of these bacterial suspensions was carried out prior to TEM analysis to preserve the biological sample. The samples were centrifuged at 3000 rpm for 15 min and then the pellet was resuspended into 1.5 mL of sterile PBS. Another centrifugation at 3000 rpm for 15 minutes was carried out and the pellet containing the bacteria was resuspended in 1.5 mL of 2.5 % glutaraldehyde in phosphate buffer 10 mM at pH 7.2 for fixation of the cells. The samples were incubated for 2 h on a Ferris wheel and then washed once with 1 mL of sterile phosphate-buffered saline (PBS) at pH 7.4 and three times with sterile distilled water with centrifugations at 3000 rpm for 15 min between washes for cell recovery and to remove excess glutaraldehyde. The pellets were resuspended in 1.5 mL of sterile MilliQ water and kept at 4 °C for further analysis. 2 µL of each sample were deposited on a

Methodology

carbon-coated copper grid (Cu200 mesh) and left to dry at room temperature overnight.

4.3.3.3. Optical microscopy

Cell viability was also analysed by epifluorescence microscopy with a LIVE/DEAD® fluorescence assay. A bacterial inoculum (1×10^7 CFU/mL) of *E. coli* (in LB media) and *B. subtilis* (in NB media), was supplemented with MgO NPs at a final concentration of 1.5 mg/mL. A sample without MgO NPs was also included in the assay as negative control. After 24 hours of incubation at 37 °C with stirring, the solutions were stained with the LIVE/DEAD® BacLight™ Bacterial Viability Kit in a 1:500 dilution and incubated for 15 minutes in the dark. Then 10 µL of the stained samples were extended over a slide and the bacteria were visualized with a Nikon ECLIPSE Ti epifluorescence microscope.

4.4. Coatings on real heritage samples

4.4.1. XVIII Century paper coating with MgO NPs

Four different paper samples from the last third of the 18th century were used in this study. The papers were obtained from the leftovers of the Herbarium sheets conserved in the Archives of the Real Jardín Botánico (CSIC) in Madrid, Spain, and differ in colour, thickness, and roughness. For the antibacterial assays there were used paper 1, 2 and 3. Paper numbers 1 and 3 were used to keep dried plants, whereas paper number 2 was the usual text document accompanying the plant samples. Paper 4, also used to keep dried plants, was used in the antifungal experiments. To avoid contamination the papers were sterilized in an autoclave before any assay performed with them.

To do the coating the MgO NPs were dispersed in sterile distilled water at a final concentration of 10 mg/mL and were applied over the paper samples in small drops using a micropipette. Then the coated papers were sterilized under UV for 15 min and they were allowed to dry in a sterile environment. This process was performed twice on each paper to ensure a homogenous coating of MgO NPs. A control paper without coating was included in all the assays. This control was treated in the same way, using a sterile distilled water instead of a MgO NPs solution.

4.4.1.1. Colorimetric measurement after the MgO NPs coating

Colour change of the 18th century papers after the coating with a 10 mg/mL MgO NPs solution (in distilled water) was measured with a Chroma Meter CR-400 (Konica Minolta) during 4 days post-application of the MgO NP coating. Measurements were performed on two paper samples (4x4 cm) before and after the coating, measuring five points for each paper to account for sample heterogeneity. The result of the chromatic change (ΔE^*_{ab}), given by the three colorimetric coordinates (L^* , a^* , b^*), was determined by the following equation, where ΔE^*_{ab} represents the total colour difference, ΔL^* the lightness difference, Δa^* the difference in redness or greyness and Δb^* denotes blueness-yellowness differences:

$$\Delta E = \sqrt{\Delta L^2 + \Delta a^2 + \Delta b^2}$$

4.4.1.2. Paper coating visualization by ESEM

The homogeneity of the MgO NPs coating over the paper samples was analysed by electron microscopy in a Quanta FE6-250 (FEI Company) field emission ESEM for high-resolution imaging working at low vacuum mode.

4.4.1.3. Inductively coupled plasma mass spectrometry (ICP–MS)

The amount of MgO NPs on the paper after the coating was analysed by ICP–MS. 1x1 cm squares of 18th century paper were coated with 10 mg/mL MgO NPs solution (uncoated samples were used as a control). All the paper samples were digested in 100 μ L of piranha solution for 15 minutes at room temperature and then 300 μ L of *aqua regia* were added and incubated for 2 hours at room temperature followed by 15 minutes at 60 °C. Afterwards, the samples were diluted in Milli-Q water to a final volume of 20 mL. ICP–MS measurements were carried out with a quadrupole Agilent 7500 series ICP–MS instrument (Agilent Technologies, CA, USA), equipped with a Babington nebulizer and a double pass spray chamber. Magnesium quantification was performed using a calibration curve ranging from 1 and 1000 ng/g (ppb) Mg (I) in ultra-pure water. The data acquisition parameters for both calibration curve and samples were set to the single particle mode for detecting the presence of magnesium (^{24}Mg , ^{25}Mg , and ^{26}Mg), in a full quantitative mode, with 1 point per spectral peak, an integration time of 0.2 s per point and 10 repeats per sample, giving a total acquisition time

Methodology

of 40.2 s. Digested paper and paper with MgO NPs samples were measured in triplicate and quintuplicate, respectively. The control paper samples were diluted 1/10 and the MgO coated paper samples were diluted 1/100 to adjust the concentration to the calibration curve.

4.4.2. Stone surfaces coated with POM-ILs

Two mineral-based building materials were used to test the antimicrobial activity of the POM-IL 1 and POM-IL 2.

Pommery cellar stones. Chalky stone from the Pommery Champagne cellar was used to study the growth inhibition of lampenflora on POM-IL coated stones. The stone is a homogeneous coccolithic limestone with a high porosity (40.4 %), with 98.7 % of micropores with a diameter less than 1 μm and most of them at 0.25 μm . Stone slabs (5 x 5 x 1 cm) were coated with different concentrations of the POM-ILs (0.1, 0.2 and 0.4 g) by brush, and the quantity of biocide applied on each stone sample has been controlled by weighing. Then the stone samples were let 48 h drying and weighed again to calculate the effective quantity of coating remained on stone for the biocidal assays.

19th century historical bricks. The POM-ILs were also studied as disinfectant agents on already contaminated bricks samples (5 x 2 x 1 cm³), that came from the demolition of a 19th century residential building. The antifungal activity of the POM-ILs was examined against a mixed culture of moulds (*Engyodontium album*, *Cladosporium cladosporioides*, *Alternaria alternata* and *Aspergillus fumigatus*) isolated from the surfaces of the historical brick barracks at the Auschwitz II-Birkenau State Museum in Oświęcim, Poland. The 19th century brick samples were inoculated with the mixed culture of moulds and afterwards the POM-ILs were spray-coated up to three times to study the disinfectant effect.

4.4.3. DOTMG-1 films

POM-IL DOTMG-1 was used to study the antimicrobial activity when embedded on polymethylmetacrylate (PMMA) at different ratios. There were prepared four films based on the different POM-IL/PMMA weight ratios: film A (0/100), film B (20/80), film C (35/65) and film D (50/50). A PMMA solution (100 mg/mL in toluene) was mixed with the POM-IL DOTMG-1 at the corresponding amounts to achieve the desired concentrations for each film. Then, the POM-IL/PMMA solution was spin-coated on a silicon wafer.

4.5. Determination of the antimicrobial activity *in situ*

4.5.1. MgO NPs paper coating antimicrobial activity evaluation

A modified Kirby-Bauer disk diffusion technique was chosen as the first assay to determine the release capacity of the papers and the diffusion ability of the particles. The 18th century papers were cut in 6mm discs, and they were impregnated with a 15 mg/mL MgO NPs solution. Another 18th century paper of each kind of paper was impregnated with an antibiotic solution (100 µg/mL Ampicillin). The diffusion ability of the particles was tested by impregnating Whatman® Antibiotic Assay Discs (6 mm) with the 15 mg/mL MgO NPs solution. As a positive control, a Whatman® Disc was impregnated with the Ampicillin solution (100 µg/mL) and, as a negative control, a non-impregnated Whatman® Disc were added to the assay. All the paper samples and the Whatman® Discs were placed in an agar plate previously inoculated with an *E. coli* lawn (10⁷ CFU/mL). The plate was incubated at 37 °C for 24 h and the inhibition halo was measured.

4.5.1.1. MgO NPs *in situ* activity against *E. coli*

To test the antimicrobial activity of the MgO NPs coating, the papers were cut in 4x4 cm squares and placed in a sterile Petri dish. Each paper was impregnated with 500 µL of a 10 mg/mL MgO NPs solution as described in **Section 4.4.1**. Once the papers were dry, an *E. coli* solution (10⁴ CFU/mL) was sprayed, twice, over the paper samples with MgO NPs and over the negative control samples (papers without MgO NPs). To detect the bacterial growth over the paper samples TBX agar was used, which contains X-β-D-glucuronide, a chromogenic compound hydrolyzed by the β-glucuronidase, an *E. coli* enzyme, which makes the *E. coli* colonies turn green-blue on an agar plate. A first layer of TBX agar was added over all the paper samples covering all the surface of the paper. When the medium solidified, a second layer was added. The papers were then incubated for 48 h at 37 °C whereupon the bacterial colonies were clearly observable with the naked eye.

4.5.1.2. Antifungal activity under optimal growth conditions

The 18th century paper samples were cut in 5 cm diameter discs and placed into a 5.5 cm Petri dish, where were then impregnated twice with 800 µL of a 10 mg/mL MgO NPs solution (as described in **Section 4.4.1**. When the papers were

Methodology

completely dry, 500 μL of a fungi inoculum (10^3 conidia/mL, in distilled water) was added to the coated papers and over a positive growth control paper sample without MgO NPs. Then, SDA culture media was added until the paper was completely covered. Plates were incubated at 35 °C for *A. niger* and *T. reesei* and at 25 °C for *C. cladosporioides*. The fungal growth was monitored for 6 days.

4.5.1.3. *In situ* antifungal activity under more realistic growth conditions

The 18th century paper samples were cut in 2x2 cm squares, placed into a 6 well plate and impregnated twice with 100 μL of a 10 mg/mL MgO NP solution (dissolved in RPMI) using a micropipette. When the papers were completely dry, 100 μL of a fungi inoculum (10^3 conidia/mL in RPMI) was added to the coated papers and over a positive growth control paper sample without MgO NPs. Afterwards, plates were incubated in a humidity chamber at the respective temperature for each fungus. Fungal growth was monitored during 2 weeks. In order to visualize the samples with ESEM, the papers were washed with 2 mL of saline and fixed with a 2 mL of cacodylate buffer 0.1 M for 1 h and 30 minutes at 37 °C. Then the samples were dehydrated with methanol (5 min with methanol 30%, 5 min with methanol 50%, 5 min with methanol 70%, 10 min with methanol 100% and 5 min with methanol 100%) and kept at room temperature. The samples were visualized on a Quanta FEG-250 (FEI Company) field emission SEM for high-resolution imaging working in ESEM mode using a GSED detector under high relative humidity conditions.

4.5.1.4. Evaluating the cellulose degradation capacity of moulds

Inhibition of cellulase activity by the MgO NPs. To study the effect of the MgO NPs in the cellulase activity of the two cellulase producing moulds *A. niger* and *T. reesei*, cellulase extracts from these two moulds were incubated with different MgO NPs concentrations (1/16, 1/8, 1/4, 1/2, 1x and 2x MIC) for 1 h at 37 °C with agitation. After incubation, 1 mL of cellulase solutions was mixed with 4 mL of a cellulose 5% (w/v) solution and incubated at 37 °C for 120 min with vigorous stirring to determine the cellulase activity. All the reagents were prepared in 50 mM sodium acetate buffer pH 5. Cellulase activity, expressed as enzymatic units (one unit (U) will liberate 1.0 μmole of glucose from cellulose in one hour at pH 5 at 37 °C), was determined by quantifying the release of reducing sugars produced after the incubation period as reported in the DNS method, using glucose as standard.¹⁷⁹

Inhibition of fungal adhesion to the paper. To verify the anti-cellulase activity of the MgO NPs, *A. niger* and *T. reesei* were forced to use the cellulose from the 18th century paper in this assay. The 18th century paper samples were incubated in 10 mL fermentation medium containing 1 mL of an *A. niger* and *T. reesei* inoculum (10^5 conidia/mL, prepared in liquid medium) and MgO NPs at the 1/4, 1/2, 1x and 2x MIC value which corresponds to the following concentrations: 1.5, 3, 6, 12 mg/mL for *A. niger* and 0.75, 1.5, 3, 6 mg/mL for *T. reesei*. Three paper samples of 1x3 cm were used for each sample, in addition with a positive growth control sample without MgO NPs and a negative control without fungi. Samples were incubated four days at 35 °C with agitation. After incubation, paper samples were removed from the culture, washed with sterile saline solution and dried at 50 °C until a constant weight was achieved.

4.5.2. POM-ILs coating on stone surfaces

4.5.2.1. Pommery chalk slabs

The antimicrobial activity of POM-IL 1 and POM-IL 2 against algae and cyanobacteria was studied on chalky stone slabs. There were performed four biocidal assays to establish the amount of POM-IL necessary to avoid the biocolonization of the stones by phototrophic microorganisms, study the coating effect when applied on wet stones and the ability to prevent re-colonizations. One cyanobacteria (*Timaviella* sp.) and three green algae (*Diplosphaera* sp., *Chromochloris zofingiensis* and *Pseudostichococcus monallantoides*), isolated from the bas-reliefs of the Pommery Champagne cellar, were used in this study. The four biocidal assays are summarized in Table 5.

Table 5. Summary of the conditions of the four biocidal assays

Assay	Aim of the assay	Stone	Inoculated microorganisms	Incubation conditions	Concentration	
					POM-ILs	PR80
1	Evaluation of the biocidal coatings	Dry	<i>Chromochloris</i> sp.	7 weeks	0.1 g	0.2 g
			<i>Pseudostichococcus</i> sp.	20°C 80 % R.H.	0.2 g	
2	Optimize the biocidal coating	Dry	<i>Pseudostichococcus</i> sp.	5 weeks 20°C 80 % R.H.	0.4 g	0.4 g

3	Effectiveness of			5 weeks	0.1 g	
	the coating on	Wet	<i>Pseudostichococcus</i> sp.	20°C	0.2 g	0.2 g
	wet stones			80 % R.H.	0.4 g	0.4 g
4	Biocidal effect		<i>Pseudostichococcus</i> sp.	5 weeks	0.1 g	
	after re-	Wet	<i>Diplosphaera</i> sp.	20°C	0.2 g	0.4 g
	inoculation		<i>Timaviella</i> sp.	80 % R.H.	0.4 g	

4.5.2.2. 19th century historical bricks

The antifungal activity of the POM-IL 2 and its homologue formed with the full kegging structure, [SiW₁₂O₄₀][THTDA]₄), was studied by ESEM analysis of the contaminated bricks after one, two and three applications of the POM-ILs. Briefly, the 19th century brick samples were inoculated with 10⁶ CON/mL of the mixed culture of moulds (*E. album*, *C. cladosporioides*, *A. alternata* and *A. fumigatus*) and after three weeks incubation they were spray-coated with the POM-ILs up to three times. The antifungal activity of POM-ILs was evaluated according to a calibration scale and the moulds morphology after the treatment with the POM-ILs was studied on a Quanta FEG-250 (FEI Company, Hillsboro, OR, USA) field emission SEM for high-resolution imaging working in ESEM mode, using a gaseous secondary electron detector (GSED) detector under high relative humidity conditions.

4.5.2.3. Surface antimicrobial activity of the POM-IL DOTMG-1

The surface antimicrobial activity of the POM-IL DOTMG-1 was studied by two different assays. First, the POM-IL was applied as a coating on 2 × 2 cm sterilised glass slides, using a modified Japanese Industrial Z 2801 Standard (Reference number: JIS Z 2801: 2000 (E); ICS 07.100.10; 11.100), and was tested against *E. coli* DH5α, VTEC, *B. subtilis* and *L. monocytogenes*. The POM-IL was dissolved in acetone and applied over the glass slides to obtain a final concentration of 1, 2, 4, 8 and 16 µg cm⁻². The coated glass slides were dried under a UV light for 20 min to avoid any external contamination and then 50 µL of a 10⁷ CFU/mL bacterial suspension were added over the coated slides and over a control slide without coating. A coverslip was put on top of each sample to ensure comparable contact surfaces. The samples were incubated at 37 °C for 24 h in a humidity chamber and after the incubation time the bacteria were extracted by vortexing the samples inside a 50 mL falcon tube with 20 mL of liquid media for 1 min. The liquid media containing the extracted bacteria was then diluted and sown on the appropriate solid media for each microorganism. The colonies grown on the

Methodology

plates were counted after incubation at 37 °C for 24 h. The percentage of bacterial growth reduction was obtained by comparing the number of colonies present in the plates from the coated samples and the colonies present in the plates from the control sample.

The surface antimicrobial activity of the was also studied embedding the POM-IL in PMMA spin-coated on a silicon wafer. The four films (A, B, C and D) were tested against *E. coli* DH5 α , *B. subtilis* and *L. monocytogenes*. First, the films were placed in a 6-well plate and inoculated with 50 μ L of a 10⁶ CFU/mL inoculum of the different bacteria. After 4 h incubation at 37 °C in a humidity chamber, the films were rinsed with saline, and the rinsed suspension was plated on the appropriated solid media, which was incubated 24 h at 37 °C to count the colonies. After a final wash with sterile distilled water, the films incubated with *L. monocytogenes* were fixed with glutaraldehyde (due to the pathogenicity of these bacteria) and all the film samples were visualized on a Quanta FEG-250 (FEI Company) field emission SEM for high-resolution imaging working in ESEM mode using a GSED detector. Due to the repeated washes (specially for the fixed sample), almost all the bacteria were removed from the surface of the silicon wafer.

5. Results and Discussion

5.1. MgO NPs to prevent heritage paper colonization

Magnesium-oxide nanoparticles (MgO NPs) are a good alternative to other traditional chemicals to prevent the biodeterioration due to their low-cost production, low eco-toxicity and low cytotoxicity.^{123,180} Until recently, their exact mechanism of action was still unknown, and was cited to arise from the production of reactive oxygen species (ROS), that generates oxidative stress and can lead to lipid peroxidation on the bacteria membrane, and interaction with the cell wall of microorganisms.¹¹⁵ Furthermore, their ability to increase the pH may cause an alkaline effect that helps to induce cell death.¹¹⁶

Here we explore the synthesis and antimicrobial activity of MgO NPs along with their potential mechanisms of action and evaluate their activity as protective coatings to prevent the bio-colonization and -degradation of paper heritage.

5.1.1. Synthesis and characterization of MgO NPs

The MgO NPs were synthesized using a sol-gel method, which was selected due to the reproducibility, scalability, simplicity, and low cost of the synthesis, which also guarantees a degree of control over the diameter of the nanoparticles. Briefly, magnesium methoxide, $\text{Mg}(\text{OCH}_3)_2$, was used as the precursor, and after addition of ethanol and water under ultrasonication for 30 min the sol was formed. After correct gelation, the mixture was heated and stirred in an oil bath, then the solvent was evaporated and a fine magnesium dihydroxide powder was obtained. The MgO NPs were obtained by oxidation of the $\text{Mg}(\text{OH})_2$ powder at 600 °C for 30 minutes.

The MgO NPs were deposited on a TEM grid and after solvent evaporation they were analysed by BF-TEM. Their size and shape were determined by measuring the diameters of the nanoparticles in the TEM images. As observed in Figure 7, the mean diameter of the particles is 12 nm, in a range that goes from 8 to 20 nm. There were also observed some aggregates of 5–10 NPs (100 nm in diameter), which can come from the sample preparation.¹⁸¹

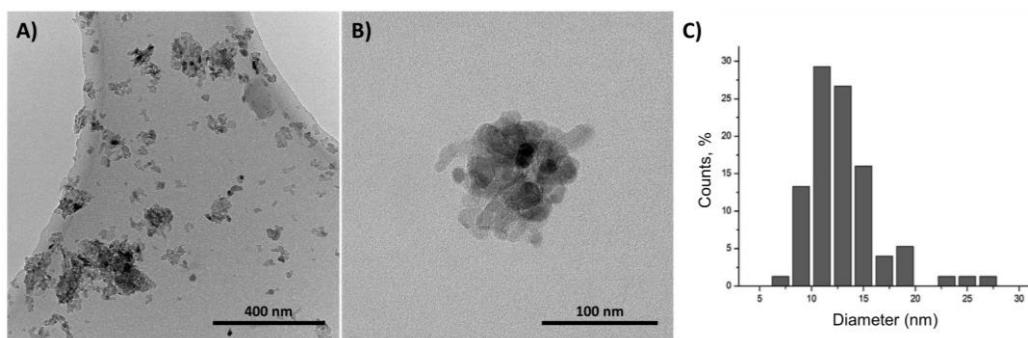


Figure 7. BF-TEM images of MgO NPs ((B) is a magnification of an area selected in (A) where an aggregate can be observed) and estimated size dispersion histogram (C).

5.1.2. Antimicrobial activity of the MgO NPs

The antimicrobial activity of the MgO NPs was studied against several bacterial and fungal strains using standardized protocols to determine the MIC and the MBC of the particles. It is crucial to determine the corresponding MIC and MBC values before using the nanoparticles as a preventive coating on heritage paper because the concentration which needs to be applied must first be determined. In addition, the effect of the MgO NPs on the bacterial morphology was studied by electron microscopy techniques.

5.1.2.1. Microbial proliferation and viability in presence of the MgO NPs

The antimicrobial effect of the MgO NPs was determined against two bacterial strains (*Escherichia coli* and *Bacillus subtilis*) and three moulds (*Aspergillus niger*, *Cladosporium cladosporioides* and *Trichoderma reesei*) in a microbial proliferation assay, complemented with a colorimetric viability assay to corroborate the antimicrobial concentrations. We chose *E. coli* as Gram-negative model and *B. subtilis* as Gram-positive model due to their high relevance in the research field. *E. coli* represents the most studied organism on the planet,¹⁸² and *B. subtilis* has served as a model microorganism for many decades, and is usually considered as the Gram-positive equivalent of *E. coli*.¹⁸³ Besides their relevance in the research field, both bacterial genera have been found colonising heritage paper due to cross-contamination during restoration works.¹¹ The three fungal strains were chosen as representative contaminating microorganisms found in heritage artefacts, especially *A. niger* and *T. reesei*, that were chosen not only for their prevalence but also for their cellulase activity, which leads into the degradation of the paper fibres.^{20,184–186}

Results and Discussion

A broth microdilution assay was used to determine the minimum inhibitory concentration (MIC) of the MgO NPs against the model bacterial strains. Briefly, an inoculum of each bacterium, in their appropriate culture media, was incubated with a dispersion of the MgO NPs at final concentrations ranging from 0.1, 0.25, 0.5, 0.75, 1 and 1.5 mg/mL. After the incubation time (24 h at 37 °C), the optical density of the samples was measured to study the cell growth, which is determined by the culture turbidity (Figure 8). The proliferation of *E. coli* and *B. subtilis* were both affected by the MgO NPs. *B. subtilis* being the most susceptible strain, which possessed a MIC corresponding to 0.75 mg/mL of the MgO NPs dispersion, whereas for *E. coli* 1.5 mg/mL was required to obtain full inhibition (Table 6). These results are reasonably close to the data reported in the literature, where 20-25 nm MgO NPs present antibacterial activity in a range between 0.5 and 1 mg/mL. The differences in the MIC value could be explained due to the differences in the particles size and the initial inoculum of bacteria.^{113,187} The MIC results were complemented with a resazurin cell viability assay, in which the minimum bactericidal concentration (MBC) was obtained, matching the MIC values (Figure 8). The bactericidal concentration was then confirmed by sub-culturing 10 μ L of the culture on solid media.

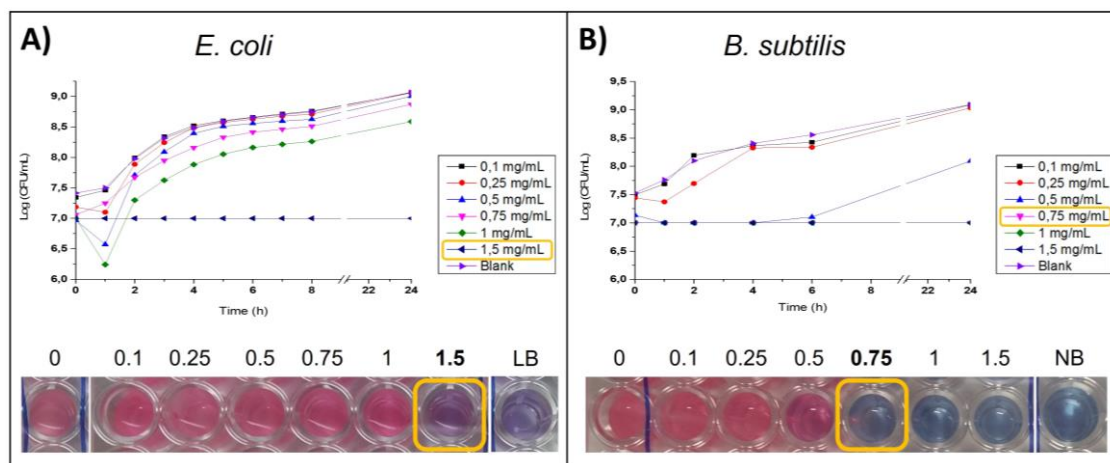


Figure 8. *E. coli* (A) and *B. subtilis* (B) growth curves starting from a concentration of 10^7 CFU/mL in LB (or NB) medium at different MgO NPs concentrations, and a control sample (blank) without MgO NPs. The minimum inhibitory concentration (MIC) was 1.5 mg/mL for *E. coli* and 0.75 mg/mL for *B. subtilis*. The minimum bactericidal concentration (MBC) was confirmed with a resazurin colorimetric cell viability assay, obtaining the same values. Antibacterial assays were repeated on several occasions and replicated a total of six times to calculate mean values and associated standard deviations.

To study the antifungal activity a broth microdilution assay was also used to determine the MIC.¹⁷⁸ As in the antibacterial assay, an inoculum of fungal spores

Results and Discussion

was incubated with different concentrations of the MgO NPs and after 48 h of incubation (at the appropriate temperature for each mould) the MIC was determined visually (Table 6). The optical density value was also obtained, and a colorimetric cell viability assay (XTT) was carried out to confirm these results. *T. reesei* was the most susceptible mould to the MgO NPs, with the lowest MIC value equal to 3 mg/mL, followed by *A. niger* (6 mg/mL), while the most resistant mould was *C. cladosporioides* (MIC equal to 12 mg/mL) (Table 6). The amount of MgO NPs needed to inhibit the fungal growth was marginally higher than those reported in the literature. For example, MIC values for *A. niger* have been reported as between 1 and 4 mg/mL.^{106,188} Importantly, the most susceptible moulds are those which can cause most damage to the paper (the cellulase producing *A. niger* and *T. reesei*), indicating that a relatively low concentration of MgO NPs can be used for the paper coating.

Table 6. Minimum Inhibitory Concentration (MIC) of the MgO NPs (in mg/mL) against the bacterial and fungal strains.

Microorganism		MIC in mg/mL
Gram-negative bacteria	<i>E. coli</i>	1.5
Gram-positive bacteria	<i>B. subtilis</i>	0.75
Moulds	<i>A. niger</i>	6
	<i>T. reesei</i>	3
	<i>C. cladosporioides</i>	12

5.1.2.2. Study of the bacterial cell viability and morphology after treatment with the MgO NPs

In order to complement the quantitative results obtained in the microbiological assays, the viability and the bacterial cell morphology was also studied by microscopy. The bacterial viability of *E. coli* and *B. subtilis* after incubation with the MgO NPs was studied using a commercial Live/Dead assay. The samples were stained with a LIVE/DEAD® BacLight™ Bacterial Viability Kit and then visualized with an epifluorescence microscope. The LIVE/DEAD® BacLight™ Bacterial Viability kit is conformed by two dyes, the green one, that enters both dead and alive cells, and the red one, that only enters dead cells with a disrupted membrane, allowing the differentiation between alive cells (in green) and dead

Results and Discussion

cells (in red). Although no quantification of alive and dead cells could be performed due to convergence of the two fluorescent channels, in the Figure 9A can be observed how the samples incubated with the MgO NPs present lower bacterial density than the bacterial culture without the exposure to the particles, what corroborated the antiproliferative effect of these nanoparticles.

Once the minimum inhibitory concentration (MIC) for each bacterial strain had been established, both bacteria were incubated with the MgO NPs at their respective MICs and visualized by Environmental Scanning Electron Microscopy (ESEM). With this technique we can visualize the morphology and health of the bacteria cells after the treatment with the nanoparticles, to obtain visual indication on the effect of the nanoparticles. The ESEM images show how both bacterial strains are affected after incubation with the MgO NPs (Figure 9B). The cells incubated with these particles showed evidence of stress and damage including general loss of cell shape, cell membrane damage and leakage of cytoplasmic material. Furthermore, *B. subtilis* showed signs of sporulation, which is an indicator of cell stress.¹⁸⁹

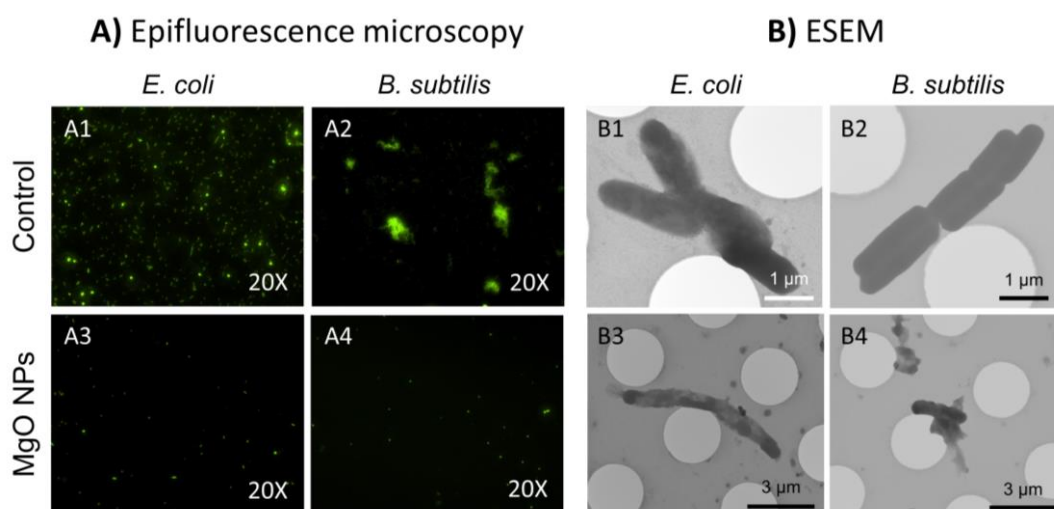


Figure 9. (A) *E. coli* and *B. subtilis* were incubated with the MgO NPs at 1.5 mg/mL (A3 and A4) and dye with a LIVE/DEAD® BacLight™ Bacterial Viability Kit to determine the viability of the bacteria after the incubation. The samples incubated with the particles present less bacterial density than the bacterial culture without the MgO NPs (control A1 and A2) due to the antiproliferative effect of the MgO. (B) Environmental ESEM images of control *E. coli* and *B. subtilis* (B1 and B2, respectively) and incubated with MgO NPs at 1.5 mg/mL for *E. coli* (B3) and 0.75 mg/mL for *B. subtilis* (B4) Both *E. coli* and *B. subtilis* incubated at their corresponding bactericidal concentrations (B3 and B4, respectively) showed evidence of stress and damage including general loss of cell shape, cell membrane damage and leakage of cytoplasmic material.

For a better understanding of the mechanism of action, Transmission Electron Microscopy (TEM) was used to determine the interaction of the MgO NPs with

one of the bacterial strains (*E. coli*). In order to elucidate how the interaction between MgO NPs and bacteria occurs, the bacteria were incubated with the nanoparticles and after the fixation protocol they were embedded in epoxy resin and sliced into 10 μm slivers to characterize using TEM. *E. coli* was incubated with sub-MIC concentrations of the particles (0.5 and 1 mg/mL) because at MIC concentration (1.5 mg/mL) the growth was completely inhibited and for embedding in the resin a relatively high concentration of bacteria in the sample is required. The aim of the assay was to attempt to identify the location of MgO NPs internalised within the bacteria or associated with the cell surface, but due to the low electron density of magnesium atoms the particles could not be distinguished from the vast amount of carbon in the bacterial cells. Due to the increase of the pH caused by the MgO NPs, a control of *E. coli* incubated in medium at pH 9 was also added. The bacteria incubated with the nanoparticles show damage of the bacterial envelope and condensation of the cytoplasmic material, as previously observed with ESEM, which could be addressed to the increase of the pH of the medium. But in the Figure 4 of the Article 2 it can be observed how at higher NP concentrations the cells present permeabilization of the bacterial envelope and leakage of the cytoplasmic material, which is not observed on the bacteria incubated at pH 9 without the particles.

5.1.3. Characterization of the MgO NPs coating on real heritage samples

To test the protective effect of the MgO NPs on real heritage paper samples, a variety selection of 18th century paper samples was obtained from the Archives of the Real Jardín Botánico (Madrid). Four paper samples covering a variety of coarseness and porosity were selected, three of them were used in the antibacterial assays and the last one was used in the antifungal assays. The MgO NPs have been already used to avoid paper acidification,^{190–193} but in this study we wanted to focus on the antimicrobial protecting when applied as a coating on the papers. Studying the MgO NPs antimicrobial activity *in situ* was one of the key priorities of this research, therefore there were developed different methods of evaluating the microbial growth on the paper surfaces.

Maintaining the original appearance of a heritage object is imperative in the field of conservation and restoration. Any intervention must not alter the aesthetic properties of the object, therefore the papers treated with MgO NPs should not display any change in their appearance. To confirm that the coating was not visibly altering the color of the paper samples, colorimetric measurements were

Results and Discussion

performed before and after the MgO NP coating. As shown in Figure 10B, the MgO NP coating did not produce any significant changes in the luminosity (ΔL^*) or colour (ΔE^*_{ab}), commensurate with results reported by Huang *et al.*¹⁹³ The total colour variation (ΔE^*_{ab}) produced by the coating was 2.55, which is below the generally established ΔE limit value ($\Delta E^*_{ab} \leq 3$) and could not be detected by the naked eye.^{194,195}

The homogeneity of the MgO NPs coating was studied by Environmental Scanning Electron Microscopy (Figure 10A). The images obtained confirmed that the MgO NPs provide a homogeneous dispersion over the surface of the papers, where particles were clearly visible penetrating the pores and fibres of the paper to provide a deep protective coating layer.

To confirm the presence and quantify the amount of nanoparticles on the paper, the Mg in the paper samples was quantified by Inductively Coupled Plasma Mass Spectrometry (ICP-MS). The control untreated samples contained only 77 μg of Mg per g, while the MgO NPs coated paper samples were found to contain 0.86 mg of Mg per g (Figure 10C).

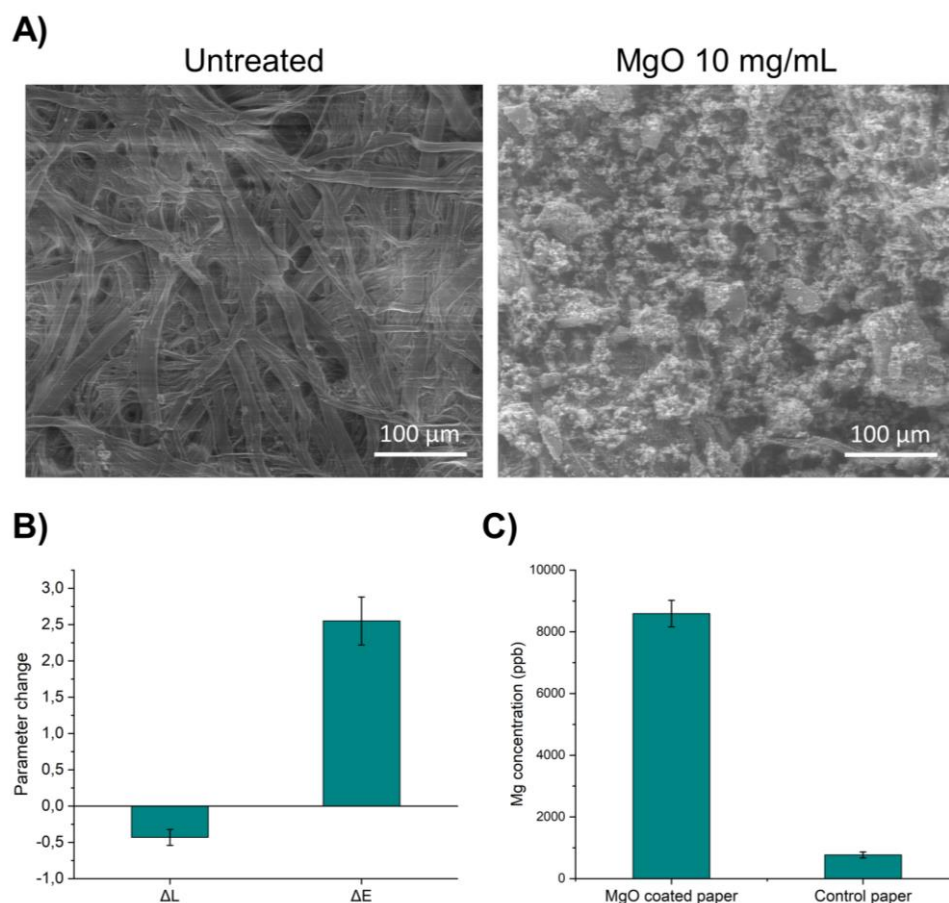


Figure 10. A) ESEM images of 18th century papers. On the left, an untreated sample where only the cellulose fibres are observed. On the right, an image of a coated paper with a 10 mg/mL MgO NP solution, showing the homogeneity of the nanoparticles over the paper surface. B) Luminosity change (ΔL^*) and colour change (ΔE^*_{ab}) of the paper samples after coating with the 10 mg/mL MgO NP dispersion. The values obtained verify the coating did not produce any significant changes in the luminosity (ΔL^*) or colour (ΔE^*_{ab}). C) Inductively Coupled Plasma Mass Spectrometry (ICP-MS) of the magnesium (Mg) content of the 18th century papers coated with 10 mg/mL MgO NPs (and uncoated as control paper samples). The MgO NP coated paper samples contained ten times more Mg content than the uncoated control paper samples.

5.1.4. Antimicrobial performance of the MgO NP on paper samples

5.1.4.1. Diffusion ability of the MgO NPs

In the first instance, the papers were cut into circles to perform a modified Kirby-Bauer disk diffusion technique. All the papers, including two circles of Whatman® Antibiotic Assay Discs were impregnated with an MgO NP suspension (disc 1) and with an Ampicillin solution (disc 2) as a control. After the incubation over an *E. coli* lawn, the only sample which generated an inhibition halo was the Whatman® disc impregnated in Ampicillin. Thus, it can be deduced that the MgO NPs do not diffuse on the agar meaning that there was no release

of the MgO NPs from the Real Jardín Botánico papers into the agar medium (Figure S6, Article 2).

Due to the lack of diffusion of the particles into the agar, three different assays were developed to study the bacterial and fungal growth inhibition *in situ* by the MgO NPs over the paper samples.

5.1.4.2. MgO NPs *in situ* activity against *E. coli*

For the antibacterial activity *in situ* we established a TBX agar method as a convenient means of detecting and quantifying the growth of *E. coli* on the paper samples. TBX Agar contains X- β -D-glucuronide, a chromogenic compound hydrolyzed by the *E. coli* enzyme β -glucuronidase, making the *E. coli* colonies turn green-blue on a conventional agar plate. The papers were therefore cut into 4×4 cm squares and placed in a sterile Petri dish, where were then impregnated with a 10 mg/mL MgO NPs solution and allowed to dry. Once dry the papers were sprayed twice with a 10⁴ CFU/mL *E. coli* suspension. In our methodology the papers were each covered by a fine layer of TBX agar and when the medium solidified the process was repeated to obtain a complete homogeneous covering. The papers were then incubated for 48 h at 37 °C. Afterwards the treated and untreated papers were compared and counting of the green-blue *E. coli* colonies clearly illustrated the efficacy of the MgO NPs for preventing colonisation of the paper samples. As it can be observed in the Figure 11, the MgO NPs treated samples do not present any bacterial growth over the surface of the paper, while the control untreated paper samples are covered by a lot of green-blue *E. coli* colonies.

5.1.4.3. Antifungal activity under optimal growth conditions

For the first antifungal assay performed in heritage paper samples, 5 cm diameter circles were coated with an aqueous dispersion of MgO NPs (10 mg/mL) as in the antibacterial *in situ* assay. Once dry, the paper samples were covered with a thin Sabouraud Dextrose Agar (SDA) layer and incubated at their optimum growth temperatures for six days. As observed in Figure 11, after 72 hours of incubation (*48 h for *A. niger*), fungal growth is clearly visible in the control samples, while no growth was observed in paper samples treated with MgO NPs. After longer incubation times of up to six days, *A. niger* and *T. reesei* failed to display any growth (fungicidal action), however *C. cladosporioides* began to proliferate on the MgO NP treated samples. Given that the MgO NPs were applied at 10 mg/mL

Results and Discussion

and the MIC value for the *C. cladosporioides* is 12 mg/mL, a fungistatic action was not fully obtained, leading to the initiation of fungal growth after six days. Although a full fungal inhibition was not obtained, the growth of *C. cladosporioides* was clearly lesser in the paper treated with MgO NPs and it started with some delay in comparison with the untreated paper, meaning the nanoparticles are able to partially inhibit growth of this mould. Nevertheless, the MgO NPs turned out to be more effective against the two fungal strains that are more relevant in this specific research (*A. niger* and *T. reesei*), due to their production of the hydrolytic cellulase enzyme, which is able to degrade cellulose into glucose.

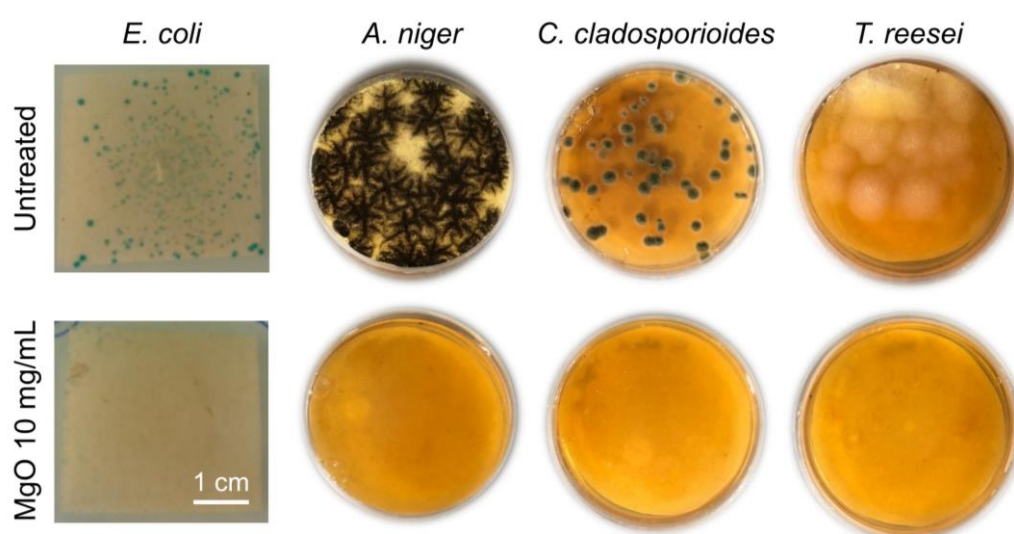


Figure 11. Images of 18th century papers inoculated with *E. coli*, *A. niger*, *C. cladosporioides* and *T. reesei*, covered with solid culture media and incubated for 48 h (*E. coli* and *A. niger*) and 72 h (*C. cladosporioides* and *T. reesei*). While the MgO NPs coated samples did not present any growth (at this incubation times), the untreated samples are fully colonised by the different microorganisms. For the *E. coli* assay TBX agar was used to easily detect the growth of the bacteria over the surface. Blue spots are colonies of *E. coli* stained with the chromogenic compound from TBX agar.

5.1.4.4. *In situ* antifungal activity under more realistic growth conditions

The second antifungal activity assay was developed to evaluate the *in situ* activity of the MgO NPs under conditions that more closely mimic the real conditions under which mould might grow in paper samples (in a hot and humid environment). To do so, 2 x 2 cm sterile paper samples were coated with 10 mg/mL MgO NPs and then inoculated with 10³ conidia/mL of each mould. To facilitate the fungal growth all the dilutions were made in RPMI (both the MgO NPs solution and the fungal inoculum) and then the samples were incubated in a humidity chamber with high relative humidity (100 %) at 35 °C for *A. niger* and

Results and Discussion

T. reesei and at 25 °C for *C. cladosporioides*. Fungal growth was monitored by macroscopic inspection of paper samples as well as microscopic observation (Environmental Scanning Electron Microscopy (ESEM) and optical microscopy). The brown-black fungal growth of *A. niger* and *C. cladosporioides* was easily observed in the untreated samples while *T. reesei* presented a yellow coloured growth (Figure S4, Article 3). The images obtained by optical microscopy (Figure S5, Article 3) and ESEM (Figure 12) confirmed that the untreated paper samples were covered with fungi mycelium for all three moulds, with a significant number of spores in the case of *A. niger*, while MgO NP treated paper samples showed no fungal growth over the paper surface and only cellulose fibres were observed (Figure 12). It is interesting to highlight the fact that the untreated paper inoculated with *T. reesei* (the most cellulase producing fungi) broke while manipulating it after the assay, due to the lack of consistency caused by the cellulase activity, while the MgO NPs treated paper had the same stiffness as at the beginning of the experiment.

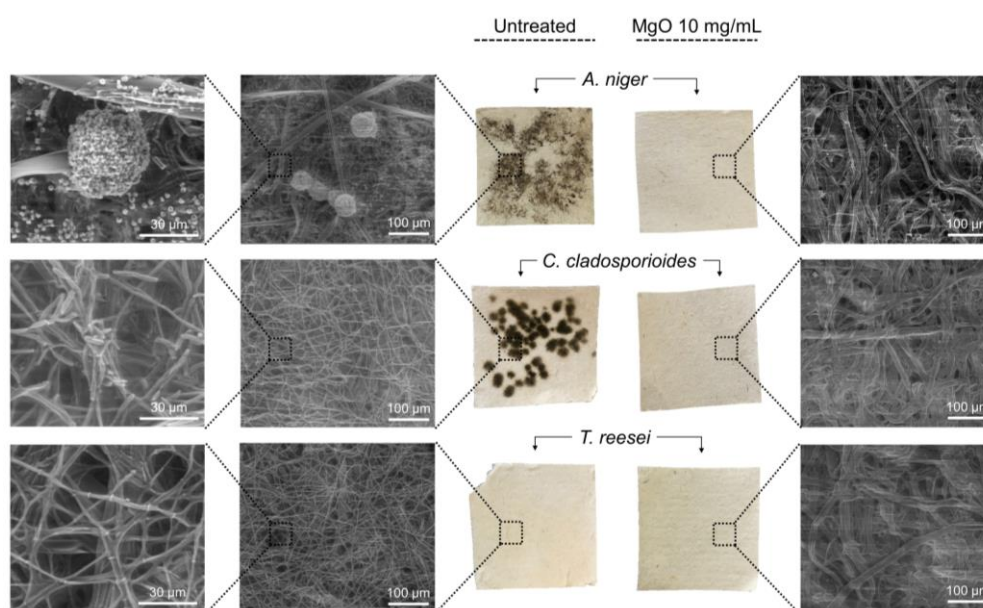


Figure 12. *In situ* antifungal activity of MgO NPs. The untreated papers (left) present fungal growth visible by the naked eye and confirmed by ESEM imaging, where the growth of all three fungal strains (*A. niger*, *C. cladosporioides* and *T. reesei*) are clearly observable on top of the cellulose fibres of the untreated papers, but are absent from the MgO NP treated papers (right).

From these two *in situ* assays we can conclude that MgO NPs deposited on the 18th century paper samples at 10 mg/mL are capable of inhibiting the fungal growth of the selected fungi, with a fungicidal action against *A. niger* and *T. reesei* (the two cellulase producing strains responsible for paper degradation) and a fungistatic action against *C. cladosporioides*.

5.1.4.5 Ability of MgO NP to prevent cellulose degradation by moulds

A. niger and *T. reesei* are both producers of cellulase, an enzyme responsible for catalysing cellulolysis, the decomposition of cellulose and related polysaccharides into simple monosaccharides for energy purposes. Fungal growth on artefacts made from cellulosic materials can undergo rapid and severe biodeterioration as the colonizing microbes consume cellulose for energy.

To evaluate the MgO NPs anticellulase activity, two methodologies were carried out. First, we evaluated the inhibition of the cellulase enzyme by the particles, and then we evaluated the efficacy of the particles prevent fungal colonization when inoculated moulds were forced to use the cellulase of the paper as their energy source.

The anticellulase activity of the MgO NPs was analysed by incubating the particles with commercial *A. niger* and *T. reesei* cellulase extracts. Cellulase activity decreased with increasing MgO NP concentration, where concentrations of $\frac{1}{2}$ MIC were able to reduce the cellulase enzymatic activity by half, with only residual enzymatic activity being observed at the MIC concentration for each fungal strain (Figure 13A and 13B).

The last assay was designed to assess the adhesion of fungal cells to the paper samples as a function of MgO NP concentration and evaluate the cellulose prevention capacity of the MgO NPs on heritage paper samples. The MgO NP concentration dependent fungal cell adhesion to the paper was evaluated by incubating different concentrations of MgO NP treated paper samples ($\frac{1}{4}$, $\frac{1}{2}$, 1x and 2x the MIC value) with *A. niger* and *T. reesei*. By weighing the papers after the incubation with the fungi, their adhesion to the papers and subsequent growth can be determined by comparing the dry weight of the positive control papers (incubated without MgO NPs) with the dry weight of the MgO NP-treated papers (Figure 4, Article 3). Figure 13C and 13D reports how the MgO NPs inhibit the adhesion and growth of *A. niger* and *T. reesei* at concentrations lower than the MIC value. At the lowest MgO NPs concentration ($\frac{1}{4}$ MIC), both fungi are capable of growing on papers, but at concentrations greater than $\frac{1}{2}$ MIC, fungal adhesion and growth are highly diminished and even completely inhibited.

Results and Discussion

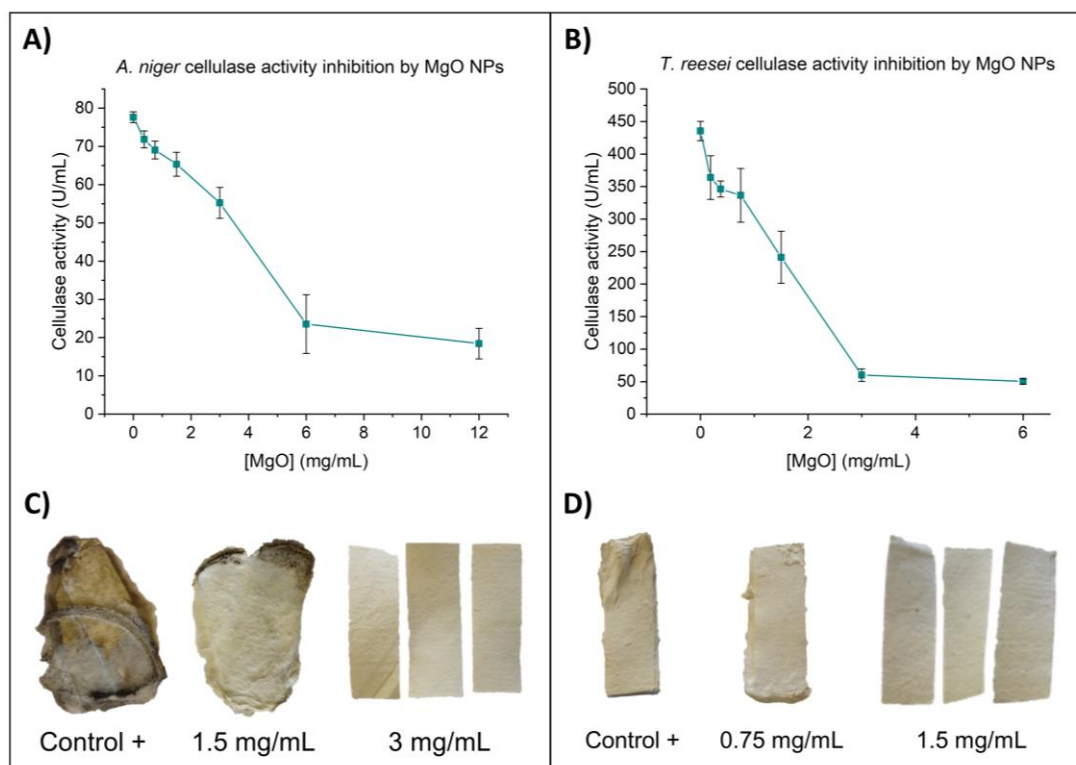


Figure 13. Enzymatic activity of cellulase from *A. niger* (A) and *T. reesei* (B) incubated with MgO NPs at concentrations of 1/16, 1/8, 1/4, 1/2, 1x and 2x the corresponding MIC values for each fungus. Error bars correspond to SD values of three independent assays. C) and D) correspond to the ‘paper adhesion inhibition’ test. The control samples from both *A. niger* and *T. reesei* are completely covered by the fungi, and the three papers of each sample adhere to each other due to the fungal growth over the paper. At the lowest concentration of MgO NPs (1.5 mg/mL for *A. niger* and 0.75 mg/mL for *T. reesei*) the fungi are still able to get attach to the paper surface and proliferate, but at the next concentration (3 mg/mL for *A. niger* and 1.5 mg/mL for *T. reesei*) the papers are completely free of fungal growth.

Newly publications obtained similar results immersing paper samples in a MgO NPs solution and testing the treated papers against four moulds (*Aspergillus niger*, *Trichoderma viride*, *Penicillium funiculosum* and *Chaetomium globosum*). The coating had no influence on the aesthetics of the treated paper sample and, although a total fungal inhibition was not achieved (probably due to the lower concentration applied (2 mg/mL)), there were observed few moulds compared with the untreated papers.¹⁹⁶ Other recent studies have demonstrated that Ag NPs and ZnO NPs can be also used to prevent paper degradation due to their antifungal activity against *A. niger* and other environmental and cellulase producing moulds as *Alternaria alternata*, opening the door to the use of this kind of nanoparticles to preserve paper and avoid biodeterioration.¹⁹⁷

5.1.5. Conclusions

This work has demonstrated the applicability of MgO NPs as protective coatings for heritage paper. The 12 nm-diameter MgO NPs can be synthesised by an easy and cheap sol-gel method and can be applied as a colourless and homogeneous coating to protect various paper from bacterial and fungal colonization. The combination of different antimicrobial assays has shown that the particles can inhibit both bacterial and fungal growth *in vitro* and *in situ*. Furthermore, microscopy studies have shown that the particles cause oxidative stress, cell membrane leakage and cell death on the bacteria. The application of a 10 mg/mL coating of the MgO NPs on 18th century papers demonstrate their inhibitory effect against *E. coli* bacterial growth and against three filamentous fungal strains, *T. reesei*, *A. niger* and *C. cladosporioides*. Additionally, the MgO NPs also display anticellulase activity at sub-MIC concentrations, avoiding the cellulose degradation of the paper by cellulase producing *A. niger* and *T. reesei*. These results highlight the potential and the multifunctionality of the MgO NPs to preserve heritage paper, not only preventing the paper colonisation due to their biocidal activity, but also inhibiting the cellulase activity of the most harmful moulds and increasing the pH to avoid paper acidification.

Article 2: Protection of 18th century paper using antimicrobial nano-magnesium oxide

International Biodeterioration & Biodegradation 141 (2019) 79–86



Contents lists available at ScienceDirect

International Biodeterioration & Biodegradation

journal homepage: www.elsevier.com/locate/ibiod



Protection of 18th century paper using antimicrobial nano-magnesium oxide

Isabel Franco Castillo^{a,1}, Laura De Matteis^{b,*}, Clara Marquina^{a,c}, Esther García Guillén^d,
Jesús Martínez de la Fuente^a, Scott G. Mitchell^{a,**}

^a Instituto de Ciencia de Materiales de Aragón (ICMA), Consejo Superior de Investigaciones Científicas (CSIC)-Universidad de Zaragoza and CIBER-BBN, C/ Pedro Cerbuna 12, 50009 Zaragoza, Spain

^b Instituto de Nanociencia de Aragón (INA), Universidad de Zaragoza and CIBER-BBN, C/ Mariano Esquillor s/n, 50018 Zaragoza, Spain

^c Departamento de Física de la Materia Condensada, Universidad de Zaragoza, C/ Pedro Cerbuna 12, 50009 Zaragoza, Spain

^d Real Jardín Botánico, Consejo Superior de Investigaciones Científicas (CSIC), Madrid, Spain

ARTICLE INFO

Keywords:
Magnesium oxide
Nanoparticles
Paper heritage
Antimicrobial activity
Oxidative stress

ABSTRACT

Magnesium oxide nanoparticles (MgO NPs) have attracted considerable interest as antimicrobial agents in a wide variety of applications. We report a simple synthetic route towards MgO NPs (average diameter 10 nm) possessing potent antibacterial activity against both Gram-negative and Gram-positive bacteria. Detailed electron microscopy studies show how these particles induce oxidative stress, cell membrane leakage and cell death in bacteria at low NP concentrations, but remain non-toxic to eukaryotic cells. Applying a homogeneous dispersion of these nanoparticles on 18th century paper proved to be a highly effective means of preventing bacterial colonisation without altering the appearance of the paper samples, thus opening the doors to the use of these colourless, low-cost, and scalable nanoparticles for preventing biodeterioration in a range of paper-based objects and surfaces.

1. Introduction

The enduring threat of microbial contamination to historical and contemporary objects of art in archives and in museums remains to be one of the principal problems of cultural heritage conservation. Microbes can penetrate deep within the microstructures of materials causing material loss from acid corrosion, enzymatic degradation and mechanical attack, all of which induce esthetical spoiling of paintings, sculptures, textiles, ceramics, metals, books and manuscripts alike (Sterflinger and Piñar, 2013). Regular decontamination of infected artefacts, exhibition areas and storage rooms/deposits results in significant expenditures for museums, local authorities and private collectors. Ultimately, material loss brought about by prolonged microbial attack can result in loss of the cultural and historical value of paintings, books and manuscripts – the socioeconomic cost of which is inestimable (Sterflinger and Pinzari, 2012; La Russa et al., 2014). Furthermore, microbial contamination in libraries, museums and their storage rooms/deposits can also represent a serious threat to the health and occupational safety of restorers, museum personnel and the general public (Skórá et al., 2015).

Metal oxide nanoparticles for example ZnO, MgO, CuO and CaO are

being studied as novel inorganic antimicrobial agents for potential applications in food, the environment and healthcare (Hajipour et al., 2012; Dizaj et al., 2014). Nanostructured inorganic materials possess unique tuneable physicochemical properties and, moreover, the combination of their large surface area and dimensions allows them to interact and internalise within cells, respectively, meaning that they display a broad spectrum of antibacterial activity. Moreover, their modular nature means that a library of relatively low cost materials with different sizes, shapes, surface properties, and chemical compositions can be developed leading to a great potential for developing effective antimicrobial agents with high stability under harsh environmental conditions. Despite the advance of this field of research in recent years, the antibacterial mechanism of action of metal oxide nanoparticles is in most cases not entirely understood. Magnesium oxide nanoparticles (MgO NPs) have received significant attention as antibacterial agents in recent years due to their high stability and low cost based on their preparation from economical precursors (He et al., 2016; Tang et al., 2012). The mechanism of antibacterial activity of MgO NPs has been attributed to the production of reactive oxygen species (ROS), which induce oxidative stress and lipid peroxidation in bacteria (Tang and Lv, 2014) as well as non-ROS mediated bacterial toxicity

* Corresponding author.

** Corresponding author.

E-mail addresses: lauradem@unizar.es (L. De Matteis), scott@unizar.es (S.G. Mitchell).

¹ These authors contributed equally.

<https://doi.org/10.1016/j.ibiod.2018.04.004>

Received 18 December 2017; Received in revised form 9 February 2018; Accepted 11 April 2018

Available online 06 September 2018

0964-8305/ © 2018 Elsevier Ltd. All rights reserved.

mechanisms (Leung et al., 2014). It is important to note that the antibacterial effect is often species and genus dependent and depends upon the size, shape, chemical composition and surface properties (e.g. hydrophobicity) of the nanoparticles (Raghupathi et al., 2011; Hajipour et al., 2012).

Although MgO NPs are generally regarded as safe (Ge et al., 2011), the application of any antibacterial nanomaterial and its nanotoxicological profile is a major concern. Currently, MgO NPs are used as additives in heavy fuel-oil (Park et al., 2006), for the cleaning of fuel-oil pipelines, avoidance of sludge formation in storage tanks and protection of boilers against corrosion. MgO has been used as a mineral supplement source for magnesium, an essential nutrient for the human body (Srinivasan et al., 2017) and they are also used for diverse applications in medicine, e.g. for the relief of cardiovascular disease and stomach problems and as anti-cancer therapy (Krishnamoorthy et al., 2012). As already mentioned, toxic effects are highly dependent on the physicochemical properties of each individual nanoparticle as well as on the types of cells tested (Reddy et al., 2007). It therefore follows that an extensive evaluation of nanoparticles on different biological systems is needed to determine their toxicity. As an illustration, despite the aforementioned examples showing the low cytotoxicity of MgO NPs, they have been shown to display toxicity on early developmental and larval stages of zebrafish (Ghobadian et al., 2015). One of the great challenges of nanotechnology is the corresponding environmental health and safety implications of the widespread use of nanomaterials, since the properties of engineered nanomaterials are potentially highly hazardous to the human population due to their potential for high ecotoxicity. The widespread use of nanoparticles and their inevitable release into the general environment ultimately means that they will find their way into terrestrial, aquatic and atmospheric environments where their toxicity, behaviour and ultimate fate are largely unknown (Bondarenko et al., 2013).

Recently, there has been a drive for greater use of nanomaterials in the conservation of cultural heritage (Baglioni et al., 2015; La Russa et al., 2012, 2016). Recent examples include their use for protecting stone monuments (Sierra-Fernandez et al., 2017a), textiles (Pietrzak et al., 2017), murals (Baglioni et al., 2012), glass (Shirakawa et al., 2016) and paper (Asghar Ariafar et al., 2017). Both silver (Koizhaiganova et al., 2015) and nano-silver (Li et al., 2017) are studied frequently and some studies have even thoroughly evaluated the sensitivity of museum microbes to nanosilver (Gutarowska et al., 2012), but cheaper more readily available metal-oxide particles have been shown to serve as alternative solutions to biodeterioration issues (Ruffolo et al., 2010 and Sierra-Fernandez et al., 2017b).

The aim of the research presented herein was to study the use of nano-magnesium oxide particles to protect a variety of 18th century papers from the Archives of the Real Jardín Botánico in Madrid (Spain) from microbial contamination. These papers have been selected as a representative sample of different paper qualities that were used as herbarium materials at the end of the 18th century to keep plant specimens (herbarium sheets) dried for other purposes. They are part of the old herbarium paper sheets kept in the RJB archive before plants were stored with standardized herbarium paper sheets (c. 1980). They arrived at the RJB between 1785 and 1800 and have been kept here since, in a rather dry environment, but without further specific preserving measures (controlled humidity and temperature). Furthermore, we wished to demonstrate how a combination of antibacterial assays (solution-based quantification of cell viability) and high resolution electron microscopy imaging (qualitative analysis of the microbial cell morphology and internal structure) could be used together to elucidate conceivable mechanisms of action.

2. Materials and methods

2.1. Materials

2.1.1. Reagents

Milli-Q water has been used throughout. Magnesium methoxide, 7–8% in methanol, was obtained from Alfa-Aesar; absolute ethanol was purchased from Panreac. 3-(4,5-Dimethylthiazol-2-yl)-2,5-diphenyltetrazolium bromide (MTT) was purchased from Invitrogen. Resazurin sodium salt and TBX agar from Sigma-Aldrich.

2.1.2. Eukaryotic cells

Vero cells (monkey kidney epithelial cells) were purchased from the American Type Culture Collection (ATCC, Manassas, VA, USA, number CCL-81). Dulbecco's modified Eagle's medium (DMEM), Phosphate-Buffered Saline (PBS), Dulbecco's Phosphate-Buffered Saline (DPBS) were purchased from Lonza.

2.1.3. Microorganisms

Escherichia coli DH5-alpha as Gram-negative (G-) bacteria and *Bacillus subtilis* 1904-E as Gram-positive (G+) bacteria were used in the assays. Luria-Bertani (LB) liquid medium (Miller's formulation) and Nutrient Broth (NB) liquid medium were freshly prepared and sterilized by autoclave. Trypticase Soy Agar plates were purchased from Thermo Scientific™.

2.1.4. Test papers

Three different paper samples from the last third of the 18th century were used in this study. The papers differ in colour, thickness and roughness.

2.2. Methods summary

2.2.1. Bacterial growth curves

Bacterial growth was recorded measuring the optical density (OD) of the samples at 600 nm every one hour (0–8 h) using a microplate reader (Thermo Scientific MULTISKAN GO). Results were compared with the OD variation of a control culture containing only bacteria. All controls and antibacterial assays were replicated in sextuplet to verify the reproducibility of the results and to calculate the mean values and standard deviations.

2.2.2. Cell viability assays

Cell viability was measured using a Thermo Scientific Multiskan GO plate reader. Each measurement was repeated five times to obtain the mean values and standard deviations.

2.2.3. Environmental scanning Transmission Electron Microscopy (ESTEM)

Data were collected on a Quanta FE6-250 (FEI Company) field emission SEM for high-resolution imaging working at low vacuum mode using a STEM detector.

2.2.4. Powder X-Ray Diffraction (PXRD)

The crystalline phase of the nanoparticles was verified using PXRD spectra obtained using a D-Max Rigaku instrument equipped with a rotating Cu anode and a graphite monochromator (therefore working with $K_{\alpha 1} = 1.5405 \text{ \AA}$). The diffractometer worked at 40 kV and 80 mA. Data were recorded in the 2θ range between 10° and 90° by using a step of 0.03° and 1 s/step.

2.2.5. Scanning electron microscopy (SEM)

SEM images and energy dispersive X-ray spectroscopy (EDX) spectra were acquired using a field emission SEM Inspect F50 with an EDX system INCA PentaFETx3 (FEI Company, Eindhoven, The Netherlands) in the energy range 0–30 keV.

2.2.6. Transmission Electron Microscopy (TEM)

Preliminary observation of the synthesized particles was carried out by Bright Field (BF) imaging in a FEI Tecnai T20 microscope operating at 200 kV. The samples were prepared by resuspending the powder in ethanol under sonication, putting a drop of the suspension directly on a TEM carbon grid, and letting it dry in air atmosphere. From different TEM images, an estimation of the diameter distribution has been obtained using Digital Micrograph® (Gatan Inc., Pleasanton, TX, USA) and OriginLab® (OriginLab, Northampton, MA, USA) software to measure the diameters of more than 100 NPs and for the frequency count statistical analysis respectively. Observation of microbial cells after incubation with nanoparticles was carried out using the same machine operating at 80 kV. The biological samples were prepared by fixation with glutaraldehyde, embedding in resin and cutting with a microtome.

2.3. Nanoparticle synthesis

MgO nanoparticles were synthesized by sol-gel method through a modification of protocols already reported in literature (Bokhimi et al., 1995). Briefly, 3.6 mL of magnesium methoxide, $\text{Mg}(\text{OCH}_3)_2$, (2.4 mmol) were added to 20 mL of absolute ethanol under ultrasonication and subsequently 0.9 mL of water (50 mmol) were added to the mixture. The sol was left in the ultrasonic bath for 30 min. The mixture was then kept under gentle stirring for 36 h to facilitate gelification.

The water/ethanol gel suspension was stirred in an oil bath and underwent a progressive increase of the temperature from 70 to 90 °C over a period of 5 h, before being completely dried in air until a fine magnesium dihydroxide powder was obtained. The final step involved annealing this powder at 600 °C for 30 min to obtain the complete oxidation of $\text{Mg}(\text{OH})_2$ to MgO. Yield = 87 mg (dry particles).

2.4. Eukaryotic cell viability assay in presence of MgO nanoparticles

Vero cells were cultured in Dulbecco's modified Eagle's medium (DMEM), supplemented with 10% foetal bovine serum (FBS), 5% glutamine and 5% penicillin/streptomycin. Cell cultures were maintained at 37 °C and equilibrated in 5% CO_2 and air. Cell viability and proliferation in the presence of MgO NPs were analysed by 3-(4,5-dimethylthiazol-2-yl)-2,5-diphenyl tetrazolium bromide (MTT) assay (Carmichael et al., 1987; Mai et al., 2012). For the cytotoxicity assay 5×10^5 cells were seeded a 96-well plate and grown for 24 h, then the medium was replaced with fresh medium containing the MgO NPs at various concentrations. At the end of the 24 h incubation period, the medium was replaced with fresh medium and 20 μL of MTT dye solution (5 mg/mL in PBS) was added to each well. After 3 h of incubation at 37 °C and 5% CO_2 , the medium was removed and formazan crystals were dissolved in 100 μL of DMSO. The absorbance of each well was read on a microplate reader at 570 nm. The relative cell viability (%) related to control wells containing cells incubated without nanoparticles was calculated by $\text{ABS}_{\text{test}}/\text{ABS}_{\text{control}} \times 100$. Each measurement was repeated five times to obtain the mean values and the standard deviation.

2.5. Bacterial cell proliferation assays in presence of MgO nanoparticles

The experiments were performed with two bacterial strains, *Escherichia coli* DH5- α and (Gram -) *Bacillus subtilis* 1904-E (Gram +). The bacteria was pre-inoculated in culture medium (Luria-Bertani (LB) medium for *E. coli* and Nutrient Broth (NB) for *B. subtilis*) and kept under shaking (180 rpm) at 37 °C for 15 h. A dilution from this culture was used for the following tests, corresponding to an inoculum of 1×10^7 CFU/mL. Firstly, culture medium was supplemented with the required amounts of MgO NPs in order to obtain the desired concentration in the sample suspension. MgO NPs were therefore dispersed previously in the corresponding medium for 30 min under

ultrasonication. Thereafter bacterial inoculum was added to the MgO NP/culture medium dilutions and the bacterial growth curves were recorded over a period of 24 h by measuring the optical density (OD) of the samples at 600 nm. Results were compared with the OD variation of a control culture containing *E. coli* or *B. subtilis* without any NPs. To verify the data, the colony-forming ability (cell viability) of *E. coli* or *B. subtilis* incubated with different concentrations of MgO NPs was tested by plating properly diluted aliquots of the samples in the logarithmic phase (4 h incubation) on nutrient agar plates and incubating the plates at 37 °C overnight.

2.6. Resazurin cell viability assays

Cell viability was analysed using a Resazurin (7-Hydroxy-3H-phenoxazin-3-one 10-oxide) assay in a 96-well plate. A bacterial inoculum (1×10^7 CFU/mL) of *E. coli* (in LB media) and *B. subtilis* (in NB media) was supplemented with different concentrations of MgO NPs as in the growth inhibition assay and a blank sample (bacteria without MgO NPs) was also included in the assay as negative control. Once the microbial cultures had been grown for a total of 24 h, 30 μL of 0.1 mg/mL Resazurin (in LB or NB medium) was added to each well and incubated in the dark at 37 °C for 1 h under stirring.

2.7. LIVE/DEAD® assay

Cell viability was analysed also by a LIVE/DEAD® fluorescence assay. A bacterial inoculum (1×10^7 CFU/mL) of *E. coli* (in LB media) and *B. subtilis* (in NB media), was supplemented with MgO NPs at a final concentration of 1.5 mg/mL. A sample without MgO NPs was also included in the assay as negative control. After 24 h of incubation at 37 °C with stirring, the solutions were stained with the LIVE/DEAD® BacLight™ Bacterial Viability Kit in a 1:500 dilution and incubated for 15 min in the dark. Then 10 μL of the stained samples were extended over a slide and the bacteria were visualized with a Nikon ECLIPSE Ti epifluorescence microscope. The experiments were performed with three different samples of paper (differing in their colour, thickness and roughness) from the 18th century from the Archives of Real Jardín Botánico-CSIC (Madrid, Spain).

2.8. Agar diffusion test

A modified Kirby-Bauer disk diffusion technique was used. In order to test the particle release capacity of the paper samples, each of the three papers were cut in 6 mm discs and they were impregnated with a 15 mg/mL MgO NPs solution. Another disc of each paper was impregnated with a 100 μg /mL Ampicillin solution as a positive control. To test the diffusion ability of the MgO NPs, also a Whatman® Antibiotic Assay Discs (6 mm) was impregnated with the 15 mg/mL MgO NPs solution and another one with the 100 μg /mL Ampicillin solution. All these papers, together with a non-impregnated Whatman® Disc as negative control, were placed in an agar plate previously inoculated with an *E. coli* lawn. After 24 h of incubation at 37 °C, the inhibition halo around the samples was measured.

2.9. Inductively coupled plasma atomic emission spectroscopy (ICP-AES) analysis of nanoparticle interaction with microbial cells

E. coli and *B. subtilis* samples of 1×10^7 CFU/mL in LB or NB medium, respectively were incubated with 1.5 mg/mL of NPs overnight. Bacterial cells were then separated from the supernatant by centrifugation. Both pellet and supernatant were digested with a 3:1 HCl/HNO₃ mixture and the Mg concentration was evaluated by ICP-AES analysis. Each sample was measured in triplicate to obtain mean values.

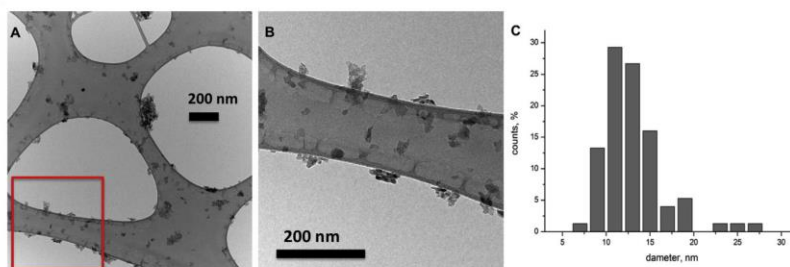


Fig. 1. BF-TEM images of MgO NPs (B is a magnification of the area selected in A) and estimated size dispersion histogram (C).

2.10. Antimicrobial assays on paper samples

18th century paper samples were obtained from the leftovers of the Herbarium sheets conserved in the Archives of the Real Jardín Botánico (Madrid, Spain). Paper numbers 1 and 3 were used to keep dried plants, whereas paper number 2 was the usual text document accompanying the plant samples. These paper samples were cut in 4×4 cm squares and each paper was placed in a sterile Petri dish. Each paper was impregnated with 500 μ L of a 10 mg/mL MgO NPs solution in small drops using a micropipette, before being sterilized under UV for 15 min and allowed to dry in a sterile environment. This process was performed twice on each paper to ensure a homogenous coating of MgO NPs. Once the papers were dry, an *E. coli* solution (10^4 CFU/mL) was sprayed, twice, over the paper samples with MgO NPs and over the negative control samples (papers without MgO NPs). To detect the bacterial growth over the paper samples TBX agar was used, which contains X- β -D-glucuronide, a chromogenic compound hydrolyzed by the β -glucuronidase, an *E. coli* enzyme, which makes the *E. coli* colonies turn green-blue on an agar plate. A first layer of TBX agar was added over all the paper samples covering all the surface of the paper. When the medium solidified, a second layer was added. The papers were then incubated for 48 h at 37 °C whereupon the bacterial colonies were clearly observable with the naked eye.

2.11. Environmental scanning electron microscopy (ESEM) analyses

ESEM was used to analyse both bacterial cell morphology, after incubation with the MgO NPs, and the appearance of paper samples, after covering with MgO NPs. All samples were analysed in a Quanta FE6-250 (FEI Company) field emission ESEM for high-resolution imaging working at low vacuum mode. Bacterial cell samples were prepared in the same way as in the fluorescence assay, including also a negative control of bacteria culture without MgO NPs, and after the 24 h of incubation they were fixed using the following procedure: They were centrifuged 10 min at 1400 rpm (300 G), the supernatant was removed and the pellet was resuspended into 1.5 mL of sterile PBS. This procedure was repeated twice and the pellet was finally resuspended into 1.5 mL phosphate buffer 10 mM pH 7.2 + 2.5% glutaraldehyde. Bacteria were incubated with this solution for two hours in a wheel at room temperature and they were washed twice with 1.5 mL of PBS. Finally they were resuspended in water. The sample was analysed without any previous treatment directly from water suspension.

3. Results and discussion

A sol-gel method was chosen for the synthesis of the MgO NPs since it represents a simple, cheap, reproducible and scalable synthetic process, which also allows for a reasonable control of the size of the nanoparticles and their subsequent properties. The synthetic conditions

were optimized in terms of reactant amounts, pH conditions, reaction time and temperature to obtain the desired product, as reported in the Experimental Section. After the condensation step of the sol-gel process and the first drying step, $\text{Mg}(\text{OH})_2$ NPs were obtained and a proper annealing process was necessary to convert this product into crystalline MgO NPs. X-Ray Diffraction (XRD) analysis was performed before and after the annealing to determine the final crystalline structure of the material. The complete transformation into MgO crystalline phase was confirmed, excluding any presence of $\text{Mg}(\text{OH})_2$ phase, and demonstrating that an annealing temperature of 600 °C, maintained during 30 min, was necessary to obtain the cubic MgO structure observed in the XRD spectrum. XRD spectrum of MgO NPs is reported in Fig. S1 in the Supplementary Information. From this spectrum it is also possible to estimate the average size of the crystallites by means of the Scherrer formula $d = k\lambda/\beta\cos(\theta)$, where λ is the Cu-K α_1 X-ray wavelength, β is the full width at half-maximum, and k is the shape factor. The calculated average size for the synthesized NPs was 10 nm.

The size and shape of the MgO NPs were analyzed by BF-TEM (Fig. 1). Fig. 1A is a BF-TEM image of the nanoparticles deposited on a carbon film TEM grid after solvent evaporation, while Fig. 1B is a magnification of the previous one, reported for sake of comprehension. Fig. 1C shows an estimation of the NP size obtained from a statistical frequency count of the particle diameters measured from TEM images. As observed from the figure, particle sizes range from 8 to 20 nm, with 9–15 nm being the most prevalent population. This estimation is coherent with the size calculated from the XRD spectrum through Scherrer equation. From the TEM image, it can also be observed that NPs tend to form small aggregates of about 5–10 NPs with an aggregate size of about 100 nm but it could not be excluded that this effect could be produced during the sample preparation as a drying artifact (Domingos et al., 2009).

The antibacterial effect of the MgO NPs was verified using two methods: by studying how their presence affected bacterial growth (cell proliferation assays) and determining the bactericidal concentration of the particles using a colorimetric resazurin cell viability assay (Fig. S2). These studies investigated the antimicrobial effect of MgO NPs at different concentrations against the Gram-negative bacteria *Escherichia coli* (*E. coli*) and the Gram-positive *Bacillus subtilis* (*B. subtilis*) using dispersions of MgO NPs in Luria-Bertani (LB) or Nutrient Broth (NB) growth medium, respectively. The study of growth curves of bacterial cells in suspension measures the turbidity of the culture suspension as optical density (OD) of the medium and allows the determination of the rate of bacterial growth over the 24 h incubation period (Fig. 2). The dispersed MgO NPs showed high antiproliferative activity against both strains of bacteria. Full inhibition of bacterial growth was observed at concentrations of 1.50 mg/mL and 0.75 mg/mL for *E. coli* and *B. subtilis* respectively. The results obtained from optical density analyses were commensurate with the bactericidal concentrations from the spectrophotometric resazurin cell viability assays, which clearly show that

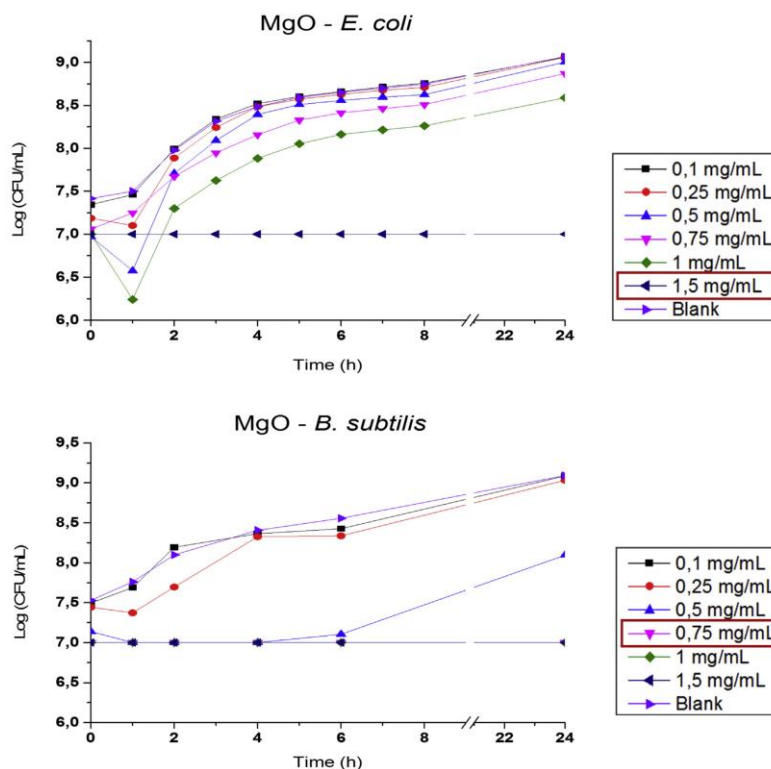


Fig. 2. *E. coli* and *B. subtilis* growth curves starting from a concentration of 10^7 CFU/mL in LB (or NB) medium at different MgO NP concentrations. Bactericidal concentration for *E. coli* is 1.5 mg/mL while the bactericidal for *B. subtilis* is lower, 0.75 mg/mL. The blank control references in both graphs refer to *E. coli* or *B. subtilis* (starting from a concentration of 10^7 CFU/mL) in culture medium. Antibacterial assays were repeated on several occasions and replicated a total of six times to calculate mean values and associated standard deviations.

MgO NPs are bactericidal and how Gram + *B. subtilis* was more susceptible to the MgO NPs than Gram - *E. coli*.

Importantly, we have also demonstrated that the particles did not produce cytotoxic effects in a kidney epithelial cell line (Vero cell line) over the same concentration range (Fig. S3). This evidence is commensurate with the aforementioned literature, which indicates that MgO NPs are not cytotoxic to mammalian cell lines and are safe to use, at least to the highest tested concentration of 1 mg/mL.

In order to complement these results, both *E. coli* and *B. subtilis* were incubated with the MgO NPs and stained with a LIVE/DEAD® BacLight™ Bacterial Viability Kit to determine the viability of the bacteria after the incubation. The samples incubated with the particles present lower bacterial density than the bacterial culture without the MgO NPs due to the antiproliferative effect of the MgO (Fig. S4).

Although the antibacterial assays already stated the potent antibacterial activity of the MgO NPs, Electron Microscopy observations were performed to obtain in-depth information about the effect of the NPs on bacterial cells. Environmental Scanning Transmission Electron Microscopy (ESEM) imaging of bacteria incubated with the MgO NPs can provide additional visible insight into bacteria morphology and health. ESEM demonstrated how the MgO NPs clearly elicited distinct responses from the bacterium cells, indicative of different

particle-bacterium interactions (Fig. 3). Both bacterial strains incubated with MgO NPs showed evidence of stress and damage including general loss of cell shape, cell membrane damage and leakage of cytoplasmic material. *B. subtilis* appeared to show signs of sporulation, an indicator of cell stress.

Initial Electron Paramagnetic Resonance spectroscopy (data not shown) showed that reactive oxygen species (ROS) were not produced under the *in vitro* conditions reported herewithin. Thus, to begin to understand the mechanism of action, Transmission Electron Microscopy (TEM) was used to determine the interaction of the MgO NPs with *E. coli* in particular (Fig. 4). Bacteria were incubated with different concentrations of MgO NPs for a 24 h period whereupon the cells were post-fixed, dehydrated, embedded in epoxy resin and sliced into 10 μ m slivers using a microtome. Our initial aim was to attempt to identify the location of MgO NPs (or aggregates thereof) internalised within the bacteria or associated with the cell surface. Unfortunately, and as may be expected, the low electron density of magnesium atoms meant that this particular element could not be distinguished from the vast amount of carbon in the bacterial cells. In Fig. 4 images of cells treated with 0.5 and 1 mg/mL of MgO NPs are reported (c and d) together with a control of untreated cells (a) and a control of cells grown in a medium at pH 9. This control is necessary due to the increase of the pH of the medium

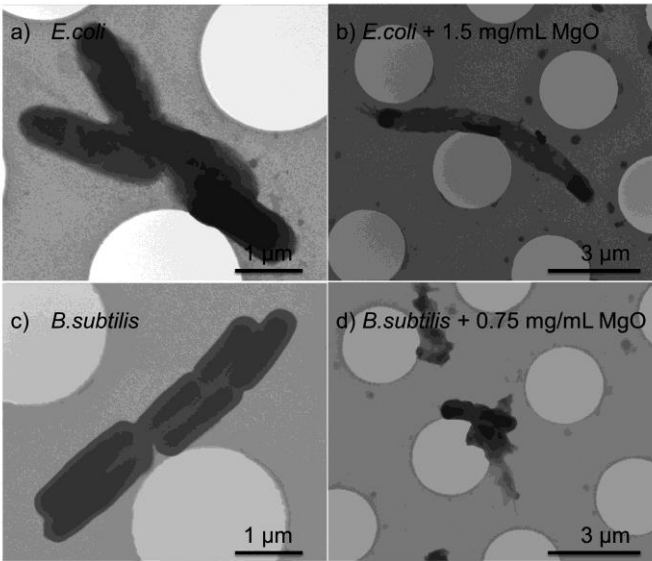


Fig. 3. Environmental STEM images of *E. coli* and *B. subtilis* incubated with MgO NPs at the corresponding bactericidal concentrations, where a) *E. coli* control cells; b) *E. coli* incubated with 1.5 mg/mL MgO NPs; c) *B. subtilis* control cells and d) *B. subtilis* incubated with 0.75 mg/mL MgO NPs.

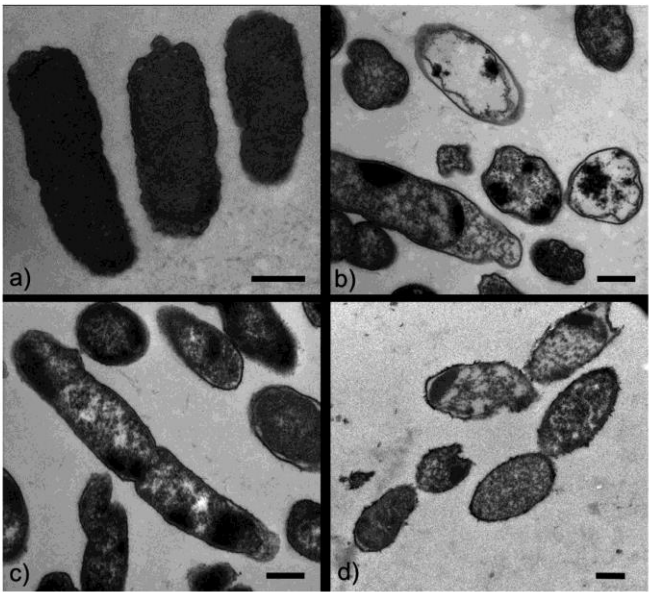


Fig. 4. Transmission Electron Microscopy (TEM) images of *E. coli* culture submitted to different treatments: control cells without any treatment (a); cells growth in the medium at pH 9 (b); cells incubated with 0.5 mg/mL MgO NPs (c) and cells incubated with 1 mg/mL MgO NPs (d). The predominant effect exerted on the bacterium cells by the MgO NPs is the loss of normal healthy shape and condensation of the cytoplasmic material (c); however, leakage of the cytoplasmic material also occurs (d). Scale bars correspond to 500 nm.

I.F. Castillo et al.

International Biodeterioration & Biodegradation 141 (2019) 79–86

Table 1
ICP-AES elemental quantification of the Mg content of *E. coli* and *B. subtilis* cells incubated with MgO NPs along with negative control samples (bacteria without MgO NPs).

Sample	Mg (mg/L)	% Mg w.r.t inoculation
MgO NPs	13.5	100
<i>E. coli</i> + MgO NPs	3.3	24.7
<i>B. subtilis</i> + MgO NPs	< 0.2	2.4
<i>E. coli</i> (control)	< 0.02	< 0.2
<i>B. subtilis</i> (control)	0.02	0.2

induced by the presence of MgO NPs. TEM imaging of MgO NP-treated bacteria emphasised the general damage of the bacterial envelope, as previously observed with ESEM. Some damage could be addressed to the increase of the pH of the medium, for example condensation of the cytoplasmic material that can be observed in Fig. 4b and c and that is in agreement with the literature. Although the increase in the pH value was responsible for some damages to the bacterial cells, it is clear from Fig. 4d that at higher NP concentrations the effect of NPs caused a permeabilisation of the bacterial envelope and leakage of the cytoplasmic material. A concentration of 1 mg/mL NPs has been used in this experiment (below the bactericidal concentration of 1.5 mg/mL) because this represents the highest NP concentration at which the observation of bacterial cells was still possible, since at higher concentrations their growth was completely inhibited.

The significant interaction of MgO NPs with bacterial cells was demonstrated by elemental analysis of bacteria incubated with MgO NPs, with *E. coli* displaying the most prominent magnesium content, retaining as much as 25% of the MgO NPs added to the medium (Table 1). Based on these results, it remains to be determined whether the MgO NPs interact with the cell membrane or actually internalise inside the bacteria, although this void currently forms part of our ongoing research efforts.

A variety of 18th century paper samples were obtained from the

Archives of the Real Jardín Botánico (Madrid) in order to test the applicability of the MgO NPs in real samples (Fig. S5). Three paper samples covering a variety of coarseness and porosity were selected from those provided. Establishing an efficient means of evaluating the activity of the particles *in situ* was one of the key priorities of this research and various different methods of evaluating and quantifying the microbial growth on the paper surfaces were investigated. In the first instance, the papers were cut into circles to perform a modified Kirby-Bauer disk diffusion technique. All the papers, including two circles of Whatman® Antibiotic Assay Discs were impregnated with an MgO NP suspension (disc 1) and with an Ampicillin solution (disc 2) as a control. After the incubation over an *E. coli* lawn, the only sample which generated an inhibition halo was the Whatman® disc impregnated in Ampicillin. Thus, it can be deduced that the MgO NPs do not diffuse on the agar meaning that there was no release of the MgO NPs from the Real Jardín Botánico papers into the agar medium (Fig. S6). We established a TBX agar method as a convenient means of detecting and quantifying the growth of *E. coli* on the paper samples. TBX Agar contains X-β-D-glucuronide, a chromogenic compound hydrolyzed by the β-glucuronidase (an *E. coli* enzyme) making the *E. coli* colonies turn green-blue on a conventional agar plate. The papers were therefore cut into 4 × 4 cm squares and placed in a sterile Petri dish and was impregnated with a 10 mg/mL MgO NPs solution and allowed to dry (see Materials & Methods). Once dry the papers were sprayed twice with a 10⁴ CFU/mL *E. coli* suspension. In our methodology the papers were each covered by a fine layer of TBX agar and when the medium solidified the process was repeated to obtain a complete homogeneous covering. The papers were then incubated for 48 h at 37 °C. Afterwards the treated and untreated papers were compared and counting of the green-blue *E. coli* colonies clearly illustrated the efficacy of the MgO NPs for preventing colonisation of the paper samples (Fig. 5). In addition, ESEM images of 18th century papers 1–3 treated with MgO NPs confirmed that the MgO NPs provide a homogeneous dispersion over the surface of the papers, where particles were clearly visible penetrating the pores and fibres of

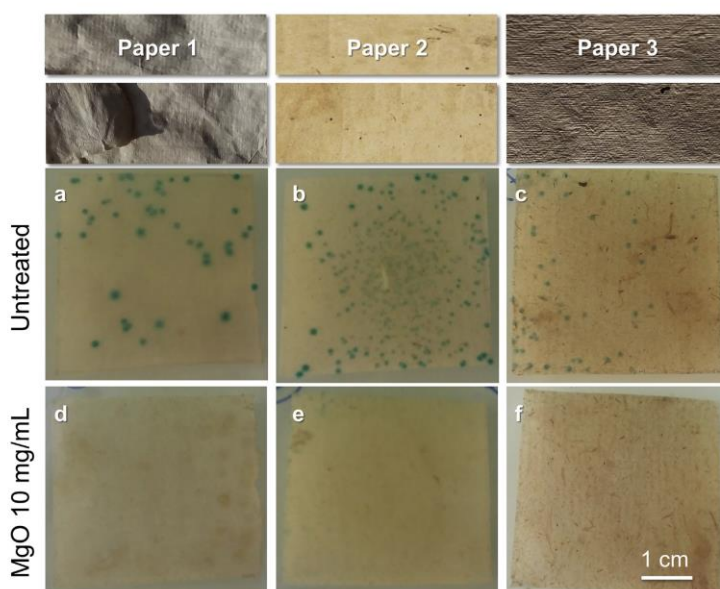


Fig. 5. Images of 18th century papers 1–3 contaminated with *E. coli* and incubated at 37 °C for 48 h. Panels a–c: untreated papers 1–3; panels d–f: papers 1–3 treated previously with a MgO NP suspension. Blue spots are colonies of *E. coli* stained with a chromogenic compound from TBX agar. Papers 1–3 treated with a suspension of MgO NPs resist *E. coli* colonisation. (For interpretation of the references to colour in this figure legend, the reader is referred to the Web version of this article.)

I.F. Castillo et al.

International Biodeterioration & Biodegradation 141 (2019) 79–86

the paper to provide a deep protective coating layer (see Fig. S7).

4. Conclusions

The powerful antibacterial activity of nano-magnesium oxide particles was used to protect various 18th century papers from bacterial colonisation. The combination of antibacterial assays and high resolution electron microscopy imaging has shown how the particles cause oxidative stress, cell membrane leakage and cell death and furthermore, this methodology has verified that the paper surfaces were covered by a homogenous nanoparticle coating which does not alter the aesthetics of the paper. Our on-going research efforts are currently centred on evaluating and understanding the bactericidal and fungicidal activity of these nanoparticles against different strains of bacteria and fungi that are common to museums, archives and library collections.

Acknowledgements

Financial support by the Fundación General CSIC (S.G.M., Programa ComFuturo), Fondo Social Europeo-Gobierno de Aragón (J.M.F, L.D.M., I.F.C. & S.G.M.) is gratefully acknowledged. Access to and use of the Advanced Microscopy Laboratory (University of Zaragoza) and to the XRD facility of the Servicio General de Apoyo a la Investigación de la Universidad de Zaragoza is gratefully acknowledged. The authors also thank Mario Soriano (Centro de Investigación Principe Felipe, Valencia, Spain), Rodrigo Fernández-Pacheco and Carlos Cuestas (Laboratorios de Microscopia Avanzada de la Universidad de Zaragoza) for their valuable technical support in electron microscopy experiments.

Appendix A. Supplementary data

Supplementary data related to this article can be found at <http://dx.doi.org/10.1016/j.ibiod.2018.04.004>.

References

- Asghar Afrafiar, A., Afsharpour, M., Samanian, K., 2017. Use of TiO₂/chitosan nanoparticles for enhancing the preservative effects of carboxymethyl cellulose in paper-art-works against biodeterioration. *Int. Biodeterior. Biodegrad.* in press (corrected proof). <https://doi.org/10.1016/j.ibiod.2017.04.025>.
- Baglioni, M., Giorgi, R., Berti, D., Baglioni, P., 2012. Smart cleaning of cultural heritage: a new challenge for soft nanoscience. *Nanoscale* 4, 42–53. <http://dx.doi.org/10.1039/C1NR10911A>.
- Baglioni, P., Carretti, E., Chelazzi, D., 2015. Nanomaterials in art conservation. *Nature Nano* 10, 287–290. <http://dx.doi.org/10.1038/nnano.2015.38>.
- Bokhim, X., Morales, A., Lopez, T., Gomez, R.J., 1995. Crystalline structure of MgO prepared by the sol-gel technique with different hydrolysis catalysts. *Solid State Chem.* 115, 411–415. <https://doi.org/10.1006/jssc.1995.1152>.
- Bondarenko, O., Juganson, K., Ivask, A., et al., 2013. Toxicity of Ag, CuO and ZnO nanoparticles to selected environmentally relevant test organisms and mammalian cells in vitro: a critical review. *Arch. Toxicol.* 87 (1181). <https://doi.org/10.1007/s00204-013-1079-4>.
- Carmichael, J., Degraff, W.G., Gazdar, A.F., Minna, J.D., Mitchell, J.B., 1987. Evaluation of a tetrazolium-based semiautomated colorimetric assay: assessment of radio-sensitivity. *Cancer Res.* 47, 936–946.
- Dizaj, S.M., Lotfipour, F., Barzegar-Jalali, M., Zarrintan, M.H., Adibkia, K., 2014. Antimicrobial activity of the metals and metal oxide nanoparticles. *Mater. Sci. Eng. C: Mater. Biol. Appl.* 44, 278–284. <https://doi.org/10.1016/j.msec.2014.08.031>.
- Domingos, R.F., Baaloucha, M.A., Ju-Nam, Y., Reid, M.M., Tufenkji, N., Lead, J.R., Leppard, G.G., Wilkinson, K.J., 2009. Characterizing manufactured nanoparticles in the environment: multimethod determination of particle sizes. *Environ. Sci. Technol.* 43, 7277–7284. <http://dx.doi.org/10.1021/es900249m>.
- Ge, S., Wang, G., Shen, Y., Zhang, Q., Jia, D., Wang, H., 2011. Cytotoxic effects of MgO nanoparticles on human umbilical vein endothelial cells in vitro. *IET Nanobiotechnol.* 5, 36–40. <http://ieeexplore.ieee.org/document/5754012/>.
- Ghobadian, M., Nabiani, M., Parivar, K., Fathi, M., Pazooki, J., 2015. Toxic effects of magnesium oxide nanoparticles on early developmental and larval stages of zebrafish (*Danio rerio*). *Ecotoxicol. Environ. Saf.* 122, 260–267. <https://doi.org/10.1016/j.ecoenv.2015.08.009>.
- Gutarowska, B., Skora, J., Zduniak, K., Rembisz, D., 2012. Analysis of the sensitivity of microorganisms contaminating museums and archives to silver nanoparticles. *Int. Biodeterior. Biodegrad.* 68, 7–17. <https://doi.org/10.1016/j.ibiod.2011.12.002>.
- Hajipour, M.J., Fromm, K.M., Ashkarran, A.A., Jiménez de Aberasturi, D., de Larramendi, I.R., Rojo, T., 2012. Antibacterial properties of nanoparticles. *Trends Biotechnol.* 30, 499–511. <https://doi.org/10.1016/j.tibtech.2012.06.004>.
- He, Y., Ingudam, S., Reed, S., Gehring, A., Strobaugh Jr., T.P., Irwin, P., 2016. Study on the mechanism of antibacterial action of magnesium oxide nanoparticles against foodborne pathogens. *J. Nanobiotechnology* 14 (54). <https://doi.org/10.1186/s12951-016-0202-0>.
- Koizhaiganova, M., Yasa, I., Gülümser, G., 2015. Assessment of antibacterial activity of lining leather treated with silver doped hydroxyapatite. *Int. Biodeterior. Biodegrad.* 105, 262–267. <https://doi.org/10.1016/j.ibiod.2015.09.017>.
- Krishnamoorthy, K., Moon, J.Y., Hyun, H.B., Cho, S.K., Kim, S.-J., 2012. Mechanistic investigation on the toxicity of MgO nanoparticles toward cancer cells. *J. Mater. Chem.* 22, 24610–24617. <http://dx.doi.org/10.1039/C2JM35087D>.
- La Russa, M.F., Ruffolo, S.A., Rovella, N., Belfiore, C.M., Palermo, A.M., Guzzi, M.T., Crisci, G.M., 2012. Multifunctional TiO₂ coatings for cultural heritage. *Prog. Org. Coat.* 74, 186–191. <https://doi.org/10.1016/j.porgcoat.2011.12.008>.
- La Russa, M.F., Macchia, A., Ruffolo, S.A., De Leo, F., Barberio, M., Barone, P., Crisci, G.M., Urzì, C., 2014. Testing the antibacterial activity of doped TiO₂ for preventing biodeterioration of cultural heritage building materials. *Int. Biodeterior. Biodegrad.* 96, 87–96. <https://doi.org/10.1016/j.ibiod.2014.10.002>.
- La Russa, M.F., Rovella, N., Alvarez de Buero, M., Belfiore, C.M., Pezzino, A., Crisci, G.M., Ruffolo, S.A., 2016. Nano-TiO₂ coatings for cultural heritage protection: the role of the binder on hydrophobic and self-cleaning efficacy. *Prog. Org. Coat.* 91, 1–8. <https://doi.org/10.1016/j.porgcoat.2015.11.011>.
- Leung, Y.H., Ng, A.M., Xu, X., Shen, Z., Gethings, L.A., Wong, M.T., 2014. Mechanisms of antibacterial activity of MgO: non-ROS mediated toxicity of MgO nanoparticles towards *Escherichia coli*. *Small* 10, 1171–1183. <http://dx.doi.org/10.1002/smll.201302434>.
- Li, W.-R., Sun, T.-L., Zhou, S.-L., Ma, Y.-K., Shi, Q.-S., Xie, X.-B., Huang, X.-M., 2017. A comparative analysis of antibacterial activity, dynamics, and effects of silver ions and silver nanoparticles against four bacterial strains. *Int. Biodeterior. Biodegrad.* 123, 304–310. <https://doi.org/10.1016/j.ibiod.2017.07.015>.
- Mai, T.-T., Moon, J.-Y., Song, Y.-W., Viet, P.-Q., Phuc, P.-V., Lee, J.-M., Yi, T.-H., Cho, M., Cho, S.-K., 2012. Ginsenoside F2 induces apoptosis accompanied by protective autophagy in breast cancer stem cells. *Cancer Lett.* 321, 144–153. <http://dx.doi.org/10.1016/j.canlet.2012.01.045>.
- Park, J.-Y., Lee, Y.-J., Jun, K.-W., Baeg, J.-O., Yim, D.J., 2006. Chemical synthesis and characterization of highly oil dispersed MgO nanoparticles. *J. Ind. Eng. Chem.* 12, 882–887. <https://www.ccheric.org/PDF/JIEC/IE12/IE12-6-0882.pdf>.
- Pietrzak, K., Puchalski, M., Otlewska, A., Wrzosek, H., Gulamet, P., Piotrowska, M., Gutarowska, B., 2017. Microbial diversity of pre-Columbian archaeological textiles and the effect of silver nanoparticles mixing disinfection. *J. Cult. Herit.* 23, 138–147. <https://doi.org/10.1016/j.culher.2016.07.007>.
- Raghupathi, K.R., Koodali, R.T., Manma, A.C., 2011. Size-dependent bacterial growth inhibition and mechanism of antibacterial activity of zinc oxide nanoparticles. *Langmuir* 27 (7), 4020–4028. <http://pubs.acs.org/doi/abs/10.1021/ja104825u>.
- Reddy, K.M., Feris, K., Bell, J., Wingett, D.G., Hanley, C., Punnoose, A., 2007. Selective toxicity of zinc oxide nanoparticles to prokaryotic and eukaryotic systems. *Appl. Phys. Lett.* 90, 2139021–2139023. <https://doi.org/10.1063/1.2742324>.
- Ruffolo, S.A., La Russa, M.F., Malagodi, M., Oliviero Rossi, C., Palermo, A.M., Crisci, G.M., 2010. ZnO and ZnTiO₂ nanopowders for antimicrobial stone coating. *Appl. Phys. A* 100, 829–834. <https://doi.org/10.1007/s00339-010-5658-4>.
- Shirakawa, M.A., John, V.M., Mocelin, A., Zilles, R., Toma, S.H., Araki, K., Toma, H.E., Thomaz, A.C., Gaylarde, C.C., 2016. Effect of silver nanoparticle and TiO₂ coatings on biofilm formation on four types of modern glass. *Int. Biodeterior. Biodegrad.* 108, 175–180. <https://doi.org/10.1016/j.ibiod.2015.12.025>.
- Sierra-Fernandez, A., Gomez-Villalba, L.S., Rabanal, M.E., Fort, R., 2017a. New nanomaterials for applications in conservation and restoration of stony materials: a review. *Mater. Construcción* 67, e107. <https://doi.org/10.3989/mc.2017.07616>.
- Sierra-Fernandez, A., De la Rosa-García, S.C., Gomez-Villalba, L.S., Gómez-Cornelio, S., Rabanal, M.E., Fort, R., Quintana, P., 2017b. Synthesis, photocatalytic, and antifungal properties of MgO, ZnO and Zn/Mg oxide nanoparticles for the protection of calcareous stone heritage. *ACS Appl. Mater. Interfaces* 9, 24873–24886. <http://pubs.acs.org/doi/abs/10.1021/acsami.7b06130>.
- Skóra, J., Gutarowska, B., Pielech-Przybylska, K., Stepień, L., Pietrzak, K., Piotrowska, M., Piotrowski, P., 2015. Assessment of microbiological contamination in the work environments of museums, archives and libraries. *Aerobiologia* 31, 389–401. <https://doi.org/10.1007/s10453-015-9372-8>.
- Sterflinger, K., Pinzari, F., 2012. The revenge of time: fungal deterioration of cultural heritage with particular reference to books, paper and parchment. *Environ. Microbiol.* 14, 559–566. <http://dx.doi.org/10.1111/j.1462-2920.2011.02584.x>.
- Sterflinger, K., Piñar, G., 2013. Microbial deterioration of cultural heritage and works of art - tilting at windmills? *Appl. Microbiol. Biotechnol.* 97, 9637–9646.
- Srinivasan, V., Bhavan, P.S., Rajkumar, G., Satgurunathan, T., Muralisankar, T., 2017. Dietary supplementation of magnesium oxide (MgO) nanoparticles for better survival and growth of the freshwater prawn *Macrobrachium rosenbergii* post-larvae. *Biol. Trace Elem. Res.* 177 (1), 196–208. <http://dx.doi.org/10.1007/s12011-016-0855-4>.
- Tang, Z.-X., Fang, X.-J., Zhang, Z.-L., Zhou, T., Zhang, X.-Y., Shi, L.-E., 2012. Nanosize MgO as antibacterial agent: preparation and characteristics. *Braz. J. Chem. Eng.* 29, 775–781. <https://doi.org/10.1590/S0104-66322012000400009>.
- Tang, Z.-X., Lv, B.F., 2014. MgO nanoparticles as antibacterial agent: preparation and activity. *Braz. J. Chem. Eng.* 31, 591–601. <http://dx.doi.org/10.1590/0104-6632.20140313s00002813>.

Protection of 18th century paper using antimicrobial nano-magnesium oxide

Isabel Franco Castillo,^{1†} Laura De Matteis,^{2**†} Clara Marquina,³ Esther García Guillén⁴,
Jesús Martínez de la Fuente,¹ Scott G. Mitchell^{1*}

1. Instituto de Ciencia de Materiales de Aragón (ICMA), Consejo Superior de Investigaciones Científicas (CSIC)-Universidad de Zaragoza and CIBER-BBN, C/ Pedro Cerbuna 12, 50009 Zaragoza (Spain).

2. Instituto de Nanociencia de Aragón (INA), Universidad de Zaragoza and CIBER-BBN, C/ Mariano Esquillor s/n, 50018 Zaragoza (Spain).

3. Departamento de Física de la Materia Condensada, Universidad de Zaragoza, C/ Pedro Cerbuna 12, 50009 Zaragoza (Spain).

4. Real Jardín Botánico, Consejo Superior de Investigaciones Científicas (CSIC), Madrid (Spain).

[†] These authors contributed equally

* E-mail: lauradem@unizar.es and scott@unizar.es

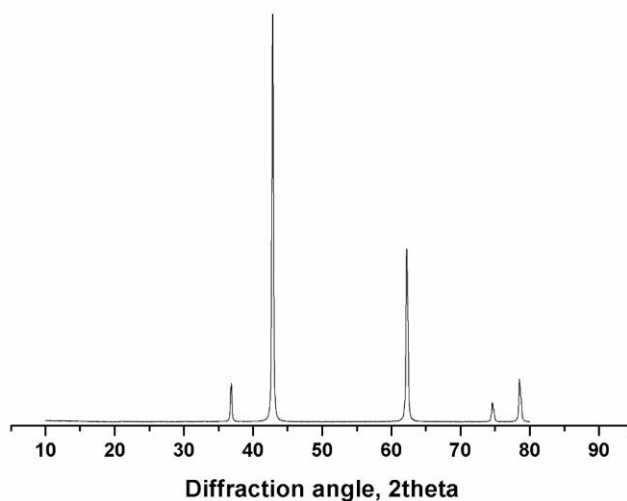


Figure S1. XRD analysis of MgO nanoparticles after annealing.

Supporting Information

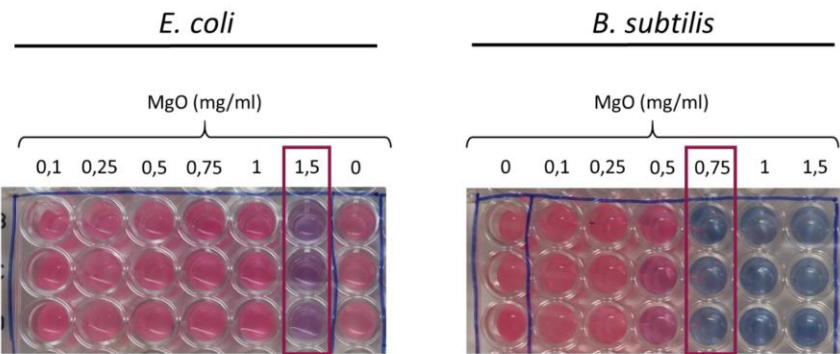


Figure S2. The antimicrobial effect of the MgO NPs was verified by determining the bactericidal concentration by resazurin colorimetric cell viability assay. The bactericidal concentration was 1.5 mg/mL in *E. coli* (left image) and 0.75 mg/mL in *B. subtilis*.

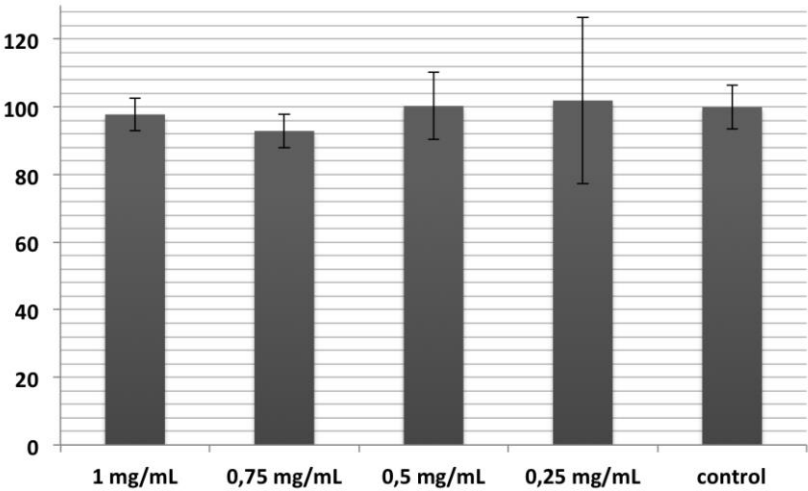


Figure S3. Cell viability assay in Vero cells after 24 hours incubation with MgO NPs at different concentrations.

Supporting Information

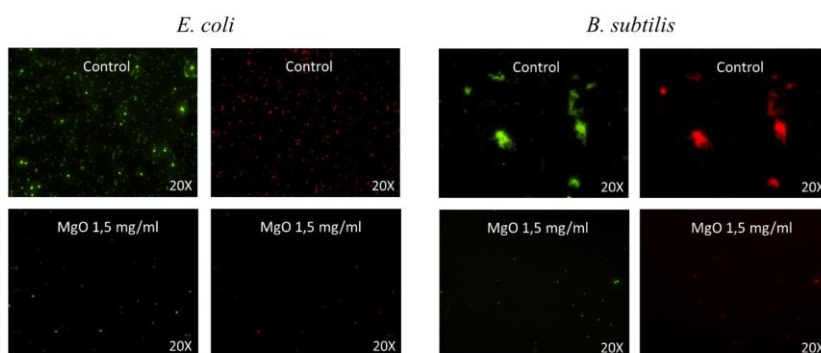


Figure S4. *E. coli* and *B. subtilis* were incubated with the MgO NPs and dye with a LIVE/DEAD® BacLight™ Bacterial Viability Kit to determine the viability of the bacteria after the incubation. The samples incubated with the particles present less bacterial density than the bacterial culture without the MgO NPs (control) due to the antiproliferative effect of the MgO.

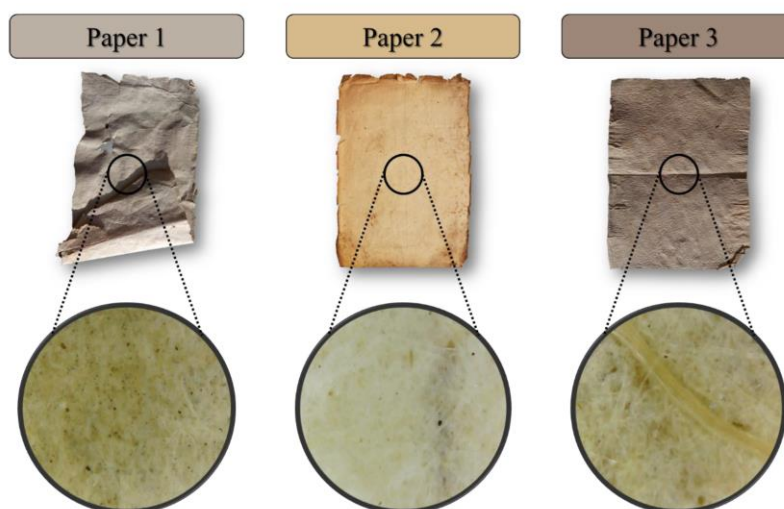


Figure S5. Papers from the 18th century obtained from the Archives of the Real Jardín Botánico (Madrid). The three paper samples exhibit a variety of coarseness and porosity. Each paper was visualized with an optical microscope to observe the fibre contain in more detail.

Supporting Information

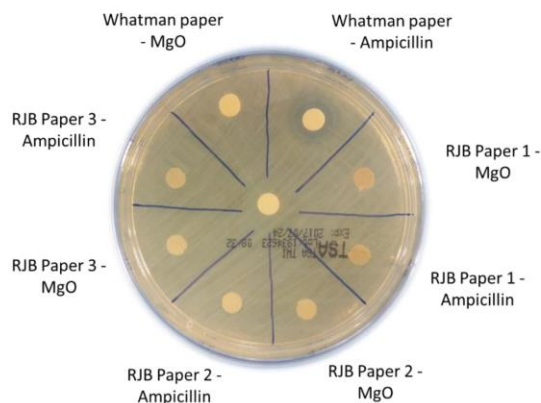


Figure S6. The RJB papers were cut into circles to perform a modified Kirby-Bauer disk diffusion technique. All the papers (Paper 1, Paper 2 and Paper 3), including two circles of Whatman® Antibiotic Assay Discs were impregnated with an MgO NP suspension (15 mg/mL) and with an Ampicillin solution (100 µg/mL) as a control. After the incubation over an *E. coli* lawn, the only sample which generated an inhibition halo was the Whatman® disc impregnated in Ampicillin. Thus, it can be deduced that the MgO NPs do not diffuse on the agar meaning that there was no release of the MgO NPs from the Real Jardín Botánico papers into the agar medium.

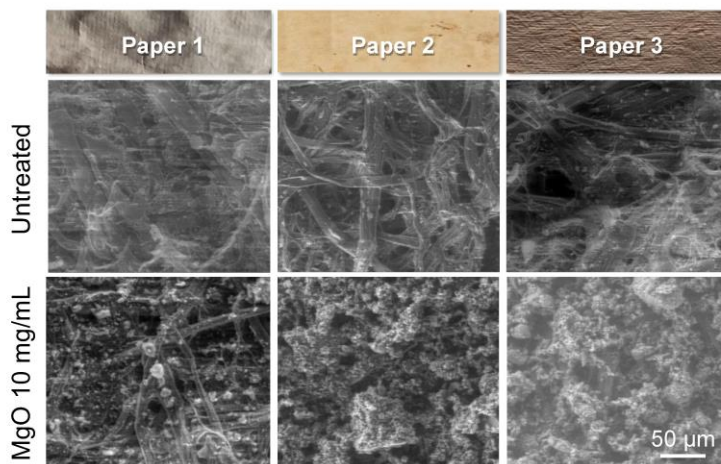


Figure S7. ESEM images of 18th century papers 1-3 in their natural state and treated with a MgO NP suspension. The images show the homogeneous coating of MgO NPs over the surface of the papers as well as the integration of the particles into the pores and fibres of the paper.

Article 3: Preventing fungal growth on heritage paper with antifungal and cellulase inhibiting magnesium oxide nanoparticles

Journal of Materials Chemistry B



PAPER

View Article Online
View Journal



Cite this: DOI: 10.1039/c9tb00992b

Preventing fungal growth on heritage paper with antifungal and cellulase inhibiting magnesium oxide nanoparticles†

Isabel Franco Castillo,^{ab} Esther García Guillén,^c Jesús M. de la Fuente,^{ab} Filomena Silva^{*de} and Scott G. Mitchell^{†ab}

Microorganisms such as bacteria, fungi, algae and moulds are highly proficient at colonizing artistic and architectural heritage. The irreparable damage they cause to unique artefacts results in immeasurable cultural and societal losses to our shared cultural heritage, which represent an important social and economic resource for Europe. With the overall aim of preventing fungal deterioration of paper artefacts, we report the use of magnesium oxide nanoparticles (MgO NPs) of average diameter 12 nm as potent antifungal agents against fungi commonly found colonising paper heritage: *A. niger*, *C. cladosporioides* and *T. reesei*. Dispersions of MgO NPs on original 18th century paper samples from the Archives of the Spanish Royal Botanic Garden were effective at preventing fungal colonisation without altering the appearance of the paper artefacts. Importantly, MgO NPs also inhibit cellulase activity in the filamentous fungi *T. reesei* and *A. niger*, two of the principle biodeteriogens of cellulosic materials. In addition, our report provides three simple new procedures for studying the fungal colonisation prevention properties of nanomaterials on paper samples. Overall this opens the door to the use of colourless, low-cost, and scalable nanomaterials for preventing biodeterioration in cellulose-based artefacts.

Received 16th May 2019,
Accepted 20th June 2019

DOI: 10.1039/c9tb00992b

rsc.li/materials-b

Introduction

Much of our shared tangible cultural heritage is based on paper objects: from books and documents, to maps, paintings, drawings and other works of art.¹ The organic composition of paper-based heritage artefacts means that they are highly susceptible to irreversible biodeterioration – “any undesirable change in the properties of a material caused by the vital activities of organism”.^{2,3} Protecting and preserving such heritage from colonisation by microorganisms is therefore a matter of great importance.^{4,5}

Filamentous fungi are considered to be some of the most hazardous microorganisms for cultural heritage objects,⁶ and cellulolytic fungi are particularly harmful for paper objects.^{7,8}

Fungi not only affect aesthetic aspects of the object or artefact, resulting in effects such as foxing or discoloration; they also produce organic acids and degrading enzymes, such as cellulases or proteases,⁹ which damage the structural integrity of the object.¹⁰ During cellulose degradation, the hydrolysis of glycosidic bonds and oxidation of glucopyranose rings results in the formation of acids which further catalyse paper degradation by breaking cellulose chains, transforming the paper into a delicate and brittle object. The *Trichoderma* and *Aspergillus* genera are two prolific cellulase producers that often threaten paper heritage.^{11,12} Furthermore, certain fungi that are often found colonizing museum spaces, archives and libraries – such as those from *Aspergillus*, *Fusarium* and *Penicillium* – may be dangerous to professionals and visitors alike due to the production of mycotoxins, which can be inhaled causing immune system issues and allergic diseases, mycotoxicosis and organ mycoses.^{13–17}

To combat paper degradation, conservators and restorers use a variety of different methods that have been changing radically in recent years.¹⁸ Ethanol (70%) is one of the most effective short-term disinfectant solutions,¹⁹ nonetheless a typical spray application, which is common and convenient for restorers, does not remove all types of microorganisms and recolonization is frequent.²⁰ Over the last century chemical agents such as quaternary ammonium salts, ethylene oxide, alcohols or formaldehyde have been used to disinfect objects.^{21,22} However, potent

^a Instituto de Ciencia de Materiales de Aragón (ICMA), Consejo Superior de Investigaciones Científicas (CSIC)-Universidad de Zaragoza, C/Pedro Cerbuna 12, 50009 Zaragoza, Spain. E-mail: scott@unizar.es

^b CIBER-BBN, Instituto de Salud Carlos III, Madrid, Spain

^c Real Jardín Botánico, Consejo Superior de Investigaciones Científicas (CSIC), Madrid, Spain

^d ARAD – Agencia Aragonesa para la Investigación y el Desarrollo, Av. Ranillas, 1D, 2B, 50018 Zaragoza, Spain

^e Universidad de Zaragoza, Facultad de Veterinaria, Calle Miguel Servet 117, 50013 Zaragoza, Spain

† Electronic supplementary information (ESI) available: Additional photos, optical and electron microscopy images. See DOI: 10.1039/c9tb00992b

antifungal compounds like these pose a direct risk to human health due to their high overall cytotoxicity. For example ethylene oxide, which is a carcinogenic and mutagenic gas, can cause severe allergic reactions.^{23,24} One widely used and effective physical method is gamma radiation, which kills fungi and their spores; however, the required fungicidal doses are higher than those needed for bactericidal action.²⁵ Moreover, this radiation can affect the cellulose fibres and paper structure and important health and safety consideration must also be given to the operator.⁸ As a result, new potent antifungal treatments that are simultaneously safe to human health must be developed.

To this end, restorers have frequently turned to using aqueous calcium hydroxide or calcium carbonate²⁶ solutions to neutralize acids and simultaneously serve as a local alkali reserve to prevent further colonization to prevent the degradation of historical paper. During the last decade, nanoparticles (NPs) as nanosols, alcohol dispersions and powders have been used to prevent the degradation of paper, stone, paintings and wood heritage.^{27,28} NPs provide an alternative to other common antimicrobials, and their effectiveness lies in their ability to interact with DNA and proteins and pass through the cell membrane.^{29,30} One of the most widely used are silver nanoparticles (Ag NPs),^{31,32} which offer high antimicrobial properties at low concentrations and multiple mechanisms of action (*e.g.* Ag inhibits the replication of DNA, disrupts respiratory processes and disturbs the electrical potential of the cell membrane, among others).^{32–34} Ag NPs are used commercially as active ingredients in health, cosmetics and packaging due to their multifunctional mode of action, broad spectrum antibacterial activity and the unlikelihood of development of resistance.³⁵ Nevertheless, silver is toxic to cells of higher animals³⁶ and can disturb the ecological balance in natural systems.³⁷ Furthermore, from a heritage conservation perspective, highly coloured noble metal particles present their own limitations. Other nanoparticles alternative include nanostructured zinc oxide (ZnO), which is antibacterial and antifungal activity but bio-safe and bio-compatible, as well as the nanometric form of TiO₂, which is characterized by its broad-spectrum biocidal activity and low cytotoxicity.^{38,39} However, the photocatalytic antimicrobial activity of nano-TiO₂ means that it is light dependent, and loses its effectiveness in environments with limited or no UV light³⁰ and it has been found to be less effective against fungi than against bacteria or viruses.⁴⁰

The advantages of these nanostructured inorganic materials resides in their tuneable physicochemical properties and modular nature, which allow us to obtain a library of materials with different sizes, shapes and surface properties.^{41,42} In the context of paper conservation, the high surface area of nanoparticles means that they can effectively cover paper and penetrate into the network of cellulose fibres to neutralize acids and protect paper from cellulose hydrolysis. Currently, the most common analytical techniques used to study the antimicrobial properties of NPs on heritage surfaces are based on optical and electron microscopies and colorimetry, but these methods are limited and do not characterise the medium-to-long-term influence of antimicrobial nanoparticles.⁴³

Here we present a combination of three rapid procedures to comprehensively characterise the antifungal properties and

biodeterioration prevention activity of nanomaterials for heritage paper conservation. We have demonstrated these using magnesium oxide nanoparticles (MgO NPs) as antifungal agents to prevent the fungal colonization of a variety of 18th century paper samples from the Archives of the Spanish Royal Botanic Garden in Madrid (Spain). Although there have been several studies concerning the antibacterial activity of MgO NPs, their exact mechanism is still unknown. Different antibacterial mechanisms have been proposed, such as the formation of reactive oxygen species (ROS) and non-ROS mediated interaction with the cell wall or the cell membrane of the bacteria as well as an alkaline effect due to the increase of the pH mediated by the MgO NPs.^{41,44,45} However, their antifungal activity has not been comprehensively reported in the literature. In this report the antifungal activity of MgO NPs has been studied against three different moulds that frequently contaminate heritage paper: *Aspergillus niger* (genera *Aspergillus* represents 29%), *Cladosporium cladosporioides* (genera *Cladosporium* represents 5–7%) and *Trichoderma reesei* (genera *Trichoderma* represents 4%).⁴ *A. niger* causes black stains due to the production of melanin.^{46,47} It is particularly harmful to paper because of its ability to grow on substrates with low (7–8%) moisture content,⁴⁸ and it is an important producer of cellulase, an enzyme capable of degrading cellulose fibres into glucose.¹² *C. cladosporioides* affects paper by producing melanoidines which cause stains^{47,49} and *T. reesei* is one of the most prominent cellulase-producing fungi triggering irreparable damage to cellulose containing heritage objects.^{11,50}

Results and discussion

Magnesium oxide nanoparticles (MgO NPs) were synthesised by a sol-gel method and used as antifungal agents on 18th century heritage paper samples. The 12 nm diameter MgO NPs were

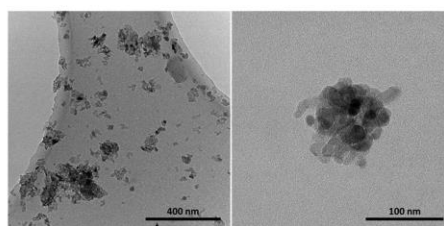


Fig. 1 TEM images of magnesium oxide nanoparticles (MgO NPs) ca. 12 nm diameter prepared by sol-gel synthesis.

Table 1 MgO NP minimum inhibitory concentration (MIC) values against *A. niger*, *C. cladosporioides* and *T. reesei*

	Fungal species		
	<i>A. niger</i>	<i>C. cladosporioides</i>	<i>T. reesei</i>
MIC value (mg mL ⁻¹)	6	12	3

prepared using a sol-gel synthesis⁵¹ according to our previously reported experimental procedure,⁵² which provided sufficient control of the nanoparticle size and morphology (Fig. 1). Further characterization of the nanoparticles can be found in our previous report.⁵² MgO NPs are particularly interesting due to

their low cost and environmental friendly characteristics.⁵³ They possess antibacterial properties resulting from two proposed mechanisms of action: one mediated by the production of reactive oxygen species (ROS), which induces oxidative stress and lipid peroxidation in bacteria,⁴⁴ and non-ROS mediated mechanisms.⁵⁴ Cell viability assays have demonstrated the absence of cytotoxicity of these nanoparticles.^{52,55}

Three representative fungal strains, *Aspergillus niger* (*A. niger*), *Cladosporium cladosporioides* (*C. cladosporioides*) and *Trichoderma reesei* (*T. reesei*), were chosen based on their prevalence in heritage artefacts and their cellulose degradation activity.^{4,11,46,49} The antifungal activity of MgO NPs was determined using an antifungal broth microdilution assay to determine the minimal inhibitory concentration (MIC) values of NPs that are able to inhibit fungal growth.⁵⁶ *C. cladosporioides* was the most resistant to MgO NPs with a MIC value of 12 mg mL⁻¹, followed by *A. niger* (6 mg mL⁻¹); whereas *T. reesei* proved to be the most susceptible to MgO NPs, with the lowest MIC value equal to 3 mg mL⁻¹ (Table 1).

Given the *in vitro* antifungal activity that was observed, a series of assays were designed to evaluate the *in situ* activity of the MgO NPs on original 18th paper samples from the Archives of the Spanish Royal Botanic Garden (CSIC) in Madrid (Fig. S1, ESI[†]). In total, three different *in situ* antifungal procedures were designed to establish the antifungal mode of action of the MgO NPs on paper samples and gain insight into longevity of action. The homogeneity of the MgO NPs coating was studied by

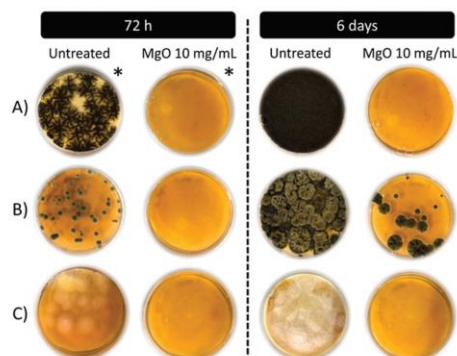


Fig. 2 Antifungal activity of MgO NPs against *A. niger* (A), *C. cladosporioides* (B) and *T. reesei* (C) on paper samples under optimal growth conditions after 72 h (*48 h for *A. niger*) and 6 days of incubation.

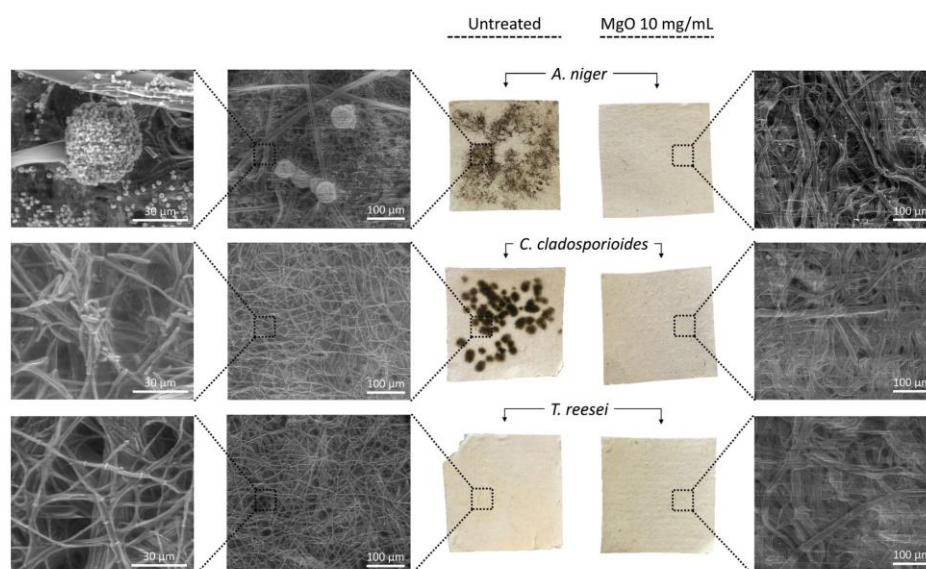


Fig. 3 *In situ* antifungal activity of MgO NPs. The untreated papers (left) present fungal growth visible by the naked eye and confirmed by ESEM imaging, where the growth of all three fungal strains (*A. niger*, *C. cladosporioides* and *T. reesei*) are clearly observable on top of the cellulose fibres of the untreated papers, but are absent from the MgO NP treated papers (right).

Environmental Scanning Electron Microscopy (Fig. S2, ESI†) and the amount of MgO NPs coating the papers was quantified by Inductively Coupled Plasma Mass Spectrometry (ICP-MS). The 18th century papers coated with a MgO NP solution were found to contain 0.86 mg of Mg per g, while the amount of Mg on the untreated paper samples was found to be 77 µg per g (Fig. S3, ESI†).

For the first antifungal assay performed in heritage paper samples, 5 cm diameter circles were coated with an aqueous dispersion of MgO NPs (10 mg mL⁻¹). This concentration was selected to ensure a satisfactory antifungal activity based on the MIC values for the fungal strains. Once dry, the paper samples were covered with a thin Sabouraud Dextrose Agar (SDA) layer and incubated at their optimum growth temperatures for six days. As observed in Fig. 2, after 72 hours of incubation (*48 h for *A. niger*), fungal growth is clearly visible in the control samples, while no growth was observed in paper samples treated with MgO NPs. After longer incubation times of up to six days, *A. niger* and *T. reesei* failed to display any growth (fungicidal action), however *C. cladosporioides* began to proliferate on the MgO NP treated samples. Given that the MgO NPs were applied at 10 mg mL⁻¹ and the MIC value for the *C. cladosporioides* is 12 mg mL⁻¹, a fungistatic action was not obtained, leading to the initiation of fungal growth after six days.

The antifungal activity was also evaluated *in situ*, where 2 × 2 cm sterile paper samples were coated with 10 mg mL⁻¹ MgO NPs and incubated in a humidity chamber. Fungal growth was monitored by macroscopic inspection of paper samples as well as microscopic observation (Environmental Scanning Electron Microscopy (ESEM) and optical microscopy). The brown-black fungal growth of *A. niger* and *C. cladosporioides* was easily observed in the untreated samples while *T. reesei* presented a yellow coloured growth (Fig. 3 and Fig. S4, ESI†). The images obtained by optical microscopy (Fig. S5, ESI†) and ESEM (Fig. 3 and Fig. S6, ESI†) confirmed that the untreated paper samples were covered with fungi mycelium for all three moulds, with a significant amount of spores in the case of *A. niger*, while MgO

NP treated paper samples showed no fungal growth over the paper surface and only cellulose fibres were observed (Fig. 3). From these two *in situ* assays we can conclude that MgO NPs deposited on the 18th century paper samples at 10 mg mL⁻¹ are capable of inhibiting the fungal growth of the selected fungi, with a fungicidal action against *A. niger* and *T. reesei* (the two cellulose producing strains responsible for paper degradation) and a fungistatic action against *C. cladosporioides*.

A. niger and *T. reesei* are both producers of cellulase, an enzyme responsible for catalysing cellulolysis, the decomposition of cellulose and related polysaccharides into simple monosaccharides for energy purposes. Fungal growth on artefacts made from cellulosic materials can undergo rapid and severe biodeterioration as the colonizing microbes consume cellulose for energy. Consequently, the third and final assay was designed to assess the adhesion of fungal cells to the paper samples and evaluate the cellulase prevention capacity of the MgO NPs on heritage paper samples. The MgO NP concentration dependent fungal cell adhesion to the paper was evaluated by incubating different concentrations of MgO NP treated paper samples (1/4, 1/2, 1× and 2× the MIC value) with *A. niger* and *T. reesei*. By weighing the papers after the incubation with the fungi, their adhesion to the papers and subsequent growth can be determined

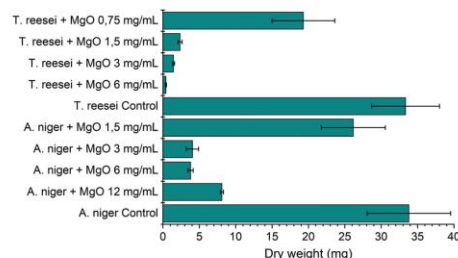


Fig. 4 Mean dry weight of the paper samples (error bars correspond to SD values of three independent assays) incubated with *A. niger* and *T. reesei* in presence of MgO NPs. The MgO NPs inhibit fungal growth and adhesion to the paper at 3 mg mL⁻¹ for *A. niger* and at 1.5 mg mL⁻¹ for *T. reesei* (concentrations that are equal to 1/2 of the MIC of MgO NPs for each fungal strain).

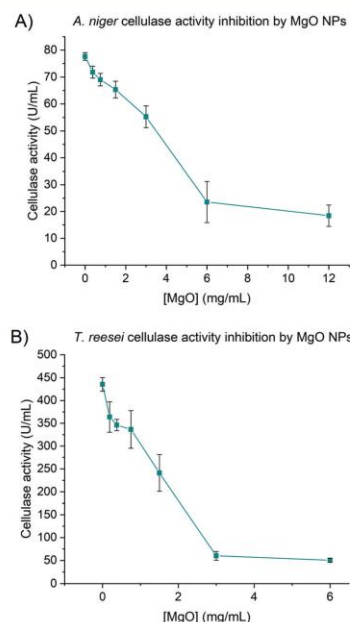


Fig. 5 Enzymatic activity of cellulase from *A. niger* (A) and *T. reesei* (B) incubated with MgO NPs at concentrations of 1/16, 1/8, 1/4, 1/2, 1× and 2× the corresponding MIC values for each fungus. Error bars correspond to SD values of three independent assays.

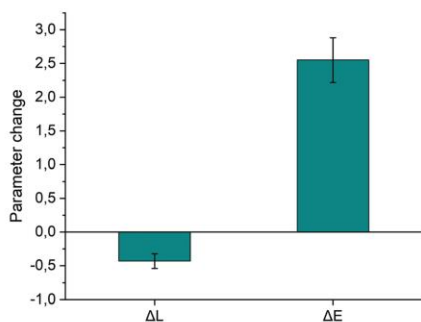


Fig. 6 Luminosity change (ΔL) and colour change (ΔE) of the paper samples after coating with the 10 mg mL⁻¹ MgO NP dispersion.

by comparing the dry weight of the positive control papers (incubated without MgO NPs) with the dry weight of the MgO NP-treated papers (Fig. S7, ESI†). Fig. 4 reports how the MgO NPs inhibit the adhesion and growth of *A. niger* and *T. reesei* at concentrations lower than the MIC value. At the lowest MgO NP concentration (1/4 MIC), both fungi are capable of growing on papers, but at concentrations greater than 1/2 MIC, fungal adhesion and growth are highly diminished and even completely inhibited.

The anticellulase activity of the MgO NPs was analysed by incubating the particles with commercial *A. niger* and *T. reesei* cellulase extracts. Cellulase activity decreased with increasing MgO NP concentration, where concentrations of 1/2 MIC were able to reduce the cellulase enzymatic activity by half, with only residual enzymatic activity being observed at the MIC concentration for each fungal strain (Fig. 5).

To confirm that the MgO nanoparticles were not visibly altering the appearance of the paper samples, colorimetric measurements were performed before and after the MgO NP coating. As shown in Fig. 6, the MgO NP coating did not produce any significant changes in the luminosity (ΔL) or colour (ΔE). The ΔE mean value was 2.55, which is far below the ΔE limit value where chromatic changes become visible to the naked eye ($\Delta E = 5$).⁵⁷

Conclusions

In this research we have demonstrated how cheap, colourless and scalable dual-functional magnesium oxide nanoparticles (MgO NPs) can be used to protect original heritage papers from fungal biodeterioration via antifungal and cellulose inhibition. *In vitro* studies showed that the small 12 nm-diameter MgO NPs possessed fungistatic activity against three filamentous fungal strains, *T. reesei*, *A. niger* and *C. cladosporioides*, at concentrations between 3 and 12 mg mL⁻¹. A series of *in situ* antifungal studies were developed to confirm the antifungal properties of the MgO NPs on original 18th century paper samples. A homogeneous 10 mg mL⁻¹ dispersion of MgO NPs provided complete

inhibition of all three fungal strains while simultaneously avoiding any unwanted colour changes to the paper. Importantly, the fungal adhesion to the paper was inhibited at MgO NP concentrations as low as 1.5 mg mL⁻¹ for *T. reesei* and 3 mg mL⁻¹ and for *A. niger*. Furthermore, the MgO NPs inhibit *A. niger* and *T. reesei* cellulase enzymes, meaning that these nanoparticles prevent degradation of the cellulose fibres as well as fungal colonization. These results illustrate how a combination of rapid antifungal procedures and high-resolution environmental electron microscopy techniques can be used to comprehensively characterise the biodeterioration prevention properties of nanomaterials and pave the way for the rapid screening of other potential antifungal nanomaterials for heritage conservation.

Experimental

Reagents

Magnesium methoxide, 7–8% in methanol (Alfa-Aesar); absolute ethanol (PanReac AppliChem); Cellulase extract from *T. reesei* and *A. niger*; Sigmacell cellulose; 3,5-dinitrosalicylic acid (DNS), 2,3,5-triphenyltetrazoliumchlorid (XTT), menadione, sodium cacodylate trihydrate, sucrose, glutaraldehyde 25% and NaCl (all from Sigma-Aldrich).

Test papers

18th century paper samples were obtained from the leftovers of the Herbarium sheets conserved in the Archives of the Real Jardín Botánico (CSIC) in Madrid, Spain.

Microorganisms and growth conditions

Two moulds from the Colección Española de Cultivos Tipo (CECT) were tested in the antifungal assays: *Aspergillus niger* CECT 2088, *Cladosporium cladosporioides* CECT 2111. *Trichoderma reesei* RUT C-30 was kindly provided by the CICS-UBI – Health Sciences Research Centre, University of Beira Interior, Portugal. Fungal spore suspensions were stored in 0.1% Tween, 20% glycerol at –80 °C prior to use. Before each assay, fungal cells were inoculated in SDA plates and slants (Sabouraud Dextrose Agar (supplemented with chloramphenicol, Scharlab, S.L.)) and grown at 35 °C for 5 days.

For the fungal adhesion assays, the following liquid medium was used: 2.0 g L⁻¹ KH₂PO₄; 1.4 g L⁻¹ (NH₄)₂SO₄; 0.0027 g L⁻¹ FeSO₄·7H₂O; 0.0016 g L⁻¹ MnSO₄·H₂O; 0.0014 g L⁻¹ ZnSO₄·H₂O; 0.0037 g L⁻¹ CoCl₂·6H₂O; 0.6 g L⁻¹ MgSO₄·7H₂O; 0.4 g L⁻¹ CaCl₂·2H₂O; 0.75 g L⁻¹ peptone; 2.0 g L⁻¹ Tween 80; 0.3 g L⁻¹ urea; and 5 g L⁻¹ glucose in formate buffer 50 mM pH = 4.8.⁵⁸

Methods

Environmental scanning electron microscopy (ESEM). Data were collected on a Quanta FEG-250 (FEI Company) field emission SEM for high-resolution imaging working in ESEM mode using a GSED detector under high relative humidity conditions.

Fungi proliferation assay. Fungal growth was recorded by measuring the optical density (OD) of the samples at 620 nm after 48 h of incubation using a microplate reader (Thermo

Scientific MULTISKAN GO). A XTT assay was performed to confirm the results, measuring the absorbance at 450 nm using a microplate reader (Thermo Scientific MULTISKAN GO). Results were compared with the OD variation of a control culture containing only fungi. The assays were replicated four times and the modal value was chosen as the minimal inhibitory concentration (MIC).

Transmission electron microscopy (TEM). Magnesium oxide nanoparticles (MgO NP) were resuspended in ethanol under sonication and visualized by Bright Field (BF) imaging in a FEI Tecnai T20 microscope operating at 200 kV. More than 100 NPs were measured and an estimation of the diameter has been obtained using Digital Micrograph[®] (Gatan Inc., Pleasanton, TX, USA) and OriginLab[®] (OriginLab, Northampton, MA, USA).

Nanoparticle synthesis. MgO nanoparticles were synthesized by sol-gel method through a modification of protocols already reported in literature.⁵² Briefly, 7.2 mL of magnesium methoxide, $\text{Mg}(\text{OCH}_3)_2$, (4.8 mmol) were added to 40 mL of absolute ethanol under ultrasonication and subsequently 1.8 mL of water (100 mmol) were added to the mixture. The sol was sonicated for 30 minutes and then kept for 36 h under gentle stirring to facilitate gelification. The water/ethanol gel suspension was heated in an oil bath under a progressive increase of the temperature from 70 to 90 °C during a period of 5 h. Then a fine magnesium dihydroxide powder was obtained by evaporating the solvent and finally this $\text{Mg}(\text{OH})_2$ powder was completely oxidised to MgO by heating at 600 °C for 30 minutes. Yield = 120 mg (dry particles).

Inductively coupled plasma mass spectrometry (ICP-MS). The amount of MgO NPs on the paper after the coating was analysed by ICP-MS. 1×1 cm squares of 18th century paper were coated with 10 mg mL⁻¹ MgO NPs solution (uncoated samples were used as a control). All the paper samples were digested in 100 µL of piranha solution for 15 minutes at room temperature and then 300 µL of aqua regia were added and incubated for 2 hours at room temperature followed by 15 minutes at 60 °C. Afterwards, the samples were diluted in Milli-Q water to a final volume of 20 mL. ICP-MS measurements were carried out with a quadrupole Agilent 7500 series ICP-MS instrument (Agilent Technologies, CA, USA), equipped with a Babington nebulizer and a double pass spray chamber. Magnesium quantification was performed using a calibration curve ranging from 1 and 1000 ng g⁻¹ (ppb) Mg(i) in ultra-pure water. The data acquisition parameters for both calibration curve and samples were set to the single particle mode for detecting the presence of magnesium (²⁴Mg, ²⁵Mg, and ²⁶Mg), in a full quantitative mode, with 1 point per spectral peak, an integration time of 0.2 s per point and 10 repeats per sample, giving a total acquisition time of 40.2 s. Digested paper and paper with MgO NPs samples were measured in triplicate and quintuplicate, respectively. The control paper samples were diluted 1/10 and the MgO coated paper samples were diluted 1/100 to adjust the concentration to the calibration curve.

Fungi growth inhibition assay. The determination of the minimum inhibitory concentration of MgO NPs was performed using a broth microdilution method according to the EUCAST

guidelines (E.DEF 9.3.1).⁵⁶ The experiments were performed with three moulds, *A. niger*, *C. cladosporioides* and *T. reesei*. Fungi spores were incubated for five days in SDA plates at 35 °C for *A. niger* and *T. reesei* and at 25 °C for *C. cladosporioides*. By picking the aerial part of the fungi, a suspension of 10⁶ conidia per mL was prepared in sterile water with 0.1% Tween. This suspension was diluted to 10⁵ conidia per mL in distilled sterile water and added to a 96 well plate to a final concentration of 5×10^4 conidia per mL. Geometric two-fold dilutions of MgO NPs [0.09375, 0.1875, 0.375, 0.75, 1.5, 3, 6, 12 mg mL⁻¹] were made by dispersing them in RPMI and sonicated for 30 minutes before adding them to the 96 well-plate. Positive control contained only fungal inocula and culture media while the negative control contained only MgO NPs dispersed in culture medium. After an incubation period of 48 h, at 35 °C for *A. niger* and *T. reesei* and at 25 °C for *C. cladosporioides*, according to CECT recommendations, the minimum inhibitory concentration (MIC) values were determined as the lowest MgO concentration able to inhibit fungal growth detectable to the naked eye. MIC values were further confirmed by measuring the OD₆₂₀ and fungal metabolic activity using XTT and menadione. The colorimetric assay based on XTT was carried out by adding 50 µL of saline containing 1 mg of XTT per mL and 20.2 µg of menadione per mL (previously dissolved in acetone at a concentration of 430 µg mL⁻¹ and then diluted 1/10 in saline) was added to each well to obtain a final concentration of 200 µg of XTT per mL and 4.3 µg of menadione per mL (25 µM). Following an incubation period of 2 h in the dark to allow conversion of the XTT to its formazan derivative, the absorbance at 450 nm was measured.

Antifungal assays on paper samples

Antifungal activity under optimal growth conditions. The 18th century paper samples were cut in 5 cm diameter discs and sterilized by autoclaving. After drying, sterilized papers were placed into a 5.5 cm Petri dish and impregnated with 800 µL of a 10 mg mL⁻¹ MgO NPs solution in sterile distilled water. The papers were allowed to dry at room temperature and the MgO impregnation protocol was repeated to ensure a homogeneous coating. When the papers were completely dry, 500 µL of a fungi inoculum (10³ conidia per mL, in distilled water) was added to the coated papers and over a positive growth control paper sample without MgO NPs. Then, SDA culture media was added until the paper was completely covered. Plates were incubated at 35 °C for *A. niger* and *T. reesei* and at 25 °C for *C. cladosporioides*. The fungal growth was monitored for 6 days.

In situ antifungal activity. The 18th century paper samples were cut in 2×2 cm squares and sterilized by autoclaving. Sterile paper samples were placed into a 6 well plate and impregnated with 100 µL of a 10 mg mL⁻¹ MgO NP solution (dissolved in RPMI) using a micropipette. The papers were let to dry and the impregnation protocol was repeated to ensure a homogeneous coating. When the papers were completely dry, 100 µL of a fungi inoculum (10³ conidia per mL in RPMI) was added to the coated papers and over a positive growth control paper sample without MgO NPs. Afterwards, plates were incubated in

a humidity chamber at the respective temperature for each fungus. Fungal growth was monitored during 2 weeks. In order to visualize the samples with ESEM, the papers were washed with 2 mL of saline and fixed with a 2 mL of cacodylate buffer 0.1 M for 1 h and 30 minutes at 37 °C. Then the samples were dehydrated with methanol (5 min with methanol 30%, 5 min with methanol 50%, 5 min with methanol 70%, 10 min with methanol 100% and 5 min with methanol 100%) and kept at room temperature for further analysis.

Inhibition of fungal adhesion. 18th century paper samples were incubated in 10 mL fermentation medium containing 1 mL of an *A. niger* and *T. reesei* inoculum (10^5 conidia per mL, prepared in liquid medium) and MgO NPs at the 1/4, 1/2, 1× and 2× MIC value which corresponds to the following concentrations: 1.5, 3, 6, 12 mg mL⁻¹ for *A. niger* and 0.75, 1.5, 3, 6 mg mL⁻¹ for *T. reesei*. Three paper samples of 1 × 3 cm were used for each sample, in addition with a positive growth control sample without MgO NPs and a negative control without fungi. Samples were incubated four days at 35 °C with agitation. After incubation, paper samples were removed from the culture, washed with sterile saline solution and dried at 50 °C until a constant weight was achieved.

Cellulase activity. Cellulase extracts from *A. niger* and *T. reesei* were incubated with different MgO NPs concentrations (1/16, 1/8, 1/4, 1/2, 1× and 2× MIC) for 1 h at 37 °C with agitation. After incubation, 1 mL of cellulase solutions was mixed with 4 mL of a cellulose 5% (w/v) solution and incubated at 37 °C for 120 min with vigorous stirring to determine the cellulase activity. All the reagents were prepared in 50 mM sodium acetate buffer pH 5. Cellulase activity, expressed as enzymatic units (one unit (U) will liberate 1.0 μmole of glucose from cellulose in one hour at pH 5 at 37 °C), was determined by quantifying the release of reducing sugars produced after the incubation period as reported in the DNS method, using glucose as standard.⁵⁹

Colorimetric measurements. Colour changes of the 18th century papers after the coating with a 10 mg mL⁻¹ MgO NPs solution (in distilled water) was measured with a Chroma Meter CR-400 (Konica Minolta). Measurements were performed on two paper samples (4 × 4 cm) before and after the coating, measuring five points for each paper to account for sample heterogeneity. The result of the chromatic change (ΔE), given by the three colorimetric coordinates (L^* , a^* , b^*), was determined by the following equation:

$$\Delta E = \sqrt{\Delta L^2 + \Delta a^2 + \Delta b^2}$$

Conflicts of interest

There are no conflicts to declare.

Acknowledgements

Financial support by the Fundación General CSIC (SGM, Programa ComFuturo) and Fondo Social Europeo-Gobierno de Aragón is gratefully acknowledged. IFC acknowledges the

Gobierno de Aragón for a doctoral scholarship (2018–2022). The authors thank Prof. Fernanda Domingues from the Health Sciences Research Centre, Portugal for providing *T. reesei* RUT C-30 strain. The authors also wish to thank The Advanced Microscopy Laboratory (Universidad de Zaragoza) for access to their instrumentation and expertise. The authors would like to thank Dr Jesús Salafranca for his assistance with the ICP-MS measurements.

References

- 1 C. Roman, R.-M. Diaconescu, L. Scripcariu and A. Grigoriu, *Eur. J. Sci. Theol.*, 2013, **9**, 263–271.
- 2 M. Area and H. Cheradame, *Bioresources*, 2011, **6**, 5307–5337.
- 3 D. Allsopp, K. J. Seal, C. C. Gaylarde, D. Allsopp, K. J. Seal and C. C. Gaylarde, *Introduction to Biodeterioration.*, 2010, pp. 13–14.
- 4 D. Melo, S. O. Sequeira, J. A. Lopes and M. F. Macedo, *J. Cult. Herit.*, 2019, **35**, 161–182.
- 5 Off. J. European Union, 2014, **183**, 36–38.
- 6 M. L. Coutinho, A. Z. Miller, A. Phillip, J. Mirão, L. Dias, M. A. Rogerio-Candellera, C. Saiz-Jimenez, P. M. Martin-Sanchez, L. Cerqueira-Alves and M. F. Macedo, *Constr. Build. Mater.*, 2019, **212**, 49–56.
- 7 A. A. Fabbri, A. Ricelli, S. Brasini and C. Fanelli, *Int. Biodeterior. Biodegrad.*, 1997, **39**, 61–65.
- 8 K. Sterflinger, *Fungal Biol. Rev.*, 2010, **24**, 47–55.
- 9 H. Arai, *Int. Biodeterior. Biodegrad.*, 2000, **46**, 181–188.
- 10 A. B. Strzelczyk, *Int. Biodeterior. Biodegrad.*, 2004, **53**, 151–156.
- 11 F. C. Domingues, J. A. Queiroz, J. M. S. Cabral and L. P. Fonseca, *Enzyme Microb. Technol.*, 2000, **26**, 394–401.
- 12 R. P. de Vries and J. Visser, *Microbiol. Mol. Biol. Rev.*, 2001, **65**, 497–522.
- 13 N. Mesquita, A. Portugal, S. Videira, S. Rodriguez-Echeverria, A. M. L. Bandeira, M. J. A. Santos and H. Freitas, *Int. Biodeterior. Biodegrad.*, 2009, **63**, 626–629.
- 14 K. F. Nielsen, *Fungal Genet. Biol.*, 2003, **39**, 103–117.
- 15 B. Gutarowska, M. Sulyok and R. Krska, *Indoor Built Environ.*, 2010, **19**, 668–675.
- 16 B. Gutarowska, M. Kosmowska, M. Wiszniewska, C. Palczyński and J. Walusiak-Skorupa, *Indoor Built Environ.*, 2012, **21**, 253–263.
- 17 S. López-Aparicio, J. Smolík, L. Mašková, M. Součková, T. Grøntoft, L. Ondráčková and J. Stankiewicz, *Build. Environ.*, 2011, **46**, 1460–1468.
- 18 S. O. Sequeira, E. J. Cabrita and M. F. Macedo, *Restaurator*, 2014, **35**, 181–199.
- 19 S. O. Sequeira, A. J. L. Phillips, E. J. Cabrita and M. F. Macedo, *Stud. Conserv.*, 2017, **62**, 33–42.
- 20 M. Nittérus, *Restaurator*, 2000, **21**, 101–115.
- 21 F. H. Hengemihle, N. Weberg and C. Shahani, *Preserv. Res. Test. Ser. No. 9502*.
- 22 W. A. Rutala and D. J. Weber, *J. Hosp. Infect.*, 1999, **43**, S43–S55.
- 23 M. S. Rakotonirainy, F. Fohrer and F. Flieder, *Int. Biodeterior. Biodegrad.*, 1999, **44**, 133–139.

- 24 M. S. Rakotonirainy and B. Lavédrine, *Int. Biodeterior. Biodegrad.*, 2005, **55**, 141–147.
- 25 M. Nittérus, *Restaurator*, 2000, **21**, 25–40.
- 26 G. Poggi, N. Toccafondi, L. N. Melita, J. C. Knowles, L. Bozec, R. Giorgi and P. Baglioni, *Appl. Phys. A: Mater. Sci. Process.*, 2014, **114**, 685–693.
- 27 R. Giorgi, M. Baglioni, D. Berti and P. Baglioni, *Acc. Chem. Res.*, 2010, **43**, 695–704.
- 28 G. Poggi, N. Toccafondi, D. Chelazzi, P. Canton, R. Giorgi and P. Baglioni, *J. Colloid Interface Sci.*, 2016, **473**, 1–8.
- 29 L. Wang, C. Hu and S. Longquan, *Int. J. Nanomed.*, 2017, **12**, 1227–1249.
- 30 B. O. Ortega-Morales, M. M. Reyes-Estebanez, C. C. Gaylarde, J. C. Camacho-Chab, P. Sanmartín, M. J. Chan-Bacab, C. A. Granados-Echegoyen and J. E. Pereañez-Sacarias, *Adv. Mater. Conserv. Stone*, 2018, 277–298.
- 31 J. S. Kim, E. Kuk, K. N. Yu, J.-H. Kim, S. J. Park, H. J. Lee, S. H. Kim, Y. K. Park, Y. H. Park and C.-Y. Hwang, *Nanomedicine*, 2007, **3**, 95–101.
- 32 M. Rai, A. Yadav and A. Gade, *Biotechnol. Adv.*, 2009, **27**, 76–83.
- 33 Q. L. Feng, J. Wu, G. Q. Chen, F. Z. Cui, T. N. Kim and J. O. Kim, *J. Biomed. Mater. Res.*, 2000, **52**, 662–668.
- 34 I. Sondi and B. Salopek-Sondi, *J. Colloid Interface Sci.*, 2004, **275**, 177–182.
- 35 X. Zhang, H. Niu, J. Yan and Y. Cai, *Colloids Surf., A*, 2011, **375**, 186–192.
- 36 Y.-H. Hsin, C.-F. Chen, S. Huang, T.-S. Shih, P.-S. Lai and P. J. Chueh, *Toxicol. Lett.*, 2008, **179**, 130–139.
- 37 S. A. Blaser, M. Scheringer, M. MacLeod and K. Hungerbühler, *Sci. Total Environ.*, 2008, **390**, 396–409.
- 38 A. C. Janaki, E. Sailatha and S. Gunasekaran, *Spectrochim. Acta, Part A*, 2015, **144**, 17–22.
- 39 S. A. Ruffolo, M. F. La Russa, M. Malagodi, C. Oliviero and A. M. Palermo, *Appl. Phys. A: Mater. Sci. Process.*, 2010, **100**, 829–834.
- 40 P. Munafò, G. B. Goffredo and E. Quagliarini, *Constr. Build. Mater.*, 2015, **84**, 201–218.
- 41 Y. He, S. Ingudam, S. Reed, A. Gehring, T. P. Strobaugh and P. Irwin, *J. Nanobiotechnol.*, 2016, **14**, 54.
- 42 Z.-X. Tang, X.-J. Fang, Z.-L. Zhang, T. Zhou, X.-Y. Zhang and L.-E. Shi, *Braz. J. Chem. Eng.*, 2012, **29**, 775–781.
- 43 D. Pinna, B. Salvadori and M. Galeotti, *Sci. Total Environ.*, 2012, **423**, 132–141.
- 44 Z.-X. Tang and B.-F. Lv, *Braz. J. Chem. Eng.*, 2014, **31**, 591–601.
- 45 N. Y. T. Nguyen, N. Grelling, C. L. Wetteland, R. Rosario and H. Liu, *Sci. Rep.*, 2018, **8**, 1–23.
- 46 T. R. Jørgensen, J. Park, M. Arentshorst, A. M. van Welzen, G. Lamers, R. A. Damveld, C. A. M. van den Hondel, K. F. Nielsen, J. C. Frisvad and A. F. J. Ram, *Fungal Genet. Biol.*, 2011, **48**, 544–553.
- 47 D. C. de Melo, Master's thesis, Universidade Nova de Lisboa, 2017.
- 48 O. S. G. Caneva and M. Nugari, *Biology in the Conservation of Works of Art*, Rome, 1991.
- 49 D. E. Eveleigh, *Appl. Microbiol.*, 1970, **19**, 872.
- 50 R. Peterson and H. Nevalainen, *Microbiology*, 2012, **158**, 58–68.
- 51 R. Mbarki, A. Mnif and A. H. Hamzaoui, *Mater. Sci. Semi-cond. Process.*, 2015, **29**, 300–306.
- 52 I. Franco Castillo, L. De Matteis, C. Marquina, E. García, J. Martínez de la Fuente and S. G. Mitchell, *Int. Biodeterior. Biodegrad.*, 2019, **141**, 79–86.
- 53 N. Salehifar, Z. Zarghami and M. Ramezani, *Mater. Lett.*, 2016, **167**, 226–229.
- 54 Y. H. Leung, A. M. C. Ng, X. Xu, Z. Shen, L. A. Gethings, M. T. Wong, C. M. N. Chan, M. Y. Guo, Y. H. Ng, A. B. Djurišić, P. K. H. Lee, W. K. Chan, L. H. Yu, D. L. Phillips, A. P. Y. Ma and F. C. C. Leung, *Small*, 2014, **10**, 1171–1183.
- 55 K. Krishnamoorthy, J. Y. Moon, H. B. Hyun, S. K. Cho and S. J. Kim, *J. Mater. Chem.*, 2012, **22**, 24610–24617.
- 56 M. C. Arendrup, J. Meletiadis, J. W. Mouton, K. Lagrou, P. Hamal and J. Guinea, EUCAST Guidel. (E.DEF 9.3.1), DOI: 10.2134/agronj2016.07.0440.
- 57 I. D. Van der Werf, N. Ditaranto, R. A. Picca, M. C. Sportelli and L. Sabbatini, *Heritage Sci.*, 2015, **3**, 1–9.
- 58 S. M. P. Ferreira, A. P. Duarte, J. A. Queiroz and F. C. Domingues, *Electron. J. Biotechnol.*, 2009, **12**, 1–9.
- 59 G. L. Miller, *Anal. Chem.*, 1959, **31**, 426–428.

Electronic Supplementary Material (ESI) for Journal of Materials Chemistry B.
This journal is © The Royal Society of Chemistry 2019

Supporting Information

Preventing fungal growth on heritage paper with antifungal and cellulase inhibiting magnesium oxide nanoparticles

Isabel Franco Castillo,^{a,b} Esther García Guillén,^c Jesús M. de la Fuente,^{a,b} Filomena Silva,^{*d,e} Scott G. Mitchell^{*a,b}

^a Instituto de Ciencia de Materiales de Aragón (ICMA), Consejo Superior de Investigaciones Científicas (CSIC)-Universidad de Zaragoza, C/ Pedro Cerbuna 12, 50009 Zaragoza (Spain).

^b CIBER-BBN, Instituto de Salud Carlos III, Madrid (Spain)

^c Real Jardín Botánico, Consejo Superior de Investigaciones Científicas (CSIC), Madrid (Spain).

^d ARAID – Agencia Aragonesa para la Investigación y el Desarrollo, Av. Ranillas, 1D, 2B, 50018 Zaragoza, Spain

^e Universidad de Zaragoza, Facultad de Veterinaria, Calle Miguel Servet 117, 50013 Zaragoza (Spain)

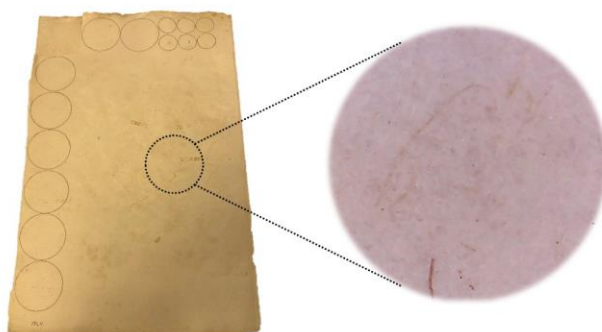


Figure S1. 18th century paper sample from the Real Jardín Botánico (CSIC), Madrid. On the left, a paper sample with pencil marks to cut for the antifungal assays. The right image corresponds to a magnified section of the paper.

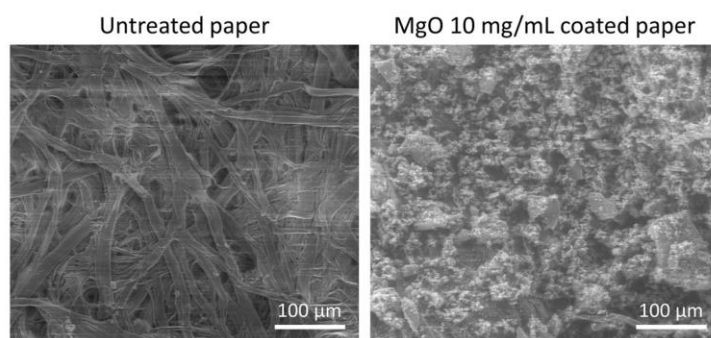


Figure S2. ESEM images of 18th century papers. On the left, an untreated sample where only the cellulose fibres are observed. On the right, an image of a coated paper with a 10 mg/mL MgO NP solution, showing the homogeneity of the nanoparticles over the paper surface.

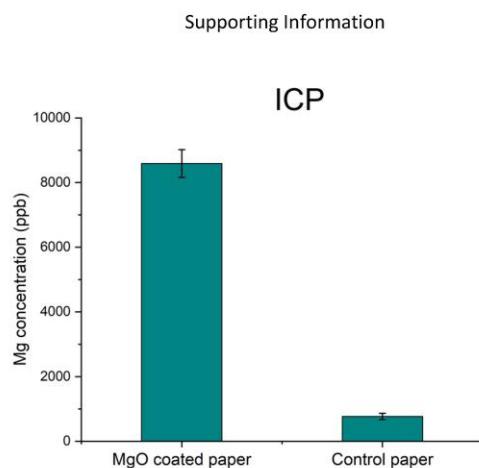


Figure S3. The magnesium (Mg) content of 18th century papers coated with 10 mg/mL MgO NPs (and uncoated as control paper samples) was analysed by Inductively Coupled Plasma Mass Spectrometry (ICP–MS). The MgO NP coated paper samples contained ten times more Mg content than the uncoated control paper samples.

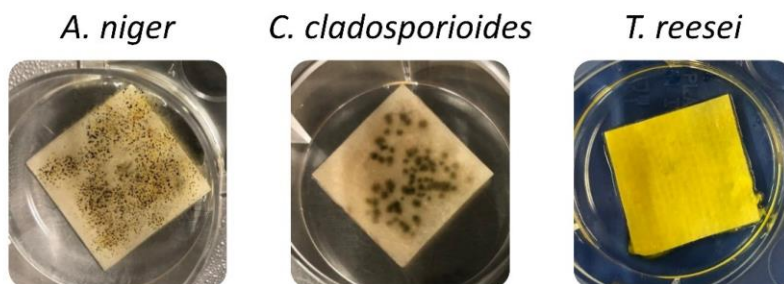


Figure S4. Untreated 18th century paper samples incubated with *A. niger*, *C. cladosporioides* and *T. reesei*. In absence of MgO NPs the three molds grow over the papers. The *A. niger* sample presents a blackish colour due to the sporulation of the fungus. The *C. cladosporioides* sample present green colonies formed mostly by the mycelium. The *T. reesei* paper is full covered by the fungus mycelium, which gives it the yellow colour, and it has lost some of its integrity due to the high production of cellulases by *T. reesei*.

Supporting Information

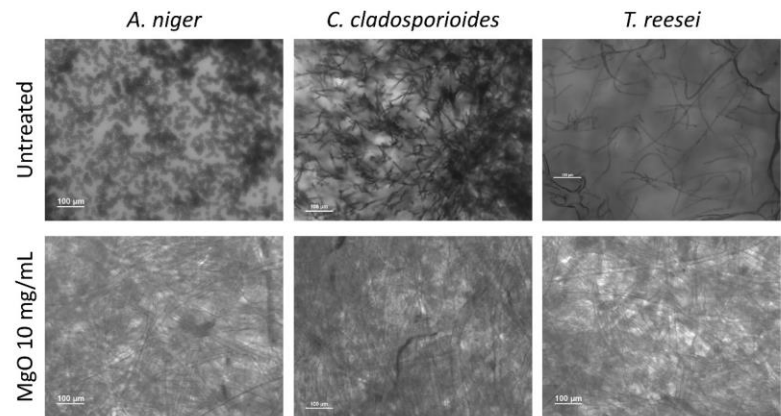


Figure S5. Optical microscopy images of 18th century papers (untreated and coated with 10 mg/mL of MgO NPs) inoculated with *A. niger*, *C. cladosporioides* and *T. reesei*. The untreated samples present a high growth of the fungi over the paper, which can be seen covered in spores (in the *A. niger* sample) and by the fungal mycelium (in the *C. cladosporioides* and *T. reesei* samples). Only cellulose fibres are observed in papers coated with MgO NPs.

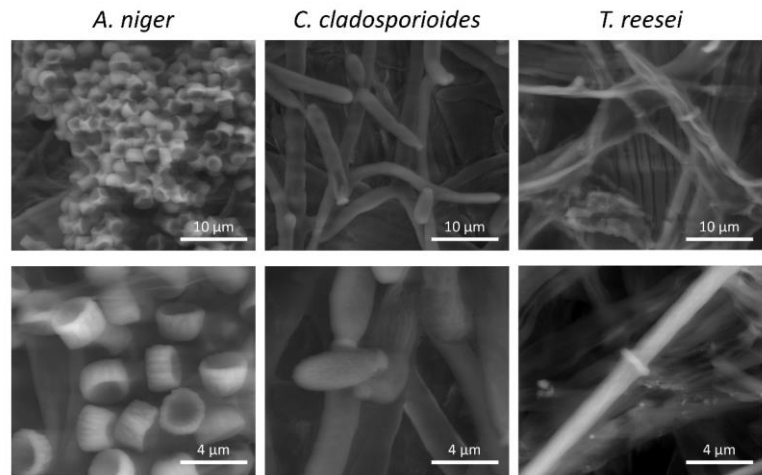


Figure S6. ESEM images of the 18th century papers colonized by *A. niger*, *C. cladosporioides* and *T. reesei*. The *A. niger* sample is riddled with fungal spores and the mycelium is hidden beneath them. In the *C. cladosporioides* sample both mycelium and spores can be observed. *T. reesei* is the least sporulating of the moulds and only the fungal mycelium is observed.

Supporting Information

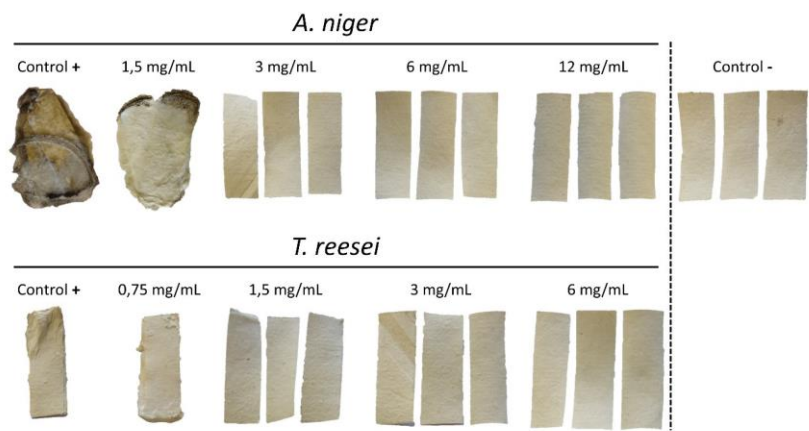


Figure S7. Papers obtained from the ‘paper adhesion inhibition’ test. The control samples from both *A. niger* and *T. reesei* are completely covered by the fungi, and the three papers of each sample adhere to each other due to the fungal growth over the paper. At the lowest concentration of MgO NPs (1.5 mg/mL for *A. niger* and 0.75 mg/mL for *T. reesei*) the fungi are still able to get attach to the paper surface and proliferate, but at the next concentration (3 mg/mL for *A. niger* and 1.5 mg/mL for *T. reesei*) the papers are completely free of fungal growth.

5.2. Polyoxometalate-ionic liquids (POM-ILs) as broad-spectrum antimicrobial coatings to protect stone materials from microbial contamination

Polyoxometalate-ionic liquids (POM-ILs) are composed of an anionic metal-oxide cluster (polyoxometalate, POM) and an organic cation. These ionic liquids (salts with a melting point below 100 °C) present interesting characteristics and properties that makes them highly suitable candidates to be applied on the heritage field. They present anticorrosive properties,¹⁴⁴ high antimicrobial activity,¹⁴⁸ and hydrophobicity and offer the advantage of being highly modulable (both cation and anion can be independently tuned), allowing the synthesis of multifunctional materials which can be applied at low concentrations, enabling the application as a colourless coating that will not affect the aesthetics of the heritage surface.

In this PhD thesis, the antimicrobial activity of three different POM-ILs (POM-IL 1, POM-IL 2 and POM-IL DOTMG-1) has been studied against a range of bacteria and moulds. The three POM-ILs are constituted by the POM $[\alpha\text{-SiW}_{11}\text{O}_{39}]^{8-}$,¹⁷⁵ and combined with three different antimicrobial cations: two quaternary alkylammonium cations (tetraheptylammonium (THA) $((n\text{-C}_7\text{H}_{15})_4\text{N}^+)$ to give POM-IL 1 and trihexyl tetradecyl ammonium (THTDA) $((n\text{-C}_6\text{H}_{13})_3(\text{C}_{14}\text{H}_{29})\text{N}^+)$ to give POM-IL 2)¹⁷⁶ and one quaternary alkylguanidinium cation (N, N, N', N'-tetramethyl-N'', N''-dioctylguanidinium, $(\text{C}_{21}\text{H}_{46}\text{N}_3)\text{Br}$) to give POM-IL DOTMG-1.^{138,177}

Although the three POM-ILs have good antimicrobial performance, based on previous studies, where POM-IL 1 and POM-IL 2 demonstrated that can be applied as a coating and prevent biofilm formation and corrosion of natural limestones,⁹⁹ we decided to use POM-IL 1 and POM-IL 2 in “Article 5” and “Article 6” as protective and disinfectant agents on chalk stone from the Pommery Champagne cellar and 19th century bricks, respectively.

5.2.1. Antimicrobial activity of the POM-ILs against bacteria and fungi

5.2.1.1. Microbial proliferation and viability in presence of the POM-ILs

The antimicrobial activity of the POM-ILs was first studied by determining the antiproliferative effect of the compounds against a variety of microorganisms. To assess bactericidal activity, we used a colorimetric cell viability assay (based in

Results and Discussion

resazurin), which was then confirmed by subculture in solid media. The corresponding minimum inhibitory concentration (MIC) and the minimum bactericidal concentration (MBC) of each POM-IL variant was determined using a combination of these assays.

The POM-IL DOTMG-1 was studied against four bacterial strains (*E. coli* DH5 α , Verotoxigenic *E. coli* (VTEC), *B. subtilis* and *L. monocytogenes*) and against four fungal strains (*A. niger*, *A. ochraceus*, *C. cladosporioides* and *P. expansum*). DOTMG-1 exhibited antimicrobial activity against all the bacterial and fungal strains at low concentrations, obtaining MICs from 1.95 $\mu\text{g/mL}$ for the most sensitive bacterium (*B. subtilis*) to 250 $\mu\text{g/mL}$ for the most resistant mould (*A. niger*) (Table 7). The most sensitive bacteria were the Gram-positive bacteria (*B. subtilis* and *L. monocytogenes*), followed by the Gram-negative bacteria (*E. coli* DH5 α and VTEC), suggesting that the mechanism of action of the DOTMG-1 may involve damage to the cell membrane. The differences in the cell wall between the Gram-positive (composed of a thick, multi-layered peptidoglycan sheath outside of the cytoplasmic membrane) and Gram-negative bacteria (composed of a thin peptidoglycan cell wall located within the periplasmic space between an inner cytoplasmic cell membrane and a bacterial outer membrane) can affect their susceptibility to a certain compound, making the Gram-positive ones more sensitive to the POM-IL. The bacterial cell growth was also monitored by measuring the optical density (OD₆₂₀) of the bacterial culture containing increasing DOTMG-1 concentrations. Figure 14 shows how the bacterial growth was inhibited for concentrations corresponding to the MIC value and higher, while the cultures containing the compound at concentrations below the MIC presented a growth curve similar to the negative control sample containing only bacteria in growth medium.

The results obtained studying the bactericidal activity confirmed that the MBC values of DOTMG-1 against *E. coli* DH5 α , VTEC and *L. monocytogenes* were commensurate with the MIC values: 125, 125 and 31.25 $\mu\text{g/mL}$, respectively (Table 7). On the other hand, the MBC for *B. subtilis* (3.91 $\mu\text{g/mL}$) was two times higher than its MIC value (1.95 $\mu\text{g/mL}$), but even so this bacterium was still the most susceptible microorganism (Figure 14).

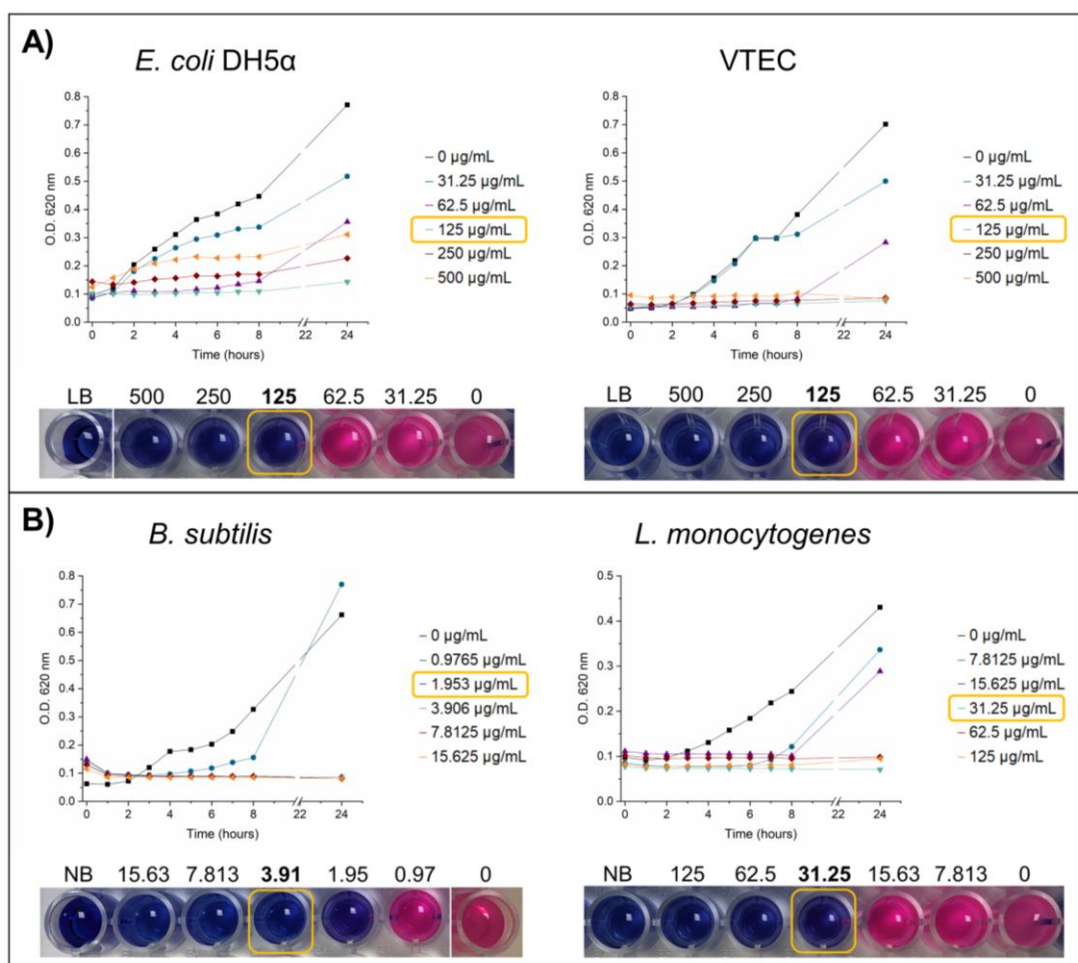


Figure 14. A) Gram-negative (*E. coli* DH5 α , VTEC) and B) Gram-positive (*B. subtilis* and *L. monocytogenes*) bacteria growth curves, starting with a 10^7 CFU/mL inoculum, in the presence of different DOTMG-1 concentrations (ranging from 0.9765 to 500 $\mu\text{g/mL}$). The minimum inhibitory concentration (MIC) obtained for the different bacteria was: 125 $\mu\text{g/mL}$ for *E. coli* DH5 α and VTEC; 31.25 $\mu\text{g/mL}$ for *L. monocytogenes* and 1.95 $\mu\text{g/mL}$ for *B. subtilis*. The apparent increase of turbidity in the *E. coli* DH5 α graph at the higher concentrations is due to the precipitation of the compound in the culture media. The minimum bactericidal concentration (MBC) was confirmed with a resazurin colorimetric cell viability assay, obtaining the same values for *E. coli* DH5 α , VTEC and *L. monocytogenes* (125, 125 and 31.25 $\mu\text{g/mL}$, respectively). The MBC of *B. subtilis* was 3.91 $\mu\text{g/mL}$, two times higher than its MIC value.

The moulds presented a MIC ranging from 31.25 $\mu\text{g/mL}$ to 250 $\mu\text{g/mL}$. As expected, the pervasive and resistant mould *A. niger* was the most resilient of the assayed microorganisms against DOTMG-1; but even so, the MIC was found to just 250 $\mu\text{g/mL}$. All the corresponding MIC values are summarized in Table 7.

The antimicrobial activities of POM-IL 1 and POM-IL 2 have been reported previously.⁹⁹ Both POM-ILs display high antimicrobial activity, with POM-IL 1 being the most active, possessing MICs of 50 $\mu\text{g/mL}$ for *E. coli* DH5 α and 0.5 $\mu\text{g/mL}$ for *B. subtilis*. The MBC values of each bacterium were equal to the MIC

Results and Discussion

values. This higher susceptibility of the Gram-positive bacteria commensurate with the DOTMG-1 results and with previous studies were three different POM-ILs (POM-IL 1 among them) displayed higher antimicrobial activity against the Gram-positive bacterial strains.¹⁴⁸ The MIC values of POM-IL 1 and 2 against *E. coli* and *B. subtilis* are summarized in Table 7.

Table 7. Minimum Inhibitory Concentration (MIC) of the POM-IL DOTMG-1, 1 and 2, and the POM K₈[α -SiW₁₁O₃₉] against different microorganisms.

MICs of the POM-ILs and the POM in $\mu\text{g/mL}$					
Microorganism		DOTMG-1	1	2	K ₈ [α -SiW ₁₁ O ₃₉]
Gram - bacteria	<i>E. coli</i> DH5 α	125	50	500	> 12680
	VTEC	125	ND	ND	-
Gram + bacteria	<i>B. subtilis</i>	1.95	0.5	5	12680
	<i>L. monocytogenes</i>	31.25	ND	ND	-
Moulds	<i>A. niger</i>	250	ND	ND	2000
	<i>A. ochraceus</i>	125	ND	ND	2000
	<i>C. cladosporioides</i>	31.25	ND	ND	2000
	<i>P. expansum</i>	31.25	ND	ND	1000

*ND: Not Determined

To complement the study, the MIC of the POM K₈[α -SiW₁₁O₃₉] was also determined against *E. coli*, *B. subtilis*, *A. niger*, *A. ochraceus*, *C. cladosporioides* and *P. expansum* (Table 7). As expected, the POM didn't display high antimicrobial activity at pharmacologically acceptable concentrations, obtaining MIC values ranging from 2000 to >12680 $\mu\text{g/mL}$. Similar values were reported for MRSA (methicillin-resistant *Staphylococcus aureus*) and VRSA (vancomycin-resistant *Staphylococcus aureus*) strains. Different lacunary POMs were tested against these bacterial strains and the MICs were found to be between 2000 and 12800 $\mu\text{g/mL}$.¹⁴⁷ Moulds turned out to be more sensitive than the bacteria to the POM (with MIC values between 1000 and 2000 $\mu\text{g/mL}$). These lower MIC values obtained for the moulds may provide insight into the mechanism of action of the POM. The POM Ag₃PW₁₂O₄₀ was stated to inhibit the biosynthesis of ergosterol (a sterol found in cell membranes of fungi and protozoa), hence this selective

Results and Discussion

target could explain the differences on the antimicrobial activity between bacteria and fungi.^{198,199}

Given these results, we can conclude that almost all the activity came from the cation. Both guanidine derivatives and quaternary ammonium compounds are known to be effective biocides. The antibiotic streptomycin and the disinfectant and antiseptic chlorhexidine gluconate possess a guanidinium core,²⁰⁰ and the biocides benzalkonium chloride and cetrimide are both classified as a quaternary ammonium compounds.²⁰¹ Thus, it is not surprising the high activity shown by the POM-ILs in comparison with the lacunary POM.

5.2.1.2. Study of the microbial morphology after treatment with the POM-IL DOTMG-1

The microbial response to DOTMG-1 was studied by electron microscopy. The four bacteria (*E. coli* DH5 α , VTEC, *B. subtilis* and *L. monocytogenes*) and the four moulds (*A. niger*, *A. ochraceus*, *C. cladosporioides* and *P. expansum*) were incubated with the compound at concentrations corresponding with the MIC and $\frac{1}{2}$ MIC in order to study the morphology of the microbial cells after the treatment. Transmission electron microscopy (TEM) of the bacteria indicated different signs of stress at both of the tested concentrations. At sub-MIC concentrations ($\frac{1}{2}$ MIC) all bacterial strains displayed indications of replication, as expected, but there signs of damage to the cell wall and accumulation of the cytoplasmic content in the cell ends were also observed. At concentrations corresponding to the MIC value, bacterial cell growth for the four bacterial strains appeared to be completely inhibited and cells displayed loss of their structural integrity (Figure 15A). Remarkably, both *E. coli* strains were completely covered by POM-IL aggregates, probably due to the characteristics of the outer cell membrane. The outer membrane of Gram-negative bacteria is composed of lipopolysaccharides (LPS), a large molecule consisting of a Lipid A and an inner and outer core oligosaccharide. This membrane provides an effective barrier against potentially harmful compounds, what could explain the higher MIC values of the Gram-negative bacterial strains.^{202,203}

The effect of the POM-IL DOTMG-1 on the morphology of the four moulds (*A. niger*, *A. ochraceus*, *C. cladosporioides* and *P. expansum*) was also studied by electron microscopy. In the same way as for the bacteria, each mould was incubated with DOTMG-1 at the MIC concentration and $\frac{1}{2}$ MIC, and then the samples were

Results and Discussion

analysed by Environmental Scanning Electron Microscopy (ESEM) (Figure 15B). Both concentrations ($\frac{1}{2}$ MIC and MIC) were able to affect the mould structure and decrease the sporulation. The MIC concentration was especially harmful to the fungal hyphae and conidia, and some morphological alterations were observed, probably due to the effect of the POM-ILs on the ergosterol, that plays a very important role in cellular membranes of the cell (Figure 15B). As discussed above, the POMs can inhibit the biosynthesis of ergosterol.¹⁹⁸ It has been also described that different gemini surfactants (based on quaternary ammonium compounds) can rapidly reduce the total number of conidia and hinder the synthesis of ergosterol.²⁰⁴ The combination of a POM and a quaternary ammonium cation on the POM-IL could explain this toxicity against the four fungal strains, affecting the germination of the conidia and the ergosterol content in the mycelium.

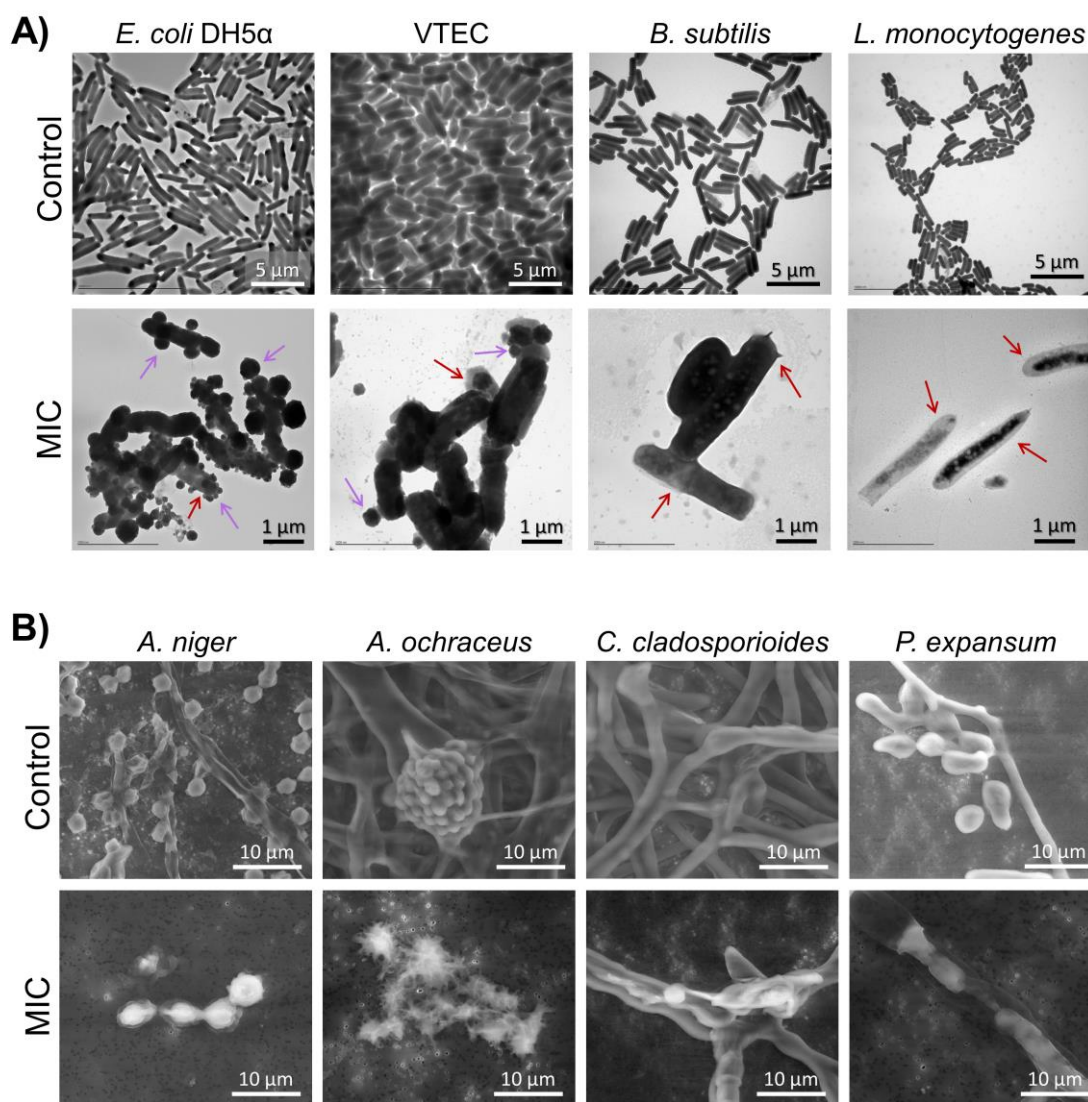


Figure 15. A) TEM images of the bacterial response to DOTMG-1 at concentrations corresponding to the MIC for each bacterial strain (*E. coli* DH5α, VTEC, *B. subtilis*, and *L. monocytogenes*) and bacteria in the absence of DOTMG-1 (control). At MIC concentration, bacterial cells are no longer capable of dividing, and most bacteria show cell damage and alterations in their morphology (red arrows). Both Gram-negative bacteria (*E. coli* DH5α and VTEC) are covered by POM-IL aggregates (purple arrows), probably due to interaction between the compound and the characteristic outer cell membrane of these bacteria. B) ESEM images of the four moulds (*A. niger*, *A. ochraceus*, *C. cladosporioides*, and *P. expansum*) in the absence of antimicrobial DOTMG-1 (control) and inoculated with DOTMG-1 at the corresponding MIC concentration for each fungal strain. At MIC concentration the compound was highly harmful to the fungal hyphae and conidia, and some morphological alterations were observed.

5.2.1.3. Surface antimicrobial activity of the POM-ILs

The surface antimicrobial activity of the POM-ILs was studied using a modified JIS Z 2801 standard, a method that tests the ability of plastics, metals, ceramics and other antimicrobial surfaces to inhibit the growth of microorganisms or kill them. The POM-IL DOTMG-1 was diluted at different concentrations (1, 2, 4, 8

Results and Discussion

and $16 \mu\text{g cm}^{-2}$) and applied as a coating on a glass surface to study the antimicrobial and antibiofilm activity against four bacterial strains (*E. coli* DH5 α , VTEC, *B. subtilis* and *L. monocytogenes*). In agreement with the MIC/MBC results, we observed a 100 % bacterial growth reduction in Gram-positive bacteria at lower concentrations of DOTMG-1 than for the Gram-negative *E. coli* strains. DOTMG-1 achieved a 100 % bacterial cell reduction at low concentrations, ranging from $2 \mu\text{g cm}^{-2}$ to $8 \mu\text{g cm}^{-2}$ (Table 8).

Table 8. Concentration of DOTMG-1 surface coating (in $\mu\text{g cm}^{-2}$) required for 100 % bacterial reduction.

Microorganism	DOTMG-1 (100 % bacterial reduction)
<i>E. coli</i> DH5 α	$8 \mu\text{g cm}^{-2}$
VTEC	$4 \mu\text{g cm}^{-2}$
<i>B. subtilis</i>	$2 \mu\text{g cm}^{-2}$
<i>L. monocytogenes</i>	$2 \mu\text{g cm}^{-2}$

POM-IL 1 and POM-IL 2 was previously studied as antimicrobial coatings on real heritage stones, obtaining significant bacterial reduction, especially for the non-porous stones. Besides, they have also shown high acid corrosion protection, preserving the integrity of all the stones, and preventing the structural collapse of the most porous one.⁹⁹ The acid corrosion can come from air pollution, but also from microorganisms that produce organic acids, such as *A. niger*, that was found to be responsible of metal corrosion via the production of oxalic acid.^{41,44} Due to the good performance of these two POM-ILs to prevent biodeterioration on real stone samples, we choose these compounds to prevent lampenflora biocolonisation of chalk stone described in “Article 5”.

5.2.2. POM-ILs antimicrobial performance as stone coatings to prevent lampenflora growth

Several halls of the Pommery Champagne cellar are decorated with monumental bas-reliefs carved in the chalk (listed as UNESCO World Heritage) and are visited every day by tourists. This tourism has increased the artificial lighting, that disrupts the natural ecosystem and promotes the growth of lampenflora on the bas-reliefs, causing greenish and reddish biofilms that not only affects the beauty

of the bas-reliefs but also contributes to their deterioration.^{205–208}. To inhibit the growth of lampenflora on chalk stones, we explore the activity of POM-IL 1 and POM-IL 2, along with the commercially product Preventol RI80 (PR80), as protective coatings against lampenflora colonisation of natural chalk stones.

First, the lampenflora species colonising the bas-reliefs were identified by molecular techniques. One cyanobacteria (*Timaviella* sp.) and three green algae (*Diplosphaera* sp., *Chromochloris zofingiensis* and *Pseudostichococcus monallantoides*) were identified in the samples. Once the colonising species were identified, four different assays were developed to study the antimicrobial effect of the three compounds when applied as a coating on dry and wet chalk stones. The first two assays were designed to establish the appropriate amount of product to be applied on dry stone, the third assay consisted of the study of the antimicrobial coatings applied on wet stones, and the last assay evaluated the ability of the coatings to prevent a re-colonisation of the surface by a mixture of algae and cyanobacteria. Prior to the antimicrobial activity characterization of the coatings, the colour change produced by the compounds was evaluated to assure the coating was not changing the aesthetics of the substrate.

5.2.2.1. Evaluation of the colour change after application of the coatings

Since any treatment applied on a surface must not change the aesthetics of the object, the colour change produced by the coating of the two POM-ILs and the commercial Preventol RI80 (PR80) was measured with a colorimeter. None of the compounds yielded a colour change significantly high after the coating, with values below $\Delta E^*_{ab} < 3$ (CIELAB units), except for the PR80 coating on the wet stones, which achieved a value of $\Delta E^*_{ab} = 3.3$ for the highest concentration (0.4 g). It is also important to consider the stone itself (the control without coating) presents a colour variation of 1.5 for the dry stone and 2.9 for the wet stone. Large differences in ΔE^*_{ab} between the dry and wet stones indicates that the colour variation depends on the humidity of the stone when the coating is applied. For the dry stones, POM-IL 1 is the product that showed higher colour variation, followed by POM-IL 2 and PR80, while for the wet stones PR80 produced the greatest colour variation, followed thereafter by POM-IL 1 and POM-IL2. All the ΔE^*_{ab} values are summarized in Table 9. The colour variations produced by both POM-ILs are below the generally established ΔE limit value ($\Delta E^*_{ab} \leq 3$)^{194,195} and could not be detected with the naked eye. These data confirm a low visual impact for all coatings, regardless the quantity and the condition of application.

Results and Discussion

Table 9. Colour change (ΔE^*_{ab} in CIELAB units) before (Control) and after the coating with POM-IL 1, POM-IL 2 and PR80 at different concentrations (g) applied on dry and wet stones.

	Control	POM-IL 1 (g)			POM-IL 2 (g)			PR80 (g)	
		0.1	0.2	0.4	0.1	0.2	0.4	0.2	0.4
Dry stones	1.5	ND	2.6	2.9	ND	0.9	1.4	0.6	0.6
Wet stones	2.9	2.8	2.7	2.3	2.0	1.9	2.6	3.2	3.3

*ND: Not Determined

5.2.2.2. Biocidal performance of the coatings against lampenflora

The biocidal activity of POM-IL 1, POM-IL 2 and PR80 was evaluated at different conditions to establish the best antimicrobial performance of the compounds. To do so, the progressive greening of the stone surfaces, due to the algal and cyanobacterial growth and biocolonisation, was monitored by measuring the Δa^* value with a colorimeter every week since the inoculation. Δa^* negative values indicate the surface is becoming greener, meaning the photosynthetic microorganisms are colonising the surface. The chlorophyll a fluorescence, a non-invasive technique used to detect damages in photosynthetic organisms before visible damages are noticeable, was also monitored every week to assess the effectiveness of the biocides.²⁰⁹ The cyanobacteria (*Timaviella* sp.) and three green algae (*Diplosphaera* sp., *Chromochloris zofingiensis* and *Pseudostichococcus monallantoides*) used in the study were isolated from the bas-reliefs of the Pommery Champagne cellar.

First, the colonisation inhibition effect of the biocides was studied on dry stones (Assay 1 and 2). A control stone without coating, and the stones coated with the POM-ILs (at 0.1 and 0.2 g), and the commercially PR80 (at 0.2) were inoculated with two green algae (*C. zofingiensis* and *P. monallantoides*) and incubated for seven weeks. The control stones showed greening just one week after the inoculation and were completely colonised by both algae after seven weeks, being *P. monallantoides* the algae that presented higher so quicker growth. POM-IL 1 displayed strong biocidal activity against *C. zofingiensis* but failed on the inhibition of *P. monallantoides* after first three weeks of incubation (Figure 16A and 16B). The stones coated with POM-IL 2 presented an early greening, indicating poor and short biocidal effect on both algae strains. PR80 showed better biocidal effect than POM-IL 2, but not enough to avoid stones colonisation, which were completely covered by *C. zofingiensis* and *P. monallantoides* after the incubation period (Figure 16A and 16B). After this first attempt, the amount of

Results and Discussion

product applied was increased up to 0.4 g and the effect on *P. monallantoides* (the fastest growing algae) growth during five weeks was studied (Figure 16C). The stones coated with POM-IL 1 and POM-IL 2 showed no greening after the five-week incubation time, indicating high biocidal activity. Besides, the coatings also revealed strong inhibition of the photosynthetic activity of the algae. On the other hand, the biocidal effect of PR80 was only effective for three weeks, suggesting that a higher amount of the product is needed to avoid completely the algae colonisation for longer periods. This was a quite unexpected result due to the good anti-biocolonisation performance of the PR80 on previous studies, where PR80 was efficient at avoiding algae and cyanobacteria colonisation for two months in an accelerated growing assay,²¹⁰ and at removing fungi and bacteria²¹¹⁻²¹⁴ as well as algae and lichens²¹⁵⁻²¹⁷ on cultural heritage.

For the following assays (**Assay 3** and **4**) the coating was applied on wet stone to replicate the more drastic natural environmental conditions of the Pommery cellar. Water saturated stone can limit the penetration of the compounds into the stone pores. To start, the biocidal activity of the coating during five weeks, applied on wet stones at the same quantity as in the previous assay (0.1, 0.2 and 0.4 g for the POM-ILs, and 0.2 and 0.4 g for PR80), was evaluated against *P. monallantoides* (**Assay 3**). The lower concentrations of both POM-ILs were able to inhibit the algal growth, while the PR80 compound failed to prevent the biocolonisation at 0.2 g at week four. For the higher amount (0.4 g) all the compounds displayed good biocidal activity and no greening was detected on the stones (Figure 16D). The next step, to mimic the natural environmental conditions, was to re-inoculate coated slabs which gave a good biocidal performance in a previous assay with two algae (*P. monallantoides* and *Diplosphaera* sp.) and a cyanobacteria (*Timaviella* sp.) (**Assay 4**). Due to the lack of biocidal activity of PR80 at 0.2 g in the previous assay, only stones coated with 0.4 g were re-inoculated. Unfortunately, the greening of these stones was very similar to the control stones without coating, denoting the ineffectiveness of this compound after a re-inoculation of algae. A slight decrease in the Δa^* value was detected after five-week incubation of the 0.1 and 0.2 g POM-IL 1 coated stones, but so close to 0 that no greening was developed on the surface. The 0.4 g coated stones confirmed the long-term biocidal effect of POM-IL 1, where no growth was developed (Figure 16E). While POM-IL 2 present good biocidal activity at the highest amount of product (0.4 g) (Figure 16E), where no greening was

Results and Discussion

detected on the re-inoculated stones, the lower quantities (0.1 and 0.2 g) failed to inhibit the microbial growth over the stones. At 0.2 g the stone remained unaltered until week 3, but the photosynthetic microorganisms started to colonise the surface at week 4. At 0.1 g it was also observed some delay of the greening until week 2, along with a different biological growth. POM-IL 2 seemed to have better biocidal activity against the algae, leading to more development of the cyanobacteria (as opposite of the growth of the controls, where the algae were dominant).

As it can be observed in the Figure 16E, both POM-ILs have been more efficient and presented higher long-term activity than PR80, which was not able avoid a second biocolonisation at the concentration of product applied. It is important to consider that, despite the good performance of POM-IL 1 and POM-IL 2 at 0.4 g in wet stones, the application of such quantity creates a glossy effect which was visually detectable. This glossy effect was also detectable at 0.2 g, therefore the desired antimicrobial effect and the preservation of the aesthetics of the material should be considered to reach an agreement that satisfies these aspects.

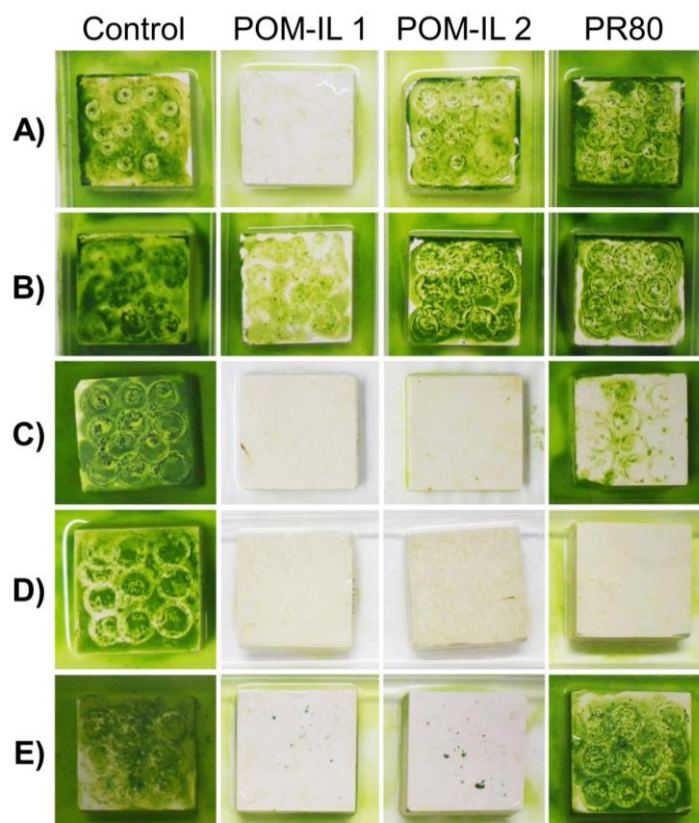


Figure 16. Photos of controls and coated chalk slabs with POM-IL 1, POM-IL 2 and Preventol RI80 (PR80), inoculated with algae and cyanoacteria. A) Photos of inoculated control and coated dry chalk slabs (0.2 g) with *C. zoofingiensis* at week 7 of incubation (Assay 1). B) Photos of inoculated

Results and Discussion

control and coated dry slabs (0.2 g) with *P. monallantoides* at week 7 of incubation (Assay 1). C) Photos of inoculated control and coated dry chalk slabs (0.4 g) with *P. monallantoides* at week 5 of incubation (Assay 2). D) Photos of inoculated control and coated wet chalk slabs (0.4 g) with *P. monallantoides* at week 5 of incubation (Assay 3). E) Photos of re-inoculated control and coated wet chalk slabs with two algae (*P. monallantoides* and *Diplosphaera* sp.) and a cyanobacteria (*Timaviella* sp.) after 5 weeks of incubation (Assay 4).

5.2.3. POM-ILs as disinfectant agents of 19th bricks

The antimicrobial activity of eight phosphotungstate and silicotungstate-based POM-ILs was studied against a mixed culture of four moulds (*Engyodontium album*, *Cladosporium cladosporioides*, *Alternaria alternata* and *Aspergillus fumigatus*) isolated from the surfaces of the historical brick barracks at the Auschwitz II-Birkenau State Museum in Oświęcim, Poland. First, the antimicrobial activity was determined by a disc diffusion method, but due to the limitations of this technique for hydrophobic compounds, the biocidal effect was studied directly on 19th century brick samples. The 19th century bricks were inoculated with the four moulds and incubated for three weeks (at 28 °C and 80 % relative humidity) to allow the colonisation of the bricks. After the incubation time, the POM-ILs were spray-coated up to three times and the disinfection effect was analysed by a contact plate method. Only two compounds showed very high antifungal activity after the third application, [SiW₁₁O₃₉][THTDA]₈ (POM-IL 2) and [SiW₁₂O₄₀][THTDA]₄ (Figure 17). Another POM-IL ([SiW₁₁O₃₉][TOA]₈, which differs from POM-IL 1 in just one carbon on the alkyl chain of the cation, also displayed good antimicrobial activity after the third application.

The bricks sprayed with [SiW₁₁O₃₉][THTDA]₈ (POM-IL 2) and [SiW₁₂O₄₀][THTDA]₄ (the ones with the highest antimicrobial activity) were analysed by ESEM to study the effect of the compounds on the morphology of the fungal mycelium and conidia. Although one application of the POM-IL was not enough to have a full biocidal effect, the POM-IL covered the mycelium and conidia and could penetrate deep into the spatial moulds structure. The third application led to a homogeneously covered surface, which implied a higher biocidal performance (Figure 17). The ESEM images indicated toxic effects of both POM-ILs on fungal conidia, which presented a spherical shape, an indicative of membrane damage and collapse, while the untreated moulds from the control brick samples presented some indications of dehydration due to the ESEM conditions. These results agree with previous studies, where quaternary phosphonium ionic liquids were involved in damaging conidia plasma

Results and Discussion

membrane,²¹⁸ which is consistent with the mechanism of action of the ionic liquids that, due to their amphiphilic character, allows their insertion into the phospholipid bilayer of plasma membranes.²¹⁹ These interactions lead to plasma membrane damage, leakage of intracellular content, and, in consequence, to cell death.²²⁰ The cation plays a key role in the antimicrobial performance of the POM-ILs, and substantial damages to conidia and hyphae provoked by the long alkyl chains were also reported in moulds.²²¹ Although the exact antifungal mode of action of POMs is still not understood, it has been described that the negative charge of POMs can cause impairments of vital cell functions in bacteria (such as interaction with proteins,¹⁴⁷ and interference with bacterial electron transfer, thereby affecting respiration processes).²²²

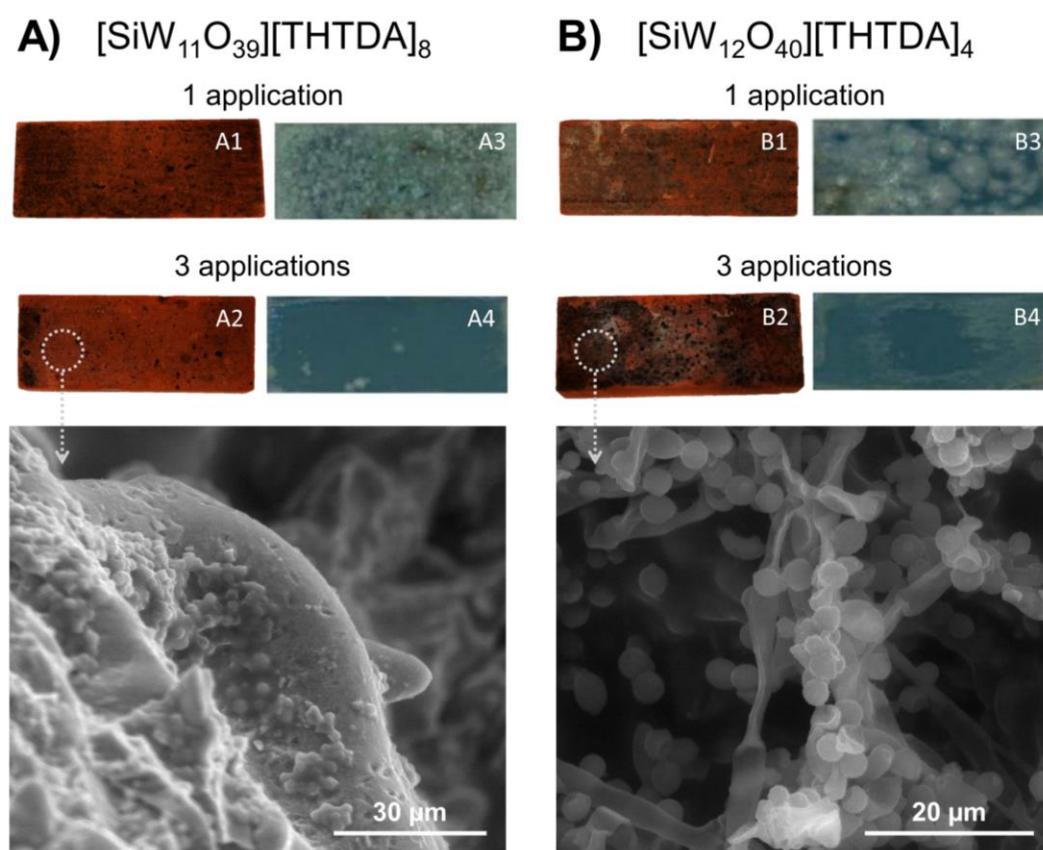


Figure 17. Antifungal activity of POM-ILs A) $[\text{SiW}_{11}\text{O}_{39}][\text{THTDA}]_8$ (POM-IL 2) and B) $[\text{SiW}_{12}\text{O}_{40}][\text{THTDA}]_4$ on brick samples inhabited by mixed culture of moulds (*Engyodontium album*, *Cladosporium cladosporioides*, *Alternaria alternata* and *Aspergillus fumigatus*). The contaminated bricks were sprayed once (A1 and B1) and three times (A2 and B2) with the POM-ILs and the disinfection effect was analysed by a contact plate method (A3, A4, B3 and B4). Environmental scanning electron microscopy (ESEM) images of the historical brick samples after three applications of POM-IL 2 ($[\text{SiW}_{11}\text{O}_{39}][\text{THTDA}]_8$) and $[\text{SiW}_{12}\text{O}_{40}][\text{THTDA}]_4$.

5.2.4. Conclusions

Here we presented the use of polyoxometalate-ionic liquids (POM-ILs) as antimicrobial agents against a wide variety of microorganisms. One of the biggest advantages of these compounds is the high modularity, which allows the combination of different anions (POMs) with different cations, obtaining broad-spectrum antimicrobials. In this work the lacunary Keggin POM [α -SiW₁₁O₃₉]⁸⁻ was used in combination with different cations to obtain three POM-ILs (DOTMG-1, POM-IL 1 and POM-IL 2). DOTMG-1 was tested against four bacterial strains (non-pathogenic *E. coli* DH5 α and *B. subtilis* and pathogenic *L. monocytogenes* and VTEC) and four moulds (*A. niger*, *A. ochraceus*, *C. cladosporioides* and *P. expansum*) and exhibited good antimicrobial activity at low concentrations. It is remarkable that the three POM-ILs, possessed higher antibacterial activity against the Gram-positive strains compared with the Gram-negative strains, suggesting that the mechanism of action is linked to the structure of the bacterial cell wall. The three POM-ILs displayed high surface antimicrobial activity, but only POM-IL 1 and POM-IL 2 were selected to prevent biodeterioration on heritage stones, due to the good performance showed in previous studies.⁹⁹ These POM-ILs were applied on chalk stone as a preventive coating, and they proved to be more effective than a commercial biocide (Preventol RI80) against algal strains isolated from the bas reliefs of the Pommery Champagne cellar, especially POM-IL 1, that maintained the antimicrobial activity even after a re-colonisation of the surface. Aside from the preventive effect, POM-IL 2 was also used as a disinfectant agent on 19th century bricks colonised by a mixture of moulds, causing toxic effects on the fungal conidia. These promising results open the door to the use of POM-ILs on mineral-based building materials as broad-spectrum antimicrobial agents to inhibit colonisation of the surface by microorganisms, herein preventing the biodeterioration.

Article 4: Hybrid Antimicrobial Films Containing a Polyoxometalate-Ionic Liquid

ACS APPLIED
POLYMER MATERIALS

pubs.acs.org/acsapm



Article

Hybrid Antimicrobial Films Containing a Polyoxometalate-Ionic Liquid

Ana G. Enderle,[○] Isabel Franco-Castillo,[○] Elena Atrián-Blasco, Rafael Martín-Rapún, Leonardo Lizarraga, María J. Culzoni, Mariela Bollini, Jesús M. de la Fuente, Filomena Silva, Carsten Streb,* and Scott G. Mitchell*



Cite This: *ACS Appl. Polym. Mater.* 2022, 4, 4144–4153



Read Online

ACCESS |

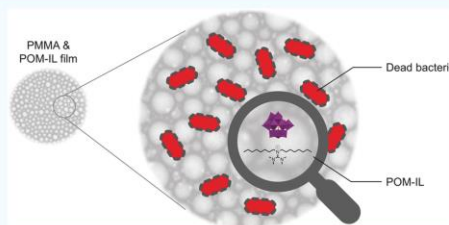
Metrics & More

Article Recommendations

Supporting Information

ABSTRACT: The increasing resistance of pathogenic microorganisms against common treatments requires innovative concepts to prevent infection and avoid long-term microbe viability on commonly used surfaces. Here, we report the preparation of a hybrid antimicrobial material based on the combination of microbicidal polyoxometalate-ionic liquids (POM-ILs) and a biocompatible polymeric support, which enables the development of surface coatings that prevent microbial adhesion. The composite material is based on an antibacterial and antifungal room-temperature POM-IL composed of guanidinium cations (*N,N,N',N'*-tetramethyl-*N*", *N*"-dioctylguanidium) combined with lacunary Keggin-type polyoxotungstate anions, [α -SiW₁₁O₃₉]⁸⁻. Integration of the antimicrobial POM-IL into the biocompatible, flexible, and stable polymer poly(methyl methacrylate) (PMMA) results in processable films, which are suitable as surface coatings or packaging materials to limit the proliferation and spread of pathogenic microorganisms (e.g., on public transport and hospital surfaces, or in ready-to-eat-food packaging).

KEYWORDS: polyoxometalate, polyoxometalate-ionic liquid, guanidinium, antimicrobial, antibiofilm



1. INTRODUCTION

The development of antimicrobial resistance in pathogens is a global public health challenge. Research efforts worldwide are underway to establish different types of treatments and concepts to prevent humans from contracting (contagious) diseases based on pathogenic microbes such as Methicillin-resistant *Staphylococcus aureus* (MRSA).¹ Of particular importance in this context is the transfer of microbes between human beings via surface contacts, e.g., door handles, tables, shared utensils, food packaging, etc. Thus, there is a great need to develop surface-active antimicrobial coatings, which can be employed in various application scenarios, such as hospitals, care-homes, or communal spaces, e.g., offices, public offices, transport, etc.^{2–4}

Recently, ionic liquids and their composites have attracted widespread interest as antimicrobial agents, which could overcome challenges related to acquired antibiotic resistance.^{5,6} Ionic liquids (ILs) are salts with a melting point below 100 °C and are often based on an organic bulky cation and an inorganic anion.⁷ For most applications, room-temperature ILs are the most desirable as they retain their liquidity under typical operating temperatures and can lead to advanced surface coatings. In addition, variation of the cation and anion

can be used to target and optimize specific properties including viscosity, solubility, and bioactivity.

Some of us have recently explored polyoxometalate-ionic liquids (POM-ILs) as bioactive surface coatings, where organic ammonium cations are combined with anionic metal oxo clusters, polyoxometalates (POMs) to obtain POM-ILs.^{8–10} The concept was inspired by earlier studies where the synergistic effects of POMs and known antibiotics and organic bioactive compounds have been explored.¹¹ In 2006, the activity of several POMs in combination with oxacillin against methicillin- and vancomycin-resistant *S. aureus* was reported, and the authors proposed that the cell proliferation suppression observed was due to synergism between the POM and the oxacillin.^{12,13} In 2017, the synthesis and characterization of POM-based silver(I) phenylethyne compounds with antibacterial and antifungal activities were

Received: January 19, 2022

Accepted: April 2, 2022

Published: April 12, 2022



ACS Publications

© 2022 The Authors. Published by
American Chemical Society

4144

<https://doi.org/10.1021/acsapm.2c00110>
ACS Appl. Polym. Mater. 2022, 4, 4144–4153

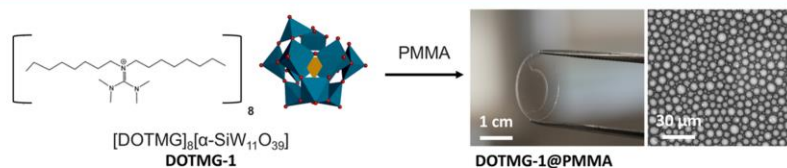


Figure 1. Polyoxometalate-ionic liquid (POM-IL) DOTMG-1 based on the cation N,N,N',N' -tetramethyl- N'' -diocetylguanidium (DOTMG) and monolacunary Keggin anion $[\alpha\text{-SiW}_{11}\text{O}_{39}]^{8-}$ incorporated into polymethylmethacrylate (PMMA) films (DOTMG-1@PMMA film). Photograph and scanning electron microscopy (SEM) image of transparent Film D, DOTMG-1@PMMA 50/50.

reported.¹⁴ The results showed that these compounds have low toxicity in both human and animal cell lines and that their antibacterial and antifungal properties were comparable to those of common antibiotic drugs. In general, the bioactivity of POMs is generally suggested to arise from interactions with amino acids of proteins that lead to biological responses affecting the viability of the bacterial cell.¹¹

POM-ILs based on Keggin-type anions ($[\alpha\text{-SiW}_{11}\text{O}_{39}]^{8-}$) and tetraalkylammonium ions as active cationic species are reported to be effective antimicrobials against important human pathogens such as *Escherichia coli*, *Pseudomonas aeruginosa*, and especially against the Gram-positive *S. aureus*.¹⁵ These POM-ILs feature tetra- n -heptylammonium or tetra- n -octylammonium chains, which interact with the lipid membranes of the bacterial cell. Furthermore, the antibacterial and antifungal activities of POM-ILs were retained, even after loading on silica and deposition as transparent coatings on mineral stone surfaces.^{10,16,17}

Thus far, the majority of bioactive POM-ILs have focused on alkylammonium cations; therefore, we reasoned that introducing cations with higher antimicrobial efficiency would be a promising route to improve the broad-spectrum antimicrobial activity of the POM-ILs and related materials. In this respect, guanidine derivatives are known to be effective biocides:¹⁸ the antibiotics streptomycin and chlorhexidine gluconate possess a guanidinium core, while some commercial disinfectants contain dodecyl guanidinium salts.¹⁹ We proposed incorporating a guanidinium-containing POM-IL into polymeric films could lead to hybrid polymeric materials with broad-spectrum antimicrobial and antibiofilm properties. To this end, here, we report a synthetic route to transform the cation N,N,N',N' -tetramethyl- N'' -diocetylguanidium (DOTMG) into a POM-IL (DOTMG-1) and demonstrate how DOTMG-1 can be incorporated into a poly(methyl methacrylate) (PMMA) films (Figure 1). The antimicrobial activity of the DOTMG-based POM-IL DOTMG-1 and resulting polymeric DOTMG-1@PMMA materials against different bacterial and fungal microorganisms reported herein, demonstrate how a new class of bioactive POM-IL composites can be obtained and highlight where further development is required.

2. EXPERIMENTAL SECTION

2.1. Instrumentation. Elemental analysis was performed on a Carlo Erba 1108 elemental analyzer. Inductively coupled plasma atomic emission spectroscopy (ICP-AES) was performed on a PerkinElmer Plasma 400 spectrometer. ^1H and ^{13}C NMR spectra were recorded on Bruker Avance 600 (1H: 400.13 MHz; 13C: 100.62 MHz) and Bruker Avance 500 spectrometers (1H: 500.14 MHz, 13C: 125.76 MHz). For the POM, Fourier transform infrared (FT-IR) spectroscopy was performed on a Bruker Vector 22 FTIR instrument. Samples were prepared as KBr pellets. For the films, FT-IR

spectroscopy was performed in a Jasco 4700 spectrometer using a magnetic film holder. Signals are given as wavenumbers in cm^{-1} using the following abbreviations: vs = very strong, s = strong, m = medium, w = weak and b = broad. Thermogravimetric analysis (TGA) was performed in a Shimadzu TGA-51 instrument; samples of ca. 10 mg were heated at a rate of 10 $^\circ\text{C}/\text{min}$ under an air atmosphere (flow rate, 30 mL/min) in the range of 30–800 $^\circ\text{C}$. SEM images were acquired using a Phenom Pro scanning electron microscope (SEM). For all images, the working distance was 2.5 ± 0.5 mm. The films were supported on Si wafers and were not sputter-coated. For film A, the study was performed using an accelerating voltage of 5 kV and a charge reduction holder (CRH). These parameters were set to obtain high-quality images of the sample as the film only consisted of PMMA. For films B, C, and D, the study was performed using an accelerating voltage of 5 kV and a standard holder (SH). Atomic force microscopy (AFM) images were acquired using a Bruker multimode 8 SPM (Santa Barbara, CA) with a nanoScope V controller (Santa Barbara, CA). The AFM images were acquired in the intermittent mode using silicon tips doped with antimony, with a spring constant of 42 N/m and a resonance frequency of 320 kHz. Typically, areas of $15 \mu\text{m} \times 15 \mu\text{m}$ were scanned. The image analysis was performed using Gwyddion version 2.46 (Brno, Czech Republic). Average surface roughness (R_a) was determined from AFM height images. For each height image, a reference plane (mean plane) was defined, and a Z-axis, perpendicular to that plane, was considered, where $Z = 0$ was on the plane. Z-values were calculated from the images in a discrete manner, where Z_j was defined as the height of the j th pixel from the mean plane. Positive Z-values are associated with protrusions above the mean plane, while negative Z-values are associated with depressions below the plane. The R_a of each AFM image was determined as the average deviation of height values from the mean plane when considering M pixels in each image ($M = 262,144$).²⁰

2.2. Synthesis. All chemicals were purchased from Sigma-Aldrich, ABCR, or Acros Organics and were of reagent grade. The chemicals were used without further purification.

2.2.1. Synthesis of $K_4[\alpha\text{-SiW}_{11}\text{O}_{39}]\cdot 13\text{H}_2\text{O}$. The synthesis is a modification of the literature procedure.²¹ Sodium metasilicate (0.50 g, 4.09 mmol) was dissolved at room temperature in 10 mL of distilled water and filtered (solution A). In a 100 mL beaker, sodium tungstate (8.26 g, 25.18 mmol) was dissolved in 3 mL of boiling distilled water (solution B). To the boiling solution B, an aqueous solution of HCl 4 mol/L (8.25 mL) was added dropwise over 5 min with vigorous stirring to dissolve the local precipitate of tungstic acid. Solution A was added, quickly followed by the addition of 2.50 mL of 4 mol/L aqueous hydrochloric acid. The solution was kept boiling for 1 h. After cooling to room temperature, the solution was filtered. KCl (6.80 g, 91.2 mmol) was added to the stirred solution. The resulting white precipitate was collected on a sintered glass funnel (medium porosity), washed with two 20 mL portions of an aqueous KCl solution (1.0 M), then washed with 50 mL of cold water, and finally dried in air (yield: 5.10 g, 1.58 mmol, 69.7% based on Si). FT-IR (cm^{-1}): 3420 (b), 2364 (w), 2037 (m), 1624 (m), 995 (s), 917 (s), 888 (vs), 793 (vs), 512 (s), 480 (s). ICP-AES (calculated values within brackets): Si 0.86 (0.87), W 64.31 (62.78).

2.2.2. Synthesis of $(\text{C}_{21}\text{H}_{40}\text{N}_3\text{Br})$ (DOTMG-Br). The synthesis is a modification of the literature procedure.²² Tetramethylguanidine

(1.15 g, 10 mmol), *n*-octylbromide (1.93 g, 20 mmol), potassium carbonate (1.38 g, 10 mmol), and tetra-*n*-butylammonium bromide (0.06 g, 0.20 mmol) was refluxed in MeCN (40 mL) for 36 h and then cooled to room temperature. Then, the filtrate was collected. *N*-Hexane and water were added, and the mixture was vigorously stirred. The organic layer was separated, and the solvent was evaporated. After removal of solvent traces under vacuum, DOTMG-Br was obtained as a yellow viscous liquid (yield: 0.70 g, 1.66 mmol, 17%). FT-IR (cm^{-1}): 3420 (b), 2931 (s), 2848 (m), 2360 (m), 2314 (m), 1600 (s), 1558 (vs), 1458 (m), 1401 (vs), 1375 (m), 1152 (w), 1068 (w), 895 (m), 832 (s), 723 (m). ^1H NMR (600 MHz, $\text{DMSO}-d_6$) δ 3.16 (m, 2H, CH_2N), 3.07 (m, 2H, CH_2N), 2.89–2.86 (m, 12H, CH_2N), 1.55 (m, 2H, $\text{CH}_2\text{CH}_2\text{N}$), 1.39 (m, 2H, $\text{CH}_2\text{CH}_2\text{N}$), 1.26 (m, 20H, CH_2), 0.86 (t, 6 H, $J = 7.2$, CH_3). ^{13}C NMR (151 MHz, $\text{DMSO}-d_6$) δ 162.4, 48.7, 39.6 (overlapping with DMSO), 31.2, 28.6, 28.5, 27.0, 26.1, 22.0, 13.9 (Figures S1 and S2).

2.2.3. Synthesis of $(\text{C}_{21}\text{H}_{46}\text{N}_2)_2[\alpha\text{-SiW}_{11}\text{O}_{39}]$ (DOTMG-1). The synthesis is based on a modified literature procedure.^{23,24} In a round-bottom flask, $\text{K}_8[\alpha\text{-SiW}_{11}\text{O}_{39}] \times 13\text{H}_2\text{O}$ (0.16 g, 0.05 mmol, 1.00 equiv) was dissolved in water (50 mL), and DOTMG-Br (0.4 mmol, 8.00 equiv) was dissolved in dichloromethane (80 mL). The biphasic mixture was vigorously stirred for 15 min. The organic layer was separated, the solvent was removed under reduced pressure, and a light yellow highly viscous liquid was obtained in quantitative yield. $M_w = 5399$ g/mol. FT-IR (cm^{-1}): 3450 (b), 2962 (s), 2925 (s), 2853 (m), 2361 (w), 1739 (w), 1595 (s), 1562 (s), 1463 (m), 1407 (m), 1375 (m), 1262 (s), 1097 (s), 1018 (s), 970 (m), 920 (m), 881 (w), 801 (s), 660 (w), 530 (m). EA: % (calculated values in brackets): C 36.6 (37.37), H 7.1 (6.86), N 6.0 (6.22). ^1H NMR (600 MHz, $\text{DMSO}-d_6$) δ 3.14 (m, 2H, CH_2N), 3.09 (m, 2H, CH_2N), 2.89–2.86 (m, 12H, CH_2N), 1.55 (m, 2H, $\text{CH}_2\text{CH}_2\text{N}$), 1.38 (m, 2H, $\text{CH}_2\text{CH}_2\text{N}$), 1.24 (m, 20H, CH_2), 0.85 (t, 6 H, $J = 7.2$, CH_3). ^{13}C NMR (151 MHz, $\text{DMSO}-d_6$) δ 162.3, 48.8, 39.6, 39.5, 31.2, 28.6, 28.5, 27.0, 26.1, 22.0, 13.9 (Figures S3 and S4). TGA, (in air, 30–800 °C): mass loss observed: 50.2 wt % (observed), 50.5 wt % (calculated) (Figure S5).

2.2.4. Preparation of DOTMG-1/PMMA Films. Silicon wafer substrates (University Wafers) were cleaned with water, ethanol, and air plasma (Zepto, Diener GmbH) before deposition. Four films based on different POM-IL/PMMA weight ratios were prepared: 0/100 (film A), 20/80 (film B), 35/65 (film C), 50/50 (film D). To this end, PMMA (50 mg, $M_w \sim 350,000$) was dissolved in toluene (0.5 mL) and stirred and heated (60–70 °C) for 3 h to have a homogeneous solution of 10% w/v (Solution A). This PMMA solution was mixed with the corresponding amount of DOTMG-1 and dissolved in toluene to prepare DOTMG-1 and PMMA blends, which corresponds to 20:80, 35:65, and 50:50 of the mass composition to DOTMG-1 in PMMA for film B, C, and D, respectively (Table S1).

After shaking for 1 h with an orbital shaker (270 rpm), 20 μL of each solution was deposited by spin-coating onto the center of a squared silicon wafer (15 mm \times 15 mm) with the help of a micropipette. For film A (PMMA film), the rate of revolution was 250 rpm for a duration of 5 s, and it was then stepped up to 3200 rpm for a duration of 15 s. For POM-IL composite films, the rate of revolution was set to 300 rpm (A), 330 (B), 360 (C), or 390 (D) for 5 s with an acceleration rate of 120 rpm/s. Then, the rate of revolution was increased to 1200 rpm with an acceleration rate of 500 rpm/s for 15 s. These procedures were set based on the dryness of the films required.

2.3. Biological Analysis. **2.3.1. Materials.** Resazurin sodium salt, sodium phosphate monobasic, sodium phosphate dibasic, sodium cacodylate trihydrate, glutaraldehyde 25%, DMSO, NaCl, and phosphate-buffered saline (PBS) were each purchased from Sigma-Aldrich. All culture media were purchased from Scharlab, S.L. (Spain). For the bacterial assays, the following culture media were used: Tryptone Soy Agar (TSA), Mueller Hinton Agar supplemented with chloramphenicol (MHAclo) and brain heart infusion agar (BHIA) as solid media; Luria-Bertani (LB) and nutrient broth (NB) as liquid media. For the fungal assays, the following culture media were used: Sabouraud dextrose agar supplemented (SDA) with chloramphenicol,

yeast malt agar (YMA), and potato dextrose agar (PDA) as solid media; RPMI 1640 (with L-glutamine and a pH indicator, without bicarbonate) supplemented with glucose to a final concentration of 2% and 3-(*N*-morpholino) propanesulfonic acid (MOPS) at a final concentration of 0.165 mol/L, pH 7.0, yeast malt broth (YMB) and malt dextrin peptone (MEP) as liquid media.

2.3.2. Microorganisms and Growth Conditions. Four bacterial strains were tested in the antibacterial assays: *E. coli* DH5 α and *E. coli* O157:H7 (verotoxigenic *E. coli* (VTEC)) CECT 5947 as Gram-negative models, *Bacillus subtilis* 1904-E and *Listeria monocytogenes* CECT 911 as Gram-positive models. Four molds from the colección española de cultivos tipo (CECT) were tested in the antifungal assays: *Aspergillus niger* CECT 2088, *Cladosporium cladosporioides* CECT 2111, *Aspergillus ochraceus* CECT 2093, and *Penicillium expansum* CECT 2275. Fungal spore suspensions were stored in 0.1% Tween and 20% glycerol at -80 °C prior to use. All bacterial and fungal growth conditions are summarized in Table S2. Briefly, all bacteria were incubated for 24 h at 37 °C, LB was the selected liquid media for the Gram-negative strains, and NB was used for the Gram-positive strains. Three different solid media were used for the bacterial cultures, TSA for *E. coli* DH5 α and *B. subtilis*, MHA for verotoxigenic *E. coli*, and BHIA for *L. monocytogenes*. All of the fungal strains were incubated for 4 days to prepare the inoculum at 35 °C for *A. niger* and at 25 °C for *A. ochraceus*, *C. cladosporioides*, and *Paspalum expansum*. RPMI was used as liquid media for *A. niger* and *C. cladosporioides*, MEP for *A. ochraceus*, and YMB for *P. expansum*. Three different solid media were used for mold incubation, SDA for *A. niger* and *C. cladosporioides*, YMA for *A. ochraceus*, and PDA for *P. expansum*.

2.3.3. Cytotoxicity Assays. Cytotoxicity assays were performed using CellTiter-Glo Luminescent Cell Viability Assay (Promega), a CO_2 incubator steri-cult 3311 (Thermo Scientific), and Orion II microplate luminometer (Titertek-Herthold, Germany), according to the manufacturer's instructions. The cell lines used were HEK293T (human embryonic kidney cell line, used for transient transfection) obtained via the ATCC (CRL-3216TM), and TZM-bl (HeLa cell derivative used as reporter cell line for human immunodeficiency virus (HIV) infection) obtained via the National Institute of Health (NIH) Acquired Immune Deficiency Syndrome (AIDS) reagent program (catalogue number 8129). To assess the potential cytotoxic activity, 100 mg of DOTMG-1 and DOTMG-Br was initially dissolved in 1 mL of dimethyl sulfoxide (DMSO). This solution was then diluted 1:200 into PBS, to avoid any DMSO-related cytotoxic effect. HEK293T and TZM-bl cells were seeded into a 96-well plate in 100 μL of Dulbecco's modified Eagle's medium (DMEM) to have 30–40% of cells confluency at the time of seeding. The next day, the cells were incubated with a serial dilution of DOTMG-1 and DOTMG-Br, with DMSO as the only negative control and Triton-X100 as a positive control for cell death. The cells were incubated for 2 days at 37 °C, and cell viability was assessed with the CellTiter-Glo assay by measuring the total amount of adenosine triphosphate (ATP). Determination of the cytotoxic concentration 50 (CC50) was done using the log(inhibitor) vs response-variable slope (four parameters) nonlinear regression option available in the GraphPad Prism 7.03 software (La Jolla, California).

2.3.4. Microbial Growth Inhibition Assay in the Presence of DOTMG-1. Bacterial and fungal growth was recorded by measuring the optical density (OD) of the samples at 620 nm over a 24 h period using a microplate reader (Thermo Scientific MULTISKAN GO). Results were compared with the OD variation of a positive control culture containing only bacteria or fungi and a negative control containing the compound in culture media. All control and antibacterial assays were replicated in sextuplet to calculate the mean values and standard deviations, and each experiment was repeated on four separate occasions to verify the reproducibility of the results. The modal value was chosen as the minimum inhibitory concentration (MIC).

2.3.4.1. Bacterial Growth Inhibition Assay. The minimum inhibitory concentration (MIC) of the POM-IL DOTMG-1 was determined against the four bacterial strains (*E. coli* DH5 α , VTEC, *B. subtilis*, and *L. monocytogenes*). The bacteria were thawed and

incubated in the appropriated solid culture media for 24 h at 37 °C. An inoculum of 10^7 CFU/mL was prepared in the appropriate liquid media, and 100 μ L was added to a 96-well plate containing 98 μ L of the appropriate liquid media and 2 μ L of the POM-IL dissolved in DMSO at the desired concentration (500, 250, 125, 62.5, 31.25, 15.62, 7.81, 3.91, 1.95, and 0.98 μ g/mL). Positive controls contained bacteria and liquid media, while the negative controls contained only DOTMG-1 dissolved in culture media. The bacterial growth curves were recorded over a 24 h period by measuring the optical density (OD) of the samples at 620 nm. Results were compared with the OD variation of a control culture containing bacteria without POM-IL.

2.3.4.2. Bacterial Cell Viability Assay. Bacterial cell viability after the treatment with DOTMG-1 was analyzed using a Resazurin (7-Hydroxy-3H-phenoxazin-3-one 10-oxide) assay. A 10^7 CFU/mL bacterial inoculum was incubated with different concentrations of DOTMG-1 as in the bacterial growth inhibition assay (Section 2.3.4.1) on a 96-well plate. A positive (bacteria and liquid media) and a negative control (liquid media and POM-IL) were also included. After the incubation of the plates for 24 h at 37 °C, 0.1 mg/mL Resazurin (dissolved in LB for *E. coli* DHS α and VTEC and in NB for *B. subtilis* and *L. monocytogenes*) was added into each well and incubated at 37 °C in the dark for 1 h under stirring. The Resazurin compound (blue) turns pink in the presence of viable microorganisms as a result of their metabolic activity; therefore, pink wells after the incubation time will indicate live, viable bacteria, while blue wells indicate a loss of metabolic activity, which is one of the first cascade events in the mechanism of cell death. The bacterial viability was also confirmed by subculturing 10 μ L of each well on solid media. After incubating the plates for 24 h at 37 °C, the MBC values obtained with Resazurin were compared with the lack of colonies on the solid media.

2.3.4.3. Fungal Growth Inhibition Assay. The determination of the minimum inhibitory concentration (MIC) of the POM-IL DOTMG-1 against the four fungal strains (*A. niger*, *A. ochraceus*, *C. cladosporioides*, and *P. expansum*) was performed using a broth microdilution method according to the European Committee on Antimicrobial Susceptibility Testing Guidelines (E.DEF 9.3.1).²⁵ Fungi spores were incubated for 5 days in solid media at the corresponding temperature for each mold. The aerial part of the fungi was recovered with a swab and resuspended in distilled sterile water with 0.1% tween to obtain a suspension of 10^6 conidia/mL. This suspension was then diluted to 10^5 conidia/mL in distilled sterile water. To determine the MIC, DOTMG-1 was dissolved in DMSO at the desired concentrations (2000, 1000, 500, 250, 125, 62.5, 31.25, 15.625 μ g/mL) and 2 μ L of each solution was added to each well of a 96-well plate containing 98 μ L of culture media and 100 μ L of the 10^5 conidia/mL suspension. The positive control contained only fungal spores and culture media, while the negative control contained only DOTMG-1 dissolved in culture media. After an incubation period of 48 h, at 35 °C for *A. niger* and at 25 °C for *A. ochraceus*, *C. cladosporioides*, and *P. expansum*, according to CECT recommendations, the minimum inhibitory concentration (MIC) values were determined as the lowest POM-IL concentration able to inhibit fungal growth visible to the naked eye. The results were confirmed by measuring the optical density (OD) of the samples at 620 nm and compared with the OD of the positive control (only bacteria without POM-IL).

2.3.5. Surface Antimicrobial Activity. The surface antimicrobial activity of the POM-IL DOTMG-1 was studied using a modified JIS Z 2801 standard (Reference number: JIS Z 2801: 2000 (E); ICS 07.100.10; 11.100); 2 cm \times 2 cm sterilized glass slides were coated with DOTMG-1, dissolved in acetone, at different concentrations (1, 2, 4, 8, and 16 μ g/cm²). The coated slides were dried under ultraviolet (UV) light for 20 min to avoid any external contamination and then 50 μ L of a 10^7 CFU/mL bacterial suspension were added over the coated slides and over a control slide without coating. A coverslip was put on top of each sample to ensure comparable contact surfaces. The samples were incubated at 37 °C for 24 h in a humidity chamber, and after the incubation time, the bacteria were extracted by vortexing the samples inside a 50 mL falcon tube with 20 mL of liquid media for 1 min. The liquid media containing the extracted bacteria

was then diluted and sown on the appropriate solid media for each microorganism. The colonies grown on the plates were counted after incubation at 37 °C for 24 h. The percentage of bacterial growth reduction was obtained by comparing the number of colonies present in the plates from the coated samples and the colonies present in the plates from the control sample.

2.3.6. Electron Microscopy Studies on Microbial Response to DOTMG-1 and DOTMG-1@PMMA. Transmission electron microscopy (TEM) images were acquired by depositing fixed bacteria on a TEM grid and visualizing the samples using bright-field imaging in an FEI Tecnai T20 microscope operating at 200 kV. Environmental scanning electron microscopy (ESEM) data were collected on a Quanta FEG-250 (FEI Company) field emission SEM for high-resolution imaging working in ESEM mode using a gaseous secondary electron detector (GSED) under high relative humidity conditions.

2.3.6.1. TEM Analysis of the Bacteria Incubated with DOTMG-1. Bacterial morphology after the treatment with the POM-IL DOTMG-1 was studied by TEM. A 10^7 CFU/mL bacterial suspension of each bacterium (*E. coli* DHS α , VTEC, *B. subtilis*, and *L. monocytogenes*) was incubated with the compound at DOTMG-1 concentrations corresponding to the MIC and 1/2 MIC values for each of them. The assay was performed on a 12-well plate, where each well contained 1 mL of the bacteria suspension, 980 μ L of liquid media, and 20 μ L of the compound at the corresponding concentration. Then, the plate was incubated at 37 °C for 24 h with agitation in an incubator. Fixation of these bacterial suspensions was carried out prior to TEM analysis to preserve the biological sample. The samples were centrifuged at 3000 rpm for 15 min, and then the pellet was resuspended into 1.5 mL of sterile PBS. Another centrifugation at 3000 rpm for 15 min was carried out and the pellet containing the bacteria was resuspended in 1.5 mL of 2.5% glutaraldehyde in phosphate buffer 10 mM at pH 7.2 for fixation of the cells. The samples were incubated for 2 h on a Ferris wheel and then washed once with 1 mL of sterile phosphate-buffered saline (PBS) at pH 7.4 and three times with sterile distilled water with centrifugations at 3000 rpm for 15 min between washes for cell recovery and to remove excess glutaraldehyde. The pellets were resuspended in 1.5 mL of sterile Milli-Q water and kept at 4 °C for further analysis. Each sample (2 μ L) was deposited on a carbon-coated copper grid (Cu200 mesh) and left to dry at room temperature overnight. TEM images were obtained in a TECNAI T20 electron microscope (FEI) operating at 60 kV.

2.3.6.2. ESEM Visualization of the Molds Incubated with the DOTMG-1. The effect of the POM-IL on fungal cells was also studied by environmental scanning electron microscopy (ESEM), which avoids the need for cell fixation. First, a suspension of 10^5 conidia/mL was prepared as described in Section 2.3.4.3. This suspension (1 mL) was then incubated with the compound at concentrations corresponding to the MIC and 1/2 MIC values for each mold, by adding 20 μ L of DOTMG-1 DMSO solution (100 \times the desired final DOTMG-1 concentration) and 980 μ L of liquid media to ensure a maximum DMSO concentration of 2% in the culture medium. The solution was incubated on a glass vial for 48 h at the corresponding temperature for each mold. After the incubation time, the samples were centrifuged at 10,000 rpm for 10 min and the supernatant was discarded. The pellet, containing the mold, was resuspended into 1 mL of saline and filtered through a sterile polycarbonate membrane (13 mm diameter, pore size 0.22 μ m). Afterward, the membranes containing the molds were placed on a 12-well plate and fixed. The fixation protocol was performed as follows: the membranes were washed once with 2 mL of saline and then fixed with 2 mL of cacodylate buffer 0.1 M at 37 °C for 90 min. To dehydrate the molds, increasing concentrations of methanol were used (5 min with methanol 30%, 5 min with methanol 50%, 5 min with methanol 70%, 10 min with methanol 100%, and 5 min with methanol 100%). The fixed samples were visualized on a Quanta FEG-250 (FEI Company) field emission SEM for high-resolution imaging operating in ESEM mode using a GSED detector.

2.3.7. Biological Performance of the Films. The antibacterial activity of the four different films (A, B, C, and D) was tested against

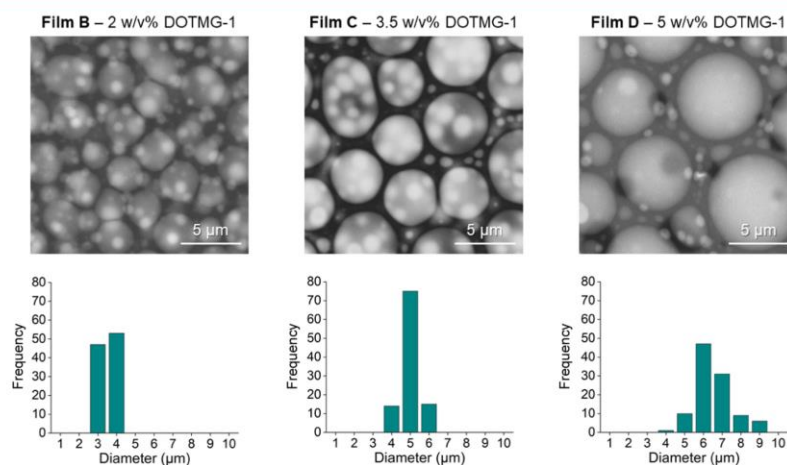


Figure 2. SEM micrographs of the films DOTMG-1@PMMA films B, C, and D prepared with 2, 3.5, and 5 w/v % DOTMG-1, respectively. Scale bar = 5 μm .

Gram-positive *B. subtilis* and *L. monocytogenes* as well as Gram-negative *E. coli* DHS α . Films were placed in a six-well plate, inoculated with 50 μL of a 10^8 CFU/mL inoculum of the different bacteria, and incubated at 37 $^{\circ}\text{C}$ for 4 h in a humidity chamber. After the incubation time, the films were rinsed with 1 mL of saline, which was then diluted and plated on TSA plates. The films were rinsed again with 1 mL of distilled sterile water to remove any remaining salts and visualized using ESEM.

2.3.7.1. Environmental Scanning Electron Microscopy (ESEM) Visualization of the Inoculated Films. The effect of the film on the bacteria was also studied by ESEM. The films (after being rinsed) were visualized on a Quanta FEG-250 (FEI Company) field emission SEM for high-resolution imaging working in ESEM mode using a GSED detector. Note that due to the pathogenicity of *L. monocytogenes*, these samples required fixation with glutaraldehyde. Unfortunately, during the fixation process and subsequent washing protocols, the bacteria were removed repeatedly from the silicon wafer surface, and despite a number of attempts, these issues could not be resolved.

3. RESULTS AND DISCUSSION

3.1. Synthesis and Characterization of DOTMG-1. The POM-IL DOTMG-1 was synthesized by a modification of a previously reported cation metathesis route and was obtained in quantitative yield. The sample composition and purity were confirmed by NMR and FT-IR spectroscopies as well as elemental analyses (refer to the Supporting Information for further details).

3.2. Preparation of DOTMG-1@PMMA Films. DOTMG-1@PMMA films were obtained by preparing a solution of DOTMG-1 and PMMA in toluene and spin-coating these solutions on silicon wafers as substrates. The hybrid films were obtained by air-drying the samples; for more details, see Section 2.2.4. Herein, four hybrid DOTMG-1@PMMA films are discussed in detail, varying in their POM-IL/PMMA weight ratio: film A (0/100, POM-IL/PMMA), film B (20/80), film C (35/65), film D (50/50).

3.3. Characterization of DOTMG-1@PMMA Films. The chemical makeup of the films was characterized by FT-IR

spectroscopy, which confirmed the presence of the POM, DOTMG, and PMMA signals (see Figure S5 for details). SEM analysis of the films shows that film A (purely PMMA-based) has a smooth surface and has a homogeneous structure (Figure S6). In contrast, films B, C, and D (2, 3.5, and 5 w/v % DOTMG-1, respectively) show a rough surface structure and a biphasic composition, which we assign to (partial) phase separation during the drying process (Figures S7–S9). SEM data also show that increasing the POM-IL content in the films also increases the size of the spherical structures embedded within the polymeric matrix. The diameter of these structures is equal to 3.05 ± 0.30 nm in film B (2 w/v %) and increases to 4.40 ± 0.52 nm in film C (3.5 w/v %) and to 5.85 ± 0.95 nm in film D (5 w/v %) (Figure 2). We attribute this larger and more “relaxed” droplet size to the fact that the DOTMG-1 was less confined by the polymeric matrix at higher POM-IL:PMMA concentration ratios.

Atomic force microscopy (AFM) was used to further probe the DOTMG-1@PMMA films and verified that increasing the POM-IL content in the films increased the size of the POM-IL assemblies embedded within the PMMA matrix (Figure 3). For further AFM data of films B, C, and D, including characterization of the surface roughness, refer to Figures S10–S13 in the Supporting Information.

3.4. Cytotoxicity of DOTMG-1. The cytotoxicity and cell viability assays were performed to study the toxic effect of the compounds on the cells. The concentration-dependent cytotoxic effect of DOTMG-1 and DOTMG-Br, along with a positive and negative control (Triton-X100 and DMSO, respectively), was measured in HEK293T cells and TZM-bl cells (Figures S14 and S15). Cell viability decreases as the concentration of the POM-ILs increases. As can be seen in Table 1, according to the calculated CC_{50} for the ILs in both cell lines, the formation of the POM-IL DOTMG-1 decreases the cytotoxicity of the precursor DOTMG-Br (as seen by the $\mu\text{g}/\text{mL}$ data in Table 1), highlighting that the combination of organo-cation and POM anion leads to improved biocompat-

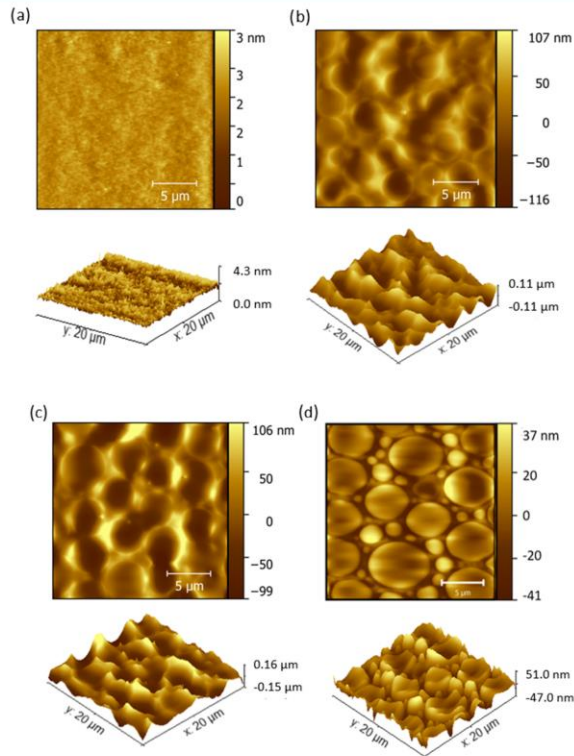


Figure 3. AFM images of POM-DOTMG-1 films prepared (a) without POM-IL DOTMG-1 and with (b) 2 w/v %, (c) 3.5 w/v %, and (d) 5 w/v % DOTMG-1, respectively.

Table 1. CC₅₀ Values of DOTMG-1 and DOTMG-Br

compounds	CC ₅₀ (μg/mL)		CC ₅₀ (μM)	
	HEK293T cells	TZM-bl cells	HEK293T cells	TZM-bl cells
DOTMG-Br	2.46	0.59	5.85	1.40
DOTMG-1	14.20	2.72	2.63	0.50

ibility, which is likely due to the reduction in the aqueous solubility of the POM-IL.

3.5. Antimicrobial Activity of DOTMG-1. **3.5.1. Microbial Growth Inhibition in the Presence of DOTMG-1.** **3.5.1.1. Bacterial and Fungal Growth Inhibition Assay.** The antimicrobial activity of DOTMG-1 was first studied by determining the minimum inhibitory concentration (MIC) of the compound against four bacterial strains (*E. coli* DH5α, VTEC, *B. subtilis*, and *L. monocytogenes*) and against four fungal strains (*A. niger*, *A. ochraceus*, *C. cladosporioides*, and *P. expansum*). DOTMG-1 exhibited antimicrobial activity against all of the bacterial and fungal strains at low concentrations (from 1.95 μg/mL for the most sensitive bacterium to 250 μg/mL for the most resistant mold; see Table 2). The Gram-positive bacterial cell wall is composed of a thick, multilayered

Table 2. Minimum Inhibitory Concentration (MIC) and Minimum Bactericidal Concentration (MBC) of DOTMG-1 against Different Microorganisms^a

microorganism		MIC (μg/mL)	MIC (μM)	MBC (μg/mL)
Gram-negative bacteria	<i>E. coli</i> DH5α	125	23.15	125
	VTEC	125	23.15	125
Gram-positive bacteria	<i>B. subtilis</i>	1.95	0.36	3.91
	<i>L. monocytogenes</i>	31.25	5.78	31.25
molds	<i>A. niger</i>	250	46.30	ND
	<i>A. ochraceus</i>	125	23.15	ND
	<i>C. cladosporioides</i>	31.25	5.78	ND
	<i>P. expansum</i>	31.25	5.78	ND

^aND: Not determined.

peptidoglycan sheath outside of the cytoplasmic membrane, while the Gram-negative cell wall is composed of an outer membrane linked by lipoproteins to thin, mainly single-layered peptidoglycan. The peptidoglycan is located within the periplasmic space that is created between the outer and

inner membranes. It therefore follows that the most sensitive microorganism was Gram-positive *B. subtilis*, with a MIC value of 1.95 $\mu\text{g/mL}$, while the MIC of DOTMG-1 against pathogenic bacteria *L. monocytogenes* was equal to 31.25 $\mu\text{g/mL}$. The Gram-negative bacteria *E. coli* DH5 α and VTEC were more resistant to DOTMG-1, both possessed MICs corresponding to 125 $\mu\text{g/mL}$. Such differences in MIC between the Gram-negative and Gram-positive bacteria suggest that the mechanism of action of the DOTMG-1 may involve damage to the cell membrane. The MIC of DOTMG-1 against molds *C. cladosporioides* and *P. expansum* corresponded to 31.25 $\mu\text{g/mL}$, while *A. ochraceus* equaled 125 $\mu\text{g/mL}$. As expected, the pervasive and resistant mold *A. niger* was the most resilient of the assayed microorganisms against DOTMG-1, but even so, the MIC was found to be low, at just 250 $\mu\text{g/mL}$. All of the corresponding MIC values are summarized in Table 2.

Bacterial cell growth in the presence of the antimicrobial DOTMG-1 was monitored via the optical density of the bacterial culture containing increasing DOTMG-1 concentrations. Figure S17 shows how the bacterial growth was inhibited for concentrations corresponding to the MIC value and higher, while the cultures containing the compound at concentrations below the MIC presented a growth curve similar to the negative control sample containing only bacteria in the growth medium.

3.5.1.2. Bacterial Cell Viability Assay. The minimum bactericidal concentration (MBC) of DOTMG-1 against the four bacterial strains was obtained by a Resazurin cell viability assay (Figure S18) and confirmed by subculturing in solid culture media. The results obtained confirmed that the MBC values of DOTMG-1 against *E. coli* DH5 α , VTEC, and *L. monocytogenes* were commensurate with the MIC values: 125, 125, and 31.25 $\mu\text{g/mL}$, respectively (Table 2). On the other hand, the MBC for *B. subtilis* (3.91 $\mu\text{g/mL}$) was 2 times higher than its MIC value (1.95 $\mu\text{g/mL}$) (Table 2). Importantly, these data confirm that DOTMG-1 POM-IL is not only inhibiting bacterial cell growth but is also killing bacterial cells.

3.5.2. Surface Antimicrobial Activity of DOTMG-1. The surface antimicrobial activity of DOTMG-1, which can be related to its ability to prevent bacterial adhesion and, consequently, biofilm formation of the four bacterial strains (*E. coli* DH5 α , VTEC, *B. subtilis*, and *L. monocytogenes*), was studied using a modified JIS Z 2801 standard. To obtain the percentage of bacterial reduction, the number of colonies counted on the plates from the POM-IL DOTMG-1-coated samples were compared with the colonies counted on the plates from the control samples without coating. In agreement with the MIC/MBC results, we observed a 100% bacterial growth reduction in Gram-positive bacteria at lower concentrations of DOTMG-1 than for the Gram-negative *E. coli* strains. DOTMG-1 achieved a 100% bacterial cell reduction at low concentrations ranging from 2 to 8 $\mu\text{g/cm}^2$ (Table 3).

3.5.3. Electron Microscopy Studies on the Microbial Response to DOTMG-1. **3.5.3.1. TEM Analysis of the Bacteria Incubated with DOTMG-1.** Transmission electron microscopy (TEM) was performed on samples of *E. coli* DH5 α , VTEC, *B. subtilis*, and *L. monocytogenes*, to study the morphology of the bacterial cells incubated with DOTMG-1 at concentrations corresponding to its MIC and 1/2 MIC for each of the bacterial strains. At sub-MIC concentrations (1/2 MIC), although all bacterial strains displayed indications of

Table 3. Concentration of DOTMG-1 Surface Coating (in $\mu\text{g/cm}^2$) Required for 100% Bacterial Reduction

microorganism	DOTMG-1 (100% bacterial reduction)
<i>E. coli</i> DH5 α	8 $\mu\text{g/cm}^2$
VTEC	4 $\mu\text{g/cm}^2$
<i>B. subtilis</i>	2 $\mu\text{g/cm}^2$
<i>L. monocytogenes</i>	2 $\mu\text{g/cm}^2$

replication, there were several signs of stress. Notably, *E. coli* DH5 α , *B. subtilis*, and *L. monocytogenes* cultures showed signs of damage to the cell wall and there was an appreciable accumulation of the cytoplasmic content in the cell ends in the case of VTEC (Figure 4). At concentrations corresponding to the MIC value, bacterial cell growth for the four bacterial strains appeared to be completely inhibited and cells displayed a loss of their structural integrity. Both Gram-negative bacterial cells (*E. coli* DH5 α and VTEC) were completely covered by POM-IL aggregates, probably due to the outer cell membrane containing lipopolysaccharides, which also could protect them against the DOTMG-1 compound, explaining the higher MIC values of these strains (Figure 4).

3.5.3.2. ESEM Visualization of the Molds Incubated with DOTMG-1. The effect of the POM-IL on mold morphology was studied by incubating each of the four molds (*A. niger*, *A. ochraceus*, *C. cladosporioides*, and *P. expansum*) with DOTMG-1 at the MIC concentration and 1/2 MIC, and then analyzing the samples by environmental scanning electron microscopy (ESEM). At both MIC and 1/2 MIC concentrations, mold structure was affected. Additionally, there was noticeably less sporulation, damage to the fungal hyphae and conidia, including morphological alterations (Figure 5).

3.5.4. Biological Performance of the DOTMG-1@PMMA Films. DOTMG-1 was embedded in a PMMA matrix to obtain antimicrobial and antibiofilm surfaces. The antimicrobial effect of the hybrid DOTMG-1@PMMA films against *E. coli* DH5 α , *B. subtilis*, and *L. monocytogenes* was studied by inoculating the films with a bacterial culture, incubating them for 4 h, and plating the culture that was isolated from the rinsing of the samples. As expected, for the control film ($A = 100\%$ PMMA; no DOTMG-1), the bacterial concentration remained constant at $\sim 10^6$ CFU/mL following the 4 h incubation period. On the other hand, the hybrid DOTMG-1@PMMA films containing the DOTMG-1 POM-IL at 2, 3.5, and 5 w/v % (B, C, and D, respectively) all displayed a 100% reduction for each of the three bacteria that were assayed. To infer the mechanism of action, the material–microbe interactions in the hybrid DOTMG-1@PMMA films incubated with nonpathogenic *E. coli* DH5 α and *B. subtilis* were studied by ESEM (Figure S19). Due to the high antimicrobial and antibiofilm activity displayed by the DOTMG-1@PMMA films, very few bacterial cells were observed on the surface of the samples, indicating low adhesion and/or death of the bacterial cells that come into contact with the polymer surface. Unfortunately, due to the low number of cells adhering to the DOTMG-1@PMMA surface, we cannot draw any definitive conclusion about the mechanism of action of the POM-IL@PMMA films. Based on our initial findings, we hypothesize that embedding POM-ILs in PMMA could act to reduce the cytotoxicity of the DOTMG-1, but further experiments will be required to confirm if hybrid POM-IL@PMMA films do indeed present lower cytotoxicity than the parent POM-IL.

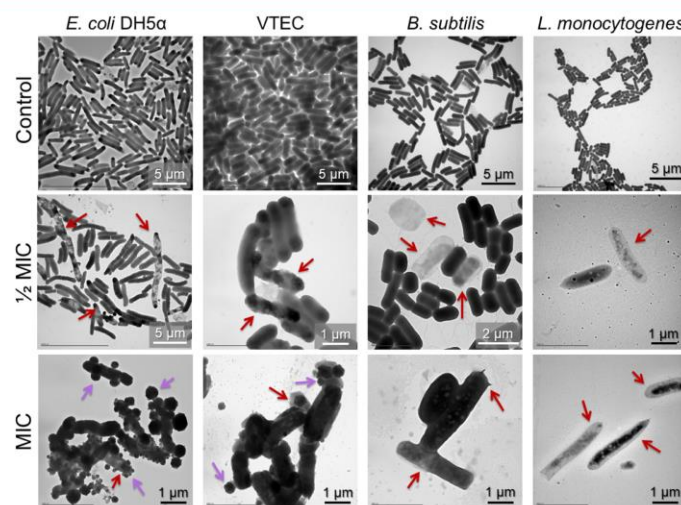


Figure 4. TEM images of the bacterial response to **DOTMG-1** at concentrations corresponding to its 1/2 MIC and MIC for each bacterial strain (*E. coli* DH5 α , VTEC, *B. subtilis*, and *L. monocytogenes*) as well as TEM images of these bacteria in the absence of **DOTMG-1** (control). At a sub-MIC concentration, bacteria are still able to reproduce, but cell damage is already observed (red arrows). At MIC concentration, bacterial cells are no longer capable of dividing, and most bacteria show cell damage and alterations in their morphology (red arrows). At MIC concentration, both Gram-negative bacteria (*E. coli* DH5 α and VTEC) are covered by POM-IL aggregates (purple arrows), probably due to interaction between the compound and the characteristic outer cell membrane of these bacteria.

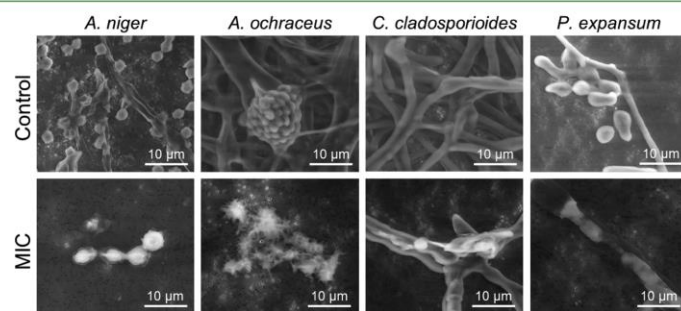


Figure 5. ESEM images of the four molds (*A. niger*, *A. ochraceus*, *C. cladosporioides*, and *P. expansum*) in the absence of antimicrobial **DOTMG-1** (control) and inoculated with **DOTMG-1** at the corresponding MIC concentration for each fungal strain.

4. CONCLUSIONS

The sterically demanding cation of the bio-based family of alkyl-guanidinium cations, **DOTMG**, combined with the lacunary Keggin POM [α -SiW₁₁O₃₉]⁷⁻, formed an ionic liquid, **DOTMG-1**, which exhibits broad-spectrum antimicrobial properties at low concentrations. The **DOTMG-1** POM-IL was found to be highly effective against different bacterial strains, including nonpathogenic *E. coli* DH5 α and *B. subtilis* as well as pathogenic *L. monocytogenes* and VTEC. The compound possessed higher antibacterial activity against the Gram-positive strains *B. subtilis* and *L. monocytogenes* compared with the Gram-negative strains *E. coli* strains, suggesting that the mechanism of action is linked to the structure of the

bacterial cell wall. Importantly, **DOTMG-1** provided a 100% reduction of bacterial colonization of surfaces and prevents subsequent biofilm formation of the same model bacterial strains. Pathogenic molds are reemerging as an increasingly serious threat to human health globally and **DOTMG-1** also possessed high antifungal activity against the model mold strains *A. niger*, *A. ochraceus*, *C. cladosporioides*, and *P. expansum*.

As a proof of concept of the general applicability of the antimicrobial guanidinium POM-IL, the fabrication of multifunctional films showed that such composite materials could be further developed to produce polymeric antimicrobial layers for different surfaces. The **DOTMG-1** POM-IL was embedded

in a PMMA polymer matrix and morphological changes in the surface of the films changed with respect to the amount of POM-IL incorporated in the matrix. Antibacterial assays on the films showed that the microbicidal DOTMG-1 coating completely prevents bacterial growth and biofilm formation, even at the lowest ratio of DOTMG-1/PMMA of 20:80. The results of this work endorse a number of potential future directions for these hybrid materials in the development and implementation of biocompatible antimicrobial surfaces for preventing undesired microbial adhesion.

■ ASSOCIATED CONTENT

● Supporting Information

The Supporting Information is available free of charge at <https://pubs.acs.org/doi/10.1021/acsapm.2c00110>.

NMR spectrum of the POM-IL DOTMG-1; characterization of the DOTMG-1 PMMA films; cytotoxicity of the POM-IL DOTMG-1; and data from additional antibacterial assays (PDF)

■ AUTHOR INFORMATION

Corresponding Authors

Carsten Streb — *Institute of Inorganic Chemistry I, Ulm University, 89081 Ulm, Germany*; Email: carsten.streb@uni-ulm.de

Scott G. Mitchell — *Instituto de Nanociencia y Materiales de Aragón (INMA-CSIC), Consejo Superior de Investigaciones Científicas-Universidad de Zaragoza, 50009 Zaragoza, Spain; CIBER de Bioingeniería, Biomateriales y Nanomedicina, Instituto de Salud Carlos III, 28029 Madrid, Spain*; orcid.org/0000-0003-4848-414X; Email: scott.mitchell@csic.es

Authors

Ana G. Enderle — *Institute of Inorganic Chemistry I, Ulm University, 89081 Ulm, Germany; Centro de Investigaciones en Bionanociencias (CIBION), CONICET, C1425FQD Ciudad de Buenos Aires, Argentina; Laboratorio de Desarrollo Analítico y Quimiometría (LADAQ), Universidad Nacional del Litoral—CONICET, Ciudad Universitaria, S3000 Santa Fe, Argentina*

Isabel Franco-Castillo — *Instituto de Nanociencia y Materiales de Aragón (INMA-CSIC), Consejo Superior de Investigaciones Científicas-Universidad de Zaragoza, 50009 Zaragoza, Spain; CIBER de Bioingeniería, Biomateriales y Nanomedicina, Instituto de Salud Carlos III, 28029 Madrid, Spain*

Elena Atrián-Blasco — *Instituto de Nanociencia y Materiales de Aragón (INMA-CSIC), Consejo Superior de Investigaciones Científicas-Universidad de Zaragoza, 50009 Zaragoza, Spain; CIBER de Bioingeniería, Biomateriales y Nanomedicina, Instituto de Salud Carlos III, 28029 Madrid, Spain*

Rafael Martín-Rapún — *Instituto de Nanociencia y Materiales de Aragón (INMA-CSIC), Consejo Superior de Investigaciones Científicas-Universidad de Zaragoza, 50009 Zaragoza, Spain; CIBER de Bioingeniería, Biomateriales y Nanomedicina, Instituto de Salud Carlos III, 28029 Madrid, Spain*; orcid.org/0000-0003-0702-8260

Leonardo Lizarraga — *Centro de Investigaciones en Bionanociencias (CIBION), CONICET, C1425FQD Ciudad de Buenos Aires, Argentina*

Maria J. Culzoni — *Laboratorio de Desarrollo Analítico y Quimiometría (LADAQ), Universidad Nacional del Litoral—CONICET, Ciudad Universitaria, S3000 Santa Fe, Argentina*; orcid.org/0000-0002-6313-3447

Mariela Bollini — *Centro de Investigaciones en Bionanociencias (CIBION), CONICET, C1425FQD Ciudad de Buenos Aires, Argentina*; orcid.org/0000-0002-8718-6236

Jesús M. de la Fuente — *Instituto de Nanociencia y Materiales de Aragón (INMA-CSIC), Consejo Superior de Investigaciones Científicas-Universidad de Zaragoza, 50009 Zaragoza, Spain; CIBER de Bioingeniería, Biomateriales y Nanomedicina, Instituto de Salud Carlos III, 28029 Madrid, Spain*; orcid.org/0000-0003-1081-8482

Filomena Silva — *ARAID—Agencia Aragonesa para la Investigación y el Desarrollo, 50018 Zaragoza, Spain; Facultad de Veterinaria, Universidad de Zaragoza, 50013 Zaragoza, Spain*

Complete contact information is available at: <https://pubs.acs.org/doi/10.1021/acsapm.2c00110>

Author Contributions

○A.G.E. and I.F.C. contributed equally to this publication. S.G.M., C.S., F.S., A.G.E., and I.F.C. designed the experiments. A.G.E., I.F.C., and E.A.-B. performed the experiments. All authors analyzed the experimental data and discussed the results. The manuscript was written through contributions of all authors. All authors gave their approval to the final version of the manuscript.

Notes

The authors declare no competing financial interest.

■ ACKNOWLEDGMENTS

This research was supported by Deutscher Akademischer Austauschdienst DAAD (A.G.E.); Ministerio de Ciencia Innovación y Universidades (Spain) Proyectos I + D + I, PID2019-109333RB-I00 (S.G.M. & R.M.-R.); CSIC i-Link + 2019 project LINK20270 (S.G.M. & R.M.-R.); European Union's Horizon 2020 research and innovation program (Marie Skłodowska-Curie grant agreement no. 845427) (E.A.B. and S.G.M.); Programa Operativo Aragón de Fondo Social Europeo 2014–2020 (I.F.C.); Agencia Nacional de Promoción Científica y Tecnológica, Argentina (National Agency for Scientific and Technological Promotion, ANP-CYT): PICT 2017-3767 (M.B.) and PICT 2017-0340 (M.J.C.); the Consejo Nacional de Investigaciones Científicas y Técnicas (National Scientific and Technical Research Council); and the Universidad Nacional del Litoral, CAI + D 50620190100020LI (M.J.C.) and Gobierno de Aragón (Project LMP49-18). The authors acknowledge the use of the Advanced Microscopy Laboratory (University of Zaragoza) for access to their instrumentation and for their expertise and Servicio General de Apoyo a la Investigación-SAI, University of Zaragoza.

■ ABBREVIATIONS

CFU, colony-forming units; DOTMG, N,N,N',N'-tetramethyl-N'',N''-dioctylguanidinium; POM, polyoxometalate; POM-IL, polyoxometalate-ionic liquid; PMMA, poly(methyl methacrylate); MIC, minimum inhibitory concentration; MBC, minimum bactericidal concentration

■ REFERENCES

- (1) Singh, S. B.; Young, K.; Silver, L. L. What Is an "Ideal" Antibiotic? Discovery Challenges and Path Forward. *Biochem. Pharmacol.* **2017**, *133*, 63–73.
- (2) Luo, L.; Li, G.; Luan, D.; Yuan, Q.; Wei, Y.; Wang, X. Antibacterial Adhesion of Borneol-Based Polymer via Surface Chiral Stereochemistry. *ACS Appl. Mater. Interfaces* **2014**, *6*, 19371–19377.
- (3) Hu, W.; Peng, C.; Luo, W.; Lv, M.; Li, X.; Li, D.; Huang, Q.; Fan, C. Graphene-Based Antibacterial Paper. *ACS Nano* **2010**, *4*, 4317–4323.
- (4) Lin, W.; Ni, Y.; Pang, J. Microfluidic Spinning of Poly (Methyl Methacrylate)/Konjac Glucomannan Active Food Packaging Films Based on Hydrophilic/Hydrophobic Strategy. *Carbohydr. Polym.* **2019**, *222*, No. 114986.
- (5) Ferraz, R.; Silva, D.; Dias, A. R.; Dias, V.; Santos, M. M.; Pinheiro, L.; Prudêncio, C.; Noronha, J. P.; Petrovski, Z.; Branco, L. C. Synthesis and Antibacterial Activity of Ionic Liquids and Organic Salts Based on Penicillin G and Amoxicillin Hydrolysate Derivatives against Resistant Bacteria. *Pharmaceutics* **2020**, *12*, No. 221.
- (6) Zakrewsky, M.; Lovejoy, K. S.; Kern, T. L.; Miller, T. E.; Le, V.; Nagy, A.; Goumas, A. M.; Iyer, R. S.; Del Sesto, R. E.; Koppisch, A. T.; Fox, D. T.; Mitragotri, S. Ionic Liquids as a Class of Materials for Transdermal Delivery and Pathogen Neutralization. *Proc. Natl. Acad. Sci. U.S.A.* **2014**, *111*, 13313–13318.
- (7) Hallett, J. P.; Welton, T. Room-Temperature Ionic Liquids: Solvents for Synthesis and Catalysis. *2. Chem. Rev.* **2011**, *111*, 3508–3576.
- (8) Herrmann, S.; Seliverstov, A.; Streb, C. Polyoxometalate-Ionic Liquids (POM-ILs)—The Ultimate Soft Polyoxometalates? A Critical Perspective. *J. Mol. Eng. Mater.* **2014**, *02*, No. 1440001.
- (9) Misra, A.; Zambrycki, C.; Kloker, G.; Kotyba, A.; Anjass, M. H.; Franco Castillo, L.; Mitchell, S. G.; Güttel, R.; Streb, C. Water Purification and Microplastics Removal Using Magnetic Polyoxometalate-Supported Ionic Liquid Phases (MagPOM-SILPs). *Angew. Chem., Int. Ed.* **2020**, *59*, 1601–1605.
- (10) Misra, A.; Franco Castillo, L.; Müller, D. P.; González, C.; Eyssautier-Chuine, S.; Ziegler, A.; de la Fuente, J. M.; Mitchell, S. G.; Streb, C. Polyoxometalate-Ionic Liquids (POM-ILs) as Anticorrosion and Antibacterial Coatings for Natural Stones. *Angew. Chem., Int. Ed.* **2018**, *57*, 14926–14931.
- (11) Bijelic, A.; Aureliano, M.; Rempel, A. The Antibacterial Activity of Polyoxometalates: Structures, Antibiotic Effects and Future Perspectives. *Chem. Commun.* **2018**, *54*, 1153–1169.
- (12) Inoue, M.; Suzuki, T.; Fujita, Y.; Oda, M.; Matsumoto, N.; Iijima, J.; Yamase, T. Synergistic Effect of Polyoxometalates in Combination with Oxacillin against Methicillin-Resistant and Vancomycin-Resistant *Staphylococcus aureus*: A High Initial Inoculum of 1×10^8 CFU/mL for in Vivo Test. *Biomed. Pharmacother.* **2006**, *60*, 220–226.
- (13) Inoue, M.; Suzuki, T.; Fujita, Y.; Oda, M.; Matsumoto, N.; Yamase, T. Enhancement of Antibacterial Activity of β -Lactam Antibiotics by $[P_2W_{18}O_{62}]^{6-}$, $[SiMo_{12}O_{40}]^{4-}$, and $[PTi_2W_{10}O_{40}]^{7-}$ against Methicillin-Resistant and Vancomycin-Resistant *Staphylococcus aureus*. *J. Inorg. Biochem.* **2006**, *100*, 1225–1233.
- (14) Hu, T.; Li, Y. H.; Kuang, X. F.; Lu, C. Z. Synthesis and Characterization of Polyoxometalate-Based Silver(I) Phenylethyne Compounds with Antibacterial and Antifungal Activities. *CrystEngComm* **2017**, *19*, 3445–3454.
- (15) Kubo, A.-L.; Kremer, L.; Herrmann, S.; Mitchell, S. G.; Bondarenko, O. M.; Kahru, A.; Streb, C. Antimicrobial Activity of Polyoxometalate Ionic Liquids against Clinically Relevant Pathogens. *ChemPlusChem* **2017**, *82*, 867–871.
- (16) Herrmann, S.; De Matteis, L.; de la Fuente, J. M.; Mitchell, S. G.; Streb, C. Removal of Multiple Contaminants from Water by Polyoxometalate Supported Ionic Liquid Phases (POM-SILPs). *Angew. Chem., Int. Ed.* **2017**, *56*, 1667–1670.
- (17) Rajkowska, K.; Koziróg, A.; Otlewska, A.; Piotrowska, M.; Atrián-Blasco, E.; Franco-Castillo, L.; Mitchell, S. G. Antifungal Activity of Polyoxometalate-Ionic Liquids on Historical Brick. *Molecules* **2020**, *25*, No. 5663.
- (18) Sivov, N. A. Biocide Guanidine Containing Polymers. In *Synthesis, Structure and Properties*; CRC Press: London, 2006; p 156.
- (19) Zhou, Z.; Wei, D.; Guan, Y.; Zheng, A.; Zhong, J.-J. Extensive in Vitro Activity of Guanidine Hydrochloride Polymer Analogs against Antibiotics-Resistant Clinically Isolated Strains. *Mater. Sci. Eng., C* **2011**, *31*, 1836–1843.
- (20) Cabrera, J.; Ruiz, M.; Fascio, M.; D'Accorso, N.; Mincheva, R.; Dubois, P.; Lizarraga, L.; Negri, R. Increased Surface Roughness in Polydimethylsiloxane Films by Physical and Chemical Methods. *Polymers* **2017**, *9*, No. 331.
- (21) Ginsberg, A. P. *Inorganic Syntheses*; John Wiley & Sons, 2009.
- (22) Qiao, L.; Lu, K.; Qi, M.; Fu, R. Separation Performance of Guanidinium-Based Ionic Liquids as Stationary Phases for Gas Chromatography. *J. Chromatogr. A* **2013**, *1276*, 112–119.
- (23) Herrmann, S. *New Synthetic Routes to Polyoxometalate Containing Ionic Liquids: An Investigation of Their Properties*; Springer, 2015.
- (24) Herrmann, S.; Kostzewa, M.; Wierschem, A.; Streb, C. Polyoxometalate Ionic Liquids as Self-Repairing Acid-Resistant Corrosion Protection. *Angew. Chem., Int. Ed.* **2014**, *53*, 13596–13599.
- (25) Arendrup, M. C.; Meletiadis, J.; Mouton, J. W.; Guinea, J.; Cuenca-Estrella, M.; Lagrou, K.; Howard, S. J.; et al. EUCAST Technical Note on Isavuconazole Breakpoints for Aspergillus, Itraconazole Breakpoints for Candida and Updates for the Antifungal Susceptibility Testing Method Documents. *Clin. Microbiol. Infect.* **2016**, *22*, S71.e1–S71.e4.

Supporting Information

Hybrid antimicrobial films containing a
polyoxometalate-ionic liquid

*Ana G. Enderle,^{†a,b,c} Isabel Franco-Castillo,^{†d,e} Elena Atrián-Blasco,^{d,e} Rafael Martín-Rapún,^{d,e} Leonardo Lizarraga,^b María J. Culzoni,^c Mariela Bollini,^b Jesús M. de la Fuente,^{d,e} Filomena Silva,^{f,g} Carsten Streb^{*a} and Scott G. Mitchell^{*d,e}*

a. Institute of Inorganic Chemistry I, Ulm University, Albert-Einstein-Allee 11, 89081 Ulm, Germany.

*Email: carsten.streb@uni-ulm.de

b. Centro de Investigaciones en Bionanociencias (CIBION), CONICET, Godoy Cruz, 2390, C1425FQD Ciudad de Buenos Aires, Argentina.

c. Laboratorio de Desarrollo Analítico y Quimiometría (LADAQ), Universidad Nacional del Litoral – CONICET, Ciudad Universitaria, Paraje El Pozo, CC242, S3000 Santa Fe, Argentina

d. Instituto de Nanociencia y Materiales de Aragón (INMA-CSIC), Consejo Superior de Investigaciones Científicas-Universidad de Zaragoza, c/ Pedro Cerbuna 12, 50009 Zaragoza, Spain.

e. CIBER de Bioingeniería, Biomateriales y Nanomedicina, Instituto de Salud Carlos III, 28029 Madrid, Spain.

*Email: scott.mitchell@csic.es

f. ARAID – Agencia Aragonesa para la Investigación y el Desarrollo, Av. Ranillas, 1D, 2B, 50018 Zaragoza, Spain.

g. Universidad de Zaragoza, Facultad de Veterinaria, Calle Miguel Servet 117, 50013 Zaragoza, Spain.

† These authors have contributed equally to this publication.

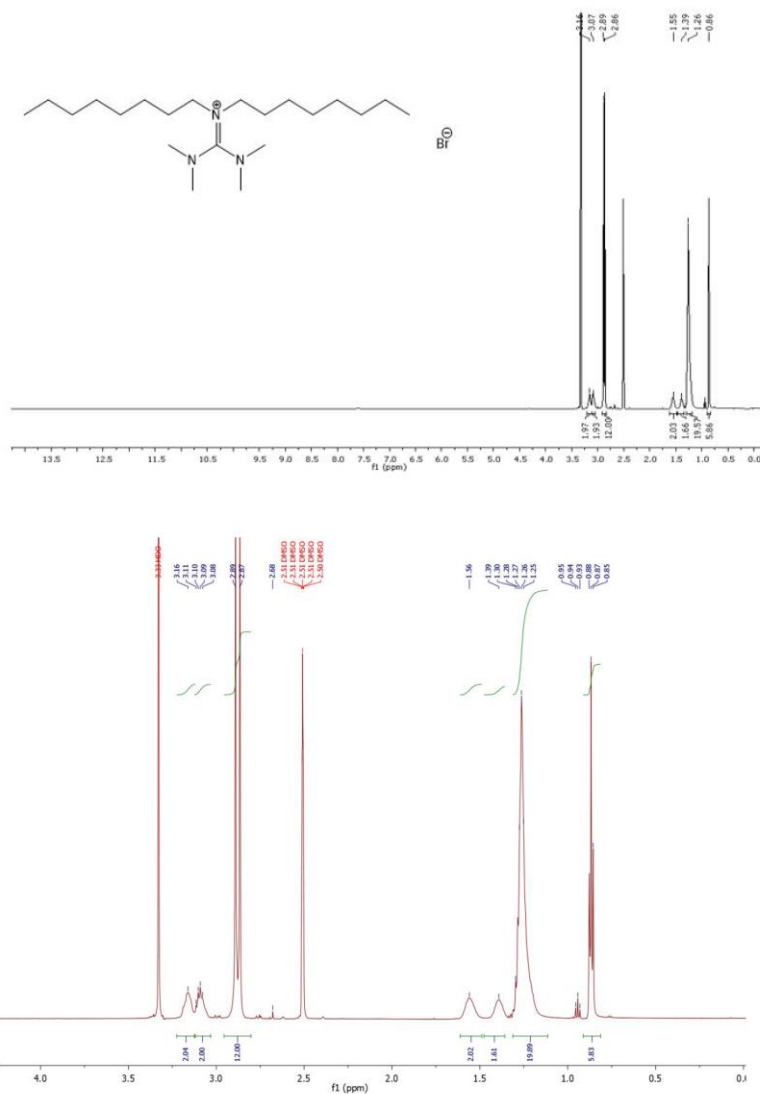
S1

Supporting Information**Table of Contents**

1. NMR spectrum of the POM-IL DOTMG-1	S3
2. TGA of POM-IL DOTMG-1	S6
3. Preparation and characterization of the DOTMG-1 PMMA films	S7
4. Cytotoxicity of the POM-IL DOTMG-1	S12
5. Antibacterial Studies	S13

Supporting Information

1. NMR spectrum of the POM-IL

Figure S1. ¹H-NMR spectrum of DOTMG-Br in DMSO-d₆.

Supporting Information

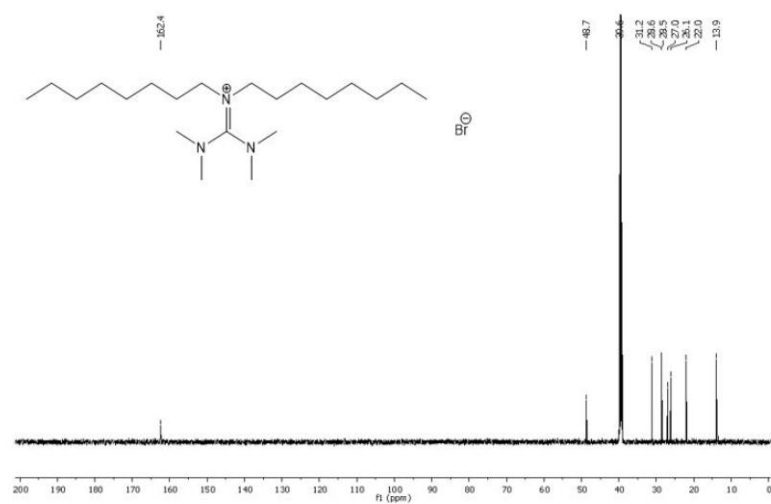


Figure S2. ^{13}C -NMR spectrum of DOTMG-Br in DMSO- d_6 .

[illegible]

Figure S3. ^1H -NMR spectrum of DOTMG-1 in DMSO- d_6 .

Chemical structure of the [SiW₁₁O₃₉] complex is shown above the spectrum. The structure consists of a central silicon atom (Si) bonded to three oxygen atoms (O) and a central tungsten atom (W). The tungsten atom is bonded to three oxygen atoms (O) and a central silicon atom (Si). The entire complex is enclosed in brackets with a subscript 8, indicating the number of repeating units.

The ¹³C NMR spectrum shows the following chemical shifts (ppm):

- 162.3
- 39.6
- 39.6
- 33.2
- 33.2
- 33.5
- 33.5
- 27.0
- 27.0
- 22.0
- 22.0
- 11.9

2. TGA graph of the POM-IL DOTMG-1

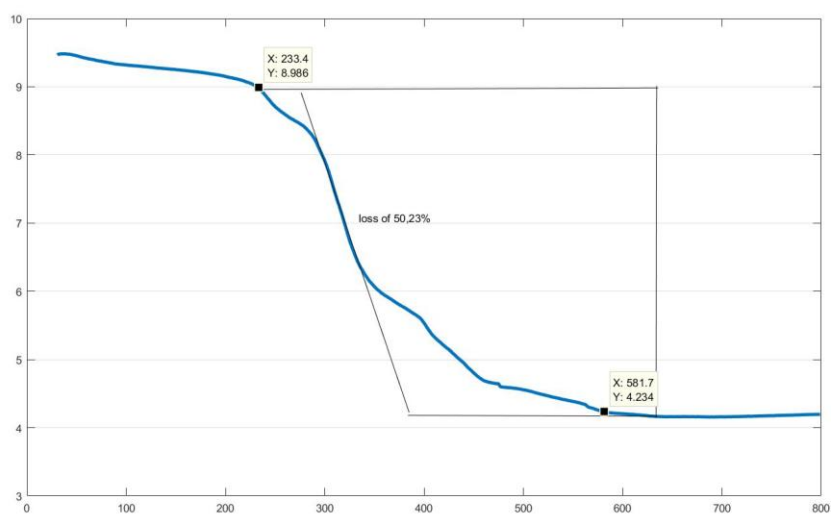


Figure S5. TGA graph of DOTMG-1.

Supporting Information

3. Preparation and characterization of the DOTMG-1 PMMA films

Table S1. Composition of the films

Film	DOTMG-1 (mg)	Toluene (mL)	Solution A (mL)
B	4	0.04	0.16
C	7	0.07	0.13
D	10	0.10	0.10

• FT-IR analysis

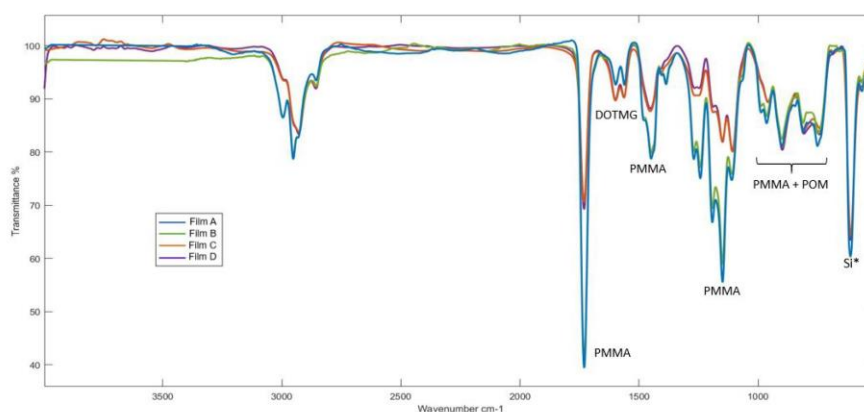


Figure S6. FT-IR analysis of films A, B, C and D.

It is possible to visualize the changes in the signals corresponding to PMMA and DOTMG-1 when increasing the POM-IL content on the films from B to C. The peaks at 610 cm^{-1} and 1115 cm^{-1} correspond to the Si lattice phonons and to Si-O2 complexes, respectively.³² The main peaks of PMMA are observed at 1713 cm^{-1} , 1425 cm^{-1} , 1125 cm^{-1} and in the region between 1000 to 750 cm^{-1} .³³ It can be observed that the region corresponding to the 750-1000 cm^{-1} is an overlapping zone of POM and PMMA signals. Two peaks corresponding to the cation in 1603 cm^{-1} and 1562 cm^{-1} are more visible on the spectra corresponding to films C and D. SEM studies

Supporting Information

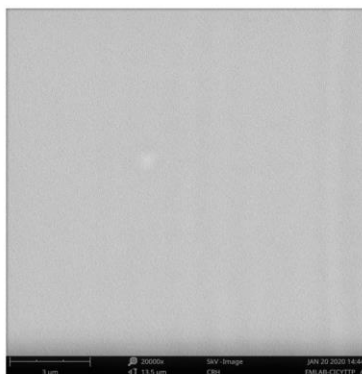


Figure S7. SEM micrographs of Film A. Scale bar 3 μm.

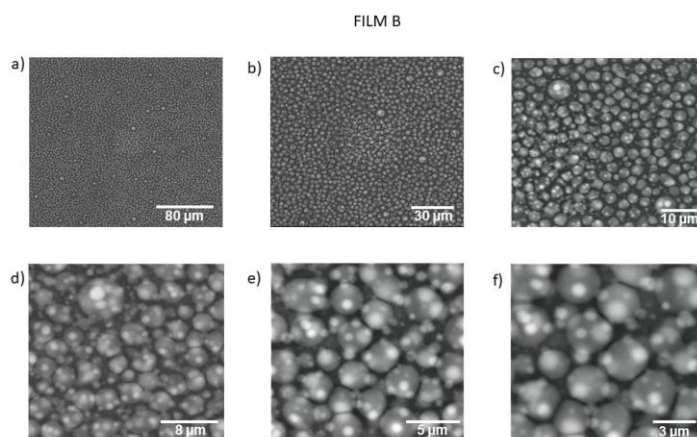


Figure S8. SEM micrographs of film B. Magnifications: a) 1000x; b) 2000x; c) 5000x; d) 10000; e) 15000x; f) 20000x

Supporting Information

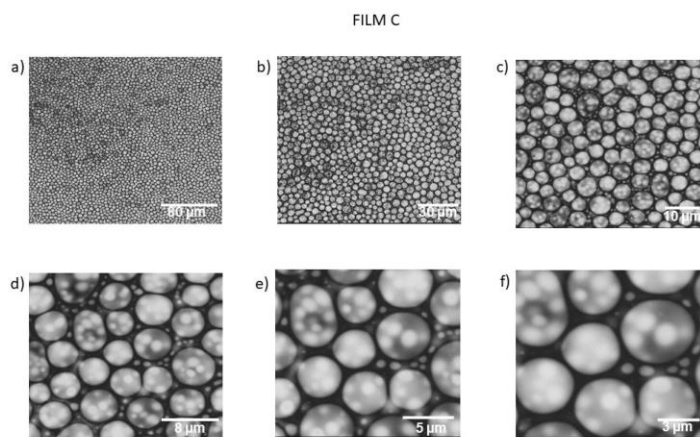


Figure S9. SEM micrographs of film C. Magnifications: a) 1000x; b) 2000x; c) 5000x; d) 10000; e) 15000x; f) 20000x.

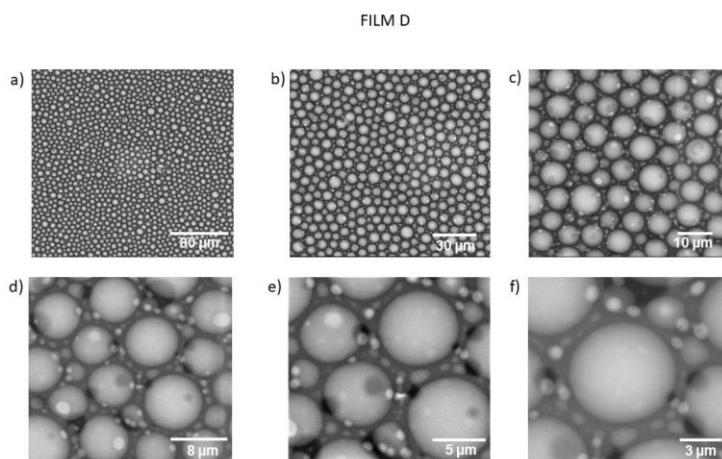


Figure S10. SEM micrographs of film D. Magnifications: a) 1000x; b) 2000x; c) 5000x; d) 10000; e) 15000x; f) 20000x.

Supporting Information

AFM images

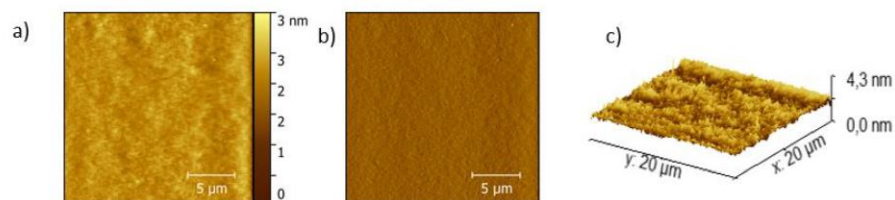


Figure S11. AFM image of Film A, a) Height image, b) phase image, and c) 3D height image.

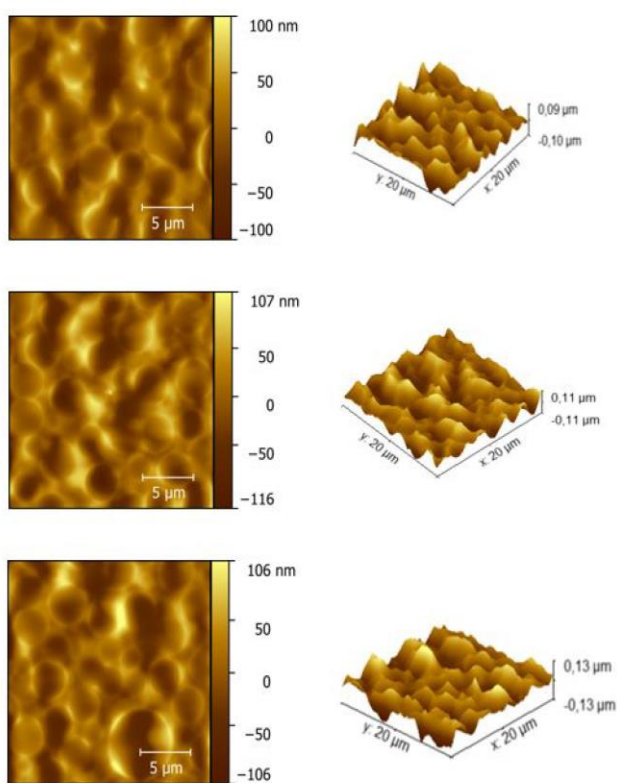


Figure S12. AFM images of Film B; Left: Height images; right: 3D height images (different positions).

Supporting Information

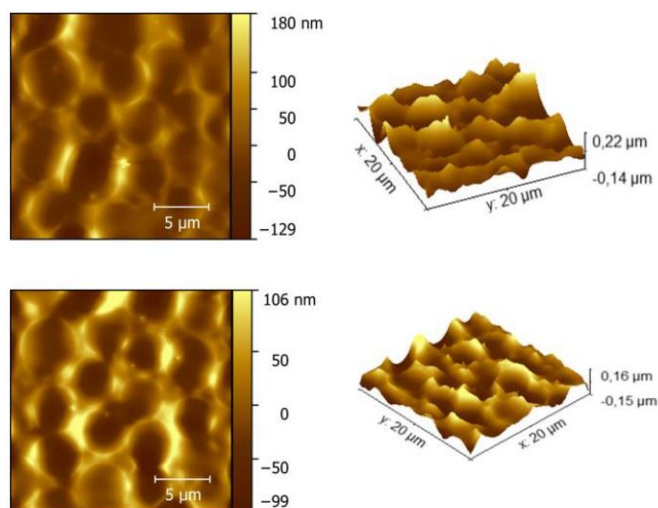


Figure S13. AFM images of Film C; Left: Height images; right: 3D height images (different positions).

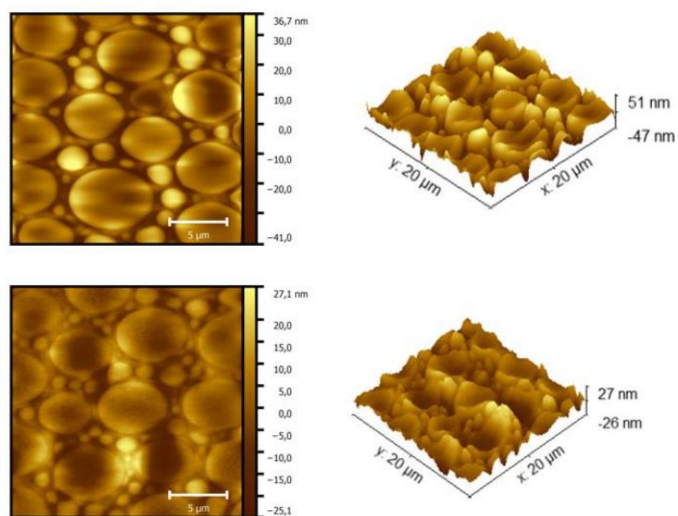


Figure S14. AFM images of Film D; Left: height images; right: 3D height images (different positions).

Supporting Information

From the height profile of the samples studied by AFM, it is possible to calculate the surface roughness. In film D, the droplets are larger, but the surface is flatter, and the roughness decreases compared with films C and B. From the comparison of the roughness of B and C, it is observed that this value increases when the content of the IL increases (Table S2).

Table S2. Root mean square roughness of the films (Sq)

Film	Sq (nm)
A	0.4
B	33.8 +/- 0.1
C	36.7 +/- 0.2
D	9.4 +/- 0.1

4. Cytotoxicity of the POM-IL DOTMG-1

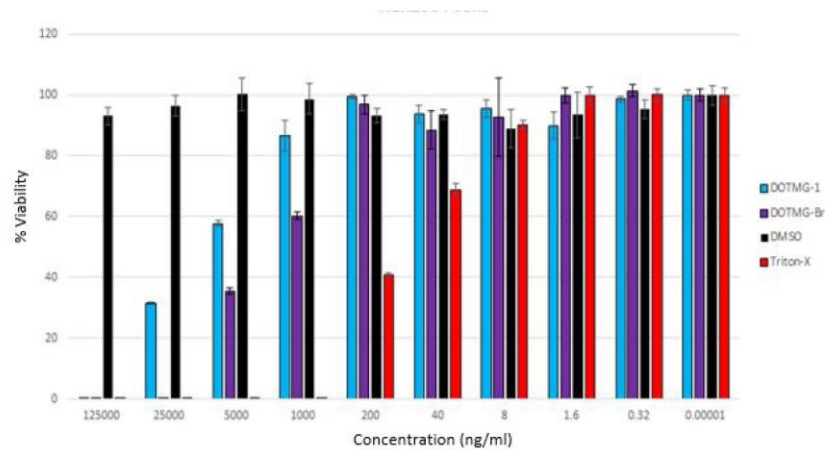


Figure S15. Concentration dependent *in vitro* cytotoxic effect of DOTMG-1 and DOTMG-Br on the viability of HEK293T cells.

Supporting Information

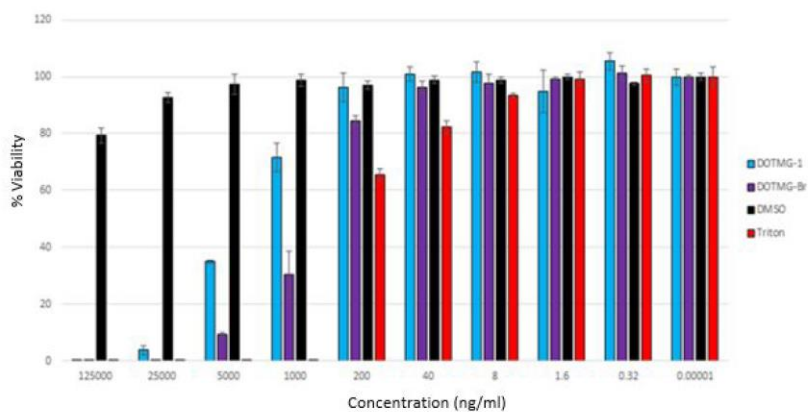


Figure S16. Concentration dependent *in vitro* cytotoxic effect of DOTMG-1 and DOTMG-Br on the viability of T2M-bl cells.

5. Antibacterial Studies

Table S3. Microorganisms and growth conditions.

Microorganisms	Solid media	Liquid media	Incubation Temperature	Inoculum incubation
Bacteria				
<i>E. coli</i> DH5α	TSA	LB	37 °C	24 hours
VTEC	MHA	LB	37 °C	24 hours
<i>B. subtilis</i>	TSA	NB	37 °C	24 hours
<i>L. monocytogenes</i>	BHIA	NB	37 °C	24 hours
Fungi				
<i>A. niger</i>	SDA	RPMI	35 °C	4 days
<i>A. ochraceus</i>	YMA	MEP	25 °C	4 days
<i>C. cladosporioides</i>	SDA	RPMI	25 °C	4 days
<i>P. expansum</i>	PDA	YMB	25 °C	4 days

Supporting Information

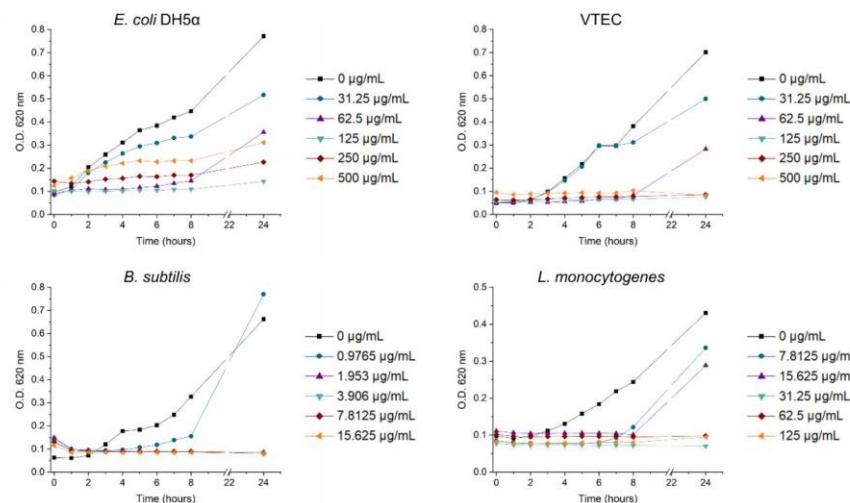


Figure S17. *E. coli* DH5α, VTEC, *B. subtilis* and *L. monocytogenes* growth curves, starting with a 10^7 CFU/mL inoculum, in the presence of different DOTMG-1 concentrations (ranging from 0.9765 to 500 µg/mL). The minimum inhibitory concentration (MIC) obtained for the different bacteria was: 125 µg/mL for *E. coli* DH5α and VTEC; 31.25 µg/mL for *L. monocytogenes* and 1.95 µg/mL for *B. subtilis*. The apparent increase of turbidity in the *E. coli* DH5α graph at the higher concentrations is due to the precipitation of the compound in the culture media. These results were confirmed with the Resazurin assay and by subculturing in solid culture media, as described in section 3.5.1.2. Bacterial cell viability assay.

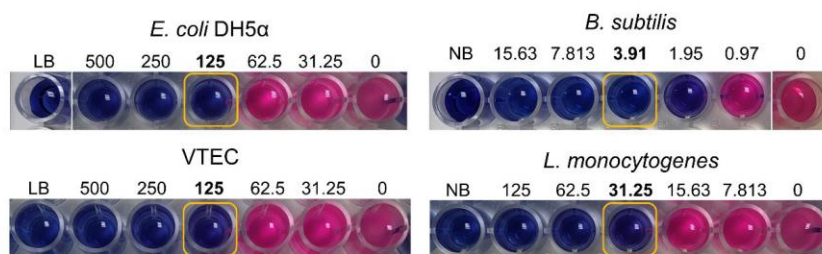


Figure S18. Resazurin cell viability assay for *E. coli* DH5α, VTEC, *B. subtilis* and *L. monocytogenes*, incubated with different concentrations of DOTMG-1 (in µg/mL). The Resazurin compound (blue) turns pink in presence of viable bacteria as a result of their metabolic activity, therefore pink wells indicate alive bacteria, while blue wells indicate a loss of metabolic activity, which is one of the first cascade events in the mechanism of cell death.

Supporting Information

The results were confirmed by subculturing on solid media and colony counting. Hence, the minimum bactericidal concentration (MBC) for both *E. coli* (*E. coli* DH5 α and VTEC) is 125 $\mu\text{g/mL}$, 3.91 $\mu\text{g/mL}$ for *B. subtilis* and 31.35 $\mu\text{g/mL}$ for *L. monocytogenes*. The MBC values of both *E. coli* strains and *L. monocytogenes* agree with the MIC value, while *B. subtilis* presents a MBC value twice that of the corresponding MIC.

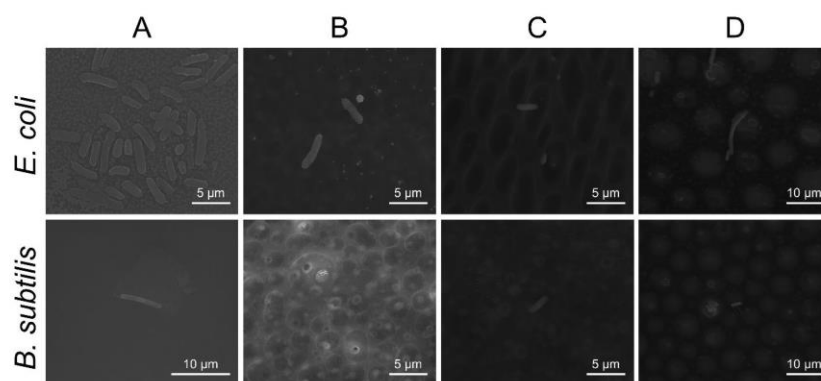


Figure S19. ESEM images of the DOTMG-1@PMMA films after incubation with *E. coli* and *B. subtilis*. All the samples were rinsed after the incubation time in order to sow the planktonic bacteria and determine the antimicrobial performance of the films. The PMMA film without DOTMG-1 (A) presented regular *E. coli* growth over the surface and the bacteria exhibited good morphology. Very few bacteria were found on the surface of the DOTMG-1@PMMA films (B, C, and D). In the case of *B. subtilis*, hardly any bacteria were found, even in the films without POM-IL (A), probably due to low adhesion of the bacterial cells to this surface of the PMMA.

Article 5: New protective coatings against lampenflora growing in the Pommery Champagne cellar

New protective coatings against lampenflora growing in the Pommery Champagne cellar

Isabel Franco-Castillo^{1,2}, Archismita Misra³, Sébastien Laratte⁴, Maxime Gommeaux⁴, Robin Perarnau⁴, Nathalie Vaillant-Gaveau⁵, Clément Pierlot⁶, Carsten Streb³, Scott G. Mitchell^{1,2*}, Stéphanie Eyssautier-Chuine^{4*}

¹ Instituto de Nanociencia y Materiales de Aragón (INMA-CSIC), Consejo Superior de Investigaciones Científicas-Universidad de Zaragoza, c/ Pedro Cerbuna 12, 50009 Zaragoza, Spain.

² CIBER de Bioingeniería, Biomateriales y Nanomedicina, Instituto de Salud Carlos III, 28029 Madrid, Spain.

* Email: scott.mitchell@csic.es

³ Institute of Inorganic Chemistry I, Ulm University, Albert-Einstein-Allee 11, 89081 Ulm, Germany

⁴ Groupe d'Étude sur les Géomatériaux et les Environnements Naturels Anthropiques et Archéologiques 3795 (GEGENAA) - SFR Condorcet FR CNRS 3417 – 2, Esplanade Roland Garros, Université de Reims Champagne-Ardenne, 51100 cedex, Reims, France.

* Email: stephanie.eyssautier@univ-reims.fr

⁵ Unité de Recherche EA 4707 Résistance Induite et Bioprotection des Plantes (RIBP), SFR Condorcet FR CNRS 3417, UFR Sciences Exactes et Naturelles, Université de Reims Champagne-Ardenne, Reims, France.

⁶ Vranken-Pommery Monopole, 5 Place du Général Gouraud, BP1049, 51689, Reims, cedex 2, France

Abstract

Phototrophic microorganisms such as cyanobacteria and microalgae can proliferate readily in underground heritage sites where the introduction of artificial illumination equipment has significantly altered previously stable environmental conditions. The extended lampenflora biofilm growth on the bas-reliefs carved in the underground Pommery Champagne cellar in Reims (France) represents a recurring biocolonisation problem which requires periodic cleaning. The aim of this work was to limit the growth of lampenflora on chalk substrates using preventative biocidal treatments based on polyoxometalate ionic liquids (POM-ILs). Biocidal assays carried out in laboratory showed how two different colourless POM-IL coatings were more effective than commercial Preventol RI80 against two algal strains isolated from the Pommery bas reliefs, *Pseudostichococcus monallantoides* and *Chromochloris zofingiensis*. However, only one POM-IL variant was capable of sustained prevention of biofilm growth when applied to wet chalk, which replicates the more drastic natural environmental conditions of the cellar and can limit the performance of the biocidal coatings. Crucially, coating concentration studies demonstrate how POM-IL-coated slabs from previous experiments retain their biocidal activity and can prevent subsequent recolonisation following the re-inoculation of coated slabs with algae and cyanobacteria. Consequently, POM-ILs represent excellent candidates to eliminate lampenflora growth on the chalk bas-reliefs in the unique subterranean environment of the Pommery Champagne cellar.

Keywords

Polyoxometalate-ionic liquid (POM-IL), Preventol RI80, Biocide, Lampenflora, Biodeterioration

Highlights

- Lampenflora colonises chalky bas-reliefs in the underground Pommery Champagne cellar.
- This study evaluates and compares two different POM-ILs and commercial Preventol RI80.
- Biocidal assays showed how POM-ILs are more effective than Preventol RI80 over a seven-week period.
- When applied to wet chalk, only one POM-IL variant was capable of sustained prevention of biofilm growth.

1. Introduction

The mechanical fracturing and disintegration of natural stone substrates by lithobionts and corrosion through the metabolic processes of microorganisms represent the greatest biodeterioration threats to the conservation of stone-based cultural heritage, however, undesired biological colonisation of stone materials can also lead to unwanted aesthetic changes such as unsightly discoloration that covers art details (Warscheid and Braams, 2000; Charola et al., 2011; Dias et al., 2020; Favero-Longo and Viles, 2020). The open-air conditions of exposure of buildings and monuments induce a large influence of climatic factors on the bioweathering by changing of sunlight radiation, temperatures and rainfall which vary with respect to their geographical location and ongoing climate change. Underground cultural heritage like caves, in the natural state, generally have a weak connection with the external atmosphere (Sanchez-Moral et al., 2021) and are considered to be extreme environments for microbial growth, due to the low nutrient availability (Simon et al., 2007). In such environments, chemolithoautotrophic organisms can thrive on stone surfaces as a result of stable conditions, constant air and water temperature, high moisture and solute-rich groundwater (Bastian and Alabouvette, 2009). However, underground caves now represent appealing tourist attractions (Cigna and Forti, 2013) and the introduction of lighting equipment can rapidly and significantly alter previously stable environmental conditions by increasing ambient temperature and CO₂ concentration, and decreasing relative humidity (Mulec et al., 2012; Baquedano Estévez et al., 2019; Caneva et al., 2020). Furthermore, intensified human activity also brings organic matter and new strains of microorganisms from outside which gradually adapt to subterranean environments (Mulec, 2014; Marques et al., 2016). One reason for this is that increased geotourism can foster the perfect combination of microbes that typically thrive on the surface along with the need for well-lit and illuminated areas, meaning that phototrophic organisms (primarily cyanobacteria and microalgae) proliferate readily (Mulec and Kosi, 2009). As a result, the biocolonisation of paintings and artifacts by the lampenflora (Dobat, 1969) has led to an irretrievable loss of historical heritage and an extinction of original cave-dwelling organisms (Bastian et al., 2010; Albertano, 2012; Perez, 2018).

One such example of this is the extended lampenflora growth on the bas-reliefs carved in the prestigious underground Pommery Champagne cellar in Reims located in a French region called Grand Est. Wells act as a weak source of natural sunlight, but it is the artificial lights - first with candles and then through electric illumination - that are the primary disruptors of the natural ecosystem. Several halls are decorated with monumental bas-reliefs carved in the chalk by a French sculptor, Gustave Navlet, between 1882 and 1885 and are listed as UNESCO World

Heritage (Fig. 1a-b). Many tourist visits are organised every day to present Champagne cellar galleries and halls where chalk bas-reliefs are highlighted by incandescent lamps which have been replaced latterly by LED. Moreover, contemporary art works have also been exhibited in halls over the last 13 years, which have enhanced the need for artificial light. In addition, some of them are luminous which generate excess light (Fig. 1c-d). The inappropriate increase of artificial light and increase in tourism have raised the outside air-current and led to the growth of lampenflora on bas-reliefs. The progressive spread of the lampenflora has formed extensive greenish and reddish biofilms which disturb the beauty of the bas-reliefs and contributes to their deterioration (Albertano and Urzi, 1999; Borderie et al., 2014; Bruno et al., 2019; Nikolić et al., 2020). The microbial communities are removed every six months using a classic cleaning procedure involving a soft airbrush with bicarbonate, but the lampenflora biofilms rapidly recolonise bas-reliefs, which has increased the need for periodic cleaning and more extreme measures. In this respect, the bas-reliefs have had to be repaired frequently in recent years and have left visible “scars” indicating where biocolonisation once caused physical alterations to the stone carvings.

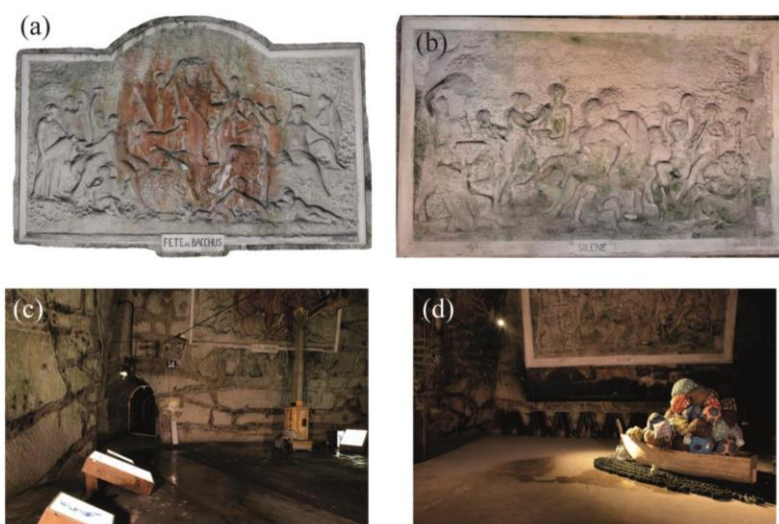


Figure 1. “Fête de Bacchus” (5 x 8 m) (a) and “Silène” (15 x 5 m) (b) bas-reliefs carved by the French sculptor Gustave Navlet in the Pommery Champagne Cellar between 1882 and 1885. Images were built by photogrammetry from respectively 94 and 153 photos (Coolpix B700) by Agisoft Metashape v.1.7.2 software (S. Laratte). Photos of the cellar room with “Fête de Bacchus” and lighting contemporary artworks (c); cellar room with “Silène” and a contemporary artwork lighted by a spot. Formerly a ramp with 10 spots distributed under and along the bas-relief (d) (S. Laratte).

The aim of this work was to limit the growth of lampenflora on chalk substrates. Drastic solutions such as the closure of the site to tourists, similar to the case of Lascaux cave in 1963 and others since, is improbable in the Pommery Champagne cellar context because the cellar tours represent a key factor for the promotion of Champagne and provide important income. In many subterranean sites (e.g., caves, catacombs, and hypogea), the common cleaning procedure consists of curative methods with hypochlorites which rapidly degrade organic substances through oxidation. But this approach can release poisonous chlorine gas, which has a harmful consequence on the environment and, in the case of the chalk which constitutes the Pommery cellar, the release of chloride ions could also lead to a dissolution of the stone and to the reddish colouring of the bas-reliefs *via* the oxidation of Fe^{2+} present in the chalk. Hydrogen peroxide is also used but it has a strong oxidising effect and produces corrosion of the material (Mulec and Kosi, 2009). Biocides like quaternary ammonium salts are also effective on many microorganisms (e.g., fungi, algae, and lichen) (Ascaso et al., 2002; Urzi et al., 2016; Vannini et al., 2018; Li et al., 2020) as a curative treatment but the challenge here was to provide a long-lasting biocidal effect to avoid the lampenflora growth despite an subterranean environment which meets favourable conditions to promote it.

Recently, polyoxometalate-ionic liquids (POM-ILs) have gained attention in the heritage field as protective antimicrobial coatings, due to their tailorable antimicrobial properties, offered by their structural and compositional versatility (Hallett and Welton, 2011; Zakrewsky et al., 2014). These compounds, which are salts with a melting point below 100°C , are composed of an anionic metal-oxide cluster (polyoxometalate, POM for short) and an organic cation (typically a quaternary ammonium or phosphonium cation) and have been previously reported as effective antimicrobials against different microorganisms (Kubo et al., 2017; Misra et al., 2018). Their hydrophobicity, high antimicrobial and anticorrosion activity combined with generally colourless nature, means that they can be applied at low concentrations as transparent coatings to prevent biodeterioration in heritage objects and architecture (Franco-Castillo et al., 2021). We have demonstrated how POM-ILs can prevent biofilm formation and corrosion of natural limestone of varying porosity (Misra et al., 2018). Recently, we also reported how POM-ILs can act as disinfectant agents to eliminate mould colonisation over brick surfaces (Rajkowska et al., 2020). Others have evaluated their ability to inhibit bacterial colonising of wall paintings (Li et al., 2021).

Here we explore the activity of two different POM-ILs as protective coatings against lampenflora colonisation of natural stones and compare their activity with the commercially available Preventol RI80 (PR80). The aim of this research is to evaluate the use of POM-IL 1

and POM-IL2 against algae and cyanobacteria present in the bas-reliefs as well as their mode-of-application and duration of action. Both POM-ILs are based on the same Keggin-type anion, $[\alpha\text{-SiW}_{11}\text{O}_{39}]^{8-}$, and two different tetraalkylammonium ions (tetraheptylammonium and trihexyl tetradecyl ammonium, POM-IL1 and POM-IL2, respectively).

2. Materials and methods

2.1 Presentation of the Pommery cellar's stone

Pommery Champagne cellar is located in the basement of Reims city and is made of Chalk. This stone belongs to the Senonian age (89.8 – 66 My) of Cretaceous Period and represents 5 % of the bedrock surface of West-Central Europe (Ballesteros et al., 2021). In Reims, Chalk has been quarried as a construction material from 10th to 15th centuries for the building of religious monuments. This stone was then replaced by Lutetian limestones in churches, but it is still employed for castles and private houses (Fronteau, 2000). Chalky quarries have been used age Champagne wine since the 19th century. The Pommery Champagne cellar is situated at a depth of 30 m depth and is composed of 18 km of underground galleries and halls. The temperature was respectively 17.6 °C and 18.6 °C in “Fête de Bacchus” and in “Silène” rooms in June 2020 and 92 % of relative humidity in both rooms. In February 2021, the temperature was 14.1 °C and 15 °C in “Fête de Bacchus” and “Silène” rooms with the relative humidity of 95 %. The high fracturing of the stone provides a wetness inside the stone and increases the relative humidity in the cellar, especially in rainy seasons like in winter.

The stone is a homogeneous coccolithic limestone with a high porosity (40.4 %). The porous network was analysed by mercury (Hg) intrusion measurements and is characterised by 98.7 % of micropores with a diameter less than 1 µm (most of them *ca.* 0.25 µm). The strong capillary coefficient of 352.5 g.m⁻².s^{-1/2} highlights a very good connection of pores and a high water saturation (94.4 %). Therefore, these results indicate that, *a priori*, chalk is a material with a high bioreceptivity due to the fact that it can absorb and release a large amount of water (over long periods of time), making it readily available to lampenflora microorganisms colonising the cellar walls (Miller et al., 2012).

2.2 Biocides

POM-ILs 1 and 2 were synthesised according to a previously reported synthetic procedure (Misra et al., 2018). Preventol RI80 is a solution of quaternary ammonium salts as Benzalkonium chloride (alkyl-dimethylbenzylamine chloride (80 %) and isopropanol (2 %)) - Lanxess, Köln, Germany. Quaternary ammonium compounds are widely used as antiseptics

and disinfectants in medical and industrial fields (Gilbert and Moore, 2005). In cultural heritage, those components are commonly used during cleaning procedures by professional restorers (Stupar et al., 2014; Favero-Longo et al., 2018). The efficiency of Preventol RI80 was proven in many studies as a curative treatment to eliminate a wide spectrum of microorganisms, such as fungi and bacteria (Blazquez et al., 2000; Maxim et al., 2012). It was also proven to be efficient against photosynthetic microorganisms such as algae, cyanobacteria, lichen (Ascaso et al., 2002; Vannini et al., 2018; Genova et al., 2020), complex biofilms on outdoor monuments (Coutinho et al., 2016; Sanmartín et al., 2020) and in subterranean environments (Nugari et al., 2009; Urzi et al., 2016). For our study, biocides were applied on non-colonised stone samples, as preventive treatments to avoid the settlement of the lampenflora microorganisms. For this purpose, both POM-IL1 and 2 were diluted in acetone for a concentration of 100 mg/mL and 2 % of Preventol RI80 was diluted in distilled water (as recommended).

2.3 Biocide coating on stone samples

Diluted solutions were applied by brush on stone slabs measuring 5 x 5 x 1 cm. The quantity of biocide applied on each stone sample was controlled by weighing to obtain similar quantity for triplicates. After 48 h of drying, slabs were weighed to calculate the effective quantity of coating remained on stone for the biocidal assays (Table S1). For assay 1 and 2, liquid coatings were applied on dry stones while for assay 3 and 4, each stone was saturated with 9 mL of distilled water before the application in order to simulate to the real application on the cellar walls, which are close to saturation. Under such conditions, the biocidal coating remained on the surface of the stone without being absorbed and penetrating the pores of the chalk. Accordingly, three different amounts of POM-ILs solutions were brushed (0.1, 0.2, and 0.4 g) and two different amounts of Preventol RI80 (0.2 and 0.4 g) since its biocidal effect was weaker, even at the highest tested concentration of 0.4 g in assay 2.

2.4 Identification of algae and cyanobacteria for biocidal assays

The sampling of biofilms was carried out from a visual selection on the coloured areas and on the non-coloured area (Fig. S1). The biofilm samples collected from both bas-reliefs of the Champagne cellar were cultured on agar plates with Hoagland medium to isolate algae and cyanobacteria species. DNeasy PowerBiofilm kit (Qiagen) was used for DNA extraction following the manufacturer's instructions. The 18S rRNA genes were amplified by PCR using eukaryote-specific primers, the forward primer NS1F (5'-GTAGTCATATGCTTGCTC-3') and the reverse primer NS8R (5'-TCCGCAGGTTACCTACGGA-3'), the thermal cycling

profile started by an initial denaturation at 95 °C for 5 min, then 30 cycles at 95 °C for 30 s, 59 °C for 30 s and 72 °C for 1 min 30 s, followed by a final extension at 72 °C for 10 min. Only one alga species was identified with the universal primers (Table S2) and for better results, *rbcL* genes of the plastid genome were used as forward primer S1F (5'-ATGTCACCACAAACAGAGACTAAAGC-3'), reverse primer S1R (5'-GAAACGGTCTCTCCAACGCAT-3') (Radha et al., 2013). The protocol for the thermal cycling was: 95 °C for 2 min, then 35 cycles of 95 °C for 30 s, hybridation at 58 °C for 30 s and extension at 72 °C for 1 min, followed by a final extension at 72 °C for 10 min.

For cyanobacteria, 16S rRNA genes were amplified by PCR with the forward primer 8F (5'-AGAGTTTGATCCTGGCTCAG-3') (Turner et al., 1999) and the reverse primer 1351R (5'-GACGGGCGGTGTGTRCA-3'). The thermal cycling profile was 5 min at 95 °C then 25 cycles of 30 s at 95 °C, 30 s at 57 °C and 1 min at 72 °C, a final extension at 72 °C for 10 min.

The PCR product was sent to Genoscreen (France) for primer removal and for further sequencing using an automatic DNA sequencer (model 3730xl; Applied Biosystems). The nucleotide sequences were aligned with the closest relative sequences of representatives in the GenBank database by means of BLASTN (Basic Local Alignment Search Tool), an algorithm using the CLUSTALW program (Thompson et al., 2002) and available at the National Center for Biotechnology Information (NCBI). They were subsequently deposited in the NCBI database (refer to Table S2 accession numbers). DNA sequences blasted in NCBI were able to lead to both *Pseudostichococcus monallantoides* and *Diplosphaera* sp., and the microscopic observations of the cultures clearly displayed distinct algae morphologies (Fig. 2).

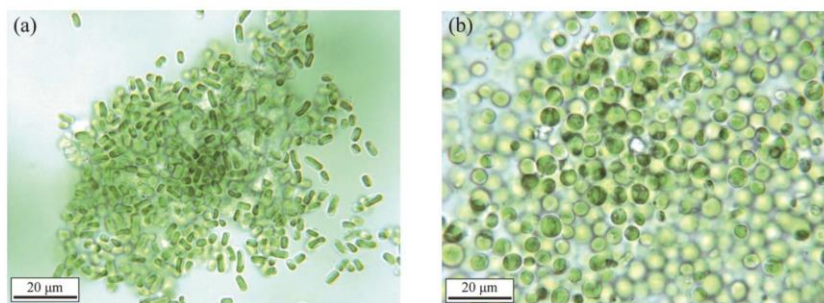


Figure 2. Optical microscopy images of *Pseudostichococcus monallantoides* (a) and *Diplosphaera* sp. (b).

2.5 Biocidal assays

Four biocidal assays consisted of an accelerated biocolonisation of stone slabs in a climatic chamber which were carried out sequentially to adapt the protocol in function of the results and to evaluate biocides in progressively more drastic conditions. In assay 1, two different batches of slabs were inoculated with the algal colonizers of the bas-reliefs, *Chromochloris zofingiensis* and *Pseudostichococcus monallantoides*. Assay 2 consisted of increasing the quantity of biocidal product on slabs to optimise the efficiency. In Assay 3 and 4, the biocidal products were applied on water-saturated stones which represented more drastic and realistic conditions in which to evaluate the performance of biocides. Assay 3 consisted of the same biocolonisation protocol as Assay 2 but performed on stones saturated with water. Finally, Assay 4 evaluated the performance of the coatings on wet stone after a second inoculation of algae and cyanobacteria in order to be closer to the natural environmental conditions, where the seeding occurs continuously all the time.

The protocol of the accelerated biocolonisation consisted of inoculating slabs with a suspension of green algae isolated from biofilms growing on both bas-reliefs of the Pommery Champagne cellar. Algae were isolated and cultured in laboratory in stirred flasks with a liquid medium composed of sterile distilled water and Hoagland medium (Table S3). Cultures were incubated at 20 °C under a fluorescent light (Sylvania Gro-Lux-15 W lamp, PAR = 15 mmol (photons) m⁻². s⁻¹). An aliquot of algae was transferred every month into fresh medium.

For **assay 1 and 2**, algal suspension was diluted to obtain a similar concentration of around 50 cells/0.1 µL and checked by the chlorophyll *a* absorbance control at 665 nm using spectrophotometry (Thermo Fisher Scientific Genesys 10-S). Stone slabs were placed in Plexiglass cups; 2 mL of algal suspension was spread out on each stone surface and 20 mL of Hoagland medium was put at the bottom of samples after the inoculation and 5 mL of this solution was added regularly over the entire incubation period to ensure the wetness of the stones by means of capillary absorption.

For **assay 3**, algal suspension was diluted to get around 100 cells/0.1 µL and only 1 mL was spread on the slab's surface because stones were already saturated with water.

For **assay 4**, a mix of two algae (*Pseudostichococcus* sp. and *Diplosphaera* sp.) and a cyanobacteria (*Timaviella* sp.) were inoculated. An algal suspension was diluted to around 200 cells/0.1 µL, and 1 mL was spread on slabs and 400 µL of a cyanobacteria suspension was spread for a concentration of around 100 cells/0.1 µL.

The biocolonisation was carried out in a climatic chamber which displayed a constant temperature at 20 °C and 80 % of relative humidity. Two neon lights (Sylvania Gro-Lux)

released a PAR (Active photosynthetic radiation) between 20 and 30 $\mu\text{mol photons.m}^{-2}.\text{s}^{-1}$ for 12 h every day. The stone and incubating conditions, the coating concentration and the algae and cyanobacteria inoculated on each assay are summarised in Table 1.

Table 1. Summary of the conditions of the four assays.

Assay	Aim of the assay	Stone	Inoculated microorganisms	Incubation conditions	Concentration	
					POM-ILs	PR80
1	Evaluation of the biocidal coatings	Dry	<i>Chromochloris</i> sp. <i>Pseudostichococcus</i> sp.	7 weeks 20°C 80 % R.H.	0.1 g 0.2 g	0.2 g
2	Optimize the biocidal coating	Dry	<i>Pseudostichococcus</i> sp.	5 weeks 20°C 80 % R.H.	0.4 g	0.4 g
3	Effectiveness of the coating on wet stones	Wet	<i>Pseudostichococcus</i> sp.	5 weeks 20°C 80 % R.H.	0.1 g 0.2 g 0.4 g	0.2 g 0.4 g
4	Biocidal effect after re-inoculation	Wet	<i>Pseudostichococcus</i> sp. <i>Diplosphaera</i> sp. <i>Timaviella</i> sp.	5 weeks 20°C 80 % R.H.	0.1 g 0.2 g 0.4 g	0.4 g

2.6 Evaluation of the biocidal effect

2.6.1 Colourimetry

The progressive greening of the stone surfaces, due to the algae biocolonisation, was followed by the measurement of the colour by a Chroma Meter CR-400 from Konica-Minolta with a light projection tube CR-A33c of 11 mm diameter. The calibration was performed with three flashes on a white ceramic plate CR-A43. Then 10 measurements were carried out on the upper face of every 5 x 5 cm sample before and after coating in the aim to estimate the colour variation of the stone impacted by coatings. Moreover, the algal growth during the biofouling assays was monitored by measuring the surface colour after the inoculation of the algae suspension (T0) and every week for the duration of the assay that means seven weeks for the first assay and five weeks for the other followed assays.

The device provides three parameters which are coordinates located in the CIELAB colour space (European committee for Standardisation, 2008). L* is lightness (0 = absolute black, 100 = absolute white), and a* and b* are the chromaticity coordinates located on the

equatorial plane of the colour sphere: a^* is the axis of green ($a^* < 0$) and red/magenta ($a^* > 0$); b^* is the axis perpendicular to a^* and it is the axis of blue ($b^* < 0$) and yellow ($b^* > 0$).

For colour analysis, the mean was calculated for each slab (assay 1) or each triplicate (for the other assays) and the CIELAB lightness and chroma differences were calculated: ΔL^* , Δa^* , Δb^* ; they are between the mean at every week during the test period and the starting of the assay (T0). Δa^* was chosen to monitor the stone greening during the biofouling assay and the global colour variation (ΔE^*_{ab}) was calculated before and after coating as follows (1) for the estimation of the coating impact on stone colour.

$$\Delta E^*_{ab} = \sqrt{\Delta L^{*2} + \Delta a^{*2} + \Delta b^{*2}} \quad (1)$$

2.6.2 Chlorophyll *a* fluorescence

The chl. *a* fluorescence is non-invasive technique used to detect damages occurring in photosynthetic organisms before visible damages caused by natural environmental stresses or initiated by biocides. It is widely employed in every fields of biology (Van Kooten and Snel, 1990; Maxwell and Johnson, 2000; Lazár et al., 2006), aquatic pollutants (Choi et al., 2012; Dewez et al., 2018) and in cultural heritage to monitor the effectiveness of biocides used to eradicate stone dwelling phototrophs (Tomaselli et al., 2002; Tretiach et al., 2010; Pfendler et al., 2018b).

a) Monitoring with Junior PAM fluorometer

A handheld photosynthesis yield analyser, Junior PAM Chlorophyll Fluorometer (Walz, Effeltrich, Germany) was coupled to WinControl-3 Software, the device was used with the pulse-amplitude modulated (PAM) in combination with saturating pulse analysis of fluorescence quenching. Ten measurements were performed over the whole sample surface (25 cm²), by means of a visible blue power LED (470 nm) for pulse modulated and saturating pulses. It is released with the fibre-optic probe of the fluorometer applied onto the surface. Samples were pre-conditioned half an hour in the dark, then the measurements were achieved in a room lighted by a green light which is not absorbed by plants. This environmental condition is required to measure the minimal (F_0) and maximal fluorescence (F_M) yields which were obtained with a saturating flash (1 s, 10 kHz). From these two parameters, the maximal quantum yield of Photosystem II, F_v/F_M , was calculated with the formula (2). It is a reliable indicator of the maximum photochemical quantum efficiency (Baruffo and Tretiach, 2007) and has been used to investigate the biocidal impact of the coatings on the photosynthesis activity thus the

physiological state of algae (Gladis et al., 2010; Manso et al., 2014; Dewez et al., 2018; Pfendler et al., 2018a; Pozo-Antonio and Sanmartín, 2018).

$$F_v/F_m = \frac{F_m - F_0}{F_m} \quad (2)$$

b) Monitoring with Imaging PAM fluorometer

Imaging PAM fluorometer (Walz, Effeltrich, Germany) was used at the end of the assay 4 in the aim to supplement Junior PAM which provided only F_v/F_m . Imaging-PAM was used to measure the kinetics of Chl. a fluorescence through the mapping heterogeneity in algal colonisation with the parameter Φ_{PSII} and the analysing fluorescence quenching, q_N and q_P outlined below, which provide information on plant adaptation to stress induced by biocides. The measuring system uses a fixed array of blue light-emitting diodes (LEDs) (peak wavelength = 470 nm) for saturating light pulses. The frequency of the pulses was adjusted to 10 Hz. Measurements were carried out at a distance of 11 cm between the camera and the slab's surface, corresponding to a 34×25 mm area. The image captured by the CCD camera was composed of 640×480 pixels. Slabs were previously conditioned in the dark for 30 min, the measured area was located on the central part of the slabs. The maximal fluorescence (F_m) yield was obtained with a saturating flash (1 s) as the device Junior PAM. The actinic light was then activated ($PAR = 25 \mu\text{mol photon.m}^{-2}.\text{s}^{-1}$, which was PAR released by fluorescence lights in the climate chamber) and finally a second saturating flash was triggered. Thereby the relative quantum yield of PSII (Φ_{PSII}) was calculated as $(F_m - F_s)/F_m$, where F_s and F_m are, respectively, steady-state fluorescence and maximum fluorescence in the light. Photochemical quenching (q_P), which represents the photochemical energy conversion of PSII reactions centres when Q_A the electron acceptor of PSII is oxidised, and non-photochemical quenching (q_N) which indicates the energy dissipation through heat, were calculated according to (Van Kooten and Snel, 1990).

2.6.3 Statistical analyses

For the analyses of the biocidal assays, Δa^* (colour parameter) and F_v/F_m (fluorescence parameter) were tested statistically using the non-parametric Mann and Whitney U test. Asterisk (*) indicates no statistically significant difference between control and coated slab measurements ($n=10$ in assay 1 and $n=30$ in assays 2, 3 and 4) at the 0.05 probability level.

3 Results and discussion

3.1 Evaluation of the colour change after application of the coatings

All biocides were tested as preventive treatments. Since they are applied as permanent coatings on the stones, they must have a minimum visual impact on the stone colour (Sasse and Snethlage, 1996). Here ΔE^*_{ab} of the dry chalk without coating was 1.5 ± 0.9 (CIELAB units) which displayed a natural colour variation (Fig. 3a). It was compared to ΔE^*_{ab} calculated from coated stones before and after every coating. For Assay 1 and 2, for which products were brushed on dry stones, ΔE^*_{ab} was equal to 2.6 and 2.9 for 0.2 g and 0.4 g of POM-IL1, respectively. Such low colour variation is below the generally established ΔE limit value ($\Delta E^*_{ab} \leq 3$ (Moreau et al., 2008; Burgos-Cara et al., 2017) and could not be detected with the naked eye. Stones coated with POM-IL2 had a lower colour variation, with $\Delta E^*_{ab} = 0.9$ and 1.4 for 0.2 g and 0.4 g, respectively. Preventol RI80 possessed the lowest colour variation, with $\Delta E^*_{ab} = 0.6$ for both quantities of liquid product. All ΔE^*_{ab} data are given in CIELAB units.

The coating applied on water-saturated stones (Assays 3 and 4) has led to higher colour variations. The colour variation produced by the POM-IL1 coating (ΔE^*_{ab} of 2.8, 2.7 and 2.3 at 0.1 g, 0.2 g and 0.4 g, respectively) was similar to the colour variation of the natural uncoated stones, with a ΔE^*_{ab} of 2.9 ± 0.7 . The POM-IL2 coating displayed less colour variation, with ΔE^*_{ab} of 2.0, 1.9 and 2.6 at 0.1 g, 0.2 g and 0.4 g, respectively. On the other hand, the Preventol RI80 applied to wet stone led to the highest colour variation, with a ΔE^*_{ab} of 3.2 and 3.3 at 0.2 g and 0.4 g, respectively. Therefore, the colour variation depends on the humidity of the stone when the coating is applied, with POM-IL1 producing the greatest colour variation when applied on dry stones (Assays 1 and 2), followed by the POM-IL2 and the PR80. When applied on wet stones (Assays 3 and 4), PR80 is the product that shows higher colour variation, followed by POM-IL1 and POM-IL2. Crucially, the colour variation, $\Delta E^*_{ab} < 3$, confirms a low visual impact for all coatings, regardless the quantity and the condition of application.

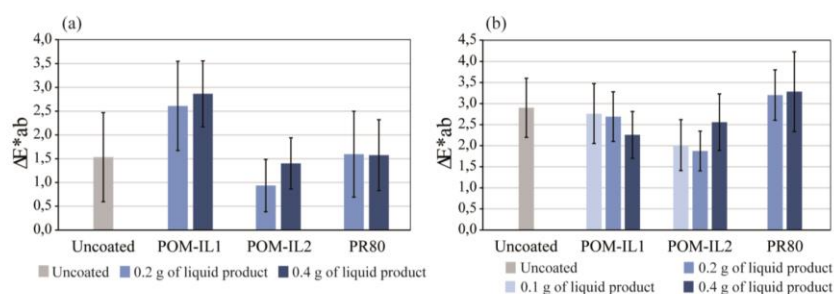


Figure 3. Global colour variation (ΔE^*_{ab}) of natural uncoated stone compared with stones coated by POM-IL1, POM-IL2, and Preventol RI80 in dry (a) and wet conditions (b).

3.2 Biocidal performance

3.2.1. Evaluation of biocidal coatings on dry stone over a seven-week period (Assay 1)

In this seven-week assay, the biocidal activity of POM-IL1, POM-IL2 and Preventol RI80 were evaluated against two algal strains isolated from the Pommery bas reliefs, *Pseudostichococcus monallantoides* and *Chromochloris zofingiensis*. Briefly, one control chalk slab (i.e. uncoated stone) was compared with slabs coated with POM-IL1, POM-IL2 or Preventol RI80, by inoculating each slab with *Chromochloris* sp. or *Pseudostichococcus* sp. (Fig. 4).

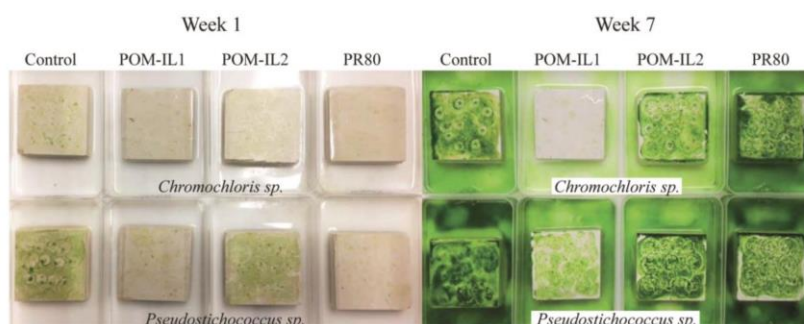


Figure 4. Photos of inoculated controls and coated chalk slabs with *Chromochloris* sp. (upper slabs) and *Pseudostichococcus* sp. (lower slabs) at week 1 and week 7 of incubation.

After one week of incubation, the comparison of control stones colonised by algae displayed a net variation of growth between both algae (Fig. 5 a-b). The Δa^* was -14.0 with *Pseudostichococcus* sp. whereas it was -3.3 with *Chromochloris* sp. The negative values showed a greening of stones for both algae because at the beginning of the incubation, all a^* were between 0 and 0.3 for slabs inoculated with *Pseudostichococcus* sp. and between 0.4 and 0.6 for slabs inoculated with *Chromochloris* sp. At the same time of the assay, the strong negative values with *Pseudostichococcus* sp. indicated higher so quicker growth than with *Chromochloris* sp. For *Pseudostichococcus* sp. growth, Δa^* had decreased to -20.2 by week 2 and remained low until week 7, -21.1. The *Chromochloris* sp. growth decreased progressively until reaching a value of -17.6 at week 5 and -14.6 at the end of the essay on week 7. Thus, the stones colonised by *Chromochloris* sp. were less green than by *Pseudostichococcus* sp. which supposed a slower growth with *Chromochloris* sp.

Nonetheless, the fluorescence parameter, F_v/F_m started at 0.28 with *Pseudostichococcus* sp. and 0.47 with *Chromochloris* sp. (Fig. 5c). Despite inoculating the slabs with the same

number of cells, *Chromochloris* sp. had a higher maximum photochemical quantum yield than *Pseudostichococcus* sp. and thus a higher photosynthetic activity. Moreover, the maximum F_v/F_m value of 0.61 for *Chromochloris* sp. was reached at week 1, which was in accordance with results obtained with *Chlorella vulgaris* where the maximum value of F_v/F_m was reached at week 1 with 0.70 (Eyssautier et al. 2015). The maximum F_v/F_m value of 0.62 for *Pseudostichococcus* sp. was measured at week 2 (Fig. 5d), which was later than the maximum of F_v/F_m for *Chlorella vulgaris*. The maximum of fluorescence of *Chromochloris* sp. seemed closer to *Chlorella vulgaris* than that of *Pseudostichococcus* sp. This result could be surprising since *Pseudostichococcus* sp. belongs to Trebouxiophyceae class like *Chlorella vulgaris* and *Chromochloris* sp. has a more distant taxonomy. Moreover, data from the two algae seemed similar to results obtained with *Dunaliella tertiolecta* where F_v/F_m was 0.6-0.7 but only after 5 days (Young and Beardall, 2003).

Pseudostichococcus sp. was slower than *Chromochloris* sp. at reaching a similar maximum photochemical efficiency despite showing a faster greening of slabs. After the maximum photochemical efficiency was achieved, F_v/F_m decreased gradually for both algae until reaching values of 0.39 for *Chromochloris* sp. and 0.44 for *Pseudostichococcus* sp. at the end of the assay. The decrease of PSII activity could be explained by the ageing of the algae with steady senescence of the first algae (Eyssautier-Chuine et al., 2015).

Accordingly, despite *Chromochloris* sp. having a maximum quantum yield higher and quicker than *Pseudostichococcus* sp. at the start of the assay, the greening of stones had been earlier and more intense with the *Pseudostichococcus* sp. algae, which is commensurate with a more rapid proliferation.

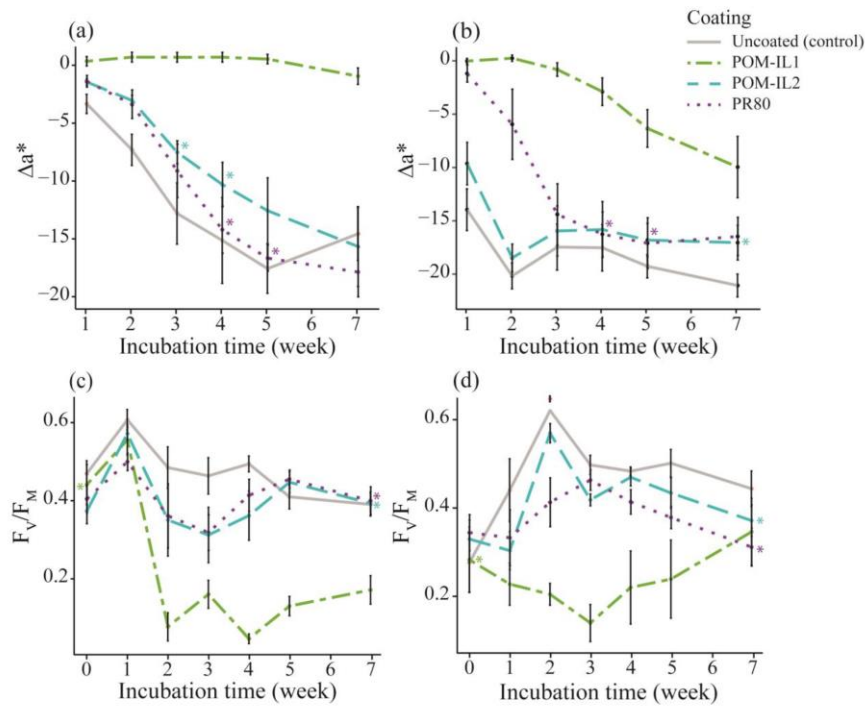


Figure 5. Greening monitored by the colour variation Δa^* and chlorophyll fluorescence F_v/F_m monitored on controls and coated stones inoculated by *Chromochloris* sp. (a-c) and *Pseudostichococcus* sp. (b-d) during 7 weeks of incubation. * indicates no statistically significant difference between control and coated slab measurements (n=10).

The two different POM-IL coatings displayed different impacts on algae. The Δa^* for was between 0.35 and -0.94 and displayed nearly no greening of slabs by *Chromochloris* sp. during the whole assay. The photosynthetic activity of algae increased only at week 1 with F_v/F_m at 0.58 then it fell strongly and remained low until the end of the assay. Therefore, POM-IL1 had a strong biocidal impact on the *Chromochloris* sp. growth. With *Pseudostichococcus* sp., Δa^* was close to 0 until week 2 whereupon it decreased to -0.82 (at week 3), suggesting greening, which decreased until Δa^* equalled -9.96 at week 7. F_v/F_m started at 0.28 and decreased gradually until reaching 0.14 at week 3 which suggested a weaker photosynthetic activity and thus inhibition of algal growth. Nonetheless, from week 4, F_v/F_m increased from 0.22 to 0.35, indicating a resumption of the algal proliferation. Thus POM-IL1 was efficient during the first three weeks, it seemed less efficient against *Pseudostichococcus* sp. than against

Chromochloris sp. nonetheless the results might have been similar if *Chromochloris* sp. grew faster than *Pseudostichococcus* sp.

Results of the colonisation of *Chromochloris* sp. on POM-IL2 coated stones showed how Δa^* was negative at week 1 (-1.45) suggesting an early greening of stones which decreased until Δa^* was equal to -15.66 at week 7. Meanwhile, F_v/F_m started at 0.38 and increased at 0.57 after just one week of incubation, the rise of the maximum photochemical quantum yield showed a strong photosynthetic activity and a net growth of algae. Nonetheless F_v/F_m decreased at weeks 2 and 3 (0.35 and 0.31, respectively) indicating an inhibition of microorganisms by POM-IL2 but this decline was also observed for controls. Moreover, F_v/F_m increased from week 4 to 7 and was found to be 0.40, the same as the control slabs. Thus POM-IL2 had a short effect on the photosynthesis of *Chromochloris* sp. The colour variation Δa^* monitored on stones inoculated with *Pseudostichococcus* sp. showed a similar trend to the controls and the chalk slabs were green already at week 1 (-9.64), decreased rapidly to -18.47 at week 2 and remained weak until the end of the test. This fast greening was highlighted by a rise of the maximum photochemical quantum yield at week 2 with F_v/F_m at 0.57. These values then decreased to between 0.35 and 0.40 over the remainder of the test period, indicating that POM-IL2 did not disturb the photosynthetic activity of *Pseudostichococcus* sp.

The biocidal effect of Preventol RI80 on chalk slabs inoculated with *Chromochloris* sp. was poor. Greening began at week 1 with a Δa^* at -1.38 and continued to decrease over the test period and was measured to be -17.87 at week 7, thus the greening was as intense as that of controls. The photosynthetic activity of *Chromochloris* sp. followed a similar trend to POM-IL2 coated stones, F_v/F_m reached a maximum of 0.50 at week 1 like all incubated stones, controls and coated stones, then it decreased at weeks 2 and 3 to 0.36 and 0.32, respectively. The short-lived antiproliferative effect of Preventol RI80 during these two weeks did not last since values became as high as POM-IL2 and controls by week 7. However, the effect of Preventol RI80 on the *Pseudostichococcus* sp. growth was different to POM-IL2. Δa^* was weakly negative (-1.20) that supposed a weak greening whereas with POM-IL2 it was already at -9.64 thus the slabs were greener. At weeks 2 and 3, Δa^* decreased at -5.95 and -14.40 that displayed a greening of slabs but it remained weaker than POM-IL2 slabs at the time. Then it still decreased to the end of the assay with -16.47 at week 7 which was similar to POM-IL2 results. The maximum photochemical quantum yield, F_v/F_m , was weak and constant at 0.33 the first week. This stagnation of photosynthetic activity suggested a lack of algal growth and a biocidal action of Preventol RI80 but it did not last since F_v/F_m increased up to 0.46 which was a maximum at week 3 and showed a resumption of the algae development. Preventol RI80 had

a better biocidal effect than POM-IL2 but not enough to avoid the greening of stones which were as green as POM-IL2 stones from week 4 to 7.

Consequently, POM-IL1 had an efficient biocidal impact on both species of algae over the seven-week test period; unlike POM-IL2 and Preventol RI80 which had a shorter biocidal effect on both algae. These results indicated that the biocidal effect could be improved by increasing the amount of product applied. Therefore, the second assay aimed to determine an optimal amount of POM-IL1 and improve the biocidal effect of POM-IL2 and Preventol RI80.

3.2.2. Optimising the biocidal effect of the coatings (Assay 2)

Pseudostichococcus sp. was the only algae used for the assay 2 due to its faster growth on chalk slabs, compared with that of *Chromochloris* sp.. With the aim of optimising the biocidal effect of all coatings, the amount of biocide treatment was increased to 0.4 g of liquid solution on triplicates used for each coating and control. Slabs were incubated in a climatic chamber for five weeks (Fig. 6).

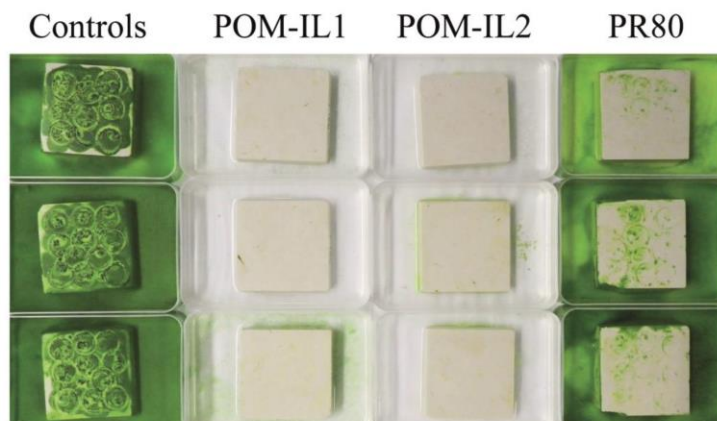


Figure 6. Photos of inoculated triplicates of controls and coated slabs with *Pseudostichococcus* sp. at week 5 of incubation.

After the inoculation, results of colour displayed a weak positive a^* which was at 0.5 for controls, 0.6 for POM-IL1 slabs and 0.5 for POM-IL2 and PR80 slabs. After one week of incubation, the calculation of Δa^* showed a net greening of control slabs which started with a Δa^* at -2.1 then a strong negative Δa^* (-15.7) at week 2 showed the definitive settlement of algae (Fig. 7a). This was corroborated by the maximum photosynthetic activity, F_v/F_m , that

highly increased during the two first weeks (Fig. 7b). Thereafter, as greening intensified, Δa^* continued to decrease until reaching a value of -19.1 after five weeks. On the other hand, POM-IL1 and POM-IL2 showed constant Δa^* close to 0 throughout the duration of the five-week assay, indicating no greening of coated slabs. Moreover, F_v/F_m , started at 0.15 and 0.12 respectively for POM-IL1 and POM-IL2; it decreased from week 1 at 0.06 and 0.05 and remained close to 0 to the end of the assay which revealed the strong inhibition of the photosynthetic activity of algae by both coatings. For slabs treated with Preventol RI80, the colour variation Δa^* was measured to be between 0.2 and 0.4 indicating no greening. The photosynthetic activity monitored by F_v/F_m decreased progressively from 0.14 at the starting of the assay to 0.02 at week 3 which revealed an inhibition of the photosystem II in the photosynthetic chain. Nonetheless, F_v/F_m increased during weeks four and five and Δa^* was negative, indicating a resumption of algae growth. The biocidal effect of Preventol RI80 was effective for only three weeks, despite the good anti-biocolonisation preventive results of benzalkonium chloride for a longer time as two months in an accelerated growing assay with a mixing of green algae and cyanobacteria (Barriuso et al., 2017). Moreover, Preventol RI80 was efficient on cultural heritage to remove fungi and bacteria (Urzi et al., 2016; Favero-Longo et al., 2018; Li et al., 2020; Rugnini et al., 2020) as well as algae and lichens (Nugari et al., 2009; De los Ríos et al., 2012; Pfendler et al., 2018b). Furthermore, many studies have demonstrated antimicrobial activity for a curative action in a short time in most of case and in a longer time when lichen was previously soaked for 1 hour in Preventol RI80 (Coutinho et al., 2016; Vannini et al., 2018). A long-term efficiency of this biocide probably needs a more significant amount whereas POM-ILs performed with a lower amount. Nonetheless, the performance of any biocide can vary significantly as a function of the concentration and amount of product that is applied, which furthermore depends on the absorption of this product by the surface substrate material.

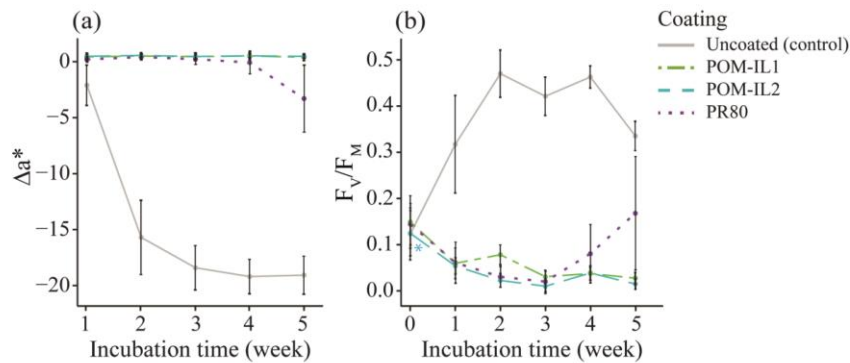


Figure 7. *Pseudostichococcus* sp. growth on control and coated slabs over five weeks monitored by the colour variations with Δa^* (a) and the chlorophyll fluorescence F_v/F_m (b). * indicates no statistically significant difference between control and coated slab measurements (n=30).

3.2.3. Application of the coatings to wet stone (Assay 3)

The aim of this assay was to evaluate the application of the biocides on wet stone, which replicates the more drastic natural environmental conditions of the Pommery cellar. Such conditions can limit the performance of the biocidal coatings due to a number of factors, including poor substrate penetration and polymerisation. In this assay, the chalk slabs were inoculated by *Pseudostichococcus* sp. in the same conditions as assay 2 (Fig. 8).

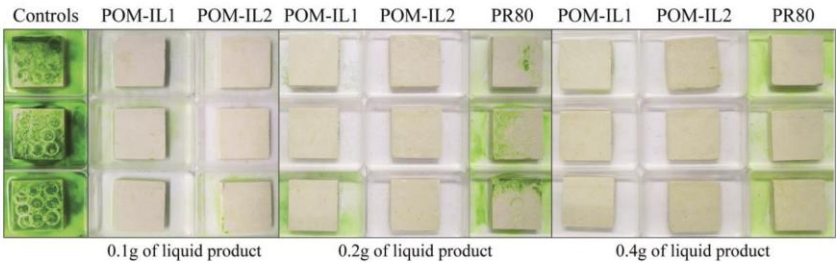


Figure 8. Photos of inoculated triplicates of controls and coated slabs 5 weeks after inoculation with *Pseudostichococcus* sp.

After the inoculation of algae, a^* was between 0.2 to 0.8 and the calculation of Δa^* for the control slabs showed significant greening after five-week incubation period, where Δa^* changed from -7.0 to -19.2. For the highest amount of coating (0.4 g), Δa^* remained close to 0 over the test time for every coating and the photosynthetic activity F_v/F_m of *Pseudostichococcus* sp.

remained low (between 0.02 and 0.14) demonstrating good biocidal activity for every coating (Fig. 9a-b).

With 0.2 g of product on slabs, POM-IL1 and POM-IL2 Δa^* were also close to 0, therefore no greening appeared during the assay. In addition, F_v/F_m remained low between 0.04 and 0.19 which displayed a weak photosynthetic activity of algae and no real growth (Fig. 9c-d). For slabs coated with Preventol RI80, Δa^* was positive and close to 0 like the other coated slabs but at week 4, it was negative (-0.8) and still decreased at -2.7 at the last week which meant the greening settled on slabs (Fig. 9c). Meanwhile, F_v/F_m remained low for all coated slab, however, at week 5, the Preventol RI80-coated slabs increased to 0.20 suggesting a resumption of photosynthetic activity; whereas F_v/F_m remained weak for POM-IL-coated slabs (0.06). All coatings had a net biocidal effect compared to controls, but the greening developed with Preventol RI80 at the end of the assay, showing less biocidal effect of this compound in comparison with the POM-ILs coatings (Fig. 9d).

The monitoring of the colonisation of slabs coated with 0.1 g of POM-IL1 and POM-IL2 displayed a lack of greening through Δa^* which remained close to 0, from 0.7 to 0.5 for POM-IL1 slabs and from 0.4 to 0.3 for POM-IL2 (Fig. 9e). This result was confirmed with a weak maximal photochemical efficiency of the PSII for all the duration of the assay, between 0.05 and 0.18 for POM-IL1 slabs and between 0.04 and 0.14 for POM-IL2 (Fig. 9f). Thereby, the low chlorophyll fluorescence of algae revealed the inhibition of the PSII in the photosynthetic chain by biocides that led to a lack of the algal growth over the five weeks of the assay.

Consequently, both POM-IL1 and POM-IL2 had a net biocidal impact on algae even under drastic application conditions as water saturated stones which avoided the penetration in the porosity and limited the amount of product to be applied. It is worth noting that the application of 0.2 g and 0.4 g of liquid POM-ILs only on the surface has indeed generated a thicker coating which did not change the stone colour but it was visually detectable by a glossy aspect. Therefore, the lower amount of POM-ILs at 0.1 g is preferable since it has not been detected by naked eye and it kept a good biocidal performance.

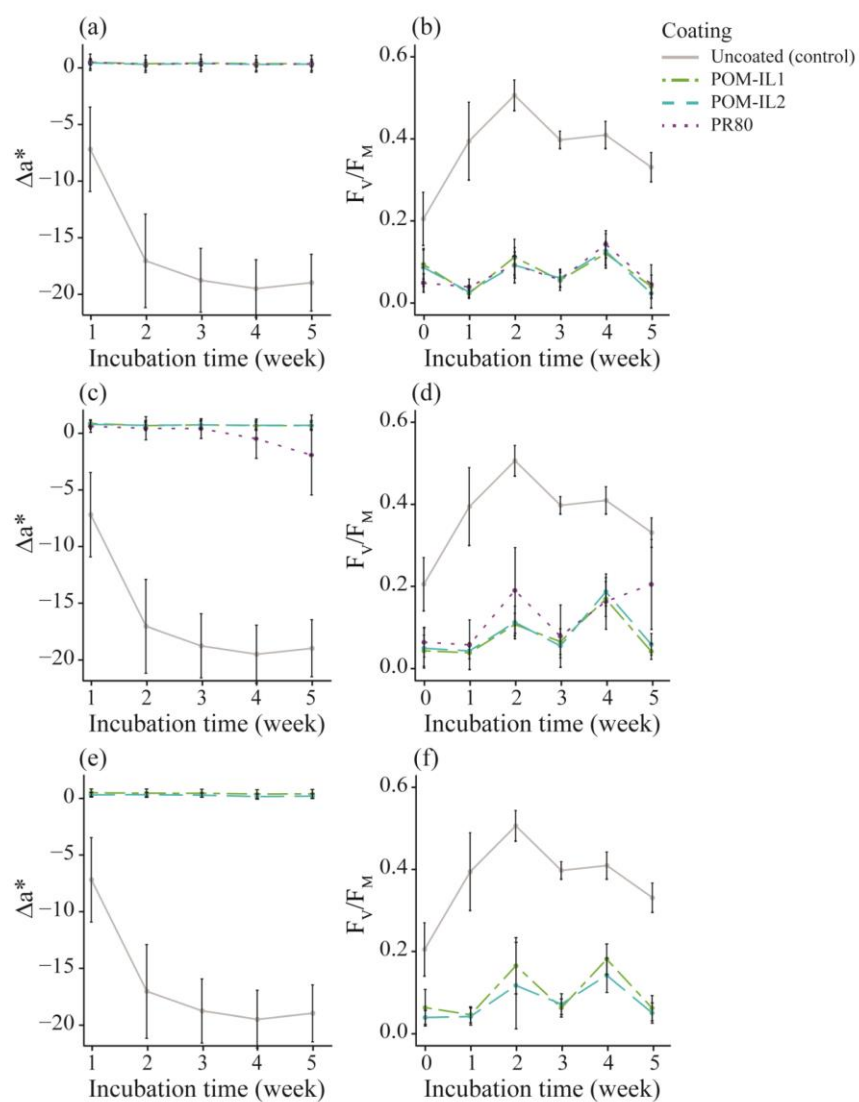


Figure 9. *Pseudostichococcus* sp. growth during the five-week assay monitored by the colour variation Δa^* and the chlorophyll fluorescence F_v/F_m on wet stones brushed with 0.4 g (a-b), 0.2 g (c-d) and 0.1 g of liquid products (e-f).

3.2.4. Re-inoculation of coated slabs with algae and cyanobacteria (Assay 4)

The aim of the final assay was to simulate natural environmental conditions by reusing coated slabs which gave a good biocidal performance in a previous assay and seeding them with a second inoculation of algae and cyanobacteria (Fig. 10).

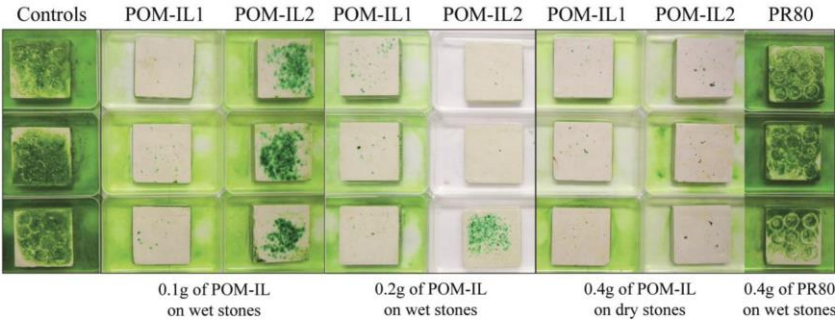


Figure 10. Photos of inoculated triplicates of controls and coated slabs 5 weeks after inoculation with two algae (*Pseudostichococcus* sp. and *Diplosphaera* sp.) and a cyanobacteria (*Timaviella* sp.).

For this last assay, Chl. *a* fluorescence was monitored every week with Junior PAM to calculate F_v/F_m then, at the end of the assay, Imaging-PAM was used for mapping heterogeneity in algal colonisation with the parameter Φ_{PSII} and for analysing fluorescence quenching, q_N and q_P , as previously described. The fluorescence mapping highlighted a gap between the fluorescence signal which did not match with the biological growth (Fig. 11). This result was induced by a gap analysis of the cyanobacterial fluorescence. The pulse-modulated excitation LED lamps from Imaging-PAM with a peak emission at 470 nm was only adapted to the main fluorescence from chlorophyll pigments in land plants and algae. Those pigments mostly absorb blue light (around 400 and 480 nm) and red light (around 650-700 nm) whereas in cyanobacteria, the principal light-harvesting complexes are phycobilisomes which absorb mainly yellow/orange light (around 500-680 nm) (Schreiber et al., 1995; Campbell et al., 1998; Ogawa et al., 2017). In consequence, Chlorophyll fluorescence analysis did not display the fluorescence emitted by the cyanobacteria growth but only the fluorescence from algae.

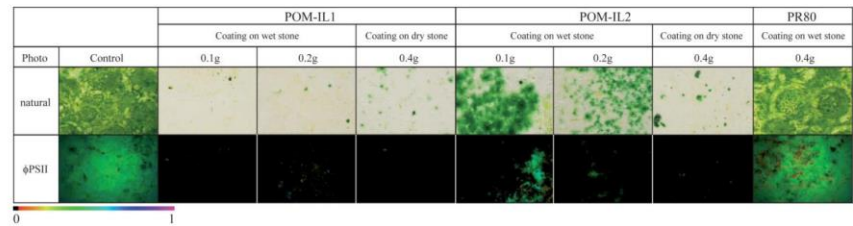


Figure 11. Natural and Chl. fluorescence (ϕ_{PSII}) imaging of one stone at 5 weeks of inoculation for control and coated stones.

As a result, a^* measured after the inoculation was weakly positive, between 0.3 and 0.6. The monitoring of the controls displayed a greening through Δa^* started the first week with -4.8, but this decreased drastically to -18.5 at week 2 and there was a strong greening which remained visible until the end of the assay (Fig. 12a). Photosynthetic activity of algae was monitored on controls as a regular algal growth on stones, through the chl. fluorescence every week with F_v/F_m . It started at 0.14 and reached a maximum value of 0.58 at week 3 (Fig. 12b). The calculation of the other parameters from the mapping of the fluorescence at week 5, showed the effective quantum yield, Φ_{PSII} , was 0.44 and similar for the three slabs considering a very minor standard deviation (0.01). q_P was 0.84 which was high and reflected a high electron flow away from PSII for the photochemistry and the reaction centre opening whereas q_N is weaker (0.39) which displayed a thermal dissipation of excess energy (Fig. 13b).

On PR80-treated slabs, the colour variation was very similar to controls with the decrease of Δa^* over time (from -3.89 to -16.15), thus the algal growth has not been avoided by the biocide. Moreover, F_v/F_m increased progressively from 0.17 at week 0 to 0.56 at week 5 which displayed a photosynthetic activity as effective as that of controls but the effective quantum yield (Φ_{PSII}) was 0.34, so weaker than controls (0.44) which further confirmed the ineffectiveness of PR80 on the algal growth (Fig. 13a). Moreover, the increase of q_N at 0.87 showed heat dissipation which reflected a stress induced by the biocidal effect.

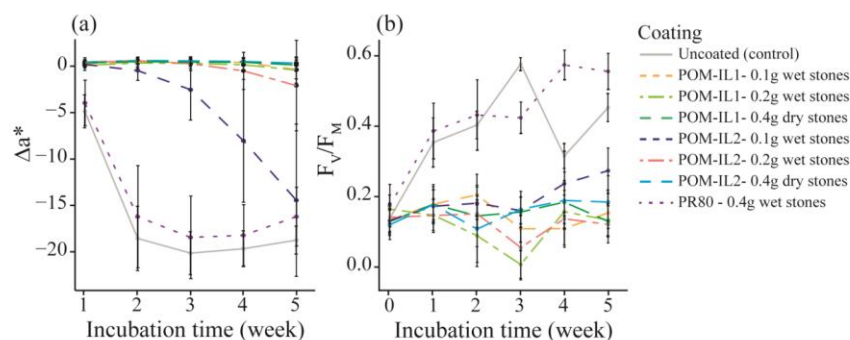


Figure 12. Algal and cyanobacterial growth monitored during 5 assay weeks on treated stones and controls through the colour variations with Δa^* (a) and F_v/F_m measured the chlorophyll fluorescence of the algal growth (b).

On POM-IL1 treated stones, the colour variation remained close to 0 for the three batches, which suggested no greening during the assay. A slight decrease was detected at week 5 for POM-IL1 at 0.1 g and at 0.2 g where Δa^* were respectively -0.30 and -0.35, compared to POM-IL1 at 0.4 g which remained stable. The chl. fluorescence showed that F_v/F_m for POM-IL1 throughout the duration of the assay was between 0.01 to 0.18, which was very low compared to the control samples. In consequence, POM-IL1 had a real long-term biocidal effect despite the wet condition of application on stones. In detail, Φ_{PSII} images were black because the detection of the fluorescence was very weak, 0.08, 0.17 and 0.07 respectively for 0.1 g, 0.2 g and 0.4 g, considering few algae remained alive. Nonetheless, q_p was substantial with 0.67 for 0.1 g and 0.2 g POM-IL1 and 0.50 for 0.4 g which indicated a photosynthetic activity with the electron transfer and the opening of the PSII centres, but the high deviation standards suggested a big heterogeneity of the fluorescence signal from triplicates. In addition, the thermal dissipation, q_N was 0.33 for 0.4 g POM-IL1 and showed that the increase of POM-IL1 on stones generated some form of oxidative stress on the algae cells.

Results of the colonisation of slabs treated with POM-IL2 were more moderate. With a quantity of 0.1 g of product on slab, Δa^* started positive with 0.26 at week 1 then it was negative from week 2 with -0.41 and decreased week-on-week thereafter until -14.38 at week 5. Thus, stones were progressively green and biocolonised by both algae and cyanobacteria. With a quantity of 0.2 g of product on slab, Δa^* was positive from week 1 to week 3 then it started to decrease and to be negative at week 4 with -0.44 and at week 5 with -2.03. With 0.2 g of product, there was a delay of greening, POM-IL2 had a better efficiency. For the last batch with 0.4 g of

product, Δa^* remained positive from 0.42 to 0.19 during the whole duration of the assay thus no greening was detected on stones. POM-IL2 with 0.4 g applied on dry stones was more efficient than a weaker amount of product applied on wet stones. The chl. fluorescence monitored with F_v/F_m every week, remained weak for all batches but for slabs with 0.1 g of POM-IL2, it increased slightly at week 4 and 5 with 0.24 and 0.27. Indeed, Φ_{PSII} images displayed a fluorescence signal which was lower than could suggest the real biological growth since it did not record cyanobacteria fluorescence, but it indicated a definite development of algae with a Φ_{PSII} of 0.20 but that remained lower than controls. The biocidal impact of POM-IL2 at 0.1 g has not been optimum but it led to a delay of the greening and a different biological growth where cyanobacteria rather developed than algae which were dominant on controls. Thus, rather the biocide seemed to act on algae than on cyanobacteria. Moreover, q_N was higher than control q_N ; this increase of the heat dissipation by algae suggested a stress generated by the biocide. In addition, q_P was lower than controls which indicated a decrease of PSII primary photochemistry and of electron transport activity (Fig. 13c). At week 5, the effective quantum yield, Φ_{PSII} was of 0.20 with 0.1 g, 0.12 with 0.2 g and 0.07 with 0.4 g, thus it progressively decreased with the amount of POM-IL2 applied on stones despite the heterogeneity of values. This result supposed a stronger biocidal effect with the increasing of the dose. In consequence, despite POM-IL2 at 0.4 g applied on wet stones has not been tested a second time in assay 4, the result suggested that at 0.4 g of biocide on slabs, the impact of POM-IL2 on the photosynthesis could have been more significant than at 0.2 g.

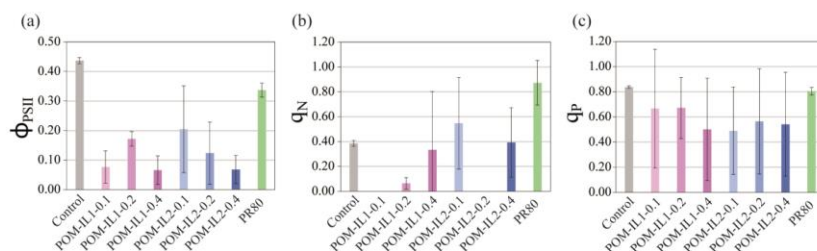


Figure 13. Histogram plots of mean and standard deviation of Φ_{PSII} (a), q_N (b) and q_P (c) as chl. fluorescence parameters measured at 5 weeks after inoculation in controls and stones coated with 0.1 g and 0.2 g of product in wet condition and 0.4 g in dry condition ($n=3$).

Finally, POM-IL1 and 2 were found to be more efficient than Preventol RI80 at avoiding a second biocolonisation of chalk stones by *Pseudostichococcus* sp., *Diplosphaera* sp. and *Timaviella* sp.. POM-IL1 possessed an optimal biocidal effect at 0.1, 0.2 and 0.4 g applied on

dry and wet stones, and it proved its long-lasting efficiency in assay 4. POM-IL2 provided a poorer performance since its efficiency was optimal with 0.4 g of product on dry stones, but it failed for the second seeding with lower amount applied on wet stones. Thus, POM-IL1 outperformed POM-IL2 in more drastic experimental conditions.

Such results on POM-ILs are promising to eliminate lampenflora on bas-reliefs, nonetheless the recent environment of the Pommery Champagne cellar can be improved to prevent the biocolonisation. Artificial lighting promotes the growth of photosynthetic biofilms by the intensity, wavelength and temperature it generates (Mulec et al., 2008; Havlena et al., 2021), it is the only parameter which can be improved in the context of Pommery Champagne cellar. The illumination equipment has changed for the two last decades and the gradual installation firstly aimed to highlight bas-reliefs by incandescent then halogen lamps. Recently the number of spots decreased and light emitted diode (LED) are lit temporarily to limit the amount of energy and the temperature increasing (D'Agostino et al., 2015). Nevertheless, contemporary art works are still exposed in the halls where bas-reliefs have been curved and need lights to be highlighted with tourists, some of them are even luminous and provide a weak but constant lighting to lampenflora which adapts to a weak light emission. Indeed, cyanobacteria and some eukaryotic algae have phycobiliproteins as pigments in addition of chlorophyll, which expand the absorption spectrum of primary pigments and enable phototrophic microorganisms survival even at low light intensities (Chaneva et al., 2007; Mulec et al., 2008; Baquedano Estévez et al., 2019). Consequently, the reduction of light intensity is not enough for a preventive strategy to limit lampenflora growth. Effort must be spent on the selection of lights whose wavelengths are less favourable for cyanobacteria like a band around 500 nm and above 700 nm (Bruno and Valle, 2017) and for overall photosynthetic organisms like 560 nm (Baquedano Estévez et al., 2019). Nonetheless, controlling the development of photosynthetic biofilms by using a spectral light emission the less adapted to the photonic assimilation performance of microorganisms was studied for the Nerja cave by both empirical and theoretical methodologies to select LED lighting systems limiting photosynthesis but the variation of results between those methodologies and the in-situ data highlighted the complexity to find an adapted lighting system due to the presence of various biofilms made of a diversity of photosynthetic microorganisms with different pigmentary compositions and able to adjust the pigment content to a short shift in the light emission (Muñoz-Fernández et al., 2021).

4. Conclusions

The unique underground environment of the Pommery Champagne cellar leads to extended lampenflora biofilm growth on the UNESCO listed bas-reliefs carved in chalk in the cellar walls. These conditions are representative of a habitual problem in biodeterioration, where periodic cleaning is required to mitigate against poorly performing commercial biocides. Our results show that preventative biocidal treatments based on polyoxometalate-ionic liquids (POM-ILs) were more effective than commercial Preventol RI80 against algal strains isolated from the bas reliefs. One variant (POM-IL1) was capable of sustained prevention of biofilm growth when applied to wet chalk. It is important to note that while the microorganisms used in this study are representative microflora that were isolated from the bas-reliefs, our ongoing work is currently focussed on an in-depth evaluation of the microflora responses to these biocidal treatments applied *in situ* on the walls of the Pommery champagne cellar. Our current hypothesis is that the most effective strategy will involve combining this chemical biocide approach with UV-C irradiation as a multi-mode strategy to prevent biocolonisation.

5. Acknowledgements

This research was supported by the Ministerio de Ciencia Innovación y Universidades (Spain) Proyecto I+D+i, PID2019-109333RB-I00 (S.G.M), Gobierno de Aragón and Programa Operativo Aragón de Fondo Social Europeo 2014-2020 (I.F.C.) and Vranken-Pommery Monopole. The authors acknowledge Rachel Ouviaha De Oliveira and Clément Pierlot of Pommery Champagne cellar for access and support. S.G.M. and S.E.C. would like to acknowledge the University of Reims Champagne-Ardenne for visiting professorships.

6. References

- Albertano, P., 2012. Cyanobacterial biofilms in monuments and caves, in: Ecology of Cyanobacteria II. Springer, pp. 317–343.
- Albertano, P., Urzì, C., 1999. Structural Interactions among Epilithic Cyanobacteria and Heterotrophic Microorganisms in Roman Hypogea. *Microb Ecol* 38, 244–252. <https://doi.org/10.1007/s002489900174>
- Ascaso, C., Wierzbos, J., Souza-Egipsy, V., de los Ríos, A., Rodrigues, J.D., 2002. In situ evaluation of the biodeteriorating action of microorganisms and the effects of biocides on carbonate rock of the Jeronimos Monastery (Lisbon). *International Biodeterioration & Biodegradation* 49, 1–12. [https://doi.org/10.1016/S0964-8305\(01\)00097-X](https://doi.org/10.1016/S0964-8305(01)00097-X)
- Ballesteros, D., Painchault, A., Nehme, C., Todisco, D., Varano, M., Mouralis, D., 2021. Normand chalkstone (France): geology and historical uses from quarries to monuments. *Episodes-Journal of International Geoscience* 44, 31–42.
- Baquedano Estévez, C., Merino, L.M., Román, A. de la L., Valsero, J.D., 2019. The lampenflora in show caves and its treatment: an emerging ecological problem.

- International Journal of Speleology 48 (3), 4. <https://doi.org/10.5038/1827-806X.48.3.2263>
- Barriuso, B.C., Botticelli, G., Cuzman, O.A., Osticioli, I., Tiano, P., Matteini, M., 2017. Conservation of calcareous stone monuments: Screening different diammonium phosphate based formulations for countering phototrophic colonization. *Journal of Cultural Heritage* 27, 97–106. <https://doi.org/10.1016/j.culher.2017.03.002>
- Baruffo, L., Tretiach, M., 2007. Seasonal variations of F o, F m, and F v/F m in an epiphytic population of the lichen *Punctelia subrudecta* (Nyl.) Krog. *The Lichenologist* 39, 555–565.
- Bastian, F., Alabouvette, C., 2009. Lights and shadows on the conservation of a rock art cave: the case of Lascaux Cave. *International Journal of Speleology* 38, 55–60.
- Bastian, F., Jurado, V., Nováková, A., Alabouvette, C., Sáiz-Jiménez, C., 2010. The microbiology of Lascaux cave. *Microbiology* 156, 644–652.
- Blazquez, A.B., Lorenzo, J., Flores, M., Gomez-Alarcon, G., 2000. Evaluation of the effect of some biocides against organisms isolated from historic monuments. *Aerobiologia* 16, 423–428.
- Borderie, F., Alaoui-Sehmer, L., Boust, F., Alaoui-Sossé, B., Aleya, L., 2014. Cellular and molecular damage caused by high UV-C irradiation of the cave-harvested green alga *Chlorella minutissima*: Implications for cave management. *International Biodeterioration & Biodegradation* 93, 118–130. <https://doi.org/10.1016/j.ibiod.2014.05.014>
- Bruno, L., Rugnini, L., Spizzichino, V., Caneve, L., Canini, A., Ellwood, N.T.W., 2019. Biodeterioration of Roman hypogea: the case study of the Catacombs of SS. Marcellino and Pietro (Rome, Italy). *Annals of Microbiology* 69, 1023–1032.
- Bruno, L., Valle, V., 2017. Effect of white and monochromatic lights on cyanobacteria and biofilms from Roman Catacombs. *International Biodeterioration & Biodegradation* 123, 286–295. <https://doi.org/10.1016/j.ibiod.2017.07.013>
- Burgos-Cara, A., Ruiz-Agudo, E., Rodriguez-Navarro, C., 2017. Effectiveness of oxalic acid treatments for the protection of marble surfaces. *Materials & Design* 115, 82–92. <https://doi.org/10.1016/j.matdes.2016.11.037>
- Caneva, G., Isola, D., Lee, H.J., Chung, Y.J., 2020. Biological risk for hypogea: Shared data from Etruscan tombs in Italy and ancient tombs of the Baekje dynasty in Republic of Korea. *Applied Sciences* 10, 6104.
- Chaneva, G., Furnadzhieva, S., Minkova, K., Lukavsky, J., 2007. Effect of light and temperature on the cyanobacterium *Arthonema africanum*-a prospective phycobiliprotein-producing strain. *Journal of Applied Phycology* 19, 537–544.
- Charola, A.E., McNamara, C., Koestler, R.J., 2011. Biocolonization of Stone: Control and Preventive Methods: Proceedings from the MCI Workshop Series. Smithsonian. *Contrib. Mus. Conserv.*, Washington D.C., pp. 1–115. <http://dx.doi.org/10.5479/si.19492359.2.1>
- Choi, C.J., Lowe, J.A., Young, E.B., 2012. Rapid effects of diverse toxic water pollutants on chlorophyll a fluorescence: variable responses among freshwater microalgae. *water research* 46, 2615–2626.
- Cigna, A.A., Forti, P., 2013. Caves: the most important geotouristic feature in the world. *Tourism and Karst areas* 6, 9–26.
- Coutinho, M.L., Miller, A.Z., Martin-Sanchez, P.M., Mirão, J., Gomez-Bolea, A., Machado-Moreira, B., Cerqueira-Alves, L., Jurado, V., Saiz-Jimenez, C., Lima, A., 2016. A multiproxy approach to evaluate biocidal treatments on biodeteriorated majolica glazed tiles. *Environmental microbiology* 18, 4794–4816.

- D'Agostino, D., Beccarisi, L., Camassa, M., Febroriello, P., 2015. Microclimate and microbial characterization in the Zinzulusa show cave (South Italy) after switching to led lighting. *Journal of Cave and Karst Studies* 77, 133–144. <https://doi.org/10.4311/2014EX0123>
- De los Ríos, A., Pérez-Ortega, S., Wierzbos, J., Ascaso, C., 2012. Differential effects of biocide treatments on saxicolous communities: Case study of the Segovia cathedral cloister (Spain). *International Biodeterioration & Biodegradation* 67, 64–72. <https://doi.org/10.1016/j.ibiod.2011.10.010>
- Dewez, D., Goltsev, V., Kalaji, H.M., Oukarroum, A., 2018. Inhibitory effects of silver nanoparticles on photosystem II performance in *Lemna gibba* probed by chlorophyll fluorescence. *Current Plant Biology* 16, 15–21. <https://doi.org/10.1016/j.cpb.2018.11.006>
- Dias, L., Rosado, T., Candeias, A., Mirão, J., Caldeira, A.T., 2020. Linking ornamental stone discolouration to its biocolonisation state. *Building and Environment* 180, 106934. <https://doi.org/10.1016/j.buildenv.2020.106934>
- Dobat, K., 1969. Die Lampenflora der Barenhöhle., in: Die Barenhöhle von Erpfingen. Gemeinde Erpfingen, Germany, pp. 29–35.
- Eyssautier-Chuine, S., Vaillant-Gaveau, N., Gommeaux, M., Thomachot-Schneider, C., Pleck, J., Fronteau, G., 2015. Efficacy of different chemical mixtures against green algal growth on limestone: A case study with *Chlorella vulgaris*. *International Biodeterioration & Biodegradation* 103, 59–68. <https://doi.org/10.1016/j.ibiod.2015.02.021>
- Favero-Longo, S.E., Brigadeci, F., Segimiro, A., Voyron, S., Cardinali, M., Girlanda, M., Piervittori, R., 2018. Biocide efficacy and consolidant effect on the mycoflora of historical stuccos in indoor environment. *Journal of Cultural Heritage* 34, 33–42.
- Favero-Longo, S.E., Viles, H.A., 2020. A review of the nature, role and control of lithobionts on stone cultural heritage: Weighing-up and managing biodeterioration and bioprotection. *World Journal of Microbiology and Biotechnology* 36, 1–18.
- Franco-Castillo, I., Hierro, L., Jesús, M., Seral-Ascaso, A., Mitchell, S.G., 2021. Perspectives for antimicrobial nanomaterials in cultural heritage conservation. *Chem.* 7 (3), 629–669.
- Fronteau, G., 2000. Comportements télogénétiques des principaux calcaires de Champagne-Ardenne: en relation avec leur facies de dépôt et leur séquençage diagénétique (PhD Thesis). University of Reims Champagne Ardenne, France.
- Genova, C., Fuentes, E., Sanmartín, P., Favero, G., Prieto, B., 2020. Phytochemical Compounds as Cleaning Agents on Granite Colonized by Phototrophic Subaerial Biofilms. *Coatings* 10, 295. <https://doi.org/10.3390/coatings10030295>
- Gilbert, P., Moore, L.E., 2005. Cationic antiseptics: diversity of action under a common epithet. *Journal of applied microbiology* 99, 703–715.
- Gladis, F., Eggert, A., Karsten, U., Schumann, R., 2010. Prevention of biofilm growth on man-made surfaces: evaluation of antialgal activity of two biocides and photocatalytic nanoparticles. *Biofouling* 26, 89–101.
- Hallett, J.P., Welton, T., 2011. Room-temperature ionic liquids: solvents for synthesis and catalysis. 2. *Chemical reviews* 111, 3508–3576.
- Havlena, Z., Kieft, T.L., Veni, G., Horrocks, R.D., Jones, D.S., 2021. Lighting effects on the development and diversity of photosynthetic biofilm communities in Carlsbad Cavern, New Mexico. *Applied and environmental microbiology* 87, 1–19.

- Kubo, A.-L., Kremer, L., Herrmann, S., Mitchell, S.G., Bondarenko, O.M., Kahru, A., Streb, C., 2017. Antimicrobial activity of polyoxometalate ionic liquids against clinically relevant pathogens. *ChemPlusChem* 82, 867–871.
- Lazár, D., Sušila, P., Nauš, J., 2006. Early detection of plant stress from changes in distributions of chlorophyll a fluorescence parameters measured with fluorescence imaging. *Journal of fluorescence* 16, 173–176.
- Li, Q., Hu, Y., Zhang, B., 2021. Polyoxometalate-Ionic Liquids (ILs) and Polyvinyl Alcohol/Chitosan/ILs Hydrogels for Inhibiting Bacteria Colonising Wall Paintings. *Carbohydrate Polymers* 256, 1–12. <http://doi.org/10.1016/j.carbpol.2020.117592>.
- Li, T., Hu, Y., Zhang, B., 2020. Evaluation of efficiency of six biocides against microorganisms commonly found on Feilaifeng Limestone, China. *Journal of Cultural Heritage* 43, 45–50. <https://doi.org/10.1016/j.culher.2019.11.006>
- Manso, S., De Muynck, W., Segura, I., Aguado, A., Steppe, K., Boon, N., De Belie, N., 2014. Bioreceptivity evaluation of cementitious materials designed to stimulate biological growth. *Science of the Total Environment* 481, 232–241. <https://doi.org/10.1016/j.scitotenv.2014.02.059>
- Marques, E.L.S., Dias, J.C.T., Silva, G.S., Pirovani, C.P., Rezende, R.P., 2016. Effect of organic matter enrichment on the fungal community in limestone cave sediments. *Genet Mol Res* 15, 1-7. <http://dx.doi.org/10.4238/gmr.15038611>
- Maxim, D., Bucşa, L., Moza, M.I., Chachula, O., 2012. Preliminary antifungal investigation of ten biocides against moulds from two different church frescoes. *Ann RSCB* 17, 139–146.
- Maxwell, K., Johnson, G.N., 2000. Chlorophyll fluorescence - A practical guide. *Journal of Experimental Botany* 51, 659–668. <https://doi.org/10.1093/jxb/51.345.659>
- Miller, A.Z., Sanmartín, P., Pereira-Pardo, L., Dionísio, A., Saiz-Jimenez, C., Macedo, M.F., Prieto, B., 2012. Bioreceptivity of building stones: A review. *Science of The Total Environment* 426, 1–12. <https://doi.org/10.1016/j.scitotenv.2012.03.026>
- Misra, A., Franco Castillo, I., Müller, D.P., González, C., Eyssautier-Chuine, S., Ziegler, A., de la Fuente, J.M., Mitchell, S.G., Streb, C., 2018. Polyoxometalate-Ionic Liquids (POM-ILs) as Anticorrosion and Antibacterial Coatings for Natural Stones. *Angewandte Chemie International Edition* 57, 14926–14931.
- Moreau, C., Vergès-Belmin, V., Leroux, L., Orial, G., Fronteau, G., Barbin, V., 2008. Water-repellent and biocide treatments: Assessment of the potential combinations. *Journal of Cultural Heritage* 9, 394–400. <https://doi.org/10.1016/j.culher.2008.02.002>
- Mulec, J., 2014. Human impact on underground cultural and natural heritage sites, biological parameters of monitoring and remediation actions for insensitive surfaces: Case of Slovenian show caves. *Journal for Nature Conservation* 22, 132–141. <https://doi.org/10.1016/j.jnc.2013.10.001>
- Mulec, J., Kosi, G., 2009. Lampenflora algae and methods of growth control. *Journal of cave and karst studies* 71, 109–115.
- Mulec, J., Kosi, G., Vrhovšek, D., 2008. Characterization of cave aerophytic algal communities and effects of irradiance levels on production of pigments. *Journal of Cave and Karst Studies* 70, 3–12.
- Mulec, J., Vaupotič, J., Walochnik, J., 2012. Prokaryotic and Eukaryotic Airborne Microorganisms as Tracers of Microclimatic Changes in the Underground (Postojna Cave, Slovenia). *Microb Ecol* 64, 654–667. <https://doi.org/10.1007/s00248-012-0059-1>

- Muñoz-Fernández, J., Del Rosal, Y., Álvarez-Gómez, F., Hernández-Mariné, M., Guzmán-Sepúlveda, R., Korbee, N., Figueroa, F.L., 2021. Selection of LED lighting systems for the reduction of the biodeterioration of speleothems induced by photosynthetic biofilms in the Nerja Cave (Malaga, Spain). *Journal of Photochemistry and Photobiology B: Biology* 217, 1–10. <https://doi.org/10.1016/j.jphotobiol.2021.112155>.
- Nikolić, N., Zarubica, N., Gavrilović, B., Predojević, D., Trbojević, I., Subakov-Simić, G., Popović, S., 2020. Lampenflora and the entrance biofilm in two show caves: Comparison of microbial community, environmental, and biofilm parameters. *Journal of Cave and Karst Studies* 82, 69–81. <https://doi.org/10.4311/2018EX0124>
- Nugari, M.P., Pietrini, A.M., Caneva, G., Imperi, F., Visca, P., 2009. Biodeterioration of mural paintings in a rocky habitat: The Crypt of the Original Sin (Matera, Italy). *International Biodeterioration & Biodegradation* 63, 705–711. <https://doi.org/10.1016/j.ibiod.2009.03.013>
- Perez, R.E., 2018. Study and remediation of environmental problems caused due to the growth of algae in speleothems of calcareous caves adapted for tourism- a case of success in Spain. *J Environ Geol* 02, 20–27. <https://doi.org/10.4172/2591-7641.1000013>
- Pfendler, S., Alaoui-Sossé, B., Alaoui-Sossé, L., Bousta, F., Aleya, L., 2018a. Effects of UV-C radiation on *Chlorella vulgaris*, a biofilm-forming alga. *Journal of Applied Phycology* 30, 1607–1616. <https://doi.org/10.1007/s10811-017-1380-3>
- Pfendler, S., Borderie, F., Bousta, F., Alaoui-Sossé, L., Alaoui-Sossé, B., Aleya, L., 2018b. Comparison of biocides, allelopathic substances and UV-C as treatments for biofilm proliferation on heritage monuments. *Journal of Cultural Heritage* 33, 117–124. <https://doi.org/10.1016/j.culher.2018.03.016>
- Pozo-Antonio, J.S., Sanmartín, P., 2018. Exposure to artificial daylight or UV irradiation (A, B or C) prior to chemical cleaning: an effective combination for removing phototrophs from granite. *Biofouling* 34, 851–869. <http://dx.doi.org/10.1016/j.scitotenv.2016.07.090>
- Rajkowska, K., Koziróg, A., Otlewska, A., Piotrowska, M., Atrián-Blasco, E., Franco-Castillo, I., Mitchell, S.G., 2020. Antifungal Activity of Polyoxometalate-Ionic Liquids on Historical Brick. *Molecules* 25, 5663. <https://doi.org/10.3390/molecules25235663>
- Rugini, L., Migliore, G., Tasso, F., Ellwood, N.T.W., Sprocati, A.R., Bruno, L., 2020. Biocidal Activity of Phyto-Derivative Products Used on Phototrophic Biofilms Growing on Stone Surfaces of the Domus Aurea in Rome (Italy). *Applied Sciences* 10, 6584. <https://doi.org/10.3390/app10186584>
- Sanchez-Moral, S., Jurado, V., Fernandez-Cortes, A., Cuezva, S., Martin-Pozas, T., Gonzalez-Pimentel, J.L., Ontañón, R., Saiz-Jimenez, C., 2021. Environment-driven control of fungi in subterranean ecosystems: the case of La Garma Cave (northern Spain). *Int Microbiol* 24, 573–591. <https://doi.org/10.1007/s10123-021-00193-x>
- Sanmartín, P., Rodríguez, A., Aguiar, U., 2020. Medium-term field evaluation of several widely used cleaning-restoration techniques applied to algal biofilm formed on a granite-built historical monument. *International Biodeterioration & Biodegradation* 147, 1–8. <https://doi.org/10.1016/j.ibiod.2019.104870>
- Sasse, H.R., Snethlage, R., 1996. Methods for evaluation of stone conservation treatments., in: *Report of the Dahlem Workshop: Saving Our Heritage: The*

- Conservation of Historic Stone Structures. Baer, N.S., Snethlage, R., Berlin 12, 223–243.
- Simon, K.S., Pipan, T., Culver, D.C., 2007. A conceptual model of the flow and distribution of organic carbon in caves. *Journal of Cave and Karst Studies* 69, 279–284.
- Stupar, M., Grbić, M.Lj., Džamić, A., Unković, N., Ristić, M., Jelikić, A., Vukojević, J., 2014. Antifungal activity of selected essential oils and biocide benzalkonium chloride against the fungi isolated from cultural heritage objects. *South African Journal of Botany* 93, 118–124. <https://doi.org/10.1016/j.sajb.2014.03.016>
- Thompson, J.D., Gibson, T.J., Higgins, D.G., 2002. Multiple sequence alignment using ClustalW and ClustalX. *Current protocols in Bioinformatics* 00, 2.3.1–2.3.22 <https://doi.org/10.1002/0471250953.bi0203s00>
- Tomaselli, L., Lamenti, G., Tiano, P., 2002. Chlorophyll fluorescence for evaluating biocide treatments against phototrophic biodeteriogens. *Annals of microbiology* 52, 197–206.
- Tretiach, M., Bertuzzi, S., Salvadori, O., 2010. Chlorophyll a fluorescence as a practical tool for checking the effects of biocide treatments on endolithic lichens. *International Biodeterioration & Biodegradation* 64, 452–460.
- Urzi, C., De, L., Krakova, L., Pangallo, D., Bruno, L., 2016. Effects of biocide treatments on the biofilm community in Domitilla's catacombs in Rome. *Science of the Total Environment* 572, 252–262. <https://doi.org/10.1016/j.scitotenv.2016.07.195>
- Van Kooten, O., Snel, J.F., 1990. The use of chlorophyll fluorescence nomenclature in plant stress physiology. *Photosynthesis research* 25, 147–150.
- Vannini, A., Contardo, T., Paoli, L., Scattoni, M., Favero-Longo, S.E., Loppi, S., 2018. Application of commercial biocides to lichens: Does a physiological recovery occur over time? *International Biodeterioration & Biodegradation* 129, 189–194. <https://doi.org/10.1016/j.ibiod.2018.02.010>
- Warscheid, Th., Braams, J., 2000. Biodeterioration of stone: a review. *International Biodeterioration & Biodegradation, Biodeterioration of Cultural Property* 2, Part 2 46, 343–368. [https://doi.org/10.1016/S0964-8305\(00\)00109-8](https://doi.org/10.1016/S0964-8305(00)00109-8)
- Young, E.B., Beardall, J., 2003. Photosynthetic Function in *Dunaliella Tertiolecta* (chlorophyta) During a Nitrogen Starvation and Recovery Cycle. *Journal of Phycology* 39, 897–905. <https://doi.org/10.1046/j.1529-8817.2003.03042.x>
- Zakrewsky, M., Lovejoy, K.S., Kern, T.L., Miller, T.E., Le, V., Nagy, A., Goumas, A.M., Iyer, R.S., Del Sesto, R.E., Koppisch, A.T., 2014. Ionic liquids as a class of materials for transdermal delivery and pathogen neutralization. *Proceedings of the National Academy of Sciences* 111, 13313–13318.

Supporting Information**New protective coatings against lampenflora
growing in the Pommery Champagne cellar**

Isabel Franco-Castillo^{1,2}, Archismita Misra³, Sébastien Laratte⁴, Maxime Gommeaux⁴, Robin Perarnau⁴, Nathalie Vaillant-Gaveau⁵, Clément Pierlot⁶, Carsten Streb³, Scott G. Mitchell^{1,2*}, Stéphanie Eyssautier-Chuine^{4*}

¹ Instituto de Nanociencia y Materiales de Aragón (INMA-CSIC), Consejo Superior de Investigaciones Científicas-Universidad de Zaragoza, c/ Pedro Cerbuna 12, 50009 Zaragoza, Spain.

² CIBER de Bioingeniería, Biomateriales y Nanomedicina, Instituto de Salud Carlos III, 28029 Madrid, Spain.

* Email: scott.mitchell@csic.es

³ Institute of Inorganic Chemistry I, Ulm University, Albert-Einstein-Allee 11, 89081 Ulm, Germany

⁴ Groupe d'Étude sur les Géomatériaux et les Environnements Naturels Anthropiques et Archéologiques 3795 (GEGENAA) - SFR Condorcet FR CNRS 3417 – 2, Esplanade Roland Garros, Université de Reims Champagne-Ardenne, 51100 cedex, Reims, France.

* Email: stephanie.eyssautier@univ-reims.fr

⁵ Unité de Recherche EA 4707 Résistance Induite et Bioprotection des Plantes (RIBP), SFR Condorcet FR CNRS 3417, UFR Sciences Exactes et Naturelles, Université de Reims Champagne-Ardenne, Reims, France.

⁶ Vranken-Pommery Monopole, 5 Place du Général Gouraud, BP1049, 51689, Reims, cedex 2, France

Supporting Information



Figure S1. Localisation of the sampling locations for the identification of the biofilm microorganisms.

Table S1. Applied quantity of liquid product on each slab and equivalent dry weight for the three biocidal assays.

Assay	Weight of liquid coating/slab (g)			Weight of dry coating/slab (g)		
	POM-IL1	POM-IL2	PR80	POM-IL1	POM-IL2	PR80
1	0.24 ± 0.01	0.21 ± 0.01	0.28 ± 0.03	0.04 ± 0.01	0.03 ± 0.01	0.15 ± 0.02
2	0.42 ± 0.01	0.40 ± 0.01	0.44 ± 0.01	0.08 ± 0.02	0.09 ± 0.01	0.24 ± 0.01
3	0.10 ± 0.03	0.12 ± 0.01	0.11 ± 0.01			
	0.20 ± 0.04	0.22 ± 0.03	0.23 ± 0.02			
	0.41 ± 0.02	0.40 ± 0.01	0.41 ± 0.01			

Supporting Information

Table S2. Identification of algae and cyanobacteria species by the closest affiliation in NCBI BlastN with primer, similarity percentage. The nucleotide sequence data have been deposited NCBI nucleotide sequence database under accession number. *CR_GenBank accession number.

Phylogenetic closest affiliation of isolates	Primer	Similarity (%)	Accession number*
<i>Chromochloris zofingiensis</i> strain ACSSI	18S rRNA	98.19	OK217227.1
<i>Pseudostichococcus monallantoides</i> strain UTEX 2249	rbcL	98.46	OK432519
<i>Diplosphaera</i> sp. cort12	rbcL	98.28	OK432520
<i>Timaviella</i> sp.	16S rRNA	98.00	OK422863

Table S3. Hoagland medium composition.

Hoagland - Component	Stock Solution	Stock Solution ml / L
2M KNO ₃	202 g/L	2.5
2M Ca(NO ₃) ₂ •4H ₂ O	472 g/L	2.5
2M MgSO ₄ •7H ₂ O	493 g/L	1
1M KH ₂ PO ₄	136 g/L	1
H ₃ BO ₃	2.86 g/L	1
MnCl ₂ •4H ₂ O	1.81 g/L	1
ZnSO ₄ •7H ₂ O	0.22 g/L	1
CuSO ₄ •5H ₂ O	0.08 g/L	1
Na ₂ MoO ₄ •2H ₂ O ☆	0.12 g/L	1
Iron(III)-EDTA	0.14 g/L	1.5

Supporting Information

Table S4. Δa^* and F_V/F_M average and standard deviation for Assay 1.

coating	Time (week)	<i>Chromochloris</i> sp. inoculation				<i>Pseudostichococcus</i> sp. inoculation			
		Δa^* average	Δa^* SD	F_V/F_M average	F_V/F_M SD	Δa^* average	Δa^* SD	F_V/F_M average	F_V/F_M SD
NO	0			0.47	0.03			0.28	0.07
	1	-3.3	0.8	0.61	0.03	-14.0	2.0	0.44	0.07
	2	-7.3	1.3	0.49	0.05	-20.2	1.2	0.62	0.01
	3	-12.8	2.6	0.47	0.05	-17.5	2.2	0.50	0.02
	4	-15.1	3.7	0.50	0.02	-17.5	2.2	0.48	0.01
	5	-17.6	2.1	0.41	0.03	-19.3	1.1	0.50	0.03
	7	-14.6	2.3	0.39	0.03	-21.1	1.1	0.44	0.04
POM-IL1	0			0.44	0.05			0.28	0.07
	1	0.3	0.4	0.56	0.04	0.0	0.2	0.23	0.05
	2	0.7	0.4	0.08	0.04	0.2	0.3	0.20	0.02
	3	0.7	0.4	0.16	0.04	-0.8	0.6	0.14	0.04
	4	0.7	0.4	0.05	0.01	-2.9	1.3	0.22	0.08
	5	0.5	0.4	0.13	0.02	-6.3	1.8	0.24	0.09
	7	-0.9	0.7	0.17	0.04	-10.0	2.9	0.35	0.08
POM-IL2	0			0.38	0.03			0.33	0.04
	1	-1.4	0.3	0.57	0.02	-9.6	2.0	0.30	0.04
	2	-3.0	0.4	0.35	0.09	-18.5	1.3	0.57	0.02
	3	-7.5	1.0	0.31	0.07	-16.0	2.4	0.42	0.01
	4	-10.3	1.9	0.36	0.06	-15.8	2.6	0.47	0.02
	5	-12.6	2.8	0.45	0.03	-16.8	1.6	0.43	0.03
	7	-15.7	3.4	0.40	0.03	-17.0	1.6	0.37	0.04
PR80	0			0.41	0.04			0.34	0.04
	1	-1.4	0.5	0.50	0.02	-1.2	0.8	0.33	0.06
	2	-3.4	1.2	0.36	0.08	-5.9	3.3	0.41	0.06
	3	-9.1	2.3	0.32	0.05	-14.4	2.9	0.46	0.02
	4	-14.2	2.0	0.42	0.04	-16.3	2.1	0.41	0.03
	5	-16.7	1.1	0.46	0.02	-17.1	2.4	0.38	0.03
	7	-17.9	2.1	0.40	0.04	-16.5	1.8	0.31	0.04

Supporting Information

Table S5. Δa^* and F_V/F_M average and standard deviation for Assay 2.

coating	Time (week)	Δa^* average	Δa^* SD	F_V/F_M average	F_V/F_M SD
NO	0			0.12	0.06
	1	-2.1	1.8	0.32	0.11
	2	-15.7	3.3	0.47	0.05
	3	-18.4	2.0	0.42	0.04
	4	-19.2	1.5	0.46	0.02
	5	-19.1	1.7	0.33	0.03
POM-IL1	0			0.15	0.06
	1	0.4	0.3	0.06	0.03
	2	0.5	0.3	0.08	0.02
	3	0.5	0.3	0.03	0.01
	4	0.5	0.3	0.04	0.01
	5	0.4	0.3	0.03	0.01
POM-IL2	0			0.12	0.05
	1	0.5	0.2	0.05	0.02
	2	0.6	0.2	0.02	0.02
	3	0.5	0.2	0.01	0.02
	4	0.5	0.2	0.04	0.02
	5	0.5	0.2	0.01	0.01
PR80	0			0.14	0.04
	1	0.2	0.2	0.06	0.04
	2	0.4	0.2	0.03	0.02
	3	0.2	0.5	0.02	0.02
	4	-0.1	1.0	0.08	0.06
	5	-3.3	3.0	0.17	0.12

Supporting Information

Table S6. Δa^* and F_V/F_M average and standard deviation for Assay 3.

coating	Time (week)	Δa^* average	Δa^* SD	F_V/F_M average	F_V/F_M SD
NO	0			0.21	0.06
	1	-7.0	3.9	0.39	0.09
	2	-17.2	4.3	0.51	0.04
	3	-19.0	2.9	0.40	0.02
	4	-19.7	2.6	0.41	0.03
	5	-19.2	2.6	0.33	0.04
POM-IL1 0.1g	0			0.06	0.04
	1	0.7	0.4	0.05	0.02
	2	0.6	0.5	0.16	0.07
	3	0.6	0.4	0.06	0.02
	4	0.5	0.5	0.18	0.04
	5	0.5	0.5	0.06	0.03
POM-IL2 0.1g	0			0.04	0.02
	1	0.4	0.2	0.04	0.02
	2	0.5	0.2	0.12	0.11
	3	0.4	0.2	0.07	0.03
	4	0.2	0.3	0.14	0.04
	5	0.3	0.3	0.05	0.02
POM-IL1 0.2g	0			0.04	0.04
	1	1.0	0.4	0.04	0.01
	2	0.7	0.4	0.11	0.03
	3	0.8	0.4	0.06	0.03
	4	0.7	0.4	0.17	0.04
	5	0.7	0.4	0.04	0.02
POM-IL2 0.2g	0			0.05	0.05
	1	0.9	0.5	0.04	0.02
	2	0.8	0.6	0.11	0.04
	3	0.8	0.5	0.05	0.03
	4	0.8	0.6	0.19	0.03
	5	0.8	0.6	0.06	0.03
PR80 0.2g	0			0.06	0.04
	1	0.6	0.7	0.06	0.06
	2	0.4	1.3	0.19	0.10
	3	0.4	1.1	0.08	0.08
	4	-0.8	2.3	0.16	0.07
	5	-2.7	4.6	0.20	0.11

Supporting Information

coating	Time (week)	Δa^* average	Δa^* SD	F_V/F_M average	F_V/F_M SD
POM- IL1 0.4g	0			0.09	0.04
	1	1.0	0.7	0.02	0.01
	2	0.8	0.8	0.11	0.04
	3	0.9	0.8	0.06	0.02
	4	0.8	0.8	0.12	0.03
	5	0.8	0.8	0.04	0.05
POM- IL2 0.4g	0			0.09	0.05
	1	0.8	0.5	0.03	0.02
	2	0.7	0.5	0.09	0.04
	3	0.8	0.5	0.06	0.02
	4	0.7	0.5	0.13	0.04
	5	0.7	0.5	0.02	0.01
PR80 0.4g	0			0.05	0.02
	1	1.0	0.2	0.04	0.02
	2	0.8	0.3	0.09	0.03
	3	0.9	0.2	0.06	0.02
	4	0.8	0.2	0.14	0.03
	5	0.8	0.3	0.05	0.02

Supporting Information

Table S7. Δa^* and F_V/F_M average and standard deviation for Assay 4.

coating	Time (week)	Δa^* average	Δa^* SD	F_V/F_M average	F_V/F_M SD
NO	0			0.14	0.04
	1	-4.8	1.8	0.35	0.07
	2	-18.5	3.5	0.40	0.04
	3	-20.1	2.3	0.58	0.02
	4	-19.6	1.9	0.32	0.04
	5	-18.7	1.5	0.45	0.04
POM-IL1 0.1g wet	0			0.13	0.04
	1	0.3	0.4	0.18	0.05
	2	0.5	0.5	0.20	0.06
	3	0.5	0.5	0.11	0.04
	4	0.5	0.4	0.11	0.05
	5	-0.3	1.0	0.15	0.06
POM-IL2 0.1g wet	0			0.13	0.03
	1	0.3	0.4	0.17	0.05
	2	-0.4	1.0	0.18	0.05
	3	-2.5	3.3	0.16	0.04
	4	-8.0	6.6	0.24	0.09
	5	-14.4	8.2	0.27	0.06
POM-IL1 0.2g wet	0			0.16	0.04
	1	0.1	0.5	0.15	0.04
	2	0.4	0.6	0.09	0.09
	3	0.4	0.6	0.01	0.04
	4	0.2	0.8	0.16	0.05
	5	-0.4	1.4	0.13	0.05
POM-IL2 0.2g wet	0			0.14	0.04
	1	0.5	0.5	0.15	0.05
	2	0.6	0.4	0.15	0.04
	3	0.3	0.7	0.06	0.09
	4	-0.4	2.0	0.14	0.08
	5	-2.0	4.9	0.12	0.05
POM-IL1 0.4g dry	0			0.13	0.04
	1	0.5	0.3	0.18	0.06
	2	0.7	0.3	0.15	0.09
	3	0.6	0.3	0.16	0.04
	4	0.6	0.4	0.18	0.06
	5	0.4	0.6	0.13	0.04
POM-IL2 0.4g dry	0			0.12	0.04
	1	0.4	0.3	0.18	0.04
	2	0.6	0.2	0.11	0.09
	3	0.5	0.3	0.16	0.05
	4	0.5	0.4	0.19	0.08
	5	0.2	0.6	0.18	0.07

Supporting Information

PR80 0.4g wet	0			0.17	0.06
	1	-3.9	2.5	0.39	0.08
	2	-16.2	5.5	0.43	0.10
	3	-18.4	4.4	0.42	0.04
	4	-18.2	3.3	0.57	0.04
	5	-16.2	3.2	0.56	0.05

Article 6: Antifungal Activity of Polyoxometalate-Ionic Liquids on Historical Brick



Article

Antifungal Activity of Polyoxometalate-Ionic Liquids on Historical Brick

Katarzyna Rajkowska ^{1,*}, Anna Koziróg ¹, Anna Otlewska ¹, Małgorzata Piotrowska ¹, Elena Atrián-Blasco ^{2,3}, Isabel Franco-Castillo ^{2,3} and Scott G. Mitchell ^{2,3,*}

¹ Institute of Fermentation Technology and Microbiology, Lodz University of Technology, Wólczńska 171/173, 90-924 Lodz, Poland; anna.kozirog@p.lodz.pl (A.K.); anna.otlewska@p.lodz.pl (A.O.); malgorzata.piotrowska@p.lodz.pl (M.P.)

² Instituto de Nanociencia y Materiales de Aragón (INMA), Consejo Superior de Investigaciones Científicas-Universidad de Zaragoza, 50009 Zaragoza, Spain; elenaab@unizar.es (E.A.-B.); isabelfrancocastillo@gmail.com (I.F.-C.)

³ Center for Biomedical Research Network-Bioengineering, Biomaterials and Nanomedicine (CIBER-BBN) CIBER-BBN, Instituto de Salud Carlos III, 28029 Madrid, Spain

* Correspondence: katarzyna.rajkowska@p.lodz.pl (K.R.); scott.mitchell@csic.es (S.G.M.)

Academic Editor: Derek J. McPhee

Received: 6 November 2020; Accepted: 26 November 2020; Published: 1 December 2020



Abstract: Moulds inhabiting mineral-based materials may cause their biodeterioration, contributing to inestimable losses, especially in the case of cultural heritage objects and architectures. Fungi in mouldy buildings may also pose a threat to human health and constitute the main etiological factor in building related illnesses. In this context, research into novel compounds with antifungal activity is of high importance. The aim of this study was to evaluate the antifungal activity of polyoxometalate-ionic liquids (POM-ILs) and their use in the eradication of moulds from historical brick. In the disc diffusion assay, all the tested POM-ILs inhibited growth of a mixed culture of moulds including *Engyodontium album*, *Cladosporium cladosporioides*, *Alternaria alternata* and *Aspergillus fumigatus*. These were isolated from the surfaces of historical brick barracks at the Auschwitz II-Birkenau State Museum in Oświęcim, Poland. POM-IL coatings on historical brick samples, under model conditions, showed that two compounds demonstrated very high antifungal activity, completely limiting mould growth and development. The antifungal activity of the POM-ILs appeared to stem from their toxic effects on conidia, as evidenced by environmental scanning transmission electron microscopy observations. The results herein indicated that POM-ILs are promising disinfectant materials for use not only on historical objects, but probably also on other mineral-based materials.

Keywords: polyoxometalate ionic liquids; antifungal activity; historical brick; biodeterioration; environmental scanning transmission electron microscopy

1. Introduction

The susceptibility of brick, concrete, mortar, stone and other mineral-based building materials to colonisation by various organisms is defined as bioreceptivity. This concept was introduced by Guillet [1] and included chemical and physical parameters such as mineralogical composition, water availability, temperature, pH, surface porosity and roughness influence on biological succession [2,3]. From a biological point of view, mineral-based building materials represent an extreme microniche for microbial growth due to large variations in environmental parameters and higher desiccation conditions in vertical and subvertical surfaces [3]. Bacteria and fungi inhabit pits, cracks and fissures on the surface of mineral-based materials, and they often may interact with substrate causing their deterioration [4]. Microorganisms, especially fungi, as a result of metabolic activity, secrete different corrosive organic

acids (e.g., oxalic, citric, formic, fumaric, gluconic acid), which lead to increased solubilisation of material components in water and consequently to structural damage. Moreover, the mineral matrix structure may be mechanically destroyed by the penetrative growth of fungal hyphae [5]. *Aspergillus* spp. (*A. fumigatus*, *A. versicolor*, *A. niger*), *Penicillium* spp. (*P. chrysogenum*, *P. frequentans*, *P. simplicissimum*), *Cladosporium herbarum*, *Fusarium oxysporum*, *Mucor hiemalis*, *Alternaria alternata* and *Rhizopus oryzae* are important deteriorogenic fungi known to flourish on stone materials [5,6]. Nevertheless, the literature focusing on microbial colonisation of mineral-based building materials, especially brick, is very limited.

It is important to note that fungi-induced biodeterioration is observed not only on cultural heritage architectures and artefacts, but also on modern buildings, museums, storerooms and a variety of other materials [6–8]. This deteriorative phenomenon is also problematic from a health and safety perspective, because the excessive development of moulds in damp building materials and poorly ventilated buildings means that the resulting air contamination poses a serious risk factor for the health of building users [9]. Although moulds rarely cause serious diseases in healthy individuals, mostly affecting only those with weakened immune systems, however, continuous living in damp and mouldy buildings can have detrimental long-term effects in healthy people and is associated with an increased risk of developing asthma, rhinitis, allergies, dyspnoea, wheeze, cough, hypersensitivity pneumonitis, superficial and systemic infections (mycoses) and mycotoxicosis [9–11]. In the human body, moulds elicit an immune response through cytotoxic effects and the production of mediators of inflammatory reactions. Allergic reactions to *Alternaria*, *Cladosporium*, *Aspergillus*, *Penicillium* and *Fusarium* are the most often clinically detected allergies [12,13]. Moreover, *Aspergillus*, *Penicillium* and *Stachybotrys* genera produce mycotoxins, which can form aerosols and enter the human body through inhalation along with fungal spores. Mycotoxins are compounds with mutagenic, teratogenic, carcinogenic, dermatotoxic, hepatotoxic, neurotoxic properties [14,15]. Furthermore, it has been demonstrated that moulds play a major role in Sick Building Syndrome (SBS) or chronic fatigue syndrome [11], which is characterised by non-specific symptoms such as fatigue, nausea, drowsiness, headache, dizziness, irritability, concentration and memory disorders, as well as asthma-like symptoms [9,15]. In such cases, spores and fragments of mycelium hyphae serve as carriers of allergenic proteins and mycotoxins, nano-particulates, structural components of cells, as well as enzymes or volatile metabolites that are secreted into the environment [13,16].

Polyoxometalates (POMs) are an important and diverse class of nanoscale molecular metal oxides, which are characterised by a wide and versatile range of physicochemical properties that can be tuned on the molecular level [17]. Their redox properties and high oxidation activity also make them useful to a wide variety of applications, from catalysis [18] to medicine [19]. POMs cross lipid membranes, interact with proteins and are producers of reactive oxygen species, so they also display important antibacterial activity [20]. Furthermore, polyoxometalate-ionic liquids (POM-ILs), where molecular POM anions are fused with bulky and functional organic cations, e.g., organic ammonium or phosphonium cations, often result in room-temperature ionic liquids. Ionic liquids (ILs) are salts with a melting point <100 °C, whose structure can be tuned to access physicochemical properties such as wide electrochemical window, high thermal stability and null vapour pressure [21–23]. Importantly, unique properties of POM-ILs have been harnessed for universal pollutant removal [24] and reactive surface protecting anti-corrosion coatings [25–27] because both the anion and cation can be tailored to target biological, organic and inorganic pollutants including microbes, acids and reactive oxygen species [28]. Their rheological properties and hydrophobicity can also be tuned by chemical design, which are important to obtain surface coatings. Prototype POM-ILs have demonstrated excellent biofilm and corrosion protection on natural stones [27], but the broad-spectrum antimicrobial activity of these materials against different bacteria, yeast and moulds still needs to be evaluated.

The aim of this study was to assess the antifungal activity of POM-ILs and their usefulness in eradication of moulds inhabiting historical brick. Although antibacterial effects of water insoluble POM-ILs have been reported previously [26,27], however, to the best of our knowledge, this is the first study to investigate their antifungal activity and application in brick conservation.

2. Results and Discussion

A total of eight silicotungstate and phosphotungstate-based POM-ILs were synthesized based on previously reported experimental procedures. Please refer to Supplementary Materials for further details on synthesis and Tables S1–S4 for characterisation data. Table 1 provides a summary of the eight different POM-ILs employed in this study.

Table 1. Summary of the POM-ILs.

POM-IL	POM-IL Short Name
$[\text{PW}_{12}\text{O}_{40}][(\text{C}_6\text{H}_{13})_4\text{N}]_3$	$[\text{PW}_{12}\text{O}_{40}][\text{THeXa}]_3$
$[\text{PW}_{12}\text{O}_{40}][(\text{C}_7\text{H}_{15})_4\text{N}]_3$	$[\text{PW}_{12}\text{O}_{40}][\text{THepA}]_3$
$[\text{PW}_{12}\text{O}_{40}][(\text{C}_8\text{H}_{17})_4\text{N}]_3$	$[\text{PW}_{12}\text{O}_{40}][\text{TOctA}]_3$
$[\text{SiW}_{11}\text{O}_{39}][(\text{C}_6\text{H}_{13})_3(\text{C}_{14}\text{H}_{29})\text{N}]_8$	$[\text{SiW}_{11}\text{O}_{39}][\text{THTDA}]_8$
$[\text{SiW}_{12}\text{O}_{40}][(\text{C}_6\text{H}_{13})_3(\text{C}_{14}\text{H}_{29})\text{N}]_4$	$[\text{SiW}_{12}\text{O}_{40}][\text{THTDA}]_4$
$[\text{SiW}_{11}\text{O}_{39}][(\text{C}_8\text{H}_{17})_4\text{N}]_8$	$[\text{SiW}_{11}\text{O}_{39}][\text{TOctA}]_8$
$[\text{SiW}_{11}\text{O}_{39}][(\text{CH}_3)_3(\text{C}_8\text{H}_{17})\text{N}]_8$	$[\text{SiW}_{11}\text{O}_{39}][\text{TMOA}]_8$
$[\text{SiW}_{12}\text{O}_{40}][(\text{CH}_3)_3(\text{C}_8\text{H}_{17})\text{N}]_4$	$[\text{SiW}_{12}\text{O}_{40}][\text{TMOA}]_4$

A disc diffusion method was used to assess the in vitro antifungal activity of eight different but closely related POM-ILs and their capacity to prevent or inhibit mould growth on historical brick samples. The antifungal activity was examined against a mixed culture of moulds consisting of *Engyodontium album*, *Cladosporium cladosporioides*, *Alternaria alternata* and *Aspergillus fumigatus*, that were isolated from the surfaces of historical brick barracks at the Auschwitz II-Birkenau State Museum in Oświęcim, Poland. The use of mixed culture of moulds is especially important since masonry building parts are usually inhabited not by one single strain but by a mixture of microorganisms [29]. Moreover, the environmental strains which were isolated from historical brick objects were adapted to nutrient-poor materials.

In the disc diffusion assay, all the tested POM-ILs inhibited mould growth, despite their poor aqueous solubility, although clear differences in diameters of inhibition growth zones were observed (Figure 1). The highest antifungal activity was exhibited by $[\text{PW}_{12}\text{O}_{40}][\text{THepA}]_3$, $[\text{SiW}_{12}\text{O}_{40}][\text{THTDA}]_4$ and $[\text{PW}_{12}\text{O}_{40}][\text{THeXa}]_3$. Other compounds acted only when the disc was in direct contact with the mould cultures, and then the growth inhibition zones equalled 6 mm. None of the anionic controls of POM-ILs showed activity against moulds, while cationic controls were highly active. The highest activity was found for $[\text{THepA}]^+$ and $[\text{THeXa}]^+$ (Figure 1). These results indicate that diffusion-based antifungal activity of POM-ILs resulted mostly from activity of the cation species, which is consistent with previous findings of Kubo et al. [26], who explained that the antibacterial activity of these compounds arises primarily from the cationic action.

While the diffusion method is a standard method for evaluating antimicrobial compounds and materials, however, its principal limitation is that the assay requires the diffusion of compounds out of the discs and into the agar nutrient medium. In the case of hydrophobic compounds and water insoluble compounds, their diffusion and delivery to microbial cells in aqueous media may be hampered [30,31]. The POM-ILs in this report are characterised by high viscosity and water immiscibility [27].

Considering the water immiscibility and high viscosity of these POM-ILs, their antifungal activity was also determined on historical brick samples under model conditions with high mould content ($>10^6$ cfu/cm²). Briefly, 19th century brick samples were inoculated with moulds and allowed to colonise the brick surface in a climate chamber (80% relative humidity and 28 °C) for three weeks. Afterwards, POM-ILs were spray-coated up to three times and the number of microorganisms after successive POM-IL applications was determined by the contact plate method whereby the antifungal activity of POM-ILs was evaluated according to a calibration scale (please refer to Materials and Methods figure). In contrast to the disc diffusion studies, the historical brick studies demonstrated that two compounds, $[\text{SiW}_{11}\text{O}_{39}][\text{THTDA}]_8$ and $[\text{SiW}_{12}\text{O}_{40}][\text{THTDA}]_4$, showed very high antifungal

activity after three successive applications (according to our calibration scale), by completely inhibiting the growth of moulds (Figure 2). Good activity was also exhibited by $[\text{SiW}_{11}\text{O}_{39}][\text{TOA}]_8$ after the third application, where the brick surface contamination by fungi was reduced approximately by 50%. Mould growth inhibition was also found in other POM-ILs, i.e., $[\text{SiW}_{11}\text{O}_{39}][\text{TMOA}]_8$ and $[\text{SiW}_{12}\text{O}_{40}][\text{TMOA}]_4$. The results indicate that POM-ILs, especially $[\text{SiW}_{11}\text{O}_{39}][\text{THTDA}]_8$ and $[\text{SiW}_{12}\text{O}_{40}][\text{THTDA}]_4$, can be effectively used in disinfection of historical brick, although the following key issues should be considered.

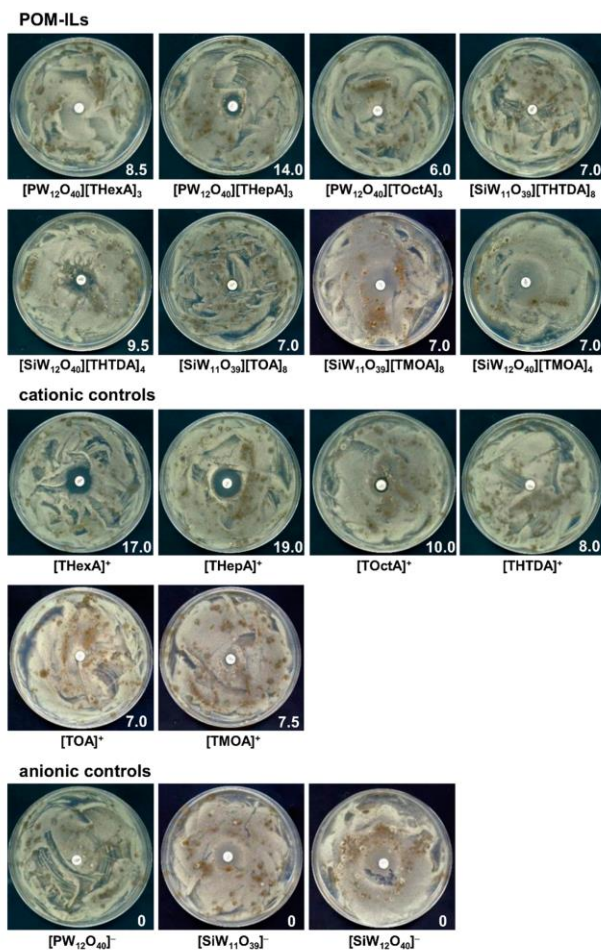


Figure 1. Zones of inhibition of mould growth by disc-diffusion method; the zone's diameter (mm) is shown in white in the lower right corner of each image.

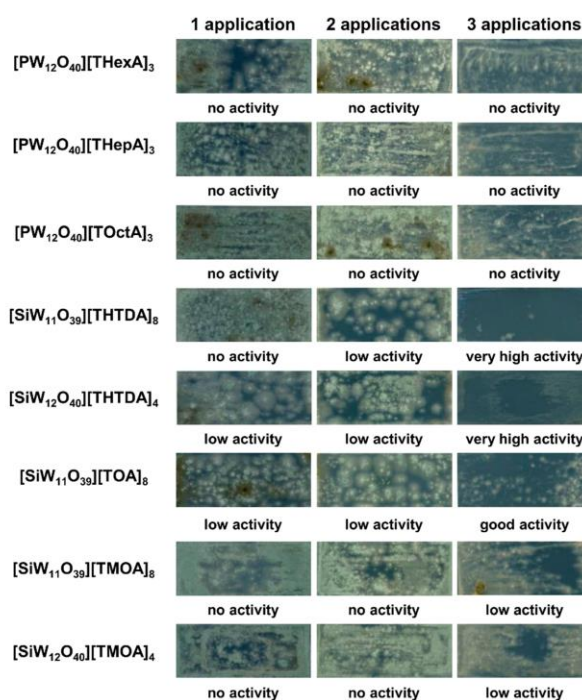


Figure 2. Antifungal activity of POM-ILs on brick samples inhabited by mixed culture of moulds.

In this study, POM-ILs solutions were applied by spraying and this method was chosen to minimise the risk of mechanical removal of fungal mycelium from the surface of bricks. Consequently, this method can result in a heterogeneous coverage of the compounds on the brick surface. For this reason, if POM-ILs are to be used as protective antimicrobial coatings, it is preferable to use the brush-coating method to protect the surface of materials against the development of microorganisms, as has been reported for POM-IL coatings on natural stones [27].

Other important factors determining the activity of biocides are their concentration, the number of applications, type of material and, what is particularly important, the intensity of microbial growth already present on the material surface. Only in objects heavily contaminated by microorganisms and in favourable environmental conditions, macroscopic signs of microbial growth are visible and the number of moulds exceeds 10^6 cfu/cm², as is seen in this study. In general, for historical objects, fungi were detected at a lower level of 10^1 – 10^3 cfu/100 cm² [32], and on building materials characterised by spore presence and active mould growth, the fungal contamination is estimated at 10^4 – 10^5 cfu/m² [33]. Therefore, the real-world use of POM-ILs as antifungal agents in situ is expected to be more effective than under the more extreme model conditions reported here.

In this context, the results obtained for the tested POM-ILs are very promising in the aspect of effective use on masonry surfaces of buildings, including historical objects. In addition to the potent antimicrobial activity of the quaternary ammonium cations that largely affected the conidia plasma membranes, we hypothesised that POM-IL coatings interfere with electron transfer and respiration processes and the overall applicability and potential as protective surface coatings are also closely related to the viscosity and hydrophobicity of the material. To further analyse the antifungal activity of

the most active POM-ILs from this study, environmental scanning transmission electron microscopy (ESTEM) was used to study the effect of $[\text{SiW}_{11}\text{O}_{39}][\text{THTDA}]_8$ and $[\text{SiW}_{12}\text{O}_{40}][\text{THTDA}]_4$ POM-ILs on fungal mycelium and conidia.

After the first application, solutions not only covered the mycelium and conidia, but also penetrated deep into the spatial moulds structure. After three applications, POM-ILs homogeneously covered the surface of the material together with the developed mycelium (Figure 3). ESTEM observations indicated toxic effects of $[\text{SiW}_{11}\text{O}_{39}][\text{THTDA}]_8$ and $[\text{SiW}_{12}\text{O}_{40}][\text{THTDA}]_4$ on fungal conidia (Figure 3 and Figure S1). In control images, conidia were collapsed as a result of moderate dehydration and a loss of turgor pressure under the ESTEM sample collection conditions. Such morphological changes are typical for conidia with intact membranes [34]. After the POM-ILs application, conidia were generally spherical, which is indicative of membrane damage and collapse. Similar results have been published previously for quaternary phosphonium ionic liquids, the mechanism of action of which are involved in damaging conidia plasma membrane [35].

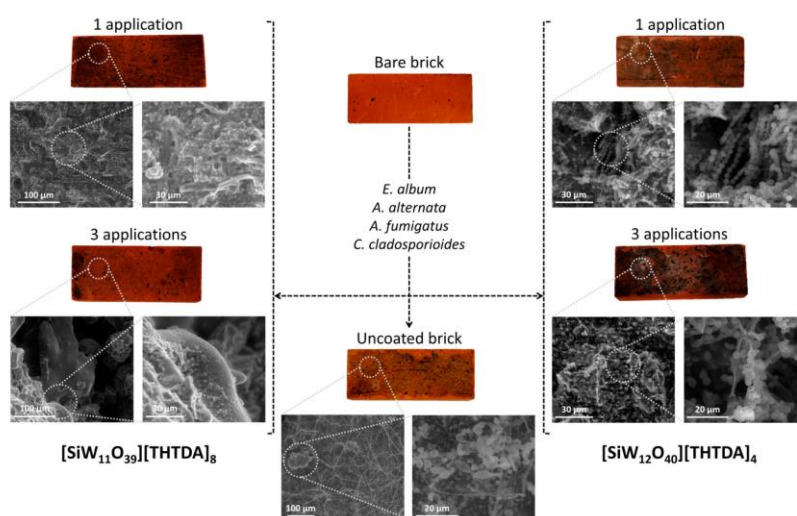


Figure 3. Environmental scanning transmission electron microscopy (ESTEM) images of antifungal activity of $[\text{SiW}_{11}\text{O}_{39}][\text{THTDA}]_8$ and $[\text{SiW}_{12}\text{O}_{40}][\text{THTDA}]_4$ POM-ILs on historical brick samples.

The results presented herein for POM-ILs are consistent with those reported for ionic liquids; this reinforces the theorem on the key role of cation species in antifungal activity. The antimicrobial mechanism of ionic liquids results from their amphiphilic character allows their insertion into the phospholipid bilayer of plasma membranes [36]. These interactions lead to plasma membrane damage, leakage of intracellular content, and, in consequence, to cell death [37]. In moulds, substantial damages to conidia and hyphae provoked by long alkyl chains were also documented [38]. The severe ultrastructural changes in cells were associated with membrane destruction, distending of cell wall structure, formation of residual organelles in the form of membranous structures and multivesicular bodies. On the other hand, the high negative charge of polyoxometalates means that they do not readily penetrate through cytoplasmic membranes, but they can cause impairments of vital cell functions in bacteria by interaction with the proteins involved in signal-transducing systems [20]. Furthermore, POMs can interfere with bacterial electron transfer, thereby affecting respiration processes [39]. The combination of two active components in the POM-IL molecule is clearly an important antimicrobial

activity enhancing property, however, the exact antifungal mode of action of POMs is still not understood and will require further detailed mechanistic experimentation.

3. Materials and Methods

3.1. Synthesis and Characterisation of POM-ILs

POM-ILs were synthesised according to previously reported synthetic procedures [26,27]. Briefly, a desired amount of POM was dissolved in 50 mL of pre-heated distilled water at 50 °C. The mixture was stirred until complete dissolution. In a beaker, the appropriate amount of the corresponding ionic liquid was dissolved in 80 mL of the solvent and stirred until complete dissolution. Then, the POM solution was slowly added to the IL solution and the mixture was stirred for 3 h at room temperature. After this time, the mixture was transferred to a separation funnel and once the two phases were clearly separated, the organic phase—including the POM-IL—was extracted into a round bottom flask. The organic solvent was removed in a rotatory evaporator, and the product was isolated in the form of powder or viscous liquid at room temperature.

All POM-ILs were characterised by thermogravimetric analysis (TGA Q5000, TA Instruments–Waters Corporation, New Castle, DE, USA), elemental analysis (Thermo Flash 1120, Thermo Fisher Scientific Inc., Waltham, MA, USA) and Fourier transform infrared spectroscopy (FT-IR JASCO FT/IR- 4100, Jasco Analytica Spain, Madrid, Spain). Please refer to Supplementary Materials Tables S1–S4 for characterisation data.

3.2. Assessment of Antifungal Activity of POM-ILs by Disc Diffusion Method

In the assay, four mould strains in a mixed culture were used, i.e., *Engyodontium album* LOCK 0590, *Cladosporium cladosporioides* LOCK 0592, *Alternaria alternata* LOCK 0594 and *Aspergillus fumigatus* LOCK 0596. All moulds were isolated from the surfaces of historical brick barracks at the Auschwitz II-Birkenau State Museum in Oświęcim, Poland. Antifungal activity was determined for POM-ILs solutions in dimethyl sulfoxide (DMSO) at a concentration of 5 mg/mL, by the disc diffusion method. Briefly, after spreading 100 µL of mixed culture of moulds in sterile saline (10^6 conidia/mL) on malt extract agar (MEA, Merck KGaA, Darmstadt, Germany), paper discs with 20 µL of POM-ILs were placed on the agar surface. DMSO (100%) served as a control. Plates were incubated for up to 5 days at 28 °C. The results were expressed as diameters of growth inhibition zones including the diameter of the disc (Ø 6 mm).

3.3. Evaluation of Antifungal Activity on Brick Samples

Antifungal activity of POM-ILs was assessed on historical brick under model conditions, as described previously [40]. One millilitre of mixed culture of moulds (10^6 conidia/mL) in the medium ((NH_4)₂SO₄ 0.075%, K₂HPO₄ 0.025%, MgSO₄·7H₂O 0.125%, yeast extract 0.125%, glucose 0.5%, agar 0.1%, pH 6.0) was applied on the surface of brick. Brick samples (50 × 20 × 10 mm³) came from the demolition of a 19th century residential building. The samples inoculated with moulds were incubated in a constant climate chamber with a relative humidity of 80% for 21 days at 28 °C. Afterwards, POM-ILs were applied up to three times at an interval of 24 h, using the spraying method. The number of microorganisms after successive applications of POM-ILs was determined by the contact plate method in MEA medium. Plates were incubated for 5 days at 28 °C. The antifungal activity of POM-ILs was evaluated according to a calibration scale (Figure 4).

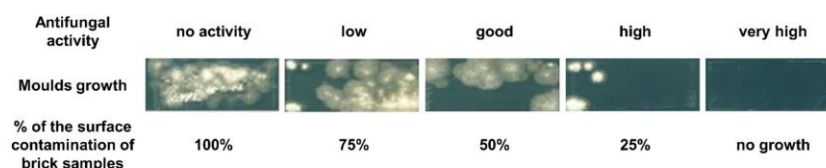


Figure 4. The scale of assessment of antifungal activity exhibited by POM-ILs.

3.4. Environmental Scanning Electron Microscopy (ESEM)

Data were collected on a Quanta FEG-250 (FEI Company, Hillsboro, OR, USA) field emission SEM for high-resolution imaging working in ESEM mode, using a gaseous secondary electron detector (GSED) detector under high relative humidity conditions.

4. Conclusions

The tested POM-ILs as part of this project showed high antifungal activity against a mixed culture of moulds that are well-adapted to the extreme conditions of mineral-based building materials. The inhibition of mould growth by POM-ILs occurs through toxic effects on conidia, and by coating the surface of the brick material, which may consequently limit the access to oxygen and nutrients. Although the antimicrobial activity of POM-ILs was mostly associated with cations, the combination of two components in the molecule gives them unique properties such as water immiscibility and creates the opportunity to design compounds with the desired characteristics for reducing microbially induced biodeterioration.

As a result of these promising features, POM-ILs could be used as antifungal agents in a variety of applications, not limited to historical brick, as described in this current study. Furthermore, the use of POM-ILs to disinfect or form protective coatings on other mineral-based building materials or historical objects, as well as in residential buildings can also be envisaged.

Supplementary Materials: The followings are available online, Figure S1: Environmental scanning transmission electron microscopy (ESEM) images of antifungal activity of the $[\text{SiW}_{11}\text{O}_{39}][\text{THTDA}]_8$ and $[\text{SiW}_{12}\text{O}_{40}][\text{THTDA}]_4$ POM-ILs on historical brick samples, taken at 642 \times and 3000 \times magnification. Table S1: Summary of the POM-ILs used in this work, their POM and ionic liquid precursors and the solvent used for their synthesis. Table S2: Thermogravimetric analysis of POM-ILs (MW = molecular weight). Table S3: Elemental analysis of POM-ILs. The values are given as mass percentages (%). Table S4: FT-IR analysis of POM-ILs (cm^{-1}).

Author Contributions: Conceptualization, K.R., S.G.M., A.K., A.O. and M.P.; synthesis and characterization, S.G.M. and E.A.-B.; methodology, K.R., A.K., A.O. and M.P.; validation, K.R.; investigation, K.R.; ESEM: S.G.M. and I.F.-C.; resources, K.R., S.G.M., E.A.-B., A.K., A.O. and M.P.; writing—original draft preparation, K.R., S.G.M., E.A.-B., A.K., A.O. and M.P.; visualization, K.R., A.O. and S.G.M.; writing—review and editing, all authors. All authors have read and agreed to the published version of the manuscript.

Funding: E.A.-B. and S.G.M. acknowledge the European Union's Horizon 2020 research and innovation program for the Marie Skłodowska-Curie grant agreement No 845427. S.G.M. acknowledges funding from Ministerio de Ciencia e Innovación (Spain) (PID2019-109333RB-I00). I.F.-C. is supported by a Gobierno de Aragón doctoral fellowship.

Acknowledgments: The microscopy characterisation has been conducted at the Laboratorio de Microscopias Avanzadas (LMA) at the Universidad de Zaragoza. Authors acknowledge the LMA for offering access to their instruments and expertise. SGM acknowledges professional support from the CSIC Interdisciplinary Thematic Platform Open Heritage: Research and Society (PTI-PAIS).

Conflicts of Interest: The authors declare no conflict of interest.

References

- Guillitte, O. Bioreceptivity and biodeterioration of brick structures. In *Conservation of Historic Brick Structures*, 1st ed.; Baer, N.S., Fitz, S., Livingston, R.A., Eds.; Taylor & Francis: New York, NY, USA, 1998; pp. 69–84.

2. Gómez-Cornelio, S.; Mendoza-Vega, J.; Gaylarde, C.C.; Reyes-Estebanez, M.; Morón-Ríos, A.; De la Rosa-García, S.; Ortega-Morales, B.O. Succession of fungi colonizing porous and compact limestone exposed to subtropical environments. *Fungal Biol.* **2012**, *116*, 1064–1072. [\[CrossRef\]](#) [\[PubMed\]](#)
3. Salvadori, O.; Mucichia, A.C. The Role of fungi and lichens in the biodeterioration of stone monuments. *Open Conf. Proc. J.* **2016**, *7*, 39–54. [\[CrossRef\]](#)
4. Cwalina, B. Biodeterioration of concrete, brick and other mineral-based building materials. In *Understanding Biocorrosion. Fundamentals and Applications*, 1st ed.; Liengen, T., Feron, D., Basseguy, R., Beech, I.B., Eds.; Woodhead Publishing Ltd.: Sawston, UK, 2014; pp. 281–312.
5. Sterflinger, K. Fungi as geologic agents. *Geomicrobiol. J.* **2000**, *17*, 97–124. [\[CrossRef\]](#)
6. Abdel Ghany, T.M.; Omar, A.M.; Elwkeel, F.M.; Al Abboud, M.A. Fungal deterioration of limestone false-door monument. *Heliyon* **2019**, *5*, e02673. [\[CrossRef\]](#) [\[PubMed\]](#)
7. Lan, W.; Li, H.; Wang, W.D.; Katayama, Y.; Gu, J.D. Microbial community analysis of fresh and old microbial biofilms on Bayon temple sandstone of Angkor Thom, Cambodia. *Microb. Ecol.* **2010**, *60*, 105–115. [\[CrossRef\]](#)
8. Gu, J.D.; Kigawa, R.; Sato, Y.; Katayama, Y. Addressing the microbiological problems of cultural property and archive documents after earthquake and tsunami. *Int. Biodeterior. Biodegrad.* **2013**, *85*, 345–346. [\[CrossRef\]](#)
9. Thrasher, J.D. Fungi, bacteria, nano-particulates, mycotoxins and human health in water-damaged indoor environments. *J. Community Public Health Nurs.* **2016**, *2*, 1000115.
10. Järvi, K.; Hyvärinen, A.; Täubel, M.; Karvonen, A.M.; Turunen, M.; Jalkanen, K.; Patovirta, R.; Syrjänen, T.; Pirinen, J.; Salonen, H.; et al. Microbial growth in building material samples and occupants' health in severely moisture-damaged homes. *Indoor Air* **2018**, *28*, 287–297. [\[CrossRef\]](#)
11. Baxi, S.N.; Portnoy, J.M.; Larenas-Linnemann, D.; Phipatanakul, W.; Barnes, C.; Baxi, S.; Grimes, C.; Horner, W.; Kennedy, K.; Levetin, E.J.; et al. Exposure and health effects of fungi on humans. *J. Allergy Clin. Immunol. Pract.* **2016**, *4*, 396–404. [\[CrossRef\]](#)
12. Sharpe, R.A.; Bearman, N.; Thornton, C.R.; Husk, K.; Osborne, N.J. Indoor fungal diversity and asthma: A meta-analysis and systematic review of risk factors. *J. Allergy Clin. Immunol.* **2015**, *135*, 110–122. [\[CrossRef\]](#)
13. Nevalainen, A.; Täubel, M.; Hyvärinen, A. Indoor fungi: Companions and contaminants. *Indoor Air* **2015**, *25*, 125–136. [\[CrossRef\]](#) [\[PubMed\]](#)
14. Nielsen, K.F. Mycotoxin production by indoor mold. *Fungal Genet. Biol.* **2003**, *39*, 103–117. [\[CrossRef\]](#)
15. Salin, J.T.; Salkinoja-Salonen, M.; Salin, P.J.; Nelo, K.; Holma, T.; Ohtonen, P.; Syrjäälä, H. Building-related symptoms are linked to the in vitro toxicity of indoor dust and airborne microbial propagules in schools: A cross-sectional study. *Environ. Res.* **2017**, *154*, 234–239. [\[CrossRef\]](#) [\[PubMed\]](#)
16. Rylander, R.; Lin, R. (1→3)- β -D-glucan—Relationship to indoor air-related symptoms, allergy and asthma. *Toxicology* **2000**, *152*, 47–52. [\[CrossRef\]](#)
17. Gumerova, N.I.; Rempel, A. Polyoxometalates in solution: Speciation under spotlight. *Chem. Soc. Rev.* **2020**. [\[CrossRef\]](#)
18. Streb, C. New trends in polyoxometalate photoredox chemistry: From photosensitisation to water oxidation catalysis. *Dalton Trans.* **2012**, *41*, 1651–1659. [\[CrossRef\]](#)
19. Yamase, T. Anti-tumor, -viral, and -bacterial activities of polyoxometalates for realizing an inorganic drug. *J. Mater. Chem.* **2005**, *15*, 4773–4782. [\[CrossRef\]](#)
20. Bijelic, A.; Aureliano, M.; Rempel, A. The antibacterial activity of polyoxometalates: Structures, antibiotic effects and future perspectives. *Chem. Commun.* **2018**, *54*, 1153–1169. [\[CrossRef\]](#)
21. Murugesan, S.; Quintero, O.A.; Chou, B.P.; Xiao, P.; Park, K.; Hall, J.W.; Jones, R.A.; Henkelman, G.; Goodenough, J.B.; Stevenson, K.J. Wide electrochemical window ionic salt for use in electropositive metal electrodeposition and solid state Li-ion batteries. *J. Mater. Chem. A* **2014**, *2*, 2194–2201. [\[CrossRef\]](#)
22. Mezzetta, A.; Perillo, V.; Guazzelli, L.; Chiappe, C. Thermal behavior analysis as a valuable tool for comparing ionic liquids of different classes. *J. Therm. Anal. Calorim.* **2019**, *138*, 3335–3345. [\[CrossRef\]](#)
23. Aschenbrenner, O.; Supasitmongkol, S.; Taylor, M.; Styring, P. Measurement of vapour pressures of ionic liquids and other low vapour pressure solvents. *Green Chem.* **2009**, *11*, 1217–1221. [\[CrossRef\]](#)
24. Herrmann, S.; De Matteis, L.; de la Fuente, J.M.; Mitchell, S.G.; Streb, C. Removal of multiple contaminants from water by polyoxometalate supported ionic liquid phases (POM-SILPs). *Angew. Chem. Int. Ed.* **2017**, *56*, 1667. [\[CrossRef\]](#) [\[PubMed\]](#)
25. Herrmann, S.; Kostrzewa, M.; Wierschem, A.; Streb, C. Polyoxometalate ionic liquids as self-repairing acid-resistant corrosion protection. *Angew. Chem. Int. Ed. Engl.* **2014**, *53*, 13596–13599. [\[CrossRef\]](#) [\[PubMed\]](#)

26. Kubo, A.-L.; Kremer, L.; Herrmann, S.; Mitchell, S.G.; Bondarenko, O.M.; Kahru, A.; Streb, C. Antimicrobial activity of polyoxometalate ionic liquids against clinically relevant pathogens. *ChemPlusChem* **2017**, *82*, 867–871. [\[CrossRef\]](#) [\[PubMed\]](#)
27. Misra, A.; Castillo, I.F.; Müller, D.P.; González, C.; Eyssautier-Chuine, S.; Ziegler, A.; de la Fuente, J.M.; Mitchell, S.G.; Streb, C. Polyoxometalate-ionic liquids (POM-ILs) as anticorrosion and antibacterial coatings for natural stones. *Angew. Chem. Int. Ed.* **2018**, *57*, 14926–14931. [\[CrossRef\]](#) [\[PubMed\]](#)
28. Misra, A.; Zambrycki, C.; Kloker, G.; Kotyba, A.; Anjass, M.H.; Franco Castillo, I.; Mitchell, S.G.; Güttel, R.; Streb, C. water purification and microplastics removal using magnetic polyoxometalate-supported ionic liquid phases (magPOM-SILPs). *Angew. Chem. Int. Ed. Engl.* **2020**, *59*, 1601–1605. [\[CrossRef\]](#)
29. Rajkowska, K.; Otlewska, A.; Koziróg, A.; Piotrowska, M.; Nowicka-Krawczyk, P.; Hachulka, M.; Wolski, G.J.; Kunicka-Styczyńska, A.; Gutarowska, B.; Żydzik-Bialek, A. Assessment of biological colonization of historic buildings in the former Auschwitz II-Birkenau concentration camp. *Ann. Microbiol.* **2014**, *64*, 799–808. [\[CrossRef\]](#) [\[PubMed\]](#)
30. Kemme, M.; Heinzel-Wieland, R. Quantitative assessment of antimicrobial activity of PLGA films loaded with 4-hexylresorcinol. *J. Funct. Biomater.* **2018**, *9*, 4. [\[CrossRef\]](#)
31. Hage-Hülsmann, J.; Grünberger, A.; Thies, S.; Santiago-Schübel, B.; Klein, A.S.; Pietruszka, J.; Binder, D.; Hilgers, F.; Domröse, A.; Drepper, T.; et al. Natural biocide cocktails: Combinatorial antibiotic effects of prodigiosin and biosurfactants. *PLoS ONE* **2018**, *13*, e0200940. [\[CrossRef\]](#)
32. Piotrowska, M.; Otlewska, A.; Rajkowska, K.; Koziróg, A.; Hachulka, M.; Nowicka-Krawczyk, P.; Wolski, G.J.; Gutarowska, B.; Kunicka-Styczyńska, A.; Żydzik-Bialek, A. Abiotic determinants of the historical buildings biodeterioration in the former Auschwitz II-Birkenau concentration and extermination camp. *PLoS ONE* **2014**, *9*, e109402. [\[CrossRef\]](#)
33. Gutarowska, B.; Żakowska, Z. Elaboration and application of mathematical model for estimation of mould contamination of some building materials based on ergosterol content determination. *Int. Biodeterior. Biodegrad.* **2002**, *49*, 299–305. [\[CrossRef\]](#)
34. Kaminsky, S.G.; Dahms, T.E. High spatial resolution surface imaging and analysis of fungal cells using SEM and AFM. *Micron* **2008**, *39*, 349–361. [\[CrossRef\]](#) [\[PubMed\]](#)
35. Petkovic, M.; Hartmann, D.O.; Adamova, G.; Seddon, K.R.; Rebelo, L.P.N.; Pereira, C.S. Unravelling the mechanism of toxicity of alkyltributylphosphonium chlorides in *Aspergillus nidulans* conidia. *New J. Chem.* **2012**, *36*, 56–63. [\[CrossRef\]](#)
36. Yoo, B.; Shah, J.K.; Zhua, Y.; Maginn, E.J. Amphiphilic interactions of ionic liquids with lipid biomembranes: A molecular simulation study. *Soft Matter* **2014**, *10*, 8641–8651. [\[CrossRef\]](#)
37. Egorova, K.S.; Gordeev, E.G.; Ananikov, V.P. Biological activity of ionic liquids and their application in pharmaceuticals and medicine. *Chem. Rev.* **2017**, *117*, 7132–7189. [\[CrossRef\]](#)
38. Koziróg, A.; Otlewska, A.; Gapińska, M.; Michlewska, S. Influence of gemini surfactants on biochemical profile and ultrastructure of *Aspergillus brasiliensis*. *Appl. Sci.* **2019**, *9*, 245. [\[CrossRef\]](#)
39. Inoue, M.; Suzuki, T.; Fujita, Y.; Oda, M.; Matsumoto, N.; Yamase, T. Enhancement of antibacterial activity of beta-lactam antibiotics by $[P_2W_{18}O_{62}]^{6-}$, $[SiMo_{12}O_{40}]^{4-}$, and $[PTi_2W_{10}O_{40}]^{7-}$ against methicillin-resistant and vancomycin-resistant *Staphylococcus aureus*. *J. Inorg. Biochem.* **2006**, *100*, 1225–1233. [\[CrossRef\]](#)
40. Rajkowska, K.; Koziróg, A.; Otlewska, A.; Piotrowska, M.; Nowicka-Krawczyk, P.; Brycki, B.; Kunicka-Styczyńska, A.; Gutarowska, B. Quaternary ammonium biocides as antimicrobial agents protecting historical wood and brick. *Acta Biochim. Pol.* **2016**, *63*, 153–159. [\[CrossRef\]](#)

Sample Availability: Samples of the compounds are available from the authors.

Publisher's Note: MDPI stays neutral with regard to jurisdictional claims in published maps and institutional affiliations.



© 2020 by the authors. Licensee MDPI, Basel, Switzerland. This article is an open access article distributed under the terms and conditions of the Creative Commons Attribution (CC BY) license (<http://creativecommons.org/licenses/by/4.0/>).

- Supporting Information -

Antifungal activity of polyoxometalate-ionic liquids on historical brick

Katarzyna Rajkowska,^{1,*} Anna Koziróg,¹ Anna Otlewska,¹ Małgorzata Piotrowska,¹ Elena Atrián-Blasco,^{2,3} Isabel Franco-Castillo^{2,3} and Scott G. Mitchell^{*2,3}

¹ Institute of Fermentation Technology and Microbiology, Lodz University of Technology, Wólczńska 171/173, 90-924 Lodz, Poland

² Instituto de Nanociencia y Materiales de Aragón (INMA), Consejo Superior de Investigaciones Científicas-Universidad de Zaragoza, 50009 Zaragoza, Spain

³ CIBER-BBN, Instituto de Salud Carlos III, Madrid, Spain

* Correspondence: katarzyna.rajkowska@p.lodz.pl and scott.mitchell@csic.es

Contents

1. Instrumentation
2. Synthesis and characterization
3. Environmental scanning transmission electron microscopy (ESTEM) images
4. References

- Supporting Information -

1. Instrumentation

Elemental Analysis: Elemental analyses (CHN) were performed by Interdepartmental Investigation Service (SIDI, Universidad Autónoma de Madrid) on a LECO CHNS-932 Elementary Chemical Analyzer.

FT-IR spectroscopy: FT-IR spectra were recorded on a Jasco FTIR 4100 spectrometer equipped with an ATR accessory. The samples were measured directly on the ATR, in a frequency range of 4000 – 600 cm⁻¹ and a resolution of 2 cm⁻¹.

Thermogravimetric analysis: thermogravimetric analyses were recorded on a TGA Q5000 from TA Instruments in air.

2. Synthesis and characterization

For the synthesis of the eight different POM-ILs, three different Keggin-type POM precursors were used (see **Table S1**). Phosphotungstic acid, H₃PW₁₂O₄₀, and quaternary ammonium salts were purchased from Sigma Aldrich. K₄SiW₁₂O₄₀ and K₈SiW₁₁O₃₉ were prepared according to the procedure described in the literature.[1]

Table S1. Summary of the POM-ILs used in this work, their POM and ionic liquid precursors and the solvent used for their synthesis.

POM-IL	POM	Ionic Liquid	Solvent
[PW ₁₂ O ₄₀][THexA] ₃	H ₃ PW ₁₂ O ₄₀	[(C ₆ H ₁₃) ₄ N]Br	dichloromethane
[PW ₁₂ O ₄₀][THepA] ₃	H ₃ PW ₁₂ O ₄₀	[(C ₇ H ₁₅) ₄ N]Br	dichloromethane
[PW ₁₂ O ₄₀][TOctA] ₃	H ₃ PW ₁₂ O ₄₀	[(C ₈ H ₁₇) ₄ N]Br	chloroform
[SiW ₁₁ O ₃₉][THTDA] ₈	K ₈ [α-SiW ₁₁ O ₃₉]	[(C ₆ H ₁₃) ₃ (C ₁₄ H ₂₉)N]Br	toluene
[SiW ₁₂ O ₄₀][THTDA] ₄	K ₄ [α-SiW ₁₂ O ₄₀]	[(C ₆ H ₁₃) ₃ (C ₁₄ H ₂₉)N]Br	chloroform
[SiW ₁₁ O ₃₉][TOctA] ₈	K ₈ [α-SiW ₁₁ O ₃₉]	[(C ₈ H ₁₇) ₄ N]Br	dichloromethane
[SiW ₁₁ O ₃₉][TMOA] ₈	K ₈ [α-SiW ₁₁ O ₃₉]	[(CH ₃) ₃ (C ₈ H ₁₇)N]Br	dichloromethane
[SiW ₁₂ O ₄₀][TMOA] ₄	K ₄ [α-SiW ₁₂ O ₄₀]	[(CH ₃) ₃ (C ₈ H ₁₇)N]Br	dichloromethane

General procedure for the synthesis of POM-ILs

A desired amount of POM was dissolved in 50 mL of pre-heated distilled water at 50 °C. The mixture was stirred until complete dissolution. In a beaker, the appropriate amount of the corresponding ionic liquid was dissolved in 80 mL of the solvent (see Table S1) and stirred until complete dissolution. Then, the POM solution was slowly added to the IL solution and the mixture was stirred for 3 h. After this time, the mixture was poured into a separation funnel and once the two phases are clearly separated, the organic phase –

- Supporting Information -

including the POM-IL – is extracted into a round bottom flask. The organic solvent was removed in a rotatory evaporator, and the product was isolated.

Table S2. Thermogravimetric analysis of POM-ILs (MW = molecular weight).

POM-IL	MW (POM)	MW (IL) x n	MW (POM-IL)	% m IL, calculated	% m IL, experimental
[PW ₁₂ O ₄₀][THexA] ₃	2877.03	1064.02	3941.05	27.00	30.70
[PW ₁₂ O ₄₀][THepA] ₃	2877.03	1232.34	4109.37	29.99	32.67
[PW ₁₂ O ₄₀][TOctA] ₃	2877.03	1400.66	4277.69	32.74	33.15
[SiW ₁₁ O ₃₉][THTDA] ₈	2674.30	3735.09	6409.39	58.28	57.64
[SiW ₁₂ O ₄₀][THTDA] ₄	2874.14	1867.54	4741.68	39.39	38.30
[SiW ₁₁ O ₃₉][TOA] ₈	2674.30	3735.09	6409.39	58.28	59.10
[SiW ₁₁ O ₃₉][TMOA] ₈	2674.30	1378.64	4052.94	34.02	31.89
[SiW ₁₂ O ₄₀][TMOA] ₄	2874.14	689.32	3563.46	19.34	25.88

Table S3. Elemental analysis of POM-ILs. The values are given as mass percentages (%).

POM-IL	calculated			experimental		
	C	H	N	C	H	N
[PW ₁₂ O ₄₀][THexA] ₃	21.94	3.99	1.07	24.30	4.30	1.20
[PW ₁₂ O ₄₀][THepA] ₃	24.55	4.41	1.02	26.50	4.60	1.10
[PW ₁₂ O ₄₀][TOctA] ₃	26.95	4.81	0.98	27.55	4.72	0.96
[SiW ₁₁ O ₃₉][THTDA] ₈	47.97	8.55	1.75	48.16	8.59	2.02
[SiW ₁₂ O ₄₀][THTDA] ₄	32.42	5.78	1.18	41.00	7.00	1.40
[SiW ₁₁ O ₃₉][TOA] ₈	47.97	8.55	1.75	48.09	8.76	1.89
[SiW ₁₁ O ₃₉][TMOA] ₈	26.08	5.17	2.76	20.88	4.34	2.03
[SiW ₁₂ O ₄₀][TMOA] ₄	14.83	2.94	1.57	16.22	3.60	1.64

Table S4. FT-IR analysis of POM-ILs (cm⁻¹).

POM-IL	ν P-O / Si-O	ν W=O	ν, δ W-O-W
[PW ₁₂ O ₄₀][THexA] ₃	1078 (s)	974 (s)	893 (s), 801 (vs), 727 (w)
[PW ₁₂ O ₄₀][THepA] ₃	1077 (s)	977 (s)	890 (s), 800 (vs), 726 (w)
[PW ₁₂ O ₄₀][TOctA] ₃	1079 (s)	974 (s)	896 (s), 813 (vs), 724 (w)
[SiW ₁₁ O ₃₉][THTDA] ₈	1081 (w)	993 (w), 953 (s)	897 (s), 813 (w), 750 (s), 693 (s), 657 (s)
[SiW ₁₂ O ₄₀][THTDA] ₄	1080 (w)	965 (s)	951 (w), 917 (s), 844 (m), 792 (s), 729 (m)
[SiW ₁₁ O ₃₉][TOA] ₈	1075 (w)	997 (m), 954 (m)	900 (s), 807 (s), 532 (m)
[SiW ₁₁ O ₃₉][TMOA] ₈	1073 (w)	978 (s), 936 (s)	861 (vs), 787 (vs), 722 (vs), 670 (s), 632 (s)
[SiW ₁₂ O ₄₀][TMOA] ₄	1080 (w)	988 (s)	935 (s), 870 (sh), 861 (vs), 788

- Supporting Information -

			(vs), 711 (vs), 655 (w), 649 (w), 640 (w), 626 (w)
--	--	--	---

3. Environmental scanning transmission electron microscopy (ESTEM)

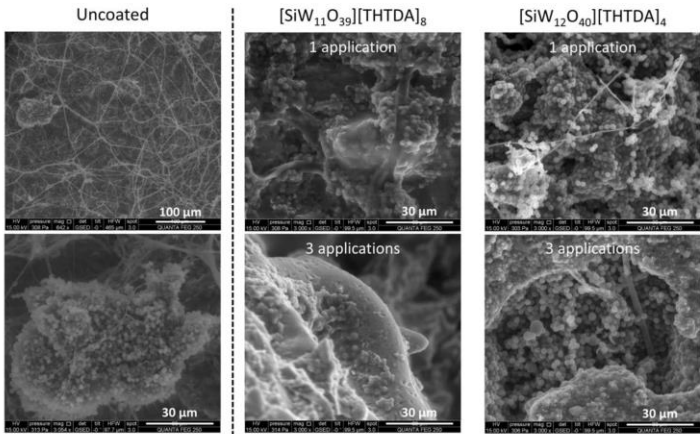


Figure S1. Environmental scanning transmission electron microscopy (ESTEM) images of antifungal activity of the [SiW₁₁O₃₉][THTDA]₈ and [SiW₁₂O₄₀][THTDA]₄ POM-ILs on historical brick samples, taken at 642 x and 3000 x magnification.

4. References

1. Tézé, A.; Hervé, G.; Finke, R.G.; Lyon, D.K. α -, β -, and γ -Dodecatungstosilicic Acids: Isomers and Related Lacunary Compounds. *Inorganic Syntheses*; 1990; pp. 85–96, Online ISBN: 9780470132586; Print ISBN: 9780471509769.

6. Conclusions

This doctoral thesis has studied the synthesis, characterisation and application of metal-oxide nanomaterials as antimicrobial coatings to prevent biodeterioration of heritage paper and stones. One of the most important challenges in this research field is the need to develop multifunctional antimicrobial agents that target specific microorganisms and meet the needs of the substrate heritage material. In this aspect, nanomaterials can provide alternatives to the traditional or commercial antimicrobial products. In this doctoral thesis, two different kinds of nanomaterials, magnesium oxide nanoparticles (MgO NPs) and the polyoxometalate-ionic liquids (POM-ILs), were applied as protective coatings on heritage paper and on mineral-based building materials, respectively, without significantly altering the appearance of the object. Importantly, both materials were demonstrated to possess antimicrobial activity against a wide variety of bacteria and moulds.

In vitro assays demonstrated how 12 nm-diameter MgO NPs can cause oxidative stress and cell membrane leakage, leading to cell death. *In situ* experiments on 18th century papers obtained from the archives of the Royal Botanical Gardens in Madrid also demonstrated the antimicrobial activity of the MgO NPs coating against prevented colonisation of the paper by *E. coli* and three filamentous fungal strains (*T. reesei*, *A. niger* and *C. cladosporioides*). What is more, these nanoparticles not only prevent growth of the microorganisms; they also inhibit the cellulase activity of *A. niger* and *T. reesei* at sub-MIC concentrations, preventing the degradation of the paper. Furthermore, the MgO NPs present some advantages in comparison with other nanoparticles frequently used in heritage. On the one hand, they increase the pH, preventing acidification of the paper, and once dissolved and applied as a coating do not change the appearance of the paper, in contrast with high coloured nanoparticles such as Ag NPs or Cu NPs, which can alter the aesthetics of the objects.⁹⁷ On the other hand, no photoactivation is needed (e.g., UV light for TiO₂ NPs), thus presenting activity in both light and dark conditions.⁹⁷ However, the amount of MgO NPs needed to stop mould growth *in vitro* (in a standard broth microdilution method) is quite high, reaching a concentration of 12 mg/mL against *C. cladosporioides*. Even the concentration needed to kill *E. coli* (1.5 mg/mL) can be considered too high. For comparison, antimicrobial plant extracts and antimicrobial peptides are highly

Conclusions

active with MICs below 100 µg/mL, and MICs ranging from 1 to 2 mg/mL are considered to have low activity.^{223–225}

The need of multifunctional coatings, with high antimicrobial activity and long-lasting effect, has increased in the last years. Research carried out during this doctoral thesis has demonstrated that polyoxometalate-ionic liquids (POM-ILs) could meet all such requirements. Due to their high modularity, a wide library of POM-ILs with different properties can be developed. In this thesis, three POM-ILs, based on the lacunary Keggin POM [α -SiW₁₁O₃₉]⁸⁻, have been synthesised to prevent biodeterioration in chalk stones and heritage bricks. The POM-IL DOTMG-1 was tested against four bacterial strains (non-pathogenic *E. coli* DH5 α and *B. subtilis* and pathogenic *L. monocytogenes* and VTEC) and four moulds (*A. niger*, *A. ochraceus*, *C. cladosporioides* and *P. expansum*) and exhibited good antimicrobial activity at low concentrations against all the microbial strains. In work not presented in this thesis, we reported how POM-IL 1 and POM-IL 2 display excellent antimicrobial activity against *E. coli* and *B. subtilis*.⁹⁹ Interestingly, the Gram-positive bacteria were more susceptible than the Gram-negative ones for the three POM-ILs, suggesting the mechanism of action could be associated to the structure of the bacterial cell wall. Regarding the antimicrobial activity of the coating on chalk stones, both POM-IL 1 and POM-IL 2 proved to be more effective than a commercial biocide (Preventol RI80) against lampenflora, a mixture of algal and cyanobacterial strains isolated from the UNESCO heritage bas-reliefs of the Pommery Champagne cellar. POM-IL 1 even displayed long-lasting effect, preventing a second re-colonisation of the surface. The disinfectant effect of POM-IL 2 was also studied on 19th century bricks colonised by mould. This POM-IL decreased the number of viable fungi present on the bricks, causing toxic effects on the fungal conidia and inhibiting further colonisation. As seen from latest studies in the field, POM-ILs represent promising multifunctional compounds with broad-spectrum antimicrobial activity, hydrophobicity, and anticorrosive properties.^{99,148} These characteristics agree with the needs of restorers, however, the high cytotoxicity shown by some POM-ILs must be studied and considered to ensure the safety of the application.²²⁶ Although biocidal at low concentrations, POM-IL DOTMG-1 displayed high cytotoxicity in two human cell lines at similar concentrations, meaning that they pose a potential risk to restorers in close contact with the compound and effective HSE measures would be required. Therefore, more

Conclusions

extensive studies on the cytotoxicity, along with the ecotoxicological aspects of the POM-ILs, should be considered to comprehensively assess the use of these materials in heritage objects.

6. Conclusiones

En esta tesis doctoral se ha estudiado la síntesis, caracterización y aplicación de diferentes nanomateriales de óxidos metálicos como recubrimientos antimicrobianos para prevenir el biodeterioro de papel y piedras patrimoniales. Uno de los desafíos más importantes en este campo de investigación es el desarrollo de agentes antimicrobianos multifuncionales y selectivos frente a microorganismos específicos, y que además cumplan con las necesidades del material a tratar. En este aspecto, los nanomateriales pueden ser una buena alternativa a los productos antimicrobianos comerciales tradicionales. Durante esta tesis doctoral se han utilizado dos tipos diferentes de nanomateriales como recubrimientos protectores, las nanopartículas de óxido de magnesio (MgO NP), aplicadas en papeles del siglo XVIII, y los líquidos iónicos de polioxometalatos (POM-ILs), aplicados en piedras de yeso y ladrillos. Es importante destacar que se demostró que ambos materiales poseen actividad antimicrobiana contra una amplia variedad de bacterias y mohos, y que no modifican la apariencia del objeto una vez aplicados.

Con los ensayos *in vitro* se observó que las NPs de MgO de 12 nm de diámetro causan estrés oxidativo y daño en la membrana celular, provocando la muerte celular. Los experimentos realizados *in situ* (en papeles del siglo XVIII obtenidos de los archivos del Real Jardín Botánico de Madrid), demostraron que la actividad antimicrobiana de las NPs de MgO se mantenía una vez aplicadas como recubrimiento, inhibiendo el crecimiento de *E. coli* y tres cepas de hongos filamentosos (*T. reesei*, *A. niger* y *C. cladosporioides*) sobre los papeles tratados. Además, estas nanopartículas no solo previenen el crecimiento de los microorganismos, sino que también inhiben la actividad celulasa de *A. niger* y *T. reesei* a concentraciones por debajo de la MIC, evitando de esta forma la degradación del papel. Las NPs de MgO presentan una serie de ventajas respecto a otras nanopartículas frecuentemente utilizadas en patrimonio. Por un lado, incrementan el pH, evitando la acidificación del papel. Asimismo, una vez disueltas y aplicadas como recubrimiento, no modifican el aspecto del papel, a diferencia de otras nanopartículas muy coloreadas como las NPs de Ag o las NPs de Cu, que pueden alterar la apariencia de los objetos.⁹⁷ Por otro lado, no se necesita fotoactivación (por ejemplo, las NPs de TiO₂ necesitan luz UV para activarse), por lo que presentan actividad tanto en condiciones de luz como de oscuridad.⁹⁷ Sin embargo, la cantidad de NPs de MgO necesaria para exhibir

Conclusiones

actividad fungistática es considerablemente alta, alcanzando una concentración de hasta 12 mg/mL frente a *C. cladosporioides*. Incluso la concentración necesaria para matar *E. coli* (1,5 mg/mL) puede considerarse demasiado alta. A modo de comparación, los extractos de plantas con actividad antimicrobiana y los péptidos antimicrobianos se consideran muy activos cuando la MIC está por debajo de 100 µg/mL, y con baja actividad cuando la MIC oscila entre 1 y 2 mg/mL.^{223–225}

La necesidad de recubrimientos multifuncionales, con una actividad antimicrobiana alta y con efecto a largo plazo, ha aumentado en los últimos años. La investigación llevada a cabo durante esta tesis doctoral ha demostrado que los líquidos iónicos de polioxometalatos (POM-ILs) podrían cumplir con estos requisitos. Debido a su alta modularidad, se puede desarrollar una amplia biblioteca de POM-ILs con diferentes propiedades. En esta tesis, se han sintetizado tres POM-ILs, basados en el POM monolacunar de estructura Keggin [α -SiW₁₁O₃₉]⁸⁻, para prevenir el biodeterioro en piedras calizas y ladrillos históricos. El POM-IL DOTMG-1 se estudió frente a cuatro cepas bacterianas (*E. coli* DH5 α y *B. subtilis* (no patógenas) y *L. monocytogenes* y VTEC (patógenas)) y frente a cuatro mohos (*A. niger*, *A. ochraceus*, *C. cladosporioides* y *P. expansum*), obteniendo una buena actividad antimicrobiana a bajas concentraciones. En un trabajo no presentado en esta tesis, se demostró cómo el POM-IL 1 y POM-IL 2 poseen una excelente actividad antimicrobiana frente a *E. coli* y *B. subtilis*.⁹⁹ Es interesante mencionar que los tres POM-ILs fueron más efectivos frente a las bacterias Gram positivas, que presentaron mayor susceptibilidad al compuesto que las Gram negativas, lo que sugiere que el mecanismo de acción podría estar relacionado con la estructura de la pared celular bacteriana. En cuanto a la actividad antimicrobiana *in situ*, como recubrimiento en piedra caliza, tanto el POM-IL 1 como el POM-IL 2 demostraron ser más efectivos que un biocida comercial (Preventol RI80) frente a la lampenflora, un conjunto de algas y cianobacterias aisladas los bajorrelieves de la bodega de Champagne de Pommery, que pertenecen al patrimonio de la UNESCO. El POM-IL 1 incluso mostró un cierto efecto duradero, evitando una segunda recolonización de la superficie. Por otra parte, también se estudió el efecto desinfectante del POM-IL 2 sobre ladrillos del siglo XIX colonizados por una mezcla mohos. La aplicación de este POM-IL disminuyó el número de hongos viables sobre los ladrillos, provocando efectos tóxicos en los conidios e impidiendo una mayor colonización.

Conclusiones

Los últimos estudios en el campo corroboran que los POM-ILs son prometedores compuestos multifuncionales, con actividad antimicrobiana de amplio espectro y con propiedades hidrofóbicas y anticorrosivas.^{99,148} Estas características coinciden con las necesidades de los restauradores, sin embargo, algunos POM-ILs presentan una alta citotoxicidad, por lo que este aspecto debe tenerse en cuenta y estudiarse para garantizar una aplicación segura.²²⁶ El POM-IL DOTMG-1 resultó ser citotóxico a concentraciones muy similares a la concentración biocida, lo que podría suponer un riesgo para los restauradores en contacto estrecho con el compuesto. Esto hace que se requieran medidas de protección para garantizar la seguridad del trabajador y del medio ambiente. Por consiguiente, es imperativo considerar estos aspectos y estudiar la eco- y citotoxicidad de los POM-ILs en mayor profundidad, para poder evaluar de manera exhaustiva el uso de estos materiales en objetos del patrimonio cultural.

7. Perspectives

Over the last decade, a variety of different classes of nanomaterials have been used in heritage conservation for deacidification, consolidation, and cleaning processes.²²⁷ The antimicrobial properties, and the potential to use nanomaterials as carriers for antimicrobial agents, means that they are also being adopted to prevent biodeterioration in different heritage materials. Nevertheless, there are a number of important considerations that must be addressed to ensure the transfer of such nanomaterials from the laboratory to a possible commercial product. In broad terms, the key aspects that a new compound or product should possess can be summarised in three words: sustainability, reversibility, and safety by design.^{228,229}

Before starting any *in situ* experiments on real heritage samples, the cyto- and ecotoxicity, and the evolution of the activity after accelerated aging studies should first be determined. One of the disadvantages of some antimicrobial agents is their non-specific activity, meaning that they are not specific to a given microorganism, and could also be highly toxic to other living organisms, including humans. Studying the cytotoxicity of the newly developed compounds, the stability of the coating using climate chamber tests and the release (liberation) of the nanoparticles from the coating to the environment is essential to guarantee the suitability of the compound. The reversibility of the application should be also considered to fit conservation guidelines.²²⁹

In addition to the research results presented in this doctoral thesis, long-term studies on the application of the POM-ILs in exterior environments were initiated in Ulm (Germany) and in Reims (France). In April 2019, sandstones from the Ulm Minster were coated with POM-IL 1 and POM-IL 2 and left on the top of the cathedral to study the protection given by the coating over a three-year period. In parallel, in June 2019, DO, SA, RO, and BB limestone were also coated with POM-IL 1 and POM-IL 2 and kept in outdoor in Reims during a two-year period. We are still analysing the data from this two-year experiment, and the results will be published in due course.

One important consideration is the toxicity of some of the POM-ILs, which is a concern. For our preliminary studies embedding DOTMG-1 in a PMMA matrix to obtain antimicrobial and antibiofilm surfaces, we hypothesise that this could reduce the cytotoxicity of the DOTMG-1. First, four DOTMG-1@PMMA films

hybrids were prepared, based on different POM-IL/PMMA weight ratios: 0/100 (film A), 20/80 (film B), 35/65 (film C), 50/50 (film D). Then, the hybrid DOTMG-1@PMMA films were tested against *E. coli*, *B. subtilis* and *L. monocytogenes*, and after four hours of incubation, the bacteria remaining on the surface was rinsed and sown on solid media. As expected, for the control film (A = 100% PMMA; no DOTMG-1), the bacterial concentration remained constant (at $\sim 10^6$ CFU/mL), and all the films containing DOTMG-1 (B, C, D) displayed a 100% reduction for each of the three bacteria that were assayed. We can conclude that the POM-IL maintained its antimicrobial properties once embedded on the PMMA matrix, but further experiments will be required to confirm if hybrid POM-IL@PMMA films do indeed present lower cytotoxicity than the parent POM-IL.²²⁶

Standardised assays and protocols should be applied to study the antimicrobial properties of the compounds. This is particularly relevant because choosing the wrong antimicrobial assay may result in compounds with biocidal potential to be discarded, for example if the compound does not diffuse into agar (e.g., zone of inhibition assay), or is not soluble on the culture media (e.g., formation of micelles). On the other hand, determining the biocidal ability of a compound is essential, and often, in the literature, only the bacteriostatic or fungistatic action is studied. Applying the wrong compound, or an insufficient concentration of the correct one, to any given surface, could lead to the development of antimicrobial resistance, therefore the concentration, number of applications, type of material and the intensity of microbial growth already present on the heritage surface must be investigated.⁹⁷ The majority of the literature in this area are focused on classical heritage materials such as stone, paper, wood, textile or glass, but it should be noted that new materials classes present in contemporary artwork (mostly plastic polymers, acrylic resins, other organic substrates and varnishes) also require significant attention to prevent their biodeterioration and so appropriate new compounds and materials should be developed.²³⁰ The effect of climate change could worsen the biodeterioration problem and should also be considered. Climate changes alter the structure and function of microbial communities.³⁷ For example, an increase on the breakouts of fungi has been observed due to extremely raining days. Climate change can also indirectly affect the material deterioration due to fluctuation of temperature, rainfall and humidity.^{231–233} Therefore, adaptation of cultural heritage conservation to climate change is necessary to mitigate harmful impacts and to increase its endurance.²³⁴

Perspectives

In summary, a multidisciplinary scientific approach is required to guarantee the preservation of the wide variety of cultural heritage objects and architectures around the world. Such approaches require the collaboration of researchers from the fields of chemistry, microbiology and restoration and conservation. Only by contemplating all these aspects we will be able to protect our heritage without putting it at risk.

8. References

1. Steinbauer, M.J., Gohlke, A., Mahler, C., Schmiedinger, A., and Beierkuhnlein, C. (2013). Quantification of wall surface heterogeneity and its influence on species diversity at medieval castles - implications for the environmentally friendly preservation of cultural heritage. *J. Cult. Herit.* 14, 219–228.
2. Mitchell, R., and Clifford, J. eds. (2018). *Biodeterioration and Preservation in Art, Archaeology and Architecture* (Archetype Publications).
3. Guillitte, O. (1995). Bioreceptivity: a new concept for building ecology studies. *Sci. Total Environ.* 167, 215–220.
4. Hueck, H.J. (1965). The biodeterioration of materials as a part of hylobiology. *Mater. und Org.* 1, 5–34.
5. Allsopp, D., Seal, K.J., and Gaylarde, C.C. (2004). *Introduction To Biodeterioration* (Cambridge university press).
6. Strzelczyk, A.B. (2004). Observations on aesthetic and structural changes induced in Polish historic objects by microorganisms. *Int. Biodeterior. Biodegrad.* 53, 151–156.
7. de la Torre, M.A., Gomez-Alarcon, G., Melgarejo, P., and Saiz-Jimenez, C. (1991). Fungi in weathered sandstone from Salamanca cathedral, Spain. *Sci. Total Environ.* 107, 159–168.
8. Martino, P.D. (2016). What About Biofilms on the Surface of Stone Monuments? *Open Conf. Proc. J.* 7, 14–28.
9. Crispim, C.A., Gaylarde, P.M., and Gaylarde, C.C. (2003). Algal and cyanobacterial biofilms on calcareous historic buildings. *Curr. Microbiol.* 46, 79–82.
10. Gutarowska, B., Skora, J., Zduniak, K., and Rembisz, D. (2012). Analysis of the sensitivity of microorganisms contaminating museums and archives to silver nanoparticles. *Int. Biodeterior. Biodegrad.* 68, 7–17.
11. Piñar, G., Sclocchi, M.C., Pinzari, F., Colaizzi, P., Graf, A., Sebastiani, M.L., and Sterflinger, K. (2020). The Microbiome of Leonardo da Vinci's Drawings: A Bio-Archive of Their History. *Front. Microbiol.* 11, 1–22.
12. Havlena, Z., Kieft, T.L., Veni, G., Horrocks, R.D., and Jones, D.S. (2021). Lighting effects on the development and diversity of photosynthetic biofilm communities in Carlsbad Cavern, New Mexico. *Appl. Environ. Microbiol.* 87, e02695-20.
13. Mulec, J. (2014). Human impact on underground cultural and natural

References

- heritage sites, biological parameters of monitoring and remediation actions for insensitive surfaces: Case of Slovenian show caves. *J. Nat. Conserv.* 22, 132–141.
14. Franco-Castillo, I., Misra, A., Laratte, S., Gommeaux, M., Perarnau, R., Vaillant-Gaveau, N., Pierlot, C., Streb, C., Mitchell, S.G., and Eyssautier-Chuine, S. (2022). New protective coatings against lampenflora growing in the Pommery Champagne cellar. *Int. Biodeterior. Biodegradation*.
 15. Jurado, V., Laiz Trobajo, L., Sánchez Moral, S., and Sáiz-Jiménez, C. (2014). Pathogenic microorganisms related to human visits in Altamira Cave, Spain.
 16. Macedo, M.F., Vilarigues, M.G., and Coutinho, M.L. (2021). Biodeterioration of glass-based historical building materials: An overview of the heritage literature from the 21st century. *Appl. Sci.* 11.
 17. Pinzari, F., Pasquariello, G., and De Mico, A. (2006). Biodeterioration of paper: A SEM study of fungal spoilage reproduced under controlled conditions. *Macromol. Symp.* 238, 57–66.
 18. Sterflinger, K., and Pinzari, F. (2012). The revenge of time: Fungal deterioration of cultural heritage with particular reference to books, paper and parchment. *Environ. Microbiol.* 14, 559–566.
 19. Szczepanowska, H.M., Jha, D., and Mathia, T.G. (2015). Morphology and characterization of Dematiaceous fungi on a cellulose paper substrate using synchrotron X-ray microtomography, scanning electron microscopy and confocal laser scanning microscopy in the context of cultural heritage. *J. Anal. At. Spectrom.* 30, 651–657.
 20. Domingues, F.C., Queiroz, J.A., Cabral, J.M.S., and Fonseca, L.P. (2000). The influence of culture conditions on mycelial structure and cellulase production by *Trichoderma reesei* Rut C-30. *Enzyme Microb. Technol.* 26, 394–401.
 21. P. de Vries, R., and Visser, J. (2001). *Aspergillus* Enzymes Involved in Degradation of Plant Cell Wall Polysaccharides. *Microbiol. Mol. Biol. Rev.* 65, 497–522.
 22. Pinzari, F., and Gutarowska, B. (2021). Extreme colonizers and rapid profiteers: the challenging world of microorganisms that attack paper and parchment. In *Microorganisms in the deterioration and preservation of cultural heritage*, E. Joseph, ed. (Springer Nature), pp. 79–113.
 23. Stokland, J.N., Siitonen, J., and Jonsson, B.G. (2012). *Biodiversity in dead wood* (Cambridge university press).

References

24. Alfieri, P.V., García, R., Rosato, V., and Correa, M.V. (2016). Biodegradation and biodeterioration of wooden heritage: Role of fungal succession. *Int. J. Conserv. Sci.* 7, 607–614.
25. Blanchette, R.A. (1991). Delignification by wood-decay fungi. *Annu. Rev. Phytopathol.* Vol. 29, 381–398.
26. Blyskal, B., Lenart-Borod, A., and Borod, P. (2017). Approaches to taxonomic studies of actinomycetes isolated from historic and contemporary materials. *J Pure Appl Microbiol* 11, 637–648.
27. Florian, M.-L.E. (2007). Protein facts: fibrous proteins in cultural and natural history artifacts.
28. Pinzari, F., Cialei, V., and Piñar, G. (2012). A case study of ancient parchment biodeterioration using variable pressure and high vacuum scanning electron microscopy. *Hist. Technol. Mater. Conserv. SEM Microanal.* Meeks N, Cart. C, Meek A, Mongiatti A (eds). Archetype Publ. Acad. Proj. 1.
29. Pinzari, F., Colaizzi, P., Maggi, O., Persiani, A.M., Schütz, R., and Rabin, I. (2012). Fungal bioleaching of mineral components in a twentieth-century illuminated parchment. *Anal. Bioanal. Chem.* 402, 1541–1550.
30. Pinzari, F. (2018). Microbial processes involved in the deterioration of paper and parchment. *Biodeterior. Preserv. art, Archaeol. Archit.* Archetype Publ. London, 33–56.
31. Rubeziene, V., Varnaite, S., Baltusnikaite, J., and Padleckiene, I. (2012). Effects of light exposure on textile durability. *Underst. Improv. Durab. Text.* Woodhead Publ. Oxford, 104–125.
32. Mazzoli, R., and Pessione, E. (2021). Ancient Textile Deterioration and Restoration: Bio-Cleaning of an Egyptian Shroud Held in the Torino Museum. *Microorg. Deterior. Preserv. Cult. Herit.*, 199–216.
33. Mazzoli, R., Giuffrida, M.G., and Pessione, E. (2018). Back to the past—forever young: cutting-edge biochemical and microbiological tools for cultural heritage conservation. *Appl. Microbiol. Biotechnol.* 102, 6815–6825.
34. Rowe, L., and Howard, G.T. (2002). Growth of *Bacillus subtilis* on polyurethane and the purification and characterization of a polyurethanase-lipase enzyme. *Int. Biodeterior. Biodegradation* 50, 33–40.
35. Gutarowska, B., Pietrzak, K., Machnowski, W., and Milczarek, J.M. (2017). Historical textiles—a review of microbial deterioration analysis and disinfection methods. *Text. Res. J.* 87, 2388–2406.

References

36. Mazzoli, R., Giuffrida, M.G., and Pessione, E. (2018). Back to the past: “find the guilty bug—microorganisms involved in the biodeterioration of archeological and historical artifacts.” *Appl. Microbiol. Biotechnol.* *102*, 6393–6407.
37. Pinna, D. (2021). Microbial Growth and its Effects on Inorganic Heritage Materials. In *Microorganisms in the Deterioration and Preservation of Cultural Heritage*, E. Joseph, ed. (Springer Nature), pp. 3–35.
38. Beech, I.B., and Sunner, J. (2004). Biocorrosion: towards understanding interactions between biofilms and metals. *Curr. Opin. Biotechnol.* *15*, 181–186.
39. Kadukova, J., and Pristas, P. (2018). Biocorrosion—Microbial Action. In *Encyclopedia of interfacial chemistry: surface science and electrochemistry* (Elsevier), pp. 20–22.
40. Gu (2019). Corrosion, microbial. In *Encyclopedia of microbiology*, S. T, ed. (Elsevier), pp. 762–771.
41. Aramendia, J., Gomez-Nubla, L., Bellot-Gurlet, L., Castro, K., Arana, G., and Madariaga, J.M. (2015). Bioimpact on weathering steel surfaces: Oxalates formation and the elucidation of their origin. *Int. Biodeterior. Biodegradation* *104*, 59–66.
42. Zanardini, E., Cappitelli, F., Ranalli, G., and Sorlini, C. (2008). Biodeterioration processes in relation to cultural heritage materials - metals. In *Plant biology for cultural heritage: biodeterioration and conservation*, G. Caneva, M. Nugari, and O. Salvadori, eds. (Getty Publications), pp. 153–156.
43. Kinzler, K., Gehrke, T., Telegdi, J., and Sand, W. (2003). Bioleaching—a result of interfacial processes caused by extracellular polymeric substances (EPS). *Hydrometallurgy* *71*, 83–88.
44. Dai, X., Wang, H., Ju, L.-K., Cheng, G., Cong, H., and Newby, B.Z. (2016). Corrosion of aluminum alloy 2024 caused by *Aspergillus niger*. *Int. Biodeterior. Biodegradation* *115*, 1–10.
45. del Junco, A.S., Moreno, D.A., Ranninger, C., Ortega-Calvo, J.J., and Sáiz-Jiménez, C. (1992). Microbial induced corrosion of metallic antiquities and works of art: a critical review. *Int. Biodeterior. Biodegradation* *29*, 367–375.
46. Salvadori, O., and Municchia, A.C. (2016). The role of fungi and lichens in the biodeterioration of stone monuments. In *The Open Conference Proceedings Journal*, pp. 39–54.
47. Sterflinger, K. (2006). Black yeasts and meristematic fungi: ecology,

References

- diversity and identification. In *Biodiversity and ecophysiology of yeasts* (Springer), pp. 501–514.
48. Selbmann, L., De Hoog, G.S., Mazzaglia, A., Friedmann, E.I., and Onofri, S. (2005). Fungi at the edge of life: cryptoendolithic black fungi from Antarctic desert. *Stud Mycol* 51, 1–32.
 49. Miller, A.Z., Sanmartín, P., Pereira-Pardo, L., Dionísio, A., Saiz-Jimenez, C., Macedo, M.F., and Prieto, B. (2012). Bioreceptivity of building stones: A review. *Sci. Total Environ.* 426, 1–12.
 50. Sterflinger, K. (2010). Fungi: Their role in deterioration of cultural heritage. *Fungal Biol. Rev.* 24, 47–55.
 51. Sterflinger, K. (2000). Fungi as geologic agents. *Geomicrobiol. J.* 17, 97–124.
 52. Scheerer, S., Ortega-Morales, O., and Gaylarde, C. (2009). Microbial deterioration of stone monuments—an updated overview. *Adv. Appl. Microbiol.* 66, 97–139.
 53. Gadd, G.M. (2007). Geomycology: biogeochemical transformations of rocks, minerals, metals and radionuclides by fungi, bioweathering and bioremediation. *Mycol. Res.* 111, 3–49.
 54. Gadd, G.M., Bahri-Esfahani, J., Li, Q., Rhee, Y.J., Wei, Z., Fomina, M., and Liang, X. (2014). Oxalate production by fungi: significance in geomycology, biodeterioration and bioremediation. *Fungal Biol. Rev.* 28, 36–55.
 55. Sterflinger, K., and Piñar, G. (2013). Microbial deterioration of cultural heritage and works of art - Tilting at windmills? *Appl. Microbiol. Biotechnol.* 97, 9637–9646.
 56. Bastian, F., and Alabouvette, C. (2009). Lights and shadows on the conservation of a rock art cave: the case of Lascaux Cave. *Int. J. Speleol.* 38, 55–60.
 57. Diakumaku, E., Gorbushina, A.A., Krumbein, W.E., Panina, L., and Soukharjevski, S. (1995). Black fungi in marble and limestones—an aesthetical, chemical and physical problem for the conservation of monuments. *Sci. Total Environ.* 167, 295–304.
 58. Ghany, T.M.A., Omar, A.M., Elwkeel, F.M., Al Abboud, M.A., and Alawlaqi, M.M. (2019). Fungal deterioration of limestone false-door monument. *Heliyon* 5, e02673.
 59. Lan, W., Li, H., Wang, W.-D., Katayama, Y., and Gu, J.-D. (2010). Microbial community analysis of fresh and old microbial biofilms on Bayon temple sandstone of Angkor Thom, Cambodia. *Microb. Ecol.* 60, 105–115.

References

60. Vítek, P., Ascaso, C., Artieda, O., and Wierzechos, J. (2016). Raman imaging in geomicrobiology: endolithic phototrophic microorganisms in gypsum from the extreme sun irradiation area in the Atacama Desert. *Anal. Bioanal. Chem.* *408*, 4083–4092.
61. Lombardozzi, V., Castrignanò, T., D'antonio, M., Municchia, A.C., and Caneva, G. (2012). An interactive database for an ecological analysis of stone biopitting. *Int. Biodeterior. Biodegradation* *73*, 8–15.
62. Stomeo, F., Portillo, M.C., Gonzalez, J.M., Laiz, L., and Sáiz-Jiménez, C. (2008). Pseudonocardia in white colonizations in two caves with Paleolithic paintings. *Int. Biodeterior. Biodegradation* *62*, 483–486.
63. Portillo, M.C., Saiz-Jimenez, C., and Gonzalez, J.M. (2009). Molecular characterization of total and metabolically active bacterial communities of “white colonizations” in the Altamira Cave, Spain. *Res. Microbiol.* *160*, 41–47.
64. Diaz-Herraz, M., Jurado, V., Cuezva, S., Laiz, L., Pallecchi, P., Tiano, P., Sanchez-Moral, S., and Saiz-Jimenez, C. (2013). The actinobacterial colonization of Etruscan paintings. *Sci. Rep.* *3*, 1–6.
65. Alonso, L., Pommier, T., Kaufmann, B., Dubost, A., Chapulliot, D., Doré, J., Douady, C.J., and Moënné-Loccoz, Y. (2019). Anthropization level of Lascaux Cave microbiome shown by regional-scale comparisons of pristine and anthropized caves. *Mol. Ecol.* *28*, 3383–3394.
66. McNamara, C.J., and Mitchell, R. (2005). Microbial deterioration of historic stone. *Front. Ecol. Environ.* *3*, 445–451.
67. Abdulla, H., May, E., Bahgat, M., and Dewedar, A. (2008). Characterisation of actinomycetes isolated from ancient stone and their potential for deterioration. *Pol J Microbiol* *57*, 213–220.
68. Shaw, A.K., Narayanan, N., and Stanton, D.E. (2021). Let's move out together: a framework for the intersections between movement and mutualism. *Ecology* *102*, e03419.
69. van Bergeijk, D.A., Terlouw, B.R., Medema, M.H., and van Wezel, G.P. (2020). Ecology and genomics of Actinobacteria: new concepts for natural product discovery. *Nat. Rev. Microbiol.* *18*, 546–558.
70. Saiz-Jimenez, C., Cuezva, S., Jurado, V., Fernandez-Cortes, A., Porca, E., Benavente, D., Cañaveras, J.C., and Sanchez-Moral, S. (2011). Paleolithic art in peril: policy and science collide at Altamira Cave. *Science* *334*, 42–43.
71. Unković, N., Erić, S., Šarić, K., Stupar, M., Savković, Stanković, S., Stanojević, O., Dimkić, I., Vukojević, J., and Ljaljević Grbić, M. (2017).

References

- Biogenesis of secondary mycogenic minerals related to wall paintings deterioration process. *Micron* 100, 1–9.
72. Liu, W., Zhou, X., Jin, T., Li, Y., Wu, B., Yu, D., Yu, Z., Su, B., Chen, R., Feng, Y., et al. (2022). Multikingdom interactions govern the microbiome in subterranean cultural heritage sites. *Proc. Natl. Acad. Sci. U. S. A.* 119, 1–9.
73. Rodrigues, A., Gutierrez-Patricio, S., Miller, A.Z., Saiz-Jimenez, C., Wiley, R., Nunes, D., Vilarigues, M., and Macedo, M.F. (2014). Fungal biodeterioration of stained-glass windows. *Int. Biodeterior. Biodegrad.* 90, 152–160.
74. Gaylarde, C.C., and Morton, L.H.G. (1999). Deteriogenic biofilms on buildings and their control: A review. *Biofouling* 14, 59–74.
75. Mesquita, N., Portugal, A., Videira, S., Rodríguez-Echeverría, S., Bandeira, A.M.L., Santos, M.J.A., and Freitas, H. (2009). Fungal diversity in ancient documents. A case study on the Archive of the University of Coimbra. *Int. Biodeterior. Biodegrad.* 63, 626–629.
76. Nielsen, K.F. (2003). Mycotoxin production by indoor molds. *Fungal Genet. Biol.* 39, 103–117.
77. Gutarowska, B., Sulyok, M., and Krska, R. (2010). A study of the toxicity of moulds isolated from dwellings. *Indoor Built Environ.* 19, 668–675.
78. Gutarowska, B., Kosmowska, M., Wiszniewska, M., Pałczyński, C., and Walusiak-Skorupa, J. (2012). An investigation of allergenic proteins produced by moulds on building materials. *Indoor Built Environ.* 21, 253–263.
79. López-Aparicio, S., Smolík, J., Mašková, L., Součková, M., Grøntoft, T., Ondráčková, L., and Stankiewicz, J. (2011). Relationship of indoor and outdoor air pollutants in a naturally ventilated historical building envelope. *Build. Environ.* 46, 1460–1468.
80. Arai, H. (2000). Foxing caused by fungi: Twenty-five years of study. *Int. Biodeterior. Biodegrad.* 46, 181–188.
81. Paulus, W. (2005). *Directory of microbicides for the protection of materials: a handbook* (Springer Science & Business Media).
82. Palla, F., and Barresi, G. (2017). *Biotechnology and conservation of cultural heritage* (Springer).
83. Kakakhel, M.A., Wu, F., Gu, J.-D., Feng, H., Shah, K., and Wang, W. (2019). Controlling biodeterioration of cultural heritage objects with biocides: A review. *Int. Biodeterior. Biodegradation* 143, 104721.

References

84. Puerto, M.S. (2018). El biodeterioro en edificios del patrimonio cultural: Metodología de evaluación de tratamientos biocidas.
85. Caneva, G., Nugari, M.P., Pinna, D., and Salvadori, O. (1996). Il controllo del degrado biologico: i biocidi nel restauro dei materiali lapidei.
86. Favero-Longo, S.E., Benesperi, R., Bertuzzi, S., Bianchi, E., Buffa, G., Giordani, P., Loppi, S., Malaspina, P., Matteucci, E., and Paoli, L. (2017). Species-and site-specific efficacy of commercial biocides and application solvents against lichens. *Int. Biodeterior. Biodegradation* 123, 127–137.
87. Fonseca, A.J., Pina, F., Macedo, M.F., Leal, N., Romanowska-Deskins, A., Laiz, L., Gómez-Bolea, A., and Saiz-Jimenez, C. (2010). Anatase as an alternative application for preventing biodeterioration of mortars: Evaluation and comparison with other biocides. *Int. Biodeterior. Biodegrad.* 64, 388–396.
88. Coutinho, M.L., Miller, A.Z., Martin-Sanchez, P.M., Mirão, J., Gomez-Bolea, A., Machado-Moreira, B., Cerqueira-Alves, L., Jurado, V., Saiz-Jimenez, C., Lima, A., et al. (2016). A multiproxy approach to evaluate biocidal treatments on biodeteriorated majolica glazed tiles. *Environ. Microbiol.* 18, 4794–4816.
89. Blazquez, A.B., Lorenzo, J., Flores, M., and Gomez-Alarcon, G. (2000). Evaluation of the effect of some biocides against organisms isolated from historic monuments. *Aerobiologia* 16, 423–428.
90. Rutala, W.A., and Weber, D.J. (1999). Infection control: The role of disinfection and sterilization. *J. Hosp. Infect.* 43, 43–55.
91. Nugari, M.P., and Salvadori, O. (2017). Biodeterioration control of cultural heritage: Methods and products. In *Molecular biology and cultural heritage* (Routledge), pp. 233–242.
92. Wawrzyk, A., Rybitwa, D., Rahnama, M., and Wilczyński, S. (2020). Microorganisms colonising historical cardboard objects from the Auschwitz-Birkenau State Museum in Oświęcim, Poland and their disinfection with vaporised hydrogen peroxide (VHP). *Int. Biodeterior. Biodegradation* 152, 104997.
93. Arney, J.S., and Pollack, L.B. (1980). The Retention of Organic Solvents in Paper. *J. Am. Inst. Conserv.* 19, 69–74.
94. Sequeira, S.O., Phillips, A.J.L., Cabrita, E.J., and Macedo, M.F. (2017). Ethanol as an antifungal treatment for paper: short-term and long-term effects. *Stud. Conserv.* 62, 33–42.
95. Palla, F., Bruno, M., Mercurio, F., Tantillo, A., and Rotolo, V. (2020).

References

- Essential oils as natural biocides in conservation of cultural heritage. *Molecules* 25, 730.
96. Fidanza, M.R., and Caneva, G. (2019). Natural biocides for the conservation of stone cultural heritage: A review. *J. Cult. Herit.* 38, 271–286.
 97. Franco-Castillo, I., Hierro, L., de la Fuente, J.M., Seral-Ascaso, A., and Mitchell, S.G. (2021). Perspectives for antimicrobial nanomaterials in cultural heritage conservation. *Chem* 7, 629–669.
 98. Cappitelli, F., Cattò, C., and Villa, F. (2020). The control of cultural heritage microbial deterioration. *Microorganisms* 8, 1–20.
 99. Misra, A., Franco-Castillo, I., Müller, D.P., González, C., Eyssautier-Chuine, S., Ziegler, A., de la Fuente, J.M., Mitchell, S.G., and Streb, C. (2018). Polyoxometalate-Ionic Liquids (POM-ILs) as Anticorrosion and Antibacterial Coatings for Natural Stones. *Angew. Chemie Int. Ed.* 57, 14926–14931.
 100. Franco-Castillo, I., Matteis, L. De, Marquina, C., García, E., Martínez de la Fuente, J., and Mitchell, S.G. (2019). Protection of 18th century paper using antimicrobial nano-magnesium oxide. *Int. Biodeterior. Biodegrad.* 141, 79–86.
 101. Franco-Castillo, I., García Guillén, E., M. de la Fuente, J., Silva, F., and Mitchell, S.G. (2019). Preventing fungal growth on heritage paper with antifungal and cellulase inhibiting magnesium oxide nanoparticles. *J. Mater. Chem. B* 7, 6412–6419.
 102. Sattler, K.D. (2016). *Handbook of nanophysics: nanoparticles and quantum dots* (CRC press).
 103. Khan, F.A. (2020). *Biotechnology fundamentals* (CRC Press).
 104. Panyam, J., Dali, M.M., Sahoo, S.K., Ma, W., Chakravarthi, S.S., Amidon, G.L., Levy, R.J., and Labhasetwar, V. (2003). Polymer degradation and in vitro release of a model protein from poly (D, L-lactide-co-glycolide) nano- and microparticles. *J. Control. release* 92, 173–187.
 105. Augustine, R., Hasan, A., Primavera, R., Wilson, R.J., Thakor, A.S., and Kevadiya, B.D. (2020). Cellular uptake and retention of nanoparticles: Insights on particle properties and interaction with cellular components. *Mater. Today Commun.* 25, 101692.
 106. Sierra-Fernandez, A., De La Rosa-García, S.C., Gomez-Villalba, L.S., Gómez-Cornelio, S., Rabanal, M.E., Fort, R., and Quintana, P. (2017). Synthesis, Photocatalytic, and Antifungal Properties of MgO, ZnO and Zn/Mg Oxide Nanoparticles for the Protection of Calcareous Stone

References

- Heritage. *ACS Appl. Mater. Interfaces* 9, 24873–24886.
107. Reyes-Estebanez, M., Ortega-Morales, B.O., Chan-Bacab, M., Granados-Echegoyen, C., Camacho-Chab, J.C., Pereañez-Sacarias, J.E., and Gaylarde, C. (2018). Antimicrobial engineered nanoparticles in the built cultural heritage context and their ecotoxicological impact on animals and plants: A brief review. *Herit. Sci.* 6, 1–11.
 108. Brandi, C., and De Angelis, G. (1972). Carta di Restauro, 1972 (Circolare n° 117 del 6 aprile 1972). Roma, Italy Minist. della Pubblica Istr.
 109. Harandi, D., Ahmadi, H., and Achachluei, M.M. (2016). Comparison of TiO₂ and ZnO nanoparticles for the improvement of consolidated wood with polyvinyl butyral against white rot. *Int. Biodeterior. Biodegradation* 108, 142–148.
 110. De Filipo, G., Palermo, A.M., Munno, R., Molinaro, L., Formoso, P., and Nicoletta, F.P. (2015). Gellan gum/titanium dioxide nanoparticle hybrid hydrogels for the cleaning and disinfection of parchment. *Int. Biodeterior. Biodegradation* 103, 51–58.
 111. Becerra, J., Zaderenko, A.P., Sayagués, M.J., Ortiz, R., and Ortiz, P. (2018). Synergy achieved in silver-TiO₂ nanocomposites for the inhibition of biofouling on limestone. *Build. Environ.* 141, 80–90.
 112. Zarzuela, R., Carbú, M., Gil, M.L.A., Cantoral, J.M., and Mosquera, M.J. (2017). CuO/SiO₂ nanocomposites: a multifunctional coating for application on building stone. *Mater. Des.* 114, 364–372.
 113. He, Y., Ingudam, S., Reed, S., Gehring, A., Strobaugh, T.P., and Irwin, P. (2016). Study on the mechanism of antibacterial action of magnesium oxide nanoparticles against foodborne pathogens. *J. Nanobiotechnology* 14, 54.
 114. Tang, Z.-X., Fang, X.-J., Zhang, Z.-L., Zhou, T., Zhang, X.-Y., and Shi, L.-E. (2012). Nanosize MgO as antibacterial agent: preparation and characteristics. *Brazilian J. Chem. Eng.* 29, 775–781.
 115. Tang, Z.-X., and Lv, B.-F. (2014). MgO nanoparticles as antibacterial agent: preparation and activity. *Brazilian J. Chem. Eng.* 31, 591–601.
 116. Leung, Y.H., Ng, A.M.C., Xu, X., Shen, Z., Gethings, L.A., Wong, M.T., Chan, C.M.N., Guo, M.Y., Ng, Y.H., Djurić, A.B., et al. (2014). Mechanisms of Antibacterial Activity of MgO: Non-ROS Mediated Toxicity of MgO Nanoparticles Towards Escherichia coli. *Small* 10, 1171–1183.
 117. Nguyen, N.Y.T., Grelling, N., Wetteland, C.L., Rosario, R., and Liu, H. (2018). Antimicrobial Activities and Mechanisms of Magnesium Oxide

References

- Nanoparticles (nMgO) against Pathogenic Bacteria, Yeasts, and Biofilms. *Sci. Rep.* 8, 1–23.
118. Ge, S., Wang, G., Shen, Y., Zhang, Q., Jia, D., Wang, H., Dong, Q., and Yin, T. (2011). Cytotoxic effects of MgO nanoparticles on human umbilical vein endothelial cells in vitro. *IET nanobiotechnology* 5, 36–40.
 119. Ghobadian, M., Nabiuni, M., Parivar, K., Fathi, M., and Pazooki, J. (2015). Toxic effects of magnesium oxide nanoparticles on early developmental and larval stages of zebrafish (*Danio rerio*). *Ecotoxicol. Environ. Saf.* 122, 260–267.
 120. Reddy, K.M., Feris, K., Bell, J., Wingett, D.G., Hanley, C., and Punnoose, A. (2007). Selective toxicity of zinc oxide nanoparticles to prokaryotic and eukaryotic systems. *Appl. Phys. Lett.* 90, 213902.
 121. Park, J.-Y., Lee, Y.-J., Jun, K.-W., Baeg, J.-O., and Yim, D.J. (2006). Chemical synthesis and characterization of highly oil dispersed MgO nanoparticles. *J. Ind. Eng. Chem.* 12, 882–887.
 122. Srinivasan, V., Bhavan, P.S., Rajkumar, G., Satgurunathan, T., and Muralisankar, T. (2017). Dietary supplementation of magnesium oxide (MgO) nanoparticles for better survival and growth of the freshwater prawn *Macrobrachium rosenbergii* post-larvae. *Biol. Trace Elem. Res.* 177, 196–208.
 123. Krishnamoorthy, K., Moon, J.Y., Hyun, H.B., Cho, S.K., and Kim, S.J. (2012). Mechanistic investigation on the toxicity of MgO nanoparticles toward cancer cells. *J. Mater. Chem.* 22, 24610–24617.
 124. Baglioni, P., Chelazzi, D., and Giorgi, R. (2015). Deacidification of paper, canvas and wood. In *Nanotechnologies in the Conservation of Cultural Heritage* (Springer), pp. 117–144.
 125. Böhme, N., Anders, M., Reichelt, T., Schuhmann, K., Bridarolli, A., and Chevalier, A. (2020). New treatments for canvas consolidation and conservation. *Herit. Sci.* 8, 1–10.
 126. Darčanova, O., Tamute, M., Beganskiene, A., and Kareiva, A. (2016). Synthesis of magnesium oxide nanoparticles via sol–gel method and hydrolysis and application for paper deacidification treatment. *chemija* 27, 170–178.
 127. Misra, A. (2020). Design and Environmental Applications of Polyoxometalate-Ionic Liquid (POM-IL)-based Molecular and Composite Materials.
 128. Tézé, A., Cadot, E., Bereau, V., and Herve, G. (2001). About the Keggin

References

- Isomers: Crystal Structure of $[N(C_4H_9)_4]_4[\gamma-SiW_{12}O_{40}]$, the γ -Isomer of the Keggin Ion. Synthesis and ^{183}W NMR Characterization of the Mixed γ - $[SiMo_2W_{10}O_{40}]_n$ ($n=4$ or 6). *Inorg. Chem.* **40**, 2000–2004.
129. Coronado, E., Giménez-Saiz, C., Gómez-García, C.J., and Capelli, S.C. (2004). Metallic Conductivity Down to 2 K in a Polyoxometalate-Containing Radical Salt of BEDO-TTF. *Angew. Chemie Int. Ed.* **43**, 3022–3025.
 130. Yamase, T. (1998). Photo-and electrochromism of polyoxometalates and related materials. *Chem. Rev.* **98**, 307–325.
 131. Clemente-Juan, J.M., Coronado, E., and Gaita-Ariño, A. (2012). Magnetic polyoxometalates: from molecular magnetism to molecular spintronics and quantum computing. *Chem. Soc. Rev.* **41**, 7464–7478.
 132. Cao, Z.-J., Zhao, X., He, F.-Q., Zhou, Y., Huang, K., Zheng, A.-M., and Tao, D.-J. (2018). Highly efficient indirect hydration of olefins to alcohols using superacidic polyoxometalate-based ionic hybrids catalysts. *Ind. Eng. Chem. Res.* **57**, 6654–6663.
 133. Liu, Y., Liu, S.-X., Cao, R.-G., Ji, H.-M., Zhang, S.-W., and Ren, Y.-H. (2008). Hydrothermal assembly and luminescence property of lanthanide-containing Anderson polyoxometalates. *J. Solid State Chem.* **181**, 2237–2242.
 134. Harrup, M.K., and Hill, C.L. (1994). Polyoxometalate catalysis of the aerobic oxidation of hydrogen sulfide to sulfur. *Inorg. Chem.* **33**, 5448–5455.
 135. Streb, C. (2012). New trends in polyoxometalate photoredox chemistry: From photosensitisation to water oxidation catalysis. *Dalt. Trans.* **41**, 1651–1659.
 136. Herrmann, S., De Matteis, L., de la Fuente, J.M., Mitchell, S.G., and Streb, C. (2017). Removal of Multiple Contaminants from Water by Polyoxometalate Supported Ionic Liquid Phases (POM-SILPs). *Angew. Chemie Int. Ed.* **56**, 1667–1670.
 137. Herrmann, S., Ritchie, C., and Streb, C. (2015). Polyoxometalate-conductive polymer composites for energy conversion, energy storage and nanostructured sensors. *Dalt. Trans.* **44**, 7092–7104.
 138. Herrmann, S., Kostrzewa, M., Wierschem, A., and Streb, C. (2014). Polyoxometalate Ionic Liquids as Self-Repairing Acid-Resistant Corrosion Protection. *Angew. Chemie Int. Ed.* **53**, 13596–13599.
 139. Rhule, J.T., Hill, C.L., Judd, D.A., and Schinazi, R.F. (1998).

References

- Polyoxometalates in medicine. *Chem. Rev.* 98, 327–358.
140. Li, H., Jia, Y., Wang, A., Cui, W., Ma, H., Feng, X., and Li, J. (2014). Self-Assembly of Hierarchical Nanostructures from Dopamine and Polyoxometalate for Oral Drug Delivery. *Chem. Eur. J.* 20, 499–504.
 141. Rogers, R.D., and Seddon, K.R. (2003). Ionic liquids--solvents of the future? *Science* 302, 792–793.
 142. Welton, T. (2004). Ionic liquids in catalysis. *Coord. Chem. Rev.* 248, 2459–2477.
 143. Van Rantwijk, F., and Sheldon, R.A. (2007). Biocatalysis in ionic liquids. *Chem. Rev.* 107, 2757–2785.
 144. MacFarlane, D.R., Forsyth, M., Howlett, P.C., Pringle, J.M., Sun, J., and Annat, G. (2007). Ionic liquids in electrochemical devices and processes: managing interfacial electrochemistry. *Acc. Chem Res.* 40, 1165–1173.
 145. Zhao, H. (2006). Innovative applications of ionic liquids as “green” engineering liquids. *Chem. Eng. Commun.* 193, 1660–1677.
 146. Ferraz, R., Silva, D., Dias, A.R., Dias, V., Santos, M.M., Pinheiro, L., Prudêncio, C., Noronha, J.P., Petrovski, Ž., and Branco, L.C. (2020). Synthesis and Antibacterial Activity of Ionic Liquids and Organic Salts Based on Penicillin G and Amoxicillin hydrolysate Derivatives against Resistant Bacteria. *Pharmaceutics* 12, 221.
 147. Bijelic, A., Aureliano, M., and Rompel, A. (2018). The antibacterial activity of polyoxometalates: Structures, antibiotic effects and future perspectives. *Chem. Commun.* 54, 1153–1169.
 148. Kubo, A.-L., Kremer, L., Herrmann, S., Mitchell, S.G., Bondarenko, O.M., Kahru, A., and Streb, C. (2017). Antimicrobial Activity of Polyoxometalate Ionic Liquids against Clinically Relevant Pathogens. *Chempluschem* 82, 867–871.
 149. Rajkowska, K., Koziróg, A., Otlewska, A., Piotrowska, M., Atrián-Blasco, E., Franco-Castillo, I., and Mitchell, S.G. (2020). Antifungal Activity of Polyoxometalate-Ionic Liquids on Historical Brick. *Molecules* 25, 5663.
 150. Bondarenko, O., Juganson, K., Ivask, A., Kasemets, K., Mortimer, M., and Kahru, A. (2013). Toxicity of Ag, CuO and ZnO nanoparticles to selected environmentally relevant test organisms and mammalian cells in vitro: a critical review. *Arch. Toxicol.* 87, 1181–1200.
 151. Noeiaghaei, T., Dhami, N., and Mukherjee, A. (2017). Nanoparticles surface treatment on cemented materials for inhibition of bacterial growth. *Constr. Build. Mater.* 150, 880–891.

References

152. Soria-Castro, M., De la Rosa-García, S.C., Quintana, P., Gómez-Cornelio, S., Sierra-Fernandez, A., and Gómez-Ortíz, N. (2019). Broad spectrum antimicrobial activity of $\text{Ca}(\text{Zn}(\text{OH})_3)_2 \cdot 2\text{H}_2\text{O}$ and ZnO nanoparticles synthesized by the sol-gel method. *J. Sol-Gel Sci. Technol.* 89, 284–294.
153. Graziani, L., Quagliarini, E., and D’Orazio, M. (2016). The role of roughness and porosity on the self-cleaning and anti-biofouling efficiency of TiO_2 -Cu and TiO_2 -Ag nanocoatings applied on fired bricks. *Constr. Build. Mater.* 129, 116–124.
154. Gómez-Ortíz, N., De la Rosa-García, S., González-Gómez, W., Soria-Castro, M., Quintana, P., Oskam, G., and Ortega-Morales, B. (2013). Antifungal coatings based on $\text{Ca}(\text{OH})_2$ mixed with ZnO/ TiO_2 nanomaterials for protection of limestone monuments. *ACS Appl. Mater. Interfaces* 5, 1556–1565.
155. Bellissima, F., Bonini, M., Giorgi, R., Baglioni, P., Barresi, G., Mastromei, G., and Perito, B. (2014). Antibacterial activity of silver nanoparticles grafted on stone surface. *Environ. Sci. Pollut. Res.* 21, 13278–13286.
156. Aslanidou, D., and Karapanagiotis, I. (2018). Superhydrophobic, superoleophobic and antimicrobial coatings for the protection of silk textiles. *Coatings* 8, 101.
157. Becerra, J., Mateo, M., Ortiz, P., Nicolas, G., and Zaderenko, A.P. (2019). Evaluation of the applicability of nano-biocide treatments on limestones used in cultural heritage. *J. Cult. Herit.* 38, 126–135.
158. Pietrzak, K., Puchalski, M., Otlewska, A., Wrzosek, H., Guiamet, P., Piotrowska, M., and Gutarowska, B. (2017). Microbial diversity of pre-Columbian archaeological textiles and the effect of silver nanoparticles misting disinfection. *J. Cult. Herit.* 23, 138–147.
159. Roveri, M., Gherardi, F., Goidanich, S., Gulotta, D., Castelvetro, V., Fischer, R., Winandy, L., Weber, J., and Toniolo, L. (2018). Self-cleaning and antifouling nanocomposites for stone protection: properties and performances of stone-nanomaterial systems. In *IOP Conference Series: Materials Science and Engineering* (IOP Publishing), p. 12070.
160. Ditaranto, N., van der Werf, I.D., Picca, R.A., Sportelli, M.C., Giannossa, L.C., Bonerba, E., Tantillo, G., and Sabbatini, L. (2015). Characterization and behaviour of ZnO-based nanocomposites designed for the control of biodeterioration of patrimonial stoneworks. *New J. Chem.* 39, 6836–6843.
161. Helmi, F.M., Ali, N.M., and Ismael, S.M. (2015). Nanomaterials for the inhibition of microbial growth on ancient Egyptian funeral masks. *Mediterr. Archaeol. Archaeom.* 15, 87–95.

References

162. Becerra, J., Ortiz, P., Zaderenko, A.P., and Karapanagiotis, I. (2020). Assessment of nanoparticles/nanocomposites to inhibit micro-algal fouling on limestone façades. *Build. Res. Inf.* 48, 180–190.
163. Ruffolo, S.A., Macchia, A., La Russa, M.F., Mazza, L., Urzì, C., De Leo, F., Barberio, M., and Crisci, G.M. (2013). Marine antifouling for underwater archaeological sites: TiO₂ and Ag-Doped TiO₂. *Int. J. Photoenergy* 2013.
164. Essa, A.M.M., and Khallaf, M.K. (2016). Antimicrobial potential of consolidation polymers loaded with biological copper nanoparticles. *BMC Microbiol.* 16, 1–8.
165. Rodrigues, J.D., and Grossi, A. (2007). Indicators and ratings for the compatibility assessment of conservation actions. *J. Cult. Herit.* 8, 32–43.
166. Van der Werf, I.D., Ditaranto, N., Picca, R.A., Sportelli, M.C., and Sabbatini, L. (2015). Development of a novel conservation treatment of stone monuments with bioactive nanocomposites. *Herit. Sci.* 3, 1–9.
167. Goffredo, G.B., Accoroni, S., Totti, C., Romagnoli, T., Valentini, L., and Munafò, P. (2017). Titanium dioxide based nanotreatments to inhibit microalgal fouling on building stone surfaces. *Build. Environ.* 112, 209–222.
168. Festa, G., Andreani, C., Arcidiacono, L., Grazzi, F., and Senesi, R. (2018). Neutron Diffraction and (n, γ)-based techniques for Cultural Heritage in “Nanotechnologies and Nanomaterials for Diagnostic, Conservation and Restoration of Cultural Heritage”, ed. G. Lazzara and R. Fakhruddin.
169. Possenti, E., Conti, C., Gatta, G.D., Merlini, M., Realini, M., and Colombo, C. (2020). Synchrotron radiation μ X-ray diffraction in transmission geometry for investigating the penetration depth of conservation treatments on cultural heritage stone materials. *Anal. Methods* 12, 1587–1594.
170. Creagh, D. (2007). Synchrotron radiation and its use in art, archaeometry, and cultural heritage studies. In *Physical techniques in the study of art, archaeology and cultural heritage* (Elsevier), pp. 1–95.
171. Cotte, M., Genty-Vincent, A., Janssens, K., and Susini, J. (2018). Applications of synchrotron X-ray nano-probes in the field of cultural heritage. *Comptes Rendus Phys.* 19, 575–588.
172. E-RIHS (European Research Infrastructure for Heritage -Science) <http://www.e-rihs.eu/>.
173. Bokhimi, X., Morales, A., Lopez, T., and Gomez, R. (1995). Crystalline structure of MgO prepared by the sol-gel technique with different hydrolysis catalysts. *J Solid State Chem* 115, 411–415.

References

174. Ginsberg, A.P. (1990). *Inorganic Syntheses*.
175. Weakley, T.J.R., and Malik, S.A. (1967). Heteropolyanions containing two different heteroatoms—I. *J. Inorg. Nucl. Chem.* 29, 2935–2944.
176. Buffet-Bataillon, S., Tattevin, P., Bonnaure-Mallet, M., and Jolivet-Gougeon, A. (2012). Emergence of resistance to antibacterial agents: the role of quaternary ammonium compounds—a critical review. *Int. J. Antimicrob. Agents* 39, 381–389.
177. Herrmann, S., and Streb, C. (2015). New synthetic routes to polyoxometalate containing ionic liquids: an investigation of their properties.
178. Arendrup, M.C., Meletiadis, J., Mouton, J.W., Lagrou, K., Hamal, P., and Guinea, J. (2017). EUCAST antifungal MIC method for moulds. EUCAST Guidel. (E.DEF 9.3.1).
179. Miller, G.L. (1959). Use of Dinitrosalicylic Acid Reagent for Determination of Reducing Sugar. *Anal. Chem.* 31, 426–428.
180. Salehifar, N., Zarghami, Z., and Ramezani, M. (2016). A facile, novel and low-temperature synthesis of MgO nanorods via thermal decomposition using new starting reagent and its photocatalytic activity evaluation. *Mater. Lett.* 167, 226–229.
181. Domingos, R.F., Baalousha, M.A., Ju-Nam, Y., Reid, M.M., Tufenkji, N., Lead, J.R., Leppard, G.G., and Wilkinson, K.J. (2009). Characterizing manufactured nanoparticles in the environment: multimethod determination of particle sizes. *Environ. Sci. Technol.* 43, 7277–7284.
182. Blount, Z.D. (2015). The unexhausted potential of *E. coli*. *Elife* 4, 1–12.
183. Barák, I. (2021). Special issue “*Bacillus subtilis* as a model organism to study basic cell processes.” *Microorganisms* 9, 9–11.
184. Melo, D., Sequeira, S.O., Lopes, J.A., and Macedo, M.F. (2019). Stains versus colourants produced by fungi colonising paper cultural heritage: A review. *J. Cult. Herit.* 35, 161–182.
185. Jorgensen, J., and Turnidge, J. (2015). CLSI, Methods for dilution antimicrobial susceptibility tests for bacteria that grow aerobically. *Man. Clin. microbiol*, 1253–1273.
186. Eveleigh, D.E. (1970). Fungal disfigurement of paper, and soft rot of cedar shingles. *Appl. Microbiol.* 19, 872.
187. Krishnamoorthy, K., Manivannan, G., Kim, S.J., Jeyasubramanian, K., and Premanathan, M. (2012). Antibacterial activity of MgO nanoparticles based

References

- on lipid peroxidation by oxygen vacancy. *J. Nanoparticle Res.* 14.
188. Safaei, M., and Taran, M. (2022). Preparation of Bacterial Cellulose Fungicide Nanocomposite Incorporated with MgO Nanoparticles. *J. Polym. Environ.* 30, 2066–2076.
 189. Mckenney, P.T., Driks, A., and Eichenberger, P. (2013). The *Bacillus subtilis* endospore: Assembly and functions of the multilayered coat. *Nat. Rev. Microbiol.* 11, 33–44.
 190. Baglioni, P., and Giorgi, R. (2006). Soft and hard nanomaterials for restoration and conservation of cultural heritage. *Soft Matter* 2, 293–303.
 191. Poggi, G., Giorgi, R., Toccafondi, N., Katur, V., and Baglioni, P. (2010). Hydroxide nanoparticles for deacidification and concomitant inhibition of iron-gall ink corrosion of paper. *Langmuir* 26, 19084–19090.
 192. Kwiatkowska, A., Wojech, R., and Wojciak, A. (2014). Paper deacidification with the use of magnesium oxide nanoparticles. *Ann. Warsaw Univ. Life Sci. - SGGW. For. Wood Technol.* 85, 144–148.
 193. Huang, J., Liang, G., Lu, G., and Zhang, J. (2018). Conservation of acidic papers using a dispersion of oleic acid-modified MgO nanoparticles in a non-polar solvent. *J. Cult. Herit.* 34, 61–68.
 194. Moreau, C., Vergès-Belmin, V., Leroux, L., Orial, G., Fronteau, G., and Barbin, V. (2008). Water-repellent and biocide treatments: assessment of the potential combinations. *J. Cult. Herit.* 9, 394–400.
 195. Burgos-Cara, A., Ruiz-Agudo, E., and Rodriguez-Navarro, C. (2017). Effectiveness of oxalic acid treatments for the protection of marble surfaces. *Mater. Des.* 115, 82–92.
 196. He, B., Ai, J., Qi, S., Ren, J., Zhao, L., Liu, C., and Fan, H. (2022). Highly stable nano magnesium oxide organic coatings for nondestructive protection of acidic paper documents. *Prog. Org. Coatings* 167, 106833.
 197. Fouda, A., Abdel-Maksoud, G., Abdel-Rahman, M.A., Eid, A.M., Barghoth, M.G., and El-Sadany, M.A.H. (2019). Monitoring the effect of biosynthesized nanoparticles against biodeterioration of cellulose-based materials by *Aspergillus niger*. *Cellulose* 26, 6583–6597.
 198. Zhang, X., Zhang, T., Guo, S., Zhang, Y., Sheng, R., Sun, R., Chen, L., Lv, R., and Qi, Y. (2020). In Vitro Antifungal Activity and Mechanism of Ag3PW12O40 Composites against *Candida* Species. *Molecules* 25, 1–14.
 199. Sabarinathan, C., Karthikeyan, M., Murugappan, R.M., Anthony, S.P., Shankar, B., Parthasarathy, K., and Arumuganathan, T. (2021). Polyoxometalate based ionic crystal: dual applications in selective

References

- colorimetric sensor for hydrated ZnCl₂ and antimicrobial activity. *New J. Chem.* 45, 5576–5588.
200. Zhou, Z., Wei, D., Guan, Y., Zheng, A., and Zhong, J.-J. (2011). Extensive in vitro activity of guanidine hydrochloride polymer analogs against antibiotics-resistant clinically isolated strains. *Mater. Sci. Eng. C* 31, 1836–1843.
201. Vijayakumar, R., Kannan, V.V., Sandle, T., and Manoharan, C. (2012). In vitro antifungal efficacy of biguanides and quaternary ammonium compounds against cleanroom fungal isolates. *PDA J. Pharm. Sci. Technol.* 66, 236–242.
202. Nikaido, H. (2003). Molecular Basis of Bacterial Outer Membrane Permeability Revisited. *Microbiol. Mol. Biol. Rev.* 67, 593–656.
203. Wiener, M.C., and Horanyi, P.S. (2011). How hydrophobic molecules traverse the outer membranes of Gram-negative bacteria. *Proc. Natl. Acad. Sci. U. S. A.* 108, 10929–10930.
204. Koziróg, A., Brycki, B., and Pielech-Przybylska, K. (2018). Impact of cationic and neutral gemini surfactants on conidia and hyphal forms of *Aspergillus brasiliensis*. *Int. J. Mol. Sci.* 19.
205. Albertano, P., and Urzì, C. (1999). Structural interactions among epilithic cyanobacteria and heterotrophic microorganisms in Roman hypogea. *Microb. Ecol.* 38, 244–252.
206. Borderie, F., Alaoui-Sehmer, L., Bousta, F., Alaoui-Sossé, B., and Aleya, L. (2014). Cellular and molecular damage caused by high UV-C irradiation of the cave-harvested green alga *Chlorella minutissima*: implications for cave management. *Int. Biodeterior. Biodegradation* 93, 118–130.
207. Bruno, L., Rugnini, L., Spizzichino, V., Caneve, L., Canini, A., and Ellwood, N.T.W. (2019). Biodeterioration of Roman hypogea: The case study of the Catacombs of SS. Marcellino and Pietro (Rome, Italy). *Ann. Microbiol.* 69, 1023–1032.
208. Nikolić, N., Zarubica, N., Gavrilović, B., Predojević, D., Trbojević, I., Subakov-Simić, G., and Popović, S. (2020). Lampenflora and the entrance biofilm in two show caves: Comparison of microbial community, environmental, and biofilm parameters. *J. Cave Karst Stud.* 82, 69–81.
209. Tomaselli, L., Lamenti, G., and Tiano, P. (2002). Chlorophyll fluorescence for evaluating biocide treatments against phototrophic biodeteriogens. *Ann. Microbiol.* 52, 197–206.
210. Barriuso, B.C., Botticelli, G., Cuzman, O.A., Osticioli, I., Tiano, P., and

References

- Matteini, M. (2017). Conservation of calcareous stone monuments: Screening different diammonium phosphate based formulations for countering phototrophic colonization. *J. Cult. Herit.* 27, 97–106.
211. Urzì, C., De Leo, F., Krakova, L., Pangallo, D., and Bruno, L. (2016). Effects of biocide treatments on the biofilm community in Domitilla's catacombs in Rome. *Sci. Total Environ.* 572, 252–262.
212. Favero-Longo, S.E., Brigadeci, F., Segimiro, A., Voyron, S., Cardinali, M., Girlanda, M., and Piervittori, R. (2018). Biocide efficacy and consolidant effect on the mycoflora of historical stuccos in indoor environment. *J. Cult. Herit.* 34, 33–42.
213. Li, T., Hu, Y., and Zhang, B. (2020). Evaluation of efficiency of six biocides against microorganisms commonly found on Feilaifeng Limestone, China. *J. Cult. Herit.* 43, 45–50.
214. Rugnini, L., Migliore, G., Tasso, F., Ellwood, N.T.W., Sprocati, A.R., and Bruno, L. (2020). Biocidal activity of phyto-derivative products used on phototrophic biofilms growing on stone surfaces of the domus Aurea in Rome (Italy). *Appl. Sci.* 10, 6584.
215. Nugari, M.P., Pietrini, A.M., Caneva, G., Imperi, F., and Visca, P. (2009). Biodeterioration of mural paintings in a rocky habitat: The Crypt of the Original Sin (Matera, Italy). *Int. Biodeterior. Biodegradation* 63, 705–711.
216. De los Ríos, A., Pérez-Ortega, S., Wierzechos, J., and Ascaso, C. (2012). Differential effects of biocide treatments on saxicolous communities: Case study of the Segovia cathedral cloister (Spain). *Int. Biodeterior. Biodegradation* 67, 64–72.
217. Pfendler, S., Borderie, F., Bousta, F., Alaoui-Sosse, L., Alaoui-Sosse, B., and Aleya, L. (2018). Comparison of biocides, allelopathic substances and UV-C as treatments for biofilm proliferation on heritage monuments. *J. Cult. Herit.* 33, 117–124.
218. Petkovic, M., Hartmann, D.O., Adamová, G., Seddon, K.R., Rebelo, L.P.N., and Pereira, C.S. (2012). Unravelling the mechanism of toxicity of alkyltributylphosphonium chlorides in *Aspergillus nidulans* conidia. *New J. Chem.* 36, 56–63.
219. Yoo, B., Shah, J.K., Zhu, Y., and Maginn, E.J. (2014). Amphiphilic interactions of ionic liquids with lipid biomembranes: a molecular simulation study. *Soft Matter* 10, 8641–8651.
220. Egorova, K.S., Gordeev, E.G., and Ananikov, V.P. (2017). Biological activity of ionic liquids and their application in pharmaceuticals and medicine. *Chem. Rev.* 117, 7132–7189.

References

221. Koziróg, A., Otlewska, A., Gapinska, M., and Michlewska, S. (2019). Influence of gemini surfactants on biochemical profile and ultrastructure of *Aspergillus brasiliensis*. *Appl. Sci.* 9, 245.
222. Inoue, M., Suzuki, T., Fujita, Y., Oda, M., Matsumoto, N., and Yamase, T. (2006). Enhancement of antibacterial activity of β -lactam antibiotics by [P₂W₁₈O₆₂]⁶⁻, [SiMo₁₂O₄₀]⁴⁻, and [PTi₂W₁₀O₄₀]⁷⁻ against methicillin-resistant and vancomycin-resistant *Staphylococcus aureus*. *J. Inorg. Biochem.* 100, 1225–1233.
223. Saraiva, A.M., Castro, R.H.A., Cordeiro, R.P., Peixoto Sobrinho, T.J.S., Castro, V.T.N.A., Amorim, E.L.C., Xavier, H.S., and Pisciotto, M.N.C. (2011). In vitro evaluation of antioxidant, antimicrobial and toxicity properties of extracts of *schinopsis brasiliensis* engl. (Anacardiaceae). *African J. Pharm. Pharmacol.* 5, 1724–1731.
224. Silva, A.C.O., Santana, E.F., Saraiva, A.M., Coutinho, F.N., Castro, R.H.A., Pisciotto, M.N.C., Amorim, E.L.C., and Albuquerque, U.P. (2013). Which approach is more effective in the selection of plants with antimicrobial activity? Evidence-based Complement. Altern. Med. 2013.
225. Ebbensgaard, A., Mordhorst, H., Overgaard, M.T., Nielsen, C.G., Aarestrup, F.M., and Hansen, E.B. (2015). Comparative evaluation of the antimicrobial activity of different antimicrobial peptides against a range of pathogenic Bacteria. *PLoS One* 10, 1–18.
226. Enderle, A.G., Franco-Castillo, I., Atrián-Blasco, E., Martín-Rapún, R., Lizarraga, L., Culzoni, M.J., Bollini, M., De La Fuente, J.M., Silva, F., Streb, C., et al. (2022). Hybrid Antimicrobial Films Containing a Polyoxometalate-Ionic Liquid. *ACS Appl. Polym. Mater.* 4, 4144–4153.
227. Sierra-Fernández, A., Gómez Villalba, L.S., Rabanal, M.E., and Fort González, R. (2017). New nanomaterials for applications in conservation and restoration of stony materials: A review. *Mater. construcción* 67, 107.
228. Feilden, B., and Jokilehto, J. (1998). Treatments and Authenticity.
229. Confederation, E., and Principles, G. (2003). E . C . C . O . Professional Guidelines (II).
230. Cappitelli, F., and Sorlini, C. (2008). Microorganisms attack synthetic polymers in items representing our cultural heritage. *Appl. Environ. Microbiol.* 74, 564–569.
231. Brimblecombe, P., and Grossi, C.M. (2007). Damage to buildings from future climate and pollution. *APT Bull. J. Preserv. Technol.* 38, 13–18.
232. Grossi, C.M., Brimblecombe, P., Esbert, R.M., and Alonso, F.J. (2007). Color

References

- changes in architectural limestones from pollution and cleaning. *Color Res. Appl.* Endorsed by Inter-Society Color Council. Colour Gr. (Great Britain), Can. Soc. Color. Color Sci. Assoc. Japan, Dutch Soc. Study Color. Swedish Colour Cent. Found. Colour Soc. Aust. Cent. Français la Coul. 32, 320–331.
233. Duthie, L., Hyslop, E., Kennedy, C.J., Phoenix, V., and Lee, M. (2008). Quantitative assessment of decay mechanisms in Scottish building sandstones. In 11th International Congress on Deterioration and Conservation of Stone (Nicolaus Copernicus University), pp. 73–80.
234. Sesana, E., Gagnon, A.S., Bertolin, C., and Hughes, J. (2018). Adapting cultural heritage to climate change risks: Perspectives of cultural heritage experts in Europe. *Geosci.* 8, 1–23.

Appendix

Appendix 1: Impact factor and Thematic Area of the journals

Article 1

Title: Perspectives for antimicrobial nanomaterials in cultural heritage conservation

Authors: Isabel Franco-Castillo, Lara Hierro, Jesús M. de la Fuente, Andrés Seral-Ascaso* and Scott G. Mitchell*

Year: 2021

Journal: Chem

Thematic Area: Chemistry, Multidisciplinary (9/178)

Impact Factor: 22.804

Quartile: Q1

Database: JCR

Article 2

Title: Protection of 18th century paper using antimicrobial nano-magnesium oxide

Authors: Isabel Franco Castillo,¹ Laura De Matteis*¹, Clara Marquina, Esther García Guillén, Jesús Martínez de la Fuente, Scott G. Mitchell**

¹: These authors contributed equally

Year: 2019

Journal: International Biodeterioration & Biodegradation

Thematic Area: Biotechnology & Applied Microbiology (36/156)

Impact Factor: 4.074

Quartile: Q1

Database: JCR

Article 3

Title: Preventing fungal growth on heritage paper with antifungal and cellulase inhibiting magnesium oxide nanoparticles

Authors: Isabel Franco Castillo, Esther García Guillén, Jesús M. de la Fuente, Filomena Silva* and Scott G. Mitchell*

Year: 2019

Journal: Journal of Materials Chemistry B

Thematic Area: Materials Science, Biomaterials (9/38)

Impact Factor: 5.344

Quartile: Q1

Database: JCR

Article 4

Title: Hybrid Antimicrobial Films Containing a Polyoxometalate-Ionic Liquid

Authors: Isabel Franco-Castillo,¹ Ana G. Enderle,¹ Elena Atrián-Blasco, Rafael Martín-Rapún, Leonardo Lizarraga, María J. Culzoni, Mariela Bollini, Jesús M. de la Fuente, Filomena Silva, Carsten Streb* and Scott G. Mitchell*

¹: These authors contributed equally

Years: 2022

Journal: ACS Applied Polymer Materials

Thematic Area: Polymer Science (22/90)

Impact Factor: 4.089

Quartile: Q1

Database: JCR

Article 5

Title: New protective coatings against lampenflora growing in the Pommery Champagne cellar

Authors: Isabel Franco-Castillo, Archismita Misra, Sébastien Laratte, Maxime Gommeaux, Robin Perarnau, Nathalie Vaillant-Gaveau, Clément Pierlot, Carsten Streb, Scott G. Mitchell* and Stéphanie Eyssautier-Chuine*

Years: 2022

Journal: International Biodeterioration & Biodegradation

Thematic Area: Biotechnology & Applied Microbiology (49/159)

Impact Factor: 4.320

Quartile: Q2

Database: JCR

Article 6

Title: Antifungal Activity of Polyoxometalate-Ionic Liquids on Historical Brick

Authors: Katarzyna Rajkowska*, Anna Koziróg, Anna Otlewska, Małgorzata Piotrowska, Elena Atrián-Blasco, Isabel Franco-Castillo and Scott G. Mitchell*

Years: 2020

Journal: Molecules

Thematic Area: Chemistry, Multidisciplinary (63/178)

Impact Factor: 4.412

Quartile: Q2

Database: JCR

Appendix 2: Doctoral student's contribution

Article 1: I. Franco-Castillo, L. Hierro, J. M. de la Fuente, A. Seral-Ascaso, S. G. Mitchell. "Perspectives for antimicrobial nanomaterials in cultural heritage conservation". *Chem*, **2021**, 7(3), 629-669.

The contribution of doctoral student Isabel Franco Castillo in "Article 1" was the collaboration in the initial approach of the work and the writing of the review, especially the parts which involve the biochemical techniques, the microorganisms causing biodeterioration, and use of magnesium oxide nanoparticles (MgO NPs) and polyoxometalate-ionic liquids (POM-ILs) in heritage.

Article 2: I. Franco-Castillo, L. De Matteis, C. Marquina, E. G. Guillén, J. M. de la Fuente, S. G. Mitchell. "Protection of 18th century paper using antimicrobial nano-magnesium oxide". *International Biodeterioration & Biodegradation*, **2019**, 141, 79-86.

The contribution of the doctoral student in "Article 2" was the collaboration in the approach and the accomplishment of the antimicrobial experiments to study the bactericidal activity of the MgO NPs and their ability to be applied as a protective coating on heritage paper. The specific experiments carried out by the doctoral student were: Bacterial cell proliferation assay in presence of MgO nanoparticles, Resazurin cell viability assay, Live/Dead Assay, Antimicrobial assays on paper samples and Environmental scanning electron microscopy (ESEM) analyses. The author also contributed to the writing and revision of the paper.

Article 3: I. Franco-Castillo, E. G. Guillén, J. M. de la Fuente, F. Silva, Mitchell, S. G. "Preventing fungal growth on heritage paper with antifungal and cellulase inhibiting magnesium oxide nanoparticles". *Journal of Materials Chemistry B*, **2019**, 7(41), 6412-6419.

The contribution of the doctoral student in "Article 3" was the collaboration in the initial approach of the work and the accomplishment of the experiments: the synthesis of the MgO NPs, the use of the MgO NPs as antifungal compound on *in vitro* assays, the application of the nanoparticles on heritage paper to prevent

fungus colonisation and the study of the anticellulase activity to prevent paper degradation, the study of the MgO NPs coating by Environmental scanning electron microscopy (ESEM) and Inductively Coupled Plasma Mass Spectrometry (ICP-MS), and the colour change produced, studied with a Chroma Meter. The author also contributed to the writing and revision of the paper.

Article 4: I. Franco-Castillo, A. G. Enderle, E. Atrián-Blasco, R. Martín-Rapún, L. Lizarraga, M. J. Culzoni, M. Bollini, J. M. de la Fuente, F. Silva, C. Streb, S. G. Mitchell. "Hybrid Antimicrobial Films Containing a Polyoxometalate-Ionic Liquid" *ACS Applied Polymer Materials*, **2022**, 4, 4144–4153.

The contribution of the doctoral student in "Article 4" was the collaboration in the design and perform of the antimicrobial assays to establish the biocidal activity of the POM-IL DOTMG-1: Bacterial cell viability assay, Surface antimicrobial activity of DOTMG-1, TEM (Transmission electron microscopy) Analysis of the bacteria incubated with DOTMG-1, ESEM (Environmental scanning electron microscopy) visualization of the moulds incubated with DOTMG-1, Biological Performance of the DOTMG-1@PMMA Films. The author also contributed to the writing and revision of the paper.

Article 5: I. Franco-Castillo, A. Misra, S. Laratte, M. Gommeaux, R. Perarnau, N. Vaillant-Gaveau, C. Pierlot, C. Streb, S. G. Mitchell, S. Eyssautier-Chuine. "New protective coatings against lampenflora growing in the Pommery Champagne cellar". *International Biodeterioration & Biodegradation*, **2022**.

The contribution of the doctoral student in "Article 5" was the synthesis of POM-IL 1 and POM-IL 2, and collaboration in the writing and revision of the paper.

Article 6: K. Rajkowska, A. Koziróg, A. Otlewska, M. Piotrowska, E. Atrián-Blasco, I. Franco-Castillo, S. G. Mitchell. "Antifungal activity of polyoxometalate-ionic liquids on historical brick". *Molecules*, **2020**, 25(23), 5663.

Appendix

The contribution of the doctoral student in “Article 6” was the analysis of the POM-ILs disinfectant effect by Environmental Scanning Electron Microscopy (ESEM) and collaboration in the writing and revision of the paper.

Appendix 3: Polyoxometalate-Ionic Liquids (POM-ILs) as Anticorrosion and Antibacterial Coatings for Natural Stones



Protective Coatings

 International Edition: DOI: 10.1002/anie.201809893
 German Edition: DOI: 10.1002/ange.201809893


Polyoxometalate-Ionic Liquids (POM-ILs) as Anticorrosion and Antibacterial Coatings for Natural Stones

 Archismita Misra[†], Isabel Franco Castillo[†], Daniel P. Müller, Carolina González, Stéphanie Eyssautier-Chuine, Andreas Ziegler, Jesús M. de la Fuente, Scott G. Mitchell,^{*} and Carsten Streb^{*}

Dedicated to Professor Bernd Krebs (Münster) on the occasion of his 80th birthday

Abstract: Corrosion of stone by acid rain and deterioration from biofilms are global problems for industrial and residential buildings as well as cultural heritage, such as statues or historic buildings. Herein we show how typical building stones can be protected from corrosion ("weathering") and biofilm formation ("biodegradation") by application of thin films of polyoxometalate-based ionic liquids (POM-ILs). Stone samples are coated with hydrophobic, acid resistant POM-ILs featuring biocidal properties. Exposure of the samples to simulated acid rain showed negligible corrosion compared to the significant deterioration of unprotected samples; in addition the biocidal properties of the POM-ILs suppress the formation of biofilms on coated stone slabs. A new class of modular molecular materials for protecting stones can now be developed for use in construction, environmental protection, and cultural heritage preservation.

The corrosion of stones used in building construction is a major global issue, particularly when considering the loss of cultural heritage objects, such as stone statues or ancient buildings.^[1,2] Stone corrosion can be caused by thermal and

mechanical stress (physical weathering) as well as chemical factors (chemical weathering). In this respect, acid corrosion is a major contributor and can be primarily attributed to "acid rain" based on industrial pollutants (SO_x, NO_x emissions).^[3] In addition, aesthetic changes along with physical and chemical deterioration arising from microbial colonization also plague the conservation of stone materials.^[4] Stone biodegradation occurs predominantly by formation of biofilms, which discolour the stone surface and alter the stone porosity.^[5] Exposure of stone artefacts to outdoor environments results in the need for continuous maintenance and the use of water-repelling agents as well as biocidal products to inhibit further biofilm growth. To overcome this challenge, protective coatings have been developed which either act as water repellents to prevent aqueous acid corrosion (e.g. alkoxysilanes, fluoropolymers) or as biocides to prevent biofilm formation on the stone surface.^[6] Over recent years, metal oxide nanoparticles have received increased attention as antimicrobial agents,^[6,7] as they feature higher environmental stability than organic antimicrobial agents and act against a broad range of microorganisms, reducing the development of antimicrobial resistance.^[8]

Recently, ionic liquids (ILs, that is, salts with a melting point < 100 °C)^[9] have been proposed as anti-corrosive agents^[10] owing to their remarkable performance in corrosion protection by lubrication and coating formation.^[11] ILs offer the advantage of a modular design in which cation and anion can be independently tuned, thereby enabling the formation of multifunctional materials suitable for surface coatings.

In the field of surface-active IL coatings, polyoxometalate-ionic liquids (POM-ILs) have recently received significant interest, owing to their outstanding chemical versatility and reactivity.^[12] In POM-ILs, molecular metal oxide anions (polyoxometalates, POMs)^[13] are combined with bulky organic cations (e.g. organic ammonium^[14] or phosphonium^[15] cations), often resulting in room-temperature ionic liquids.^[12] The physical, rheological and chemical properties of POM-ILs can be tuned by chemical design, so that applications in thermo-regulated epoxidation catalysis,^[16] large-scale petrochemical desulfurization,^[17] light-driven water oxidation^[18] and other technology areas have become possible.^[12] Recently, it was shown that room-temperature POM-ILs, such as ((n-C₇H₁₅)₄N)₆[α-SiW₁₁O₃₉Cu(H₂O)] are effective coatings, which prevent acid corrosion of metals.^[19] Significantly improved performance was observed compared with

^[*] M. Sc. A. Misra,^[†] M. Sc. D. P. Müller, Prof. Dr. C. Streb
 Institute of Inorganic Chemistry I
 Ulm University
 Albert-Einstein-Allee 11, 89081 Ulm (Germany)
 E-mail: carsten.streb@uni-ulm.de
 Homepage: <http://www.strebgroup.net>
 M. Sc. I. Franco Castillo,^[†] M. Sc. C. González, Dr. J. M. de la Fuente,
 Dr. S. G. Mitchell
 Instituto de Ciencia de Materiales de Aragón (ICMA-CSIC) and
 CIBER-BBN, CISC-Universidad de Zaragoza
 50019 Zaragoza (Spain)
 E-mail: scott@unizar.es
 Dr. S. Eyssautier-Chuine
 Groupe d'Etude sur les Géomatériaux et les environnements
 Naturels Anthropiques et Archéologiques (GEGENAA), Université de
 Reims Champagne-Ardenne, Centre de Recherches en Environnement
 et Agronomie
 51100 Reims (France)
 Priv.-Doz. Dr. A. Ziegler
 Central Unit Electron Microscopy, Ulm University
 Albert-Einstein-Allee 11, 89081 Ulm (Germany)

^[†] These authors contributed equally to this work.

Supporting information and the ORCID identification number(s) for the author(s) of this article can be found under:
<https://doi.org/10.1002/anie.201809893>.

commercial ILs (e.g. [hmim]Br) and with solid POM coatings (e.g. $((n\text{-C}_7\text{H}_{15})_4\text{N})_6[\alpha\text{-SiW}_{11}\text{O}_{39}\text{Cu}(\text{H}_2\text{O})]$), highlighting the unique properties of POM-ILs. Further, immobilization of POM-ILs based on antimicrobial alkylammonium cations^[20] and metal-binding POM anions on porous silica led to POM-SILPs (POM-supported ionic liquid phases) capable of removing organic, inorganic, and biological contaminants from water by simple filtration.^[21]

Herein, we explored the development of water-repellent, acid-stable POM-ILs featuring biocidal activity as multifunctional corrosion protection coatings for natural carbonate stones typically used in construction. Our study shows that the combination of long-chain quaternary alkylammonium cations with acid-stable polyoxotungstate anions can be used to access room-temperature POM-ILs which have facile application and high surface adhesion on porous and non-porous stone surfaces combined with high water repellency, acid stability and biocidal activity. Significantly increased corrosion-resistance is demonstrated when the treated materials are placed under harsh chemical conditions and exposed to typical biofilm-forming microbes, so that novel POM-IL based acid- and bio-corrosion protection now is possible.

We used an established cation metathesis route^[19–21] to combine the acid-stable polytungstate anion $[\alpha\text{-SiW}_{11}\text{O}_{39}]^{8-}$ ^[25] with two antimicrobial quaternary alkylammonium cations^[26] tetraheptylammonium ($= (n\text{-C}_7\text{H}_{15})_4\text{N}^+$) and trihexyl tetradecyl ammonium ($= (n\text{-C}_6\text{H}_{13})_3(\text{C}_{14}\text{H}_{29})\text{N}^+$), to give the respective POM-ILs **1** and **2** (Figure 1 and Table 1). The composition and purity of both compounds

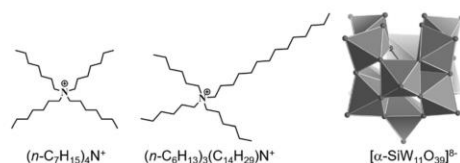


Figure 1. Illustration of the cations and anion used as components for POM-ILs **1** and **2**.

was verified by elemental analyses and FT-IR spectroscopy, see Supporting Information. Note that both compounds are room temperature ILs, they are insoluble in water but show high solubility in a wide range of polar and unipolar organic solvents. In addition, the hydrophilicity/hydrophobicity of the POM-ILs was assessed by the sessile drop method, giving values of 53.9° for **1** and 41.1° for **2** (also see Supporting Information). To assess the POM-IL performance as acid corrosion protection coatings, three typical limestone samples

Table 1: Composition and properties of the POM-ILs **1** and **2**.

POM-IL	POM-IL formula	Contact angle [°] ^[a]
1 ^[a]	$((n\text{-C}_7\text{H}_{15})_4\text{N})_8[\alpha\text{-SiW}_{11}\text{O}_{39}]$	53.9
2 ^[a]	$((n\text{-C}_6\text{H}_{13})_3(\text{C}_{14}\text{H}_{29})\text{N})_8[\alpha\text{-SiW}_{11}\text{O}_{39}]$	41.1

[a] Room-temperature ionic liquids. [b] Measured by sessile drop method, see Supporting Information.

used in the Northern part of France and in Belgium were selected. The stone samples varied in chemical composition and porosity (see Table 2).

Table 2: Three types of natural building stones used as test samples.

ID	Stone type	Chemical composition (wt%)					Porosity [%]
		CaCO ₃	SiO ₂	Al ₂ O ₃	Fe ₂ O ₃	MgO	
BB ^[22]	Belgian Blue	98.2	—	—	0.4	—	ca. 0.3
RO ^[23]	Romery	81.1	17.0	0.2	1.0	0.5	ca. 5
DO ^[24]	Dom	96.3	1.1	0.5	1.4	0.4	ca. 30

First, we examined the acid corrosion protection properties of the POM-ILs **1** and **2**. To this end, cubic samples of the stones (dimensions: $1.0 \times 1.0 \times 1.0 \text{ cm}^3$, geometric surface area: 6 cm^2) were brush-coated with a concentrated acetone solution of the respective POM-IL ($[\text{POM-IL}] = 200 \text{ mg mL}^{-1}$), giving a POM-IL loading of about 17 mg cm^{-2} or 100 mg per sample (see Supporting Information for details). Initial coating studies showed that brush coating resulted in homogeneous surface coverage whereas other methods (dip-coating, spray-coating) displayed less homogeneous POM-IL distribution.

Stone corrosion by acid vapor was then explored by exposing the samples (as well as uncoated references) to acetic acid vapor inside a closed glass vial for 72 h. Acetic acid was selected as a model corrosive agent with environmental relevance.^[27] After exposure, the stones were rinsed with water and acetone (to remove the POM-IL), oven-dried (120°C , 1 h) and the weight loss of each sample was determined. Visual inspection of the stones (Figure 2) shows that the coated samples retain the original shape, smooth surface and sharp edges of the original sample. In contrast, the uncoated references are significantly corroded, leading to notable surface damage and visible “weathering”. Strikingly, the highly porous, acid-sensitive Dom stone showed complete structural disintegration after acid vapor exposure when washed with water (also see Supporting Information video). In contrast, the Dom samples coated with **1** or **2** both show only minor corrosion and structural integrity of the stone samples is retained (Figure 2). When analysing the weight losses observed for the acid vapor tests (Table 3), both POM-ILs show significant corrosion protection compared to non-coated samples. When comparing both POM-ILs, **1** shows slightly higher corrosion protection (i.e. lower weight losses) compared with **2**, highlighting that chemical tuning of the POM-IL performance by cation modification is possible. Notably, comparative experiments using 50 % POM-IL loading (i.e. ca. 50 mg POM-IL coating per sample) showed only small increases in the amount of corrosion observed. This emphasizes that tuning of film thickness and coating procedure can be used to achieve high acid corrosion resistance even at low POM-IL loading (Table 3).

Next, we examined the integrity of the POM-IL coatings by exposing the coated stones to simulated acid rain. To this end, the samples were sprayed continuously with aqueous acetic acid (20 wt %) for 3 h at a flow rate of approximately

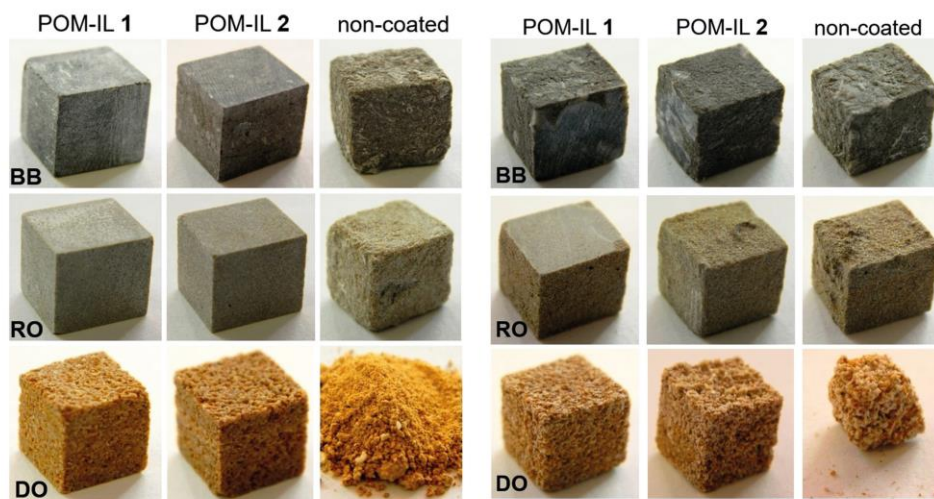


Figure 2. Acid-vapour corrosion protection of POM-IL-coated stone samples, studied by exposing the samples to acetic acid vapour for 72 h; for weight losses see Table 3. RO: Romerly stone; BB: Belgian Bluestone; DO: Dom stone.

Figure 3. Acid-rain corrosion protection of POM-IL coated stone samples. Conditions: simulated acid rain: aqueous acetic acid (20 wt%), flow rate 60 mL min⁻¹ per sample, exposure time: 3 h, for weight losses see Table 3. RO: Romerly stone; BB: Belgian Bluestone; DO: Dom stone.

60 mL min⁻¹, see Supporting Information. After the acid rain treatment, the samples were recovered, rinsed with water and acetone, oven-dried (120 °C for 1 h) and the weight loss was determined, see Figure 3 and Table 3. The acid rain tests show corrosion protection effects similar to the vapor chamber study, while the corrosion observed is overall higher owing to the harsh mechanical and chemical treatment: both POM-ILs result in significantly reduced acid corrosion. As described above, we note slightly higher corrosion protection (i.e. lower weight loss) for POM-IL 1 compared with POM-IL 2. The acid rain simulator study further highlights the POM-IL coating durability, enabling the coating to retain its structural integrity even under harsh spraying conditions.

Biofilms on stones are typically formed by groups of microorganisms bound in an extracellular biopolymer matrix,^[28] and both Gram-negative and -positive bacteria

are common in biofilms.^[29] In particular, spore-forming bacteria of the *Bacillus* and *Bacillus*-related genera have been frequently identified on monumental stones, which is perhaps unsurprising since they are commonly found in soil, and their spore-forming ability enables them to withstand extreme environments.^[30] The biodegradation activity of this genera is caused by the production of organic acids and surfactants^[31] and, moreover, examples of white fuzzy biofilm layers in deteriorated caves and catacombs indicate that they may actively participate in the precipitation of mineral phases.^[32]

To assess the bactericidal activity of POM-ILs 1 and 2, we used a combination of in vitro cell proliferation assays and colorimetric cell viability assays to quantify bacterial growth over an incubation period of 24 h. As bacterial models, we used Gram-positive *Bacillus subtilis* (*B. subtilis*) and Gram-negative *Escherichia coli* (*E. coli*). Both POM-IL 1 and 2 showed potent bactericidal activity against sporulating *B. subtilis* at concentrations of 0.5 µg mL⁻¹ and 5 µg mL⁻¹, respectively (Figures S5, S6). The bactericidal concentration of POM-IL 1 and 2 against more resistant *E. coli* was 50 µg mL⁻¹ and 500 µg mL⁻¹, respectively. In summary, POM-IL 1 was the most potent variant in vitro and *B. subtilis* was more susceptible to the

Table 3: Acid corrosion protection data for POM-ILs 1 and 2.

Stone type	Coating ^[a]	Weight loss [wt %]		Acid-rain test
		ca. 50 mg POM-IL/sample	ca. 100 mg POM-IL/sample	
BB	–	10.1 ± 0.2	10.1 ± 0.2	28.0 ± 0.4
BB	POM-IL 1	0.1 ± 0.1	0.0 ± 0.0	7.0 ± 0.5
BB	POM-IL 2	0.6 ± 0.1	0.4 ± 0.1	10.6 ± 0.4
RO	–	6.2 ± 0.2	6.2 ± 0.2	32.1 ± 0.6
RO	POM-IL 1	0.1 ± 0.1	0.1 ± 0.1	5.9 ± 0.4
RO	POM-IL 2	0.4 ± 0.1	0.3 ± 0.1	7.6 ± 0.4
DO	–	Complete breakdown	Complete breakdown	84.4 ± 0.4
DO	POM-IL 1	1.4 ± 0.06	0.4 ± 0.04	13.5 ± 0.4
DO	POM-IL 2	8.7 ± 0.3	3.4 ± 0.1	18.5 ± 0.4

[a] for details on coating procedure, see Supporting Information.

POM-ILs (see Supporting Information for further details).

We assessed the performance of both POM-ILs in preventing biofilm formation in situ on BB, RO, and DO stones. *E. coli* was chosen as a model organism, as it represents a more resistant bacterium and is also more effective at generating a biofilm in laboratory conditions. The surface biocidal activity of the POM-ILs on stone surfaces was quantified using a modified Japanese Industrial Standard (JIS).^[33] JIS Z 2801 standard analysis showed that POM-IL 1 was more effective at reducing cell viability than the POM-IL 2, reaching up to 100 % of bacterial reduction in the BB stone (Table 4). In addition, a TBX agar method was used to

and RO stones samples (Figure S7). Note that no colony forming was observed in DO stone, even after longer growth period, since bacteria embed themselves within the highly accessible pores. Moreover, water is quickly absorbed and evaporated by porous stone, resulting in less available nutrients for bacterial growth, which means that the absence of short-term bacterial proliferation in this study could therefore be due to a number of factors.

These antibacterial assays illustrate the potent biocidal and biofilm prevention properties of the POM-ILs. To further analyse biofilm growth on stone surfaces, and to obtain in-depth information about the effect of the POM-ILs on the bacterial cells we used a combination of environmental scanning transmission electron microscopy (ESEM) and fluorescence microscopy. Non-porous BB was chosen as a model stone surface because of its non-porous surface, which enables facile detection of biofilm formation (Figure 4). BB samples treated with POM-IL 1 and 2 were inoculated with *E. coli* and *B. subtilis* and stained with a LIVE/DEAD® BacLight™ Bacterial Viability Kit to determine the viability of the bacteria and assess the biofilm formation after incubation. The samples incubated with the POM-ILs display lower bacterial density than the untreated stones, highlighting the antiproliferative effect of both POM-ILs (Figures S8, S9). However, a more detailed confocal microscopy analysis of biofilm formation on glass cover slips showed greater biofilm inhibition with POM-IL 1 compared to POM-IL 2 (Figure S10), which is in line with the results obtained from the antimicrobial surface analysis (JIS Z 2801 standard, Table 4). ESEM can provide information on bacteria morphology, health and visual indicators of the extent of biofilm formation. This technique demonstrated how the POM-ILs clearly lead to distinct responses from the

Table 4: Surface antimicrobial activity data for POM-ILs 1 and 2.

Stone type	Coating ^[a]	Bacterial reduction [%]
BB	POM-IL 1	100
BB	POM-IL 2	11.4
RO	POM-IL 1	36.4
RO	POM-IL 2	24.1
DO	POM-IL 1	55.9
DO	POM-IL 2	33.9

[a] Each stone sample was coated with a 10 mg mL⁻¹ solution of the respective POM-IL, for details see Supporting Information.

detect and quantify the growth of *E. coli* on the stone samples. TBX agar contains X-β-D-glucuronide, a chromogenic compound hydrolysed by the β-glucuronidase (an *E. coli* enzyme) making the bacterial colonies turn green-blue on a conventional agar plate. The treated and untreated stones were compared and counting of the green-blue *E. coli* colonies illustrated how POM-IL 1 prevented colonization of the BB

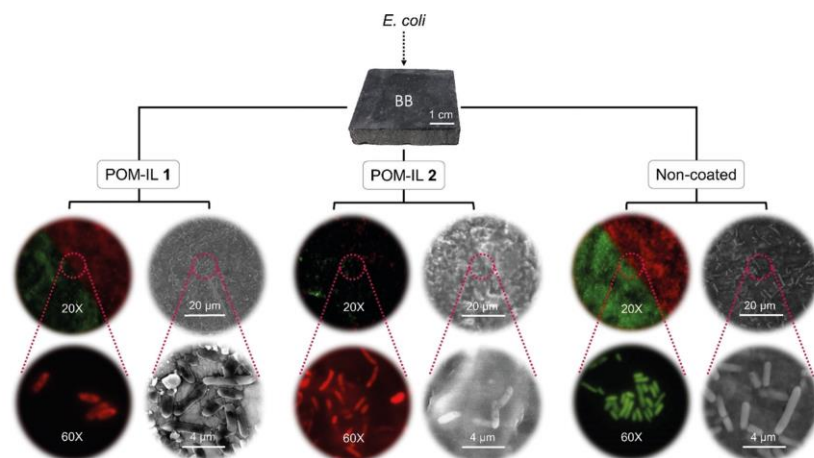


Figure 4. Environmental scanning transmission electron microscopy (ESEM) and fluorescence microscopy analyses summarizing the bactericidal effects of POM-IL 1 and 2 on BB stone for *E. coli* biofilm prevention. Green cells = live (viable) bacteria; Red cells = dead (non-viable) bacteria. See Supporting Information for additional ESEM and fluorescence microscopy images for both *E. coli* and *B. subtilis*.

bacterium cells on the stone surface (Figures 4, Figure S11). In general, both bacterial strains incubated with POM-ILs showed evidence of stress and damage including general loss of cell shape, cell membrane damage and leakage of cytoplasmic material. *B. subtilis* showed signs of sporulation, an indicator of cell stress. Both POM-ILs substantially reduced the number of bacterial cells on the stone surfaces, and higher bactericidal efficiency was observed for POM-IL **1** (Table 4, Figure S11). Importantly, images of *E. coli* on BB with POM-IL **2** appeared to show the presence of high molecular weight extracellular polymeric substances (EPSs) secreted by the *E. coli* biofilm (Figure S11), which is in line with the more dense biofilm observed by confocal microscopy (Figure S10). Finally, a modified optical density analysis of coated stones confirmed that POM-IL **1** was the more bactericidal compound against both *E. coli* and *B. subtilis* across all three types of stone (Table 4 and Figure S12).

In summary, we report a multifunctional polyoxometalate ionic liquid (POM-IL) transparent coating for natural building stones, which can easily be applied by brush-coating. We show that the POM-IL coating protects the stone surfaces from acid corrosion and biofilm formation by forming an acid-stable, biocidal surface layer. The coating is mechanically stable and is not removed even by harsh mechanical and chemical treatment (e.g. under accelerated acid rain simulation). Tuning of the rheological, physical and chemical properties of the POM-ILs is possible and our results demonstrate that modification of the cation affects the anti-corrosive properties and the biocidal activity. Future studies will explore the longer-term performance of POM-ILs under “real life” conditions (an on-site study is planned) and will optimize the POM-IL properties with a focus on antifungal activity.

Acknowledgements

Financial support by Ulm University, Fundación General CSIC (S.G.M., Programa ComFuturo), Fondo Social Europeo-Gobierno de Aragón and CIBER-BBN is gratefully acknowledged. A.M. gratefully acknowledges the Schlumberger Foundation (Faculty for the Future) for a doctoral fellowship. We gratefully acknowledge Mr. Andreas Böhm (master stone mason, Ulm Münster) for helpful discussions and The Advanced Microscopy Laboratory (University of Zaragoza).

Conflict of interest

The authors declare no conflict of interest.

Keywords: corrosion · ionic liquids · metal oxides · polyoxometalates · self-assembly

How to cite: *Angew. Chem. Int. Ed.* **2018**, *57*, 14926–14931
Angew. Chem. **2018**, *130*, 15142–15147

- [1] R. W. Revie, *Corrosion and Corrosion Control: An Introduction to Corrosion Science and Engineering*, Wiley, New York, **2008**.
- [2] Special Issue on Heritage Science: M. Strlič, *Angew. Chem. Int. Ed.* **2018**, *57*, 7260–7261; *Angew. Chem.* **2018**, *130*, 7380–7381.
- [3] A. E. Charola, R. Ware, *Geol. Soc. Spec. Publ.* **2002**, *205*, 393–406.
- [4] N. Kip, J. A. Van Veen, *ISME J.* **2015**, *9*, 542–551.
- [5] F. Gherardi, S. Goidanich, V. Dal Santo, L. Toniolo, *Angew. Chem. Int. Ed.* **2018**, *57*, 7360–7363; *Angew. Chem.* **2018**, *130*, 7482–7485.
- [6] E. Doehne, C. A. Price, *Stone Conservation: An Overview of Current Research*, 2nd ed., Getty Publications, Los Angeles, **2011**.
- [7] I. Franco Costillo, L. De Matteis, M. E. García Guillén, J. M. de la Fuente, S. G. Mitchell, *Int. Biodeterior. Biodegradation* **2018**, <https://doi.org/10.1016/j.ibiod.2018.04.004>.
- [8] K. P. Miller, L. Wang, B. C. Benicewicz, A. W. Decho, *Chem. Soc. Rev.* **2015**, *44*, 7787–7807.
- [9] R. D. Rogers, K. R. Seddon, *Science* **2003**, *302*, 792–793.
- [10] D. R. MacFarlane, M. Forsyth, P. C. Howlett, J. M. Pringle, J. Sun, G. Annat, W. Neil, E. I. Izgorodina, *Acc. Chem. Res.* **2007**, *40*, 1165–1173.
- [11] J. Arias-Pardilla, T. Espinosa, M. D. Bermúdez, *Electrochem. Ion. Liq. Vol. 2 Appl.* **2015**, *1*, 530–561.
- [12] S. Herrmann, A. Seliverstov, C. Streib, *J. Mol. Eng. Mater.* **2014**, *02*, 1440001.
- [13] Special POM themed issue: L. Cronin, A. Müller, (guest eds.), *Chem. Soc. Rev.* **2012**, *41*, 7325–7648.
- [14] A. B. Bourlino, K. Raman, R. Herrera, Q. Zhang, L. A. Archer, E. P. Giannelis, *J. Am. Chem. Soc.* **2004**, *126*, 15358–15359.
- [15] P. G. Rickert, M. R. Antonio, M. A. Firestone, K.-A. Kubatko, T. Szredner, J. F. Wishart, M. L. Dietz, *J. Phys. Chem. B* **2007**, *111*, 4685–4692.
- [16] J. Chen, L. Hua, W. Zhu, R. Zhang, L. Guo, C. Chen, H. Gan, B. Song, Z. Hou, *Catal. Commun.* **2014**, *47*, 18–21.
- [17] W. Huang, W. Zhu, H. Li, H. Shi, G. Zhu, H. Liu, G. Chen, *Ind. Eng. Chem. Res.* **2010**, *49*, 8998–9003.
- [18] G. Bernardini, A. G. Wedd, C. Zhao, A. M. Bond, *Proc. Natl. Acad. Sci. USA* **2012**, *109*, 11552–11557.
- [19] S. Herrmann, M. Kostrzewa, A. Wierschem, C. Streib, *Angew. Chem. Int. Ed.* **2014**, *53*, 13596–13599; *Angew. Chem.* **2014**, *126*, 13814–13817.
- [20] A.-L. Kubo, L. Kremer, S. Herrmann, S. G. Mitchell, O. M. Bondarenko, A. Kahru, C. Streib, S. G. Mitchell, O. M. Bondarenko, *ChemPlusChem* **2017**, *82*, 867–871.
- [21] S. Herrmann, L. De Matteis, J. M. de la Fuente, S. G. Mitchell, C. Streib, *Angew. Chem. Int. Ed.* **2017**, *56*, 1667–1670; *Angew. Chem.* **2017**, *129*, 1689–1692.
- [22] D. Pereira, F. Touneur, L. Bernaldez, A. Garcia Blazquez in *Geophys. Res. Abstr.* **2014**, pp. EGU2014-30.
- [23] C. Thomachot-Schneider, Etude et Suivi Des Altérations de l'Abbaye d'Orval, **2012**.
- [24] S. Eyssautier-Chuine, B. Marin, C. Thomachot-Schneider, G. Fronteau, A. Schneider, S. Gibaux, P. Vazquez, *Environ. Earth Sci.* **2016**, *75*, 748.
- [25] T. J. R. Weakley, S. A. Malik, *J. Inorg. Nucl. Chem.* **1967**, *29*, 2935–2944.
- [26] S. Buffet-Bataillon, P. Tattevin, M. Bonnaure-Mallet, A. Jolivet-Gougeon, *Int. J. Antimicrob. Agents* **2012**, *39*, 381–389.
- [27] A. López-Delgado, E. Cano, J. M. Bastidas, F. A. López, *J. Electrochem. Soc.* **1998**, *145*, 4140–4147.
- [28] R. M. Donlan, *Emerging Infect. Dis.* **2002**, *8*, 881–890.
- [29] F. Bellissima, M. Bonini, R. Giorgi, P. Baglioni, G. Barresi, G. Mastromei, B. Perito, *Environ. Sci. Pollut. Res. Int.* **2014**, *21*, 13278–13286.

- [30] S. Scheerer, O. Ortega-Morales, C. Gaylarde, *Adv. Appl. Microbiol.* **2009**, *66*, 97–139.
- [31] A. Stassi, E. Zanardini, F. Cappitelli, A. Schiraldi, C. Sorlini, *Ann. Microbiol. Enzimol.* **1998**, *48*, 111–120.
- [32] F. de Leo, A. Iero, G. Zammit, C. E. Urzì, *Int. J. Speleol.* **2012**, *41*, 125–136.
- [33] Japanese Standards Association, “Antibacterial products – Test for antibacterial activity and efficacy”, *Ref. number JIS Z 2801 2010 (E), First English Ed.: Publ.* **2011**, 1–15.
- Manuscript received: August 28, 2018
Accepted manuscript online: September 2, 2018
Version of record online: September 26, 2018
-

Appendix 4: Water Purification and Microplastics Removal Using Magnetic Polyoxometalate-Supported Ionic Liquid Phases (magPOM-SILPs)



Water Purification

International Edition: DOI: 10.1002/anie.201912111
German Edition: DOI: 10.1002/ange.201912111

Water Purification and Microplastics Removal Using Magnetic Polyoxometalate-Supported Ionic Liquid Phases (magPOM-SILPs)

Archismita Misra, Christian Zambrzycki, Gabriele Kloker, Anika Kotyrba, Montaha H. Anjass, Isabel Franco Castillo, Scott G. Mitchell,* Robert Güttel,* and Carsten Streb*

Abstract: Filtration is an established water-purification technology. However, due to low flow rates, the filtration of large volumes of water is often not practical. Herein, we report an alternative purification approach in which a magnetic nanoparticle composite is used to remove organic, inorganic, microbial, and microplastics pollutants from water. The composite is based on a polyoxometalate ionic liquid (POM-IL) adsorbed onto magnetic microporous core-shell $\text{Fe}_2\text{O}_3/\text{SiO}_2$ particles, giving a magnetic POM-supported ionic liquid phase (magPOM-SILP). Efficient, often quantitative removal of several typical surface water pollutants is reported together with facile removal of the particles using a permanent magnet. Tuning of the composite components could lead to new materials for centralized and decentralized water purification systems.

Access to clean water is still a major challenge in large parts of the world, and many water resources in developing countries carry high concentrations of organic pollutants, heavy metals or microbial contaminants.^[1–3] In addition, microplastic particles have recently been identified as contaminants of emerging concern (CEC) which can enter the food chain upon uptake by marine organisms.^[4,5] Micro-

plastics can bind and concentrate persistent organic pollutants (POPs), which amplifies their public health impact.^[6] Often, water purification relies on a series of operations including chemical coagulation, flocculation, sedimentation, filtration and disinfection which produce safe drinking water from contaminated surface or ground water.^[7,8]

Traditionally, different filters which target specific pollutants are connected in line to enable stepwise water purification. Filter materials typically include porous adsorbents, such as zeolites, minerals, or active carbon.^[9] However, treatment of large volumes of water or the deployment in remote areas require alternative methods which combine ease of use with minimum technological requirements and the ability to simultaneously remove multiple contaminants. Composites are promising materials to this end, as their target properties can be tuned by independent modification of each component. Recently, some of us have explored the removal of water contaminants by developing so-called polyoxometalate-supported ionic liquid phases (POM-SILPs).^[10] This composite is based on commercial porous silica particles which are surface-functionalized with water-immiscible polyoxometalate ionic-liquids (POM-ILs) capable of binding organic and inorganic contaminants.^[11] The POM-ILs^[12] combined lacunary Keggin tungstate anions featuring heavy-metal binding sites^[13,14] with long-chain quaternary organo-ammonium cations^[15,16] which act as antimicrobials. Integration of the POM-SILP composite in filter cartridges allowed the simultaneous removal of organic, inorganic, and microbial contamination from water. However, the system requires filtration processing which is limited to small water volumes, and overcoming this challenge is either energy-intensive (using pressurized systems) or materials-intensive (using more filter materials).

Herein, we propose water purification by magnetic particles as a promising alternative to filtration which could be employed in various water treatment scenarios. In contrast to filtration, magnetic water purification could facilitate the treatment of large volumes of water, and can in principle be used without further infrastructure if particle removal is possible using simple permanent magnets.^[17] Pioneering studies have explored the removal of aqueous pollutants using magnetic particles, including heavy-metal cation removal by amino acid-modified iron oxide,^[18] organic pollutant removal by graphene oxide-functionalized magnetic particles,^[19] and separation of freshwater algae using silica-coated magnetic particles.^[20] Recently, ground-breaking studies reported the use of light-driven magnetic microswimmers for the collection and removal of microplastics from water.^[21]

[*] M. Sc. A. Misra, G. Kloker, A. Kotyrba, Dr. M. H. Anjass,

Prof. Dr. C. Streb

Institute of Inorganic Chemistry I

Ulm University

Albert-Einstein-Allee 11, 89081 Ulm (Germany)

E-mail: carsten.streb@uni-ulm.de

M. Sc. C. Zambrzycki, Prof. Dr.-Ing. R. Güttel

Institute of Chemical Engineering

Ulm University

Albert-Einstein-Allee 11, 89081 Ulm (Germany)

E-mail: robert.guettel@uni-ulm.de

Dr. M. H. Anjass, Prof. Dr. C. Streb

Helmholtz Institute Ulm

Helmholtzstrasse 11, 89081 Ulm (Germany)

M. Sc. I. Franco Castillo, Dr. S. G. Mitchell

Instituto de Ciencia de Materiales de Aragón (ICMA-CSIC)

CSIC-Universidad de Zaragoza

50009 Zaragoza (Spain)

E-mail: scott@unizar.es

Supporting information and the ORCID identification number(s) for the author(s) of this article can be found under: <https://doi.org/10.1002/anie.201912111>.

© 2020 The Authors. Published by Wiley-VCH Verlag GmbH & Co. KGaA. This is an open access article under the terms of the Creative Commons Attribution License, which permits use, distribution and reproduction in any medium, provided the original work is properly cited.

Herein, we target multi-pollutant removal based on core-shell particles composed of a superparamagnetic iron oxide (Fe_3O_4 , hematite) core encased in a porous silica shell.^[22,23] We hypothesized that this architecture enables magnetic removal and at the same time stable POM-IL surface-anchoring. We demonstrate that the resulting magnetic POM-SILP (magPOM-SILP) composite effectively binds organic, inorganic, microbial, and microplastic pollutants from water, and can easily be recovered using a permanent magnet. Treatment of large water volumes therefore becomes possible. To our knowledge, this is the first report of magnetic POM-SILPs (MagPOM-SILPs), therefore their synthesis is described briefly: the magnetic iron oxide/silica core-shell precursor particles are synthesized by an adapted reverse water-in-oil microemulsion method at elevated temperature with cyclohexane as the organic phase.^[22] Reaction of the surfactant Brij 56 with aqueous Fe^{III} solution and subsequently with $\text{Si}(\text{OEt})_4$ leads to spherical $\text{Fe}_3\text{O}_4@/\text{SiO}_2$ core-shell nanoparticles which were washed, dried, and calcined (420°C) to give the microporous $\text{Fe}_2\text{O}_3@/\text{SiO}_2$ composite **1**. The average particle size of **1** was 16 nm, the BET specific surface area was approximately $270\text{ m}^2\text{ g}^{-1}$ and the BJH pore volume was $0.97\text{ cm}^3\text{ g}^{-1}$; for further characterization details, see Supporting Information. Composite **1** is used as non-modified reference compound throughout this study.

The POM-IL is synthesized as described in the literature^[10,12,24,25] by combination of the lacunary-Keggin cluster anion ($[\alpha\text{-SiW}_{11}\text{O}_{39}]^{8-}$)^[26] and the antimicrobial tetra-*n*-heptyl ammonium cation (Q^7 ($= (n\text{-C}_7\text{H}_{15})_4\text{N}^+$)^[27] (Figure 1). The magPOM-SILPs were prepared by dispersing $\text{SiO}_2@/\text{Fe}_3\text{O}_4$ particles (4.0 g) in a POM-IL solution in acetone (50 mL, $[\text{POM-IL}] = 3.36\text{ mM}$, $m(\text{POM-IL}) = 1.0\text{ g}$) and subsequent vacuum drying, giving the composite magPOM-SILP **2** with a POM-IL loading of 20 wt %, see Supporting Information for details. As a result of the partial filling of the pores in **2** with the POM-IL, the BET specific surface area of **2** was reduced to around $100\text{ m}^2\text{ g}^{-1}$ and the BJH pore volume was $0.70\text{ cm}^3\text{ g}^{-1}$; for further characterization details, see Support-

ing Information. Compound **2** was obtained as dry and free-flowing powder which can be easily handled, while the POM-IL precursor is a highly viscous liquid which would make deployment for water purification difficult.

We performed a series of water-purification tests using the magPOM-SILPs for removal of pollutants often found in water samples. Aqueous samples (5 mL) of the respective pollutant at health-relevant concentrations were prepared, and the magPOM-SILP **2** or the reference particles **1** (50 mg) were dispersed in the polluted sample and magnetically stirred. After stirring for 24 h, the magnetic particles were removed using a permanent magnet (see Supporting Video). Note that no leaching of any components of **2** into the aqueous phase was observed after stirring for 24 h using inductively coupled plasma atomic emission spectroscopy (ICP-AES) and C,H,N elemental analysis.

We explored heavy-metal removal from water using the metal-ion pollutant models^[2] Pb^{2+} , Ni^{2+} , Co^{2+} , and MnO_4^- according to the standard procedure described above (Figure 1). The metal-ion concentrations are set to levels significantly above the WHO guideline levels to test removal efficiency and simulate acute pollution scenarios (Table 1).^[28] ICP-AES analyses of the solutions after particle removal show metal removal efficiencies between 75–99 mol % for the magPOM-SILP **2**, while the non-modified reference **1** showed significantly lower removal efficiencies in the approximately 35–50 mol % range (Table 1, entries 1–5).

Table 1: Pollutant removal performance of magPOM-SILP **2** and the non-modified reference **1**.^[a]

Entry	Pollutant (conc.) [WHO guideline level] ^[28]	Pollutant removal by magPOM-SILP 2 [non-modified reference 1] ^[a]
1	Pb^{2+} (2.2 mM) [0.05 μM]	99 [48] mol %
2	Ni^{2+} (1.3 mM) [0.34 μM]	90 [52] mol %
3	Cu^{2+} (1.3 mM) [30 μM]	99 [51] mol %
4	Co^{2+} (1.3 mM) [–]	75 [35] mol %
5	MnO_4^- (1.15 mM) [0.05 μM]	99 [42] mol %
6	PBV (32 μM) ^[b] [–]	99 [6] mol %
7	PS beads, 10 μm (1 g L ⁻¹) [–]	100 [0] wt %
8	PS beads, 1 μm (1 g L ⁻¹) [–]	100 [0] wt %

[a] $V_{\text{solution}} = 5\text{ mL}$; $m_{\text{adsorbent}}$ (**1** or **2**) = 50 mg, $t_{\text{binding}} = 24\text{ h}$. [b] Patent Blue V.



Figure 1. Concept of the removal of multiple pollutants from water using magnetic polyoxometalate supported ionic liquid phases (magPOM-SILPs). Color scheme (bottom right): teal polyhedra $[\text{WO}_4]$, gray C, red O, blue N, white H.

We then explored the removal of organic pollutants from water using the triphenylmethane (trityl) dye Patent Blue V (PBV, Figure 2) as a model for textile dye pollutants.^[29] To this end, aqueous solutions of PBV were stirred with magPOM-SILP **2** using the standard experimental procedure described above. Dye removal was quantified by UV/Vis spectroscopy (Figure 2) and it was observed that the magPOM-SILP **2** removes more than 99 % of the dye while the non-modified reference **1** showed only 6 % removal (Table 1, entry 6). The increased dye removal by **2** is assigned to the high affinity of the POM-IL to interact with organic species, due to the large, hydrophobic Q^7 cations.^[11]

We hypothesized that the viscous POM-IL coating on the magnetic nanoparticle surface could be well suited for

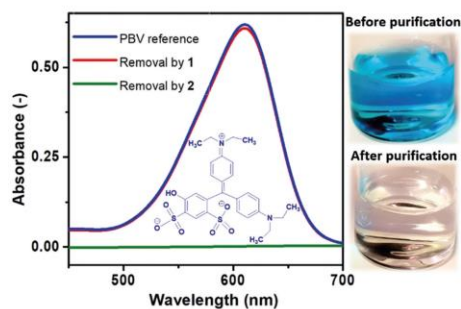


Figure 2. Removal of the water-soluble aromatic model pollutant Patent Blue V (PBV) from water. Left: UV/Vis spectra before purification (blue), after purification using reference 1 (red) and after purification using magPOM-SILP **2** (green). [PBV]₀ = 32 μM . Adsorption time: 24 h. Details see Table 1 entry 6. Inset: molecular structure of PBV. Right: photographs of the PBV solutions before and after purification (with **2**).

attaching the magPOM-SILP particles to microplastics, and thereby enable their magnetic recovery from water. To this end, we used commercial colloidal solutions of spherical polystyrene (PS) beads (diameter 1 μm and 10 μm , PS bead concentration: 0.1 wt % ($= 1 \text{ g L}^{-1}$)) as models of environmentally persistent microplastics. PS particle removal was quantified using dynamic light scattering (DLS, see Supporting Information for details). The removal experiments were carried as described above ($V_{\text{solution}} = 5 \text{ mL}$, $t_{\text{binding}} = 24 \text{ h}$). Our experiments demonstrated quantitative removal of both the 1 μm and 10 μm PS beads using magPOM-SILP **2**. In contrast, the reference **1** showed no microplastics removal, see Table 1, entries 7 and 8.

To gain some insights into the kinetics of the binding of **2** to the microplastic particles, we performed the removal experiment described above (using both PS bead sizes) at a reduced binding time of 6 h, which also resulted in quantitative PS bead removal. In addition, we demonstrated that three consecutive recycling runs using the same batch of **2** are possible, all of which show quantitative removal of both the 1 μm and the 10 μm PS beads (see Supporting Information). Next, we examined the microplastics removal capacity of **2** by performing the above experiment, but using PS bead solution volumes of 20 mL and 50 mL. For both solutions we note PS bead removal efficiencies over 90 % based on DLS analyses, see Supporting Information. This emphasizes that the magPOM-SILPs are capable of removing microplastic model compounds from large volumes of water.

To gain insights into the interactions between magPOM-SILP **2** and the PS beads, we performed scanning electron microscopy/energy-dispersive X-ray spectroscopy (SEM/EDX) of the magnetically recovered, dried samples. As shown in Figure 3, the significantly smaller particles of **2** cover large parts of the surface of the PS beads and thus render them susceptible for magnetic removal. We suggest that this surface attachment of **2** to the PS beads is due to hydrophobic interactions between the POM-IL coating and the PS surface,

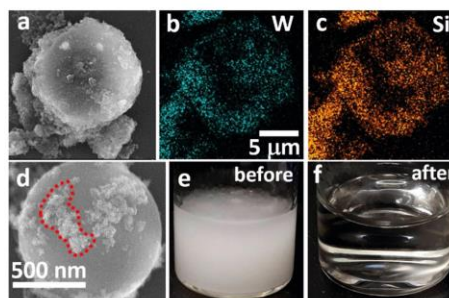


Figure 3. Microplastics removal by magPOM-SILP **2**: a)–c): SEM and EDX elemental mapping micrographs showing 10 μm polystyrene beads covered with **2** (as indicated by the W and Si signals). d) high magnification micrograph of a 1 μm polystyrene sphere coated with a smaller loading of **2** (outlined in red). e), f) photographs of test solutions before and after microplastics removal.

see Supporting Information for proposed scheme. In addition, PS bead aggregation is observed which could be induced by **2**, and further aggregation studies are currently underway to understand the surface attachment in more detail. In sum, PS microplastics removal by magnetic particle attachment could provide a means of treating larger volumes of water which are not amenable to classical filtration.^[21]

Some of our previous research has confirmed the bactericidal properties of POM-ILs,^[10,12,25] therefore we hypothesized that magPOM-SILP **2** would be able to purify water heavily contaminated with bacteria. The antibacterial water purification properties of the magPOM-SILPs were tested against gram-negative *E. coli* and gram-positive *B. subtilis*.^[12] Briefly, aqueous solutions of the microporous magPOM-SILP **2** were inoculated with 10^6 CFU mL^{-1} of *E. coli* or *B. subtilis* and incubated at 37 °C for 1 h before removing the particles with a magnet and quantifying the bacteria present in the supernatant solutions. At a magPOM-SILP **2** concentration of 1 mg mL^{-1} , the bacterial removal was 58 % for *E. coli* and 100 % for *B. subtilis*, while at a concentration of 10 mg mL^{-1} the bacterial removal efficiency was 100 % for both bacterial strains. The antibacterial effect was confirmed and characterized using electron microscopies (SEM and TEM). Figure 4B and Figures S3–S6 illustrate how the morphology of the bacteria was affected by the presence of magPOM-SILP **2**, even at concentrations below the minimum bactericidal concentration.

The reusability of the magPOM-SILP nanoparticles was tested over three cycles of inoculation with *E. coli* or *B. subtilis*, particle separation, and particle washing with water and subsequent reuse with a fresh inoculum of the bacteria. The bactericidal effect of **2** against *B. subtilis* remained unaltered after three cycles, while the effect of the particles on *E. coli* was reduced after the second cycle (Figure 4A), which is commensurate with other studies using magnetic nanoparticles for water purification.^[30,31]

In conclusion, we report the first example of magnetic polyoxometalate-supported ionic liquid phases (magPOM-

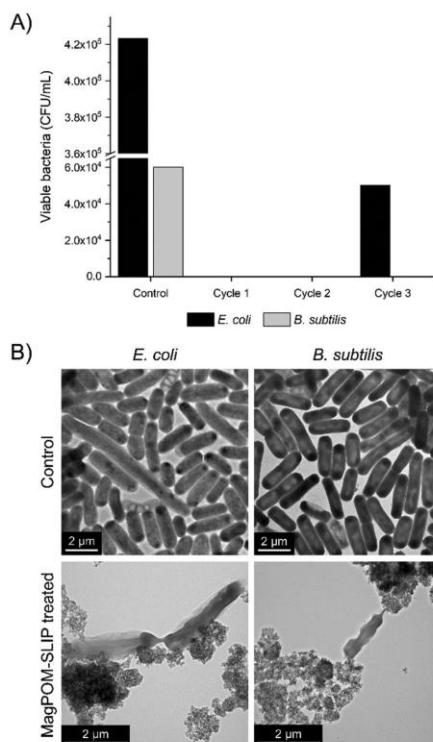


Figure 4. A) bacteria removal efficiency of magPOM-SILP 2 (10 mg mL⁻¹) over three consecutive cycles (50 min/cycle), where the initial concentration of the *E. coli* and *B. subtilis* inoculum was 10⁶ CFU mL⁻¹ (37 °C, pH 6); B) TEM images of *E. coli* and *B. subtilis* incubated with magPOM-SILP 2 at sub-bactericidal concentrations, including control bacterial cells without magPOM-SILP 2.

SILPs) and their use in water purification. The magPOM-SILP composite is capable of removing organic, inorganic, microbial, and microplastic pollutants from water using a range of target-specific removal modes. High removal efficiencies are reported together with initial insights into a new mode of microplastics removal by surface-binding of magnetic particles. In future, we will explore how optimization of the individual components can be used to improve the capacity of the systems and investigate their coupling to electromagnetic recovery systems for use under more realistic operating conditions.

Acknowledgements

C.S. and R.G. gratefully acknowledge financial support by Ulm University and the Vector Stiftung. C.S. and M.H.A. gratefully acknowledge the Helmholtz Gemeinschaft (HGF)

for financial support. A.M. gratefully acknowledges the Schlumberger Foundation (Faculty for the Future Program) for a doctoral fellowship. I.F.C. acknowledges the Gobierno de Aragón for a doctoral scholarship (2018–2022). We also thank The Advanced Microscopy Laboratory (Universidad de Zaragoza) for access to their instrumentation and expertise.

Conflict of interest

The authors declare no conflict of interest.

Keywords: ionic Liquids · microplastics · polyoxometalate · self-assembly · water purification

How to cite: *Angew. Chem. Int. Ed.* **2020**, 59, 1601–1605
Angew. Chem. **2020**, 132, 1618–1622

- [1] M. A. Shannon, P. W. Bohn, M. Elimelech, J. G. Georgiadis, B. J. Marinas, A. M. Mayes, *Nature* **2008**, 452, 301–310.
- [2] M. S. Islam, M. K. Ahmed, M. Raknuzzaman, M. Habibullah-Al-Mamun, M. K. Islam, *Ecol. Indic.* **2015**, 48, 282–291.
- [3] J. Qu, *J. Environ. Sci.* **2008**, 20, 1–13.
- [4] J. A. Ivar do Sul, M. F. Costa, *Environ. Pollut.* **2014**, 185, 352–364.
- [5] M. Cole, P. Lindeque, C. Halsband, T. S. Galloway, *Mar. Pollut. Bull.* **2011**, 62, 2588–2597.
- [6] A. L. Andrad, *Mar. Pollut. Bull.* **2011**, 62, 1596–1605.
- [7] T. Asami, H. Katayama, J. Robert, C. Visvanathan, H. Furumai, *Water Res.* **2016**, 101, 84–94.
- [8] X. Tang, H. Zheng, H. Teng, Y. Sun, J. Guo, W. Xie, Q. Yang, W. Chen, *Desalin. Water Treat.* **2016**, 57, 1733–1748.
- [9] N. B. Singh, G. Nagpal, S. Agrawal, *Environ. Technol. Innov.* **2018**, 11, 187–240.
- [10] S. Herrmann, L. De Matteis, J. M. de la Fuente, S. G. Mitchell, C. Streb, *Angew. Chem. Int. Ed.* **2017**, 56, 1667–1670; *Angew. Chem.* **2017**, 129, 1689–1692.
- [11] S. Herrmann, A. Seliverstov, C. Streb, *J. Mol. Eng. Mater.* **2014**, 02, 1440001.
- [12] A.-L. Kubo, L. Kremer, S. Herrmann, S. G. Mitchell, O. M. Bondarenko, A. Kahru, C. Streb, S. G. Mitchell, O. M. Bondarenko, *ChemPlusChem* **2017**, 82, 867–871.
- [13] POM-themed issue (Guest Eds.: L. Cronin, A. Müller), *Chem. Soc. Rev.* **2012**, 41, 7325–7648.
- [14] Y.-F. Song, R. Tsunashima, *Chem. Soc. Rev.* **2012**, 41, 7384–7402.
- [15] A. B. Bourlino, K. Raman, R. Herrera, Q. Zhang, L. A. Archer, E. P. Giannelis, *J. Am. Chem. Soc.* **2004**, 126, 15358–15359.
- [16] P. G. Rickert, M. R. Antonio, M. A. Firestone, K. A. Kubatko, T. Szeder, J. F. Wishart, M. L. Dietz, *J. Phys. Chem. B* **2007**, 111, 4685–4692.
- [17] A.-H. Lu, E. L. Salabas, F. Schüth, *Angew. Chem. Int. Ed.* **2007**, 46, 1222–1244; *Angew. Chem.* **2007**, 119, 1242–1266.
- [18] S. Guo, P. Jiao, Z. Dan, N. Duan, J. Zhang, G. Chen, W. Gao, *Chem. Eng. Res. Des.* **2017**, 126, 217–231.
- [19] Y. Lin, S. Xu, L. Jia, *Chem. Eng. J.* **2013**, 225, 679–685.
- [20] M. Cerff, M. Morweiser, R. Dillschneider, A. Michel, K. Menzel, C. Posten, *Bioresour. Technol.* **2012**, 118, 289–295.
- [21] L. Wang, A. Kaeppler, D. Fischer, J. Simmchen, *ACS Appl. Mater. Interfaces* **2019**, 11, 32937–32944.
- [22] S. Takenaka, H. Umebayashi, E. Tanabe, H. Matsune, M. Kishida, *J. Catal.* **2007**, 245, 392–400.

- [23] J. Lee, Y. Lee, J. K. Youn, H. Bin Na, T. Yu, H. Kim, S.-M. Lee, Y.-M. Koo, J. H. Kwak, H. G. Park, H. N. Chang, M. Hwang, J.-G. Park, J. Kim, T. Hyeon, *Small* **2008**, *4*, 143–152.
- [24] S. Herrmann, M. Kostrzewa, A. Wierschem, C. Streb, *Angew. Chem. Int. Ed.* **2014**, *53*, 13596–13599; *Angew. Chem.* **2014**, *126*, 13814–13817.
- [25] A. Misra, I. Franco Castillo, D. P. Müller, C. González, S. Eyssautier-Chuine, A. Ziegler, J. M. de la Fuente, S. G. Mitchell, C. Streb, *Angew. Chem. Int. Ed.* **2018**, *57*, 14926–14931; *Angew. Chem.* **2018**, *130*, 15142–15147.
- [26] T. J. R. Weakley, S. A. Malik, *J. Inorg. Nucl. Chem.* **1967**, *29*, 2935–2944.
- [27] S. Buffet-Bataillon, P. Tattevin, M. Bonnaure-Mallet, A. Jolivet-Gougeon, *Int. J. Antimicrob. Agents* **2012**, *39*, 381–389.
- [28] World Health Organization: Guidelines for Drinking-Water Quality (Ed.: N. Graham), Geneva, **2011**.
- [29] E. Forgacs, T. Cserhádi, G. Oros, *Environ. Int.* **2004**, *30*, 953–971.
- [30] F. Zhang, *Environ. Sci. Nano* **2018**, *5*, 1341–1349.
- [31] X. Zhang, J. Qian, B. Pan, *Energy Sci. Technol.* **2016**, *50*, 881–889.

Manuscript received: September 22, 2019

Revised manuscript received: October 21, 2019

Accepted manuscript online: October 22, 2019

Version of record online: November 27, 2019

Appendix 5: On-POM Ring-Opening Polymerisation of N-Carboxyanhydrides



Polymerisation Hot Paper

How to cite: *Angew. Chem. Int. Ed.* **2021**, *60*, 3449–3453

International Edition: doi.org/10.1002/anie.202013563

German Edition: doi.org/10.1002/ange.202013563



On-POM Ring-Opening Polymerisation of N-Carboxyanhydrides

Héctor Soria-Carrera, Isabel Franco-Castillo, Pilar Romero, Santiago Martín,
Jesús M. de la Fuente, Scott G. Mitchell,* and Rafael Martín-Rapún*

Abstract: The ring-opening polymerisation of α -amino acid N-carboxyanhydrides (NCAs) offers a simple and scalable route to polypeptides with predicted and narrow molecular weight distributions. Here we show how polyoxometalates (POMs)—redox-active molecular metal-oxide anions—can serve as inorganic scaffold initiators for such NCA polymerisations. This “On-POM polymerisation” strategy serves as an innovative platform to design hybrid materials with additive or synergistic properties stemming from the inorganic and polypeptide component parts. We have used this synthetic approach to synthesise a library of bactericidal poly(lysine)–POM hybrid derivatives that can be used to prevent biofilm formation. This versatile “On-POM polymerisation” method provides a flexible synthetic approach for combining inorganic scaffolds with amino acids, and the potential to tailor and improve the specificity and performance of hybrid antimicrobial materials.

Polypeptides are ubiquitous in Nature and perform crucial roles in signalling, protecting and transport in living organisms. Most often, synthetic polypeptides are obtained by biosynthesis or by means of Solid Phase Peptide Synthesis (SPPS), which reproduce the exact peptide sequence. However, the scalability of these processes remains challenging.^[1] In contrast, the Ring Opening Polymerisation (ROP) of N-carboxyanhydrides (NCAs) has emerged as an atom efficient one-pot route to polypeptides under living polymerisation conditions.^[2,3] This approach allows the scalable synthesis of peptidomimetics that gather the main features needed for

a certain function such as charge, hydrophilicity/hydrophobicity or secondary structure. Thus, its use has been explored with different naturally occurring amino acid monomers and initiators to confer specific functionality and different chemistries to the peptidic chain.^[4–6] In addition to conventional initiators as organic nucleophiles, several non-conventional platforms such as gold surfaces or metallic nanoparticles have been employed as NCA polymerisation initiators.^[7–9] The surface-initiated ROP of NCAs relies on the immobilisation of amino groups at the surface that can initiate the polymerisation. This attractive concept combines the robustness of a metallic support with the high functionality of polypeptides. Although the controlled binding and assembly of polypeptides onto inorganic substrates lies at the core of biological-materials engineering, these scaffolds are not discrete molecules and mostly comprise noble metals, minerals or metal-oxides such as hydroxyapatite, calcite, magnetite and silica.

Polyoxometalates (POMs) are molecular metal-oxides with elevated redox activity that have been employed in fields as diverse as catalysis, energy and biology.^[10–12] These cluster anions can be easily tuned to tailor the physicochemical properties for a variety of applications by varying the number and/or type of metal addenda atom or introducing organic ligands. Organic hybrids of POMs offer versatile platforms to develop new materials that potentially combine the properties of both entities.^[13–15] In particular, the well-known Mn-Anderson derivative can be functionalised with Tris-base producing bis-amino functionalised POM $[\text{MnMo}_6\text{O}_{18}((\text{OCH}_2)_3\text{CNH}_2)_2]^{3-}$ for post-reaction development.^[16,17] Cronin and co-workers paved the way towards hybrid-POM-peptidic composites via covalent attachment^[18] or introducing them in a SPPS-like workflow.^[19] Further, POMs have been also derivatised in such a way that they act as initiators of radical polymerisations^[20,21] or as repeating unit in a polymer sequence.^[22,23]

POMs have been shown to exhibit antimicrobial properties arising from their redox properties and their interaction with bacterial cell membranes, which results in membrane puncturing and cell lysis.^[24] Antimicrobial peptides (AMPs) have received increasing attention because of their rapid action and broad-spectrum antimicrobial activities. They are usually formed by sequences combining hydrophobic and cationic amino acids. The dual functionality arising from these cationic and amphiphilic properties allows AMPs to attach to the anionic microbial cell membranes, intercalate into the lipid bilayers and eventually disrupt the cell membrane.^[25] Importantly, libraries of AMPs can easily be prepared by ROP of NCAs.^[26–28]

Since both POMs and polypeptides have each been shown to exhibit potent antimicrobial properties, it therefore follows that hybrid materials based on these components emerge as

[*] H. Soria-Carrera, I. Franco-Castillo, Dr. P. Romero, Dr. S. Martín, Prof. J. M. de la Fuente, Dr. S. G. Mitchell, Dr. R. Martín-Rapún
Instituto de Nanociencia y Materiales de Aragón (INMA)
CSIC-Universidad de Zaragoza
c/ Pedro Cerbuna 12, 50009 Zaragoza (Spain)
E-mail: scott@unizar.es
rmartin@unizar.es

H. Soria-Carrera, I. Franco-Castillo, Prof. J. M. de la Fuente,
Dr. S. G. Mitchell, Dr. R. Martín-Rapún
CIBER de Bioingeniería, Biomateriales y Nanomedicina
Instituto de Salud Carlos III
28029 Madrid (Spain)
Dr. R. Martín-Rapún
Departamento de Química Orgánica, Facultad de Ciencias
Universidad de Zaragoza
c/ Pedro Cerbuna 12, 50009 Zaragoza (Spain)
Dr. S. Martín
Departamento de Química Física, Facultad de Ciencias
Universidad de Zaragoza
c/ Pedro Cerbuna 12, 50009 Zaragoza (Spain)

Supporting information and the ORCID identification number(s) for the author(s) of this article can be found under <https://doi.org/10.1002/anie.202013563>.

interesting candidates to overcome the increasing problem of bacterial resistance towards conventional antibiotics.^[29–32] The ionic combination of peptides or peptide-polymers and POMs have resulted in hybrids with better antimicrobial activities than each component alone.^[33–35] In addition, the vast combinatorial possibilities of both POMs and amino acids means that it is also possible to tune the secondary structure, molecular weight and antimicrobial properties of the hybrid.

Here we present the use of an amino-functionalised Mn-Anderson-POM as an initiator for the on-POM ROP of amino acid NCAs. We have termed the hybrid POM-peptides obtained by this polymerisation approach as POMlymers (Figure 1). In this proof-of-principle report we combine hydrophobic (*N*^ε-protected lysine) and cationic residues (lysine) to explore the antimicrobial and antibiofilm behaviour of the resulting POMlymers. To the best of our knowledge, this is the first example of ROP of NCAs using a molecular metal-oxide as initiator and inorganic molecular scaffold. From a fundamental standpoint, this “on-POM polymerisation” strategy represents a modular and controllable synthetic approach for producing libraries of POMlymers with controlled molecular weight and structure, from organo-functionalised POMs and amino acids. Such an approach could pave the way to next generation hybrid materials with additive or synergistic antimicrobial properties.

ZK NCA and TFAK NCA (*N*^ε-benzyloxycarbonyl and trifluoroacetamide protected lysine, respectively) were selected as precursor monomers to obtain, respectively, the hydrophobic and cationic residues in the final POMlymers, whereas [MnMo₆O₁₈((OCH₂)₃CNH₂)₂]^{3−} with tetrabutylammonium (TBA) as counteranions was chosen as bifunctional initiator (Figure 1). To mimic the favoured structure of an AMP, we randomly copolymerised both monomers. We anticipated that the higher number of TFAK residues

(lysine residues after deprotection) would confer a higher degree of antimicrobial activity due to the increased number of cationic residues. In consequence, we fixed the hydrophobic residue content at 30 repeating units and we set the TFAK NCA feed to 30 and 90 residues (**POMK₃₀^{TFA}** and **POMK₉₀^{TFA}**). We also prepared a short oligomer containing 10 residues of each monomer, **POMK₁₀^{TFA}**, to test whether the solubility would play an important role in the antimicrobial activity (Figure 1). As control, the synthesis of the polymers **K_n^{TFA}** without the POM moiety was initiated with *n*-butylamine. In all cases the polymerisation was performed following an adapted protocol that had previously ensured a living chain growth polymerisation with fast reaction kinetics by removing the CO₂ formed during the reaction.^[36,37] All the polymers could be isolated by precipitation in either water or diethyl ether. In the case of POMlymers, precipitation in water offered the advantage that TBA cations could be removed almost completely, which was crucial in order to perfectly isolate the contributions of the POM against bacteria, since tetraalkylammonium cations are known antibacterial agents.^[29]

After polymerisation, the composition of the polymeric scaffold was evaluated using ¹H-NMR on the POMlymers precipitated in diethyl ether (Figure 2 and S8–S10). The ratio between the comonomers reflected that of the reaction mixture as calculated from the integration of the proton signals of the trifluoroacetamide and the benzylic hydrogens of the Z protecting group (Figure 2). The methylene protons closer to the Mn^{III} core in the Tris-functionalised POM were used to determine the average degree of polymerisation, which corresponded well with that defined by the feed (Table 1). Due to the strong paramagnetic behaviour of Mn^{III} the methylene signal is subject to a large downfield chemical shift and its signal appears at ca. 65 ppm (inset in Figure 2). When precipitated in water instead of diethyl ether, TBA cations were mostly removed which led to the disappearance

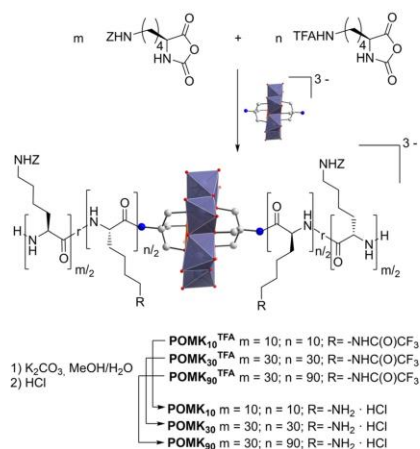


Figure 1. On-POM preparation of POMlymers **POMK_n^{TFA}** via ring-opening polymerisation (ROP) of *N*-carboxyhydride (NCA) and subsequent deprotection to obtain the positively charged POMlymers **POMK_n**.

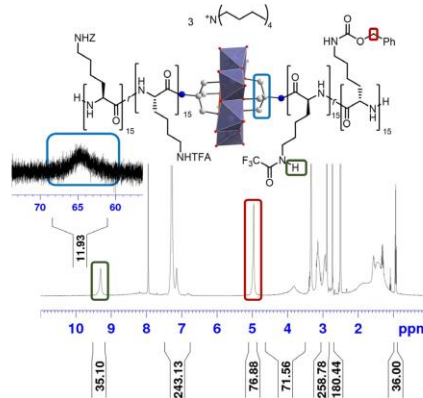


Figure 2. Structure of **POMK₃₀^{TFA}** and ¹H-NMR spectrum of **POMK₃₀^{TFA}**. Relevant signals to characterise the structure of the polymers are highlighted with colour boxes.

Table 1: Characterisation results of POMlymers **POMK_n^{TFA}** and **POMK_n**.

Feed ^[a]	$M^{[b]}$ [kg mol ⁻¹]	POMK_n^{TFA}		$M^{[d]}$ [kg mol ⁻¹]	POMK_n	
		Ratio ^[a] (NMR) ^[c]	M_n (NMR) ^[c] [kg mol ⁻¹]		M_n (GPC) ^[e] [kg mol ⁻¹]	\bar{D} (GPC)
10:10	6.0	1:11:11	6.5	5.1	—	—
30:30	15.7	1:38:35	19.0	12.9	21.0	1.19
30:90	29.2	1:38:89	31.0	20.6	29.3	1.35

[a] Expressed by the molar ratio POM:ZK:TFAK in the feed and in the polymer (NMR). [b] As calculated based on the feed but excluding TBA. [c] Calculated based on the integration of Tris signal at ca. 65 ppm. [d] As calculated based on the feed but excluding hydrochloride and TBA. [e] Relative to PMMA standards with HFIP with 3 g L⁻¹ K⁺TFA⁻ as eluent.

of the methylene signal at ca. 65 ppm. The suppression of the signal was probably due to the change in the environment of paramagnetic Mn^{III} ion as well as solvation effects, as it was recovered after treating the material with a solution of TBA bromide in diethyl ether (Figure S23).

The targeted materials (**POMK_n**) were prepared by selective cleavage of the trifluoroacetamide group under mild alkaline conditions.^[38] The successful cleavage was confirmed by the disappearance of the -CF₃ signal in ¹⁹F-NMR (Figure S22). The materials were insoluble in DMSO and H₂O, nevertheless, it was possible to solubilise them with hexafluoroisopropanol (HFIP), which is known to favour the dissolution of hydrogen bonded aggregates. ¹H-NMR spectra of **POMK_n** showed only signals belonging to the polypeptidic chain and side groups while the methylene signals of Tris ligands were suppressed (Figures S12–S14). POM decomposition or fragmentation during the deprotection step would give rise to a broader variety of polymeric structures with smaller size. In consequence we used DOSY (Diffusion Ordered Spectroscopy) ¹H-NMR as a tool to determine whether the POM was still attached to the polypeptide. **POMK_n^{TFA}** and **POMK_n** showed that the presence of the paramagnetic Mn^{III} not only affects the signal of the Tris methylene protons but also the signals along the polymeric structure, mainly α-protons: After applying the magnetic field gradients, the methylene bridges in Tris ligands and the α-proton signals were suppressed due to the interaction with the magnetic field. This effect seems to be more pronounced for **POMK_n^{TFA}** than for **POMK_n**. However, in polymers **K_n^{TFA}** and **K_n**, without POM, we did not observe this phenomenon, confirming that the paramagnetic effect is indeed transferred through the peptide backbone. When comparing DOSY spectra of both **POMK_n** and **K_n** polymers we did not observe any significant change on the pattern of the molecular diffusion (Figures S24–S29), concluding that the POM was still attached to the polymer in **POMK_n**. Additionally, the presence of the POM was verified directly by using a combination of FTIR (Figures S31–S33) and X-ray Photoelectron Spectroscopy (XPS) (Figures S37, S38). Briefly, FTIR spectra can be used to prove the presence of Mn-Anderson [MnMo₆O₁₈((OCH₂)₃CNH₂)₂]³⁻ in the final **POMK_n** materials. The Mo=O and Mo-O stretches (ca. 890 cm⁻¹ and 690 cm⁻¹, respectively) are present for MnMo₆ Mn-Anderson starting material and **POMK_n**. These bands are absent in **K_n**, which do not contain the MnMo₆ Mn-Anderson, showing that

the bands in the 1200–600 cm⁻¹ region of the spectra in the final **POMK_n** materials do not correspond to the peptidic part. (Figures S31–S33). XPS was used to identify Mn^{III} and Mo^{VI} in **POMK_n** POMlymers.

Consistent with the DOSY spectra, gel permeation chromatography traces recorded for **POMK_n** in HFIP with 3 g L⁻¹ K⁺TFA⁻ showed monomodal distributions for POMlymers **POMK₃₀** and **POMK₃₀**, with estimated molecular weights similar to the control polymers **K₃₀** and **K₃₀** (Figure 3). **POMK₁₀** exhibited scarce solubility and therefore its GPC was not measured.

Bearing in mind the importance of conformational structure for developing materials with antimicrobial properties, we used circular dichroism (CD) spectroscopy to study the differences in how the polypeptide sequence folds (in HFIP) when conjugated to the POM. For the shortest POMlymer (**POMK₁₀**) we observed that the metallic centre favoured the folding into α-helices (Figure 3), in turn, its analogue **K₁₀** did not show any particular conformation but random coil (Figure S34). This phenomenon was already described by Yvon and Ventura et al., for POM and peptide hybrids prepared by SPPS, but without any further explanation.^[19,39] In contrast, **POMK₃₀** and **POMK₃₀** adopted a random coil conformation whereas their POM-free counterparts **K₃₀** and **K₃₀** formed α-helices (Figures 3B and S34). Our hypothesis is that POM-free structures possess a longer uninterrupted peptide chain, with a larger number of ZK residues which are known to induce a helical conformation. However, when the solvent contained 3 g L⁻¹ K⁺TFA⁻ as used in GPC, α-helices were detected for all POMlymers **POMK_n** and control polymers **K_n**, even for **K₁₀** (Figures S35–S36). It therefore follows that **K₁₀** should be less prone to adopting the α-helix conformation and would lead to the coexistence of α-helix and random coil conformations in HFIP containing 3 g L⁻¹ K⁺TFA⁻. This is translated to an apparent bimodal GPC trace and broader molecular weight distribution (Table S1 and Figure S30).^[40]

The presence of poly(lysine) combined with the limited aqueous solubility make POMlymers interesting candidates for antimicrobial surface coatings to prevent biofilm formation.^[25,41] Bacteria that attach to a surface or to an interface can grow as a densely packed multicellular community of microorganisms, a biofilm, that protect them from the bactericidal effects of different antimicrobials, such as antibiotics. Biofilms are the source of persistent infections of many pathogenic microbes. The POMlymers in this report

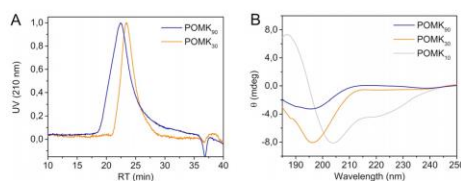


Figure 3. A) GPC profiles (UV absorbance at 210 nm) of POMlymers **POMK₃₀** and **POMK₁₀**; B) CD spectra of **POMK₃₀**, **POMK₃₀** and **POMK₁₀** as measured in HFIP (0.1 mg L⁻¹).

were evaluated against the Gram-positive *Bacillus subtilis*, which is a widely studied non-pathogenic biofilm model.^[42,43] Colorimetric cell viability assays were used to determine the bactericidal activity of the POMlymers (expressed as the concentration of the POMlymer per cm²). The bactericidal activity of **POMK₉₀** against *B. subtilis* corresponded to 31.2 µg cm⁻², while the bactericidal concentration of **POMK₁₀** was 500 µg cm⁻² (Figure S39). As control experiments, we also evaluated each counterpart individually and the combination of K₉₀ with Na₃[MnMo₆O₁₈]-((OCH₂)₃CNH₂)₂^[44] (Figures S40–S42). All antibacterial results are summarized in Table S2.

The surface antibacterial activity was also confirmed using a modified Japanese Industrial Standard (JIS Z 2801), which verified that **POMK₉₀** provided a complete bacterial cell viability reduction on surfaces at concentrations as low as 20 µg cm⁻² (Table 2). **POMK₁₀** provided surface bactericidal

Table 2: Surface antimicrobial activity of **POMK₁₀** and **POMK₉₀** determined using the Japanese Industrial Standard (JIS Z 2801).

Sample	Concentration [µg cm ⁻²]	Bacterial Reduction [%]
POMK₁₀	640	100
	160	100
	20	41
POMK₉₀	640	100
	160	100
	20	100

[a] Refer to Figure S43 for full log(CFU) reduction data.

action at concentrations of 640 and 160 µg cm⁻² while at lower concentrations of 20 µg cm⁻² the bacterial reduction was determined to be 41 % (please also refer to Figure S43 for log(CFU) reduction data).

The biofilm prevention properties of the POMlymers were also studied by Environmental Scanning Electron Microscopy (ESEM) and by Crystal Violet assays. The ESEM analysis of the biofilm growth over silicon wafers (coated with different concentrations of the POMlymers) showed how *B. subtilis* colonised the non-coated sample and developed a biofilm, while the coated samples fully inhibit biofilm development (Figure 4). Both **POMK₁₀** and **POMK₉₀** fully protect from *B. subtilis* surface colonisation; however, some bacteria aggregates were observed in the 20 µg cm⁻² **POMK₁₀** sample, commensurate with the antimicrobial results (Figure S43). A Crystal Violet assay, on the other hand, was used to evaluate the ability of the bacteria to develop a pellicle biofilm at the liquid-air interface. Spectrophotometric analysis of the intensity of the biofilm halo developed at the liquid-air interface demonstrated that both **POMK₉₀** and **POMK₁₀** inhibit biofilm formation at concentrations as low as 160 µg cm⁻² (Figure S44).

In this work we have demonstrated how hybrid POM-materials can be accessed through ring opening polymerisation (ROP) of *N*-carboxyanhydrides (NCAs) where the POM serves as the molecular metal-oxide scaffold initiator. We have designated the hybrid POM-peptides prepared using this approach as POMlymers. Here we have shown how

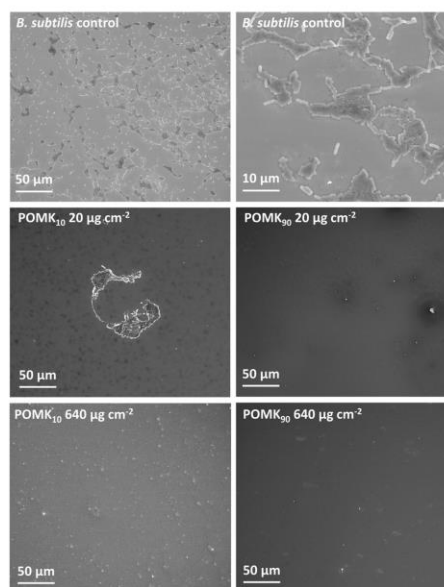


Figure 4. Environmental Scanning Electron Microscopy (ESEM) images of *B. subtilis* incubated over a silicon wafer coated with **POMK₁₀** and **POMK₉₀** at 20 and 640 µg cm⁻² (and over a non-coated sample as a biofilm positive control). Bacteria incubated over the non-coated sample are covering the surface by developing a biofilm. Some bacterial aggregates in the sample coated with 20 µg cm⁻² **POMK₁₀**, but at the highest concentration (640 µg cm⁻²) no bacteria were observed. Surfaces coated with 20 or 640 µg cm⁻² **POMK₉₀** show no biofilm growth.

a series of poly(lysine)-functionalised POMs were prepared under living polymerisation conditions by varying the number of cationic residues and the length of the polymer and that after the deprotection step in basic medium, the integrity of the POM is preserved. Some of these bactericidal POMlymers possessed surface antibacterial activity at concentrations as low as 20 µg cm⁻² (**POMK₉₀**), which completely prevented biofilm growth. The **POMK₉₀** POMlymer serves as a promising proof-of-concept candidate whose design could be improved to develop alternative antimicrobial hybrids to tackle biofilms that provide highly protective environments for pathogenic bacteria. In summary, the “on-POM polymerisation” represents a new design principle towards hybrid materials and a versatile route to produce POMlymers for combating biofilms that are highly resistant to conventional therapies.

Acknowledgements

Financial support from Ministerio de Ciencia Innovación y Universidades (Spain) through a Ramón y Cajal fellowship (RMR, RYC-2013-12570) and Proyectos I+D+i (PID2019-

109333RB-I00, PGC2018-097583-B-I00, and PID2019-105881RB-I00) and CSIC i-Link+2019 project (LINK20270). HSC and IFC are grateful for predoctoral fellowships from Ministerio de Educación Cultura y Deporte (FPU program) and Gobierno de Aragón, respectively. Further financial support from Fondo Social Europeo-Gobierno de Aragón (E15_20R, E47_20R and E31_17R) and CIBER-BBN is gratefully acknowledged. The authors would like to acknowledge the Laboratorio de Microscopías Avanzadas (LMA) at Universidad de Zaragoza for offering access to their instruments and expertise, especially Guillermo Antorrena for the XPS measurements; the use of the Unidad de Apoyo a la Investigación del CEOMA (CSIC-Universidad de Zaragoza). The authors also thank Dr. Elena Atrián-Blasco for fruitful discussions.

Conflict of interest

The authors declare no conflict of interest.

Keywords: antimicrobial activity · biofilm · polyoxometalates · polypeptides · ring-opening polymerisation

- [1] J. M. Palomo, *RSC Adv.* **2014**, *4*, 32658–32672.
- [2] H. R. Kricheldorf, *Angew. Chem. Int. Ed.* **2006**, *45*, 5752–5784; *Angew. Chem.* **2006**, *118*, 5884–5917.
- [3] J. H. Vrijsen, A. Rasines Mazo, T. Junkers, G. G. Qiao, *Macromol. Rapid Commun.* **2020**, *41*, 2000071.
- [4] T. J. Deming, *Chem. Rev.* **2016**, *116*, 786–808.
- [5] O. Zagorodko, J. J. Arroyo-Crespo, V. J. Nebot, M. J. Vicent, *Macromol. Biosci.* **2017**, *17*, 1600316.
- [6] D. Huesmann, K. Klinker, M. Barz, *Polym. Chem.* **2017**, *8*, 957–971.
- [7] S. H. Wibowo, A. Sulistio, E. H. H. Wong, A. Blencowe, G. G. Qiao, *Chem. Commun.* **2014**, *50*, 4971–4988.
- [8] S. H. Wibowo, E. H. H. Wong, A. Sulistio, S. N. Guntari, A. Blencowe, F. Caruso, G. G. Qiao, *Adv. Mater.* **2013**, *25*, 4619–4624.
- [9] G. Marcelo, A. Muñoz-Bonilla, J. Rodríguez-Hernández, M. Fernández-García, *Polym. Chem.* **2013**, *4*, 558–567.
- [10] D. Gao, R. Liu, J. Biskupek, U. Kaiser, Y. F. Song, C. Streb, *Angew. Chem. Int. Ed.* **2019**, *58*, 4644–4648; *Angew. Chem.* **2019**, *131*, 4692–4696.
- [11] D. L. Long, R. Tsunashima, L. Cronin, *Angew. Chem. Int. Ed.* **2010**, *49*, 1736–1758; *Angew. Chem.* **2010**, *122*, 1780–1803.
- [12] A. Bijelic, M. Aureliano, A. Rompel, *Angew. Chem. Int. Ed.* **2019**, *58*, 2980–2999; *Angew. Chem.* **2019**, *131*, 3008–3029.
- [13] A. Proust, B. Matt, R. Villanneau, G. Guillemot, P. Gouzerh, G. Izzet, *Chem. Soc. Rev.* **2012**, *41*, 7605–7622.
- [14] K. Kastner, A. J. Kibler, E. Karjalainen, J. A. Fernandes, V. Sans, G. N. Newton, *J. Mater. Chem. A* **2017**, *5*, 11577–11581.
- [15] A. V. Anyushin, A. Kondinski, T. N. Parac-Vogt, *Chem. Soc. Rev.* **2020**, *49*, 382–432.
- [16] P. R. Marcoux, B. Hasenknopf, J. Vaissermann, P. Gouzerh, *Eur. J. Inorg. Chem.* **2003**, 2406–2412.
- [17] A. Blazevec, A. Rompel, *Coord. Chem. Rev.* **2016**, *307*, 42–64.
- [18] J. Luo, B. Zhang, C. Yvon, M. Hutin, S. Gerislioglu, C. Wesdemiotis, L. Cronin, T. Liu, *Eur. J. Inorg. Chem.* **2019**, 380–386.

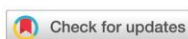
- [19] C. Yvon, A. J. Surman, M. Hutin, J. Alex, B. O. Smith, D. L. Long, L. Cronin, *Angew. Chem. Int. Ed.* **2014**, *53*, 3336–3341; *Angew. Chem.* **2014**, *126*, 3404–3409.
- [20] B. Hu, C. Wang, J. Wang, J. Gao, K. Wang, J. Wu, G. Zhang, W. Cheng, B. Venkateswarlu, M. Wang, et al., *Chem. Sci.* **2014**, *5*, 3404–3408.
- [21] Y. Han, Y. Xiao, Z. Zhang, B. Liu, P. Zheng, S. He, W. Wang, *Macromolecules* **2009**, *42*, 6543–6548.
- [22] W. K. Miao, Y. K. Yan, X. Le Wang, Y. Xiao, L. J. Ren, P. Zheng, C. H. Wang, L. X. Ren, W. Wang, *ACS Macro Lett.* **2014**, *3*, 211–215.
- [23] W. K. Miao, A. Yi, Y. K. Yan, L. J. Ren, D. Chen, C. H. Wang, W. Wang, *Polym. Chem.* **2015**, *6*, 7418–7426.
- [24] A. Bijelic, M. Aureliano, A. Rompel, *Chem. Commun.* **2018**, *54*, 1153–1169.
- [25] Q. Gao, P. Li, H. Zhao, Y. Chen, L. Jiang, P. X. Ma, *Polym. Chem.* **2017**, *8*, 6386–6397.
- [26] Y. Wu, D. Zhang, P. Ma, R. Zhou, L. Hua, R. Liu, *Nat. Commun.* **2018**, *9*, 5297.
- [27] W. Jiang, X. Xiao, Y. Wu, W. Zhang, Z. Cong, J. Liu, S. Chen, H. Zhang, J. Xie, S. Deng, et al., *Biomater. Sci.* **2020**, *8*, 739–745.
- [28] Y. Zhang, W. Song, S. Li, D. K. Kim, J. H. Kim, J. R. Kim, I. Kim, *Chem. Commun.* **2020**, *56*, 356–359.
- [29] A. Misra, I. Franco Castillo, D. P. Müller, C. González, S. Eyssautier-Chuine, A. Ziegler, J. M. de la Fuente, S. G. Mitchell, C. Streb, *Angew. Chem. Int. Ed.* **2018**, *57*, 14926–14931; *Angew. Chem.* **2018**, *130*, 15142–15147.
- [30] A. J. Park, J. P. Okhovat, J. Kim, *Clin. Basic Immunodermatology Second Ed.* **2017**, *26*, 81–95.
- [31] M. Xiong, M. W. Lee, R. A. Mansbach, Z. Song, Y. Bao, R. M. Peek, C. Yao, L.-F. Chen, A. L. Ferguson, G. C. L. Wong, et al., *Proc. Natl. Acad. Sci. USA* **2015**, *112*, 13155–13160.
- [32] P. Salas-Ambrosio, A. Tronnet, P. Verhaeghe, C. Bonduelle, *Biomacromolecules* **2020**, <https://doi.org/10.1021/acs.biomac.0c00797>.
- [33] L. P. Datta, R. Mukherjee, S. Biswas, T. K. Das, *Langmuir* **2017**, *33*, 14195–14208.
- [34] J. Li, Z. Chen, M. Zhou, J. Jing, W. Li, Y. Wang, L. Wu, L. Wang, Y. Wang, M. Lee, *Angew. Chem. Int. Ed.* **2016**, *55*, 2592–2595; *Angew. Chem.* **2016**, *128*, 2638–2641.
- [35] S. Zhang, B. Peng, P. Xue, X. Kong, Y. Tang, L. Wu, S. Lin, *Soft Matter* **2019**, *15*, 5375–5379.
- [36] J. Zou, J. Fan, X. He, S. Zhang, H. Wang, K. L. Wooley, *Macromolecules* **2013**, *46*, 17–20.
- [37] H. Soria-Carrera, A. Lucía, L. De Matteis, J. A. Aínsa, J. M. de la Fuente, R. Martín-Rapún, *Macromol. Biosci.* **2019**, *19*, 1800397.
- [38] J. R. Hernández, H. A. Klok, *J. Polym. Sci. Part A* **2003**, *41*, 1167–1187.
- [39] D. Ventura, A. Calderan, C. Honisch, S. Krol, S. Serrati, M. Bonchio, M. Carraro, P. Ruzza, *Pept. Sci.* **2018**, *110*, e24047.
- [40] D. Huesmann, A. Birke, K. Klinker, S. Türk, H. J. Räder, M. Barz, *Macromolecules* **2014**, *47*, 928–936.
- [41] J. Hasan, R. J. Crawford, E. P. Ivanova, *Trends Biotechnol.* **2013**, *31*, 295–304.
- [42] S. Arnaouteli, C. E. MacPhee, N. R. Stanley-Wall, *Curr. Opin. Microbiol.* **2016**, *34*, 7–12.
- [43] S. Gingichashvili, D. Duanis-Assaf, M. Shemesh, J. D. B. Featherstone, O. Feuerstein, D. Steinberg, *Front. Microbiol.* **2017**, *8*, 2072.
- [44] Z. He, B. Li, H. Ai, H. Li, L. Wu, *Chem. Commun.* **2013**, *49*, 8039–8041.

Manuscript received: October 8, 2020

Accepted manuscript online: December 6, 2020

Version of record online: January 19, 2021

Appendix 6: Decoupling manufacturing from application in additive manufactured antimicrobial materials



Cite this: DOI: 10.1039/d1bm00430a

Received 19th March 2021,
Accepted 10th May 2021

DOI: 10.1039/d1bm00430a

rsc.li/biomaterials-science

Decoupling manufacturing from application in additive manufactured antimicrobial materials†

Dominic J. Wales,^{a,†} Sara Miralles-Comins,^{b,§} Isabel Franco-Castillo,^{c,d}
 Jamie M. Cameron,^e Qun Cao,^a Erno Karjalainen,^a Jesum Alves Fernandes,^f
 Graham N. Newton,^e Scott G. Mitchell^{*,c,d} and Victor Sans^{*,b}

3D printable materials based on polymeric ionic liquids (PILs) capable of controlling the synthesis and stabilisation of silver nanoparticles (AgNPs) and their synergistic antimicrobial activity are reported. The interaction of the ionic liquid moieties with the silver precursor enabled the controlled *in situ* formation and stabilisation of AgNPs via extended UV photoreduction after the printing process, thus demonstrating an effective decoupling of the device manufacturing from the on-demand generation of nanomaterials, which avoids the potential aging of the nanomaterials through oxidation. The printed devices showed a multi-functional and tuneable microbicidal activity against Gram positive (*B. subtilis*) and Gram negative (*E. coli*) bacteria and against the mould *Aspergillus niger*. While the polymeric material alone was found to be bacteriostatic, the AgNPs conferred bactericidal properties to the material. Combining PIL-based materials with functionalities, such as *in situ* and photoactivated on-demand fabricated antimicrobial

AgNPs, provides a synergistic functionality that could be harnessed for a variety of applications, especially when coupled to the freedom of design inherent to additive manufacturing techniques.

Introduction

Antimicrobial resistance is a significant global health challenge around the world.¹ A potential solution that has enjoyed significant interest are materials with inherent antimicrobial properties.² One example is silver nanoparticles (AgNPs), which exhibit broad antimicrobial potential,^{3,4} and can be supported in a wide range of polymers and hydrogels.^{5–8} Such materials can be fabricated into myriad functional shapes and devices by utilising the design freedoms afforded by 3D printing,⁹ and indeed there are many examples of AgNP supporting materials that have been 3D printed.^{10–17} Typically, the AgNPs are either dispersed in the resin before 3D printing, or the AgNPs are formed during the 3D printing process, and then the materials can be used immediately. However, the disadvantage to this approach is that it does not allow for tuneable fabrication of the AgNPs so the efficacy of the device is tailored for the particular application at the point of use.

Therefore, to maintain maximal antimicrobial efficacy, whilst still allowing for a responsive bespoke personalised healthcare approach enabled by the inherent freedoms afforded by 3D printing, decoupling of the manufacture of the 3D printed part and the formation of AgNPs is needed. There are some examples of 3D printed materials containing AgNPs, wherein the fabrication is decoupled from the AgNP formation, but they typically require post-printing treatments, like energy-intensive heating steps,¹⁸ or immersion of the printed part in a reducing solution.¹⁹

A desirable alternative is a polymeric matrix that can be 3D printed, has the required mechanical properties and also maintains the silver precursor in the oxidised form to enable a controlled reductive formation of the AgNPs at the point of need. Fantino *et al.* have demonstrated on-demand photo-

^aFaculty of Engineering, University of Nottingham, University Park, Nottingham, NG7 2RD, UK

^bInstitute of Advanced Materials (INAM), Universitat Jaume I, 12071 Castellon, Spain. E-mail: sans@uji.es

^cInstituto de Nanociencia y Materiales de Aragón (INMA-CSIC), CSIC-Universidad de Zaragoza, c/Pedro Cerbuna 12, 50009 Zaragoza, Spain

^dCIBER de Bioingeniería, Biomateriales y Nanomedicina, Instituto de Salud Carlos III, 28029 Madrid, Spain. E-mail: scott.mitchell@csic.es

^eGSK Carbon Neutral Laboratory, University of Nottingham, Jubilee Campus, Nottingham, NG8 2GA, UK

^fSchool of Chemistry, University of Nottingham, University Park, Nottingham, NG7 2RD, UK

† Electronic supplementary information (ESI) available: UV-Vis spectrum of a 3D printed PIL1 part before post-printing UV photoreduction treatment; XPS spectrum, stress-strain curves, temporal UV-Vis spectra tracking photoreduction, and tabulated mechanical data for photoreduced 3D printed PIL1 parts; UV-Vis spectrum of photoreduced analogous homogeneous non-polymerisable liquid IL system; UV-Vis spectra for photoreduced 3D printed PIL2 and PIL3 parts; photographs of PIL2 and PIL3 3D printed parts before and after photoreduction; temporal UV-Vis spectra of photoreduced 3D printed PIL2 aged in ambient light. See DOI: 10.1039/d1bm00430a

‡ Present Address: Hamlyn Centre, Institute of Global Health Innovation, Imperial College London, South Kensington Campus, London, SW7 2AZ, United Kingdom.

§ These authors have contributed equally.



reductive formation of AgNPs within photocured polyethylene glycol diacrylate (PEGDA), which was decoupled from the 3D printing step. However, their system appeared to offer limited ability to stabilise AgNPs, and nanoparticle aggregation and migration were observed.²⁰ One suitable class of materials to achieve superior stabilisation ability are poly(ionic liquids), also known as polymeric ionic liquids (PILs), which are polyelectrolytes,²¹ formed from polymerisable ionic liquid monomers. PILs possess analogous properties to bulk ionic liquids in solution,^{22,23} and also enable exquisite tuning of the polymer properties through a near-infinite combination of cations and anions, together with the broad range of architecture and morphology variations inherent to polymeric materials.²⁴ There are many examples of poly(ionic liquid) functional materials such as porous electro-optic films,²⁵ ion conductive polymer films,^{26–29} dispersants,³⁰ and actuators.^{31,32} Furthermore, PILs can also be 3D printed using a range of techniques, such as inkjet printing,³³ DLP,^{34,35} and microstereolithography.³⁶ In addition, the ability of ionic liquids and PILs to stabilise and support metal nanoparticle precursor salts and nanoparticles has been well demonstrated.³⁷ Finally, ILs and PILs can be designed so as to possess inherent broad antimicrobial properties, against bacteria and fungi.^{38–41}

Therefore, we propose the use of 3D printable poly(ionic liquids) to fabricate multifunctional materials that feature three key properties; (i) on-demand photoreductive formation of the AgNPs within the material that is decoupled from the 3D printing step; (ii) an antimicrobial effect of the PIL backbone; combined with (iii) the broad antimicrobial action afforded by AgNPs. Vat photopolymerisation is selected as the 3D printing technique for proof of concept, since it allows the rapid formulation of polymerisation formulations and the generation of precise, complex geometries.

Herein we report the development of novel 3D-printable materials based on two different polymeric ionic liquids (PILs) functionalised with silver nanoparticles (AgNPs), we compare and contrast the formation and stabilisation of the silver nanoparticles in the two formulations and investigate the antimicrobial properties. The ability of each PIL to stabilise active nanomaterials *via* photoreduction is demonstrated by effective decoupling of the fabrication from the on-demand generation of low polydispersity AgNPs by subsequent exposure to UV irradiation. Furthermore, the tuneable antimicrobial activity of the AgNP@PIL printed devices against Gram-positive *Bacillus subtilis* (*B. subtilis*) and Gram-negative *Escherichia coli* (*E. coli*) bacteria, and *Aspergillus niger* (*A. niger*) and *Cladosporium cladosporioides* (*C. cladosporioides*) fungi is presented.

Results and discussion

In this work, several formulations based on combinations of different IL based monomers (mIL) and cross-linkers were investigated (Fig. 1A & B), with the aim of developing an optimised ink composition for printing AgNP@PIL materials.

Initial 3D printing experiments used the digital light processing (DLP) technique, employing a Little RP printer with a DLP projector to generate the UV light required for polymerisation. Latter 3D printing experiments were performed with a newer liquid crystal display (LCD) based printer (Elegoo Mars). The latter allowed for marginally better resolution, and had a smaller footprint, but no differences for the printing process were noticed. The first tunable 3D printing ink formulation was based on the polymerisable monomeric IL (mIL) precursor 1-butyl-3-vinylimidazolium bis(trifluoromethane)sulfonimide ([BVIM][NTf₂]) (mIL1, Fig. 1A), which was synthesised from 1-butyl-3-vinylimidazolium bromide ([BVIM][Br]) *via* anion metathesis as described in the ESI.†^{34,35} mIL1 was chosen as the polymerisable ionic liquid component as it has been previously demonstrated as a suitable poly(ionic liquid) (PIL) for stabilising and solubilising hybrid organic–inorganic polyoxometalates, and forms mechanically resistant polymers when 3D printed.^{34,35} Based on our previous experience, the initial ink formulation (PIL1, Fig. 1B) consisted of mIL1 (80 mol%), the crosslinker 1,4-butanediol diacrylate (20 mol%) and the organic photoinitiator diphenyl(2,4,6-trimethylbenzoyl)phosphine oxide (TMDPO, 1 mol%) and was a clear, very pale yellow viscous liquid. This ink composition was chosen as it was previously found to be the most effective for 3D-printing of PILs with the DLP technique. To this baseline formulation silver hexafluoroantimonate (AgSbF₆, ~1 wt%) salt was solubilised and stabilised.

The photopolymerisation of the PIL1 formulation resulted in well-defined clear and very pale yellow PIL parts (Fig. 2A, 0 min). The pale-yellow colour of the 3D printed PIL1 pieces is attributed to the polymer, thus suggesting that the encapsulated silver was still in the Ag⁺ state, despite exposure to the light during the 3D printing step. Furthermore, the UV-Visible spectra of the as printed pieces confirmed the absence of an absorption peak in the region $\lambda \approx 375\text{--}475\text{ nm}$, attributable to the LSPR band of the AgNPs (Fig. S1†),⁴² but does show the expected absorption peak features for the photoinitiator TMDPO.⁴³ Then upon exposure to UV light, the photoreduction of Ag⁺ to Ag(0) was initiated and the colour of the printed parts changed over time to increasingly darker shades of amber (Fig. 2A), and TEM analysis confirmed the presence of AgNPs (Fig. 2A, inset). The presence of Ag(0) was further confirmed by XPS characterisation, which revealed the expected peaks in the spectrum for Ag 3d_{5/2} and Ag 3d_{3/2} (Fig. S2A†).⁴⁴ Indeed, the slight asymmetry of the Ag 3d_{5/2} peak toward higher binding energies could be due to a convoluted peak that corresponds to aggregated Ag nanoparticles, which further corroborates the presence of AgNPs.⁴⁵

Mechanical analysis of parts exposed to UV photoreduction for different times indicated an increase in tensile stiffness with increasing UV exposure time (Fig. S2B†). Additionally, the corresponding $\tan \delta$ vs. temperature curves revealed the T_g values (defined as the x -axis values at each curve maximum) also increased with increasing UV exposure time (Fig. 2B), the secondary peak at low temperatures can be attributed to local chain motions or side group movements in the polymer



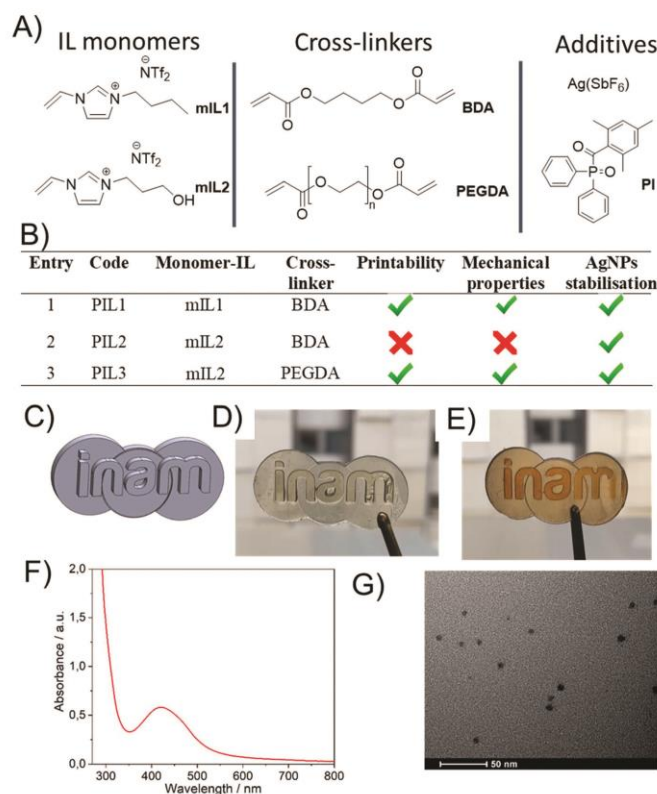


Fig. 1 This figure provides an overall visual summary of the work in this paper, and also shows the following specific results: (A) The components employed for the development of the 3D printable PIL-based formulations; (B) table summarising the formulations explored and a qualitative assessment of the properties of the materials developed. Unless indicated otherwise, 80 : 20 mol : mol, 1 mol% PI, 1 wt% AgSbF₆; (C) example CAD design that was employed as a benchmark for 3D-printing; (D) 3D-printed part with PIL3 formulation without Ag reduction; (E) 3D printed part with PIL3 formulation with AgNPs generated by post printing UV irradiation. Printed part; (F) the UV-Visible peak feature attributed to the AgNP plasmon in 3D-printed and UV-exposed PIL3 centred at 422 nm; and (G) transmission electron micrograph of a 3D printed and UV-exposed PIL3 part showing the presence of AgNPs dispersed within the PIL matrix.

chains.⁴⁶ The mechanical properties of the **PIL1** pieces are summarised in Fig. S2D.† FT-IR studies during UV exposure over time revealed only a small decrease in the intensity of the C=C stretch peak at $\sim 1660\text{ cm}^{-1}$ after 5 minutes of UV exposure, and no further change upon further UV exposure (Fig. 2C). The peak feature at $\sim 1660\text{ cm}^{-1}$ can also be attributed to the C=C bond in the imidazole ring,^{47–49} and thus the intensity of this peak would not change upon further UV exposure. Therefore, it is proposed that the increase in tensile stiffness and T_g upon increased UV exposure time is due to the continued formation of AgNPs and/or aggregation of AgNPs, both of which contribute to modifying the mechanical pro-

perties of polymer matrices.⁵⁰ UV-Vis transmission spectroscopy experiments during the UV post-printing treatment further confirmed the formation of AgNPs due to the presence of a shoulder peak centred at $\lambda \approx 450\text{ nm}$ increasing in absorbance, which is attributed to the AgNP plasmon. For comparison, an analogous liquid IL homogeneous system was prepared, where Ag(SbF₆) (1 wt%) was added to non-polymerisable 1-butyl-3-methylimidazolium bis(trifluoromethane)sulfonimide and photo-reduced under UV light ($\lambda = 395\text{ nm}$). In this case, the plasmon arising due to the presence of AgNPs, was also observed as a shoulder in the UV-Vis spectrum (see Fig. S3†). Interestingly, changing the monomer to 1-(3-hydroxy-



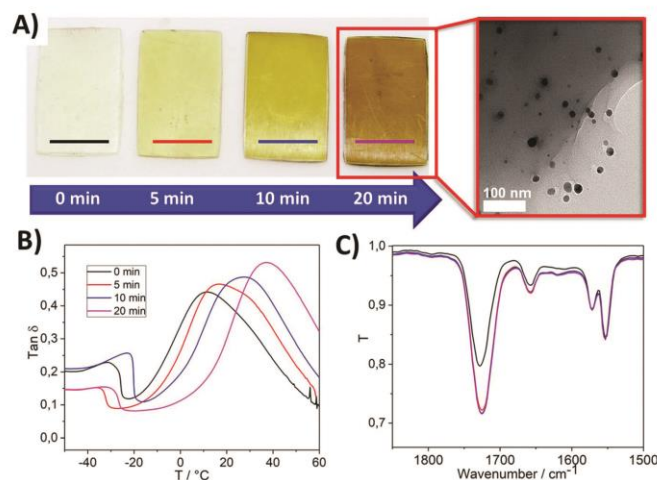


Fig. 2 (A) The PIL1 3D printed parts exhibited different colours depending on the exposure time to UV light ($\lambda = 395$ nm, 36 W, r.t.) with (red inset) a transmission electron micrograph showing the presence of nanoparticles; (B) The $\tan \delta$ vs. temperature curves, where the T_g values (defined as the x-axis values at each curve maximum) increase with increasing UV exposure time; and (C) FT-IR spectrum demonstrating little to no change in the C=C peak upon increasing UV exposure time (the curve colours are the same as per the legend inset in (B)). This suggests that further polymerisation of unpolymerised C=C bonds in the materials is not contributing to the increases in tensile stiffness and T_g upon UV exposure.

propyl)-3-vinylimidazolium bis(trifluoromethane)sulfonimide [POHVM][NTf₂] (**mIL2**, Fig. 1B) in the formulation, whilst keeping the rest of the formulation constant (**PIL2**), led to better resolved plasmons after post-curing with a well-defined plasmon (distinct absorption peak, rather than a shoulder feature) with a maximum at $\lambda = 413$ nm (Fig. S4,† blue curve).

However, it was determined that LCD-based printing of the **PIL2** formulation resulted in excessively rigid samples, which deformed and cracked during the polymerisation process. It was hypothesised that the presence of the hydroxyl group of the cation, combined with the use of 1,4-BDA as cross-linking agent, had an influence on the mechanical properties of the resulting material, which in turn affected the printability. Instead, use of poly(ethyleneglycol) diacrylate (PEGDA, $M_n = 575$ g mol⁻¹) resulted in much more flexible films (herein **PIL3**, Fig. 1B), which showed suitable mechanical properties for the polymerisation and 3D printing of suitable geometries with acceptable resolution (Fig. 1C–E and Fig. S5†). The corresponding UV-Visible peak feature attributable to AgNPs was well-defined and centred at 422 nm (Fig. 1F and Fig. S4,† red curve) and the AgNPs were well dispersed within the PIL matrix (Fig. 1G). Now that a suitable composition of PIL ink had been determined, aging experiments were performed to determine the stability of the AgNP@PIL parts over time.

To examine the photostability of the AgNP@PIL materials, **PIL2** 3D-printed parts were stored either under ambient lighting or in dark conditions. It was observed that AgNP@PIL2 materials, which had been generated by post-curing photore-

duction exhibited photo-aging when exposed to ambient light in terms of an increase in the magnitude of the absorbance peak attributed to AgNPs, suggesting the continued photoreductive formation of AgNPs (Fig. S6†). The stability of 3D-printed AgSbF₆-containing PILs to photoreduction was then investigated and it was determined that storage in dark conditions was required to prevent photo-aging. When non-photoreduced **PIL2** pieces were exposed to three weeks of ambient light a peak (centred at ~ 450 nm) in the UV-Visible transmission spectra developed, suggesting the formation of AgNPs (Fig. 3A). In contrast, non-photoreduced 3D printed **PIL2** pieces stored in the dark produced no such observable absorbance feature that could be attributed to AgNPs (Fig. 3B). Thus, for use of these materials as potential antimicrobial materials/devices, storage in dark conditions demonstrates the hypothesis that it is possible to decouple the manufacturing of devices by 3D printing from the photoreduction of active AgNPs.

The presence of hydrophobic poly(ionic liquids) combined with AgNPs make PILs interesting and highly applicable candidates for antimicrobial surface coatings to prevent biofilm formation. Ionic liquids are gaining relevance as they present some desirable characteristics highly relevant in the clinical use, such as improved bacterial resistance, antibiofilm properties, and the possibility of being 3D-printed as specific dental objects, among others.^{41,51} The antimicrobial activity of the PILs reported herein were evaluated against non-pathogenic *E. coli* and *B. subtilis* and two moulds (*A. niger* and



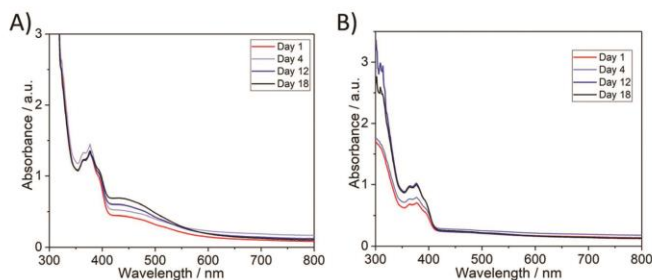


Fig. 3 (A) AgNPs@PIL2 non-reduced and then aged under ambient light highlighting the development of a peak feature at ~450 nm suggesting the formation of AgNPs; and (B) AgNPs@PIL2 non-reduced and then aged under dark conditions, showing no AgNP plasmon. In all cases the samples were exposed to ambient atmosphere.

C. cladosporioides) via zone of inhibition (Kirby-Bauer) tests and cell proliferation assays, as well as biofilm inhibition studies. In general, PIL and AgNP@PIL samples act to inhibit microbial growth, but AgNP-containing PILs (AgNP@PIL) are more effective at reducing bacterial viability.

In the first instance, a zone of inhibition test of **PIL1** and AgNPs@PIL1 revealed that only the AgNP@PIL1 displayed an inhibition halo against *E. coli* and *B. subtilis* (Fig. 4A). This inhibition of bacterial growth around the sample is due to the diffusion of the Ag⁺ ions into the agar, which is the most important factor in the antimicrobial activity of the AgNPs against bacteria.⁵¹ No inhibition halo was found with the **PIL1** samples due to the lack of silver. A delay halo—characterised for the mycelium growth but a lack of sporulation—was found around AgNP@PIL1 incubated in the plate inoculated with *A. niger*. No inhibition nor delay halo was found with the **PIL1** sample, and neither **PIL1** nor AgNP@PIL1 resulted in mycelium or sporulation inhibition for *C. cladosporioides* (Fig. 4B).

In order to determine the antibacterial activity of the samples in solution, the bacterial growth in cell culture media in the presence of the samples was monitored by optical density. **PIL1** repressed the growth of *E. coli* and *B. subtilis* in

liquid media over a 24 hour period but, interestingly, the corresponding reduction in bacterial cell viability was lower for the Gram-positive *B. subtilis* (Fig. 5A). Since hydrophobic antimicrobial compounds often act by disrupting, depolarising, and destabilising bacterial cell membranes,^{52,53} our hypothesis was that the bacteriostatic PIL samples and the associated stress to the cell membrane provokes increased proliferation in this species. Furthermore, *B. subtilis* can form protective endospores that are able to tolerate harsh environmental conditions, thus another hypothesis is that the presence of the PIL without silver can stimulate the production of endospores by *B. subtilis*, potentially explaining the differences compared with the growth of *E. coli*. This was confirmed by Environmental Scanning Electron Microscopy (ESEM), which showed a high degree of sporulation in *B. subtilis* (Fig. 5C). On the other hand, the AgNPs@PIL1 variant was found to reduce bacterial cell growth of *E. coli* and *B. subtilis* by 86% and 75%, respectively, as expected, due to the antimicrobial effect of silver. Broth and agar dilution methods are standard methods used to determine the antimicrobial effect of the compounds, but these assays are standardised for soluble compounds. Hence, performing a surface antimicrobial assay is essential when using compounds which are meant to be applied as a coating or, like in this case, they are created directly as a 3D object. Here, a modified Japanese Industrial Standard Z 2801 method was used to determine the surface antimicrobial activity of **PIL1** and AgNP@PIL1 (Table 1). **PIL1** displayed a bacterial reduction of 100% and 89% for *E. coli* and *B. subtilis*, respectively, while AgNP@PIL1 reduced 100% of the bacterial cell count. Subcultures of the supernatants confirmed the bactericidal effect of the AgNP@PIL1, while **PIL1** only displayed bactericidal effect against *E. coli*. These results are commensurate with the results in liquid medium and the ESEM images (Fig. 5A), where the samples containing Ag displayed a higher antimicrobial effect, with *B. subtilis* being the most resistant strain. The differences in antimicrobial activity between the solution and the surface activity tests show that the antimicrobial properties are based primarily on surface contact-

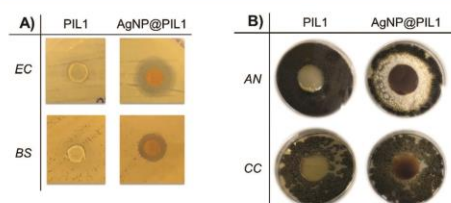


Fig. 4 (A) Zone of Inhibition test of **PIL1** and AgNPs@PIL1 against two bacterial strains (*E. coli* and *B. subtilis*) and (B) two moulds (*A. niger* and *C. cladosporioides*).



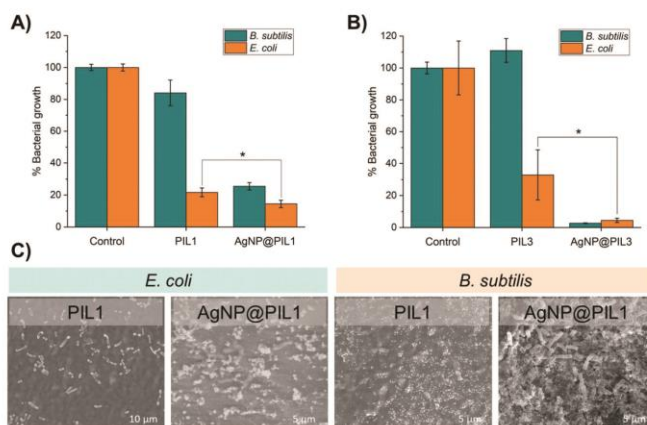


Fig. 5 (A) Bacterial cell viability of *E. coli* and *B. subtilis* incubated with PIL1 and AgNP@PIL1 and (B) PIL3 and AgNP@PIL3. (C) ESEM images of PIL1 and AgNP@PIL1 inoculated with *E. coli* and *B. subtilis*. Both PIL1 and AgNP@PIL1 affect *E. coli* morphology, disrupting the cell membrane. On the other hand, PIL1 stimulates *B. subtilis* sporulation, while the AgNP@PIL1 prevents colonisation of the polymeric surface due to a higher bactericidal effect.

Table 1 Bacterial reduction (%) after 24 hours incubation over the samples

	Bacterial reduction	
	<i>E. coli</i>	<i>B. subtilis</i>
PIL1	100%	89%
AgNP@PIL1	100%	100%

killing rather than the release of an active component, such as Ag⁺ ions, into the local environment.³¹ Evaluation of the antibacterial activity of the PIL3 formulation yielded similar results, however, AgNP@PIL3 was found to possess the highest degree of inhibition after 24 hours of incubation, resulting in a reduction of around 95% for both bacterial strains (Fig. 5B).

Conclusions

Herein, the capability of novel 3D-printed materials consisting of polymeric ionic liquids (PILs) for the controlled on-demand synthesis, and subsequent stabilisation, of silver nanoparticles (AgNPs) has been demonstrated. It was determined that the nature of the ionic liquid moieties affected the *in situ* formation of the AgNPs and enabled the controlled formation and stabilisation of AgNPs via extended UV photoreduction after the 3D printing process. This demonstrated an effective decoupling of the 3D printing fabrication step from the on-demand generation of AgNPs with narrow size dispersity by subsequent exposure to UV irradiation. Upon further investigation, it was determined that the structure of the cation of

the monomer ionic liquid had a profound effect on the formation of AgNPs, with a discrete UV-Vis peak feature attributed to the plasmon resonance of well-formed discrete AgNPs within the PILs formed from **mIL2** (AgNPs@PIL3), in contrast to a broad shoulder feature measured in the UV-Vis spectrum of AgNPs@PIL1. Thus, through careful choice of monomer ionic liquid, a suitable crosslinker for favourable mechanical properties, and a formulation that had previously been shown to be effective for 3D printing, the fabrication of materials/devices decoupled from on-demand photo-reductive formation of AgNPs for enhanced antimicrobial activity was realised. Indeed, the printed devices showed a multi-functional and tuneable microbiocidal activity against Gram positive (*B. subtilis*) and Gram negative (*E. coli*) bacteria and against the fungus *A. niger*. PIL-based materials were found to be bacteriostatic, whereas AgNPs@PIL materials possessed enhanced antimicrobial activity and bactericidal properties against the tested strains.

This work represents the first example of the novel combination of the decoupled *in situ* photoreductive fabrication of silver nanoparticles from the fabrication via 3D printing of the PIL-based materials. This *in situ* generation of nanostructured antimicrobial materials opens new routes to the development of 3D printed devices resistant to biofilm formation, for applications in the biomedical, food technology and healthcare industries. Furthermore, the near infinite combinations of cations and anions possible in PIL-based materials allows for further tuning and enhancement of the synergistic antimicrobial properties, especially when combined with the freedom of design inherent to additive manufacturing techniques.



Experimental and methods

General experimental information

Unless otherwise stated, all reagents were purchased from Sigma-Aldrich and used without further purification. BDA (90%) and 1-vinylimidazole were used after purification by passing through a short column of basic alumina (aluminium oxide).

The 3D printers used in this study were a LittleRP 3D printer and an Elegoo Mars. The Little RP 3D printer was equipped with an Acer P1500 projector (3D printer light source) that was fitted with an OSRAM P-VIP high pressure (>200 bar) Hg vapour lamp (210 W). The Elegoo Mars printed was equipped with a 2560 × 1440 2 K HD masking LCD, illuminated with 40 W UV LED backlight ($\lambda = 405$ nm). The light sources in both printers were both ~3000 lumens. UV-vis spectra were collected using an Agilent Cary 5000 UV-vis-NIR spectrophotometer. FT-IR spectra were collected on a Bruker Alpha fitted with a Platinum ATR module. ^1H NMR spectra were recorded on a Bruker AVX400 (400 MHz) spectrometer at ambient temperature. ^{13}C NMR spectra were recorded on a Bruker AVX400 (101 MHz) spectrometer at ambient temperature. Environmental Scanning Electron Microscopy (ESEM) data was collected on a Quanta FEG-250 (FEI Company) field emission SEM for high-resolution imaging working in ESEM mode using a GSED detector under high relative humidity conditions. Transmission electron microscopy (TEM) measurements were performed using a JEOL 2000-FX operated with an accelerating voltage of 200 kV. The samples were prepared using ultramicrotomy process, where sample slices of few nanometres thickness were deposited on TEM grids. The mechanical analyses were performed with a TA Q800 DMA using a tension clamp. The moduli measurements as a function of temperature were measured using a strain amplitude of 0.1% and frequency of 1 Hz. The samples were cooled to -50 °C and stabilised at -50 °C for 5 min. Finally, the sample was then heated to 200 °C at the rate of 5 °C min^{-1} . The moduli were measured during the heating run. For the stress-strain measurements, the samples were first equilibrated at 25 °C for 5 min and then the force was ramped from 0 to 18 N at the rate of 1 N min^{-1} and the stress-strain curves were recorded.

Synthesis of ionic liquids

Full synthesis details and characterisation data are given at the end of the ESI.†

Process for 3D printing imidazolium PIL networks

The process for 3D printing imidazolium PIL pieces fabricated with 80 mol% [BVIM][NTf₂] (**mIL1**) ionic liquid is given as an example. The stereolithography fabrication began by slicing a 3D computer aided design model into individual images for projecting onto the photocurable ink. Additive manufacturing software, Creation Workshop RC36, was used to create slices of a desired thickness (50 μm per layer), control the projection time of the images by the projector, and the movement of the

build plate of the LittleRP FlexVat. For the Elegoo Mars 3D printer CHITUBOX software was employed. Then the printer vat was filled with the premixed **PIL1** ink, which contained 80 mol% [BVIM][NTf₂], 20 mol% 1,4-butanediol diacrylate (BDA), 1 mol% diphenyl(2,4,6-trimethylbenzoyl)phosphine oxide (photoinitiator) and 1 wt% silver hexafluoroantimonate (AgSbF₆). Then the build plate was lowered into the ink against the transparent film of the bottom of the vat. The software then controlled the projector to show a black background with white images of each of the layers which were to be photo-cured. The UV light passed through the transparent bottom of the vat. Each layer (50 μm) was cured for 8 s. After 8 s, the printer showed a black background (negligible light was projected into the photocurable ink) whilst the build plate was automatically lifted by 50 μm . Then the software loaded the image of the next layer and turned “on” the UV light by showing the next white colour image. This process was repeated until the object was completely fabricated. After the object was fabricated, the object was isolated and copiously washed with isopropyl alcohol to remove any uncured ink.

UV-Vis absorbance measurements of 3D-printed pieces

For collection of the UV-vis absorbance spectra of the 3D printed specimen, before and after irradiation with UV light, the specimen was first affixed to a metal holder exposed to UV light for a determined fixed amount of time, then a UV-vis spectrum of this specimen was collected using the Cary 5000 UV-vis-NIR spectrophotometer. Once the UV-Vis spectrum was collected, the procedure was repeated until a total UV light exposure of the desired time was reached.

Microorganisms and growth conditions

Two bacterial strains were tested in the antibacterial assays: *Escherichia coli* DH5 α as a Gram-negative model and *Bacillus subtilis* 1904-E as a Gram-positive model. Two moulds from the “Colección Española de Cultivos Tipo (CECT)” were tested in the antifungal assays: *Aspergillus niger* CECT 2088 and *Cladosporium cladosporioides* CECT 2111. Fungal spore suspensions were stored in 0.1% Tween, 20% glycerol at -80 °C prior to use. The following culture media was used: Tryptone Soy Agar (TSA) (Thermo Scientific™), Sabouraud Dextrose Agar supplemented with chloramphenicol (SDA) (Scharlab, S. L.), as solid media; Luria-Bertani (LB) and Nutrient Broth (NB) (Scharlab, S. L.) as liquid media. The microbial growth conditions are summarised in the Table 2.

Agar diffusion test

A modified Kirby Bauer disk diffusion technique was used. The 3D printed samples (3 mm-diameter circles of PIL and AgNPs@PIL) were first sterilised with ethanol 70% and then they were placed in solid media previously inoculated with a bacterial lawn (10^7 CFU mL^{-1}) of *E. coli* or *B. subtilis*. After 24 hours of incubation at 37 °C, the inhibition halo around the samples was observed.

For the antifungal assay, the 3D printed samples (20 mm-diameter circles of PIL and AgNPs@PIL) were sterilised with



Table 2 Microorganisms and growth conditions

Microorganism	Solid medium	Liquid medium	Incubation temperature (°C)	Pre-inoculum incubation
Bacteria				
<i>E. coli</i> DH5α	TSA	LB	37	24 hours
<i>B. subtilis</i>	TSA	NB	37	24 hours
Fungi				
<i>A. niger</i>	SDA	—	35	4 days
<i>C. cladosporioides</i>	SDA	—	25	4 days

ethanol 70% and then placed in solid media previously inoculated with a spore solution (10^4 conidia mL^{-1}) of *A. niger* or *C. cladosporioides*. After 96 hours of incubation at the corresponding temperature (see Table 2), the inhibition halo around the samples was observed.

Bacterial cell proliferation assay

Bacterial growth was recorded measuring the optical density (OD) of the samples at 600 nm over a 24 hour period using a microplate reader (Thermo Scientific MULTISKAN GO). Results were compared with the OD variation of a control culture containing only *E. coli* or *B. subtilis*. The data for all control experiments and antibacterial assays are based on a total of six repeats to verify the reproducibility of the results and to calculate the mean values and the standard deviation; each experiment was repeated a minimum of three times to verify the results between different inoculations. The samples (PIL and AgNPs@PIL), previously sterilised with ethanol 70%, were placed in a 24-well plate inoculated with 1 mL of the inoculum (1×10^7 CFU mL^{-1} of *E. coli* or *B. subtilis*), incubated at 37 °C, and the antiproliferative effects induced by the samples were observed by plotting optical density (OD) vs. time. Bacterial growth was recorded measuring the optical density (OD) of 100 μL collected from each well of the 24-well plate, in a 96-well plate. Measurements at 600 nm were performed using a microplate reader, each hour during the first 8 hours and at 24 hours as a final point. To maintain the final volume (1 mL) during the experiment, the 100 μL subtracted from the wells from the 24-well plate were replaced with 100 μL of medium. Results were compared with the OD variation of a control culture containing only bacteria (*E. coli* or *B. subtilis*). Statistical analysis was performed using unpaired *t*-test. *P* values <0.05 were considered significant. Single stars denote $0.01 < P < 0.05$.

Surface antimicrobial activity

The surface antimicrobial activity was studied using a modified JIS Z 2801 standard. The protocol lasts three days. On the first day, a bacterial suspension of 1×10^7 CFU mL^{-1} was prepared and then 50 μL of this suspension was added over the surface of the samples of interest (2×2 cm) and over a reference sample with no antimicrobial activity (2×2 cm) after the sterilisation of these samples with ethanol 70%. In order to even the contact surface, a coverslip was put above the 50 μL of bacterial suspension in all the samples. The samples were incubated in a humid chamber at 37 °C for 24 h. After the 24 h of incubation, the bacteria over the samples were extracted

into liquid medium by putting the samples into a 50 mL falcon with 15 mL of culture media and shaking them one minute with a vortex. The culture media with the extracted bacteria was then diluted and sown in agar plates, which were incubated at 37 °C during 24 h. On the last day, the CFU of the cultivated agar plates were counted. The percentage of bacterial log reduction was obtained using the following formula:

$$\text{Reduction} = \log(\text{cfu reference sample}) - \log(\text{cfu antimicrobial sample})$$

Environmental scanning electron microscopy (ESEM) of the bacteria incubated over the samples

The effect of the samples (PIL and PIL@AgNPs) on the morphology of the bacteria was studied by ESEM. The samples were sterilised with ethanol 70% and inoculated with 100 μL of a 10^4 CFU mL^{-1} bacterial suspension. Then the inoculated samples were incubated in a humid chamber at 37 °C for 24 h. After the incubation time, the samples were rinsed with distilled sterile water and visualised on a Quanta FEG-250 (FEI Company) field emission SEM for high-resolution imaging working in ESEM mode using a GSED detector.

Conflicts of interest

There are no conflicts to declare.

Acknowledgements

Generalitat Valenciana (CIDEAGENT/2018/036), UJI (UJI-B2020-44) and the Agencia Valenciana of Innovacion (INNCON/2020/14) are gratefully acknowledged for funding that partially funded this work. SMC thanks the Generalitat Valenciana for a doctoral scholarship funding (ACIF/2020/338). Financial support from Ministerio de Ciencia Innovación y Universidades (Spain) through Proyecto I+D+i PID2019-109333RB-I00. We thank the Beacons of Excellence: Propulsion Futures and Green Chemicals of the University of Nottingham for financial support; the Nanoscale and Microscale Research Centre – UoN. J. M. C., V. S., and G. N. N. thank the Leverhulme Trust (RPG-2016-442). IFC thanks Gobierno de Aragón for a doctoral scholarship. Further financial support from Fondo Social Europeo-Gobierno de Aragón (E15_20R) and CIBER-BBN is gratefully acknowledged. The authors would like to acknowledge the Laboratorio de



Microscopias Avanzadas (LMA) at Universidad de Zaragoza for offering access to their instruments and expertise.

References

- 1 J. M. A. Blair, M. A. Webber, A. J. Baylay, D. O. Ogbolu and L. J. V. Piddock, *Nat. Rev. Microbiol.*, 2015, **13**, 42–51.
- 2 S. Mahira, A. Jain, W. Khan and A. J. Domb, in *Antimicrobial Materials for Biomedical Applications*, Royal Society of Chemistry, 2019, pp. 1–37, DOI: 10.1039/9781788012638-00001.
- 3 T. C. Dakal, A. Kumar, R. S. Majumdar and V. Yadav, *Front. Microbiol.*, 2016, **7**, 1831.
- 4 M. B. Estevez, S. Raffaelli, S. G. Mitchell, R. Faccio and S. Alborés, *Molecules*, 2020, **25**, 2023–2023.
- 5 N. Karak, in *Nanomaterials and Polymer Nanocomposites*, ed. N. Karak, Elsevier, 2019, pp. 47–89.
- 6 B. Tylkowski, A. Trojanowska, M. Nowak, L. Marciniak and R. Jastrzab, *Phys. Sci. Rev.*, 2017, **2**, 0024.
- 7 C. C. Piras, C. S. Mahon and D. K. Smith, *Chem. – Eur. J.*, 2020, **26**, 8452–8457.
- 8 Y. Niu, T. Guo, X. Yuan, Y. Zhao and L. Ren, *Soft Matter*, 2018, **14**, 1227–1234.
- 9 I. Gibson, D. W. Rosen and B. Stucker, *Additive Manufacturing Technologies: Rapid Prototyping to Direct Digital Manufacturing*, Springer-Verlag US, Boston, MA, U. S., 2010.
- 10 F. Afghah, M. Ullah, J. S. M. Zanjani, P. A. Sut, O. Sen, M. Emanet, B. S. Okan, M. Culha, Y. Menceoglu and M. Yildiz, *Biomed. Mater.*, 2020, **15**, 035015.
- 11 C. Bergonzi, G. Remaggi, C. Graiff, L. Bergamonti, M. Potenza, M. C. Ossiprandi, I. Zanotti, F. Bernini, R. Bettini and L. Elviri, *Nanomaterials*, 2020, **10**, 844.
- 12 S. Chen, J. Yang, Y.-G. Jia, B. Lu and L. Ren, *Materials*, 2018, **11**, 2444.
- 13 D. Podstawczyk, D. Skrzypczak, X. Polomska, A. Stargala, A. Witek-Krowiak, A. Guiseppi-Elie and Z. Galewski, *Polym. Compos.*, 2020, **41**, 4692–4705.
- 14 M. Shin, K. H. Song, J. C. Burrell, D. K. Cullen and J. A. Burdick, *Adv. Sci.*, 2020, **6**, 1901229.
- 15 G. Taormina, C. Sciancalepore, F. Bondioli and M. Messori, *Polymers*, 2018, **10**, 212.
- 16 N. Vidakis, M. Petousis, E. Velidakis, M. Liebscher and L. Tzounis, *Biomimetics*, 2020, **5**, 42.
- 17 Y. Yagci, M. Sangermano and G. Rizza, *Polymer*, 2008, **49**, 5195–5198.
- 18 E. Fantino, A. Chiappone, F. Calignano, M. Fontana, F. Pirri and I. Roppolo, *Materials*, 2016, **9**, 589–589.
- 19 Z. Wu and Y. Hong, *ACS Appl. Mater. Interfaces*, 2019, **11**, 33734–33747.
- 20 E. Fantino, A. Chiappone, I. Roppolo, D. Manfredi, R. Bongiovanni, C. F. Pirri and F. Calignano, *Adv. Mater.*, 2016, **28**, 3712–3717.
- 21 D. Mecerreyes, *Prog. Polym. Sci.*, 2011, **36**, 1629–1648.
- 22 J. Dupont, *J. Braz. Chem. Soc.*, 2004, **15**, 341–350.
- 23 V. Sans, N. Karbass, M. I. Burguete, V. Compañ, E. García-Verdugo, S. V. Luis and M. Pawlak, *Chem. – Eur. J.*, 2011, **17**, 1894–1906.
- 24 W. Qian, J. Texter and F. Yan, *Chem. Soc. Rev.*, 2017, **46**, 1124–1159.
- 25 J. Huang, C.-a. Tao, Q. An, W. Zhang, Y. Wu, X. Li, D. Shen and G. Li, *Chem. Commun.*, 2010, **46**, 967–969.
- 26 M. G. Cowan, M. Masuda, W. M. McDanel, Y. Kohno, D. L. Gin and R. D. Noble, *J. Membr. Sci.*, 2016, **498**, 408–413.
- 27 J.-S. Lee, K. Sakaushi, M. Antonietti and J. Yuan, *RSC Adv.*, 2015, **5**, 85517–85522.
- 28 S. Washiro, M. Yoshizawa, H. Nakajima and H. Ohno, *Polymer*, 2004, **45**, 1577–1582.
- 29 S. Sen, S. E. Goodwin, P. V. Barbará, G. A. Rance, D. Wales, J. M. Cameron, V. Sans, M. Mamlouk, K. Scott and D. A. Walsh, *ACS Appl. Polym. Mater.*, 2021, **3**, 200–208.
- 30 Y. Biswas, T. Maji, M. Dule and T. K. Mandal, *Polym. Chem.*, 2016, **7**, 867–877.
- 31 Q. Zhao, J. W. C. Dunlop, X. Qiu, F. Huang, Z. Zhang, J. Heyda, J. Dzubiella, M. Antonietti and J. Yuan, *Nat. Commun.*, 2014, **5**, 4293.
- 32 Q. Zhao, J. Heyda, J. Dzubiella, K. Täuber, J. W. C. Dunlop and J. Yuan, *Adv. Mater.*, 2015, **27**, 2913–2917.
- 33 E. Karjalainen, D. J. Wales, D. H. A. T. Gunasekera, J. Dupont, P. Licence, R. D. Wildman and V. Sans, *ACS Sustainable Chem. Eng.*, 2018, **6**, 3984–3991.
- 34 V. G. Maciel, D. J. Wales, M. Seferin and V. Sans, *J. Cleaner Prod.*, 2019, **214**, 29–40.
- 35 D. J. Wales, Q. Cao, K. Kastner, E. Karjalainen, G. N. Newton and V. Sans, *Adv. Mater.*, 2018, **30**, 1800159.
- 36 A. R. Schultz, P. M. Lambert, N. A. Chartrain, D. M. Ruohoniemi, Z. Zhang, C. Jangu, M. Zhang, C. B. Williams and T. E. Long, *ACS Macro Lett.*, 2014, **3**, 1205–1209.
- 37 J. Dupont and J. D. Scholten, *Chem. Soc. Rev.*, 2010, **39**, 1780–1804.
- 38 J. Guo, Q. Xu, Z. Zheng, S. Zhou, H. Mao, B. Wang and F. Yan, *ACS Macro Lett.*, 2015, **4**, 1094–1098.
- 39 A. Muñoz-Bonilla and M. Fernández-García, *Eur. Polym. J.*, 2018, **105**, 135–149.
- 40 A. Misra, I. Franco-Castillo, D. P. Müller, C. González, S. Eyssautier-Chuine, A. Ziegler, J. M. de la Fuente, S. G. Mitchell and C. Streb, *Angew. Chem., Int. Ed.*, 2018, **57**, 14926–14931.
- 41 M. D. T. Torres, S. Voskian, P. Brown, A. Liu, T. K. Lu, T. A. Hatton and C. de la Fuente-Nunez, *ACS Nano*, 2021, **15**, 966–978.
- 42 D. K. Bhui, H. Bar, P. Sarkar, G. P. Sahoo, S. P. De and A. Misra, *J. Mol. Liq.*, 2009, **145**, 33–37.
- 43 K. Ikemura, K. Ichizawa, M. Yoshida, S. Ito and T. Endo, *Dent. Mater. J.*, 2008, **27**, 765–774.
- 44 A. Heilmann, *Polymer Films with Embedded Metal Nanoparticles*, Springer-Verlag Berlin Heidelberg, Berlin, Germany, 2003.



- 45 S. V. Calderon, R. E. Galindo, N. Benito, C. Palacio, A. Cavaleiro and S. Carvalho, *J. Phys. D: Appl. Phys.*, 2013, **46**, 325303.
- 46 K. P. Menard and N. R. Menard, in *Encyclopedia of Polymer Science and Technology*, ed. H. F. Mark, Wiley, 4th edn, 2015, DOI: 10.1002/0471440264.pst102.pub2.
- 47 C. W. Duan, J. You, B. Liu, J. L. Ma, H. P. Zhou, H. B. Zhang and J. Zhang, *New J. Chem.*, 2018, **42**, 12243–12255.
- 48 B. Jamehbozorg and R. Sadeghi, *J. Chem. Eng. Data*, 2018, **63**, 331–340.
- 49 R. S. Datta, S. M. Said, S. R. Shahrir, N. Abdullah, M. F. M. Sabri, S. Balamurugan, Y. Miyazaki, K. Hayashi, N. A. Hashim, U. Habiba and A. M. Affi, *RSC Adv.*, 2015, **5**, 48217–48223.
- 50 J. Jancar, J. F. Douglas, F. W. Starr, S. K. Kumar, P. Cassagnau, A. J. Lesser, S. S. Sternstein and M. J. Buehler, *Polymer*, 2010, **51**, 3321–3343.
- 51 J. Yue, P. Zhao, J. Y. Gerasimov, M. van de Lagemaat, A. Grotenhuis, M. Rustema-Abbing, H. C. van der Mei, H. J. Busscher, A. Herrmann and Y. Ren, *Adv. Funct. Mater.*, 2015, **25**, 6756–6767.
- 52 M. D. T. Torres, S. Sothiselvam, T. K. Lu and C. de la Fuente-Nunez, *J. Mol. Biol.*, 2019, **431**, 3547–3567.
- 53 A. Valls, J. J. Andreu, E. Falomir, S. V. Luis, E. Atrián-Blasco, S. G. Mitchell and B. Altava, *Pharmaceuticals*, 2020, **13**, 482.



Appendix 7: Bacterfield - ¡Las bacterias entran en juego!

Actividad de divulgación creada por Isabel Franco Castillo y Elena Atrián Blasco

Breve resumen de la actividad

¿Quién dijo que los juegos de estrategia y educativos no podían ir juntos? ¡Esta es la idea detrás de Bacterfield! Bacterfield es un juego de mesa que usa bacterias y su comportamiento real como elementos principales del juego, para construir la dinámica de un juego clásico de estrategia.



Bacterfield comenzó como un juego de mesa desarrollado por **dos Elena Atrián Blasco e Isabel Franco Castillo, investigadoras** del INMA-CSIC/UNIZAR, para ser usado como herramienta de divulgación. El proyecto inicial contó con la financiación de la 3ª convocatoria *Cuenta la Ciencia* de la Fundación General CSIC. A partir de este proyecto han surgido otras

importantes iniciativas como la futura comercialización del juego de mesa, que estará disponible próximamente en formato de campaña de microfinanciación, o una versión *print-and-play* disponible en 24 idiomas con la colaboración de la iniciativa *Science is Wonderful! Live* de la Comisión Europea.

Fecha de realización: en activo desde enero de 2020

Lugar de realización: Zaragoza

Público destinatario de la acción divulgativa o proyecto educativo:

Bacterfield es un juego de mesa de estrategia y, por lo tanto, de interés para un público muy variado, desde estudiantes de educación secundaria hasta familias y grupos de amigos. Lo más importante, además, es que no se necesitan conocimientos previos en ciencia ni microbiología para poder jugar, sino que estos se adquieren a través del juego. Además, se está desarrollando una versión *print-and-play*, que estará disponible en los 24 idiomas oficiales de la Unión Europea, para convertir Bacterfield en un recurso educativo gratuito para todos los países de la Unión Europea. Esta versión está destinada a divulgación en colegios para estudiantes de entre 12 a 18 años.

Objetivos

Acercar el campo de la microbiología, tan desconocido, pero a la vez tan importante en nuestro día a día, a un público general, de manera sencilla y divertida.

Aunque no los veamos a simple vista, los microorganismos están presentes en nuestra vida desde que nacemos. Estuvieron aquí antes que nosotros y se han adaptado a vivir

en las condiciones más extremas, en las que ningún otro ser vivo sería capaz de sobrevivir. A pesar de que algunos pueden resultar perjudiciales para nosotros, otros muchos son capaces de hacer cosas fascinantes, como producir la enzima necesaria para realizar las ahora tan famosas PCRs o sintetizar insulina para tratar la diabetes. Es más, sin ellos la vida tal y como la conocemos no sería posible: por ejemplo, el ser humano depende de las bacterias que constituyen la flora intestinal para digerir correctamente los alimentos, y la gran mayoría de seres vivos dependen de vitaminas que únicamente pueden sintetizar las bacterias.

Entender cómo funciona este fascinante mundo microscópico nos puede ayudar a comprender y resolver problemas tan relevantes como la resistencia a los antimicrobianos, declarada por la [Organización Mundial de la Salud](#) como una de las 10 amenazas más importantes a la salud pública en el mundo, y que se está acelerando debido, en parte, a un desconocimiento sobre el correcto uso de los antibióticos.

El objetivo principal de la actividad Bacterfield es la **divulgación sobre microbiología**, acercando conceptos como la resistencia a antibióticos o la generación de *biofilm* (ecosistemas bacterianos organizados que otorgan protección a las bacterias), **a un público general** y no especializado **de una forma divertida**, usando estos conceptos como la dinámica y estrategia de un juego de mesa, lo que permite reforzar los conocimientos que se desean impartir de una manera más eficiente.

Resumen del alcance y resultados

Resultados principales:

- **Creación de un juego de mesa** de estrategia clásico que usa a las bacterias y sus acciones para generar la dinámica del juego.
- Desarrollo de **proyectos paralelos** a Bacterfield: Bacterfield *print-and-play*, versión online, campaña de microfinanciación.

Alcance actual y potencial, se estima un número de beneficiarios muy alto debido a:

- Las **acciones divulgativas** llevadas a cabo hasta el momento (más de 200 personas).
- La presencia en **redes sociales** y **medios de comunicación** y participación en **eventos**.
- La distribución del juego en 50 municipios dentro del proyecto **Ciudad Ciencia** del CSIC.
- Implementación **a nivel europeo** de Bacterfield *print-and-play* durante el 2022.
- Lanzamiento **internacional** de la campaña de microfinanciación a principios del 2022.
- El reconocimiento como “Best physical piece” dentro del concurso #MicrobeArt2021 organizado por la Federación de Sociedades Europeas de Microbiología.
- El reconocimiento como **accésit** en la categoría de Divulgación, de los **premios Tercer Milenio 2021**, organizados por el Heraldo de Aragón.

Descripción de la acción divulgativa o proyecto educativo

Bacterfield - ¡Las bacterias entran en juego! es un proyecto de divulgación cuyo objetivo es acercar el tan desconocido y a la vez tan importante mundo de la microbiología a un público general, de manera sencilla y divertida, mediante la creación de un innovador juego de mesa y la realización de numerosas actividades para su diversificación y difusión.

Este proyecto ha sido ideado y llevado a cabo por dos jóvenes investigadoras aragonesas del Instituto de Nanociencia y Materiales de Aragón.

El proyecto comenzó como una propuesta para el diseño y producción de un prototipo de juego de mesa con el que ayudar a explicar conceptos básicos de microbiología tales como el crecimiento bacteriano y la producción de *biofilm*, así como la importancia de la investigación de nuevos materiales antimicrobianos.

Durante los primeros meses del proyecto se llevó a cabo el diseño del juego de mesa, poniendo cuidado y énfasis en el rigor científico detrás de su dinámica. Por ejemplo, se ha tenido en cuenta el crecimiento exponencial de las bacterias como una de las características importantes de la estrategia del juego, así como la capacidad de generar *biofilm* para protegerse frente a diferentes agentes externos. El hecho de utilizar las bacterias y su comportamiento habitual en la vida real, aplicado a la dinámica y estrategia del juego, es una de las señas de identidad de Bacterfield.

El juego (desarrollado en español y en inglés, para facilitar su difusión a nivel internacional), de 2 a 4 jugadores, está formado por un tablero, fichas de bacterias de tres tipos diferentes, fichas de matriz de biofilm y distintos tipos de cartas de juego (Figura 1). Durante la partida, los jugadores podrán multiplicar sus bacterias para colonizar el tablero, y esto lo harán replicando el crecimiento exponencial de las bacterias. Además, las cartas de juego permitirán a nuestras bacterias protegerse o luchar contra las bacterias rivales, ganando genes de resistencia o de producción de antibióticos, produciendo matriz de biofilm para defenderse o eliminando bacterias rivales con la ayuda de agentes antimicrobianos o infectándolas con virus bacteriófagos.

La financiación inicial permitió el diseño profesional de las ilustraciones del juego, así como la producción de 40 copias del prototipo final y la realización de un vídeo explicativo.

Enlaces donde ampliar información

Página web del proyecto	www.bacterfieldthegame.com
Vídeo promocional	https://www.youtube.com/watch?v=gexY3rqUtK8
Twitter	@BacterfieldGame
Instagram	@bacterfield_game
Ganadores Premios #MicrobeArt2021	https://fems-microbiology.org/and-the-winners-of-microbeart2021-are/
Página de prelanzamiento, campaña de microfinanciación	https://www.kickstarter.com/projects/zierzolab/bacterfield
Heraldo de Aragón (03/05/2021)	https://www.heraldo.es/noticias/aragon/2021/05/03/investigadoras-del-inma-crean-bacterfield-un-juego-de-mesa-que-permite-dar-a-conocer-el-mundo-de-la-microbiologia-1489321.html
Aragón TV noticias (08/06/2021)	https://youtu.be/C6ePn9B5hTo



Figura 1. Componentes del juego de mesa Bacterfield